

**Joint-free movements in insects:
actuation and steering mechanisms observed
in ovipositors and piercing-sucking mouthparts,
and their biomimetic potential**

Dissertation

der Mathematisch-Naturwissenschaftlichen Fakultät
der Eberhard Karls Universität Tübingen
zur Erlangung des Grades eines
Doktors der Naturwissenschaften
(Dr. rer. nat.)

vorgelegt von
Benjamin Eggs, M.Sc.
aus Brig, Schweiz

Tübingen
2024

Gedruckt mit Genehmigung der Mathematisch-Naturwissenschaftlichen Fakultät der Eberhard Karls Universität Tübingen.

Tag der mündlichen Qualifikation: 11.11.2024

Dekan:	Prof. Dr. Thilo Stehle
1. Berichterstatter:	Prof. Dr. Oliver Betz
2. Berichterstatter:	Prof. Dr. James H. Nebelsick
3. Berichterstatter:	Assoc. Prof. Lars Vilhelmsen
4. Berichterstatter:	Dr. habil. Andy Sombke

Inhaltsangabe

Zusammenfassung.....	4
Abstract.....	6
Introduction.....	8
Material and methods.....	13
Material examined.....	13
Methods used.....	13
Terms.....	14
Synopses.....	15
Publication 1.....	16
Publication 2.....	45
Publication 3.....	49
Publication 4.....	78
Publication 5.....	90
Publication 6.....	142
Publication 7.....	148
Publication 8.....	171
Publication 9.....	206
Publications 10 and 11.....	219
Publication 12.....	230
Conclusions.....	247
Joint-free steering movements of terebrae of parasitoid hymenopterans.....	248
Joint-free steering movements of maxillary bundles of triatominae heteropterans.....	252
Joint-free steering movements of acicular cuticular structures in insects and their potential for biomimetic research.....	254
Outlook.....	257
References.....	258

Zusammenfassung

Tiere haben eine Vielfalt von stabförmigen Strukturen evolviert, welche aktiv verformt werden können, obschon sie keine intrinsischen klassischen Gelenke besitzen, wie sie in den Ingenieurwissenschaften üblich sind. Die zugrunde liegenden Mechanismen dieser aktiv aktuierten gelenkfreien Bewegungen sind aber bisher nur spärlich untersucht worden.

Diese Arbeit gibt einen Überblick über all die gelenkfreien Bewegungsmechanismen, welche wir bei wirbellosen Tieren finden. Der Schwerpunkt liegt auf dem sogenannten Gleit-Stopp-Mechanismus, welcher hier an den Beispielen der Terebrae (= Ovipositorschaft oder Eilegebohrer) parasitoider Hymenopteren und der stechend-saugenden Mundwerkzeuge von Raubwanzen untersucht wurde. Diese cuticulären Strukturen verfügen über keinerlei intrinsische Gelenke und werden über Muskeln im Hinterleib bzw. im Kopf ferngesteuert. Bei diesen Systemen sind zwei oder mehrere stabförmige elastische Elemente in Längsrichtung über ein Nut-und-Feder-System miteinander verfalzt. Die Elemente können dabei in Längsrichtung gegeneinander verschoben werden. Wird diese Längsverschiebung jedoch durch eine mechanische Sperre erschwert oder ganz unterbunden, so kommt es zu einer relativen und reversiblen Verbiegung der Elemente aufgrund ihrer elastische Verformung. Beim Gleit-Stopp-Mechanismus zählt daher zu den aktiven Biegemechanismen, da die Biegung ausschliesslich auf den relativen Bewegungen der Unterelemente zueinander beruht. Dem gegenüber stehen passive Biegemechanismen, welche aus der mechanischen Interaktion zwischen den einzelnen Elementen einer stabförmigen Struktur und dem Umgebungsmedium resultieren.

In mehreren Fallstudien haben wir umfassende morphologische Untersuchungen der gesamten skeletomuskulären Systeme mit Verhaltensanalysen kombiniert, um Funktionsmodelle zu erstellen und die zugrundeliegenden Mechanismen der gelenkfreien Bewegungen der cuticulären stabförmigen Strukturen zu eruieren und schlussendlich deren öko-evolutionäre Bedeutung und biomimetisches Potential zu diskutieren.

Parasitoide Wespen legen ihre Eier in oder auf andere Insekten(-larven) ab, welche oft verborgen im Pflanzengewebe leben. Biegebewegungen der Terebra sind dabei u.a. wichtig für das Aufspüren potentieller Wirte und eine präzise Eiablage. Die Terebra von Hymenopteren besteht aus einer 2. Valvula, welche über ein Nut-und-Feder-System mit den paarigen 1. Valvulae verbunden ist. Sie besitzt aber weder intrinsische Gelenke noch intrinsische Muskeln.

In dieser Arbeit wurde der Ovipositor und das Eilegeverhalten mehrerer Arten parasitoider Wespen aus den Überfamilien der Schlupfwespenartigen (Ichneumonoidea), Erzwespenartigen (Chalcidoidea) und Gallwespenartigen (Cynipoidea) untersucht. Dabei zeigte sich, dass gelenkfreie Biegebewegungen der Terebra weit verbreitet sind. Die verschiedenen Arten haben unterschiedliche aktive wie auch passive Bewegungsmechanismen entwickelt.

In unserer umfassenden und detaillierten Studie über den Ovipositor der Lagererzwespe *Lariophagus distinguendus* (Pteromalidae) konnten wir eine angepasste Version des Gleit-Stopp-Mechanismus

beschrieben. Die Terebra der Erzwespen besteht aus einer in Längsrichtung aufgespaltenen 2. Valvula, deren Hälften nur ganz an der Spitze verwachsen sind. Die beiden paarigen mit der 2. Valvula assoziierten Muskeln sind in ihrer Funktion modifiziert und dienen bei den Erzwespen primär der Biegung und Rotation der Terebra. Kontrahieren die Muskeln einer Seite, so wird die Basis einer Hälfte der 2. Valvula nach dorsad gezogen, wodurch sich eine Biegung der gesamten 2. Valvula und dadurch der gesamten Terebra ergibt. Dieser für Erzwespen einzigartige angepasste Gleit-Stopp-Mechanismus erlaubt es den Tieren, ihre Terebra aktiv in verschiedene Richtungen zu biegen und auch bis zu einem gewissen Masse zu rotieren und gleichzeitig die 1. Valvulae vor und zurück zu schieben, ohne dass letzteres die Biegung beeinflusst.

Des weiteren haben wir die erste quantitative mechanische Analyse skeletomuskulären Ovipositor-Systems einer Hymenoptere vorgenommen am Beispiel der Schlupfwespe *Venturia canescens* (Ichneumonidae).

Bei all den vorgestellten Studien über den Ovipositor parasitoider Wespen haben wir uns an die Hymenoptera Anatomy Ontology (HAO) gehalten und diese ergänzt und teilweise korrigiert sowie all die in der bisherigen Literatur gefundenen Synonyme aufgelistet. Unsere integrativen Studien über das skeletomuskuläre Ovipositor-System, welche Analysen des Eilegeverhaltens und detaillierte morphologische und biomechanische Untersuchungen des Ovipositors kombinieren, können als Referenzwerke für künftige Studien über dieses Thema dienen.

Die blutsaugenden Raubwanzen der Unterfamilie Triatominae (Reduviidae) besitzen langgezogene stechende Mundwerkzeuge, die aus paarigen Maxillen bestehen, welche von paarigen Mandibeln flankiert werden. Die linke und rechte Maxille sind über ein Nut-und-Feder-System miteinander verbunden und bilden das Maxillenbündel. Mit diesem suchen die Tiere im Gewebe ihrer Opfer nach Blutgefässen, wobei oft Biegebewegungen zu sehen sind.

In unserer integrativen Studie mit vier Arten der Triatominae haben wir herausgefunden, dass die Tiere in Gewebe passive Biegemechanismen nutzen um das Maxillenbündel zu biegen, also auf den mechanischen Widerstand des Umgebungsmediums angewiesen sind. In Flüssigkeit hingegen zeigen die Tiere Biegebewegungen der Spitze des Maxillenbündels, welche auf dem Gleit-Stopp-Mechanismus (also einem aktiven Biegemechanismus) beruhen. Dies zeigt, dass passive und aktive Biegemechanismen in demselben System vorkommen und dabei auch von denselben Muskelgruppen aktuiert werden können.

Detaillierte Fallstudien wie diese sind wichtig um die Funktion(en) und das/die Wirkprinzip(ien) eines Systems eruieren zu können. Diese beiden Konzepte sind zentral für den biomimetischen Wissenstransfer.

Sowohl die Terebrae parasitoider Wespen wie auch die Mundwerkzeuge der Raubwanzen können als geeignete biologische Vorbilder für Entwicklung miniaturisierter, nagelartiger und aktiv steuerbarer Sondierungsinstrumente dienen. Aufgrund dieses hohen Innovations- und Anwendungspotentials wäre das insbesondere für die minimal-invasive Chirurgie von Interesse. Da der Gleit-Stopp-Mechanismus jedoch sowohl eine gewisse Elastizität der Unterelemente als auch eine geringe Reibung zwischen diesen erfordert, eignen sich Ovipositoren und Stechborsten aber aufgrund von auftretenden Skalierungsproblemen in den meisten Fällen wahrscheinlich eher weniger als biologisches Vorbild für Projekte in der Architektur.

Abstract

Animals have evolved a variety of rod-shaped structures that can be actively deformed, even though they do not feature intrinsic classical joints as conventionally used in engineering. However, the underlying mechanisms of these actively actuated joint-free movements have so far only been sparsely investigated.

This thesis provides an overview of all the joint-free movement mechanisms found in invertebrates; its focus is on the so-called slide-lock mechanism, which has been investigated here by using the examples of the terebra (= ovipositor shaft) of parasitoid hymenopterans and the piercing-sucking mouthparts of haematophagous heteropterans. These cuticular structures have no intrinsic joints and are remotely controlled by muscles in the abdomen and the head, respectively. In these systems, two or more rod-shaped elastic elements are interlocked in a longitudinal direction via a tongue-and-groove mechanism. The individual elements can be moved against each other in a longitudinal direction. However, if this longitudinal displacement is restrained or fully prevented in some way by structural modifications, a relative and reversible bending of the elements results attributable to elastic deformation. The slide-lock mechanism thus belongs to the active bending mechanisms, as the bending is based exclusively on the relative movements of the sub-elements. Passive bending mechanisms, on the other hand, result from mechanical interactions between individual elements of a rod-shaped structure and the surrounding medium.

In several case studies, we have combined comprehensive morphological investigations of the musculoskeletal systems with behavioural analyses to create functional models and determine the underlying mechanisms of joint-free movements of the cuticular rod-shaped structures, and finally to discuss their eco-evolutionary significance and biomimetic potential.

Parasitoid wasps lay their eggs in or onto insect hosts (usually larvae), which often live hidden inside plant tissues. Steering movements of the terebra (*i.e.* bending and/or rotating) are thus important for locating potential hosts and precise egg laying. The hymenopteran terebra consists of a 2nd valvula that is connected with the paired 1st valvulae via a tongue-and-groove mechanism. However, the terebra has neither intrinsic joints nor intrinsic muscles.

This thesis presents an investigation of the structure of the ovipositor and the oviposition behaviour of several species of parasitoid wasps from the superfamilies Ichneumonoidea, Chalcidoidea and Cynipoidea. Joint-free steering mechanisms of the terebra are widespread with different taxa having evolved various active and passive movement mechanisms.

In our comprehensive and detailed study of the ovipositor of the chalcidoid wasp *Lariophagus distinguendus* (Pteromalidae), we have described a specific version of the slide-lock mechanism that seems to be unique for chalcidoids. The terebra of chalcidoid wasps features a longitudinally split 2nd valvula with overlapping, asymmetric halves that are fused only at the apex. The two paired muscles associated with the 2nd valvula are modified in their function and primarily serve to bend and rotate the terebra in chalcidoids. When the muscles on one side contract, the base of one half of the 2nd valvula is pulled dorsad, resulting in a bending

of the entire 2nd valvula and thus the whole terebra. This adapted slide-lock mechanisms unique to chalcidoid wasps allows them actively to bend their terebra in various directions and to rotate it to a certain degree and, at the same time, to pro- and retract the 1st valvulae without the latter affecting the bending of the whole terebra.

Furthermore, we have carried out the first quantitative mechanical analysis of the musculoskeletal ovipositor system of a hymenopteran by examining the ichneumonid wasp *Venturia canescens*.

In all the presented studies on the ovipositor of parasitoid wasps, we have applied the Hymenoptera Anatomy Ontology (HAO); we have also supplemented/corrected it and listed all the synonyms found in the literature. Our integrative studies on the musculoskeletal ovipositor system combining analyses of the oviposition behaviour with detailed morphological and biomechanical studies of the ovipositor system might thus become reference works for the study of the hymenopteran ovipositor in the future.

The haematophagous kissing bugs of the subfamily Triatominae (Reduviidae) possess elongated piercing mouthparts comprising a pair of maxillae flanked by paired mandibles. The left and right maxillae are interlocked via a tongue-and-groove mechanism and form the maxillary bundle. The animals use this bundle to search for blood vessels in the tissue of their hosts, whereby steering movements are often exhibited.

In our integrative study on four species of Triatominae, we have found that the kissing bugs employ passive bending mechanisms within a host's tissue to bend the maxillary bundle, *i.e.* they are dependent on the mechanical resistance of the surrounding medium. In liquids, however, the bugs exhibit bending movements of the apex of the maxillary bundle; these movements are based on the slide-lock mechanisms, *i.e.* on active bending mechanisms. This shows that passive and active bending mechanisms can occur within the same system and can also be actuated by the same set of muscles.

Detailed case studies as presented in this thesis are important for the determination of the function(s) and the working principle(s) of a system. These two concepts are central to knowledge transfer in the field of biomimetics.

The terebrae of hymenopterans and the mouthparts of heteropterans might be suitable biological concept generators for the development of miniaturized, needle-like and actively controllable probing tools. Such tools would be of particular interest for minimally invasive surgery because of their high level of innovation and their application potential. However, as the slide-lock mechanism requires both a certain elasticity of the individual sub-elements and low friction between them, ovipositors and piercing-sucking mouthparts are probably less suitable as biological concept generators for large-scale projects, such as those in architecture, because of possible up-scaling problems.

Introduction

Animals have evolved a variety of rod-like or tube-shaped systems capable of achieving actively actuated deformation without the need for joints conventionally used in engineering. In these systems, joint-free movements of organs, body parts or entire bodies do not involve flexible links (joints = articulations) between rigid elements (e.g. bones in vertebrates or exoskeletal parts in arthropods), but function via reversible shape-changes attributable to elastic deformation of the individual elements. In addition, adaptive stiffness occurs when single organs or body parts (usually reversibly) adjust their bending stiffness in response to changing external loads. Ideally, the systems exhibit flexibility during movement and develop an increased stiffness and strength when required. Four general principles of joint-free movement are observed in invertebrates: (1) amoeboid cell crawling, (2) hydroskeletal mechanisms, (3) muscular hydrostats and (4) slide-lock mechanisms (*sensu* Betz *et al.* 2016).

Slide-lock mechanisms involve the relative longitudinal sliding of two or more rod-like elements. If the relative sliding movement between the elements is restrained by structural modifications at the interfaces, then joint-free movements result because of the elastic deformations of the single elements. The bending stiffness of the elements depends on their geometry, *i.e.* their cross-sectional shape, and their material composition (Betz *et al.* 2016, Cerkvenik *et al.* 2018).

Several insects have evolved slender elongated needle-like cuticle structures featuring slide-lock mechanisms, consisting of longitudinally interlocked elements that lack any joints in the direction of bending; e.g. the terebrae (= ovipositor shafts *sensu* Quicke 1997, 2015) of hymenopterans (*cf.* Quicke and Fitton 1995, Quicke *et al.* 1995, Cerkvenik *et al.* 2017) or the piercing-sucking mouthparts of hemipterans (*cf.* Lavoipierre *et al.* 1959). These structures are often capable of achieving target-oriented deformations. The ability for sensing and precise steering (*i.e.* bending and/or rotational movements) enables these insects to navigate body structures through a variety of substrates without visual information and to reach targets that are hidden deep inside the substrate (Cerkvenik *et al.* 2017).

A parasitoid is an organism (usually an insect) that completes its larval development within or on a single host that is usually killed at the end of its development or whose further reproduction is prevented (Hajek and Eilenberg 2018). Parasitoid wasps are the most successful group of insect parasitoids, accounting for more than half of the known diversity of Hymenoptera and most likely most of the unknown diversity (Polaszek and Vilhemsen 2023). The parasitoid lifestyle evolved only once among basal hymenopterans more than 200 million years ago (Fig. 1) (Peters *et al.* 2017).

Oviposition is crucial for reproductive success; thus, oviposition behaviour and ovipositor structure have a central adaptive role (e.g. Gauld and Bolton 1988, Le Ralec *et al.* 1996, Belshaw *et al.* 2003, Ghara *et al.* 2011) that should directly affect fitness. In order successfully to parasitize a wide range of hosts, parasitoid wasps have evolved variety of parasitization strategies (ecto- vs endoparasitoidism, idiobiont vs koinobiont, solitary vs gregarious, hyperparasitoidism; *cf.* Quicke 1997, 2015, Polaszek and Vilhemsen 2023) with adapted oviposition behaviour and a huge morphological diversity in ovipositor structure.

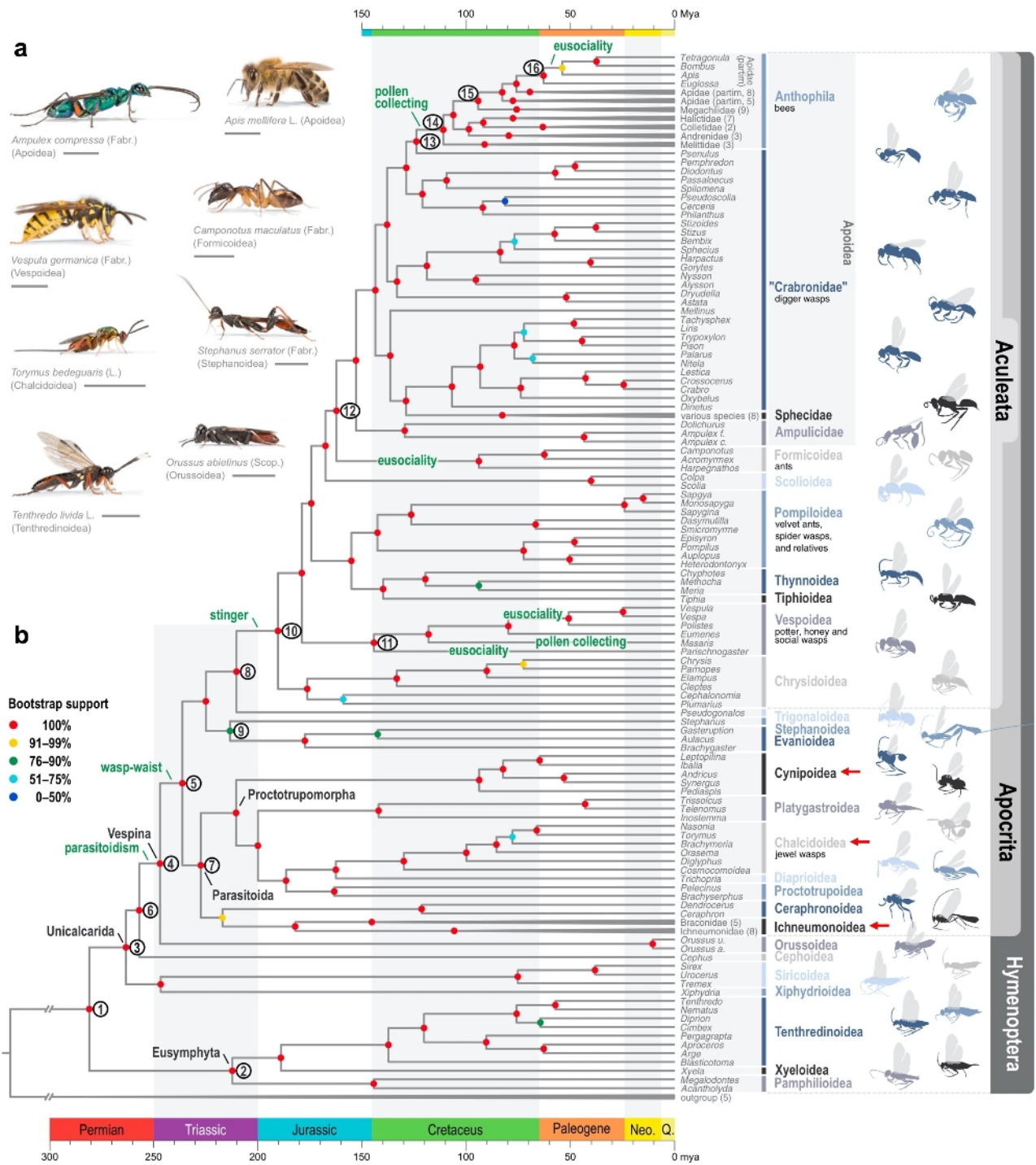


Fig. 1. Evolutionary history of Hymenoptera, highlighting the evolutionary success of parasitoid wasps (see point 7). **a** Representatives of sawflies, wasps, ants and bees (scale bars = 5 mm). **b** Phylogenetic relationships and divergence time estimates of Hymenoptera. Key evolutionary events are indicated at the respective clades. The tree was inferred under the maximum-likelihood optimality criterion. Divergence times were estimated with an independent-rates molecular clock approach and considering validated fossils. The superfamilies of the representatives studied in this thesis are marked with red arrows. From Peters *et al.* 2017, with kind permission of the authors, Elsevier license number 5623651228925.

The hymenopteran ovipositor consists of the female T9 (9th abdominal tergum), two pairs of valvifers and three pairs of valvulae derived from the 8th and 9th abdominal segments (7th and 8th metasomal segments) (Snodgrass 1933, Oeser 1961, Vilhelmsen 2000). The paired 1st valvulae (1vv; Fig. 2d,e) and the 2nd valvulae (2vv; Fig. 2d,e) enclose the egg canal (ec; Fig. 2e) and form the terebra (trb; Fig. 2 a–c). The ventral surfaces of the 2nd valvula are interlocked with both dorsal surfaces of the 1st valvulae by a sublateral longitudinal tongue called the rhachis, which runs within a corresponding groove called the aulax (au; Fig. 2d) along the dorsal surface of each of the 1st valvulae. This so-called olistheter system (oth; Fig. 2e) allows the terebra to slide longitudinally relative to each other and simultaneously prevents their unwanted separation (Oeser 1961, Quicke *et al.* 1994).

In order to reach their hosts and to permit greater control over egg placement, several parasitoid wasps are able actively to steer (*i.e.* bend and rotate) their terebra in various directions, despite the lack of intrinsic terebral musculature and joints (*cf.* Quicke and Fitton 1995, Quicke *et al.* 1995, Cerkvenik *et al.* 2017). However, putative evolutionary novelties of the hymenopteran ovipositor, such as its morphological and behavioural adaptations enabling terebra steering, its underlying mechanisms and its potential eco-evolutionary significance have hitherto not been thoroughly investigated.

Kissing bugs belonging to the subfamily Triatominae (Hemiptera: Heteroptera: Reduviidae) are known for their role as blood-sucking capillary feeding vectors of Chagas disease (*e.g.* Lavoipierre *et al.* 1959, Lent and Wygodzinsky 1979, Krenn and Aspöck 2012, Justi and Galvão 2016).

The exclusively haematophagous Triatominae possess elongated piercing mouthparts comprising a pair of mandibles that flank a pair of maxillae specialized for piercing and sucking. The maxillae are flexible half-pipes (in cross-section) tightly interlocked by a tongue and groove system that allows them to move longitudinally against each other (Wenk *et al.* 2010), while also ensuring the difficult task of forming and sealing the antidromic channels for the passage of food and salivary fluids during blood feeding (Rakitov 2019). The maxillary apices are strongly asymmetrical in shape, *i.e.* the left maxilla is spine-like, whereas the right maxilla is flagellum-like (Barth 1952, Wirtz 1987, Rakitov 2019).

While penetrating the host tissue, the animals are able to bend and rotate the maxillary bundle in various directions (*cf.* Lavoipierre *et al.* 1959), even though the maxillae are single pieced cuticular rods that are devoid of intrinsic musculature (Barth 1952). However, no studies have been presented so far about the steering movements of the stylets (mandibles and maxillae) and the mechanisms behind them.

The two systems investigated here, *i.e.* the terebrae of parasitoid wasps and the mouthparts of triatomine bugs (Fig. 2), share the following characteristics: (1) both these structures are elongated, acicular cuticle structures; (2) neither of these structures have any intrinsic musculature; (3) neither of these structures have flexible engineering-like joints in the direction of bending; (4) these structures consist of two or more longitudinally interlocked elements that are connected by a tongue-and-groove mechanism that allows them to slide against each other; and (5) these structures are capable of target-oriented bending movements that (6) are actively actuated by muscles located at the proximal end of the elements.

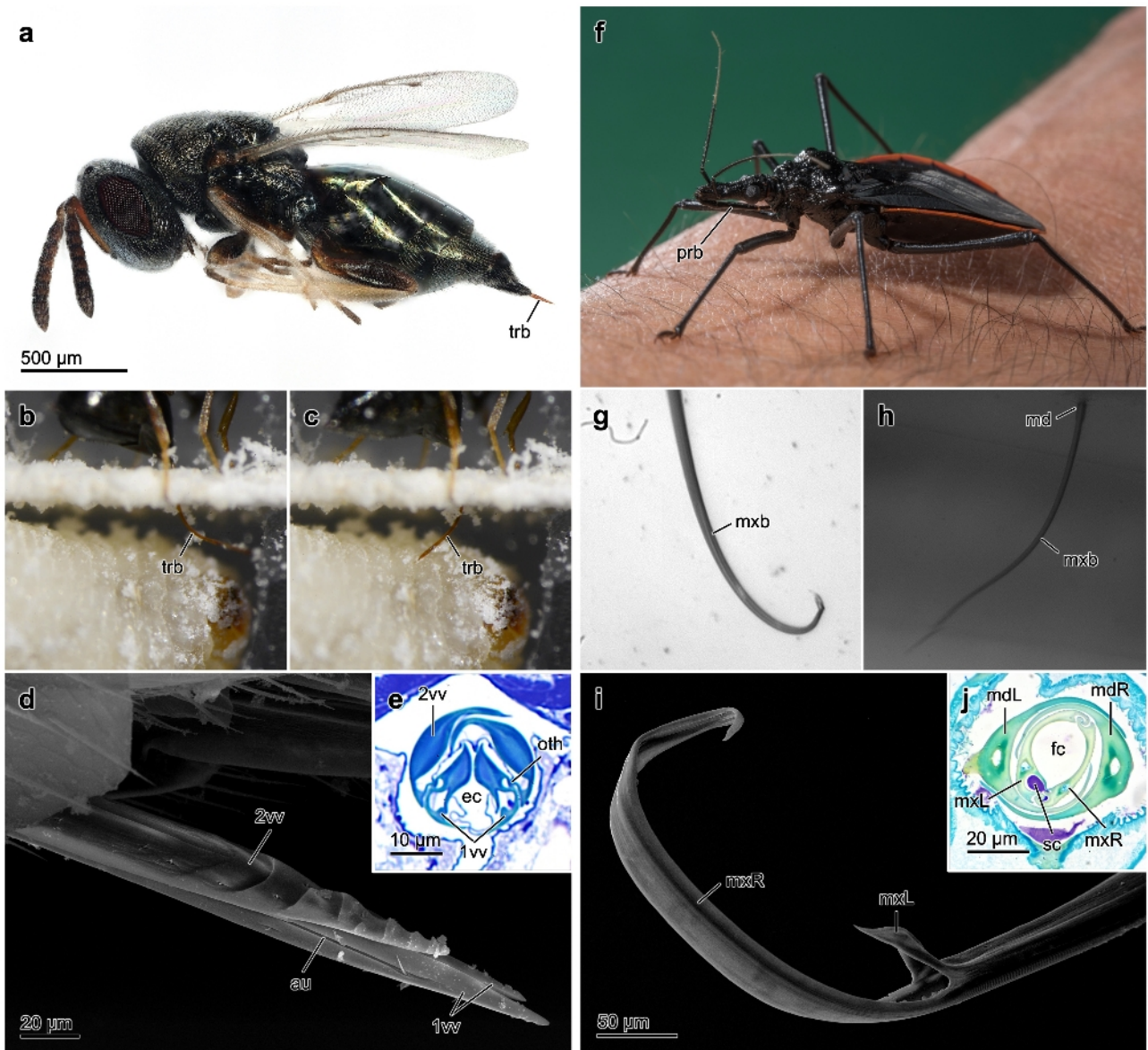


Fig. 2. Two of the systems studied: **a–e** ovipositor of the parasitoid wasp *Lariophagus distinguendus* (Chalcidoidea: Pteromalidae: Pteromalinae); **f–j** mouthparts of the haematophagous kissing bug *Dipetalogaster maxima* (Hemiptera: Heteroptera: Reduviidae: Triatominae) (lateral view). During the oviposition process, female *L. distinguendus* are able to actively to bend and rotate their terebra to assess the host and to search for a suitable place for oviposition (**b,c**; single frames of high-resolution video recordings of a wasp parasitizing a larva of *Sitophilis granarius* in an artificial chamber). The 2nd valvula and the paired 1st valvulae are interlocked via the olistheter system comprising a longitudinal tongue called the rhachis, which runs in a corresponding groove called the aulax (**d**; SEM image; **e**; light microscopical image of semithin cross section). *D. maxima* exhibits bending movements of the maxillary bundle when searching for a blood vessel (**g,h**; single frames of high-speed video recordings of the motion patterns of the maxillary bundle in artificial feeding chambers containing agar and isotonic blood saline). The mandibles are anchored at the puncture site (**h**). Opening of the food channel, whereby the left maxillae is splayed outwards forming a spine (**i**; SEM image). The maxillae are interlocked by a tongue-and-groove system and form the two antidromic channels for the passage of food and salivary fluids (**j**; light microscopical image of semithin cross section). For *L. distinguendus* see Publication 5; for *D. maxima* see Publication 7; Image 2f: Oliver Meckes. Abbreviations: 1vv: 1st valvula; 2vv: 2nd valvula; au: aulax; ec: egg canal; fc: food channel; md: mandible; mdL/mdR: left/right mandible; mxb: maxillary bundle; mxL/R: left/right maxilla; oth: olistheter; prb: proboscis; sc: salivary channel; trb: terebra

The main aims of this cumulative dissertation can be summarized as follows.

What are the functions of the joint-free bending movements of the needle-like structures?

How do these bending and/or rotating movements look like exactly?

Behavioural investigations:

- Recording and behavioural analyses (*i.e.* of the oviposition process and the employment of the terebra in parasitoid hymenopterans and the feeding process or the employment of the stylets in the triatomine heteropterans, respectively).
- Qualitative analysis of the steering movements (*i.e.* bending and rotating) of the needle-like cuticular structures (*i.e.* terebrae or maxillary bundle, respectively) *in vivo*.

Which cuticular structures and muscles are involved in the bending movements?

Morphological investigations:

- Thorough morphological descriptions of the acicular cuticular structures, including form, structure, microsculpture, ultrastructure and material composition.
- Morphological descriptions of the musculoskeletal system involved, including all relevant cuticular structures, articulations and muscles.

How are the different movements actuated?

How does joint-free bending of the terebrae and maxillary bundles work (working principles)?

Biomechanical analyses:

- Examination of the actuation of the various movements observed to create functional models.
- Determination of the underlying working principles behind the joint-free bending movements.

What adaptations and evolutionary novelties lie behind the joint-free bending movements?

What were the potential evolutionary drivers?

Eco-evolutionary analyses:

- Examination of the various mechanisms of joint-free bending movements and the underlying adaptations in morpho-physiological, behavioural, ecological and life history traits based on the aforementioned analyses.
- Examination of the eco-evolutionary significance of this system in the respective groups based on our own data and the scientific literature available.

Are these findings interesting for biomimetic research?

Biomimetic point of view:

- What are the function(s) and working principle(s) of the systems studied here?
- In which disciplines can these biological systems potentially act as suitable biological concept generators and why?

Material and methods

Material examined

In our studies on the hymenopteran ovipositor we investigated the following species: *Venturia canescens* (GRAVENHORST, 1829) (Ichneumonoidea: Ichneumonidae), *Habrobracon hebetor* (SAY, 1836) (Ichneumonoidea: Braconidae), *Microterys flavus* (HOWARD, 1881) (Chalcidoidea: Encyrtidae), *Lariophagus distinguendus* (FÖRSTER, 1841) (Chalcidoidea: Pteromalidae), and *Leptopilina heterotoma* (THOMSON, 1862) (Cynipoidea: Figitidae).

In our studies on the stylets of hemipterans we investigated the following species: *Dipetalogaster maxima* (UHLER, 1894) (Hemiptera: Reduviidae), *Rhodnius prolixus* STAL, 1859 (Hemiptera: Reduviidae), *Triatomina infestans* (KLUG, 1834) (Hemiptera: Reduviidae), and *Panstrongylus megistus* (BURMEISTER, 1835) (Hemiptera: Reduviidae).

Methods used

We combined behavioural analyses based on video recordings with various morphological and mechanical investigations based on a variety of histological, microscopical and microtomographical techniques.

High-speed and high-resolution videography were used to study the animals' behaviour *in vivo* and to describe movement patterns, e.g. the joint-free bending movements of the terebra of hymenopterans or the stylets of hemipterans, respectively.

In order to visualize and analyse the surfaces of morphological structures, we used stereomicroscopy and scanning electron microscopy (SEM). Wide-field epifluorescence microscopy (WFM) and confocal laser scanning microscopy (CLSM) were employed to analyse the material properties of the insect cuticle (*cf.* Michels and Gorb 2012). In order to examine inner structures, samples were histologically fixed and embedded to produce semi- and ultrathin serial sections with an ultramicrotome. These sections were then visualized and analysed by light microscopy (LM) or a transmission electron microscopy (TEM) for structural and ultrastructural investigations, respectively. In addition, we used non-invasive synchrotron X-ray phase contrast microtomography (SR- μ CT) to gain virtual serial sections without the destruction of the specimens under study (for a detailed description see Betz *et al.* 2007).

We used Fiji (Schindelin *et al.* 2012; <https://imagej.net/Fiji>; RRID:SCR_002285) and its plugin TrakEM2 (Cardona *et al.* 2012; RRID:SCR_003070) and GIMP (<https://www.gimp.org>; RRID:SCR_003182) for image processing, Amira version 6.0 (FEI Company, Hillsboro, OR, USA) for (pre-)segmentation, and the Biomedical Image Segmentation App "Biomedisa" (Lösel *et al.* 2020; <https://biomedisa.org>) for automated segmentation in order to create 3D models (surface meshes). Inkscape (<https://www.inkscape.org>; RRID:SCR_014479) was employed to create schematic drawings.

Terms

In the studies of Hymenoptera, the morphological terms have been strictly applied according to the Hymenoptera Anatomy Ontology (HAO; Yoder *et al.* 2010, Seltmann *et al.* 2012, Hymenoptera Anatomy Consortium 2022; <http://glossary.hymao.org>), which has also been supplemented, following modern concepts of designating morphological structures in a standardized way. We have also provided tables with a total of 210 terms relevant to the hymenopteran ovipositor system, their definitions and a total of 513 synonyms found in the literature (see appendices of Publications 1, 3 and 5).

Synopses

The published studies can be divided into three categories:

- Case studies on the structure and function of the ovipositor of parasitoid Hymenoptera (e.g. ichneumonoid, chalcidoid and cynipoid wasps): actuation and mechanisms of joint-free terebra movements and their eco-evolutionary significance (**Publications 1–6**)
- Case study on the structure and function of the mouthparts of bloodsucking kissing bugs (Triatominae, Reduviidae, Hemiptera) and the mechanisms of joint-free movements of the maxillary bundle (**Publication 7**)
- Biomimetic potential of actively actuated rod-shaped structures of animals (**Publications 8–11**)

In addition, I have also worked on a project concerning a fossil parasitoid dryinid wasp encased in Rovno amber, which I also present in this thesis:

- Description of a new dryinid species from Eocene Rovno amber (**Publication 12**)

The published PDF files of the articles and their corresponding additional files (supplementary material) are attached in the above order in the following.

Publication 1

Eggs B., Birkhold A. I., Röhrle O. and Betz O. (2018). Structure and function of the musculoskeletal ovipositor system of an ichneumonid wasp. *BMC Zoology* 3: 12. doi: 10.1186/s40850-018-0037-2

(peer-reviewed journal article)

Abstract

Background: Modifications of the ovipositor appear to have played a prominent role in defining the host range of parasitoid hymenopterans, highlighting an important contributing factor in shaping their oviposition strategies, life histories and diversification. Despite many comparative studies on the structure of the hymenopteran terebra, little is known about functional aspects of the musculoskeletal ovipositor system. Therefore, we examined all inherent cuticular elements and muscles of the ovipositor of the ichneumonid wasp *Venturia canescens* (GRAVENHORST, 1829), investigated the mechanics of the ovipositor system and determined its mode of function.

Results: We found that the movements of the ichneumonid ovipositor, which consists of the female T9 (9th abdominal tergum), two pairs of valvifers and three pairs of valvulae, are actuated by a set of six paired muscles. The posterior and the anterior 2nd valvifer-2nd valvula muscles flex and extend the terebra from its resting towards an active probing position and back. The dorsal T9-2nd valvifer muscle is modified in *V. canescens* and forms distinct bundles that, together with the antagonistically acting ventral T9-2nd valvifer muscle, change the relative position of the 2nd valvifer to the female T9. Thereby, they indirectly tilt the 1st valvifer because it is linked with both of them via intervalvifer and tergo-valvifer articulation, respectively. The 1st valvifer acts as a lever arm that transfers movements to the 1st valvula. The posterior T9-2nd valvifer muscle and the small 1st-valvifer-genital membrane muscle stabilize the system during oviposition.

Conclusions: From our examination of the elements of the musculoskeletal ovipositor system of ichneumonids, we discussed leverages and muscle forces and developed a functional model of the underlying working mechanisms adding to our understanding of a key feature that has largely determined the evolutionary success of the megadiverse Ichneumonidae with more than 24,000 hitherto described species.

Significance within the present thesis: The majority of previous studies on the ovipositors of parasitoid hymenopterans have focused solely on morphological aspects of the terebra. Studies on the form and function of the entire ovipositor system, which includes various cuticular elements, articulations and a set of muscles, are rare. Therefore, we have described the ovipositor of the ichneumonid wasp *Venturia canescens* in detail. To our knowledge, this is the first study presenting a quantitative analysis of the musculoskeletal ovipositor system of a parasitoid wasp and a calculation of its muscle forces. We have also established a

functional model. Furthermore, many previous authors have employed various terms for the same morphological structures. Therefore, we have strictly followed the Hymenoptera Anatomy Ontology (HAO; Yoder *et al.* 2010, Seltmann *et al.* 2012, Hymenoptera Anatomy Consortium 2022) and provide a list of all terms relevant to the ovipositor, including synonyms found in the literature. This investigation serves as a basis for understanding the form and function of the ovipositor and allows for an easier identification and comprehension of the specific (morphological) adaptations enabling these parasitoids to bend and steer their terebrae, as examined in the subsequent studies.

Methods used: light microscopy (LM), scanning electron microscopy (SEM), synchrotron X-ray phase-contrast microtomography (SR- μ CT), videography

Own contribution: designing the study; preparing the specimens; performing the microscopical studies; analysing and interpreting the data; writing the original version of the manuscript, preparing the figures; revising the manuscript; correspondence

RESEARCH ARTICLE

Open Access



Structure and function of the musculoskeletal ovipositor system of an ichneumonid wasp

Benjamin Eggs^{1*†}, Annette I. Birkhold^{2†}, Oliver Röhrle² and Oliver Betz¹

Abstract

Background: Modifications of the ovipositor appear to have played a prominent role in defining the host range of parasitoid hymenopterans, highlighting an important contributing factor in shaping their oviposition strategies, life histories and diversification. Despite many comparative studies on the structure of the hymenopteran terebra, little is known about functional aspects of the musculoskeletal ovipositor system. Therefore, we examined all inherent cuticular elements and muscles of the ovipositor of the ichneumonid wasp *Venturia canescens* (Gravenhorst, 1829), investigated the mechanics of the ovipositor system and determined its mode of function.

Results: We found that the movements of the ichneumonid ovipositor, which consists of the female T9 (9th abdominal tergum), two pairs of valvifers and three pairs of valvulae, are actuated by a set of six paired muscles. The posterior and the anterior 2nd valvifer-2nd valvula muscles flex and extend the terebra from its resting towards an active probing position and back. The dorsal T9-2nd valvifer muscle is modified in *V. canescens* and forms distinct bundles that, together with the antagonistically acting ventral T9-2nd valvifer muscle, change the relative position of the 2nd valvifer to the female T9. Thereby, they indirectly tilt the 1st valvifer because it is linked with both of them via intervalvifer and tergo-valvifer articulation, respectively. The 1st valvifer acts as a lever arm that transfers movements to the 1st valvula. The posterior T9-2nd valvifer muscle and the small 1st-valvifer-genital membrane muscle stabilize the system during oviposition.

Conclusions: From our examination of the elements of the musculoskeletal ovipositor system of ichneumonids, we discussed leverages and muscle forces and developed a functional model of the underlying working mechanisms adding to our understanding of a key feature that has largely determined the evolutionary success of the megadiverse Ichneumonidae with more than 24,000 hitherto described species.

Keywords: Hymenoptera, Ichneumonidae, Kinematics, Muscles, Ovipositor, Parasitoid, SEM, SR- μ CT

Background

The vast majority of hymenopterans are parasitoids of other insects. Apart from oviposition, their ovipositor serves several tasks in the parasitoid lifestyle, i.e. navigating or penetrating the substrate (if the host is concealed) or the targeted egg/puparium, assessing the host, discriminating between suitable and previously parasitized hosts, piercing the host, injecting venom, oviducting the competitors' eggs and finding a suitable place for egg laying [1]. In some species, the ovipositor is also used to form a feeding tube for host feeding or

defensive stinging [2]. Undoubtedly, modifications of the ovipositor apparatus have been one of the key factors in the evolution of the parasitoids' oviposition strategies, the life histories and the enormous diversification of this large and ecologically important insect order [2–4].

The hymenopteran ovipositor consists of the female T9 (9th abdominal tergum), two pairs of valvifers and three pairs of valvulae (cf. Figs. 1a, c, 5a) derived from the 8th and 9th abdominal segments (7th and 8th metasomal segments) (morphological terms are applied according to the Hymenoptera Anatomy Ontology (HAO) [5–7]; a table of the terms used, their definitions and synonyms is given in Table 2 in the Appendix). The basally situated valvifers accommodate the operating musculature, whereas all the valvulae are devoid of intrinsic

* Correspondence: benjamin.eggs@uni-tuebingen.de

†Benjamin Eggs and Annette I. Birkhold contributed equally to this work.

¹Evolutionary Biology of Invertebrates, Institute of Evolution and Ecology, University of Tübingen, Auf der Morgenstelle 28, 72076 Tübingen, Germany
Full list of author information is available at the end of the article



musculature [8–10]. The 1st valvifers (fusion of the 8th gonocoxites with the gonangula [10]; = gonangulum, gonangula *sensu* [1]) anterodorsally are continuous with the rami of the 1st valvulae (8th gonapophyses; = lower valves *sensu* [1]). Their posterior angles articulate dorsally with the female T9 via the tergo-valvifer articulation and ventrally with the 2nd valvifers via the intervalvifer articulation. The 2nd valvifers (9th gonocoxites) extend in the form of the 3rd valvulae (9th gonostyli; = ovipositor sheaths *sensu* [1]) and are anteroventrally articulated with the 2nd valvula (fusion of the 9th gonapophyses; = upper valve *sensu* [1]) [8, 9], which is secondarily re-separated except at the apex in some parasitoid taxa [11]. The interlocked 1st and 2nd valvulae enclose the egg canal and form the terebra (= ovipositor (shaft) *sensu* [1]), which is embraced by the 3rd valvulae when not in use. The ventral surface of the 2nd valvula is interlocked with both of the 1st valvulae by a sublateral longitudinal tongue called the rhachis, which runs within a corresponding groove called the aulax along the dorsal surface of each of the 1st valvulae. This so-called olistheter system allows the three parts of the terebra to slide longitudinally relative to each other [9, 11]. The sensillar equipment of the 1st and 2nd valvulae is highly variable among parasitoid hymenopterans [2].

Despite many descriptive studies on the comparative morphology of the hymenopteran terebra [8, 9, 11, 12], the mode of function of the musculoskeletal ovipositor system has only been described in some “symphytan” families [10, 13–15], in the aculeate *Apis mellifera* Linnaeus, 1758 (Apidae) [8] and *Cryptocheilus versicolor* (Scopoli, 1763) (Pompilidae) [16], in some species of Cynipoidea [17, 18], and in a few parasitoid species of Ceraphronoidea [19] and Chalcidoidea [20–27]. However, the underlying working mechanisms of the musculoskeletal ovipositor system of the extremely diverse and species-rich superfamily of Ichneumonoidea has remained largely unexplored so far and little is known about the actuation of the various ovipositor movements that are executed during oviposition. In this study, we investigated structural, mechanical and functional aspects of the ovipositor of *Venturia canescens* (Gravenhorst, 1829) (Hymenoptera: Ichneumonidae: Campopleginae), a cosmopolitan, synovigenic [28], non-host feeding [29], solitary, koinobiont larval endoparasitoid of several moth species (Lepidoptera) [30, 31]. The oviposition behaviour (Additional file 1) is described by Rogers [32]. These parasitoid wasps coat their eggs with virus-like particles (VLPs) to circumvent their host’s immune system [33–37] and exhibit both arrhenotokous and obligate thelytokous reproduction modes [38–41]. We aimed to (1) describe the ovipositor of *V. canescens*, including all inherent

cuticular elements and muscles, (2) examine the mechanics of this musculoskeletal system, (3) determine its mode of function and (4) discuss the process of oviposition.

Results and discussion

We combined light microscopy (LM), scanning electron microscopy (SEM), synchrotron X-ray phase-contrast microtomography (SR- μ CT) and subsequent 3D image processing with muscle and leverage analyses. Based on these microscopical and microtomographical studies, we present a thorough morphological, mechanical and functional analysis of the musculoskeletal ovipositor system (Additional file 2) that steers the various movements executed by the female ichneumonid wasp during oviposition.

Cuticular elements of the ovipositor

The paired **1st valvulae** (1vv, Figs. 1a, c, e, 2a, b, e, f, g, 4d) of *V. canescens* are terminally differentiated in five apically directed sawteeth (st; Fig. 2b) of decreasing size that are used to penetrate the substrate and the host’s skin [42, 43]. Each of the 1st valvulae has a medioventral part formed into a thickened longitudinal flap that projects inwards into the egg canal (lf1; Fig. 3a; = medio-ventral seal *sensu* [16]). These thin chitinous flaps are considered to effectively seal the crack between the 1st valvulae and prevent the loss of venom and/or oviposition fluid during oviposition [11, 44–46]. The pressure of the venom squeezes the two membranes together and thus closes the seal. A transverse flap called the valvillus (vlv; Fig. 2e) protrudes from their medial walls and projects into the central egg/venom canal (cf. [32]). Segregate valvilli are typical for taxa of Ichneumonoidea but vary in shape and number between subfamilies [11, 46]. In non-aculeate Hymenoptera, they potentially serve as a stop and release mechanism for the egg by maintaining the egg in position within the terebra and blocking the egg canal [32, 43, 46] or by pushing fluids into the ovipositor, thereby creating a hydrostatic pressure that forces the egg out of the terminal portion of the egg canal [43]. The internal microsculpture of the medial walls of the egg canal consists of distally oriented scale-like structures; leaf-like ctenidia (ct; Fig. 2f) occur from the proximal basis of the valvulae to the further distally positioned region of the valvillus, where they are replaced by spine-like subctenidial setae (scts; Fig. 2g). The ctenidia help to push the deformable egg along the egg canal by alternate movements of the 1st valvulae and prevent it from moving backwards [43, 46, 47]. They are also hypothesized to deliver forward a liquid lubricant for the moving valvulae and thus reduce

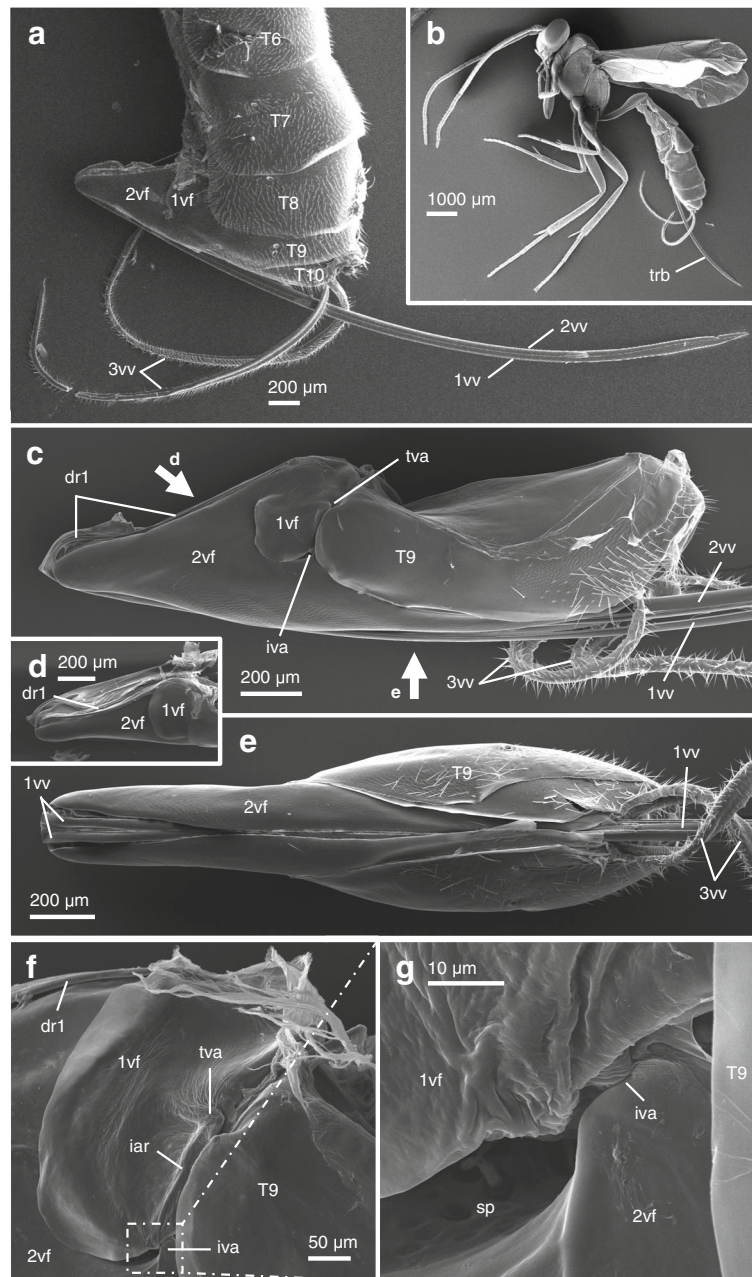


Fig. 1 SEM images of *Venturia canescens*. **a** The posterior part of the metasoma (lateral view) with the exhibited ovipositor that consists of the female T9, two pairs of valvifers and three pairs of valvulae. Because of the storage in ethanol and the drying procedure, the 3rd valvulae are coiled and do not embrace the terebra (formed by the interlocked 1st and 2nd valvulae) as in living animals (left is anterior). **b** Habitus image of *V. canescens* (lateral aspect). **c-e** Ovipositor excised from the genital chamber (left is anterior; **c**, lateral view; **d**, dorsolateral view; **e**, ventral view), so that the articulations of the 1st valvifer and the female T9 (tergo-valvifer articulation) and of the 1st valvifer with the 2nd valvifer (intervalvifer articulation) become visible. The dorsal rami of the 1st valvulae are continuous with the 1st valvifers. The fat arrows represent the direction of view of the other SEM images. **f-g** Detailed images of the tergo-valvifer and the intervalvifer articulation (lateral view, left is anterior) and the sensillar patch of the 2nd valvifer (in **g**). Abbreviations: 1vf, 1st valvifer; 1vv, 1st valvula; 2vf, 2nd valvifer; 2vv, 2nd valvula; 3vv, 3rd valvula; dr1, Dorsal ramus of the 1st valvula; iar, Interarticular ridge of the 1st valvifer; iva, Intervalvifer articulation; sp, Sensillar patch of the 2nd valvifer; T6, 6th abdominal tergum; T7, 7th abdominal tergum; T8, 8th abdominal tergum; T9, Female T9; T10, 10th abdominal tergum; tva, Tergo-valvifer articulation

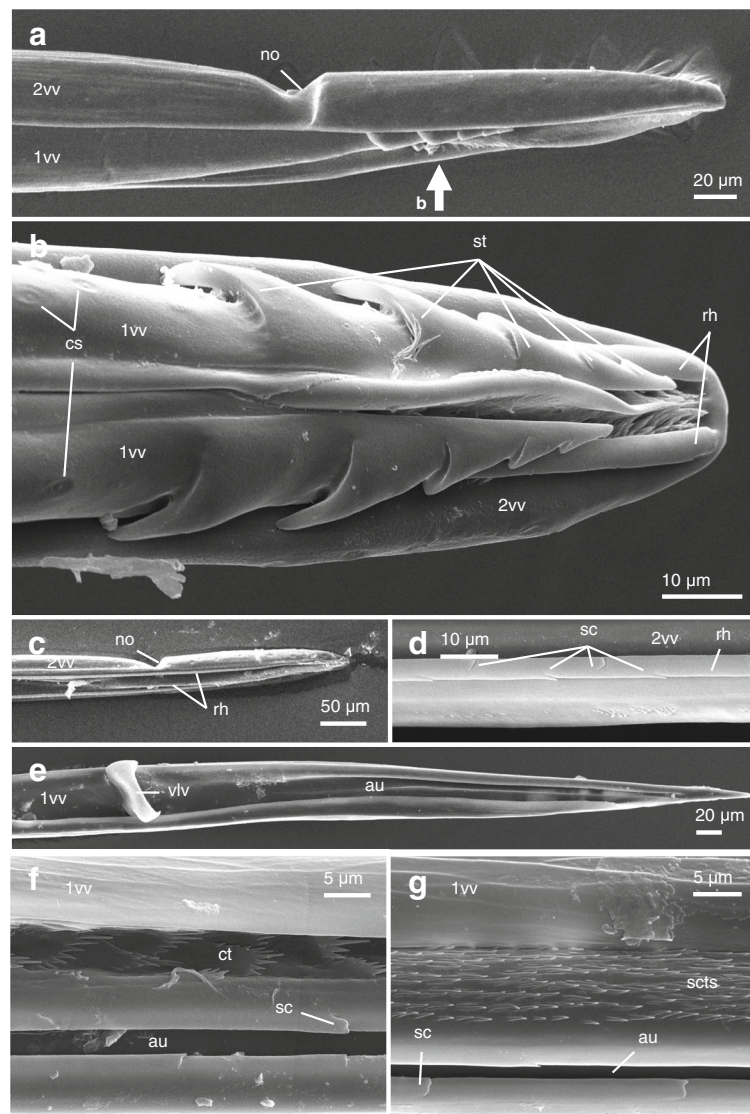


Fig. 2 SEM images of *Venturia canescens* (left is anterior). **a, b** The apex of the terebra (**a**, lateral view; **b**, ventral view; for a transverse section see Fig. 3) showing the notch and the rhachis, which ends at the very apex of the 2nd valvula, and five sawteeth directed apically and decreasing in size apically on each of the 1st valvulae. The valvulae bear various types of sensilla with the campaniform sensilla being numerous at the apices of both the 1st and the 2nd valvulae. **c** Upon removal of the 1st valvulae, the rhachises at the ventral side of the 2nd valvula become visible (ventrolateral view). **d** The rhachises show distally directed scales/serrations. **e** The inner surface of the apex of the right 1st valvula shows a single valvillus and the aulax. **f, g** The egg canal formed by the 1st and 2nd valvifers bears a microsculpture consisting of distally oriented ctenidia (**f**), which become further distally replaced by spine-like subctenidial setae (**g**) at the apex of the terebra. The aulaces of the 1st valvulae, similar to the rhachis, show distally oriented scales. The fat arrow in **a** represents the direction of view of the image in **b**. Abbreviations: 1vv, 1st valvula; 2vv, 2nd valvula; au, Aulax; cs, Campaniform sensilla; ct, Ctenidium; no, Notch; rh, Rhachis; sc, Scales; scts, Subctenidial setae; st, Sawtooth; vlv, Valvillus

friction between the valvulae during oviposition [42, 45, 46, 48].

The **2nd valvula** (2vv; Figs. 1a, c, 2a, b, c, d, 4d) is bulbous at its proximal end and basally articulated with the 2nd valvifers via the basal articulation (ba; Fig. 4i; blue region in Fig. 3). There are openings on each of the dorsolateral sides of the bulbs that presumably enable the passage of eggs, venom and other

fluids. The dorsal ramus of the 2nd valvula extends along its dorsal margin and bears the processus articularis (pra; Fig. 5h) laterally at its proximal part (anterior) and the processus musculares (prm; Fig. 5h) dorsally. On its ventral side, the 2nd valvula bears the rhachises (rh; Fig. 2b, c, d), which are interlocked with both the aulaces (au; Fig. 2e, f, g) on the dorsal side of the opposing paired 1st valvulae via the olistheter

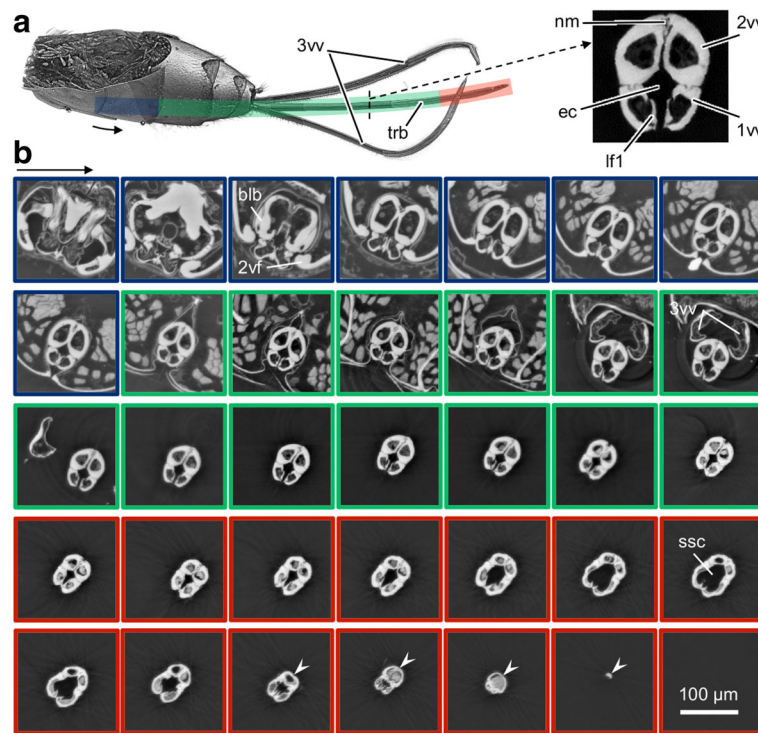
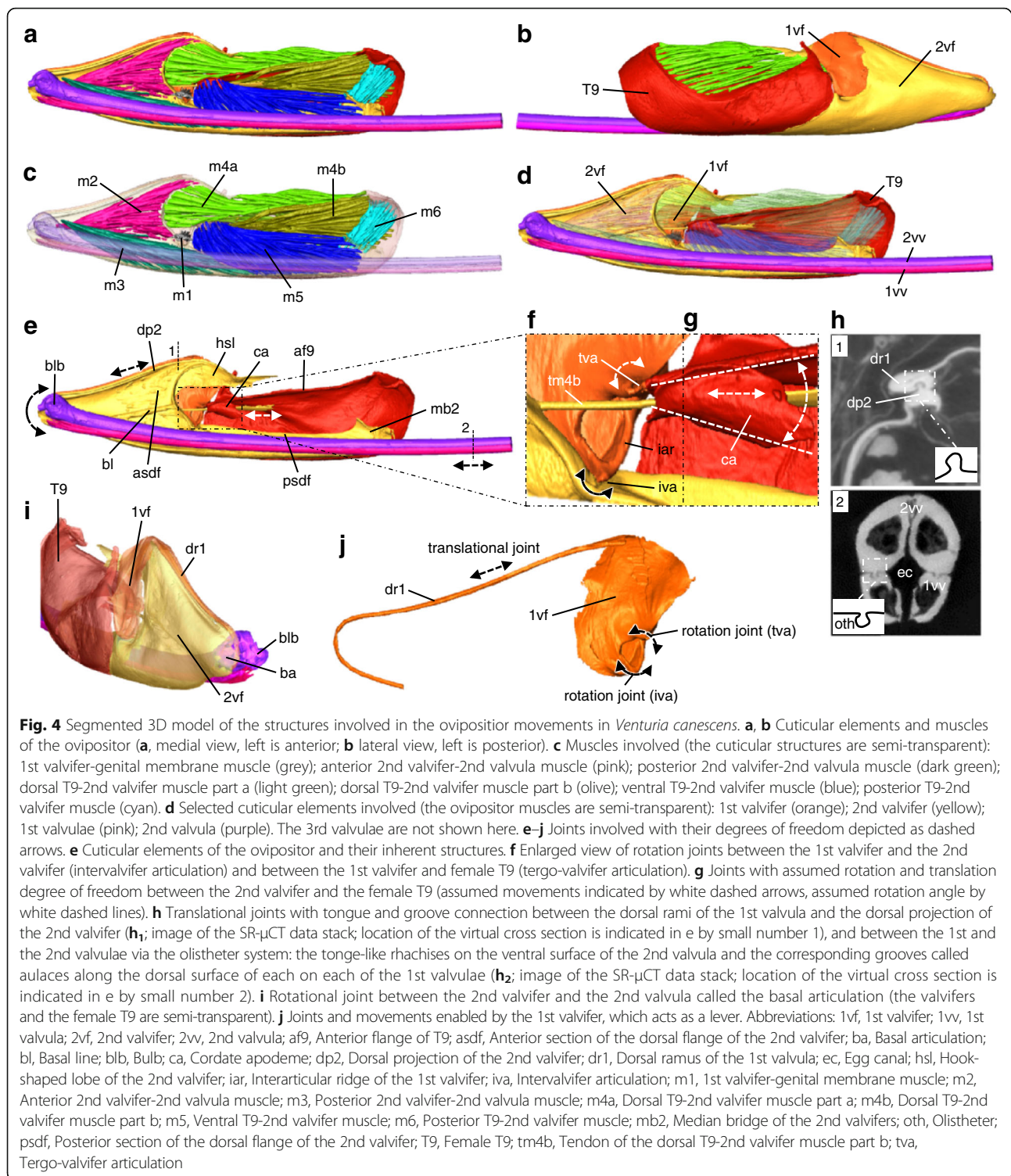


Fig. 3 SR- μ CT images of the terebra of *Venturia canescens*. **a** 3D visualization of the whole terebra in the metasoma. **b** Virtual cross sections through the terebra from proximal to distal. Proximal (blue); every 65 μ m, a cross section is displayed because of strong morphological changes such as the bulbous proximal end of the 2nd valvula. According to the limited morphological changes along the longitudinal axis, for the next part (green), a cross section is shown only every 260 μ m over the next 3380 μ m. The most distal 900 μ m (red) shows, once again, large morphological variations such as the spindle-shaped cavity formed by all three valvulae; therefore, a cross section is shown every 65 μ m. The arrows indicate the undivided distal parts of the 2nd valvula. Abbreviations: 1v1, 1st valvulae; 2v1, 2nd valvulae; 2vf, 2nd valvifer; 2vv, 2nd valvulae; 3vv, 3rd valvulae; b1b, Bulb; ec, Egg canal; lf1, Longitudinal flap of the 1st valvulae; nm, Notal membrane; ssc, Spindle-shaped cavity; trb, Terebra

system (oth; Fig. 4h₂), which extends all the way to the apex. The 2nd valvula of *V. canescens* and other ichneumonids (e.g. taxa belonging to the subfamilies of Campopleginae, Cremastinae, Ctenopelmatinae, Neorhacodinae and Tryphoninae) consists of two halves that are joined together for the most of their length by a dorsal notal membrane (nm; Fig. 3a; cf. [32, 45]) but are fused at the apex [11], so that the 2nd valvula possesses a lumen that is undivided at the apex of the terebra (arrows in red region of Fig. 3b) but that splits into two lumina for a substantial proportion of its proximal part. The blunt tip of the 2nd valvula dorsally possesses a distal notch (no; Fig. 2a, c), which is assumed to be associated with moderating penetration of the host cuticle [42] or to maintain a grip on the inner surface of the host cuticle and thereby providing a momentary clamping mechanism in the host's skin to ensure continuous engagement with the host during oviposition [43]. Almost all ichneumonid species with a pre-apical notch are larval endoparasitoids of holometabolous insects [43]. At their external surface, both the 1st and the 2nd valvulae of *V. canescens* exhibit campaniform sensilla (cs; Fig. 2b),

which are concentrated at the apices of the valvulae, especially distally of the distal notch of the 2nd valvula and posteriorly of the sawteeth of the 1st valvulae (cf. [45]). However, the sensillar equipment of the terebra was not further investigated in this study (but see [49]).

The **terebra** (trb; Fig. 1b, 3) consists of the paired 1st valvulae and the 2nd valvula, which are tightly interlocked by the olistheter (oth; Fig. 4h₂). The distally directed scales/serrations on the surfaces of both the rhachises and the walls of the aulaces (sc; Fig. 2d, f, g) potentially reduce friction forces by minimizing the contact area of the olistheter elements [46]. However, we hypothesize that these scales might also serve other functions: (1) they, analogous to the ctenidia, might forward a liquid lubricant from the metasoma to the apex of the olistheter system to reduce friction between the moving valvulae (cf. [48]), and/or (2) they might create anisotropic conditions in the olistheter by increasing frictional forces whenever a valvula is pushed in proximal direction, thereby preventing the 1st valvulae from randomly sliding back during piercing/drilling. The terebra extends far beyond the tip of



the metasoma. The diameter of the terebra decreases from the proximal to its distal end, although the part in between remains similar in diameter throughout. The cross sections of both the 1st and the 2nd valvulae are notably different across the length of the terebra

(Fig. 3b). The egg canal is largely defined by the 1st valvulae but its dorsal side is formed by the 2nd valvula (ec; Fig. 3a). At the apex of the terebra, the 1st valvulae are enlarged and form an approximately spindle-shaped cavity (ssc; red region in Fig. 3) that is

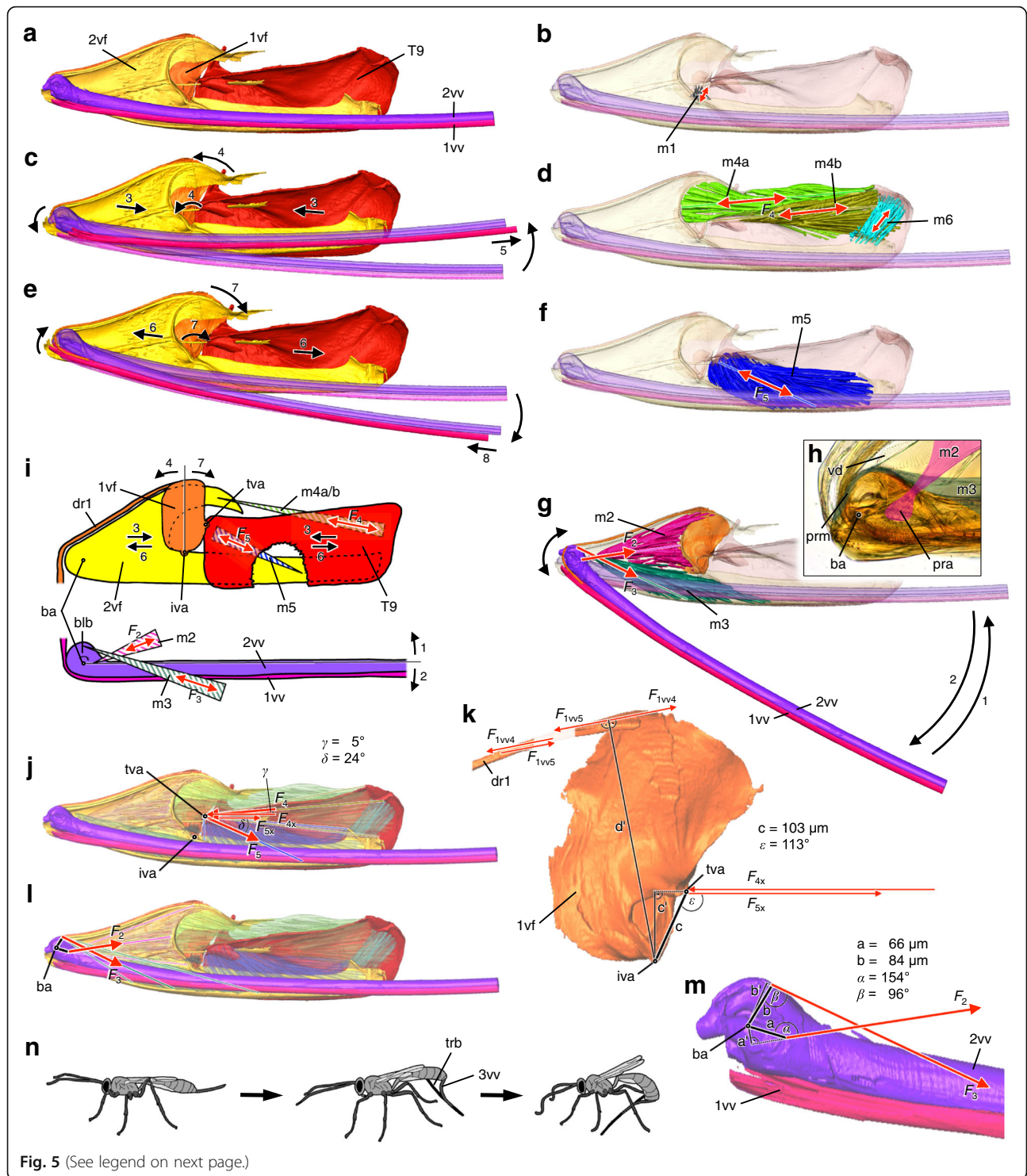


Fig. 5 (See legend on next page.)

(See figure on previous page.)

Fig. 5 Mechanics of the musculoskeletal ovipositor system of *Venturia canescens*. **a–g, i** Kinematics of the musculoskeletal ovipositor system; acting (input) muscle forces are visualized by solid red arrows (**b, d, f, g, i**) and resulting (output) movements by solid black arrows (**c, e, g, i**). **a–g, j–m** 3D model of the ovipositor system (medial view, left is anterior). **b** m1 potentially serves as a tensor muscle for stabilization of the ovipositor system during oviposition. **c, d, i** Contraction of both m4a and m4b (F_4 in **d, i**) moves the 2nd valvifer posteriorly and the female T9 anteriorly towards each other (small number 3 in **c, i**), thus indirectly causing the 1st valvifer to tilt anteriorly (small number 4 in **c, i**). This is possible because the 1st valvifer is articulated with both the 2nd valvifer and the female T9 via the intervalvifer and tergo-valvifer articulations that act as rotational joints. The 1st valvifer thereby functions as a lever arm that transfers the movement to the dorsal ramus of the 1st valvula and consequently causes the 1st valvula to slide distally relative to the 2nd valvula (small number 5 in **c**). These movements might also facilitate the extension of the terebra back towards its resting position (**c**). m6 thereby stabilizes the ovipositor system by holding the 2nd valvifer and the female T9 in position and preventing them to rotate around the articulations (**d**). **e, f, i** Contraction of m5 (F_5 in **f, i**) moves the 2nd valvifer anteriorly and the female T9 posteriorly apart from each other (small number 6 in **e, i**), thus causing the 1st valvifer to tilt posteriorly (small number 7 in **e, i**) and consequently causing the 1st valvula to slide proximally relative to the 2nd valvula (small number 8 in **e**). These movements might also facilitate the flexion of the terebra (**e**). **g, i** Contraction of m3 (F_3 in **g, i**) causes the bulbs to pivot anteriorly at the basal articulation, thus flexing the 2nd valvula and, therefore, the whole terebra (small number 2 in **g, i**). Contraction of m2 (F_2 in **g, i**) extends the terebra back towards its resting position (small number 1 in **g, i**). **h** Light microscopical image of the insertion regions of m2 and m3 at the processus articularis and the processus musculares, respectively (lateral view, left is anterior). The duct of the venom gland reservoir of the 2nd valvifer ends at the lateral openings of the bulbous region of the 2nd valvula. **i** Resulting schematic drawing of the mechanism of the tilting movements of the 1st valvifer and of the flexion/extension of the terebra (lateral view, left is anterior, not to scale). Only the two pairs of antagonistically acting muscles that are mainly responsible for these movements are represented in simplified terms (m2/m3 and m4/m5). The muscles stabilizing the system (m1 and m6) are not depicted here. **j–m** Simplified mechanical scheme of the leverages of the ovipositor in the resting position; acting (input) muscle forces are visualized by solid red arrows, their horizontal force vector components and the resulting (output) forces by thin red arrows (**j, k**), the anatomical (in)levers by solid black lines and the effective (= mechanical) levers by thin black lines, and the joint angles ($\alpha, \beta, \varepsilon$) are given (**k, m**). **j, l** Major direction of the acting muscle forces (F_2, F_3, F_4 and F_5) from a muscle's insertion point to the centre point of its origin. **j, k** Under the simplified assumption that the 2nd valvifer, which acts as the frame of reference, and the female T9 are guided and cannot twist but only move towards or apart from each other along the horizontal anterior–posterior axis, the input force vectors F_{4x} and F_{5x} act horizontally at the 1st valvifer at the tergo-valvifer-articulation. The distance between the tergo-valvifer articulation (where the force is applied) and the intervalvifer articulation (joint axis/pivot point) is the anatomical inlever c ; for torques see eqs. 4, 5. The 1st valvifer acts as a lever with the effective outlever d' , resulting in pro- or retraction forces at the dorsal ramus of the 1st valvula F_{1vw} and F_{1ws} ; see eqs. 6, 7. **l, m** Input force vectors F_2 and F_3 acting at the proximal end of the 2nd valvula with the basal articulation as joint axis and the anatomical inlevers a and b ; for torques see eqs. 2, 3. **n** Schema of a female wasp flexing its terebra to an active position for oviposition (after [32]) (Additional file 1), which might be supported by the flexible 3rd valvulae (not shown in a–m). Abbreviations: 1vf, 1st valvifer; 1vv, 1st valvula; 2vf, 2nd valvifer; 2vv, 2nd valvula; 3vv, 3rd valvula; ba, Basal articulation; blb, Bulb; dr1, Dorsal ramus of the 1st valvifer; F , Force; F_x , Horizontal vector components of a force; iva, Intervalvifer articulation; m1, 1st valvifer-genital membrane muscle; m2, Anterior 2nd valvifer-2nd valvula muscle; m3, Posterior 2nd valvifer-2nd valvula muscle; m4a, Dorsal T9-2nd valvifer muscle part a; m4b, Dorsal T9-2nd valvifer muscle part b; m5, Ventral T9-2nd valvifer muscle; m6, Posterior T9-2nd valvifer muscle; pra, Processus articularis; prm, Processus musculares; T9, Female T9; trb, Terebra; tva, Tergo-valvifer articulation; vd, Duct of the venom gland reservoir of the 2nd valvifer

partly occluded by the valvilli of each of the 1st valvulae (cf. [32]).

The paired **3rd valvulae** (3vv; Figs. 1a, c, e, 3) emerge at the posterior end of the 2nd valvifer and ensheath and protect the terebra when at rest. The lateral walls of the 3rd valvulae of *V. canescens* and other parasitoid wasps with long external terebrae are annulated by fine transversal narrow furrows (cf. [50]), which makes them flexible and allow their extensive deformation during oviposition. Since the valvulae lack intrinsic muscles, deformation must arise as a passive response to external pressures. The ability to bend the 3rd valvulae facilitates oviposition [50], however, it is not yet clear if *V. canescens* is able to support the flexion of the terebra towards an active probing position and its steering during the search for a potential host with their 3rd valvulae or if they simply follow the movements of the terebra (Fig. 5n; Additional file 1; cf. [32]). The distally directed dense microsetae on the inner surface of the 3rd valvulae (cf. [45]) are thought to be involved in cleaning the ovipositor sensilla between oviposition

episodes [2, 12, 50]. The 3rd valvulae potentially also have a sensory function [1].

The paired **1st valvifers** (1vf; Figs. 1a, c, d, f, g, 4b, d, j) of *V. canescens* and other ichneumonid species are short and show an almost oblong shape (with rounded edges) [8], unlike the bow-shaped 1st valvifers of species of Chalcidoidea [21, 23–26] or the triangularly shaped 1st valvifers of species of Apoidea [8, 9, 51, 52]. The posterior angles of the 1st valvifer are doubly movably articulated with the modified female T9 via the tergo-valvifer articulation and via its posteroventral corner with the 2nd valvifer by means of the intervalvifer articulation (tva/iva; Figs. 1c, f, g, 4f, j). A strengthened ridge called the interarticular ridge (iar; Figs. 1f, 4f) occurs between the two articulations and might mechanically stabilize the 1st valvifer during oviposition. The anterodorsal angle of the 1st valvifer is continuous with the dorsal ramus of the 1st valvula (dr1; Figs. 1c, d, f, 4h₁, i, j), which is interlocked with the dorsal projection of the 2nd valvifer (dp2; Fig. 4e, h₁) by a system analogous to the olistheter. This tight

interlocking guides the dorsal rami and prevents them from buckling when pushing forces are applied during the protraction of the 1st valvulae. The rami make acute angles around the proximal bulbous end of the 2nd valvula. The cuticle in the part of the dorsal rami that slides around the angle during pro- or retraction of the 1st valvulae needs to be flexible in the sagittal plane and might contain high proportions of the very elastic rubber-like protein resilin (cf. [53–55]).

The paired **2nd valvifers** (2vf; Fig. 1a, c, e, f, g, 4b, d) are elongated and their posterior parts are placed medially of the female T9. A conjunctiva, called the genital membrane (not shown), connects the ventral margins of both the 2nd valvifers arching above the 2nd valvula. The 2nd valvifer bears the dorsal flange, which extends upon its dorsal margin and which is divided by a sharply defined ridge called the basal line (bl; Fig. 4e) into an anterior and a posterior section. The anterior section of the dorsal flange of the 2nd valvifer (asdf; Fig. 4e) dorsally bears the dorsal projection of the 2nd valvifer (dp2; Fig. 4e, h₁) and extends upwards in a hook-shaped lobe (hsl; Fig. 4e; *sensu* [8]) at its postero-dorsal end, which might allow a greater arc of movement of the 1st valvifer and therefore a greater protraction of the 1st valvulae. The dorsal margins and the dorsal flanges are strengthened by cuticular ridges that might have a stabilizing function to prevent deformation. Sensillar patches (sp; Fig. 1g) can be seen on the 2nd valvifer near the intervalvifer and the basal articulation (cf. [56]), monitoring the movements of the 1st valvifer and therefore the connected 1st valvula or the position of the bulbs of the 2nd valvula. The posterior section of the dorsal flange of the 2nd valvifer (psdf; Fig. 4e) is elongated and oriented almost vertically. At their posterodorsal ends, the 2nd valvifers are connected by the median bridge (mb2; Fig. 4e). The duct of the venom gland reservoir (vd; Fig. 5h) is situated in between the paired 2nd valvifers.

The **female T9** (T9; Figs. 1a, c, e, f, g, 4b, d) is elongated and anterodorsally bears a hook-shaped structure. Medially at its anterior end, the T9 forms a funnel-like structure at the cordate apodeme (ca; Fig. 4e, f, g), situated posteriorly to the tergo-valvifer articulation. This structure has not yet been described in parasitoid hymenopterans. The anterodorsal and dorsal margins of the female T9 is strengthened by the anterior flange of T9 (af9; Fig. 4e) that might mechanically stabilize the female T9 during oviposition.

Joints of the musculoskeletal ovipositor system

The musculoskeletal ovipositor system possesses three main joints.

The **basal articulation** (ba; Fig. 4i) connects the laterally placed bulbs of the 2nd valvula with the thickened anteroventral parts of the 2nd valvifers via a rotational joint. This joint might also allow some limited pivoting movements of the 2nd valvula and therefore of the whole terebra.

Both the 2nd valvifer and the female T9 are connected with the 1st valvifer by the **intervalvifer articulation** and the **tergo-valvifer articulation** (iva/tva; Figs. 1c, f, g, 4f, j), respectively, forming a double joint. The tergo-valvifer articulation is situated dorsal to the intervalvifer articulation. Both of these articulations act as rotational joints; thus, the 1st valvifer is movable in the sagittal plane only.

Ovipositor muscles

The maximum tensions at constant muscle length (isometric tension) that individual insect muscles can exert greatly vary between species, ranging from 19 to 700 kPa [57, 58] (e.g. approximately 38 kPa exerted by the asynchronous dorso-ventral flight muscle in *Bombus terrestris* (Linnaeus, 1758) at 30 °C [59]). In case of parallel muscle fibres, the maximum force (F) created by a muscle can be estimated by using the specific tension (f) and the mean cross section area (CSA; Table 1) according to the equation:

$$F = \text{CSA} \cdot f \quad (\text{eq. 1})$$

However, there are, to the best of our knowledge, no studies hitherto that measured tensions of abdominal muscles of hymenopterans we could refer to.

The ovipositor of *V. canescens* possesses a set of six paired muscles (Fig. 4c; Table 1), one of them (m4) forming two distinct bundles.

The paired **1st valvifer-genital membrane muscles** (m1) are the only muscles of the 1st valvifer. They originate at the medial surface of the posteroventral part of the 1st valvifer, i.e. between the tergo-valvifer and the intervalvifer articulation, and insert anteriorly on the genital membrane. They are the smallest muscles of the ovipositor with a CSA of 0.0008 mm² each (Table 1).

The paired fan-shaped **anterior 2nd valvifer-2nd valvula muscles** (m2) arise at the medial region along the anterodorsal part of the 2nd valvifer, largely at the anterior section of the dorsal flange (asdf; Fig. 4e), and insert at the processus articularis (pra; Fig. 5h), a process that extends laterally from the proximal part of the 2nd valvula to form the medial part of the basal articulation. These muscles have a CSA of 0.0032 mm² each (Table 1).

The paired **posterior 2nd valvifer-2nd valvula muscles** (m3) originate at the medial region along the ventral part of the 2nd valvifer and insert at the

Table 1 Ovipositor muscles of *Venturia canescens*. The muscles (abbreviations in brackets), their origin, insertion and assumed function are described. In addition, the measured volume, mean length and the mean cross section area (CSA) of the single muscles are listed

muscle name (label)	origin	insertion	assumed function	volume [mm ³]	mean length [mm]	mean cross section area (CSA) [mm ²]
1st valvifer-genital membrane muscle (m1)	medial surface of the posteroventral part of the 1st valvifer, in the centre between the tergo-valvifer and the intervalvifer articulation	anteriorly on the genital membrane	tensor muscle for stabilization of the 1st valvifers during ovipositor movements	0.0001	0.175	0.0008
anterior 2nd valvifer-2nd valvula muscle (m2)	medial region along the anterodorsal part of the 2nd valvifer	at the processus articularis	extensor of the terebra (towards the resting position)	0.0015	0.455	0.0032
posterior 2nd valvifer-2nd valvula muscle (m3)	medial region along the ventral part of the 2nd valvifer	at the processus musculares	flexor of the terebra (towards the active probing position): causes the bulb to pivot anteriorly at the basal articulation	0.0029	0.760	0.0039
dorsal T9-2nd valvifer muscle part a (m4a)	lateral region along the posterodorsal part of the anterior margin of female T9	anterior section of the dorsal flange of the 2nd valvifer, partly at the dorsal hook-shaped lobe	protractor of the 1st valvulae: moves the 2nd valvifer posteriorly and the female T9 anteriorly towards each other, causing the 1st valvifer to tilt anteriorly and thus the 1st valvula to slide distally relative to the 2nd valvula	0.0047	0.950	0.0050
dorsal T9-2nd valvifer muscle part b (m4b)	medial region along the posterodorsal part of the anterior margin of female T9	anterior section of the dorsal flange of the 2nd valvifer via tendon, ventrally to m4a	retractor of the 1st valvulae: moves the 2nd valvifer anteriorly and the female T9 posteriorly apart from each other, causing the 1st valvifer to tilt posteriorly and thus the 1st valvula to slide proximally relative to the 2nd valvula	0.0029	0.740	0.0039
ventral T9-2nd valvifer muscle (m5)	medial region of the anterodorsal part of female T9, partly on the cordate apodeme	along the posterior section of the dorsal flange of the 2nd valvifer	muscle for stabilization by holding the posterior parts of the 2nd valvifers in position during ovipositor movements	0.0004	0.280	0.0015

All measurements were determined directly from the 3D muscle masks of the SR- μ CT dataset. These values potentially are lower than in living animals due to shrinking artefacts. The total muscle length was determined as the distance between the centre points of the muscle attachments. CSA was determined as muscle volume / muscle length

processus musculares (prm; Fig. 5h), namely the apodeme that extends dorsally from the proximal part of the 2nd valvula to the genital membrane. These muscles have a CSA of 0.0039 mm², which is similar to that of m2 (Table 1).

The paired **dorsal T9-2nd valvifer muscles** (m4a/b) are modified in their insertion and form two distinct muscle bundles, as it is also known to occur in the ichneumonid genus *Megarhyssa* Ashmead, 1858 [8, 60]. One part of these muscles (m4a) arises at the lateral region along the posterodorsal part of the anterior margin of female T9 and inserts at the anterior section of the dorsal flange of the 2nd valvifer (asdf; Fig. 4e) and partly on the hook-shaped lobe of the 2nd valvifer (hsl; Fig. 4e). The other part (m4b) is fan-shaped and originates at the medial region along the posterodorsal part of the anterior margin of female T9. The muscle tendons (tm4b; Fig. 4f, g) also insert at the anterior section of the dorsal flange of the 2nd valvifer, ventrally to the insertion region of m4a. The tendon of m4b thereby traverses the funnel-like structure at the cordate apodeme (ca; Fig. 4f, g) of the female T9. Muscles m4a and m4b are long thick muscles with a CSA of 0.0050 mm² and 0.0039 mm², respectively (Table 1).

The paired **ventral T9-2nd valvifer muscles** (m5) arise from the medial region of the anterodorsal part of the female T9, partly at the funnel-like structure at the cordate apodeme (ca; Fig. 4f, g), and insert along the posterior section of the dorsal flange of the 2nd valvifer (psdf; Fig. 4e). These are the largest ovipositor muscles with a CSA of 0.0077 mm².

The paired **posterior T9-2nd valvifer muscles** (m6) arise medially at the posterodorsal part of the female T9 and insert at the median bridge of the 2nd valvifers (mb2; Fig. 4e). They are the second smallest muscles of the ovipositor with a CSA of 0.0015 mm² (Table 1).

The literature concerning the musculoskeletal ovipositor system of ichneumonoid wasps is limited and some inconsistent statements have been made about certain ovipositor muscles. We describe the 1st valvifer-genital membrane muscle for the first time in an ichneumonoid species. Either this small muscle is not present in all ichneumonoid species or, more likely, previous authors (e.g. [8, 60]) might have overlooked its presence. In *Megarhyssa macrurus lunator* (Fabricius, 1781) (Hymenoptera: Ichneumonidae), Abbott [60] described the 1st valvifer-2nd valvifer muscle as 'a small muscle connecting the "runner" plate [= 2nd valvifer] with the dorsal margin of the "kidney" plate [= 1st valvifer]'. However, this muscle has neither been found in *Megarhyssa atrata* (Fabricius, 1781) (Hymenoptera: Ichneumonidae) by Snodgrass

[8] nor in *V. canescens* in the present study and might have been mistaken for the anterior 2nd valvifer-2nd valvula (m2) muscle by this author.

In general, the musculoskeletal ovipositor system of ichneumonoid wasps is similar to that of the parasitoid hymenopteran species belonging to Ceraphronoidea [19], a superfamily that is closely related to Ichneumonoidea [61]. However, the ceraphronoids lack the anterior 2nd valvifer-2nd valvula muscle [19] that is present in *V. canescens* and other ichneumonids. All chalcidoid species investigated to date with regard to the ovipositor muscles (Agaonidae [26], Aphelinidae [27], Chalcididae [20], Eurytomidae [23], Pteromalidae [21, 25] and Torymidae [24]) comprise the same set of muscles as ichneumonids but lack the 1st valvifer-genital membrane muscle. All the taxa of Chalcidoidea, Ceraphronoidea and Ichneumonoidea investigated hitherto (including our study of *V. canescens*) lack the 1st valvifer-2nd valvifer muscle, lateral T9-2nd valvifer muscle, 2nd valvifer-genital membrane muscle and T9-genital membrane muscle, which have been described in other hymenopteran taxa [7].

Mechanics and mode of function of the musculoskeletal ovipositor system

The set of six paired ovipositor muscles in *V. canescens* (Fig. 4c; Table 1) comprises two pairs of two antagonistically working muscles that are mainly responsible for the various ovipositor movements, and two muscles stabilizing the musculoskeletal system. Based on the following functional model, we assume that the anterior (m2) and the antagonistically acting posterior 2nd valvifer-2nd valvula muscles (m3) extend or flex the terebra, whereas the two parts of the dorsal T9-2nd valvifer (m4a/b) and the antagonistically acting ventral T9-2nd valvifer muscle (m5) indirectly protract or retract the 1st valvulae. The relatively small 1st valvifer-genital membrane muscle (m1) and the posterior T9-2nd valvifer muscle (m6) might predominantly serve for the stabilization of the ovipositor system during oviposition.

Flexion and extension of the terebra

The 2nd valvula of *V. canescens* is connected with the 2nd valvifers by a rotational joint called the basal articulation (ba; Figs. 4i, 5h, i, l, m). Two antagonistic muscles (m2, m3) insert at the bulbous region around this articulation (Fig. 5h). The insertion region of the posterior 2nd valvifer-2nd valvula muscle (m3) at the 2nd valvula is located dorsally of the basal articulation, whereas its region of origin at the 2nd valvifer is located posteroventrally to it. Therefore, a contraction of m3 (F_3 ; Fig. 5g, i) causes the

bulbs (blb; Fig. 4e, i) to pivot anteriorly at the basal articulation. This leads to a flexion of the 2nd valvula and the interlocked 1st valvulae from its resting position between the paired 3rd valvulae towards an active probing position (small number 2; Fig. 5g, i; Table 1). An alternate contraction of m3 on either side might also cause the terebra to rotate to a certain degree. The insertion region of the anterior 2nd valvifer-2nd valvula muscle (m2) at the 2nd valvula is situated posteroventrally of both the basal articulation and the insertion region of m3, whereas its origin at the 2nd valvifer is located posterodorsally of the articulation. Hence, when m2 (F_2 ; Fig. 5g, i) contracts, the terebra is extended towards its resting position (small number 1; Fig. 5g, i; Table 1).

The anatomical cluster comprising the 2nd valvifer, the 2nd valvula and the two muscles connecting them (Fig. 5l) is a simple mechanical system in which the 2nd valvula is a two-armed class 1 lever. The ratio of the anatomical inlevers ($a = 66 \mu\text{m}$ and $b = 84 \mu\text{m}$; Fig. 5m) is 1:1.27. The torques (M) of the muscle forces of the anterior and posterior 2nd valvifer-2nd valvula muscle (F_2 and F_3) on the basal articulation in the resting position can be estimated by using the maximum force of the muscle (F ; cf. eq. 1), the lengths of the anatomical inlever arms and the attachment angles of the muscles at the 2nd valvula ($\alpha = 154^\circ$ and $\beta = 96^\circ$; Fig. 5m) according to the equations:

$$M_2 = F_2 \cdot a \cdot \sin(\alpha) \quad (\text{eq. 2})$$

$$M_3 = F_3 \cdot b \cdot \sin(\beta) \quad (\text{eq. 3})$$

However, the lengths of the effective (= mechanical) inlever arms (a' and b' ; Fig. 5m) vary greatly with attachment angle (joint angle), i.e. during the flexion or extension of the terebra. The attachment angle of m3 in the resting position is almost 90° ; thus, the effective inlever arm is almost optimal, so that the force of m3 can be optimally transmitted to the 2nd valvula, which leads to a high torque. By contrast, the attachment angle of m2 in the resting position is far below 90° but increases when the wasp flexes its terebra towards the active probing position. This results in an increase in length of the effective inlever arm, an optimal force transmission of m2 at the basal articulation and consequently a high torque. High torques at the basal articulation might be crucial to enable the extensive movements for both the flexion and extension of the terebra, despite the relatively small anatomical inlevers.

Pro- and retraction of the 1st valvulae

Three muscles (m4–m6) connect the 2nd valvifer with the female T9, both these structures being connected with the 1st valvifer by the intervalvifer

articulation or the tergo-valvifer articulation (iva/tva; 1c, f, g, 4f, j, 5i–k), forming a double joint. The insertion regions at the 2nd valvifer of both parts of the dorsal T9-2nd valvifer muscle (m4a/b) lie anterodorsally, whereas the regions of origin at the female T9 are posterodorsally located of both articulations. A contraction of m4a and m4b (F_4 ; Fig. 5d, i) moves the 2nd valvifer posteriorly and the female T9 anteriorly towards each other (small number 3; Fig. 5c, i), whereby the tension of the posterior T9-2nd valvifer muscle (m6) presumably prevents the involved cuticular elements to rotate around the articulations. This movement causes the 1st valvifer to tilt anteriorly (small number 4; Fig. 5c, i) because it is articulated with both the 2nd valvifer and the female T9 via rotational joints (intervalvifer and tergo-valvifer articulation). The 1st valvifer acts as a one-armed class 3 lever that transfers its tilting movement to the dorsal ramus of the 1st valvula, causing the 1st valvula to slide distally relative to the 2nd valvula (small number 5; Fig. 5c). Both m4a and m4b act as protractors of the 1st valvulae (Table 1). They might also assist in extending the terebra (Fig. 5c), as a simultaneous protraction of the 1st valvulae places the terebra under unilateral tension due to friction between the olistheter elements of the 1st and 2nd valvulae. The origin of the antagonistic ventral T9-2nd valvifer muscle (m5) at the female T9 is situated posterodorsally near the intervalvifer articulation and posterior to the tergo-valvifer articulation, whereas its insertion region at the 2nd valvifer is located posteroventrally of both these articulations. Its contraction (F_5 ; Fig. 5f, i) moves the 2nd valvifer anteriorly with respect to the female T9 (small number 6; Fig. 5e, i), thus indirectly causing the 1st valvifer to tilt posteriorly (small number 7; Fig. 5e, i) and the 1st valvulae, as a direct consequence, to slide proximally relative to the 2nd valvula (small number 8; Fig. 5e). Therefore, m5 acts as a retractor of the 1st valvulae (Table 1). It might also assist in flexing the terebra (Fig. 5e), as a simultaneous retraction of both of the 1st valvulae places the terebra under a unilateral tension due to friction between the olistheter elements of the 1st and 2nd valvulae. Muscles m4a and m4b act antagonistically against m5, i.e. m4a/b protract the 1st valvulae, whereas m5 retracts them. The posterior T9-2nd valvifer muscle (m6) stabilizes the ovipositor system by holding the 2nd valvifer and the female T9 in position and prevents them to rotate around the articulations (Fig. 5d; Table 1), although some limited movements in dorso–ventral direction at their posterior ends are likely to occur (cf. Fig. 4g).

The following assumptions were made for a simplified estimation of the torques (M) of the muscle

forces of the dorsal and ventral T9-2nd valvifer muscle (F_4 and F_5): (1) The 2nd valvifer acts as the frame of reference; therefore, the intervalvifer articulation (iva; Figs. 1c, f, g, 4f, j, 5i, j, k) acts as the pivot point (= joint axis or fulcrum) at which the 1st valvifer tilts; and (2) the 2nd valvifer and the female T9 are guided and cannot twist around the articulations but only move towards to or apart from each other along the horizontal anterior–posterior axis without friction occurring. Under these assumptions, the horizontal force vector components of m4 and m5 ($F_{4x} = \cos(\gamma) \cdot F_4$ and $F_{5x} = \cos(\delta) \cdot F_5$ with $\gamma = 5^\circ$ and $\delta = 24^\circ$; Fig. 5j, k) act at the 1st valvifer at the tergo-valvifer articulation (tva; Figs. 1c, f, 4f, j, 5i, j, k). Therefore, the torque (M) of F_{4x} and F_{5x} on the intervalvifer articulation in the resting position can be estimated by using the horizontal vector component (F_x) of the maximum force of a muscle (cf. eq. 1), the length of the anatomical inlever arm ($c = 103 \mu\text{m}$; Fig. 5k)—which is the distance between tergo-valvifer and intervalvifer articulation—and the joint angle ($\varepsilon = 113^\circ$; Fig. 5k) according to the equations:

$$M_4 = F_{4x} \cdot c \cdot \sin(\varepsilon) \quad (\text{eq. 4})$$

$$M_5 = F_{5x} \cdot c \cdot \sin(\varepsilon) \quad (\text{eq. 5})$$

The 1st valvifer acts as a lever with the effective outlever (d' ; Fig. 5k), which is defined as the length between the intervalvifer articulation and the point where the 1st valvifer continues as dorsal ramus of the 1st valvula. The resulting pro- or retracting forces at the dorsal ramus of the 1st valvula (F_{vvm4} and F_{vvm5} ; Fig. 5k) can be estimated by using the horizontal vector components (F_x) of the forces acting on the 1st valvifer at the tergo-valvifer articulation, the length of the effective inlever arm ($c' = c \cdot \sin(\varepsilon) = 94.8 \mu\text{m}$; Fig. 5k) and the effective outlever arm according to the equations:

$$F_{1vv4} = (F_{4x} \cdot c') / d' \quad (\text{eq. 6})$$

$$F_{1vv5} = (F_{5x} \cdot c') / d' \quad (\text{eq. 7})$$

The distance that the 1st valvifer moves is equally transferred to the 1st valvula. Thereby, the shape of the 1st valvifer and the positions of the tergo-valvifer and the intervalvifer articulations influence the way how the 1st valvula is moved, i.e. the more closely the two articulations are situated to each other and the further they are away from the anterior angle of the 1st valvifer, the further the 1st valvula will slide relative to the 2nd valvula along the olistheter [19]. An increase of the quotient of the effective outlever to the effective inlever ($d': c'$ ratio) results in a smaller force output but an increase in the potential maximum velocity and mechanical deflection, i.e. an increase in the speed and the movement distance of the dorsal rami of the 1st valvulae. Their tight interlocking with the dorsal projection of the 2nd valvifer

prevents them from buckling and transfers the movements to the apex of the valvulae. The double joint system of the 1st valvifer enables an pro- and retraction of the 1st valvulae.

The 1st valvifer-genital membrane muscle (m1) potentially serves as a tensor muscle that stabilizes the 1st valvifers during their fast alternate movements by holding them in position laterally to the 2nd valvifers (Fig. 5a, b; Table 1).

Process of oviposition

After a female wasp has found a suitable oviposition site, the contraction of the posterior 2nd valvifer-2nd valvula muscles (m3) causes the 2nd valvula and the interlocked 1st valvulae to flex anteriorly towards the active probing position [19]. This flexing and the general employment of the terebra of *V. canescens* (as in many other ichneumonoid wasp taxa [62, 63]) might be assisted by the annulated and flexible 3rd valvulae and the generally improved manoeuvrability of the metasoma of the Apocrita [64]. The 2nd valvifer is then rotated away from the dorsal surface of the metasoma concomitantly with the terebra. During the so-called cocking behaviour (*sensu* [32]) of *V. canescens*, the 2nd valvifer and the terebra flex simultaneously. In *V. canescens*, this characteristic behaviour is always performed prior to the actual oviposition and is assumed to correlate with the egg being passed down into the spindle-shaped cavity at the apex of the terebra in readiness for oviposition [32, 45]. The parasitoid then performs localized probing movements with the unsheathed terebra in the substrate (Additional file 1). Drilling movements of the terebra are not needed, since the hosts of *V. canescens* live in soft substrates. Once a suitable host is found, stabbing movements are conducted, whereby the terebra is quickly inserted into the host caterpillar [32, 65]. Thereby, alternate contractions of the dorsal T9-2nd valvifer muscles (m4a/b) and the ventral T9-2nd valvifer muscles (m5) indirectly execute the penetration movements of the 1st valvulae (which are documented in a braconid wasp [66]). In some species of Braconidae (the sister group of Ichneumonidae), these movements of the 1st valvulae are known to enable the wasps to actively steer their terebra to some extent: asymmetrical apex forces at the terebra in a viscid medium—caused by varying its asymmetrical tip by pro- or retracting one 1st valvula with respect to the other—result in a passive bending of the terebra [66], or restrictions in inter-element displacements (e.g. strongly swollen short regions pre-apically on the rhachises) cause the terebra to bend due to tensile and compressive forces [67]. Throughout penetration,

the relative position of the valvifers and consequently of the 1st valvulae might be monitored via the sensillar patches of the 2nd valvifers situated anteriorly to the intervalvifer articulations. In addition to penetrating the substrate, the longitudinal alternate movements of the 1st valvulae presumably serve to pass the egg along the terebra. This is facilitated by the egg canal microsculpture consisting of distally oriented scales (ctenidia and subctenidial setae) that push the egg towards the apex of the terebra and hold it in position by preventing backward movements [43, 46, 47]. Shah [45] suggests that the valvilli assist in moving the egg in the terminal part of the terebra by using hydrostatic pressure for a speedy delivery of the egg into the host. In *V. canescens*, the laying of an egg into the haemocoel of the host caterpillar takes only a fraction of a second [32, 45]. After oviposition and withdrawal of the terebra, the anterior 2nd valvifer-2nd valvula muscles (m2) extend the terebra back towards its resting position between the internal concave faces of the 3rd valvulae [10]. Oviposition is commonly followed by cleaning behaviour during which the wasp especially grooms its antennae and terebra.

Conclusions

The examination of the elements of the musculoskeletal ovipositor system of *V. canescens* and its underlying working mechanisms adds to our understanding of a key feature in the evolution of parasitoid hymenopterans, a feature that has impacted the evolutionary success of ichneumonid wasps (with more than 24,000 described [68] and more than 100,000 estimated species [69]) and parasitoid hymenopterans in general (with 115,000 described and 680,000 estimated species [70]). Whereas the basic organization of the ovipositor is remarkably uniform among the Hymenoptera [8], huge variations exist in its structure [9, 11, 12], which are associated with the employment of the terebra in the different taxa of parasitoid species (cf. [62, 63, 71, 72]). Further studies that combine thorough morphological analyses of a parasitoid's musculoskeletal ovipositor system with investigations of its parasitoid-host interactions are needed in order to understand how morpho-physiological traits have influenced the evolution of behavioural, ecological and life history traits and *vice versa* in the megadiverse parasitoid Hymenoptera.

Methods

The *V. canescens* specimens used in this study originated from the thelytokous lab colony of Biologische Beratung Ltd. (Berlin, Germany) from whom we also

received larvae of the host *Ephestia kuehniella* Zeller, 1879 (Lepidoptera: Pyralidae). The wasps were kept in a glass box (20 · 30 · 20 cm) and reproduced after the addition of several pyralid larvae within a mealy substrate to the box every third week (Additional file 1). Three times a week, the imagos were fed with watered honey absorbed onto paper towels. The room was kept at a constant temperature of 24°C.

Light microscopy (LM) and scanning electron microscopy (SEM)

The ovipositor was excised and dissected from the genital chamber of ethanol-fixed animals by using fine forceps, macerated in 10% aqueous potassium hydroxide (KOH) for 12–15 h at room temperature if necessary, cleaned in distilled water and dehydrated stepwise in ethanol (C₂H₆O).

For light microscopy, specimens were mounted onto microscopic slides (76 mm · 26 mm, VWR International, Radnor, PA, USA), embedded in Euparal (Waldeck GmbH & Co. KG, Münster, Germany) and, after drying, investigated with a light microscope of the type Zeiss Axioplan (Carl Zeiss Microscopy GmbH, Jena, Germany) equipped with a Nikon D7100 single-lens reflex digital camera (Nikon Corporation, Tokyo, Japan) and the software Helicon Remote version 3.6.2.w (Helicon Soft Ltd., Kharkiv, Ukraine) (for focus stacking Helicon Focus version 6.3.7 Pro; RRID:SCR_014462).

For scanning electron microscopy (SEM), specimens were air-dried for at least one week in a desiccator. The samples were mounted with double-sided adhesive tape onto stubs, sputter-coated with 19 nm pure gold (Au) by using an Emitech K550X (Quorum Technologies Ltd., West Sussex, UK) and investigated with a scanning electron microscope of the type Zeiss EVO LS 10 (Carl Zeiss Microscopy GmbH, Jena, Germany) and the software SmartSEM version V05.04.05.00 (Carl Zeiss Microscopy GmbH, Jena, Germany).

After completion of the microscopical studies, the remaining wasps were killed by freezing them at –20°C.

Synchrotron X-ray phase-contrast microtomography (SR-μCT)

Two metasomas of ethanol-fixed female *V. canescens* were dehydrated stepwise in ethanol and critical-point-dried by using a Polaron 3100 (Quorum Technologies Ltd., West Sussex, UK) to minimize shrinking artefacts by water loss during the tomography procedure. The anterior ends of the metasomas were glued onto the tips of plastic pins, so that the ovipositor tip was oriented upright, and mounted onto the goniometer head of the sample stage for

tomography. Synchrotron X-ray phase-contrast microtomography (SR- μ CT) [73] was performed at the beamline ID19 at the European Synchrotron Radiation Facility (ESRF) (Grenoble, France) at 19 keV (wavelength $8 \cdot 10^{-11}$ m) and an effective detector pixel size of $0.68 \mu\text{m}$ with a corresponding field of view of $1.43 \cdot 1.43 \text{ mm}$; 6000 projections were recorded over the 180 degree rotation. The detector-to-sample distance was 12 mm. As the structures of interest were larger than the field of view, four separate image stacks were acquired. Therefore, the sample was repositioned in between the imaging procedure, resulting in a certain overlap of two consecutive images. The 3D voxel datasets were reconstructed from the 2D radiographs by using the filtered back-projection algorithm [74, 75] developed for absorption contrast tomography.

Registration and segmentation of SR- μ CT images

To obtain a high-resolution 3D image of the ovipositor and the inherent muscles, two consecutive images from the stack were geometrically aligned in an iterative 3D rigid registration procedure (Additional file 3). A stepwise strategy was applied for the registration. The two data sets were aligned according to the translation of the sample stage in between imaging. The images were then rigidly registered by using normalized mutual information of the grey value images as a similarity measure, with a line search algorithm for the optimization approach. A hierarchical strategy was applied to reduce the risk of finding local minima, starting at a coarse resampling of the datasets and proceeding to finer resolutions. Finally, an affine transformation by using a Lanczos interpolation (cf. [76]) was performed that interpolated both images into the same coordinate system. As a result, all four images were matched in a common coordinate system. An edge-preserving smoothing filter was applied for the segmentation of the individual structures. Segmentation was based on local differences in densities, as chitinous structures have higher densities than muscles. Therefore, grey value images were binarized by using a dual threshold approach that allowed the extraction and separation of regions with different densities.

Image processing and extraction of individual morphological structures

The obtained two masks of muscles and denser structures were further processed to differentiate them into their various morphological components. Therefore, a semi-automatic extraction of biological structural features was applied by using geometric

information. First, small islands were removed with an opening filter and, subsequently, the connected components were automatically labelled. Second, the resulting chitinous structures were manually split at the connection points between the female T9 and the valvifers and at the olistheter mechanism of the terebra, as these fine structures could not be segmented automatically because of the limited resolution of the images. For each muscle bundle, insertion regions (apodemes) were identified on the cuticular elements at both muscle ends, with the whole muscle between the apodemes being determined in a semi-automated interpolation process. This resulted in individual labels for the six muscles involved in ovipositor actuation mechanics. A Gaussian filter was applied for smoothing the 3D masks of the individual chitinous and muscular structures and 3D morphological volumetric models of the biological structures were generated.

Image processing was performed by using the software Amira version 6.0 (FEL, Hillsboro, OR, USA; RRID:SCR_014305) and the custom MATLAB scripts version R2016a (The MathWorks, Inc., Natick, MA, USA; RRID:SCR_001622).

Muscle and leverage analyses

Muscle volume, mean length and mean cross section area were determined from the 3D data sets. The obtained muscle volume values potentially are lower than in living animals due to shrinking artefacts. The total muscle length and the major direction of the muscle force was determined as the distance between the centre points of the attachments of the muscles and the direction of the line in between, respectively. The exact locations of the muscles' origins and insertions were verified with light microscopy. The mean cross section area (CSA) was determined as the muscle volume / muscle length. However, the orientation of the single muscle fibre might deviate from the direction of the main muscle force (cf. [77]), which potentially results in an underestimation of the estimated CSA of an individual muscle and thus its maximum muscle force but also an overestimation of its maximum contraction distance. The anatomical inlevers were measured from the 3D data set and the joint angles were determined. The anatomical lever was defined as the length of the line between the joint axis and the point where the muscle force is applied, i.e. the tendon attachment point. The effective lever arm, which is pivotal for the efficiency of the force transmission, is defined as the perpendicular distance between the projection of the line of action of the tendon attachment point and the joint axis.

Appendix

Table 2 Morphological terms relevant to the hymenopteran ovipositor system. The terms (abbreviations used in this article in brackets) are used and defined according to the Hymenoptera Anatomy Ontology (HAO) [5–7]; the respective Uniform Resource Identifiers (URI) and the synonyms found in the cited literature are listed

anatomical term (abbreviation)	definition/concept	URI	synonyms commonly found in literature
1st valvifer (1vf)	The area of the 1st valvifer-1st valvula complex that is proximal to the aulax, bears the 9th tergal condyle of the 1st valvifer and the 2nd valviferal condyle of the 1st valvifer and is connected to the genital membrane by muscle.	http://purl.obolibrary.org/obo/HAO_0000338	1. Valvifer [9]; fulcral plate [20–27]; gonangulum, gonangula [1]; gonocoxite 8 [18]; gonocoxite XIII [13, 14]; kidney plate [60]; triangular plate [8]; vorderer Valvifer [9]; Winkelplatte [17]
1st valvifer-1st valvula complex	The anatomical cluster that is composed of the sclerites that articulates with the 9th abdominal tergite and the 2nd valvifer.	http://purl.obolibrary.org/obo/HAO_0002158	
1st valvifer-2nd valvifer muscle	The ovipositor muscle that arises from the interarticular ridge of the 1st valvifer and inserts on the 2nd valvifer	http://purl.obolibrary.org/obo/HAO_0002189	
1st valvifer-genital membrane muscle (m1)	The ovipositor muscle that arises from the posterior part of the 1st valvifer and inserts anteriorly on the genital membrane anterior to the T9-genital membrane muscle.	http://purl.obolibrary.org/obo/HAO_0001746	anterior tergo-sternal strictor muscle [14]
1st valvula (1w)	The area of the 1st valvifer-1st valvula complex that is delimited distally by the proximal margin of the aulax.	http://purl.obolibrary.org/obo/HAO_0000339	1. Valvula [9]; gonapophysis 8 [18]; gonapophysis VIII [13, 14]; lancet [8, 60]; lower valve [1, 2, 11, 42, 44, 46, 71, 72]; Stechboiste [9, 17]; stylet [20–27]; ventral stylet [45, 49]; ventral valve [43, 47, 66, 67]; ventral valvula [45, 49]
2nd valvifer (2vf)	The area of the 2nd valvifer-2nd valvula-3rd valvula complex that is proximal to the basal articulation and to the processus musculares and articulates with the female T9.	http://purl.obolibrary.org/obo/HAO_0000927	2. Valvifer [9]; gonocoxite 9 [1, 18]; gonocoxite IX [13, 14]; hinterer Valvifer [9]; inner plate [20]; ~ inner ovipositor plate [21, 22, 24, 26, 27]; oblong plate [8]; oblonge Platte [9, 17]; runner plate [60]; ~ semicircular sheet [23, 25]
2nd valvifer-2nd valvula-3rd valvula complex	The area that is connected to the 9th tergite and the 1st valvifer via conjunctiva, is articulated to the 1st tergite, and bears the aulax.	http://purl.obolibrary.org/obo/HAO_0002175	
2nd valvifer-3rd valvula complex	The area of the 2nd valvifer-2nd valvula-3rd valvula complex that is proximal to the basal articulation.	http://purl.obolibrary.org/obo/HAO_0002181	
2nd valvifer-genital membrane muscle	The ovipositor muscle that arises anteriorly from the dorsal flange of the 2nd valvifer and inserts anteriorly on the dorsal part of the genital membrane.	http://purl.obolibrary.org/obo/HAO_0001672	
2nd valviferal condyle of the 1st valvifer	The condyle that is located on the 1st valvifer and articulates with the 1st valviferal fossa of the 2nd valvifer.	http://purl.obolibrary.org/obo/HAO_0002167	
2nd valvula (2w)	The area of the 2nd valvifer-2nd valvula-3rd valvula complex that is distal to the basal articulation and to the processus musculares and is limited medially by the median body axis.	http://purl.obolibrary.org/obo/HAO_0000928	2. Valvula [9]; dorsal valve [43, 47, 66, 67]; dorsal stylet [45, 49]; dorsal valvula [45, 49]; gonapophysis 9 [18]; gonapophysis IX [13, 14]; Schienenrinne [9, 17]; sheath [21, 22, 27]; ~ stylet [= slender distal part of the united 2nd valvulae] [8] stylet sheath [20, 23–26]; upper valve [1, 2, 11, 42, 44, 46, 71, 72]; (fused) ventral valves [60]

Table 2 Morphological terms relevant to the hymenopteran ovipositor system. The terms (abbreviations used in this article in brackets) are used and defined according to the Hymenoptera Anatomy Ontology (HAO) [5–7]; the respective Uniform Resource Identifiers (URI) and the synonyms found in the cited literature are listed (*Continued*)

anatomical term (abbreviation)	definition/concept	URI	synonyms commonly found in literature
3rd valvula (3rv)	The area of the 2nd valvifer-3rd valvula complex that is posterior to the distal vertical conjunctiva of the 2nd valvifer-3rd valvula complex.	http://purl.obolibrary.org/obo/HAO_0001012	3. Valvula [9]; articulating palps [25]; dorsal valve [60]; gonostylus [18]; gonostylus IX [13, 14]; ~ inner ovipositor plate [23]; ovipositor sheath [1, 2, 11, 43–45, 49]; palp [20]; sheath [67]; sheath lobe [8]; Stachelscheide [9, 17]; terminal palp [24]
9th tergal condyle of the 1st valvifer	The condyle that is located on the 1st valvifer and articulates with the 1st valviferal fossa of T9.	http://purl.obolibrary.org/obo/HAO_0002160	
annulus	The carina that is transverse and extends across the lateral wall of the terebra.	http://purl.obolibrary.org/obo/HAO_0001173	
anterior 2nd valvifer-2nd valvula muscle (m2)	The ovipositor muscle that arises from the anterodorsal part of the 2nd valvifer and inserts subapically on the processus articularis.	http://purl.obolibrary.org/obo/HAO_0001166	anterior gonocoxapophyseal muscle [13, 14]; gonapophysis 9 levator [18]; ramus muscle of the 2nd valvula [8]; shaft elevator muscle [27]
anterior angle of the 1st valvifer	The corner on the 1st valvifer that marks the posterior end of the 1st valvula.	http://purl.obolibrary.org/obo/HAO_0002168	
anterior area of the 2nd valvifer	The area of the 2nd valvifer which is anterior to the anatomical line that is the shortest distance from the 1st valviferal fossa of the 2nd valvifer and the ventral margin of the 2nd valvifer.	http://purl.obolibrary.org/obo/HAO_0002169	
anterior flange of the 1st valvifer	The flange that extends anteriorly on the 1st valvifer and overlaps with the posterior margin of the anterior area of the 2nd valvifer.	http://purl.obolibrary.org/obo/HAO_0002166	
anterior flange of abdominal tergum 9 (af9)	The flange that extends along the anterolateral margin of female T9.	http://purl.obolibrary.org/obo/HAO_0001171	Apodem [9]
anterior ridge of T9	The ridge that extends along the anterior margin of female T9 and receives the site of origin of the ventral and the dorsal T9-2nd valvifer muscles.	http://purl.obolibrary.org/obo/HAO_0002182	
anterior section of dorsal flange of 2nd valvifer (asdf)	The area of the dorsal flange of the 2nd valvifer that is anterior to the site of origin of the basal line.	http://purl.obolibrary.org/obo/HAO_0002173	~ semicircular sheet [23–27]
apodeme	The process that is internal.	http://purl.obolibrary.org/obo/HAO_0000142	
articular surface	The area that is located on the sclerite and that makes movable direct contact with another sclerite.	http://purl.obolibrary.org/obo/HAO_0001485	
aulax (au)	The impression that is on the 1st valvifer-1st valvula complex accommodates the rhachis.	http://purl.obolibrary.org/obo/HAO_0000152	Falze der Stechborste [17]; groove [20, 21, 25]
basal articulation (ba)	The articulation that is part of the 2nd valvifer-2nd valvula-3rd valvula complex and adjacent to the rhachis.	http://purl.obolibrary.org/obo/HAO_0001177	Basalgelenk [9]; bulbous articulation [18, 21, 25–27]
basal line of the 2nd valvifer	The line on the 2nd valvifer that extends between the pars articularis and the dorsal flange of 2nd valvifer.	http://purl.obolibrary.org/obo/HAO_0002171	

Table 2 Morphological terms relevant to the hymenopteran ovipositor system. The terms (abbreviations used in this article in brackets) are used and defined according to the Hymenoptera Anatomy Ontology (HAO) [5–7]; the respective Uniform Resource Identifiers (URI) and the synonyms found in the cited literature are listed (Continued)

anatomical term (abbreviation)	definition/concept	URI	synonyms commonly found in literature
bulb (bib)	The anterior area of the dorsal valve [composite structure of the fused 2nd valvulae] that is bulbous.	http://purl.obolibrary.org/obo/HAO_0002177	Backen [17]; bulbous basal part of the united 2nd valvulae [8]; boubulous sockets [25, 26]; pivoting process [20]; sockets [27]
carina	The process that is elongate and external.	http://purl.obolibrary.org/obo/HAO_0000188	
condyle	The articular surface that is convex and is inserted into the fossa of an adjacent sclerite.	http://purl.obolibrary.org/obo/HAO_0000220	
conjunctiva	The area of the cuticle that is weakly sclerotized, with thin exocuticle.	http://purl.obolibrary.org/obo/HAO_0000221	
cordate apodeme (ca)	The apodeme on the anterior margin of female T9. The ventral T9-2nd valvifer muscle attaches partly on the apodeme.	http://purl.obolibrary.org/obo/HAO_0001585	Apophyse [9]
distal notch of the dorsal valve (no)	The notch that is distal on the dorsal valve [composite structure of the fused 2nd valvulae].	http://purl.obolibrary.org/obo/HAO_0002179	
distal vertical conjunctiva of the 2nd valvifer-3rd valvula complex	The conjunctiva that traverses the 2nd valvifer-3rd valvula complex and is located distal to the median bridge of the 2nd valvifers.	http://purl.obolibrary.org/obo/HAO_0002180	
dorsal flange of the 2nd valvifer	The flange that extends on the dorsal margin of the 2nd valvifer. Part of the ventral T9-2nd valvifer muscle attaches to the flange.	http://purl.obolibrary.org/obo/HAO_0001577	dorsale Verdickungsleiste [9]
dorsal projection of the 2nd valvifer (dp2)	The projection that is located on the 2nd valvifer and corresponds to the proximal end of the rhachis.	http://purl.obolibrary.org/obo/HAO_0002172	~ ramus edge [23, 25, 27]
dorsal ramus of the 1st valvula (dr1)	The region that extends along the dorsal margin of the 1st valvula and bears the aulax.	http://purl.obolibrary.org/obo/HAO_0001579	1st ramus [16]; Ramus der 1. Valvula [9]; ramus of the 1st valvula [8, 51]; Stechborstenbogen [9]
dorsal ramus of the 2nd valvula	The area that extends along the dorsal margin of the 2nd valvula, bears the processus articularis anteriorly and the processus musculares on the antero-dorsal region and articulates with the 2nd valvifer via the basal articulation.	http://purl.obolibrary.org/obo/HAO_0002190	2nd ramus [16]; Ramus der 2. Valvula [9]; Schienenbögen [9, 17]
dorsal sclerite of the 1st valvifer	The sclerite of the 1st valvifer that is located dorsally of the transvalviferal conjunctiva.	http://purl.obolibrary.org/obo/HAO_0002163	
dorsal T9-2nd valvifer muscle (m4a/b)	The ovipositor muscle that arises along the posterodorsal part of the anterior margin of female T9 and inserts on the anterior section of the dorsal flanges of the 2nd valvifer.	http://purl.obolibrary.org/obo/HAO_0001569	anterior tergonocoxal muscle [13, 14]; dorsal/ventral [= part a/part b] anterior tergal muscle of the 2nd valvifer [8]; extensor muscles of lancet [60]; upper/lower [= part a/part b] protractor of gonapophysis 8 [18]; upper/lower [= part a/part b] stylet protractor muscle [27]
dorsal valve	The area that is articulated with the right and left 2nd valvifers at the basal articulation and bears the rhachises. [Term sometimes used for the composite structure of the fused 2nd valvulae.]	http://purl.obolibrary.org/obo/HAO_0001658	[cf. 2nd valvula]

Table 2 Morphological terms relevant to the hymenopteran ovipositor system. The terms (abbreviations used in this article in brackets) are used and defined according to the Hymenoptera Anatomy Ontology (HAO) [5–7]; the respective Uniform Resource Identifiers (URI) and the synonyms found in the cited literature are listed (Continued)

anatomical term (abbreviation)	definition/concept	URI	synonyms commonly found in literature
egg canal (ec)	The anatomical space that is between the left and right olistheter.	http://purl.obolibrary.org/obo/HAO_0002191	Eikanal [9]; Innenkanal [9, 17]
female T9 (T9)	The tergite that is articulated with the 1st valvifer and is connected to the 2nd valvifer via muscles.	http://purl.obolibrary.org/obo/HAO_0000075	9. Tergit [9]; 9th tergum [8]; outer ovipositor plate [21–27]; outer plate [20]; quadrate plate [8]; quadratische Platte [9, 17]; sled plate [60]; T9 [1, 10, 15, 19, 51, 52]; terga 9 [45, 49]; tergite 9 [12, 18]; tergite IX [13, 14]; tergum 9 [10, 15, 51, 52]; tergum IX [16]
flange	The projection that is lamella-like and is located on a rim, carina, apodeme or edge.	http://purl.obolibrary.org/obo/HAO_0000344	
fossa	The articular surface that is concave and accommodates the condyle of another sclerite.	http://purl.obolibrary.org/obo/HAO_0000353	
furcula	The sclerite that is proximal to the 2nd valvifer and receives the site of origin of the posterior 2nd valvifer-2nd valvula muscle.	http://purl.obolibrary.org/obo/HAO_0002498	Gabelbein [9]
genital membrane	The conjunctiva that connects the ventral margins of the 2nd valvifers arching above the 2nd valvula.	http://purl.obolibrary.org/obo/HAO_0001757	
integument	The anatomical system that forms the covering layer of the animal, ectodermal in origin and composed of epidermal cells producing the cuticle.	http://purl.obolibrary.org/obo/HAO_0000421	
interarticular ridge of the 1st valvifer (iar)	The ridge that extends along the posterior margin of the 1st valvifer between the intervalvifer and tergovavifer articulations.	http://purl.obolibrary.org/obo/HAO_0001562	
intervalvifer articulation (iva)	The articulation between the 1st valvifer and 2nd valvifer.	http://purl.obolibrary.org/obo/HAO_0001558	Intervalviferengelenk [9]
intravalvifer articulation	The articulation between the dorsal sclerite of the 1st valvifer and the ventral sclerite of the 1st valvifer.	http://purl.obolibrary.org/obo/HAO_0002165	
lateral T9-2nd valvifer muscle	The muscle arises from the posteroventral parts of the female T9 and inserts on the median bridge.	http://purl.obolibrary.org/obo/HAO_0002187	
median bridge of the 2nd valvifers (mb2)	The area that connects posterodorsally the 2nd valvifers and is the site of attachment for the posterior T9-2nd valvifer muscle.	http://purl.obolibrary.org/obo/HAO_0001780	
medial conjunctiva of the 1st valvula	The conjunctiva that extends medially along the 1st valvula.	http://purl.obolibrary.org/obo/HAO_0002192	
medial conjunctiva of abdominal tergum 9	The conjunctiva of abdominal tergum 9 that has median and longitudinal.	http://purl.obolibrary.org/obo/HAO_0002267	
notal membrane (nm)	The conjunctiva that connects the medial margins of the 2nd valvulae.	http://purl.obolibrary.org/obo/HAO_0001733	
olistheter (oth)	The anatomical cluster that is composed of the rhachis of the 2nd valvula and the aulax of the 1st valvula.	http://purl.obolibrary.org/obo/HAO_0001103	

Table 2 Morphological terms relevant to the hymenopteran ovipositor system. The terms (abbreviations used in this article in brackets) are used and defined according to the Hymenoptera Anatomy Ontology (HAO) [5–7]; the respective Uniform Resource Identifiers (URI) and the synonyms found in the cited literature are listed (Continued)

anatomical term (abbreviation)	definition/concept	URI	synonyms commonly found in literature
ovipositor	The anatomical cluster that is composed of the 1st valvulae, 2nd valvulae, 3rd valvulae, 1st valvifers, 2nd valvifers and female T9.	http://purl.obolibrary.org/obo/HAO_0000679	ovipositor mechanism [27]
ovipositor apparatus	The anatomical cluster that is composed of the ovipositor, abdominal terga 8–10, abdominal sternum 7 and muscles connecting them.	http://purl.obolibrary.org/obo/HAO_0001600	
ovipositor muscle	The abdominal muscle that inserts on the ovipositor.	http://purl.obolibrary.org/obo/HAO_0001290	
pars articularis	The articular surface that is situated anteriorly on the ventral margin of the 2nd valvifer and forms the lateral part of the basal articulation.	http://purl.obolibrary.org/obo/HAO_0001606	
posterior 2nd valvifer-2nd valvula muscle (m3)	The ovipositor muscle that arises posteroventrally from the 2nd valvifer and inserts on the processus musculares of the 2nd valvula.	http://purl.obolibrary.org/obo/HAO_0001815	gonapophysis 9 depressor [18]; muscle of the furcula [in the Ichneumonid <i>Megarhyssa</i>] [8]; posterior gonocoxapophyseal muscle [13, 14]; retractor of ventral valves [60]
posterior area of the 2nd valvifer	The area of the 2nd valvifer that is posterior to the anatomical line that is the shortest distance from the valviferal fossa of the 2nd valvifer to the ventral margin of the 2nd valvifer.	http://purl.obolibrary.org/obo/HAO_0002170	
posterior margin of 1st valvifer	The margin of the 1st valvifer that is posterior and extends between the intervalvifer articulation and the anterior angle of the 1st valvifer.	http://purl.obolibrary.org/obo/HAO_0002159	~ inner ovipositor plate [23–27]
posterior section of dorsal flange of 2nd valvifer (psdf)	The area of the dorsal flange of the 2nd valvifer that is posterior to the site of origin of the basal line.	http://purl.obolibrary.org/obo/HAO_0002174	dorsal/lateral tergo-gonostylar muscle [13, 14]; posterior dorso-ventral muscle [60]
posterior T9-2nd valvifer muscle (m6)	The ovipositor muscle that arises medially from the posterodorsal part of female T9 and inserts on the median bridge of the 2nd valvifers.	http://purl.obolibrary.org/obo/HAO_0001813	
posteroventral corner of the 1st valvifer	The corner of the 1st valvifer that is adjacent to the intervalvifer articulation.	http://purl.obolibrary.org/obo/HAO_0002239	
process	The area on the sclerite that is raised.	http://purl.obolibrary.org/obo/HAO_0000822	
processus articularis (pra)	The process that extends laterally from the proximal part of the 2nd valvula and forms the median part of the basal articulation, and corresponds to the site of attachment for the anterior 2nd valvifer-2nd valvula muscle.	http://purl.obolibrary.org/obo/HAO_0001704	
processus musculares (prm)	The apodeme that extends dorsally from the proximal part of the 2nd valvula to the genital membrane and receives the site of attachment of the posterior 2nd valvifer-2nd valvula muscle.	http://purl.obolibrary.org/obo/HAO_0001703	
rhachis (rh)	The ridge that extends along the ventral surface of the 2nd valvula that is partially enclosed by the aulax.	http://purl.obolibrary.org/obo/HAO_0000898	Leisten der Schienenrinne [17]; T-ridge of ventral valve [60]
ridge	The apodeme that is elongate.	http://purl.obolibrary.org/obo/HAO_0000899	

Table 2 Morphological terms relevant to the hymenopteran ovipositor system. The terms (abbreviations used in this article in brackets) are used and defined according to the Hymenoptera Anatomy Ontology (HAO) [5–7]; the respective Uniform Resource Identifiers (URI) and the synonyms found in the cited literature are listed (*Continued*)

anatomical term (abbreviation)	definition/concept	URI	synonyms commonly found in literature
sawtooth (st)	The process that is located along the ventral margin of the 1st valvula or the dorsal margin of the 2nd valvula.	http://purl.obolibrary.org/obo/HAO_0001681	barb, barbs [43]; teeth [23–26]; Sägezähnnchen [9, 17]; sheath teeth [21]; Zähnnchen [9]
sclerite	The area of the cuticle that is strongly sclerotized, with thick exocuticle and is surrounded by conjunctivae.	http://purl.obolibrary.org/obo/HAO_0000909	
sensillar patch of the 2nd valvifer (sp)	The patch that is composed of placoid sensilla adjacent to the intervalvifer articulation.	http://purl.obolibrary.org/obo/HAO_0001671	Sinneshärrchen des Intervalfiferengelenkes [9]
sternum	The area that is located on the integument and is ventral of the ventral diaphragm.	http://purl.obolibrary.org/obo/HAO_0000956	
T9-genital membrane muscle	The ovipositor muscle that arises from the cordate apodeme and inserts dorsally on the proximal part of the genital membrane and on the opposite cordate apodeme.	http://purl.obolibrary.org/obo/HAO_0001639	
tendon	The portion of tissue that is fibrous, strong, composed of tendon cells and connects the muscle to the integument.	http://purl.obolibrary.org/obo/HAO_0000996	
terebra (trb)	The anatomical cluster that is composed of the 1st and 2nd valvulae.	http://purl.obolibrary.org/obo/HAO_0001004	Legebohrer [17]; ovipositor [1, 11, 18, 42–44, 49, 66, 67, 71, 72]; (ovipositor) shaft [12, 21–27, 45, 47, 56]; shaft of ovipositor [8]; sting shaft [48]; stylus (of the ovipositor) [63]
tergite	The sclerite that is located on the tergum.	http://purl.obolibrary.org/obo/HAO_0001005	
tergo-valvifer articulation (tva)	The articulation that is located between the female T9 and the 1st valvifer and is composed of the 9th tergal condyle of the 1st valvifer and the 1st valviferal fossa of the 9th tergite.	http://purl.obolibrary.org/obo/HAO_0001636	Tergovalviferengelenk [9]
tergum	The area that is located on the integument and is dorsal of the ventral diaphragm.	http://purl.obolibrary.org/obo/HAO_0001006	
transvalviferal conjunctiva	The conjunctiva that transverses the 1st valvifer and separates the dorsal and ventral sclerites of the 1st valvifer.	http://purl.obolibrary.org/obo/HAO_0002162	
valvillus (vlv)	The sclerite that articulates on the 1st valvula and projects into the egg/poison canal.	http://purl.obolibrary.org/obo/HAO_0001619	Hemmplättchen [9]; projection [32]
venom gland reservoir of the 2nd valvifer	The gland reservoir that is between the 2nd valvifers.	http://purl.obolibrary.org/obo/HAO_0002176	
ventral ramus of the 1st valvula	The area that extends external to the dorsal ramus of the 1st valvula.	http://purl.obolibrary.org/obo/HAO_0000891	Ventralfortsatz [9]
ventral ramus of the 2nd valvula	The area of the 2nd valvifer-2nd valvula-3rd valvula complex that bears the rhachis.	http://purl.obolibrary.org/obo/HAO_0001107	
ventral sclerite of the 1st valvifer	The sclerite of the 1st valvifer that is ventral to the transvalviferal conjunctiva.	http://purl.obolibrary.org/obo/HAO_0002164	

Table 2 Morphological terms relevant to the hymenopteran ovipositor system. The terms (abbreviations used in this article in brackets) are used and defined according to the Hymenoptera Anatomy Ontology (HAO) [5–7]; the respective Uniform Resource Identifiers (URI) and the synonyms found in the cited literature are listed (*Continued*)

anatomical term (abbreviation)	definition/concept	URI	synonyms commonly found in literature
ventral T9-2nd valvifer muscle (m5)	The ovipositor muscle that arises from the lateral region of female T9 and inserts along the posterior part of the dorsal flange of the 2nd valvifer.	http://purl.obolibrary.org/obo/HAO_0001616	gonapophysis 8 retractor [18]; posterior tergal muscle of the 2nd valvifer [8]; posterior tergonocoxal muscle [13, 14]; retractor muscle of lancet [65]; stylet retractor muscle [27]

Additional files

Additional file 1: Video sequence of female *Venturia canescens* probing with their terebra in a mealy substrate and potential egg injection into a host larvae (*Ephestia kuehniella*). (MP4 19585 kb)

Additional file 2: Animation of the rotating segmented 3D model of the ovipositor of *Venturia canescens*. (MP4 12464 kb)

Additional file 3: Registered SR- μ CT images of the section of the metasoma of *Venturia canescens* that contains the musculoskeletal ovipositor system and animation of the surface rendering of the aligned SR- μ CT data. (MP4 11892 kb)

Abbreviations

1vf: 1st valvifer; 1vv: 1st valvula; 2vf: 2nd valvifer; 2vv: 2nd valvula; 3vv: 3rd valvula; af9: Anterior flange of T9; asdf: Anterior section of the dorsal flange of the 2nd valvifer; au: Aulax; ba: Basal articulation; bl: Basal line; blb: Bulb; ca: Cordate apodeme; cs: Campaniform sensilla; ct: Ctenidium; dp2: Dorsal projection of the 2nd valvifer; dr1: Dorsal ramus of the 1st valvula; ec: Egg canal; F: Force; F_x : Horizontal vector components of a force; hsl: Hook-shaped lobe of the 2nd valvifer; iar: Interarticular ridge of the 1st valvifer; iva: Intervalvifer articulation; lf1: Longitudinal flap of the 1st valvula; M: Torque; m1: 1st valvifer-genital membrane muscle; m2: Anterior 2nd valvifer-2nd valvula muscle; m3: Posterior 2nd valvifer-2nd valvula muscle; m4a: Dorsal T9-2nd valvifer muscle part a; m4b: Dorsal T9-2nd valvifer muscle part b; m5: Ventral T9-2nd valvifer muscle; m6: Posterior T9-2nd valvifer muscle; mb2: Median bridge of the 2nd valvifers; nm: Notal membrane; no: Notch; oth: Olistheter; pra: Processus articularis; prn: Processus musculares; psdf: Posterior section of the dorsal flange of the 2nd valvifer; rh: Rhachis; sc: Scales; scts: Subscenidial seta; SEM: Scanning electron microscopy; sp: Sensillar patch of the 2nd valvifer; SR- μ CT: Synchrotron X-ray phase-contrast microtomography; ssc: Spindle-shaped cavity in the distal part of the terebra; st: Sawtooth; T6: 6th abdominal tergum; T7: 7th abdominal tergum; T8: 8th abdominal tergum; T9: Female T9 (9th abdominal tergum); T10: 10th abdominal tergum; tm4b: Tendon of the dorsal T9-2nd valvifer muscle part b; trb: Terebra; tva: Tergo-valvifer articulation; vd: Duct of the venom gland reservoir of the 2nd valvifer; vlv: Valvillus

Acknowledgements

The authors thank the following colleagues for their help: Alexander Rack for assistance with the beamline ID19 at ESRF, Monika Meinert and Michael Csader with SEM, Paavo Bergmann, Manfred Drack and Stefan Fischer for valuable tips and inspiring discussions, Helen A. Eggenberger and Theresa Jones for improvements and linguistic corrections of the manuscript, and two referees for their useful comments.

Funding

This work was funded by the German Research Foundation (DFG) as part of the Transregional Collaborative Research Centre (SFB-TRR) 141 'Biological design and integrative structures' (project A03 'Inspired by plants and animals: actively actuated rod-shaped structures exhibiting adaptive stiffness and joint-free kinematics'). The experiment (LS-2342) at ESRF was funded by the EU. The article processing charge was covered by the DFG and the Open Access Publishing Fund of the University of Tübingen.

Availability of data and materials

All data supporting the conclusions of this article are included within the article and its additional files. The analysed raw datasets are available from the corresponding author on reasonable request.

Authors' contributions

BE, AIB, OR and OB prepared the study design. OB attained the SR- μ CT data. AIB performed the analysis of the SR- μ CT data. BE performed the LM and SEM studies, interpreted the data and wrote the manuscript. AIB, OR and OB discussed the results and revised the manuscript. All authors read and approved the final manuscript.

Ethics approval and consent to participate

No approval of research ethics committees was required to accomplish the goals of this study because experimental work was conducted with an unregulated invertebrate species.

Consent for publication

Not applicable.

Competing interests

The authors declare that they have no competing or financial interests.

Publisher's Note

Springer Nature remains neutral with regard to jurisdictional claims in published maps and institutional affiliations.

Author details

¹Evolutionary Biology of Invertebrates, Institute of Evolution and Ecology, University of Tübingen, Auf der Morgenstelle 28, 72076 Tübingen, Germany.

²Continuum Biomechanics and Mechanobiology, Institute of Applied Mechanics, University of Stuttgart, Pfaffenwaldring 7, 70569 Stuttgart, Germany.

Received: 18 March 2018 Accepted: 16 October 2018

Published online: 12 November 2018

References

1. Quicke DLJ. The braconid and ichneumonid parasitoid wasps: biology, systematics, evolution and ecology. 1st ed. Wiley-Blackwell: Chichester; 2015.
2. Quicke DLJ, LeRalec A, Vilhelmsen L. Ovipositor structure and function in the parasitic Hymenoptera with an exploration of new hypotheses. *Rendiconti*. 1999;47:197–239.
3. Quicke DLJ. Parasitic wasps. 1st ed. London: Chapman & Hall; 1997.
4. Gauld I, Bolton B, editors. The Hymenoptera. 1st ed. Oxford: Oxford University Press; 1988.
5. Yoder MJ, Mikó I, Seltmann KC, Bertone MA, Deans AR. A gross anatomy ontology for Hymenoptera. *PLoS ONE*. 2010;5:e15991.
6. Seltmann KC, Yoder MJ, Mikó I, Forshage M, Bertone MA, Agosti D, et al. A hymenopterists' guide to the Hymenoptera Anatomy Ontology: utility, clarification, and future directions. *J Hymenopt Res*. 2012;27:67–88.
7. Hymenoptera Anatomy Consortium. Hymenoptera Anatomy Ontology. 2018. <http://glossary.hymao.org>. Accessed 28 May 2018.
8. Snodgrass RE. Morphology of the insect abdomen. Part II. The genital ducts and the ovipositor. *Smithson Misc Collect*. 1933;89:1–148.
9. Oeser R. Vergleichend-morphologische Untersuchungen über den Ovipositor der Hymenopteren. *Mitt Zool Mus Berlin*. 1961;37:3–119.
10. Vilhelmsen L. The ovipositor apparatus of basal Hymenoptera (Insecta): phylogenetic implications and functional morphology. *Zool Scr*. 2000;29:319–45.
11. Quicke DLJ, Fitton MG, Tunstead JR, Ingram SN, Gaitens PV. Ovipositor structure and relationships within the Hymenoptera, with special reference to the Ichneumonoidea. *J Nat Hist*. 1994;28:635–82.
12. LeRalec A, Rabasse JM, Wajnberg E. Comparative morphology of the ovipositor of some parasitic Hymenoptera in relation to characteristics of their hosts. *Can Entomol*. 1996;128:413–33.
13. Smith EL. Evolutionary morphology of the external insect genitalia. 2. Hymenoptera. *Ann Entomol Soc Am*. 1970;63:1–27.
14. Smith EL. Biosystematics and morphology of Symphyta—III External genitalia of *Euura* (Hymenoptera: Tenthredinidae): sclerites, sensilla, musculature, development and oviposition behavior. *Int J Insect Morphol Embryol*. 1972;1:321–65.
15. Vilhelmsen L, Isidoro N, Romani R, Basibuyuk HH, Quicke DLJ. Host location and oviposition in a basal group of parasitic wasps: the subgenital organ, ovipositor apparatus and associated structures in the Orussidae (Hymenoptera, Insecta). *Zoomorphology*. 2001;121:63–84.
16. Kumpanenko AS, Gladun DV. Functional morphology of the sting apparatus of the spider wasp *Cryptocheilus versicolor* (Scopoli, 1763) (Hymenoptera: Pompilidae). *Entomol Sci*. 2018;21:124–32.
17. Frühauf E. Legeapparat und Eiablage bei Gallwespen (Cynipidae). *Z Wiss Zool*. 1924;121:656–723.
18. Fergusson NDM. A comparative study of the structures of phylogenetic importance of female genitalia of the Cynipoidea (Hymenoptera). *Syst Entomol*. 1988;13:13–30.
19. Ernst AF, Mikó I, Deans AR. Morphology and function of the ovipositor mechanism in Ceraphronoidea (Hymenoptera, Apocrita). *J Hymenopt Res*. 2013;33:25–61.

20. Hanna AD. The male and female genitalia and the biology of *Euchalcidia anyobori* Hanna (Hymenoptera, Chalcidoidea). *Trans R Entomol Soc Lond.* 1934;82:107–36.
21. King PE. The muscular structure of the ovipositor and its mode of function in *Nasonia vitripennis* (Walker) (Hymenoptera: Pteromalidae). *Proc R Entomol Soc Lond Ser A Gen Entomol.* 1962;37:121–8.
22. King PE, Copland MJW. The structure of the female reproductive system in the Mymaridae (Chalcidoidea: Hymenoptera). *J Nat Hist.* 1969;3:349–65.
23. Copland MJW, King PE. The structure of the female reproductive system in the Eurytomidae (Chalcidoidea: Hymenoptera). *J Zool.* 1972;166:185–212.
24. Copland MJW, King PE. The structure of the female reproductive system in the Torymidae (Hymenoptera: Chalcidoidea). *Trans R Entomol Soc Lond.* 1972;124:191–212.
25. Copland MJW, King PE. The structure of the female reproductive system in the Pteromalidae (Chalcidoidea: Hymenoptera). *Entomol.* 1972;105:77–96.
26. Copland MJW, King PE, Hill DS. The structure of the female reproductive system in the Agaonidae (Chalcidoidea, Hymenoptera). *J Entomol Ser A Gen Entomol.* 1973;48:25–35.
27. Copland MJW. Female reproductive system of the Aphelinidae (Hymenoptera: Chalcidoidea). *Int J Insect Morphol Embryol.* 1976;5:151–66.
28. Roberts HLS, Schmidt O. Lifetime egg maturation by host-deprived *Venturia canescens*. *J Insect Physiol.* 2004;50:195–202.
29. Casas J, Driessen G, Mandon N, Wielard S, Desouhant E, van Alphen J, et al. Energy dynamics in a parasitoid foraging in the wild. *J Anim Ecol.* 2003;72:691–7.
30. Beling I. Zur Biologie von *Nemeritis canescens* Grav. (Hymen. Ophion). I. Züchtungsverfahren und ökologische Beobachtungen. *Z Angew Entomol.* 1932;19:223–49.
31. Salt G. The hosts of *Nemeritis canescens*, a problem in the host specificity of insect parasitoids. *Ecol Entomol.* 1976;1:63–7.
32. Rogers D. The ichneumon wasp *Venturia canescens*: oviposition and avoidance of superparasitism. *Entomol Exp Appl.* 1972;15:190–4.
33. Salt G. Experimental studies in insect parasitism. XIII. The haemocytic reaction of a caterpillar to eggs of its habitual parasite. *Proc R Soc Lond Ser B Biol Sci.* 1965;162:303–18.
34. Salt G. Experimental studies in insect parasitism. XIV. The haemocytic reaction of a caterpillar to larvae of its habitual parasite. *Proc R Soc Lond Ser B Biol Sci.* 1966;165:155–78.
35. Rotheram S. The surface of the egg of a parasitic insect. I. the surface of the egg and first instar larva of *Nemeritis*. *Proc R Soc Lond Ser B Biol Sci.* 1973; 183:179–94.
36. Rotheram S. The surface of the egg of a parasitic insect. II. The ultrastructure of the particulate coat on the egg of *Nemeritis*. *Proc R Soc Lond Ser B Biol Sci.* 1973;183:195–204.
37. Feddersen I, Sander K, Schmidt O. Virus-like particles with host protein-like antigenic determinants protect an insect parasitoid from encapsulation. *Experientia.* 1986;42:1278–81.
38. Beukeboom LW, Driessen G, Luckerhoff L, Bernstein C, Lapchin L, van Alphen JJM. Distribution and relatedness of sexual and asexual *Venturia canescens* (Hymenoptera). *Proc Sect Exp Appl Entomol Neth Entomol Soc.* 1999;10:23–8.
39. Beukeboom LW, Pijnacker LP. Automictic parthenogenesis in the parasitoid *Venturia canescens* (Hymenoptera: Ichneumonidae) revisited. *Genome.* 2000; 43:939–44.
40. Schneider MV, Beukeboom LW, Driessen G, Lapchin L, Bernstein C, van Alphen JJM. Geographic distribution and genetic relatedness of sympatric thelytokous and arrhenotokous populations of the parasitoid *Venturia canescens* (Hymenoptera). *J Evol Biol.* 2002;15:191–200.
41. Amat I, Castelo M, Desouhant E, Bernstein C. The influence of temperature and host availability on the host exploitation strategies of sexual and asexual parasitic wasps of the same species. *Oecologia.* 2006;148:153–61.
42. Belshaw R, Grafen A, Quicke DLJ. Inferring life history from ovipositor morphology in parasitoid wasps using phylogenetic regression and discriminant analysis. *Zool J Linnean Soc.* 2003;213–28.
43. Boring CA, Sharkey MJ, Nychka JA. Structure and functional morphology of the ovipositor of *Homolobus truncator* (Hymenoptera: Ichneumonoidea: Braconidae). *J Hymenopt Res.* 2009;18:1–24.
44. Shaw MR. Further notes on the biology of *Pseudavga flavicoxa* Tobias, 1964 (Hymenoptera, Braconidae, Rhysipolinae). *J Hymenopt Res.* 2017;54:113–28.
45. Shah ZA, Blackwell A, Hubbard SF. Ultramorphology of the ovipositor of *Venturia canescens* (Gravenhorst) and possible mechanisms for oviposition. *Int J Agric Biol.* 2012;14:908–14.
46. Rahman MH, Fitton MG, Quicke DLJ. Ovipositor internal microsculpture in the Braconidae (Insecta, Hymenoptera). *Zool Scr.* 1998;27:319–31.
47. Austin AD, Browning TO. A mechanism for movement of eggs along insect ovipositors. *Int J Insect Morphol Embryol.* 1981;10:93–108.
48. Bender JC. Anatomy and histology of the female reproductive organs of *Habrobracon jugnalis* (Ashmead) (Hymenoptera, Braconidae). *Ann Entomol Soc Am.* 1943;36:537–45.
49. Shah ZA. Morphology, ultrastructure, and probable functions of the sense organs on the ovipositor stylets of the hymenopteran parasitoid, *Venturia canescens* (Gravenhorst). *Microsc Res Tech.* 2012;75:876–83.
50. Vilhelmsen L. Flexible ovipositor sheaths in parasitoid Hymenoptera (Insecta). *Arthropod Struct Dev.* 2003;32:277–87.
51. Matushkina NA. Sting microsculpture in the digger wasp *Bembix rostrata* (Hymenoptera, Crabronidae). *J Hymenopt Res.* 2011;21:41–52.
52. Matushkina NA, Stetsun HA. Morphology of the sting apparatus of the digger wasp *Oxybelus uniglumis* (Linnaeus, 1758) (Hymenoptera, Crabronidae), with emphasis on intraspecific variability and behavioural plasticity. *Insect Syst Evol.* 2016;47:347–62.
53. Andersen SO, Weis-Fogh T. Resilin. A rubberlike protein in arthropod cuticle. *Adv Insect Physiol.* 1964;2:1–65.
54. Qin G, Hu X, Cebe P, Kaplan DL. Mechanism of resilin elasticity. *Nat Commun.* 2012;3:1003.
55. Michels J, Gorb SN. Detailed three-dimensional visualization of resilin in the exoskeleton of arthropods using confocal laser scanning microscopy. *J Microsc.* 2012;245:1–16.
56. Dethier VG. The response of hymenopterous parasites to chemical stimulation of the ovipositor. *J Exp Zool.* 1947;105:199–207.
57. Alexander RM. The maximum forces exerted by animals. *J Exp Biol.* 1985; 115:231–8.
58. Rospars J-P, Meyer-Vernet N. Force per cross-sectional area from molecules to muscles: a general property of biological motors. *R Soc Open Sci.* 2016;3: 160313.
59. Josephson RK, Ellington CP. Power output from a flight muscle of the bumblebee *Bombus terrestris*. I. Some features of the dorso-ventral flight muscle. *J Exp Biol.* 1997;200:1241–6.
60. Abbott CE. How *Megarhyssa* deposits her eggs. *J New York Entomol Soc.* 1934;42:127–33.
61. Peters RS, Krogmann L, Mayer C, Donath A, Gunkel S, Meusemann K, et al. Evolutionary history of the Hymenoptera. *Curr Biol.* 2017;27:1013–8.
62. Heatwole H, Davis DM, Wenner AM. The behaviour of *Megarhyssa*, a genus of parasitic hymenopterans (Ichneumonidae: Ephialtinae). *Z Tierpsychol.* 1962;19:652–64.
63. Le Lannic J, Nénon J-P. Functional morphology of the ovipositor in *Megarhyssa atrata* (Hymenoptera, Ichneumonidae) and its penetration into wood. *Zoomorphology.* 1999;119:73–9.
64. Vilhelmsen L, Mikó I, Krogmann L. Beyond the wasp-waist: structural diversity and phylogenetic significance of the mesosoma in apocritan wasps (Insecta: Hymenoptera). *Zool J Linnean Soc.* 2010;159:22–194.
65. Williams JR. The factors which promote and influence the oviposition of *Nemeritis canescens* Grav. (Ichneumonidae, Ophioninae). *Proc R Entomol Soc Lond Ser A Gen Entomol.* 1951;26:49–58.
66. Cerkvenik U, van de Straat B, Gussekloo SWS, van Leeuwen JL. Mechanisms of ovipositor insertion and steering of a parasitic wasp. *Proc Natl Acad Sci USA.* 2017;114:E7822–31.
67. Quicke DLJ, Fitton MG, Harris J. Ovipositor steering mechanisms in braconid wasps. *J Hymenopt Res.* 1995;4:110–20.
68. Yu DS, van Achterberg K, Horstmann K. World Ichneumonoidea 2004. Taxonomy, biology, morphology and distribution. 2004. <http://www.taxapad.com>. Accessed 22 Jan 2018.
69. Gauld I, Sithole R, Gómez JU, Godoy C. The Ichneumonidae of Costa Rica, 4. *Mem Am Entomol Inst.* 2002;66:1–768.
70. Heraty JM. Parasitoid biodiversity and insect pest management. In: Footitt RG, Adler PH, editors. *Insect biodiversity: science and society*. 1st ed. Oxford: Wiley-Blackwell; 2009. p. 445–62.
71. Fritzen NR, Sääksjärvi IE. Spider silk felting—functional morphology of the ovipositor tip of *Clitopyga* sp. (Ichneumonidae) reveals a novel use of the hymenopteran ovipositor. *Biol Lett.* 2016;12:20160350.
72. Takasuka K, Fritzen NR, Tanaka Y, Matsumoto R, Maeto K, Shaw MR. The changing use of the ovipositor in host shifts by ichneumonid ectoparasitoids of spiders (Hymenoptera, Ichneumonidae, Pimplinae). *Parasite.* 2018;25:17.

73. Betz O, Wegst U, Weide D, Heethoff M, Helfen L, Lee WK, et al. Imaging applications of synchrotron X-ray phase-contrast microtomography in biological morphology and biomaterials science. I. General aspects of the technique and its advantages in the analysis of millimetre-sized arthropod structure. *J Microsc.* 2007;227:51–71.
74. Cloetens P, Pateyron-Salomé M, Buffière JY, Peix G, Baruchel J, Peyrin F, et al. Observation of microstructure and damage in materials by phase sensitive radiography and tomography. *J Appl Phys.* 1997;81:5878–86.
75. Cloetens P, Ludwig W, Boller E, Helfen L, Salvo L, Mache R, et al. Quantitative phase contrast tomography using coherent synchrotron radiation. In: Bonse U, editor. *Proceedings of SPIE: developments in X-ray tomography III*, vol. 4503. Bellingham, WA: SPIE Press; 2002. p. 82–91.
76. Birkhold AI, Razi H, Weinkamer R, Duda GN, Checa S, Willie BM. Monitoring in vivo (re)modeling: a computational approach using 4D microCT data to quantify bone surface movements. *Bone.* 2015;75:210–21.
77. Weihmann T, Kleinteich T, Gorb SN, Wipfler B. Functional morphology of the mandibular apparatus in the cockroach *Periplaneta americana* (Blattodea: Blattellidae) – a model species for omnivore insects. *Arthropod Syst Phylogeny.* 2015;73:477–88.

Ready to submit your research? Choose BMC and benefit from:

- fast, convenient online submission
- thorough peer review by experienced researchers in your field
- rapid publication on acceptance
- support for research data, including large and complex data types
- gold Open Access which fosters wider collaboration and increased citations
- maximum visibility for your research: over 100M website views per year

At BMC, research is always in progress.

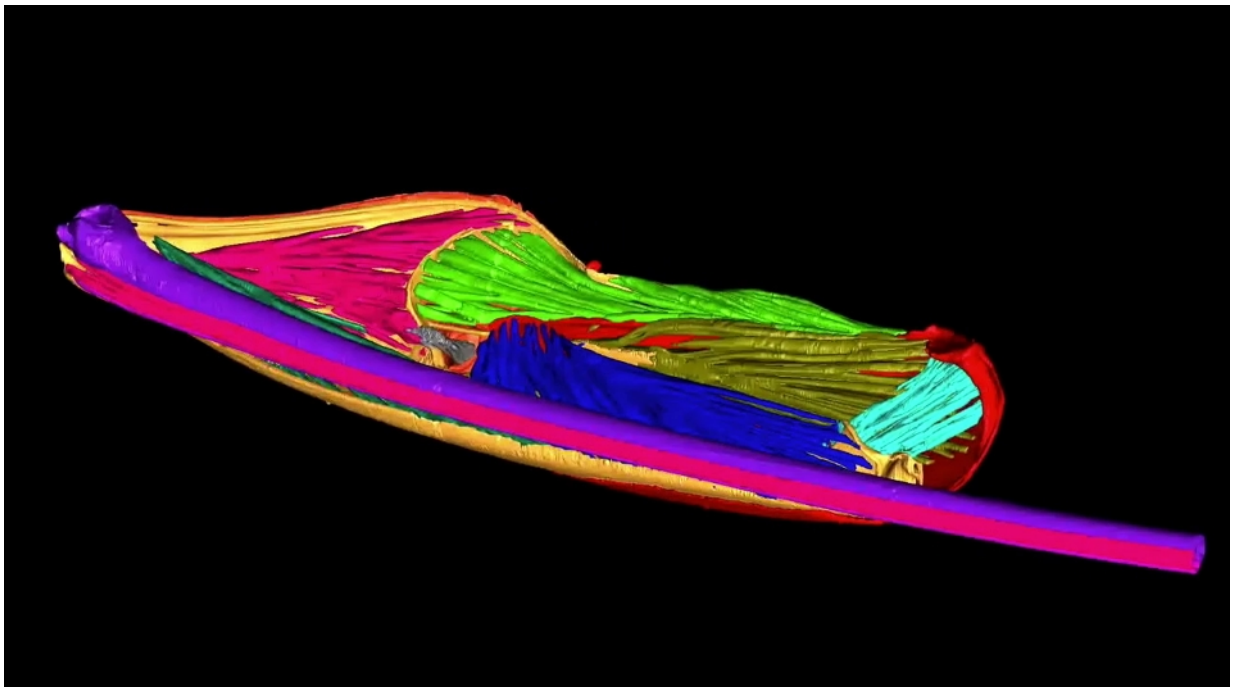
Learn more biomedcentral.com/submissions



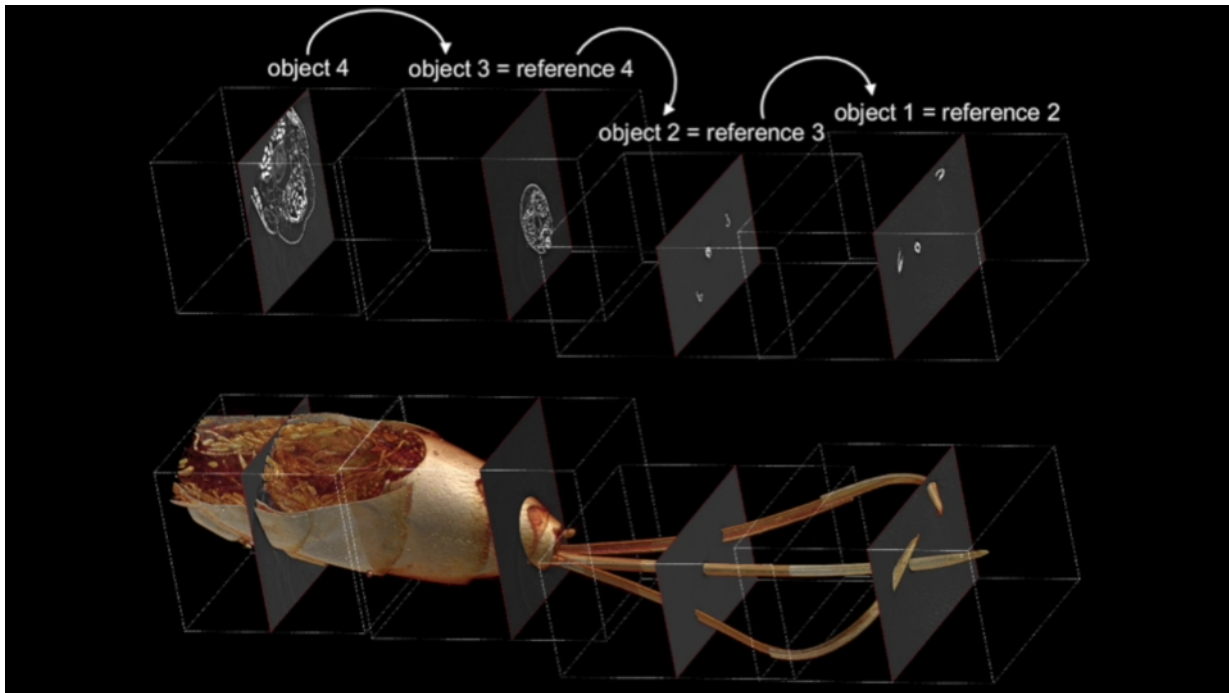
Additional files (supplementary material): video files (snapshots displayed here); files available online at <https://bmczool.biomedcentral.com/articles/10.1186/s40850-018-0037-2>



Additional file 1: Video sequence of female *Venturia canescens* probing with their terebra in a mealy substrate and potential egg injection into a host larva (*Ephestia kuehniella*). (MP4 19575 kb)



Additional file 2: Animation of the rotating segmented 3D model of the ovipositor of *Venturia canescens*. (MP4 12464 kb)



Additional file 3: Registered SR- μ CT images of the section of the metasoma of *Venturia canescens* that contains the musculoskeletal ovipositor system and animation of the surface rendering of the aligned SR- μ CT data. (MP4 11892 kb)

Publication 2

Eggs B., Birkhold A. I., Röhrle O. and Betz O. (2018). The musculoskeletal ovipositor system of an ichneumonid wasp: structural and functional aspects. *Mitteilungen des Entomologischen Vereins Stuttgart* 53 (1): 34–36.

(non-peer-reviewed conference paper; summary of the investigations presented in Publication 1 in detail)

Abstract

The vast majority of hymenopterans are parasitoids of other insects. Their ovipositor serves several tasks in the parasitoid lifestyle, *i.e.* navigating or penetrating the substrate (if the host is concealed) or the targeted puparium, assessing and piercing the host, injecting venom, oviducting the competitors' eggs, finding a suitable place for egg laying and ovipositing. Undoubtedly, modifications of the ovipositor have played a prominent role in defining the host range of parasitoid hymenopterans. Despite many comparative studies on the structure of the hymenopteran terebra (*e.g.* Snodgrass 1933; Quicke *et al.* 1994), the underlying working mechanisms of the musculoskeletal ovipositor system of the extremely diverse and species-rich Ichneumonoidea has remained largely unexplored so far and only little is known about the actuation of the various ovipositor movements. Therefore, we examined all inherent cuticular elements and muscles of the ovipositor of *Venturia canescens* (GRAVENHORST, 1829) (Hymenoptera: Ichneumonidae: Campopleginae), a solitary, koinobiont larval endoparasitoid of several moth species (Lepidoptera) (for oviposition behaviour *cf.* Rogers 1972). Furthermore, we investigated the mechanics of the ovipositor system and determined its mode of function. [...]

Significance within the present thesis: This is a summary of Publication 1, published as a conference proceeding of the “13. Hymenopterologen-Tagung” 2018 in Stuttgart, Germany.

Methods used: scanning electron microscopy (SEM)

Own contribution: writing the original version of the manuscript; preparing the figures; correspondence

The musculoskeletal ovipositor system of an ichneumonid wasp: structural and functional aspects

Benjamin Eggs^{1*}, Annette I. Birkhold², Oliver Röhrle² & Oliver Betz¹

¹Evolutionary Biology of Invertebrates, Institute of Evolution and Ecology, University of Tübingen, Auf der Morgenstelle 28, 72076 Tübingen, Germany

²Continuum Biomechanics and Mechanobiology, Institute of Applied Mechanics, University of Stuttgart, Pfaffenwaldring 7, 70569 Stuttgart, Germany

*E-Mail: benjamin.eggs@uni-tuebingen.de

The vast majority of hymenopterans are parasitoids of other insects. Their ovipositor serves several tasks in the parasitoid lifestyle, i.e. navigating or penetrating the substrate (if the host is concealed) or the targeted puparium, assessing and piercing the host, injecting venom, oviciding the competitors' eggs, finding a suitable place for egg laying and ovipositing. Undoubtedly, modifications of the ovipositor have played a prominent role in defining the host range of parasitoid hymenopterans. Despite many comparative studies on the structure of the hymenopteran terebra (e.g. Snodgrass 1933; Quicke et al. 1994), the underlying working mechanisms of the musculoskeletal ovipositor system of the extremely diverse and species-rich Ichneumonoidea has remained largely unexplored so far and only

little is known about the actuation of the various ovipositor movements. Therefore, we examined all inherent cuticular elements and muscles of the ovipositor of *Venturia canescens* (Gravenhorst, 1829) (Hymenoptera: Ichneumonidae: Campopleginae), a solitary, koinobiont larval endoparasitoid of several moth species (Lepidoptera) (for oviposition behaviour cf. Rogers 1972). Furthermore, we investigated the mechanics of the ovipositor system and determined its mode of function.

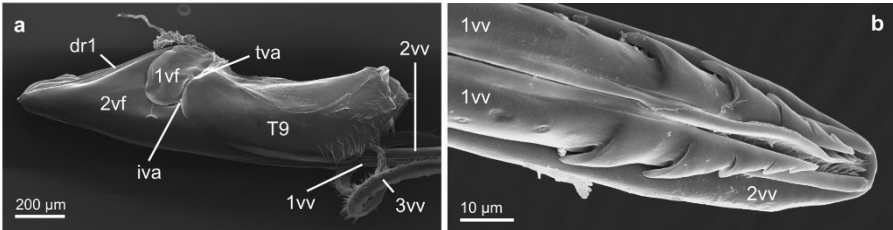


Fig. 1: SEM images. **a** Ovipositor of *Venturia canescens* excised from the genital chamber (left is anterior, lateral view). **b** Apex of the terebra (ventral view). Abbreviations: 1vf, 1st valvifer; 1vv, 1st valvula; 2vf, 2nd valvifer; 2vv, 2nd valvula; 3vv, 3rd valvula; dr1 dorsal ramus of the 1st valvula; iva, intervalvifer articulation; T9, female T9; tva, tergo-valvifer articulation

The ichneumonid ovipositor consists of the female T9 (9th abdominal tergum), two pairs of valvifers and three pairs of valvulae (Fig. 1a). The paired 1st and the 2nd valvulae are tightly interlocked by the olistheter and form the terebra (Fig. 1b). The ovipositor movements are actuated by a set of six muscles. The antagonistically acting posterior and anterior 2nd valvifer-2nd valvula muscles flex and extend the terebra from its resting towards an active probing position and back. The dorsal T9-2nd valvifer muscle is modified in *V. canescens*; it forms two distinct bundles that, together with the antagonistically acting ventral T9-2nd valvifer muscle, change the relative position of the 2nd valvifer to the female T9. This indirectly causes a tilting movement of the 1st valvifer, because it is linked with both of them via intervalvifer and tergo-valvifer articulation, respectively. The 1st valvifer acts as a lever arm, which transfers movements to the 1st valvula via the dorsal ramus. Thus, the shape of the 1st valvifer and the relative positions of the tergo-valvifer and the intervalvifer articulations influence the movements of the 1st valvula. The posterior T9-2nd valvifer muscle and the small 1st-valvifer-genital membrane muscle mainly stabilize the system during oviposition.

From the examination of the elements of the musculoskeletal ovipositor system, we discussed leverage and muscle forces and finally developed a structural and functional model of the underlying working mechanisms. This way, a better understanding of a key feature in the evolution of parasitoid hymenopterans could be attained, a feature that has impacted the evolutionary success of ichneumonid wasps (with more than 24,000 described species (Yu et al. 2004)) and parasitoid hymenopterans in general.

References

- Quicke, D.L.J., Fitton, M.G., Tunstead, J.R., Ingram, S.N. & Gaitens, P.V. (1994): Ovipositor structure and relationships within the Hymenoptera, with special reference to the Ichneumonoidea. *Journal of Natural History* 28, 635-682.
- Rogers, D. (1972): The ichneumon wasp *Venturia canescens*: oviposition and avoidance of superparasitism. *Entomologia Experimentalis et Applicata* 15, 190-194

- Snodgrass, R.E. (1933): Morphology of the insect abdomen. Part II. The genital ducts and the ovipositor. Smithsonian Miscellaneous Collections 89, 1-148
- Yu, D.S., van Achterberg, K., Horstmann, K. (2004): World Ichneumonoidea 2004. Taxonomy, biology, morphology and distribution. <http://www.taxapad.com>

Publication 3

Csader M., Mayer K., Fischer S., Betz O. and **Eggs B.** (2021). The ovipositor of the braconid wasp *Habrobracon hebetor*: structural and functional aspects. *Journal of Hymenoptera Research* 83: 73–99. doi: 10.3897/jhr.83.64018

(peer-reviewed journal article)

Abstract

The Braconidae are a megadiverse and ecologically highly important group of insects. The vast majority of braconid wasps are parasitoids of other insects, usually attacking the egg or larval stages of their hosts. The ovipositor plays a crucial role in the assessment of the potential host and precise egg laying. We used light- and electron-microscopic techniques to investigate all inherent cuticular elements of the ovipositor (the female 9th abdominal tergum, two pairs of valvifers, and three pairs of valvulae) of the braconid *Habrobracon hebetor* (SAY, 1836) in detail with respect to their morphological structure and microsculpture. Based on serial sections, we reconstructed the terebra in 3D with all its inherent structures and the ligaments connecting it to the 2nd valvifers. We examined the exact position of the paired valvilli, which are bilateral concave structures that protrude into the egg canal. In *H. hebetor*, these structures putatively divert the egg ventrally between the 1st valvulae for oviposition. We discuss further mechanical and functional aspects of the ovipositor in order to increase the understanding of this putative key feature in the evolution of braconids and of parasitoid wasps in general.

Significance within the present thesis: We investigated the form and function of the ovipositor of the braconid wasp *Habrobracon hebetor*. Our studies now include representatives of both families of the extremely diverse and species-rich Ichneumonoidea, *i.e.* the Ichneumonidae and the Braconidae.

Methods used: ultramicrotomy, light microscopy (LM), scanning electron microscopy (SEM)

Own contribution: designing and co-supervising the study; writing parts of the manuscript; discussing and revising the manuscript

Ovipositor of the braconid wasp *Habrobracon hebetor*: structural and functional aspects

Michael Csader¹, Karin Mayer¹, Oliver Betz¹, Stefan Fischer^{1,2}, Benjamin Eggs¹

1 *Evolutionary Biology of Invertebrates, Institute of Evolution and Ecology, University of Tübingen, Auf der Morgenstelle 28, 72076, Tübingen, Germany* **2** *Tübingen Structural Microscopy Core Facility (TSM), Center for Applied Geosciences, University of Tübingen, Schnarrenbergstrasse 94–96, 72076, Tübingen, Germany*

Corresponding author: Michael Csader (m.csader@web.de)

Academic editor: J. Fernandez-Triana | Received 5 February 2021 | Accepted 22 April 2021 | Published 28 June 2021

<http://zoobank.org/FEA676AD-6473-4EA3-8F74-E7F83A572234>

Citation: Csader M, Mayer K, Betz O, Fischer S, Eggs B (2021) Ovipositor of the braconid wasp *Habrobracon hebetor*: structural and functional aspects. *Journal of Hymenoptera Research* 83: 73–99. <https://doi.org/10.3897/jhr.83.64018>

Abstract

The Braconidae are a megadiverse and ecologically highly important group of insects. The vast majority of braconid wasps are parasitoids of other insects, usually attacking the egg or larval stages of their hosts. The ovipositor plays a crucial role in the assessment of the potential host and precise egg laying. We used light- and electron-microscopic techniques to investigate all inherent cuticular elements of the ovipositor (the female 9th abdominal tergum, two pairs of valvifers, and three pairs of valvulae) of the braconid *Habrobracon hebetor* (Say, 1836) in detail with respect to their morphological structure and microsculpture. Based on serial sections, we reconstructed the terebra in 3D with all its inherent structures and the ligaments connecting it to the 2nd valvifers. We examined the exact position of the paired valvilli, which are bilateral concave structures that protrude into the egg canal. In *H. hebetor*, these structures putatively divert the egg ventrally between the 1st valvulae for oviposition. We discuss further mechanical and functional aspects of the ovipositor in order to increase the understanding of this putative key feature in the evolution of braconids and of parasitoid wasps in general.

Keywords

3D reconstruction, Braconidae, functional morphology, Hymenoptera, parasitoid, SEM, serial sectioning, terebra

Introduction

Most hymenopteran species belong to the guild of parasitoids of other insects (Quicke 1997). The astonishing radiation of the most diverse parasitoid wasp lineages (i.e. Ceraphronoidea, Ichneumonoidea and Proctotrupomorpha; = Parasitoida *sensu* Peters et al. 2017) has been estimated to have occurred 266–195 million years ago. This process was presumably triggered by continuous adaptations of the parasitoid lifestyle including features such as endoparasitism, miniaturization, and/or modifications of the ovipositor (Peters et al. 2017). Adaptations in oviposition behavior and the morphological structure of the ovipositor might not only have increased the reproductive success of the wasps, but have potentially also enabled them to oviposit in a multitude of different substrates, facilitating the acquisition of new hosts and host ranges (Gauld and Bolton 1988; Quicke 1997). The ovipositor of parasitoid wasps serves a set of functions: penetration of the substrate (if the host is concealed) or of the targeted egg/puparium, the location, assessment, and piercing of the host, the injection of venom, the killing of the competitors' eggs or larvae, the finding of a suitable place for egg laying, and oviposition (Quicke et al. 1999).

The hymenopteran ovipositor is an anatomical and functional cluster that consists of the following elements: the paired 1st valvulae (8th gonapophyses), the 2nd valvula (fused 9th gonapophyses), the paired 3rd valvulae (9th gonostyli), the paired 1st valvifers (fusion of the 8th gonocoxites and gonangula (Vilhelsen 2000)), the paired 2nd valvifers (9th gonocoxites), and the female T9 (9th abdominal tergum) (Snodgrass 1933; Oeser 1961). All the morphological terms are applied according to the Hymenoptera Anatomy Ontology (HAO; Yoder et al. 2010; Hymenoptera Anatomy Consortium 2021; a table of the terms used and of their definitions is given in Table A1 in the Appendix 1). The 1st valvifer is connected to the 2nd valvifer via the intervalvifer articulation and with the female T9 via the tergo-valvifer articulation. Each of the 1st valvulae is attached to the corresponding 1st valvifer via the dorsal ramus of the 1st valvula, whereas the 2nd valvula is connected to the 2nd valvifer via the basal articulation and fine ventral rami of the 2nd valvula (cf. Bender 1943). Both the 1st and the 2nd valvulae are firmly interlocked along almost their entire length via a tongue and groove-like system called the olistheter. They form the terebra (= ovipositor shaft) and accommodate the egg canal (Oeser 1961; Quicke et al. 1994).

Despite many comparative studies on the terebra of hymenopterans (Snodgrass 1933; Oeser 1961; Quicke et al. 1994; LeRalec et al. 1996), the number of publications concerning the entire ovipositor is limited for the vast number of hymenopteran (super-)families. Studies that describe all the inherent cuticular elements and muscles of the ovipositor and (in part) also consider functional aspects include several basal 'symphytan' families (Smith 1970, 1972; Vilhelsen 2000; Vilhelsen et al. 2001), some aculeate species (i.e. *Apis mellifera* Linnaeus, 1758 (Apidae) (Snodgrass 1933), species belonging to Chryridoidea (Barbosa et al. 2021), *Sceliphron destillatorium* (Illiger, 1807) (Sphecidae), *Ampulex compressa* (Fabricius, 1781) (Ampulicidae) (Graf et al. 2021), *Vespa crabro* Linnaeus, 1758 (Vespidae) (Stetsun and Matushkina 2020),

and species belonging to the Crabronidae (Matushkina 2011; Matushkina and Stetsun 2016; Stetsun et al. 2019) and Pompilidae (Kumpanenko and Gladun 2018)), and a few parasitoid species belonging to the Cynipoidea (Frühauf 1924; Fergusson 1988), Platygastroidea (Field and Austin 1994), Chalcidoidea (Hanna 1934; King 1962; King and Copland 1969; Copland and King 1972a, 1972b, 1972c, 1973; Copland 1976), and Ceraphronoidea (Ernst et al. 2013). The musculoskeletal ovipositor system and the actuation mechanisms of ichneumonoid wasps have been described recently in the ichneumonid *Venturia canescens* (Gravenhorst, 1829) (Eggs et al. 2018) and the braconid *Diachasmimorpha longicaudata* (Ashmead, 1905) (van Meer et al. 2020), respectively. Furthermore, drawings of the braconid ovipositor including all inherent cuticular elements exist for *Atanycolus rugosiventris* (Ashmead, 1889) (Snodgrass 1933), *Apanteles congestus* (Nees, 1834) (Oeser 1961), and *Stenobracon deesae* (Cameron, 1902) (Alam 1953; Venkatraman and Subba Rao 1954).

However, knowledge about structural and functional aspects of the ovipositor system of the ecologically and morphologically extremely diverse and species-rich Braconidae remains limited.

Habrobracon hebetor (Say, 1836) (Fig. 1a, b) is a gregarious, idiobiont, larval ectoparasitoid of pyralid moths (Lepidoptera) (Paust et al. 2006) and is well known for its use in biological pest control (Paust et al. 2006; Mbata and Shapiro-ilan 2010; Sanower et al. 2018). Dweck et al. (2008) provided the first morphological descriptions of the ovipositor of this species, with a strong focus on the terebra and its sensillar equipment. In the present study, however, we aim to describe thoroughly all the inherent cuticular elements of the ovipositor of *H. hebetor* in order further to discuss their structural, mechanical, and functional aspects. We have therefore combined scanning electron microscopic (SEM) and light-microscopic studies on both complete cuticular structures and histological serial sections. Serial sections of the terebra have been used to provide a 3D reconstruction that has helped us to understand its morphology especially with regard to all its functionally clustered inherent structures. Finally, we present a structural model of the braconid ovipositor and discuss its mode of function.

Materials and methods

Study animals

The *H. hebetor* (Fig. 1a, b) specimens used in this study originated from Sauter & Stepper GmbH (Ammerbuch, Germany), where they were bred on larvae of *Ephestia kuehniella* Zeller, 1879 (Lepidoptera: Pyralidae).

Sample preparation and light microscopy

For whole mount samples, female *H. hebetor* were killed in 70 % ethanol at 45 °C. The metasoma was cut off and macerated in 10% aqueous potassium hydroxide for up

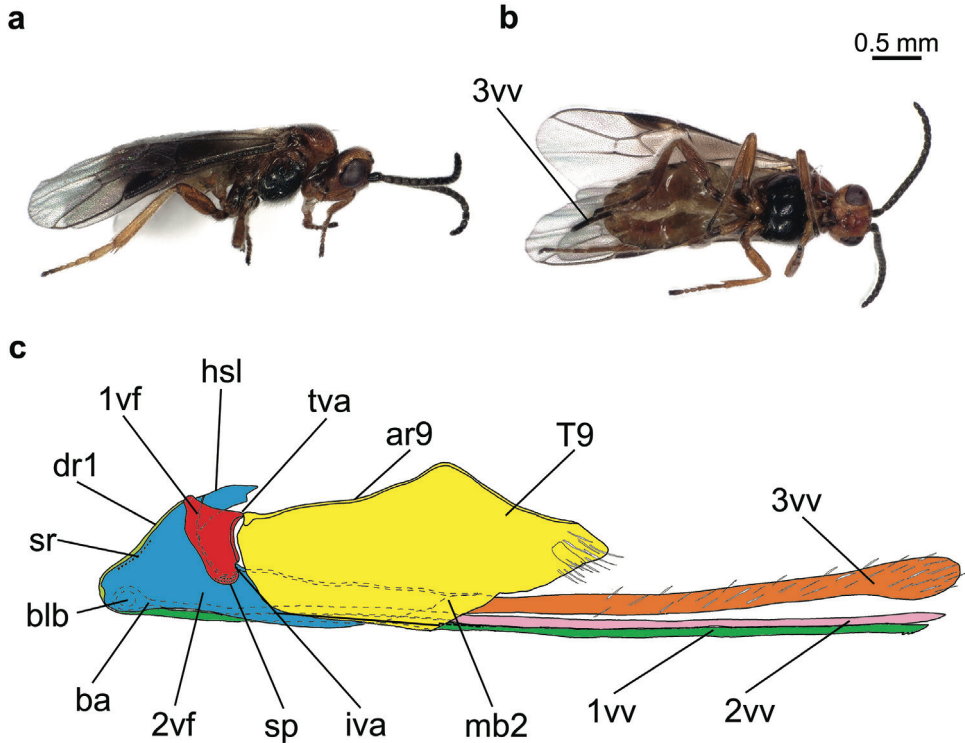


Figure 1. Habitus images of female *Habrobracon hebetor*: lateral (a) and ventral (b) aspect. Schematic drawing of the ovipositor of *H. hebetor* (lateral view) based on the light microscopic and SEM images (c). Abbreviations: 1vf = 1st valvifer; 1vv = 1st valvula; 2vf = 2nd valvifer; 2vv = 2nd valvula; 3vv = 3rd valvula; ar9 = anterior ridge of T9; ba = basal articulation; blb = bulb; dr1 = dorsal ramus of the 1st valvula; hsl = hook-shaped lobe of the 2nd valvifer; iva = intervalvifer articulation; mb2 = median bridge of 2nd valvifers; sr = sensillar row of the 2nd valvifer; sp = sensillar patch of the 2nd valvifer; T9 = female T9; tva = tergo-valvifer articulation.

to 24 h at room temperature to remove tissues, cleaned in distilled water on a mini-shaker, and dehydrated stepwise in ethanol. We then dissected the ovipositor out of the metasoma by using thin tungsten needles, mounted the specimen onto a microscope slide, and embedded it in Entellan® (Merck KGaA, Darmstadt, Deutschland).

For semithin serial sections, we anaesthetized female *H. hebetor* with carbon dioxide. The metasomas were removed and, in order to avoid autolysis, immediately submerged in a primary fixative containing 2.5% glutaraldehyde and 5% sucrose, buffered with 0.1 M cacodylate to pH 7.4. During this fixation, the samples were held in an ice bath at approximately 4 °C for 4 h. Samples were rinsed three times for 10 min in pre-chilled 0.1 M cacodylate buffer (pH 7.4) and post-fixed by using a solution of 1% osmium tetroxide in 0.1 M cacodylate buffer at 4 °C for 4 h. After being further rinsed in the same buffer, the samples were dehydrated through a graded series of ethanol with steps of 30% for 15 min and 50% for 10 min at 4 °C, three times per step, and of 70%

for 10 min, three times at room temperature. The following steps were performed at room temperature. *En bloc* staining was conducted using a saturated solution of 70% ethanolic uranyl acetate for 12 h on a rotatory shaker. Afterwards, dehydration was continued in 5% steps, three times for 10 min each. The fully dehydrated samples were washed in 100% propylene oxide twice for 1 h, and subsequently infiltrated in Spurr low-viscosity embedding resin (Polysciences Inc., Warrington, PA, USA) via a propylene oxide:resin mixture at ratios of 1:1, 1:3, and 1:7 for 1 h per step and then in pure resin for 17 h on a rotatory shaker. As a last incubation step, the samples were placed in fresh pure resin, embedded in silicon molds, and polymerized at 70 °C for 8 h.

Semithin sections of 600 nm were cut perpendicularly to the terebra of *H. hebetor* by using an ultramicrotome Leica Ultracut UTC (Leica Microsystems GmbH, Wetzlar, Germany) equipped with a diamond knife (45° knife angle; DuPont Instruments, Wilmington, DE, USA); a series was obtained with 1920 sections. Semithin sections were then mounted on a microscopic slide by using a 'Perfect Loop for Light Microscopy' (Electron Microscopy Sciences, Hatfield, PA, USA), stained with Stevenel's blue (del Cerro et al. 1980) for 40 min at 60 °C, and subsequently washed in distilled water twice for 5 min each. After being dried, the stained sections were embedded in 'Xyloolfrees Eindeckmittel' (Engelbrecht Medizin- und Labortechnik GmbH, Edermüde, Germany).

The image stack for the 3D reconstruction was generated using a Zeiss Axioplan (Carl Zeiss Microscopy GmbH, Jena, Deutschland) light microscope, equipped with a Nikon D7100 single-lens reflex digital camera (Nikon K.K., Tokio, Japan) and Helicon Remote software version 3.6.2.w (Helicon Soft Ltd, Kharkiv, Ukraine). Flawed images (missing or folded structures and staining problems) were replaced by a copy of the previous or the following image (this was the case for fewer than 3% of the images) for reconstruction purposes. Adobe Photoshop Lightroom version 6.0 (Adobe Systems, San José, CA, USA) was used for initial image processing (white balancing, color contrasting, black and white conversion), whereas Fiji (Schindelin et al. 2012; available online at <https://imagej.net/Fiji>) was employed for cropping, CLAHE filtering, and image stack calibration by using the plugin TrakEM2 (Cardona et al. 2012). A preliminary least square rigid alignment followed by an elastic alignment of the image stack was performed using the 'Elastic Stack Alignment' plugin (Saalfeld et al. 2012). The aligned image stack was then imported into Amira version 6.0 (FEI Company, Hillsboro, OR, USA). We pre-segmented the 1st and 2nd valvulae, the duct of the venom gland and the ligaments that connect the terebra and the 2nd valvifer in the software's segmentation editor by manually labeling approximately every 15th virtual slice along the terebra and every 4th virtual slice in the proximal bulbous region and assigned them to different 'materials'. The labels served as an input for automated segmentation by using the Biomedical Image Segmentation App Biomedisa (available online at <https://biomedisa.de>) (Lösel et al. 2020). The output of Biomedisa was then partially corrected manually in Amira, and a final surface model was generated.

Schematic drawings of the cross-sections of the terebra were generated in Inkscape version 0.92.4 (Inkscape Community; available online at <http://www.inkscape.org/>) based on the original light-microscopic images of the semithin sections.

For lateral and ventral habitus images, female wasps were imaged with a Keyence VHX-7000 Digital Microscope (Keyence Corporation, Osaka, Japan) using focus stacking.

Scanning electron microscopy (SEM)

For scanning electron microscopy (SEM), the specimens were air-dried in a desiccator with Silica gel blue (Carl Roth GmbH & Co. KG, Karlsruhe, Deutschland) for at least four days before being mounted with double-sided adhesive tabs onto stubs and sputter-coated with 19 nm pure gold by using an Emitech K550X (Quorum Technologies Ltd, West Sussex, UK). Images were taken with a scanning electron microscope of the type EVO LS 10 (Carl Zeiss Microscopy GmbH, Jena, Germany) and SmartSEM version V05.04.05.00 software (Carl Zeiss Microscopy GmbH, Jena Germany).

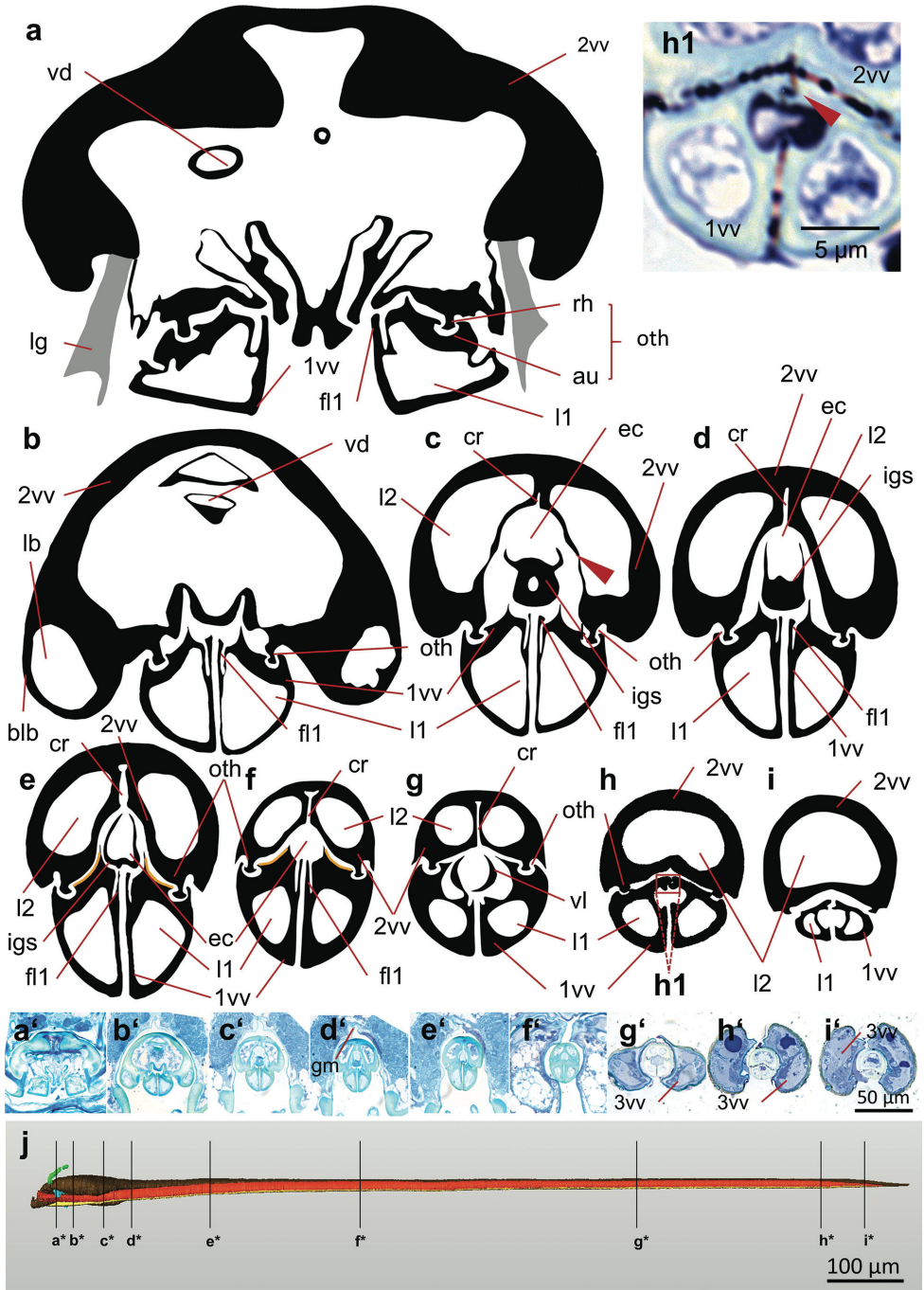
Results and discussion

As in all hymenopterans, the ovipositor of *H. hebetor* consists of three pairs of valvulae, two pairs of valvifers, and the female T9 (Fig. 1c).

Overall structure of the terebra

The 1st and 2nd valvulae form the terebra and enclose the egg canal (cf. Figs 2c–g, 3; Suppl. material 1). The terebra of *H. hebetor* extends far beyond the posterior tip of the metasoma. They are interconnected by a tongue and groove-like system, called the olistheter (oth; Fig. 2a–h). The olistheter comprises two longitudinal ridges that are called the rhachises (rh; Figs 2a, 5c, d) on both sides at the ventral surface of the 2nd valvula and that fit into corresponding T-shaped grooves termed the aulaxes (au; Figs 2a, 4b, f, h)

Figure 2. (next page) Cross sections through the terebra of *Habrobracon hebetor* (from proximal to distal); schematic drawings of the 1st and 2nd valvula (a–i) based on the light microscopic images of the presented semithin sections (a'–i' 600 nm; stained with Stevenel's blue). The drawings are of the same size ratio. The 2nd valvulae possesses, in the proximal region, two lumina that merge into one in the most distal region (h–i). The bulbs (b) and the valvilli (g) are visible. The orange lines (in e, f) mark the position of the distally pointing ctenoid structures on the dorsal surfaces of the 1st valvulae, which are in close contact with the ventral surface of the 2nd valvula. The genital membrane connects the dorsal margins of the 2nd valvifers (b'–h') c fine cuticular structures arise from the dorsal and ventral parts of the 2nd valvula and define the lumina of the bulbs (arrow) h l olistheter-like interlocking system connecting the medial surfaces of the apices of the paired 1st valvulae (arrow). Final segmented 3D reconstruction based on a semithin section series (600 nm thickness) a*–i* position of each single section marked on the final 3D reconstruction of the terebra. Abbreviations: 1vv = 1st valvula; 2vv = 2nd valvula; 3vv = 3rd valvula; au = aulax; blb = bulb; cr = longitudinal crack of 2nd valvula; ec = egg canal; fl1 = longitudinal flap of the 1st valvula; gm = genital membrane; igs = internal guiding structure; l1 = lumen of 1st valvula; l2 = lumen of 2nd valvula; lb = lumen of the bulb; lg = ligament; oth = olistheter; rh = rhachis; vd = duct of the venom gland; vl = valvillus.



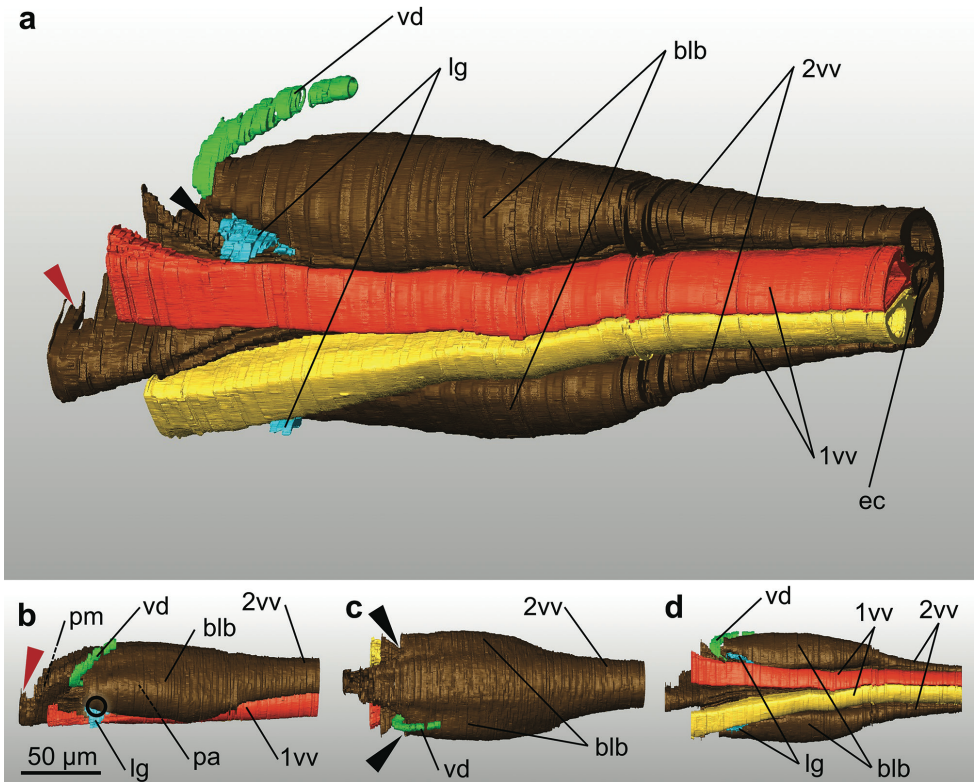


Figure 3. 3D reconstruction of the basal part of the terebra of *Habrobracon hebetor* composed of the 2nd valvulae and the paired 1st valvulae, based on a semithin section series (600 nm thickness **a** lateroventral aspect **b** lateral aspect **c** dorsal aspect **d** ventral aspect). The duct of the venom gland enters dorsoproximally on the left side only. The two ligaments connect the 2nd valvula to the anterior parts of the 2nd valvifers (not visible in these images). The black circle (**b**) indicates the rotation axis of the basal articulation. The lines of the processus articularis and processus musculares (**b**) point to their presumed position according to the results of van Meer et al. (2020). The peak-like structure at the anterior end of the 2nd valvula (red arrow in **a**, **b**) is part of the processus musculares. There are two openings (black arrows in **a**, **c**) at the proximal side of the bulbs. The duct of the venom gland enters on the left side only. Abbreviations: 1vv = 1st valvula; 2vv = 2nd valvula; blb = bulb; ec = egg canal; lg = ligament; pa = processus articularis; pm = processus musculares; vd = duct of the venom gland.

along the dorsal surface of each of the 1st valvulae. This system allows the 1st valvulae to slide longitudinally relative to each other when actuated by the corresponding operating muscles (Oeser 1961; Quicke et al. 1994). Distally pointing scale-like structures are found on both the olistheter elements and might reduce the friction forces by reducing the contact surface between the 1st valvulae and the 2nd valvula (sc; Fig. 4f) (Rahman et al. 1998).

In *H. hebetor*, the cross sections of the terebra differ notably along its length (Fig. 2a–i). A common oviduct enters the proximal bulbous part of the terebra (Bender

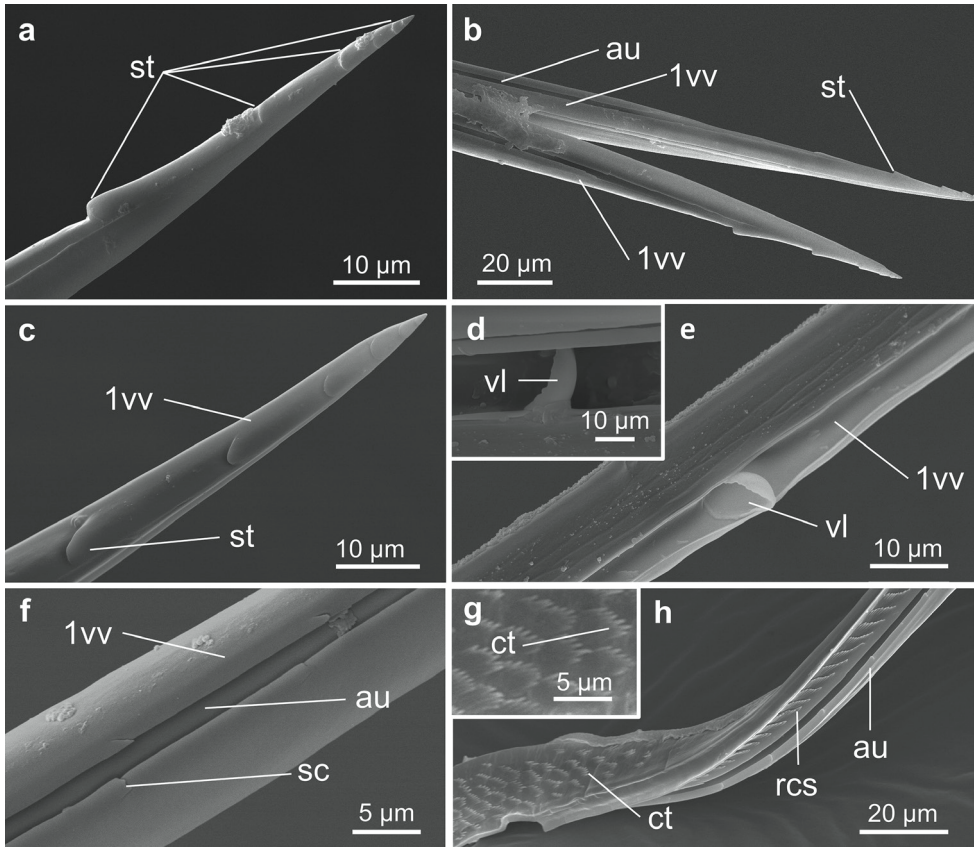


Figure 4. SEM images of the 1st valvulae of *Habrobracon hebetor* **a–c** apex of 1st valvula with sawteeth (**a** lateral aspect **b–c** dorsal aspect). The aulaces are visible (**b**) **d–e** valvillus of 1st valvula (distal is right) **f** distally oriented scale-like structures on the lateral walls of the aulax **g** leaf-like ctenidia on the medial side of 1st valvula **h** 1st valvula with distally oriented ctenoid structures on its dorsal side (contact surface with the 2nd valvula) and ctenidia on its medial side (contact surface with the opposing 1st valvula building the egg canal in the distal part of the terebra). Abbreviations: 1vv = 1st valvula; au = aulax; ct = ctenidium; rcs = row of ctenoid structures; sc = scales; st = sawtooth; vl = valvillus.

1943; Pampel 1914), where it ends at the base of the egg canal (Quicke 1997). Distally, the egg canal is largely defined by the 1st valvulae, but with the dorsal side being formed by the 2nd valvula. The diameter of the terebra decreases from proximal to distal, whereas the diameter of the egg canal remains constant for a long distance from proximal until the valvillus (see subsection ‘1st valvulae’).

1st valvulae

The paired 1st valvulae of *H. hebetor* form the ventral half of the terebra (1vv; Figs 1c, 2a–i, 3, 7a). The proximal end of each 1st valvula is continuous with its dorsal ramus

(dr1; Figs 1c, 7c, h), which is fused with the anterodorsal corner of the 1st valvifer (Figs 7a, c, e, 8).

At their apices, the 1st valvulae of *H. hebetor* possess several sawteeth, which decrease in size apically (st; Fig. 4a, b, c) (cf. Dweck et al. 2008). They probably serve to penetrate the substrate and the host's skin and tissue. Distally pointing ctenoid structures (rcs; Fig. 4h) arranged in rows can be found on the dorsal surfaces of the 1st valvulae, which are in close contact with the ventral surface of the 2nd valvula (orange line; Fig. 2e, f). These ctenoid structures potentially reduce friction forces by minimizing the contact surface between the 1st and the 2nd valvula. The aulaces do not extend all the way to the apex of the 1st valvulae but end just before the lateral sawteeth occur (au; Fig. 4b). Both 1st valvulae are separated for the most of their length. However, mediadorsally at their very apex, the two 1st valvulae become interlocked dorsally by a mechanism similar to that of the olistheter (Fig. 2h1; also see fig. 4a of Dweck et al. 2008). Such a mechanism has previously been observed in other braconids (*Zaglyptogastra* (Quicke 1991), *Aleiodes*, *Ligulibracon* and *Odontobracon* (Quicke et al. 1994), and *D. longicaudata* (van Meer et al. 2020)) and is suggested to be an adaptation to the injection of venom into the host while laying the egg externally (Dweck et al. 2008). In addition, this mechanism might also increase the stability of the apex of the terebra when the host cuticle is pierced (Quicke 2015).

A single valvillus situated on the inner surface of each 1st valvulae protrudes inside the egg canal (vl; Figs 2g, 4d, e; cf. Dweck et al. 2008). The valvillus is a bilaterally concave structure lying in the distal third of the terebra and occupies the whole diameter of the egg canal. Valvilli can be found in the Ichneumonoidea and in various families of the Apocrita (Snodgrass 1933; Quicke et al. 1992; Rahman et al. 1998). They are postulated to serve as a stop and release mechanism for the egg by maintaining the egg in position within the terebra and blocking the egg canal in Ichneumonoidea (Rogers 1972; Rahman et al. 1998; Boring et al. 2009), or for venom pumping in Apocrita (Quicke et al. 1992). However, in the ectoparasitoid *H. hebetor*, the eggs are observed to advance and even partially emerge ventrally at the base of the terebra, i.e. in between the 1st valvulae and near the genital opening (Prozell et al. 2006; Wührer et al. 2009, see also Shaw 2017). Further distally, the valvilli seem to divert the egg ventrally between the 1st valvulae and to press it out completely, since the egg does not emerge at the tip of the terebra but rather ventrally in between the 1st valvulae approximately at the region at which the valvilli are located (Prozell et al. 2006; Wührer et al. 2009). We therefore suggest that the valvilli guide the relatively large egg ventrally out in between the 1st valvulae. The latter are capable of being widely spread in this region because of the olistheter mechanism (Shaw 2017). In cross sections further apically to the valvilli, an egg canal is rarely visible or is absent (Fig. 2h, i), which suggests that at that point the egg has already left the terebra. In addition, the apical interlocking in between the two 1st valvulae (red arrow; Fig. 2h1), which is similar to that of the olistheter, prevents the canal from expanding at the very apex. Proximal to the valvillus, the walls of the egg canal carry leaf-like ctenidia (ct; Fig. 4g, h), which are arranged in rows and are directed towards the distal end of the terebra. These rows of ctenidia point distally in

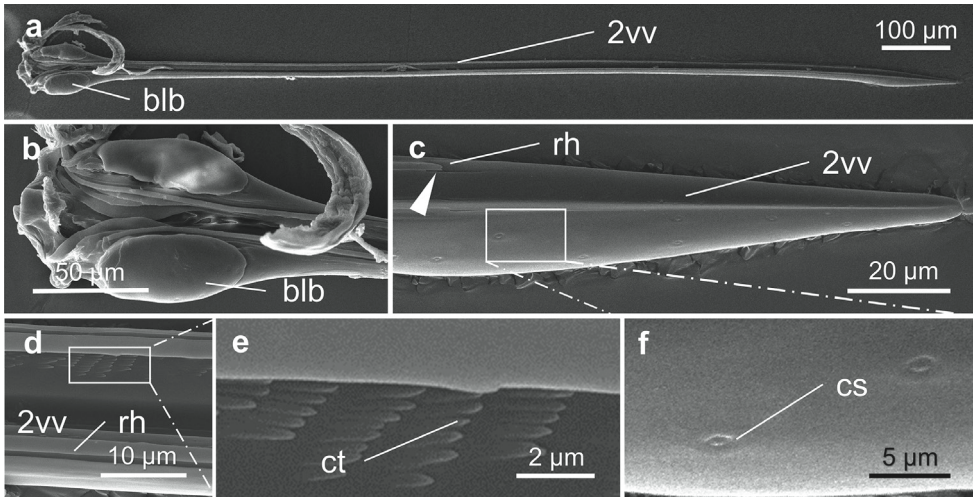


Figure 5. SEM images of the 2nd valvula of *Habrobracon hebetor* **a** overview of the 2nd valvula (ventral aspect with the interlocked 1st valvulae removed) **b** proximal part of 2nd valvula featuring the bulbs **c** apex of 2nd valvula with the ending of the rhachises (arrow) and campaniform sensillae (medioventral aspect) **d–e** middle part of the 2nd valvula showing the rhachises and distally oriented ctenidia **f** sensilla at the apex of the 2nd valvula (detail image of **c**). Abbreviations: 2vv = 2nd valvula; blb = bulb; cs = campaniform sensilla; ct = ctenidia; rh = rhachis.

the direction of egg movement and presumably prevent the regression of the egg during the oviposition process (Austin and Browning 1981). Setiform structures (= subctenidial setae *sensu* Rahman et al. 1998) are also found at the inner walls of the 1st valvulae lying distally to the valvilli. They are arranged in distinct rows.

Each 1st valvula contains a lumen (l1, Fig. 2a–i) whose cuticular walls differ along its length. Proximally, the cuticle is thin but becomes thicker towards the middle and diminishes again apical to the valvillus (Fig. 2a–i). In cross section, the shape of the 1st valvula differs between the basal region and the rest of the terebra. In the basal part, it is triangular in shape (1vv; Fig. 2a), whereas further distally, it appears more oval (1vv; Fig. 2b–i). A longitudinal flap extends along the mediodorsal edge for most of the length of the 1st valvulae and is clearly recognizable in cross sections (fl1; Fig. 2a–f). This flap is highly prominent in the proximal part of the terebra but vanishes further apically (fl1; Fig. 2g–i). It might seal the egg canal to prevent the leaking of venom, since the pressure of the venom has been suggested to squeeze the two flaps together and therefore to seal the gap (Quicke et al. 1994; Shaw 2017). It has been observed in almost all the examined braconid species (Quicke and van Achterberg 1990; Quicke et al. 1994).

2nd valvula

In *H. hebetor*, the 2nd valvula (2vv; Figs 1c, 2a–i, 3, 5a, 7a) form the dorsal half of the terebra, and its proximal bulbous end (blb; Figs 1c, 2b, 3, 5b, 7e, h; called the

bulbs in the following) is connected with the 2nd valvifer via the basal articulation (ba; Figs 1c, 7h).

The apex of the 2nd valvula is not serrated but is slightly enlarged before it narrows towards the tip (Figs 5a, c, 7a). In contrast to many ichneumonid and other braconid species (cf. Boring et al. 2009; Shah et al. 2012; Eggs et al. 2018), the 2nd valvula of *H. hebetor* does not feature a prominent apical notch. Campaniform sensilla can be found in this area (cs; Fig. 5f) (for a discussion of the sensillary equipment of the terebra of *H. hebetor*, see Dweck et al. 2008). Similar to the aulaces on the 1st valvulae, the rhachises (rh; Fig. 5c, d) do not extend all the way to the apex but end at about the same distance away from the apex as seen for the aulaces (arrow; Fig. 5c). The apical half of the ventral side of the 2nd valvula forms the dorsal wall of the egg canal and is, similar to the 1st valvulae, covered by rows of ctenidia directed distally (ct; Fig. 5e). As previously discussed for the 1st valvulae, these structures might prevent the regression of the egg during oviposition (cf. Rahman et al. 1998). Medioproximally, the bulbs feature ligaments (lg; Figs 2a, 3a, b, d) that connect the 2nd valvula with the anterior section of the 2nd valvifer. The ligament marks the region at which parts of the 2nd valvifer merge into the anterior part of the 2nd valvula. The bulbs also contain a lumen (lb; Fig. 2b). The proximal end of the 2nd valvula bears the processus articularis (pa; Figs 3b, 7h) laterally and the processus musculares (pm; Figs 3b, 7h) at the anterior peak-like structure of the 2nd valvula (red arrow; Fig. 3a, b). However, the medial 2nd valvifer-2nd valvula muscle (M-2vfl-2vlv) that might stabilize the 2nd valvifer and that was newly described in the braconid *D. longicaudata* by Meer et al. (2020) was absent in our serial sections. There are two openings (black arrows; Fig. 3a, c) at the proximal side of the bulbs. The duct of the venom gland enters the dorsoproximal area of the bulbs on the left side only (vd; Figs 2a, b, 3, Suppl. material 2) (cf. Bender 1943, who investigated the anatomy and histology of the female reproductive organs of the closely related *Habrobracon juglandis* (Ashmead, 1889)). Further distally, the closed duct of the venom gland seems to disappear and to merge with the egg canal formed by the valvulae (Suppl. material 2). In this area, the venom presumably flows into the egg channel that is formed by both the 1st and 2nd valvulae with the longitudinal flaps of the 1st valvulae acting as a seal (fl1; Fig. 2a–f).

Proximally, the 2nd valvula features a distinct longitudinal crack at the ventral side along the middle, which is clearly visible in cross-section (cr; Fig. 2c–g), presumably indicating the paired origin of the 2nd valvulae. At the basal part of the 2nd valvula, fine cuticular structures (arrow; Fig. 2c) arise from its dorsal and ventral parts and define the two lumina (l2; Fig. 2c–g) that run almost the entire length of the 2nd valvula and that fuse at the apex (Fig. 2h, i). Proximally, the ventral part of the 2nd valvula gradually changes shape and forms a U-shaped structure that extends distally into the egg canal (Suppl. material 2). This internal structure (igs; Fig. 2c–e) presumably helps in guiding the egg by forming a temporary egg canal. Without this internal guiding structure, the diameter of the egg canal would be large in this proximal region; this might lead to a lowered internal pressure and thus to problems when the egg is pushed further distally.

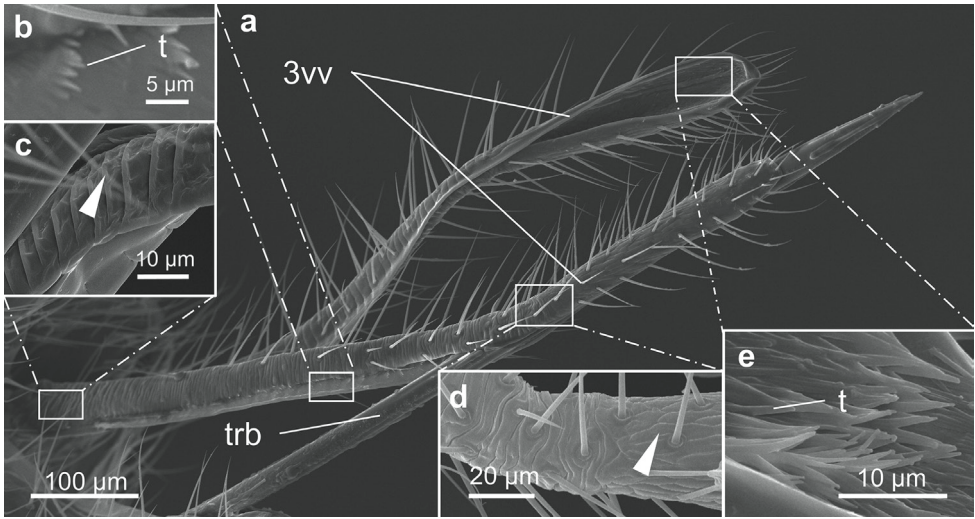
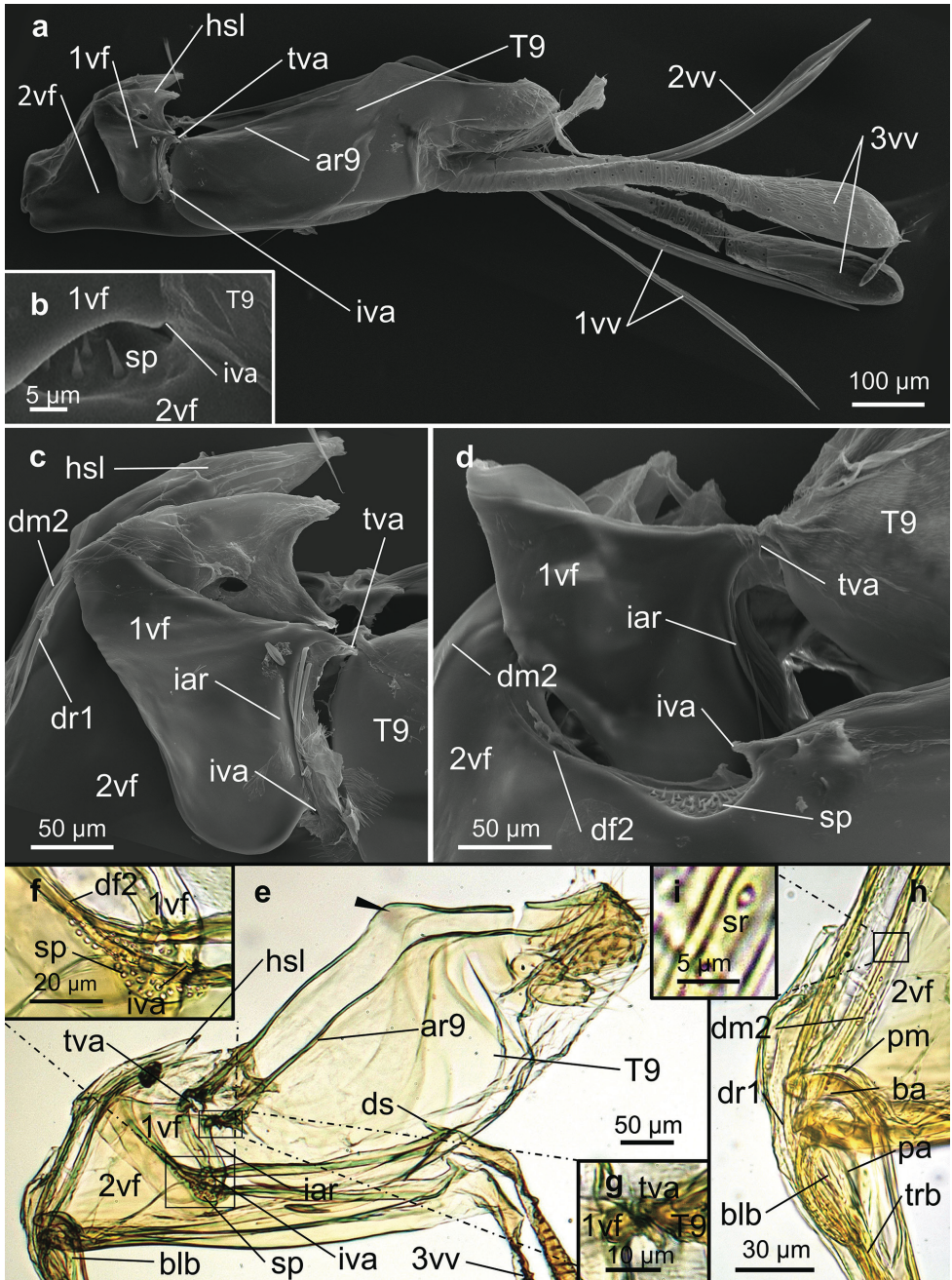


Figure 6. SEM images of 3rd valvulae of *Habrobracon hebetor* **a** the terebra is partially embraced by the 3rd valvulae **b** inner proximal surface of the 3rd valvulae with fine trichomes distally **c** outer surface of the 3rd valvulae, proximally exhibiting annulation caused by fine transverse furrows (arrow) **d** outer surface of the 3rd valvulae at the transition zone (arrow) between the distal longitudinal ridge to the proximal vertically folded surface at the region in which the 3rd valvulae expand **e** inner surface of the apex of a 3rd valvula covered by trichomes. Abbreviations: 3vv = 3rd valvula; trb = terebra; t = trichome.

3rd valvulae

The paired 3rd valvulae of *H. hebetor* originate at the distal end of the 2nd valvifers and extend far beyond the posterior tip of the metasoma towards the tip of the terebra (Figs 1b,c, 7a, e). Each is U-shaped in cross-section (3vv; Figs 2g'–i', 6a) and they completely ensheath and protect the terebra in the resting position (3vv, trb; Figs 2g'–i', 6a) (cf. Bender 1943; Dweck et al. 2008). The distal third of the 3rd valvulae is enlarged (Figs 6a, 7a), and their lateral surfaces differ over the course of their length: proximally, the 3rd valvulae are annulated by fine transverse furrows (arrow; Fig. 6c; cf. Vilhelmsen 2003; Eggs et al. 2018), whereas the enlarged distal part lacks these structures (arrow; Fig. 6d). Trichomes, which Dweck et al. (2008) have described as trichoid sensilla, cover most of the external surface of the 3rd valvulae (Fig. 6a). The density of the trichomes varies along the length of the 3rd valvulae and is highest at the apex (Fig. 6a).

The inner surface of the 3rd valvulae facing the terebra is densely covered by trichomes (t; Fig. 6b, e), particularly at the distal enlarged part (Fig. 6a, e). These structures might be involved in cleaning the terebra sensilla between oviposition episodes (Quicke et al. 1999; Vilhelmsen 2003). Observations have shown that the 3rd valvulae also play a role in stabilizing the terebra during oviposition (Prozell et al. 2006; Wührer et al. 2009; Vilhelmsen 2003; Cerkvenik et al. 2017; Eggs et al. 2018; van Meer et al. 2020).



1st valvifer

In lateral view, the paired 1st valvifers of *H. hebetor* have a compact triangular shape with rounded edges (1vf; Figs 1c, 7a, c–e, 8). The intervalvifer articulation (iva; Figs 1c, 7a, c–f), a rotational joint, is located at the rounded posteroventral side and connects the 1st valvifer to the 2nd valvifer. The ventral edge of the 1st valvifer is placed laterally of the 2nd valvifer and seems to be in contact with a sensillar patch (sp; Figs 1c, 7b, d–f) that extends dorsally at the anterior beginning of the dorsal flange of the 2nd valvifer (df2; Fig. 7d, f). The tergo-valvifer articulation (tva; Fig. 7a, c–e, g) connects the 1st valvifer to the female T9. A ridge, called the interarticular ridge of the 1st valvifer (iar; Figs 1c, 7c–e, 8), extends in between the two articulations. This ridge might mechanically stabilize the 1st valvifer and prevent it from extensive deformation. At its anterodorsal corner (arrow; Fig. 8), the 1st valvifer is fused with the dorsal ramus of the 1st valvula (dr1; Figs 1c, 7c, h, 8), which is continuous with the 1st valvula.

2nd valvifer

The paired 2nd valvifers of *H. hebetor* are elongated in the longitudinal axis (2vf; Figs 1c, 7a, e). The anteromedial socket-like part of the 2nd valvifer is connected to the laterally placed bulbs of the 2nd valvula (blb; Figs 1c, 3, 7e, h) via the ball-and-socket-like basal articulation (ba; Figs 1c, 7h). The posterior ends of both the 2nd valvifers are connected to the 3rd valvulae (3vv; Figs 1c, 7a, e). At their posterodorsal ends, the two 2nd valvifers are connected by a median bridge (mb2; suggested position indicated in Fig. 1c). A massive dorsal spike (ds; Fig. 7e), a structure that has not as yet been described in other parasitoid wasps, is present at the posterior end of the 2nd valvifer and potentially serves as an apodeme. In addition, a flexible cuticular area, a conjunctiva called the genital membrane (gm; Fig. 2d'), connects the ventral margins of the 2nd valvifers arching above the 2nd valvula.

Figure 7. (previous page) SEM (a–d) and light microscopic (e–i) images of the ovipositor of *Habrobracon hebetor* **a** overview of the ovipositor (lateral aspect; visible pore-like structures are presumably artefacts of detached trichomes) **c** 1st valvifer exhibiting the interarticular ridge and the hook-shaped lobe of the 2nd valvifer. The 1st valvifer is continuous with the dorsal rami of the 1st valvula and is articulated with the 2nd valvifer and the female T9 via the intervalvifer articulation and the tergo-valvifer articulation, respectively **d** sensillar patch of the 2nd valvifer (made visible by partly removal of the 1st valvifer) **b, f** sensillar patch of the 2nd valvifer **e** overview of the 2nd valvifer and female T9. The arrow shows the dorsal hump of the T9 **g** tergo-valvifer articulation between the 1st valvifer and female T9 **h** detail image of e. The laterally placed bulbs of the most proximal part of the 2nd valvula are articulated with the paired 2nd valvifers via the basal articulation **i** sensilla in a row at the dorsal margin of the 2nd valvifer. Abbreviations: 1vf = 1st valvifer; 1vv = 1st valvula; 2vf = 2nd valvifer; 2vv = 2nd valvula; 3vv = 3rd valvula; ar9 = anterior ridge of T9; ba = basal articulation; blb = bulb; df2 = dorsal flange of 2nd valvifer; dm2 = dorsal margin of the 2nd valvifer; dr1 = dorsal ramus of the 1st valvula; ds = dorsal spike of the 2nd valvifer; hsl = hook-shaped lobe of the 2nd valvifer; iar = interarticular ridge of the 1st valvifer; iva = intervalvifer articulation; sp = sensillar patch of the 2nd valvifer; sr = sensillar row of the 2nd valvifer; pa = processus articularis; pm = processus musculares; T9 = female T9; trb = terebra; tva = tergo-valvifer articulation.

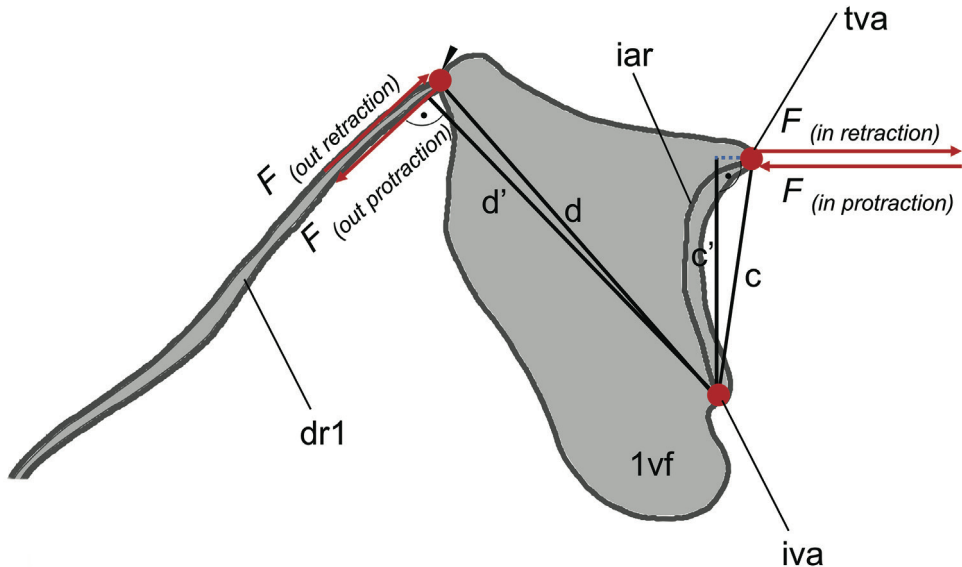


Figure 8. Functional lever model of 1st valvifer with both articulations and the beginning of the dorsal ramus of the 1st valvula (arrow) with the intervalvifer articulation acting as pivot point. c = anatomical inlever; c' = effective (= mechanical) inlever; d = anatomic outlever; d' = effective (= mechanical) outlever; $F_{(in\ protraction)}$, $F_{(in\ retraction)}$ = Force input at the 1st valvifer; $F_{(out\ protraction)}$, $F_{(out\ retraction)}$ = Force output at the 1st valvifer that is transferred to the dorsal ramus of the 1st valvula. $c' \cdot F_{(in)}$ = $d' \cdot F_{(out)}$. Abbreviations: 1vf = 1st valvifer; dr1 = dorsal ramus of the 1st valvula; iar = interarticular ridge of the 1st valvifer; iva = intervalvifer articulation; tva = tergo-valvifer articulation.

At its anterodorsal corner, the 2nd valvifer extends upwards in a hook-shaped lobe (hsl; Fig. 7a, c, e; *sensu* Snodgrass 1933), and features the elongated anterodorsal ridge of the 2nd valvifer, the so called dorsal margin of the 2nd valvifer (dm2; Fig. 7c, d, h). The dorsal projection of the 2nd valvifer, a tongue-like structure situated on the dorsal margin of the 2nd valvifer, is continuous with the olistheter. The corresponding groove is located on the dorsal side of the dorsal ramus of the 1st valvula (dr1; Fig. 7c, h; cf. fig. 4h1 of Eggs et al. 2018) and enables its back and forth movement. This hook-shaped lobe might guide and stabilize the 1st valvifer during its posterior pivoting but might also allow for a larger arc of movement of the 1st valvifer and therefore a greater retraction distance of the 1st valvulae (cf. Eggs et al. 2018).

Two main ridges are found on the 2nd valvifer, i.e. (1) the dorsal flange of the 2nd valvifer (df2; Fig. 7d, f), which expands from the sensillar patch in the direction of the hook-shaped lobe and posteriorly from the sensillar patch to the origin of the 3rd valvulae (Fig. 7e), and (2) the dorsal margin of the 2nd valvifer (dm2; Fig. 7c, d, h). The two cuticular ridges might have a stabilizing function to prevent deformation. The 2nd valvifer of *H. hebetor* does not feature a basal line (e.g. in contrast to the ichneumonid *Venturia canescens* (Gravenhorst, 1829), see fig. 4e of Eggs et al. 2018), a ridge that extends from the pars articularis to the dorsal flange of the 2nd valvifer.

Clusters of sensillae (“styloconic sensillae” according to Dweck et al. 2008) occur in two regions. The first cluster, called the sensillar patch (sp; Figs 1c, 7b, d–f), is situated ventrally of the intervalvifer articulation and is covered by the 1st valvifer laterally. The second cluster occurs at the dorsal margin of the 2nd valvifer (sr; Figs 1c, 7h, i). These sensilla are arranged in a row and are in contact with the dorsal ramus of the 1st valvula. The two sensilla clusters presumably monitor the pro- and retraction movements of the 1st valvifers and the attached 1st valvulae, respectively. The density of sensilla in the patch is much higher than that on the dorsal margin of the 2nd valvifer.

Female T9

The female T9 is unpaired and elongated (T9; Figs 1c, 7a, c, d, e). At its anterodorsal corner, it is connected to the 1st valvifer via the tergo-valvifer articulation (tva; Figs 1c, 7a, c–e, g). Dorsally, it features the anterior ridge almost throughout its length (ar9; Fig. 7e), and posteriorly, it bears a hump-shaped structure (arrow; Fig. 7e). The female T9 mostly lies inside the abdomen, and only the posterolateral part that faces the outside is covered with hairs.

Mode of function of the ovipositor

Functional models of the actuation and movement mechanisms based on thorough analyses of the musculoskeletal system of an ichneumonid and a braconid wasp have recently been described (Eggs et al. 2020, van Meer et al. 2020) and are summarized in the following. Although, in our study, we have not considered the muscles of the system, we have basically found the same arrangement of cuticular elements in the ovipositor system of *H. hebetor* as described in both of the above-mentioned studies. Hence, we assume analogous functional morphological conditions, although we point out any possible *H. hebetor*-specific modifications.

The ovipositor movements are mainly actuated by two pairs of antagonistically working muscles (further described below), i.e. (1) the depression (i.e. downward rotation to the active position) and elevation (i.e. upward rotation back to the resting position) of the terebra, and (2) the pro- and retraction of the 1st valvulae. Smaller muscles, i.e. the 1st valvifer-genital membrane muscle or the posterior T9-2nd valvifer muscle, might predominantly serve to stabilize the ovipositor system during oviposition.

(1) Depression and elevation of the terebra: The basal articulation is composed of the processus articularis (pa; Figs 3b, 7h) at the 2nd valvulae and the pars articularis at the 2nd valvifer. The pars articularis is a small area of anteroventral corners of the 2nd valvifer, whereas the processus articularis is the respective structure of the bulb. The posterior 2nd valvifer-2nd valvula muscle depresses the terebra, i.e. rotates it downwards to the active position from its resting position between the paired 3rd valvulae. The tendon of this muscle inserts at the processus musculares (pm; Figs 3b, 7h), which is situated at the peak-like posterior part of the 2nd valvula (arrow; Fig. 3a, b) and thus

increases the moment arm. However, the moment arm most probably changes over the range of motion of the terebra. In *H. hebetor*, we assume that the virtual line that can be drawn perpendicularly to the length axis of the terebra through the ligaments (lg; Figs 2a, 3a, b, d) lying anterolaterally on the bulbs (blb; Figs 2b, 5a, b, 7e, h) most likely forms the rotation axis (= joint axis, pivot point or fulcrum; black circle; Fig. 3b), since the ligaments form the connections of the 2nd valvula with the anterior parts of the 2nd valvifers and can only stretch to a limited extent. Van Meer et al. (2020) postulate that, in the braconid *D. longicaudata*, the rotation axis lies directly anterior to the bulbs. In addition, these authors have observed that, during terebra depression (towards an active probing position), the lateral bulbs are pulled out of the socket-like anterior parts of the 2nd valvifers, which are pushed slightly apart. The ball-and-socket-like connection is therefore assumed mainly to stabilize the terebra in its resting position. The antagonistically acting anterior 2nd valvifer-2nd valvula muscle inserts at the processus musculares and elevates the terebra, i.e. rotates it back upwards towards the resting position.

(2) Pro- and retraction of the 1st valvulae: The 1st valvifer, 2nd valvifer, and the female T9 form a mechanical cluster of functionally interconnected elements (for detailed functional models see fig. 5 of Eggs et al. 2018 and fig. 8 of van Meer et al. 2020). The dorsal and the antagonistically acting ventral T9-2nd valvifer muscle change the relative position of the 2nd valvifer and the female T9. Both of these structures are connected with the 1st valvifer via the intervalvifer and the tergo-valvifer articulation (Fig. 7c), respectively. Moreover, both are rotational joints that allow rotation in the sagittal plane only. The 1st valvifer acts as a lever (Fig. 8) that transfers its movements to the dorsal ramus of the 1st valvula (dr1; Figs 7c, h, 8). Contraction of the dorsal T9-2nd valvifer muscle leads to an anterior rotation of the 1st valvifer around the intervalvifer articulation. The 1st valvifer acts as a lever that transfers these movements to the dorsal ramus of the 1st valvula, thus causing the 1st valvula to slide distally relative to the 2nd valvula, i.e. to protract. *Vice versa*, contraction of the antagonistic ventral T9-2nd valvifer muscle leads to a posterior rotation of the 1st valvifer, causing the 1st valvula to slide proximally to the 2nd valvula, i.e. to retract (Eggs et al. 2018; van Meer et al. 2020). The hook-shaped lobe of the 2nd valvifer (hsl; Fig. 7a, c, e) might allow a larger arc of movement of the 1st valvifer and therefore a larger retraction distance of the 1st valvulae. During the retraction of the 1st valvula, the dorsal ramus of the 1st valvula (dr1; Fig. 7c, h) can slide along the dorsal projection of the 2nd valvifer almost until the posterior end of the hook-shaped lobe (hsl; Fig. 7a, c, e).

In the context of the described movements, the 1st valvifer acts as a one-armed class 3 lever (force arm smaller than load arm). In our lever model (Fig. 8), we use the 2nd valvifer (2vf; Fig. 1c) as a frame of reference. However, in reality, all involved cuticular elements can move relative to each other. The anatomical inlever (*c*; Fig. 8) equals the distance between the intervalvifer articulation and the tergo-valvifer articulation (where the input force is applied; $F_{(\text{in protraction})}$, $F_{(\text{in retraction})}$; Fig. 8). The distance between the intervalvifer articulation and the beginning of the dorsal ramus of the 1st valvula at the anterodorsal end of the 1st valvifer equals the anatomical outlever (*d*; Fig. 8). The ratio of effective outlever (*d'*; Fig. 8) and the effective inlever (*c'*; Fig. 8) are indicative for the potential

maximum velocity, the mechanical deflection, and the amount of force transmission to the 1st valvula. An increase of the d':c' ratio results in an increase of the potential maximum velocity and mechanical deflection but entails a smaller force output ($F_{\text{(out protraction)}}$, $F_{\text{(out retraction)}}$; Fig. 8) of the 1st valvulae. In resting position, the anatomical in- and outlever are both very similar to their respective effective levers, thereby creating high torques at the intervalvifer articulation and ensuring an optimal force transmission when pro- or retracting the 1st valvulae. During oviposition, the left and the right 1st valvulae slide back and forth alternately at a high frequency. These valvula movements are crucial for drilling and precise egg laying (Vilhelmsen 2000; Cerkvenik et al. 2017; van Meer et al. 2020).

The shape of the 1st valvifer varies between the various hymenopteran superfamilies (Oeser 1961). Ichneumonoid species such as the braconid *H. hebetor* in the present study possess a 1st valvifer with a rounded compact shape (Snodgrass 1933; Eggs et al. 2018), in contrast to the elongated and bow-shaped 1st valvifers of members of the superfamily Chalcidoidea (Copland and King 1972a, 1972b, 1972c, 1973), the triangularly shaped 1st valvifers of *Apis mellifera* (Linnaeus, 1758) and other aculeate species (Snodgrass 1933; Oeser 1961; Matushkina 2011; Matushkina and Stetsun 2016; Stetsun and Matushkina 2020; Graf et al. 2021), and the highly diverse 1st valvifers of basal hymenopterans (e.g. the robust-appearing 1st valvifers of Tentredinidae (Snodgrass 1933; Vilhelmsen 2000) or the triangular 1st valvifers in some Xyelidae (Vilhelmsen 2000)). The ecomorphological consequences of these morphological differences remain to be explored in future systematic comparative analyses with respect to the parasitization of other hosts in different substrates and habitats.

The two sensilla clusters found on the 2nd valvifer of *H. hebetor* (sp, sr; Fig. 7b, d–f, i), probably play an important role in monitoring the pro- and retraction of the 1st valvulae, since their accurate actuation is of major importance for successful egg deposition (van Meer et al. 2020). Unlike in *H. hebetor* or *V. canescens* (Eggs et al. 2018), the sensilla patch at the intervalvifer articulation of other parasitoid wasps can be extremely reduced, e.g. in Pteromalidae (Chalcidoidea) with only three single sensilla (Copland and King 1972b). The question remains as to whether both the density and number of sensilla are linked to the importance of the control of the movements involved in oviposition, and whether this correlates with the shape of the 1st valvifer.

Conclusion

All the cuticular elements of the ovipositor of *Habrobracon hebetor* play a crucial role for successful oviposition. The 2nd valvifer and the female T9 exhibit many muscle insertions, the 1st valvifer acts as a lever that transmits movements to the 1st valvulae, and the terebra serves as a device for precise venom injection, host assessment, and accurate egg laying. All the cuticular elements feature many distinct structures in addition to the microsculpture that is crucial for the performance of these tasks. Our work also has shown that a 3D reconstruction based on a histological section series preserves useful information about the exact morphology and position of inherent structures thereby enabling us to draw conclusions about their function. Future comparative examination of the inherent ovipositor

elements, their morphological structure, and the underlying mechanical and functional aspects has the potential to increase our understanding of a putative key feature in the evolution of parasitoid hymenopterans, a feature that probably has significantly impacted the evolutionary success of braconid wasps (more than 18,000 described (Quicke 2015) and about 43,000 estimated species (Jones et al. 2009)) and of parasitoid hymenopterans in general (115,000 described and 680,000 estimated species (Heraty 2009)).

Acknowledgements

We thank Paavo Bergmann for valuable hints regarding histological techniques, Monika Meinert for assistance with SEM, Verena Pietzsch and James H. Nebelsick with the Keyence digital microscope, Theresa Jones for linguistic corrections of the manuscript, and Lars Vilhelmsen and Donald L. J. Quicke for their useful comments.

This work was funded by the German Research Foundation (DFG) as part of the Transregional Collaborative Research Centre (SFB-TRR) 141 ‘Biological design and integrative structures’ (project A03 ‘Inspired by plants and animals: actively actuated rod-shaped structures exhibiting adaptive stiffness and joint-free kinematics’). The article processing charge was covered by the DFG and the Open Access Publishing Fund of the University of Tübingen.

References

- Alam SM (1953) The skeleto-muscular mechanism of *Stenobracon deesae* Cameron (Braconidae, Hymenoptera) – An ectoparasite of sugarcane and juar borers of India. Part II. Abdomen and internal anatomy. Aligarh Muslim University Publications (Zoology Series) 3: 1–75
- Austin AD, Browning TO (1981) A mechanism for movement of eggs along insect ovipositors. International Journal of Insect Morphology and Embryology 10: 93–108. [https://doi.org/10.1016/S0020-7322\(81\)80015-3](https://doi.org/10.1016/S0020-7322(81)80015-3)
- Barbosa DN, Vilhelmsen L, Azevedo CO (2021) Morphology of sting apparatus of Chrysoidea (Hymenoptera, Aculeata). Arthropod Structure & Development 60: 100999. <https://doi.org/10.1016/j.asd.2020.100999>
- Bender JC (1943) Anatomy and histology of the female reproductive organs of *Habrobracon juglandis* (Ashmead) (Hymenoptera, Braconidae). Annals of the Entomological Society of America 36: 537–545. <https://doi.org/10.1093/aesa/36.3.537>
- Boring CA, Sharkey M, Nychka J (2009) Structure and functional morphology of the ovipositor of *Homolobus truncator* (Hymenoptera: Ichneumonoidea: Braconidae). Journal of Hymenoptera Research 18: 1–24.
- Cardona A, Saalfeld S, Schindelin J, Arganda-Carreras I, Preibisch S, Longair M, Tomancak P, Hartenstein V, Douglas RJ (2012) TrakEM2 software for neural circuit reconstruction. PLoS ONE 7: e38011. <https://doi.org/10.1371/journal.pone.0038011>

- Cerkvenik U, van de Straat B, Gussekloo SWs, van Leeuwen JL (2017) Mechanisms of ovipositor insertion and steering of a parasitic wasp. *Proceedings of the National Academy of Sciences of the United States of America* 114: E7822–E7831. <https://doi.org/10.1073/pnas.1706162114>
- del Cerro M, Cogen J, del Cerro C (1980) Stevenel's blue: an excellent stain for optical microscopical study of plastic embedded tissues. *Microscopica Acta* 83: 117–121.
- Copland MJW (1976) Female reproductive system of the Aphelinidae (Hymenoptera: Chalcidoidea). *International Journal of Insect Morphology and Embryology* 5: 151–166. [https://doi.org/10.1016/0020-7322\(76\)90001-5](https://doi.org/10.1016/0020-7322(76)90001-5)
- Copland MJW, King PE (1972a) The structure of the female reproductive system in the Eurytomidae (Chalcidoidea: Hymenoptera). *Journal of Zoology* 166: 185–212. <https://doi.org/10.1111/j.1469-7998.1972.tb04085.x>
- Copland MJW, King PE (1972b) The structure of the female reproductive system in the Pteromalidae (Chalcidoidea: Hymenoptera). *The Entomologist* 105: 77–96.
- Copland MJW, King PE (1972c) The structure of the female reproductive system in the Torymidae (Hymenoptera: Chalcidoidea). *Transactions of the Royal Entomological Society of London* 124: 191–212. <https://doi.org/10.1111/j.1365-2311.1972.tb00363.x>
- Copland MJW, King PE (1973) The structure of the female reproductive system in the Agaonidae (Chalcidoidea, Hymenoptera). *Journal of Entomology Series A, General Entomology* 48: 25–35. <https://doi.org/10.1111/j.1365-3032.1973.tb00029.x>
- Dweck HKM, Gadallah NS, Darwish E (2008) Structure and sensory equipment of the ovipositor of *Habrobracon hebetor* (Say) (Hymenoptera: Braconidae). *Micron* 39: 1255–1261. <https://doi.org/10.1016/j.micron.2008.03.012>
- Eggs B, Birkhold AI, Röhrle O, Betz O (2018) Structure and function of the musculoskeletal ovipositor system of an ichneumonid wasp. *BMC Zoology* 3: 12. <https://doi.org/10.1186/s40850-018-0037-2>
- Ernst AF, Mikó I, Deans AR (2013) Morphology and function of the ovipositor mechanism in Ceraphronoidea (Hymenoptera, Apocrita). *Journal of Hymenoptera Research* 33: 25–61. <https://doi.org/10.3897/jhr.33.5204>
- Fergusson NDM (1988) A comparative study of the structures of phylogenetic importance of female genitalia of the Cynipoidea (Hymenoptera). *Systematic Entomology* 13: 13–30. <https://doi.org/10.1111/j.1365-3113.1988.tb00225.x>
- Field SA, Austin AD (1994) Anatomy and mechanics of the telescopic ovipositor system of *Scelio latreille* (Hymenoptera: Scelionidae) and related genera. *International Journal of Insect Morphology and Embryology* 23: 135–158. [https://doi.org/10.1016/0020-7322\(94\)90007-8](https://doi.org/10.1016/0020-7322(94)90007-8)
- Frühauf E (1924) Legeapparat und Eiablage bei Gallwespen (Cynipidae). *Zeitschrift für Wissenschaftliche Zoologie* 121: 656–723.
- Gauld I, Bolton B (Eds) (1988) *The Hymenoptera*. Oxford University Press, Oxford, 332 pp.
- Graf S, Willsch M, Ohl M (2021) Comparative morphology of the musculature of the sting apparatus in *Ampulex compressa* (Hymenoptera, Ampulicidae) and *Sceliphron destillatorium* (Hymenoptera, Sphecidae). *Deutsche Entomologische Zeitschrift* 68: 21–32. <https://doi.org/10.3897/dez.68.58217>

- Hanna AD (1934) The male and female genitalia and the biology of *Euchalcidia aryobori* Hanna (Hymenoptera, Chalcidinae). Transactions of the Royal Entomological Society of London 82: 107–136. <https://doi.org/10.1111/j.1365-2311.1934.tb00030.x>
- Heraty J (2009) Parasitoid biodiversity and insect pest management. In: Foottit RG, Adler PH (Eds) Insect Biodiversity: Science and Society. Wiley-Blackwell, Oxford, 445–462. <https://doi.org/10.1002/9781444308211.ch19>
- Hymenoptera Anatomy Consortium (2021) Hymenoptera Anatomy Ontology. [Accessed 12 January 2021]
- Jones OR, Purvis A, Baumgart E, Quicke DLJ (2009) Using taxonomic revision data to estimate the geographic and taxonomic distribution of undescribed species richness in the Braconidae (Hymenoptera: Ichneumonoidea). Insect Conservation and Diversity 2: 204–212. <https://doi.org/10.1111/j.1752-4598.2009.00057.x>
- King PE (1962) The muscular structure of the ovipositor and its mode of function in *Nasonia vitripennis* (Walker) (Hymenoptera: Pteromalidae). Proceedings of the Royal Entomological Society of London. Series A, General Entomology 37: 121–128. <https://doi.org/10.1111/j.1365-3032.1962.tb00002.x>
- King PE, Copland MJW (1969) The structure of the female reproductive system in the Mymaridae (Chalcidoidea: Hymenoptera). Journal of Natural History 3: 349–365. <https://doi.org/10.1080/00222936900770311>
- Kumpanenko AS, Gladun DV (2018) Functional morphology of the sting apparatus of the spider wasp *Cryptocheilus versicolor* (Scopoli, 1763) (Hymenoptera: Pompilidae). Entomological Science 21: 124–132. <https://doi.org/10.1111/ens.12288>
- LeRalec A, Rabasse JM, Wajnberg E (1996) Comparative morphology of the ovipositor of some parasitic Hymenoptera in relation to characteristics of their hosts. Canadian Entomologist 128: 413–433. <https://doi.org/10.4039/Ent128413-3>
- Lösel PD, van de Kamp T, Jayme A, Ershov A, Faragó T, Pichler O, Tan Jerome N, Aadepu N, Bremer S, Chilingaryan SA, Heethoff M, Kopmann A, Odar J, Schmelzle S, Zuber M, Wittbrodt J, Baumbach T, Heuveline V (2020) Introducing Biomedisa as an open-source online platform for biomedical image segmentation. Nature Communications 11: 5577. <https://doi.org/10.1038/s41467-020-19303-w>
- Matushkina NA (2011) Sting microsculpture in the digger wasp *Bembix rostrata* (Hymenoptera, Crabronidae). Journal of Hymenoptera Research 21: 41–52. <https://doi.org/10.3897/jhr.21.873>
- Matushkina NA, Stetsun HA (2016) Morphology of the sting apparatus of the digger wasp *Oxybelus uniglumis* (Linnaeus, 1758) (Hymenoptera, Crabronidae), with emphasis on intraspecific variability and behavioural plasticity. Insect Systematics & Evolution 47: 347–362. <https://doi.org/10.1163/1876312X-47032146>
- Mbata GN, Shapiro-Ilan DI (2010) Compatibility of *Heterorhabditis indica* (Rhabditida: Heterorhabditidae) and *Habrobracon hebetor* (Hymenoptera: Braconidae) for biological control of *Plodia interpunctella* (Lepidoptera: Pyralidae). Biological Control 54: 75–82. <https://doi.org/10.1016/j.biocontrol.2010.04.009>
- Oeser R (1961) Vergleichend-morphologische Untersuchungen über den Ovipositor der Hymenopteren. Mitteilungen aus dem Zoologischen Museum in Berlin 37: 3–119. <https://doi.org/10.1002/mmzn.19610370102>

- Pampel W (1914) Die weiblichen Geschlechtsorgane der Ichneumoniden. Zeitschrift für wissenschaftliche Zoologie 108: 290–357.
- Paust A, Reichmuth C, Büttner C, Prozell S, Adler CS, Schöller M (2006) Spatial effects on competition between the larval parasitoids *Habrobracon hebetor* (Say) (Hymenoptera: Braconidae) and *Venturia canescens* (Gravenhorst) (Hymenoptera: Ichneumonidae) parasitising the Mediterranean flour moth, *Ephestia kuehniella* Zeller. Proceedings of the 9th International Working Conference on Stored Product Protection, PS7-17-6189: 797–803.
- Peters RS, Krogmann L, Mayer C, Donath A, Gunkel S, Meusemann K, Kozlov A, Podsiadlowski L, Petersen M, Lanfear R, Diez PA, Heraty J, Kjer KM, Klopstein S, Meier R, Polidori C, Schmitt T, Liu S, Zhou X, Wappler T, Rust J, Misof B, Niehuis O (2017) Evolutionary history of the Hymenoptera. Current Biology 27: 1013–1018. <https://doi.org/10.1016/j.cub.2017.01.027>
- Prozell S, Schöller M, Wyss U (2006) Die Mehlmotte *Ephestia kuehniella* und ihr natürlicher Feind, die Mehlmottenschlupfwespe *Habrobracon hebetor*. Entofilm (Kiel).
- Quicke DLJ (1991) Ovipositor mechanics of the braconine wasp genus *Zaglyptogastra* and the ichneumonid genus *Pristomerus*. Journal of Natural History 25: 971–977. <https://doi.org/10.1080/00222939100770631>
- Quicke DLJ (1997) Parasitic Wasps. Chapman & Hall Ltd, London, 470 pp.
- Quicke DLJ (2015) The Braconid and Ichneumonid Parasitoid Wasps: Biology, Systematics, Evolution and Ecology. Wiley-Blackwell, Chichester, 681 pp.
- Quicke DLJ, van Achterberg C (1990) Phylogeny of the subfamilies of the family Braconidae (Hymenoptera: Ichneumonoidea). Zoologische Verhandlungen 258: 3–95.
- Quicke DLJ, Fitton MG, Ingram S (1992) Phylogenetic implications of the structure and distribution of ovipositor valvelli in the Hymenoptera (Insecta). Journal of Natural History 26: 587–608. <https://doi.org/10.1080/00222939200770361>
- Quicke DLJ, LeRalec A, Vilhelmsen L (1999) Ovipositor structure and function in the parasitic Hymenoptera with an exploration of new hypotheses. Rendiconti 47: 197–239.
- Quicke DLJ, Fitton MG, Tunstead JR, Ingram SN, Gaitens PV (1994) Ovipositor structure and relationships within the Hymenoptera, with special reference to the Ichneumonoidea. Journal of Natural History 28: 635–682. <https://doi.org/10.1080/00222939400770301>
- Rahman MH, Fitton MG, Quicke DLJ (1998) Ovipositor internal microsculpture and other features in doryctine wasps (Insecta, Hymenoptera, Braconidae). Zoologica Scripta 27: 333–343. <https://doi.org/10.1111/j.1463-6409.1998.tb00465.x>
- Rogers D (1972) The ichneumon wasp *Venturia canescens*: oviposition and avoidance of superparasitism. Entomologia Experimentalis et Applicata 15: 190–194. <https://doi.org/10.1111/j.1570-7458.1972.tb00195.x>
- Saalfeld S, Fetter R, Cardona A, Tomancak P (2012) Elastic volume reconstruction from series of ultra-thin microscopy sections. Nature Methods 9: 717–720. <https://doi.org/10.1038/nmeth.2072>
- Sanower W, Mbata GN, Payton ME (2018) Improvement of reproductive performance of *Habrobracon hebetor*: Consideration of diapausing and non-diapausing larvae of *Plodia interpunctella*. Biological Control 118: 32–36. <https://doi.org/10.1016/j.biocontrol.2017.12.003>
- Schindelin J, Arganda-Carreras I, Frise E, Kaynig V, Longair M, Pietzsch T, Preibisch S, Rueden C, Saalfeld S, Schmid B, Tinevez J-Y, White DJ, Hartenstein V, Eliceiri K, Tomancak

- P, Cardona A (2012) Fiji: an open-source platform for biological-image analysis. *Nature Methods* 9: 676–682. <https://doi.org/10.1038/nmeth.2019>
- Shah ZA, Blackwell A, Hubbard SF (2012) Ultramorphology of the ovipositor of *Venturia canescens* (Gravenhorst) and possible mechanisms for oviposition. *International Journal of Agriculture and Biology* 14: 908–914.
- Shaw MR (2017) Further notes on the biology of *Pseudavga flavicoxa* Tobias, 1964 (Hymenoptera, Braconidae, Rhysipolinae). *Journal of Hymenoptera Research* 54: 113–128. <https://doi.org/10.3897/jhr.54.10789>
- Smith EL (1970) Evolutionary morphology of the external insect genitalia. 2. Hymenoptera. *Annals of The Entomological Society of America* 63: 1–27. <https://doi.org/10.1093/aesa/63.1.1>
- Smith EL (1972) Biosystematics and morphology of Symphyta—III External genitalia of *Euura* (Hymenoptera: Tenthredinidae): sclerites, sensilla, musculature, development and oviposition behavior. *International Journal of Insect Morphology and Embryology* 1: 321–365. [https://doi.org/10.1016/0020-7322\(72\)90016-5](https://doi.org/10.1016/0020-7322(72)90016-5)
- Snodgrass RE (1933) Morphology of the insect abdomen. Part II. The genital ducts and the ovipositor. *Smithsonian Miscellaneous Collections* 89: 1–148.
- Stetsun H, Matushkina NA (2020) Sting morphology of the European hornet, *Vespa crabro* L., (Hymenoptera: Vespidae) re-examined. *Entomological Science* 23: 416–429. <https://doi.org/10.1111/ens.12438>
- Stetsun H, Rajabi H, Matushkina N, Gorb SN (2019) Functional morphology of the sting in two digger wasps (Hymenoptera: Crabronidae) with different types of prey transport. *Arthropod Structure & Development* 52: 100882. <https://doi.org/10.1016/j.asd.2019.100882>
- van Meer NMME, Cerkvénik U, Schlepütz CM, van Leeuwen JL, Gussekloo SWS (2020) The ovipositor actuation mechanism of a parasitic wasp and its functional implications. *Journal of Anatomy* 237: 689–703. <https://doi.org/10.1111/joa.13216>
- Venkatraman TV, Subba Rao BR (1954) The mechanisms of oviposition in *Stenobracon deesae* (Cam.) (Hymenoptera: Braconidae). *Proceedings of the Royal Society of London. Series A, General Entomology* 29: 1–8. <https://doi.org/10.1111/j.1365-3032.1954.tb01178.x>
- Vilhelmsen L (2000) The ovipositor apparatus of basal Hymenoptera (Insecta): phylogenetic implications and functional morphology. *Zoologica Scripta* 29: 319–345. <https://doi.org/10.1046/j.1463-6409.2000.00046.x>
- Vilhelmsen L (2003) Flexible ovipositor sheaths in parasitoid Hymenoptera (Insecta). *Arthropod Structure & Development* 32: 277–287. [https://doi.org/10.1016/S1467-8039\(03\)00045-8](https://doi.org/10.1016/S1467-8039(03)00045-8)
- Vilhelmsen L, Isidore N, Romani R, Basibuyuk HH, Quicke DLJ (2001) Host location and oviposition in a basal group of parasitic wasps: the subgenual organ, ovipositor apparatus and associated structures in the Orussidae (Hymenoptera, Insecta). *Zoomorphology* 121: 63–84. <https://doi.org/10.1007/s004350100046>
- Wührer B, Zimmermann O, Wyss U (2009) Lebensweise und Entwicklung des Parasitoiden *Bracon brevicornis*. *Entofim* (Kiel).
- Yoder MJ, Miko I, Seltmann KC, Bertone MA, Deans AR (2010) A gross anatomy ontology for Hymenoptera. *PloS ONE* 5: e159991. <https://doi.org/10.1371/journal.pone.0015991>

Appendix I

Table AI. Morphological terms relevant to the hymenopteran ovipositor system. The terms (abbreviations used in this article in brackets) are used and defined according to the Hymenoptera Anatomy Ontology Portal (HAO) (Yoder et al. 2010; Hymenoptera Anatomy Consortium 2021) and the according Uniform Resource Identifiers (URI) are listed.

Anatomical term (abbreviation)	definition / concept	URI
1 st valvifer (1vf)	The area of the 1 st valvifer-1 st valvulae complex that is proximal to the aulax, bears the 9 th tergal condyle of the 1 st valvifer and the 2 nd valviferal condyle of the 1 st valvifer and is connected to the genital membrane by muscle.	http://purl.obolibrary.org/obo/HAO_0000338
1 st valvifer-genital membrane muscle	The ovipositor muscle that arises from the posterior part of the 1 st valvifer and inserts anteriorly on the genital membrane anterior to the T9-genital membrane muscle.	http://purl.obolibrary.org/obo/HAO_0001746
1 st valvula, 1 st valvulae (1vv)	The area of the 1 st valvifer-1 st valvulae complex that is delimited by the proximal margin of the aulax.	http://purl.obolibrary.org/obo/HAO_0000339
2 nd valvifer (2vf)	The area of the 2 nd valvifer-2 nd valvulae-3 rd valvulae complex that is proximal to the basal articulation and to the processus musculares and articulates with the female T9.	http://purl.obolibrary.org/obo/HAO_0000927
2 nd valvula (2vv)	The area of the 2 nd valvifer-2 nd valvulae-3 rd valvulae complex that is distal to the basal articulation and to the processus musculares and is limited medially by the median body axis.	http://purl.obolibrary.org/obo/HAO_0000928
3 rd valvula, 3 rd valvulae (3vv)	The area of the 2 nd valvifer-3 rd valvulae complex that is posterior to the distal vertical conjunctiva of the 2 nd valvifer-3 rd valvulae complex.	http://purl.obolibrary.org/obo/HAO_0001012
anterior 2 nd valvifer-2 nd valvula muscle	The ovipositor muscle that arises from the anterodorsal part of the 2 nd valvifer and inserts subapically on the processus articularis.	http://purl.obolibrary.org/obo/HAO_0001166
anterior ridge of T9 (ar9)	The ridge that extends along the anterior margin of female T9 and receives the site of origin of the ventral and the dorsal T9-2 nd valvifer muscles.	http://purl.obolibrary.org/obo/HAO_0002182
anterior section of dorsal flange of 2 nd valvifer	The area of the dorsal flange of the 2 nd valvifer that is anterior to the site of origin of the basal line.	http://purl.obolibrary.org/obo/HAO_0002173
apodeme	The process that is internal.	http://purl.obolibrary.org/obo/HAO_0000142
aulax (au)	The impression that is on the 1 st valvifer-1 st valvula complex accommodates the rhachis.	http://purl.obolibrary.org/obo/HAO_0000152
basal articulation (ba)	The articulation that is part of the 2 nd valvifer-2 nd valvula-3 rd valvula complex and adjacent to the rhachis.	http://purl.obolibrary.org/obo/HAO_0001177
basal line of the 2 nd valvifer	The line on the 2 nd valvifer that extends between the pars articularis and the dorsal flange of 2 nd valvifer.	http://purl.obolibrary.org/obo/HAO_0002171
bulb (blb)	The anterior area of the dorsal valve [composite structure of the fused 2 nd valvulae] that is bulbous.	http://purl.obolibrary.org/obo/HAO_0002177
conjunctiva	The area of the cuticle that is more flexible than adjacent sclerites.	http://purl.obolibrary.org/obo/HAO_0000221
distal notch of the dorsal valve (no)	The notch that is distal on the dorsal valve [composite structure of the fused 2 nd valvulae].	http://purl.obolibrary.org/obo/HAO_0002179
dorsal flange of the 2 nd valvifer (df2)	The flange that extends on the dorsal margin of the 2 nd valvifer. Part of the ventral T9-2 nd valvifer muscle attaches to the flange.	http://purl.obolibrary.org/obo/HAO_0001577
dorsal projection of the 2 nd valvifer (dp2)	The projection that is located on the 2 nd valvifer and corresponds to the proximal end of the rhachis.	http://purl.obolibrary.org/obo/HAO_0002172
dorsal ramus of the 1 st valvula (dr1)	The region that extends along the dorsal margin of the 1 st valvula and bears the aulax.	http://purl.obolibrary.org/obo/HAO_0001579
dorsal T9-2 nd valvifer muscle	The ovipositor muscle that arises along the posterodorsal part of the anterior margin of female T9 and inserts on the anterior section of the dorsal flanges of the 2 nd valvifer.	http://purl.obolibrary.org/obo/HAO_0001569
egg canal (ec)	The anatomical space that is between the left and right olistheters.	http://purl.obolibrary.org/obo/HAO_0002191
female T9 (T9)	The tergite that is articulated with the 1 st valvifer and is connected to the 2 nd valvifer via muscles.	http://purl.obolibrary.org/obo/HAO_0000075
flange	The projection that is lamella-like and is located on a rim, carina, apodeme or edge.	http://purl.obolibrary.org/obo/HAO_0000344
genital membrane (gm)	The conjunctiva that connects the ventral margins of the 2 nd valvifers arching above the 2 nd valvula.	http://purl.obolibrary.org/obo/HAO_0001757

Anatomical term (abbreviation)	definition / concept	URI
interarticular ridge of the 1 st valvifer (iar)	The ridge that extends along the posterior margin of the 1 st valvifer between the intervalvifer and tergo-valvifer articulations.	http://purl.obolibrary.org/obo/HAO_0001562
intervalvifer articulation (iva)	The articulation between the 1 st valvifer and 2 nd valvifer.	http://purl.obolibrary.org/obo/HAO_0001558
median bridge of the 2 nd valvifers (mb2)	The area that connects posterodorsally the 2 nd valvifers and is the site of attachment for the posterior T9-2 nd valvifer muscle.	http://purl.obolibrary.org/obo/HAO_0001780
notal membrane	The conjunctiva that connects the medial margins of the 2 nd valvulae.	http://purl.obolibrary.org/obo/HAO_0001733
notch	The part of the margin of a sclerite that is concave.	http://purl.obolibrary.org/obo/HAO_0000648
olistheter (oth)	The anatomical cluster that is composed of the rhachis of the 2 nd valvula and the aulax of the 1 st valvula.	http://purl.obolibrary.org/obo/HAO_0001103
ovipositor	The anatomical cluster that is composed of the 1 st valvulae, 2 nd valvulae, 3 rd valvulae, 1 st valvifers, 2 nd valvifers and female T9.	http://purl.obolibrary.org/obo/HAO_0000679
ovipositor apparatus	The anatomical cluster that is composed of the ovipositor, abdominal terga 8-10, abdominal sternum 7 and muscles connecting them.	http://purl.obolibrary.org/obo/HAO_0001600
ovipositor muscle	The abdominal muscle that inserts on the ovipositor.	http://purl.obolibrary.org/obo/HAO_0001290
pars articularis / pars articulares	The articular surface that is situated anteriorly on the ventral margin of the 2 nd valvifer and forms the lateral part of the basal articulation.	http://purl.obolibrary.org/obo/HAO_0001606
posterior 2 nd valvifer-2 nd valvula muscle	The ovipositor muscle that arises posteroventrally from the 2 nd valvifer and inserts on the processus musculares of the 2 nd valvula.	http://purl.obolibrary.org/obo/HAO_0001815
processus articularis / processus articulares	The process that extends laterally from the proximal part of the 2 nd valvula and forms the median part of the basal articulation, and corresponds to the site of attachment for the anterior 2 nd valvifer-2 nd valvula muscle. The processus articularis is part of the sclerite.	http://purl.obolibrary.org/obo/HAO_0001704
processus musculares / processus muscularis	The apodeme that extends dorsally from the proximal part of the 2 nd valvula to the genital membrane and receives the site of attachment of the posterior 2 nd valvifer-2 nd valvula muscle.	http://purl.obolibrary.org/obo/HAO_0001703
rhachis (rh)	The ridge that extends along the ventral surface of the 2 nd valvula that is partially enclosed by the aulax.	http://purl.obolibrary.org/obo/HAO_0000898
ridge	The apodeme that is elongate.	http://purl.obolibrary.org/obo/HAO_0000899
sawtooth (st)	The process that is located along the ventral margin of the 1 st valvula of the dorsal margin of the 2 nd valvula.	http://purl.obolibrary.org/obo/HAO_0001681
sclerite	The area of the cuticle that is less flexible than adjacent conjunctivae.	http://purl.obolibrary.org/obo/HAO_0000909
sensillar patch of the 2 nd valvifer (sp)	The patch that is composed of placoid sensilla adjacent to the intervalvifer articulation.	http://purl.obolibrary.org/obo/HAO_0001671
sensillum	A sense organ embedded in the integument and consisting of one or a cluster of sensory neurons and associated sensory structures, support cells and glial cells forming a single organized unit with a largely bona fide boundary.	http://purl.obolibrary.org/obo/HAO_0000933
terebra (trb)	The anatomical cluster that is composed of the 1 st and 2 nd valvulae.	http://purl.obolibrary.org/obo/HAO_0001004
tergite	The sclerite that is located on the tergum.	http://purl.obolibrary.org/obo/HAO_0001005
tergo-valvifer articulation (tva)	The articulation that is located between the female T9 and the 1 st valvifer and is composed of the 9 th tergal condyle of the 1 st valvifer and the 1 st valvifer fossa of the 9 th tergite.	http://purl.obolibrary.org/obo/HAO_0001636
valvillus (vlv)	The sclerite that articulates on the 1 st valvula and projects into the egg/poison canal.	http://purl.obolibrary.org/obo/HAO_0001619
venom gland reservoir of the 2 nd valvifer (vd)	The gland reservoir that is between the 2 nd valvifers.	http://purl.obolibrary.org/obo/HAO_0002176
ventral ramus of the 2 nd valvula	The area of the 2 nd valvifer-2 nd valvula-3 rd valvula complex that bears the rhachis.	http://purl.obolibrary.org/obo/HAO_0001107
ventral T9-2 nd valvifer muscle	The ovipositor muscle that arises from the lateral region of female T9 and inserts along the posterior part of the dorsal flange of the 2 nd valvifer.	http://purl.obolibrary.org/obo/HAO_0001616

Supplementary material 1

Video S1

Authors: Michael Csader, Karin Mayer, Oliver Betz, Stefan Fischer, Benjamin Eggs

Data type: Video file (mp4)

Explanation note: Animation of the rotated segmented 3D reconstruction of the terebra of *Habrobracon hebetor*.

Copyright notice: This dataset is made available under the Open Database License (<http://opendatacommons.org/licenses/odbl/1.0/>). The Open Database License (ODbL) is a license agreement intended to allow users to freely share, modify, and use this Dataset while maintaining this same freedom for others, provided that the original source and author(s) are credited.

Link: <https://doi.org/10.3897/jhr.83.64018.suppl1>

Supplementary material 2

Video S2

Authors: Michael Csader, Karin Mayer, Oliver Betz, Stefan Fischer, Benjamin Eggs

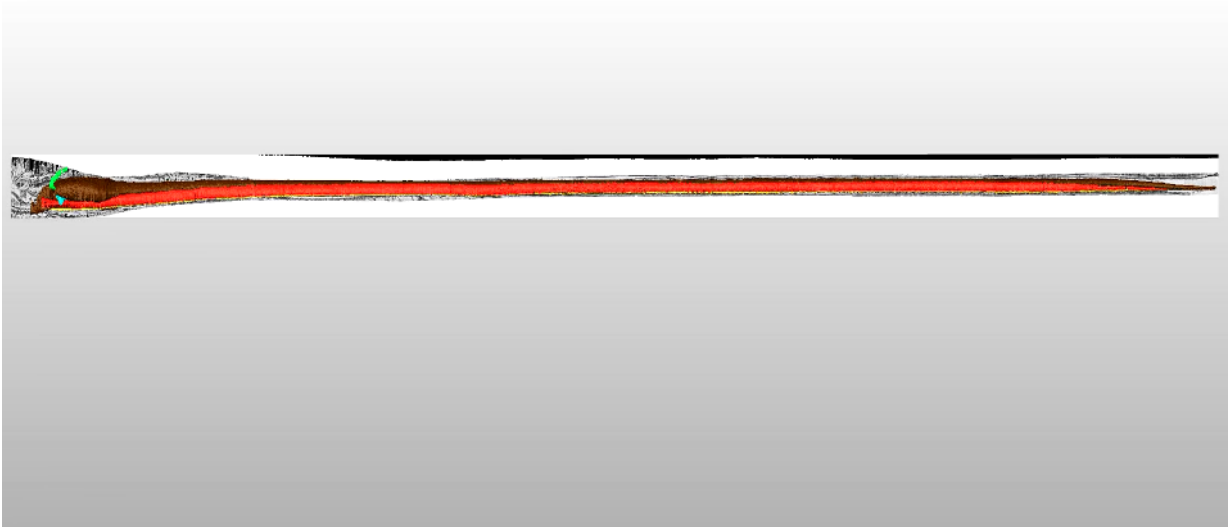
Data type: Video file (mp4)

Explanation note: Animation of the rotated segmented 3D reconstruction of the proximal region of the terebra of *Habrobracon hebetor* (cf. Fig. 3), highlighting the 1st and 2nd valvulae, the ligaments, and the duct of the venom gland.

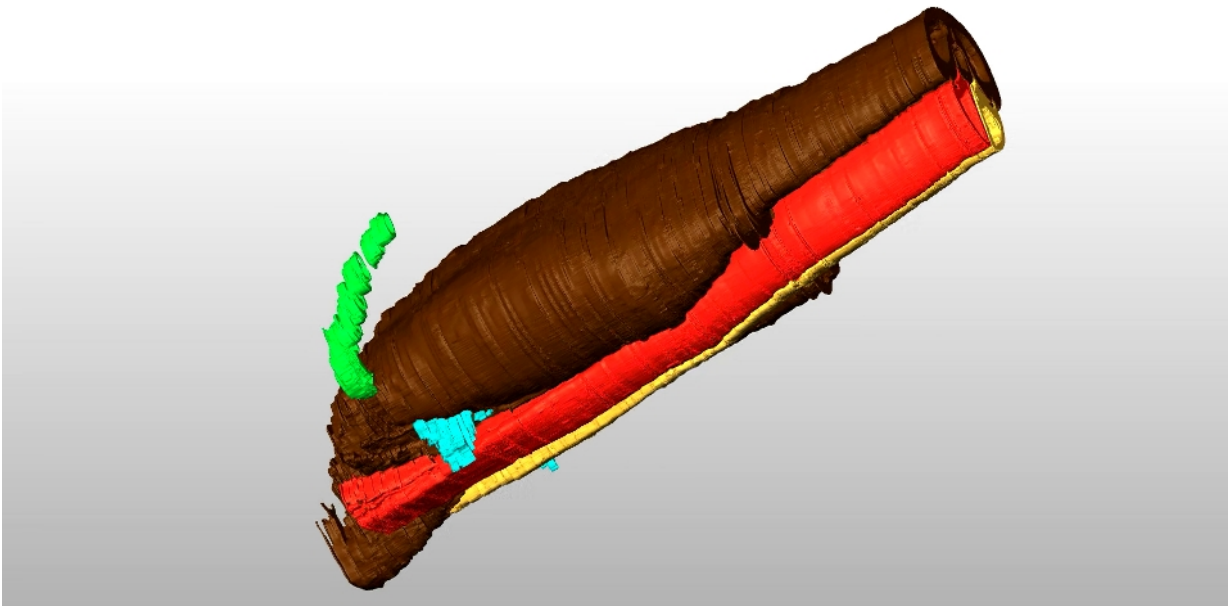
Copyright notice: This dataset is made available under the Open Database License (<http://opendatacommons.org/licenses/odbl/1.0/>). The Open Database License (ODbL) is a license agreement intended to allow users to freely share, modify, and use this Dataset while maintaining this same freedom for others, provided that the original source and author(s) are credited.

Link: <https://doi.org/10.3897/jhr.83.64018.suppl2>

Additional files (supplementary material): video files (snapshots displayed here); files available online at <https://jhr.pensoft.net/article/64018/>



Supplementary material 1 – Video S1: Animation of the rotated segmented 3d reconstruction of the terebra of *Habrobracon hebetor*. (mp4)



Supplementary material 2 – Video S2: Animation of the rotated segmented 3D reconstruction of the proximal region of the terebra of *Habrobracon hebetor* (cf. Fig. 3), highlighting the 1st and 2nd valvulae, the ligaments, and the duct of the venom gland. (mp4)

Publication 4

van de Kamp T., Mikó I., Staniczek A. H., **Eggs B.**, Bajerlein D., Faragó T., Hagelstein L., Hamann E., Spiecker R., Baumbach T., Janšta P. and Krogmann L. (2022). Evolution of flexible biting in hyperdiverse parasitoid wasps. *Proceedings of the Royal Society B: Biological Sciences* 298 (1967): 20212086. doi: 10.1098/rspb.2021.2086

(peer-reviewed journal article)



Abstract

One key event in insect evolution was the development of mandibles with two joints, which allowed powerful biting but restricted their movement to a single degree of freedom. These mandibles define the Dicondylia, which constitute over 99% of all extant insect species. It was common doctrine that the dicondylic articulation of chewing mandibles remained unaltered for more than 400 million years. We report highly modified mandibles overcoming the restrictions of a single degree of freedom and hypothesize their major role in insect diversification. These mandibles are defining features of parasitoid chalcid wasps, one of the most species-rich lineages of insects. The shift from powerful chewing to precise cutting likely facilitated adaptations to parasitize hosts hidden in hard substrates, which pose challenges to the emerging wasps. We reveal a crucial step in insect evolution and highlight the importance of comprehensive studies even of putatively well-known systems.

Significance within the present thesis: The Chalcidoidea is an extremely diverse and ecologically important group of extraordinarily diverse wasps (nearly 27,00 species described, over 500,000 species estimated) (Heraty 2017, Peters *et al.* 2018). The majority of chalcidoids are idiobiont ectoparasitoids of hosts that live in concealed cavities (in plant tissues, such as grains, or in puparia, egg shells *etc.*). However, the use of hosts living concealed within hard substrates poses challenges not only for the female wasp attempting to parasitize them (*cf.* Publication 5), but also for the emerging wasp when leaving the substrate. In this study, we present a secondary reversal to monocondylic mandibles in chalcidoid wasps, highlighting an evolutionary novelty and presumably a strong driver of diversification in this group.

Methods used: synchrotron X-ray microtomography (SR- μ CT), high-resolution videography

Own contribution: performing high resolution videography; discussing and revising the manuscript

Miscellaneous: This study appeared on the cover of the vol. 298 of *Proceedings of the Royal Society B: Biological Sciences* (see image in the top right corner).

Research



Cite this article: van de Kamp T *et al.* 2022 Evolution of flexible biting in hyperdiverse parasitoid wasps. *Proc. R. Soc. B* **289**: 20212086.
<https://doi.org/10.1098/rspb.2021.2086>

Received: 21 September 2021

Accepted: 8 December 2021

Subject Category:

Evolution

Subject Areas:

evolution, ecology

Keywords:

mandibles, functional morphology, insect diversification

Authors for correspondence:

Thomas van de Kamp

e-mail: thomas.vandekamp@kit.edu

Lars Krogmann

e-mail: lars.krogmann@smns-bw.de

Electronic supplementary material is available online at <https://doi.org/10.6084/m9.figshare.c.5762457>.

Evolution of flexible biting in hyperdiverse parasitoid wasps

Thomas van de Kamp^{1,2}, István Mikó³, Arnold H. Staniczek⁴, Benjamin Eggs⁵, Daria Bajerlein⁶, Tomáš Faragó¹, Lea Hagelstein¹, Elias Hamann¹, Rebecca Spiecker², Tilo Baumbach^{1,2}, Petr Janšta^{4,7} and Lars Krogmann^{4,8}

¹Institute for Photon Science and Synchrotron Radiation (IPS), Karlsruhe Institute of Technology (KIT), 76344 Eggenstein-Leopoldshafen, Germany

²Laboratory for Applications of Synchrotron Radiation (LAS), Karlsruhe Institute of Technology (KIT), 76131 Karlsruhe, Germany

³Department of Biological Sciences, University of New Hampshire, Durham, NH 03824, USA

⁴Department of Entomology, State Museum of Natural History Stuttgart, 70191 Stuttgart, Germany

⁵Evolutionary Biology of Invertebrates, Institute of Evolution and Ecology, University of Tübingen, 72076 Tübingen, Germany

⁶Department of Animal Taxonomy and Ecology, Adam Mickiewicz University in Poznań, 61-614 Poznań, Poland

⁷Department of Zoology, Faculty of Science, Charles University, 128 43 Prague 2, Czech Republic

⁸Institute of Biology, Systematic Entomology (190n), University of Hohenheim, 70593 Stuttgart, Germany

TvdK, 0000-0001-7390-1318; BE, 0000-0001-7618-4326; EH, 0000-0002-0623-9069; LK, 0000-0002-3724-1735

One key event in insect evolution was the development of mandibles with two joints, which allowed powerful biting but restricted their movement to a single degree of freedom. These mandibles define the Dicondylia, which constitute over 99% of all extant insect species. It was common doctrine that the dicondylic articulation of chewing mandibles remained unaltered for more than 400 million years. We report highly modified mandibles overcoming the restrictions of a single degree of freedom and hypothesize their major role in insect diversification. These mandibles are defining features of parasitoid chalcid wasps, one of the most species-rich lineages of insects. The shift from powerful chewing to precise cutting likely facilitated adaptations to parasitize hosts hidden in hard substrates, which pose challenges to the emerging wasps. We reveal a crucial step in insect evolution and highlight the importance of comprehensive studies even of putatively well-known systems.

1. Introduction

In terms of species numbers and morphological and ecological diversity, insects are by far the most diverse lineage of terrestrial organisms [1–3]. During more than 400 million years, insect mouthparts have evolved considerable modifications allowing the ecological diversification of biting/chewing, sucking or filtering lineages and contributing to the tremendous species richness of the group [4,5]. The mandibles of the earliest hexapod lineages (Collembola, Diplura and Protura) are characterized by a single posterior articulation allowing flexible movement along a ball-and-socket joint [6]. A major evolutionary step was the development of dicondylic mandibles with an additional anterior articulation to the head capsule [7], leading to the Dicondylia, which traditionally comprise all insects except the bristletails (Archaeognatha) [8]. Within Dicondylia, secondary monocondyly is known from insects, whose mouthparts are transformed into stylets (e.g. Hemiptera) [9], but all groups with chewing mouthparts are considered dicondylic. Dicondylic mandibles are generally linked to an increased biting force [10–12], which allowed insects to exploit new food sources [13]. A major consequence of this transformation was the loss of rotating

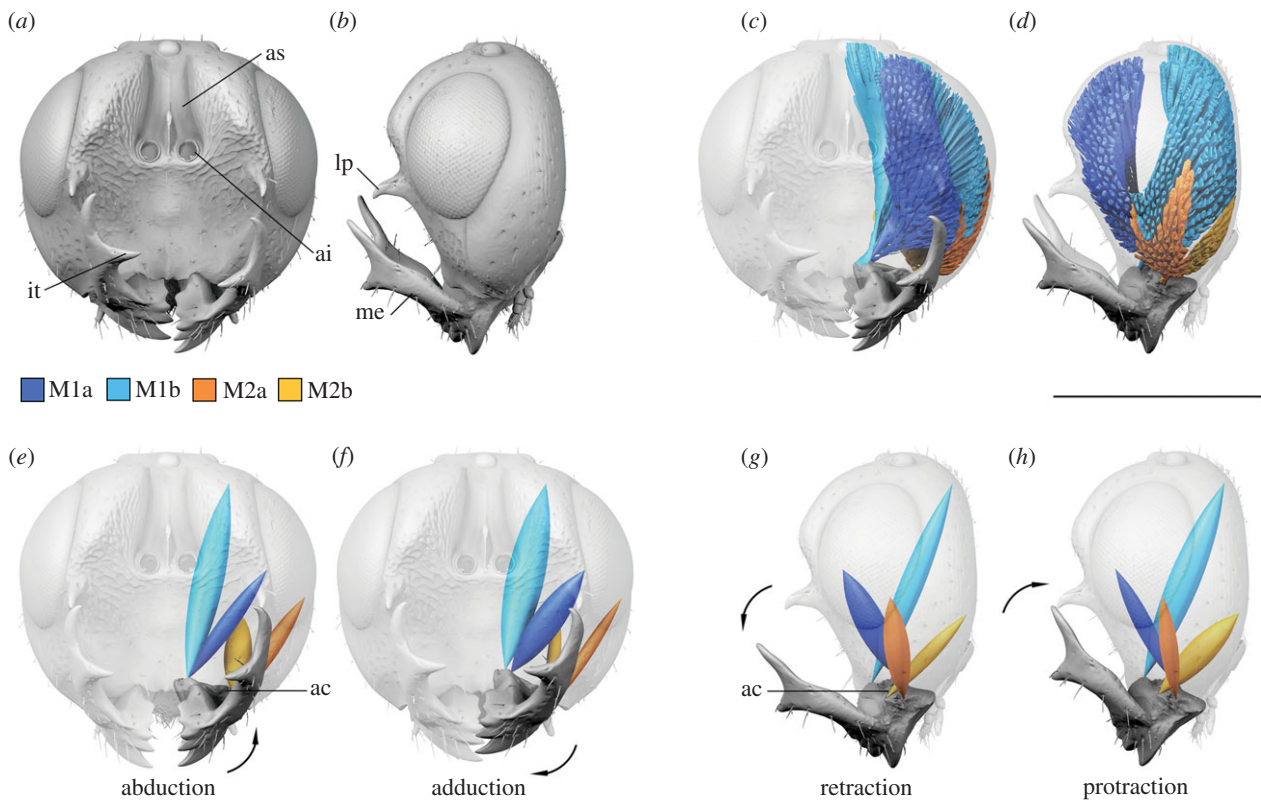


Figure 1. Head morphology and mandibular movement of *Colotrechninae* sp. (a) Head, frontal aspect. (b) Head, lateral aspect. (c,d) Original arrangement of the four mandibular muscles, M1a, M1b, M2a and M2b. (e,f) Putative biting movement. (g,h) Putative grasping movement. ac, anterior condyle; ai, antennal insertion; as, antennal scrobe; it, inner tooth; lp, lateral process; me, mandibular extension. Scale bar, 0.5 mm. (Online version in colour.)

motion of the mandibles and their confinement to movement in a single plane [12,14]. As a fixed axis of rotation requires fewer muscles to control mandibular movements, the complexity of mandibular musculature was gradually reduced from early hexapods to winged insects (Neoptera) [10]. In most derived Neoptera, mandibular movement is realized solely by two large antagonistic muscles, adductor and abductor. Both may be composed of several bundles of fibres [15,16] but insert at single attachment sites, often via sclerotized tendons.

The evolution of parasitoidism in Hymenoptera has led to one of the largest species radiations within insects [17–19]. Several morphological adaptations have been identified that triggered diversification processes during parasitoid evolution (e.g. wasp waist, venomous stinger) [20]. The role of mouthparts has mainly been studied in the context of feeding, but its role in emergence from host, mating behaviour, host handling and nest construction has also been discussed [21]. However, there were no hints that mouthpart evolution might have been a strong driver of parasitoid species radiations.

In an undescribed species of parasitoid wasps, we discovered peculiar antler-like extensions on top of otherwise ordinary-looking chewing mandibles (figure 1). These extensions correspond to forward-projecting processes on the face and potentially serve as a grasping tool. Both grasping and chewing obviously cannot be realized by dicondylic mandibular movement. We analysed the functional morphology of the mandibles of this extraordinary specimen by synchrotron X-ray microtomography and found evidence for flexible mandibular movement, contradicting the current hypothesis of largely conserved mandibular articulations and musculature in chewing insects. The undescribed species belongs to the superfamily Chalcidoidea, which comprises one of the largest

groups of insects with an estimated 500 000 predominantly parasitoid species [22]. Until now there was no convincing hypothesis which morphological features might have facilitated their unparalleled diversification [23,24].

To test whether flexible mandibular movement represents a singular evolutionary event or might play a larger role in parasitoid evolution, we analysed the occurrence of this type of mandible throughout Chalcidoidea and all major lineages of Hymenoptera and correlated the morphological characters with the most recent molecular phylogenies of Hymenoptera [25] and Chalcidoidea [24].

2. Results

(a) Mandibular morphology of *Colotrechninae* sp.

The face of *Colotrechninae* sp. is excavated and bears a pair of lateral facial processes next to the inner eye margins, which are each flanked by a single elongate seta. These processes are pointed ventrally and are slightly curved inwards. They are situated slightly below the level of the antennal insertions. The antennae are inserted high on the face within deep antennal scrobes. The mandibles possess five teeth each. Their outer surfaces feature conspicuous, distally pointed extensions, reaching distally to the lateral facial processes. Further, each mandibular extension carries a distinct inner tooth (figure 1a,b).

The mandible is loosely articulated to the head capsule by a single anterior condyle. A posterior condyle is completely absent. All mandibular muscles insert directly to the mandible and not via sclerotized tendons (figure 1c,d). Two separate pairs of muscle bundles are developed and connect the mandible to the cranium. One pair (M1) has its anterior bundle (M1a) originating from the frons and its posterior

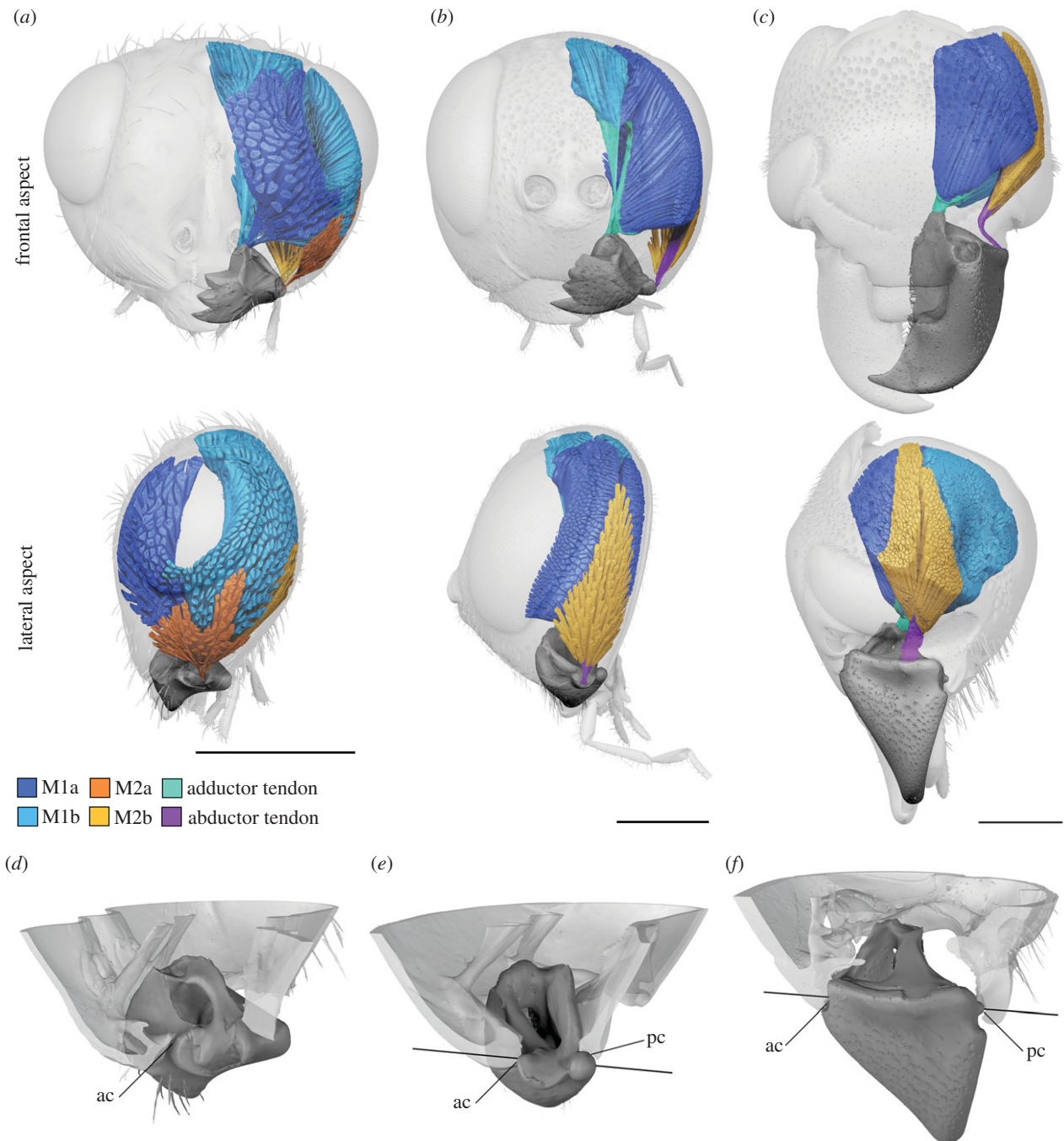


Figure 2. Comparison of mandibles and attached musculature in two wasps and a histerid beetle. (a) *Chremeurytoma* (Chalcidoidea). (b) *Zeuxevania* (Evanoidea). (c) *Margarinetus* (Coleoptera: Hydrophiloidea). (d–f) Mandibular articulations in the respective species, lateral view, cranium cut. (d) Monocondylic mandible with a single anterior articulation. (e,f) Dicondylic mandibles with anterior and posterior articulations that restrict mandibular movement to a fixed axis of rotation (indicated). ac, anterior condyle; pc, posterior condyle. Scale bars, 0.5 mm. (Online version in colour.)

bundle (M1b) from the gena. Both bundles insert at the inner angle of the mandibular base. The second pair (M2) has its anterior (M2a) and posterior bundles (M2b) originating at the ventral part of the gena and inserting to flanges of the outer margin of the mandibular base (figure 1c,d).

(b) Mandibular character distribution throughout Hymenoptera

Despite huge variation in overall mandibular shape, all other Chalcidoidea examined (figure 2a,d, 3 and 4) share the monocondylous condition found in *Colotrechninae* sp. Only in *Austrotoxeuma*, a posterior condyle is slightly indicated but not articulated to the head capsule. The

mandibular musculature of all other Chalcidoidea is also characterized by two muscles (M1 and M2) with two bundles each, which individually insert on the mandible. As in *Colotrechninae* sp., M1a originates always from the frons and M1b from the gena. In most Chalcidoidea, M2a and M2b originate from the ventral gena. A notable exception is the flattened head of *Ceratosolen* (Agaonidae), where M2a originates from the frons.

Regarding mandibular morphology, we also found a reduction of the posterior condyle in other Proctotrupomorpha, while it was distinct in all other groups (figures 2e and 5). In close relatives of Chalcidoidea (*Belytus* (Diapriidae) and *Exallonyx* (Proctotrupoidea)), the posterior condyle is completely reduced (no posterior articulation with the

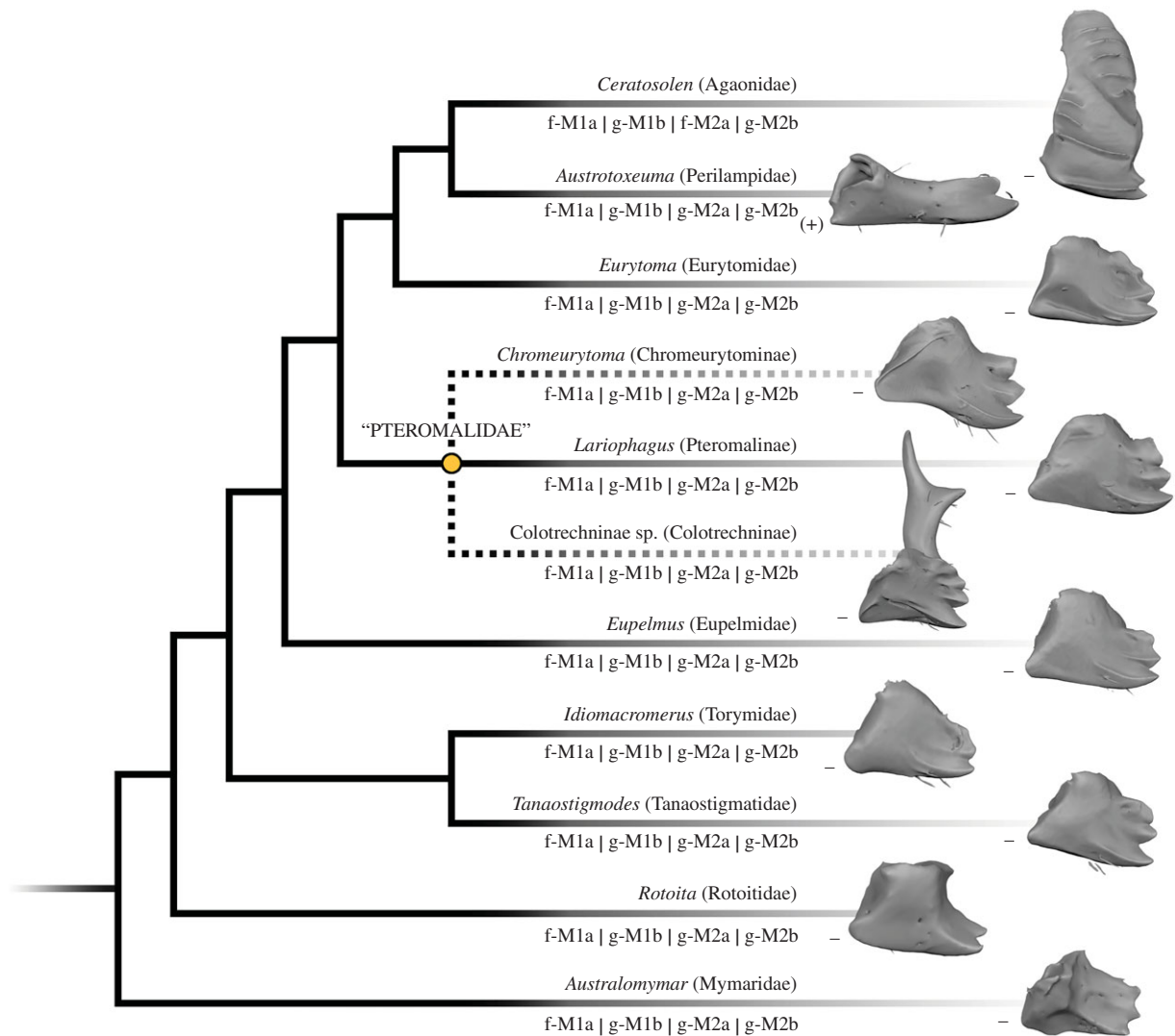


Figure 3. Characters of mandibles and mandibular musculature found in the examined taxa mapped on the molecular phylogeny of Chalcidoidea from Peters *et al.* [24]. The placement of *Rotoita* follows Heraty *et al.* [23]. Dotted lines indicate taxa of uncertain phylogenetic position. f-, originates from the frons; g-, originates from the gena; M1a, M1b, M2a, M2b, mandibular muscle bundles; (+), posterior condyle indicated; -, posterior condyle reduced.

head capsule), while it is indicated but without form closure around the condyle in the more distantly related lineages (*Telenomus* (Platygastridae) and *Andricus* (Cynipoidea)).

The mandibles in all hymenopteran lineages except Chalcidoidea have single insertion points for M1 and M2 (figures 2*b* and 6) and muscle bundles usually insert via sclerotized tendons (abductor tendon not recognizable only in *Belytus* (Diaprioidea) and *Exallonyx* (Proctotrupeoidea)). With the exception of *Netelia* (Ichneumonoidea), the tendons of M1 are split distally and attach to separate muscle bundles. Both muscles (M1 and M2) originate from the gena. This largely corresponds to the condition found in other mandibulate insects, such as beetles (figure 2*c,e*).

3. Discussion

(a) Functional interpretation

In Chalcidoidea, the mandible and its articulation as well as the associated musculature are highly modified compared to other pterygote insects, with fundamental functional consequences. The mandible is articulated to the head capsule by just a single anterior condyle, instead of two condyles as generally postulated for pterygote insects with biting mouthparts. This

abolishes a functional restriction of mandibular movement to a single plane. Instead, in combination with highly modified mandibular musculature, a flexible movement of mandibles can be achieved, including adduction, abduction, protraction, retraction, rotation and any combination of these movements. In Chalcidoidea, M1 is therefore not restricted in its function as an adductor and M2 not as abductor as in other pterygote insects. By contrast to all other groups examined, M1a originates from the frons (figures 1, 2*a* and 4), instead of the gena (figures 2*b,c* and 6). This allows the mandible to be pulled from an anterior direction, supporting mandibular movement along multiple planes. Moreover, each bundle of M1 and M2 inserts independently at the mandible, whereas in other biting insects, these bundles insert via a single sclerotized tendon [26] (figures 2*b,c* and 6). Based on the observations mentioned above we conclude that in the mandibular musculature of Chalcidoidea each muscle bundle acts as a functionally separate entity. Standard biting can still be achieved by the antagonizing bundles of M1 and M2. In this case, these pairs of muscle bundles would act as adductor (M1) and abductor (M2) (figure 1*e,f*). By contrast, flexible mandibular movement along multiple degrees of freedom is realized by the interplay of all four muscle bundles acting independently. For upward-directed movement of mandibles, the two posterior bundles

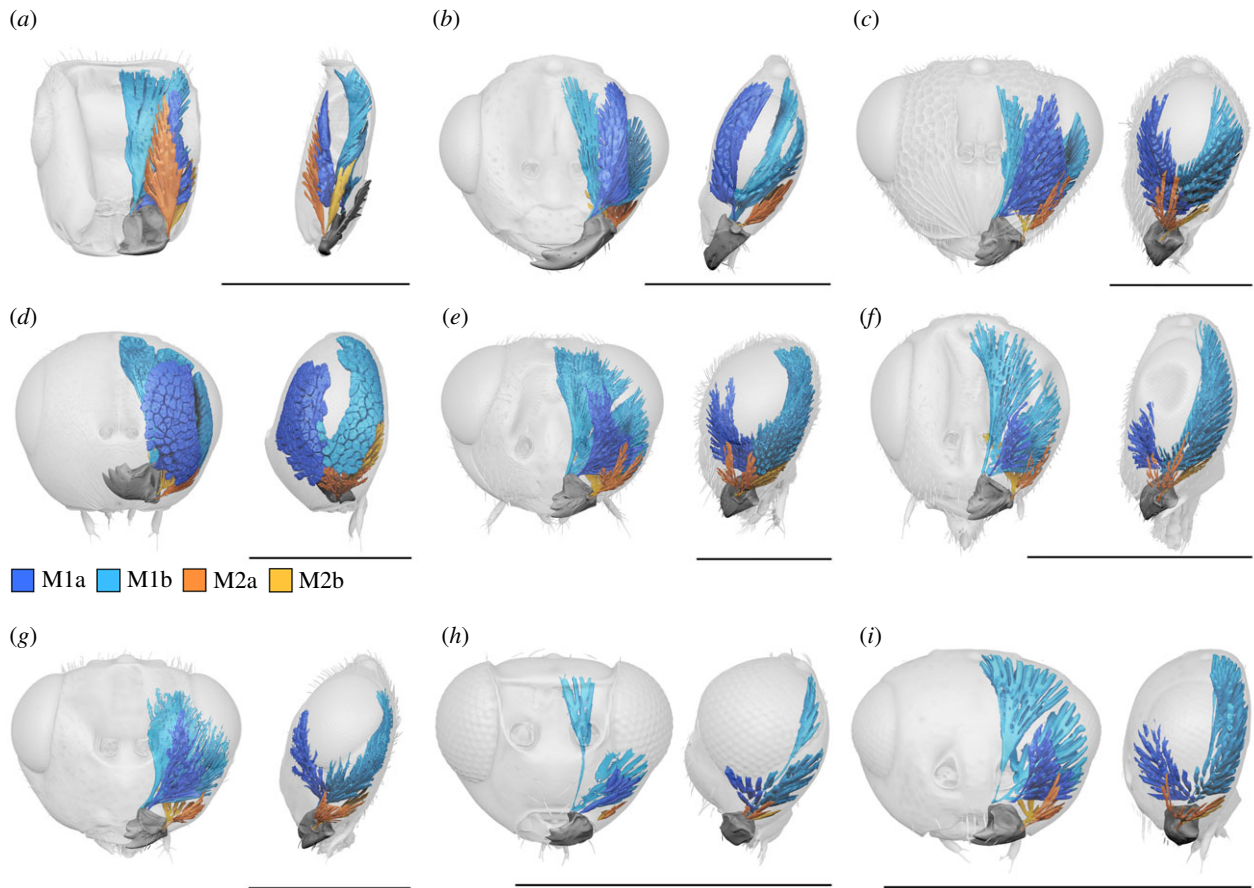


Figure 4. Mandibles and attached musculature throughout Chalcidoidea. (a) *Ceratosolen* (Agaonidae). (b) *Austrotoxeuma* (Perilampidae). (c) *Eurytoma* (Eurytomidae). (d) *Lariophagus* (Pteromalidae). (e) *Eupelmus* (Eupelmidae). (f) *Idiomacromerus* (Torymidae). (g) *Tanaostigmodes* (Tanaostigmatidae). (h) *Australomyrmar* (Myrmariidae). (i) *Rotoita* (Rotoitidae). Scale bars, 0.5 mm. (Online version in colour.)

M1b and M2b would act as protractors and their anterior counterparts M1a and M2a as retractors. In *Colotrechninae* sp., this movement allows for a closure between the tips of the mandibular antlers and the lateral facial processes (figure 1g,h; see electronic supplementary material, movie S1).

(b) Evolutionary considerations

Chalcidoidea are unique among parasitoids in targeting the largest diversity of host taxa and in exhibiting the largest number of feeding types defined for parasitoid wasps [27]. However, unlike other parasitoid wasp groups, such as Ichneumonoidea, Chalcidoidea do not often develop on free-living hosts, such as ectophytophagous larvae of butterflies, moths or beetles. A large majority of chalcid species develop on enclosed host stages with reduced mobility. Examples include wood and stem borers, leaf-miners or inhabitants of galls, seeds and fruits [27]. Interestingly, most of these host associations are displayed by ectoparasitoid chalcids, which enables the parasitoid larvae to develop within the protection of a concealed environment without being exposed to the host immune system, thereby combining advantages of endo- and ectoparasitoid lifestyles. A consequence of this strategy is the challenge of the freshly emerged wasp to escape from the concealed environment, which is usually achieved by time-consuming biting through the surrounding substrate. In this respect, the host biology of *Lariophagus distinguendus* (Förster, 1841) (Pteromalidae) is typical for the majority of chalcid wasp species. Flexible mandibular movements during its host eclosion are clearly visible (see electronic supplementary

material, movie S2): both mandibles can move independently at the same time. This allows precise cutting, as the mandibles can operate under different angles to the substrate and to each other. This flexible movement might be especially helpful in an environment with spatial constraints, where force has to be applied with minimal movements of the head itself. These constraints can either be caused by arthropod host eggs, as in the earliest chalcid lineage Myrmariidae, or by the substrate surrounding parasitoids emerging from their enclosed hosts, as in the majority of Chalcidoidea. Therefore, we assume that flexible mandibular movement played an important role in the evolution of diverse host associations.

The flexible articulation of the mandibles represents a modification unique among insects. Close relatives of Chalcidoidea (Diaprioidea and Proctotrupeoidea) already show at least a partial reduction of the posterior condyle (figure 5), which may be interpreted as an intermediate state putatively leading to increased flexibility. In a second step, the complete reduction of the posterior condyle is accompanied by modified musculature with a functional separation, different origins and insertions of abductors and adductors. This resulted in full flexibility of mandibles in Chalcidoidea. Interestingly, this case of secondary monocondyly is realized differently than in the primarily monocondylic hexapods (*Collembola*, *Diplura* and *Protura*). By contrast to the latter, only the anterior (secondary) articulation remained to facilitate mandibular movements in Chalcidoidea.

The bizarre mandibles in *Colotrechninae* sp. represent a unique evolutionary step that was facilitated by their flexible articulation. The antler-like extensions of the mandibles can

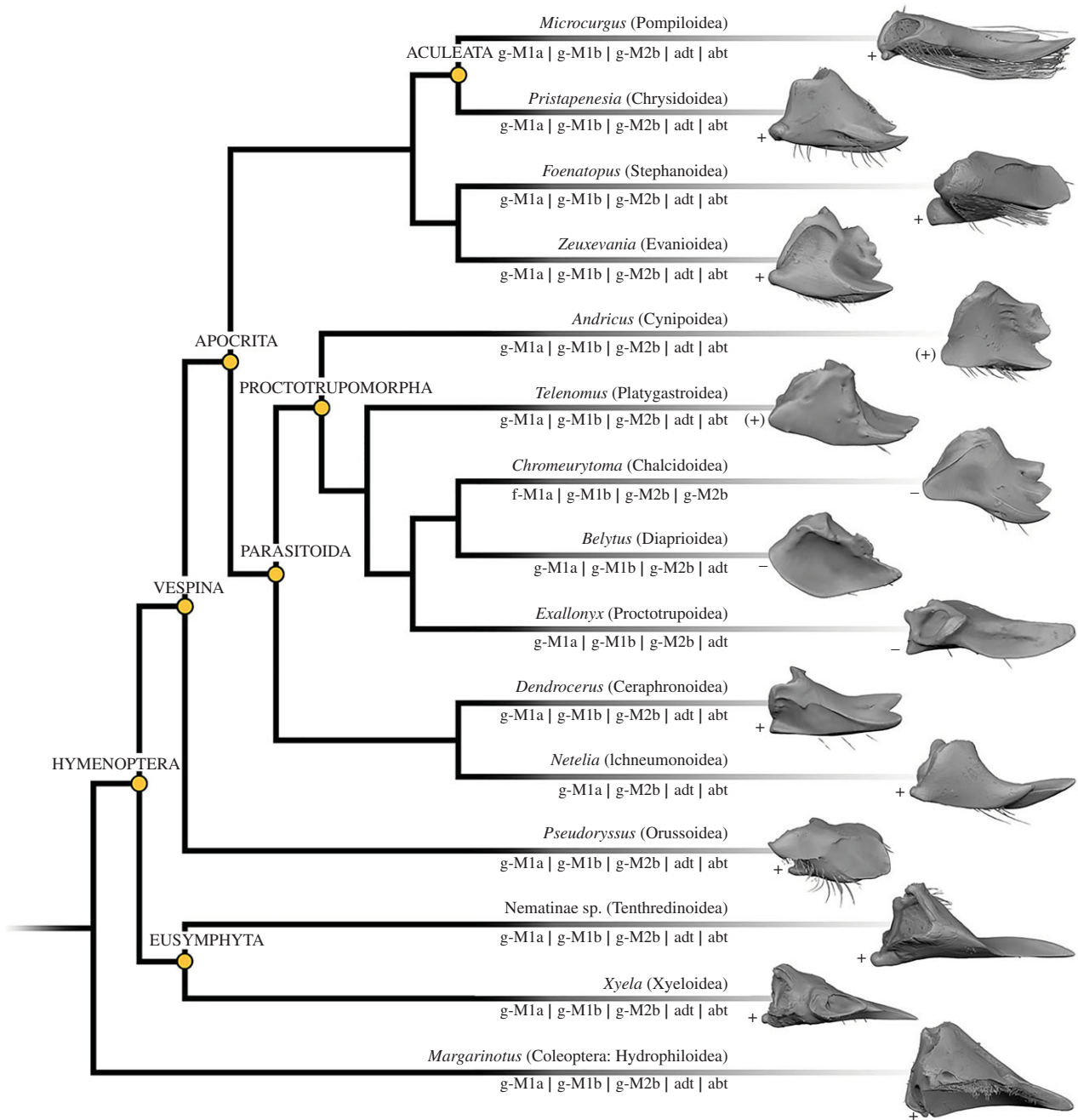


Figure 5. Characters of mandibles and mandibular musculature found in the examined taxa mapped on a molecular phylogeny of Hymenoptera [25]. abt, abductor tendon; adt, adductor tendon; f-, originates from the frons; g-, originates from the gena; M1a, M1b, M2a, M2b, mandibular muscle bundles; +, posterior condyle distinct; (+), posterior condyle indicated; -, posterior condyle reduced.

interlock with the lateral facial processes. In combination with the excavated face, this strongly hints to a grasping mechanism, while the standard biting function of the mandibles can be maintained (figure 1*e-h*, electronic supplementary material, movie S1). A potential grasping mechanism could be used for clasping the hosts prior to oviposition. Currently, the host biology of Colotrechninae sp. is obscure and the new species is only known from a single female specimen. The face and mandibular morphology of Colotrechninae sp. is unparalleled among extant insects but shows a staggering similarity to the ‘hell ants’ (Formicidae: Haidomyrmecinae) described from Cretaceous amber deposits [28]. ‘Hell ants’ were able to move their mandibles vertically to interlock with a cephalic projection, and a function as prey-capturing device has been verified based on the discovery of a fossil specimen holding its roach-like prey [29]. The mandibular articulation of ‘hell ants’ is currently not

known but the observed similarities to Colotrechninae sp. are undoubtedly the result of convergent evolution. Another similarity between Colotrechninae sp. and ‘hell ants’ is the presence of sensory organs close to the cephalic projection. In Colotrechninae sp., a single seta is situated close to each of the paired facial processes. In ‘hell ants’, the setae are more prominent and situated in a row along the outer margin of the cephalic projection. In both cases, these setae might have triggered the (potential) grasping mechanism.

(c) Mouthpart evolution triggers diversification of arthropods

The mandible of Chalcidoidea represents an evolutionary novelty that likely played an important role during an extremely large insect radiation process leading to the estimated 500 000 species of this superfamily. It has long been known that

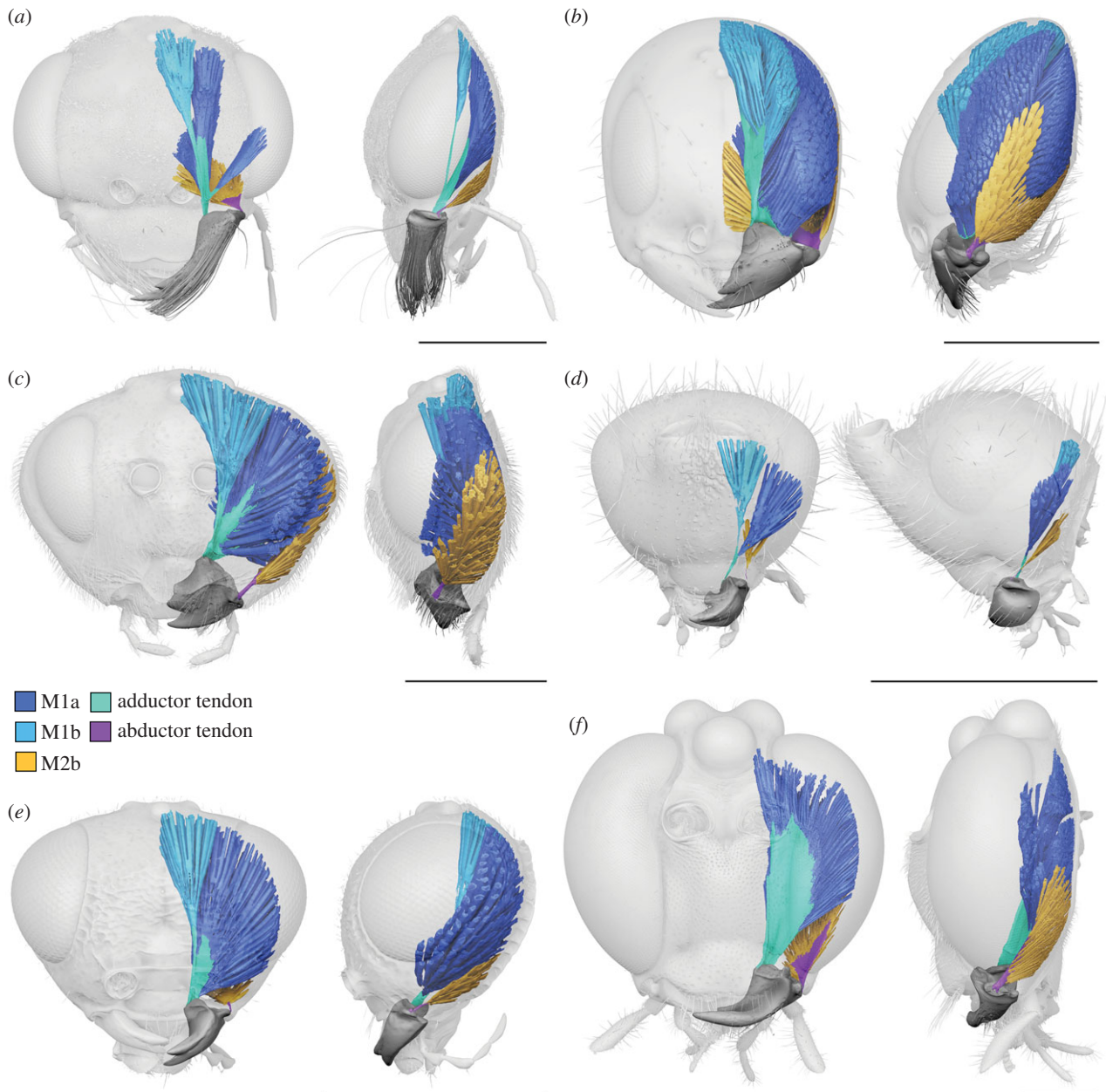


Figure 6. Mandibles and attached musculature throughout Hymenoptera. (a) *Microcurgus* (Pompiloidea). (b) *Pristapenesia* (Chrysoidea). (c) *Andricus* (Cynipoidea). (d) *Belytus* (Diapriidae). (e) *Dendrocerus* (Ceraphronidae). (f) *Netelia* (Ichneumonidae). Scale bars, 0.5 mm. (Online version in colour.)

the evolution of mandibles in the Mandibulata (the most speciose group of Arthropoda comprising millipedes, crustaceans and hexapods) and its modifications in the dicondylic insects have triggered large species radiations [13]. Our results suggest that the secondary reversal to monocondylic mandibles in Chalcidoidea (this time affecting the posterior condyle instead of the anterior typical for monocondylic hexapods) had further dramatic evolutionary consequences for parasitoids and helped them to exploit novel host systems, leading to complex niche differentiations and adaptive radiations.

4. Methods

(a) Taxon sampling

Representative taxa of ethanol-preserved Hymenoptera and one species of Coleoptera (electronic supplementary material, table S1) have been selected and studied and voucher specimens are deposited at the State Museum of Natural History, Stuttgart.

(b) Synchrotron X-ray microtomography

Tomographic scans of ethanol-preserved insect heads were performed at the UFO-I station of the Imaging Cluster at the KIT light source using a parallel polychromatic X-ray beam produced by a 1.5T bending magnet. The beam was spectrally filtered by 0.5 mm aluminium and the resulting spectrum had a peak at about 15 keV, with a full-width at a half maximum bandwidth of about 10 keV. A fast indirect detector system was employed, consisting of a 12 μm LSO:Tb scintillator [30] and a diffraction-limited optical microscope (Optique Peter) [31] coupled with a 12bit pco.dimax high speed camera with 2016 \times 2016 pixels. Scans were done by taking 3000 projections at 70 fps and an optical magnification of 10 \times , resulting in an effective pixel size of 1.22 μm . We used the control system concert [32] for automated data acquisition and online reconstruction of tomographic slices for data quality assurance. Online and final data processing included flat field correction and phase retrieval of the projections based on the transport of intensity equation [33]. X-ray beam parameters for algorithms in the data processing pipeline were computed by *syris* [34] and the execution of the pipelines,

including tomographic reconstruction, was performed by the UFO framework [35].

(c) Post-processing of tomographic data

Tomographic slices were converted to 8 bit and cropped to the region of interest. In Amira 5.6, heads, mandibles and mandibular muscles were pre-segmented in the software's segmentation editor. The labels served as input for automated segmentation, which was performed using the online platform Biomedisa (<https://biomedisa.org>) [36]. Segmentation results were again imported into Amira 5.6 and minor errors were corrected. The final labels were converted into polygon meshes, exported as OBJ files and reassembled and smoothed in CINEMA 4D R20.

(d) High-resolution videography

The specimens of *L. distinguendus* used in this study originate from the laboratory colonies of the Biologische Beratung GmbH (Berlin), where they were bred on larvae of *Sitophilus oryzae* (Linnaeus, 1763) (Coleoptera: Curculionidae) that developed in grains of the common wheat *Triticum aestivum* L. The infested wheat grains were observed and the hatching wasps were recorded using a Nikon DSC D90 camera mounted on a Leica MZ 12.5 stereomicroscope.

Data accessibility. The tomographic volumes examined in this study are available from the Dryad Digital Repository: <https://doi.org/10.5061/dryad.0rxwdb1x> [37].

Authors' contributions. T.K.: conceptualization, investigation, methodology, project administration, supervision, visualization, writing—original draft, writing—review and editing; I.M.: investigation,

writing—review and editing; A.H.S.: investigation, writing—review and editing; B.E.: investigation, methodology, writing—review and editing; D.B.: resources, writing—review and editing; T.F.: data curation, methodology, software, writing—review and editing; L.H.: investigation, methodology, writing—review and editing; E.H.: methodology, writing—review and editing; R.S.: methodology, writing—review and editing; T.B.: funding acquisition, resources, supervision, writing—review and editing; P.J.: investigation, writing—review and editing; L.K.: conceptualization, funding acquisition, investigation, project administration, supervision, writing—original draft, writing—review and editing.

All authors gave final approval for publication and agreed to be held accountable for the work performed therein.

Competing interests. We declare we have no competing interests.

Funding. Research was supported by the projects UFO 2, STROBOS-CODE and HIGH-LIFE (BMBF; 05K2012, 05K2014 and 05K2019).

Acknowledgements. We thank Gary Taylor for his help and support during fieldwork in Australia. Daniel Hänschke, Simon Bode and Simon Haaga are acknowledged for their assistance at the beamline and Stephen Doyle for improving the language of the manuscript. We thank Bob Blinn and Matthias Schöller for specimens of *Xyela minor* and *L. distinguendus*, and Oliver Betz for providing the video equipment. Tanja Schweizer is thanked for her technical support and Jessica Awad, Marina Moser and Cristina Vaselita for the determination of voucher specimens. We acknowledge the KIT light source for provision of instruments at their beamlines and we thank the Institute for Beam Physics and Technology (IBPT) for the operation of the storage ring, the Karlsruhe Research Accelerator (KARA). We gratefully acknowledge the data storage service SDS@hd supported by the Ministry of Science, Research and the Arts Baden-Württemberg (MWK) and the German Research Foundation (DFG) through grant INST 35/1314-1 FUGG and INST 35/1503-1 FUGG.

References

1. Grimaldi D, Engel MS. 2005 *Evolution of the insects*. Cambridge, UK: Cambridge University Press.
2. Misof B *et al.* 2014 Phylogenomics resolves the timing and pattern of insect evolution. *Science* **346**, 763–767. (doi:10.1126/science.1257570)
3. Footitt RG, Adler PH. 2017 *Insect biodiversity*, second edition. Chichester, England: John Wiley & Sons.
4. Nel P, Bertrand S, Nel A. 2018 Diversification of insects since the Devonian: a new approach based on morphological disparity of mouthparts. *Sci. Rep.* **8**, 3516. (doi:10.1038/s41598-018-21938-1)
5. Krenn HE (ed). 2019 *Insect mouthparts*. Cham, Switzerland: Springer Nature Switzerland.
6. Krenn H. 2019 Form and function of insect mouthparts. In *Insect mouthparts* (ed. H Krenn), pp. 9–46. Cham, Switzerland: Springer Nature Switzerland.
7. von Lieven A. 2000 The transformation from monocondylous to dicondylous mandibles in the Insecta. *Zoologischer Anzeiger*. **239**, 139–146.
8. Hennig W. 1953 Kritische Bemerkungen zum phylogenetischen System der Insekten. *Beitr. Entomol.* **3**, 1–85. (doi:10.21248/contr.entomol.3.Sonderheft.1-85)
9. Gayubo SF. 2008 Mouthparts of Hexapods. In *Encyclopedia of entomology* (ed. JL Capinera), pp. 2497–2504. Dordrecht, Germany: Springer.
10. Blanke A. 2019 The early evolution of biting–chewing performance in Hexapoda. In *Insect mouthparts* (ed. H Krenn), pp. 175–202. Cham, Switzerland: Springer Nature Switzerland.
11. Engel MS. 2015 Insect evolution. *Curr. Biol.* **25**, R868–R872. (doi:10.1016/j.cub.2015.07.059)
12. Staniczek A. 2000 The mandible of silverfish (Insecta: Zygentoma) and mayflies (Ephemeroptera): its morphology and phylogenetic significance. *Zool. Anz.* **239**, 147–178.
13. Blanke A, Machida R, Szucsich NU, Wilde F, Misof B. 2015 Mandibles with two joints evolved much earlier in the history of insects: dicondylia is a synapomorphy of bristletails, silverfish and winged insects. *Syst. Entomol.* **40**, 357–364. (doi:10.1111/syen.12107)
14. Simpson SJ, Douglas AE, Chapman RF (eds). 2013 *The insects: structure and function*. Cambridge, UK: Cambridge University Press.
15. Snodgrass RE. 1935 *Principles of insect morphology*. London/New York, NY: MacGraw-Hill.
16. Wipfler B, Machida R, Müller B, Beutel RG. 2011 On the head morphology of Grylloblattodea (Insecta) and the systematic position of the order, with a new nomenclature for the head muscles of Dicondylia. *Syst. Entomol.* **36**, 241–266. (doi:10.1111/j.1365-3113.2010.00556.x)
17. Kristensen NP. 1999 Phylogeny of the endopterygote insects, the most successful lineage of living organisms. *Eur. J. Entomol.* **96**, 237–253.
18. Vilhelmsen L. 2000 Before the wasp-waist: comparative anatomy and phylogenetic implications of the skeleto-musculature of the thoraco-abdominal boundary region in basal Hymenoptera (Insecta). *Zoomorphology* **119**, 185–221. (doi:10.1007/PL00008493)
19. Vilhelmsen L, Mikó I, Krogmann L. 2010 Beyond the wasp-waist: structural diversity and phylogenetic significance of the mesosoma in apocritan wasps (Insecta: Hymenoptera). *Zool. J. Linn. Soc.* **159**, 22–194. (doi:10.1111/j.1096-3642.2009.00576.x)
20. Quicke DLJ. 1997 *Parasitic wasps*. London, UK: Chapman & Hall Ltd.
21. Jervis M. 1998 Functional and evolutionary aspects of mouthpart structure in parasitoid wasps. *Biol. J. Linn. Soc.* **63**, 461–493. (doi:10.1111/j.1095-8312.1998.tb00326.x)
22. Heraty J. 2017 Parasitoid biodiversity and insect pest management. In *Insect biodiversity*, second edition (eds RG Footitt, PH Adler), pp. 445–462. Chichester, UK: John Wiley & Sons.
23. Heraty JM *et al.* 2013 A phylogenetic analysis of the megadiverse Chalcidoidea (Hymenoptera). *Cladistics* **29**, 466–542. (doi:10.1111/clad.12006)
24. Peters RS *et al.* 2018 Transcriptome sequence-based phylogeny of chalcidoid wasps (Hymenoptera: Chalcidoidea) reveals a history of rapid radiations, convergence, and evolutionary success. *Mol. Phylogenet. Evol.* **120**, 286–296. (doi:10.1016/j.ympev.2017.12.005)

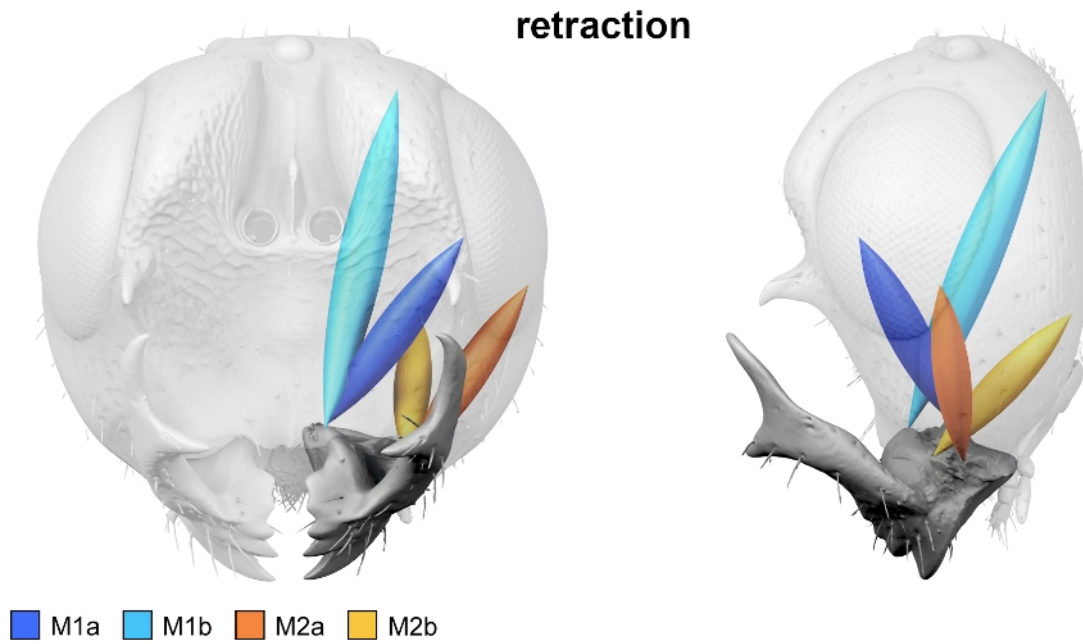
25. Peters RS *et al.* 2017 Evolutionary history of the Hymenoptera. *Curr. Biol.* **27**, 1013–1018. (doi:10.1016/j.cub.2017.01.027)
26. Beutel RG, Friedrich F, Ge S-Q, Yang X-K. 2014 *Insect morphology and phylogeny*. Boston, MA: De Gruyter.
27. Gibson GAP, Heraty JM, Woolley JB. 1999 Phylogenetics and classification of Chalcidoidea and Mymarommatoidea—a review of current concepts (Hymenoptera. Apocrita). *Zool. Scr.* **28**, 87–124. (doi:10.1046/j.1463-6409.1999.00016.x)
28. Perrichot V, Wang B, Barden P. 2020 New remarkable hell ants (Formicidae: Haidomyrmecinae stat. nov.) from mid-Cretaceous amber of northern Myanmar. *Cretaceous Res.* **109**, 104381. (doi:10.1016/j.cretres.2020.104381)
29. Barden P, Perrichot V, Wang B. 2020 Specialized predation drives aberrant morphological integration and diversity in the earliest ants. *Curr. Biol.* **30**, 1–7. (doi:10.1016/j.cub.2020.06.106)
30. Cecilia A *et al.* 2011 LPE grown LSO:Tb scintillator films for high resolution X-ray imaging applications at synchrotron light sources. *Nucl. Instrum. Methods Phys. Res., Sect. A* **648**(Suppl. 1), 321–323. (doi:10.1016/j.nima.2010.10.150)
31. Douissard P-A *et al.* 2012 A versatile indirect detector design for hard X-ray microimaging. *J. Instrum.* **7**, P09016. (doi:10.1088/1748-0221/7/09/P09016)
32. Vogelgesang M, Farago T, Morgener TE, Helfen L, dos Santos Rolo T, Myagotin A, Baumbach T. 2016. Real-time image-content-based beamline control for smart 4D X-ray imaging. *J. Synchrotron Radiat.* **23**, 1254–1263. (doi:10.1107/S1600577516010195)
33. Paganin D, Mayo SC, Gureyev TE, Miller PR, Wilkins SW. 2002 Simultaneous phase and amplitude extraction from a single defocused image of a homogeneous object. *J. Microsc.* **206**, 33–40. (doi:10.1046/j.1365-2818.2002.01010.x)
34. Faragó T, Mikulik P, Ershov A, Vogelgesang M, Hänschke D, Baumbach T. 2017 syris: a flexible and efficient framework for X-ray imaging experiments simulation. *J. Synchrotron Radiat.* **24**, 1283–1295. (doi:10.1107/S1600577517012255)
35. Vogelgesang M, Chilingaryan S, dos Santos Rolo T, Kopmann A. 2012 UFO: a scalable GPU-based image processing framework for on-line monitoring. In *Proc. of HPCC-ICISS, Liverpool, UK, 24–27 June 2012*, pp. 824–829. Piscataway, NJ: IEEE. (doi:10.1109/HPCC.2012.116)
36. Lösel P *et al.* 2020 Introducing Biomedisa as an open-source online platform for biomedical image segmentation. *Nat. Commun.* **11**, 5577. (doi:10.1038/s41467-020-19303-w)
37. van de Kamp T *et al.* 2021 Data from: Evolution of flexible biting in hyperdiverse parasitoid wasps. Dryad Digital Repository. (doi:10.5061/dryad.0rxwdb51x)

Additional files (supplementary material): PDF file and video files (snapshots displayed here); files available online at <https://royalsocietypublishing.org/doi/10.1098/rspb.2021.2086>

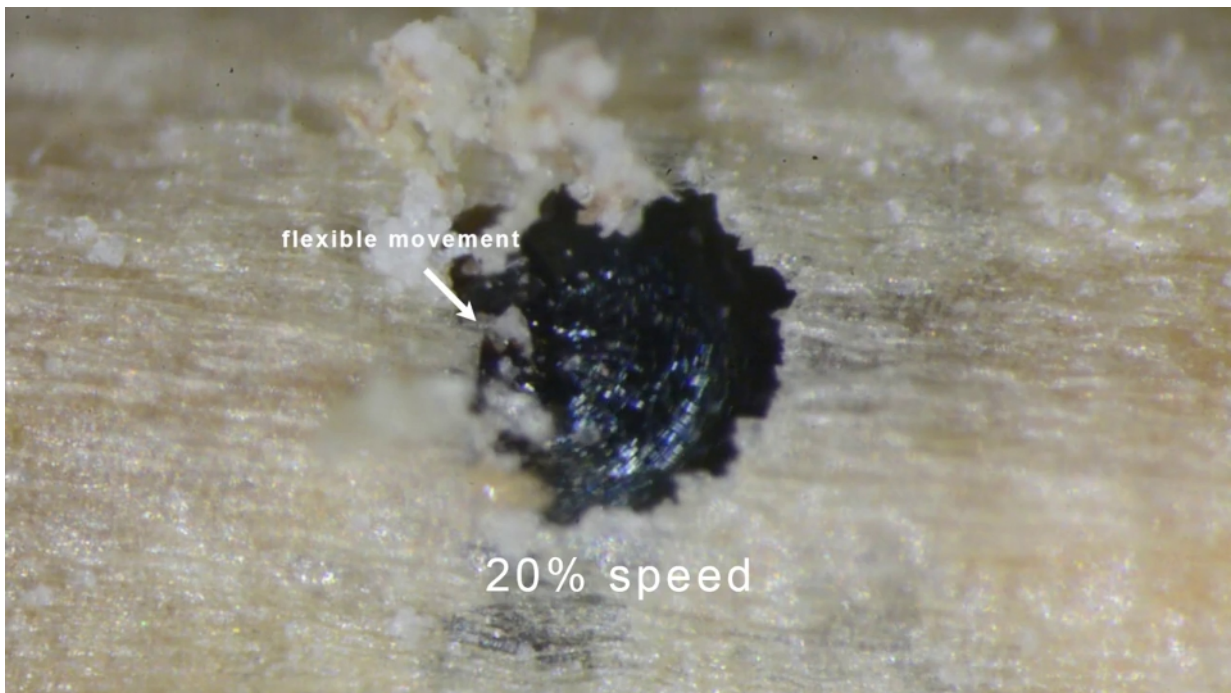
Table S1. Voucher specimens deposited at the State Museum of Natural History Stuttgart (SMNS).

Collection number	Family & species	Sex
SMNS_Hym_Aga_000001	Agaonidae: <i>Ceratosolen</i> sp.	female
SMNS_Hym_Dia_000637	Diapriidae: <i>Belytus</i> sp.	male
SMNS_Hym_Eup_000227	Eupelmidae: <i>Eupelmus</i> sp.	female
SMNS_Hym_Eur_000921	Eurytomidae: <i>Eurytoma</i> sp.	female
SMNS_Hym_Hym_013467	Scolebythidae: <i>Pristapenesia</i> sp.	female
SMNS_Hym_Hym_013479	Orussidae: <i>Pseudoryssus henschii</i>	female
SMNS_Hym_Hym_014077	Tenthredinidae: Nematinae sp. (<i>Euura/Nematus</i>)	male
SMNS_Hym_Hym_014078	Evaniidae: <i>Zeuxevania</i> sp.	female
SMNS_Hym_Hym_014097	Stephanidae: <i>Foenatopus</i> sp.	female
SMNS_Hym_Hym_014099	Cynipidae: <i>Andricus quercuscalicis</i>	female
SMNS_Hym_Meg_000035	Megaspilidae: <i>Dendrocercus</i> sp.	female
SMNS_Hym_Mym_000831	Mymaridae: <i>Australomymar</i> sp.	female
SMNS_Hym_Pom_000272	Pompilidae: <i>Microcurgus</i> sp.	female
SMNS_Hym_Per_000052	Perilampidae: <i>Austrotoxema</i> sp.	male
SMNS_Hym_Pro_000040	Proctotrupidae: <i>Exallonyx longicornis</i>	female
SMNS_Hym_Pte_008178	Pteromalidae: <i>Chromeyrtoma</i> sp.	female
SMNS_Hym_Pte_008020	Pteromalidae: Colotrechninae sp.	female
SMNS_Hym_Rot_000001	Rotoitidae: <i>Rotoita basalis</i>	female
SMNS_Hym_Sce_000668	Scelionidae: <i>Telenomus</i> sp.	female
SMNS_Hym_Tan_000006	Tanaostigmatidae: <i>Tanaostigmodes</i> sp.	male
SMNS_Hym_Tor_000507	Torymidae: <i>Idiomacromerus</i> sp.	male
SMNS_Hym_Hym_014104	Xyelidae: <i>Xyela minor</i>	male
SMNS_Hym_Pte_012303	Pteromalidae: <i>Lariophagus distinguendus</i>	female
SMNS_Hym_Hym_014102	Ichneumonidae: <i>Netelia ehippiata</i>	male
SMNS_Col_His_000001	Histeridae: <i>Margarinotus brunneus</i>	indet.

Supplementary material – Table S1: Voucher specimens deposited at the State Museum of Natural History Stuttgart (SMNS).



Supplementary material – Movie S1: Putative flexible mandibular movement of *Colotrechninae* sp.



Supplementary material – Movie S2: High-resolution video of *Lariophagus distinguendus* showing flexible biting during its emergence from a grain.

Publication 5

Eggs B., Fischer S., Csader M., Mikó I., Rack A. and Betz O. (2023). Terebra steering in chalcidoid wasps. *Frontiers in Zoology* 20: 26. doi: 10.1186/s12983-023-00503-1

(peer-reviewed journal article)

Abstract

Various chalcidoid wasps are able to actively steer their terebra (= ovipositor shaft) in different directions, despite the lack of terebral intrinsic musculature. To investigate the mechanisms of these bending and rotational movements, we combined microscopical and microtomographical techniques, together with videography, to analyse the musculoskeletal ovipositor system of the pteromalid wasp *Lariophagus distinguendus* (FÖRSTER, 1841) and the employment of its terebra during oviposition. The ovipositor consists of three pairs of valvulae, two pairs of valvifers and the female T9 (9th abdominal tergum). The paired 1st and 2nd valvulae are interlocked via the olistheter system, which allows the three parts to slide longitudinally relative to each other, and form the terebra. The various ovipositor movements are actuated by a set of nine paired muscles, three of which (*i.e.* 1st valvifer-genital membrane muscle, ventral 2nd valvifer-venom gland reservoir muscle, T9-genital membrane muscle) are described for the first time in chalcidoids. The anterior and posterior 2nd valvifer-2nd valvula muscles are adapted in function. (1) In the active probing position, they enable the wasps to pull the base of each longitudinally split and asymmetrically overlapping halves of the 2nd valvula that are fused at the apex dorsally, thus enabling lateral bending of the terebra. Concurrently, the 1st valvulae can be pro- and retracted regardless of the bend. (2) These muscles can also rotate the 2nd valvula and therefore the whole terebra at the basal articulation, allowing bending in various directions. The position of the terebra is anchored at the puncture site in hard substrates (in which drilling is extremely energy- and time consuming). A freely steerable terebra increases the chance of making contact with the potential host within a concealed cavity. The evolution of the ability actively to steer the terebra can be considered a key innovation that has putatively contributed to the acquisition of new hosts to a parasitoid's host range. Such shifts in host exploitation, each followed by rapid radiations, have probably aided the evolutionary success of Chalcidoidea (with more than 500,000 species estimated).

Significance within the present thesis: This is the core study of this thesis. In this study, we observed and recorded the oviposition behaviour and the employment of the terebra of a chalcidoid wasp; the pteromalid *Lariophagus distinguendus*. The wasp showed both bending and rotational movements of the terebra, although the latter has no intrinsic joints or muscles. In combination with a detailed description of the

musculoskeletal ovipositor, we have been able to create a functional model and determine the underlying mechanisms behind the terebra bending movements, which are based on several morphological modifications of its cuticular elements and muscle function. In addition, we discuss the various joint-free bending mechanisms found in insects and their eco-evolutionary significance. We have identified the structural adaptations that appear to be unique to the chalcidoid terebra, *i.e.* the longitudinally split and asymmetrically overlapping halves of the 2nd valvula that are fused only at the apex. We have analysed the mechanisms behind the active bending and rotation of the terebra, which are actuated by a set of two paired and functionally adapted muscles of the 2nd valvula. Both the evolution of the ability actively to steer the terebra to parasitize hosts concealed in hard substrates (*i.e.* entering the substrate) and the ability for precise cutting movement of the mandibles (*i.e.* leaving the substrate; *cf.* Publication 4) can be considered as key innovations that have probably aided the tremendous evolutionary success of the Chalcidoidea. Moreover, following modern concepts of designating morphological structures in a standardized way, we have applied and supplemented the Hymenoptera Anatomy Ontology (HAO; Yoder *et al.* 2010, Seltmann *et al.* 2012, Hymenoptera Anatomy Consortium 2022). Accordingly, we provide a comprehensive table with all 210 terms relevant to the hymenopteran ovipositor system and list their definitions and the respective uniform Resource Identifier (URI). We have also added all 515 synonyms and homonyms found in the literature (English, German, French) to facilitate future reading and to allow comparisons of findings from different studies dealing with the ovipositor system in Hymenoptera. This comprehensive study has the potential to become a reference work for future studies dealing with the hymenopteran ovipositor.

Methods used: high-resolution videography, stereomicroscopy, scanning electron microscopy (SEM), confocal laser scanning microscopy (CLSM), wide-field epifluorescence microscopy (WFM), ultramicrotomy, light microscopy (LM), transmission electron microscopy (TEM), synchrotron X-ray phase-contrast microtomography (SR- μ CT)

Own contribution: designing the study; preparing the specimens (fixation, embedding); processing of the SR- μ CT and light microscopical images; performing the ultramicrotomy, LM, WFM, TEM and high resolution videography; analysing and interpreting the data; writing the original version of the manuscript; preparing the figures; revising the manuscript; correspondence

RESEARCH

Open Access



Terebra steering in chalcidoid wasps

Benjamin Eggs^{1*} , Stefan Fischer^{1,2} , Michael Csader^{1,3} , István Mikó⁴ , Alexander Rack⁵  and Oliver Betz¹ 

Abstract

Various chalcidoid wasps can actively steer their terebra (= ovipositor shaft) in diverse directions, despite the lack of terebral intrinsic musculature. To investigate the mechanisms of these bending and rotational movements, we combined microscopical and microtomographical techniques, together with videography, to analyse the musculoskeletal ovipositor system of the ectoparasitoid pteromalid wasp *Lariophagus distinguendus* (Förster, 1841) and the employment of its terebra during oviposition. The ovipositor consists of three pairs of valvulae, two pairs of valvifers and the female T9 (9th abdominal tergum). The paired 1st and the 2nd valvulae are interlocked via the olis-theter system, which allows the three parts to slide longitudinally relative to each other, and form the terebra. The various ovipositor movements are actuated by a set of nine paired muscles, three of which (i.e. 1st valvifer-genital membrane muscle, ventral 2nd valvifer-venom gland reservoir muscle, T9-genital membrane muscle) are described here for the first time in chalcidoids. The anterior and posterior 2nd valvifer-2nd valvula muscles are adapted in function. (1) In the active probing position, they enable the wasps to pull the base of each of the longitudinally split and asymmetrically overlapping halves of the 2nd valvula that are fused at the apex dorsally, thus enabling lateral bending of the terebra. Concurrently, the 1st valvulae can be pro- and retracted regardless of this bending. (2) These muscles can also rotate the 2nd valvula and therefore the whole terebra at the basal articulation, allowing bending in various directions. The position of the terebra is anchored at the puncture site in hard substrates (in which drilling is extremely energy- and time-consuming). A freely steerable terebra increases the chance of contacting a potential host within a concealed cavity. The evolution of the ability actively to steer the terebra can be considered a key innovation that has putatively contributed to the acquisition of new hosts to a parasitoid's host range. Such shifts in host exploitation, each followed by rapid radiations, have probably aided the evolutionary success of Chalcidoidea (with more than 500,000 species estimated).

Keywords Chalcidoidea, Functional morphology, Hymenoptera, Ovipositor, Parasitoid, Pteromalidae

*Correspondence:

Benjamin Eggs

benjamin.eggs@uni-tuebingen.de; benjamin.eggs@protonmail.ch

¹ Evolutionary Biology of Invertebrates, Institute of Evolution and Ecology, University of Tübingen, Auf der Morgenstelle 28, 72076 Tübingen, Germany

² Tübingen Structural Microscopy Core Facility (TSM), University of Tübingen, Schnarrenbergstraße 94–96, 72076 Tübingen, Germany

³ State Museum of Natural History Karlsruhe, Erbprinzenstraße 13, 76133 Karlsruhe, Germany

⁴ Department of Biological Sciences, University of New Hampshire Collection of Insects and Other Arthropods, University of New Hampshire, Spaulding Hall, Durham, NH 03824, USA

⁵ ESRF – The European Synchrotron, Structure of Materials Group – ID19, CS 40220, 38043 Grenoble Cedex 9, France

Background

The evolution of parasitoidism in Hymenoptera has led to one of the largest species radiations in insects [1–5]. A large proportion of parasitoids belong to the Chalcidoidea, an extremely diverse and ecologically important group (nearly 27,000 species described, over 500,000 species estimated) of mainly minute wasps (average body size range from 1–2 mm) that are omnipresent in almost all terrestrial habitats [6–11]. Most chalcidoids are ectoparasitoids of other insects, usually attacking enclosed host stages with reduced mobility (i.e. egg or larval stages of wood and stem borers, leaf-miners



© The Author(s) 2023. **Open Access** This article is licensed under a Creative Commons Attribution 4.0 International License, which permits use, sharing, adaptation, distribution and reproduction in any medium or format, as long as you give appropriate credit to the original author(s) and the source, provide a link to the Creative Commons licence, and indicate if changes were made. The images or other third party material in this article are included in the article's Creative Commons licence, unless indicated otherwise in a credit line to the material. If material is not included in the article's Creative Commons licence and your intended use is not permitted by statutory regulation or exceeds the permitted use, you will need to obtain permission directly from the copyright holder. To view a copy of this licence, visit <http://creativecommons.org/licenses/by/4.0/>. The Creative Commons Public Domain Dedication waiver (<http://creativecommons.org/publicdomain/zero/1.0/>) applies to the data made available in this article, unless otherwise stated in a credit line to the data.

or inhabitants of galls, seeds and fruits) [12], although other life stages are also targeted [13]. The parasitization of hosts living deep within substrates allows the ectoparasitoid larvae to develop within the protection of a concealed environment and without exposure to the host immune system as occurs in endoparasitoids. An evolutionary novelty and presumably a strong driver of diversification in Chalcidoidea is the secondary reversal to monocondylic mandibles (reduction of the posterior condyle accompanied with modified musculature with functional separation), which allow the emerging wasp to bite through a hard substrate by precise cutting movements that overcome the limitations of a single degree of freedom [14]. However, the use of hosts living concealed within hard substrates poses challenges not only for the emerging wasp (i.e. in leaving the substrate), but also for females attempting to parasitize them (i.e. entering the substrate to find a potential host) [15]. In this context, the ovipositor has to fulfil several functional demands: penetration or navigation through the substrate or the target egg/puparium, assessment of the host, discrimination between suitable and previously parasitized hosts, piercing of the host, injection of venom, formation of a feeding tube for host feeding, ovicide or larvicide of the competitors' eggs or larvae, respectively, marking of the host and find a suitable place for egg laying and oviposition [16]. However, putative evolutionary novelties of the chalcidoid ovipositor system, such as morphological and behavioural adaptations that enable the steering of the terebra (= ovipositor (shaft) sensu [17–27]) and its underlying mechanisms have not been thoroughly investigated hitherto.

As in all hymenopterans, the chalcidoid ovipositor consists of the female T9 (9th abdominal tergum;=outer ovipositor plates sensu [17–25]), two pairs of valvifers and three pairs of valvulae derived from the 8th and 9th abdominal segments (7th and 8th metasomal segments). The basally situated valvifers accommodate the operating musculature, whereas all the valvulae are devoid of intrinsic musculature [28–32]. The 1st valvifers (8th gonocoxites [33, 34] or the fusion of the same with the gonangula [30];=fulcral plates sensu [17–25, 35–37];=gonangulum, gonangula sensu [26, 27]) are anteriorly continuous with the rami of the 1st valvulae (8th gonapophyses;=stylets sensu [17–25, 35–38];=lower valves sensu [26, 27]), and their posterior angles articulate dorsally with the female T9 via the tergo-valvifer articulation and ventrally with the 2nd valvifers via the intervalvifer articulation. The 2nd valvifers (9th gonocoxites;=inner ovipositor plates sensu [17–25]) extend as the 3rd valvulae (9th gonostyli;=(articulating/terminal) palps sensu [19, 20, 22, 23, 36];=ovipositor sheaths sensu [26, 27]) and are ventrally articulated with the 2nd

valvula (fusion of the 9th gonapophyses;=(stylet) sheath sensu [17–25, 36–38];=upper valve sensu [26, 27]) [28, 29], which is asymmetrically split except at the apex in all chalcidoid families [39]. The two overlapping asymmetric halves of the 2nd valvula are connected dorsally by the notal membrane, which extends almost to the apex [17, 19–25, 40]. The interlocked 1st and 2nd valvulae enclose the egg canal and form the terebra, which is embraced by the 3rd valvulae when not in use. The ventral surface of the 2nd valvula is interlocked with both of the 1st valvulae by a sublateral longitudinal tongue called the rhachis, which runs within a corresponding groove called the aulax along the dorsal surface of each of the 1st valvulae. This so-called olistheter system allows the three elements of the terebra to slide longitudinally relative to each other and simultaneously prevents their unwanted separation [29, 39].

In order to reach their hosts and permit greater control over egg placement, several parasitoid wasps are able actively to bend and rotate their terebra in any direction relative to their body axis [41–44], despite the lack of intrinsic terebral musculature. Such terebra movements have also been reported in chalcidoid wasps of the family of Pteromalidae [40, 45–47], a polyphyletic group sensu lato [6, 10, 48, 49] (over 3500 species described [8]). However, little is known about the actuation of the various ovipositor movements, with the mechanisms involved in terebra steering (i.e. bending and rotating) remaining unclear. In this study, we investigated the working mechanisms of the terebra steering movements of *Lariophagus distinguendus* (Förster, 1841) (Chalcidoidea: Pteromalidae: Pteromalinae), a cosmopolitan synanthropic synovigenic autogenous solitary idiobiont larval and pupal ectoparasitoid of several granivorous coleopteran species [50, 51]. This species exhibits extensive terebra movements during the assessment of a potential host and eventual subsequent egg placement [45, 47]. We aimed (1) to analyse the oviposition process in vivo, (2) to describe the ovipositor of *L. distinguendus*, including all inherent cuticular elements and muscles, (3) to examine the mechanics and mode of function of the musculoskeletal system, including the actuation of the various ovipositor movements, (4) to investigate the underlying working mechanisms of the terebra steering movements and (5) to discuss their eco-evolutionary significance.

Results and discussion

We combined behavioural analyses involving high-resolution video recordings with morphological investigations based on microscopical and microtomographical techniques. These studies have enabled us to present a thorough morphological and mechanical analysis of the musculoskeletal ovipositor system that steers the various



Fig. 1 Habitus image of a female *Lariophagus distinguendus* (lateral view). Abbreviations: trb: Terebra

movements executed by the female *L. distinguendus* (Fig. 1) during oviposition. In particular, we focused on the employment of the terebra and on its form, structure and material properties.

Morphological terms are applied according to the Hymenoptera Anatomy Ontology (HAO; [52–54]; a table of all 210 terms relevant to the hymenopteran ovipositor system, their definitions and 513 synonyms commonly found in literature is given in Table 2 in the Appendix 1).

In cases in which our findings have been confirmed by other studies, these are indicated below with ‘cf.’

Oviposition process and employment of the terebra

Previous studies describing the behavioural sequences of the attempts of *L. distinguendus* [45, 50, 55, 56] and other pteromalids [40, 46, 57] to oviposit have been unable to provide an analysis of the events that take place within the cavity of the substrate. Therefore, we mainly focus on the employment of the terebra and its movements in the following (Fig. 2; Additional file 1).

Search for the host’s habitat: *L. distinguendus* parasitizes concealed granivorous host larvae (Fig. 2a). The parasitoids mainly use volatile chemicals to locate the habitat of their hosts: faecal cues from the host itself and herbivory-associated chemicals in the seed induced by the mechanical damage caused by the host larvae [51, 55, 58].

Search for an infested substrate: Once *L. distinguendus* finds the host’s location (infested grains; blotting paper with the host faeces in our experimental setup), the wasp starts to walk on the substrate followed by antennal drumming with the flagellum directed towards the ground (Additional file 1, min. 0:05–0:07; cf. [45, 47, 50, 55, 56]). The female parasitoid is able to discriminate between healthy and infested grains [59].

Penetration of the substrate: Once the female wasp has selected a small spot with its antennae, it brings its terebra into the drilling position by a downward bending of the metasoma so that its tip taps the surface. The terebra is guided and stabilized by the 3rd valvulae in

order to prevent buckling despite axial compressive forces occurring during the initial puncturing of the substrate, i.e. the pericarp of the grain. Once the apex of the terebra is engaged in the substrate, the metasoma with the 2nd valvifer and the attached 3rd valvulae are lifted upwards out of the way (Fig. 2b–d; Additional file 1, min. 0:06–0:11; cf. [40, 45, 47, 50, 55, 56]). The initial puncturing (i.e. pericarp surface penetration) is necessary for the 1st and 2nd valvulae to be anchored in the substrate so that the subsequent ‘push-pull’ mechanism can be initiated. Thereby, the wasp exhibits alternate reciprocal movements of the paired 1st valvulae, which can be seen as trembling movements of the posteroventral part of the metasoma (i.e. the 2nd valvifers and the female T9). Only one of the 1st valvulae is pushed into the substrate at a time, while the other 1st valvula and the 2nd valvula, which are anchored in the substrate, are simultaneously pulled [60–62]. The apical sawteeth thereby increase the friction with the surrounding substrate. The tension in the two anchored ‘stationary’ elements increases their bending stiffness and, hence, they can serve as guides for the particular 1st valvula being pushed into the substrate [44, 60]. Small pushing movements of the 2nd valvula caused by the relative movements of the 2nd valvifers cannot be excluded (cf. [32]). The simultaneous pushing and pulling of the various terebral elements minimizes the net compressive force on the substrate and thus the chance of buckling of the terebra [32, 44, 60]. The ‘push-pull’ mechanism enables drilling without torque and with very low axial load, although these cannot be completely avoided [44, 62]. During the drilling process (Additional file 1, min. 0:12–0:20; cf. [47]), the wasp combines the ‘push-pull’ mechanism with slight rotations of the terebra [44, 60]. Moreover, a fluid is constantly secreted at the apex and also along the shaft of the terebra. This secretion putatively prevents particles from entering the terebra but might also act as a (cooling) lubricant (cf. [63, 64]).

Search for a potential host within the substrate: As soon as the wasp has penetrated the grain in which a potential host larva is living, it attempts to locate the host larva in its concealed cavity with its terebra (Additional file 1, min. 4:02–4:32). Thereby, the metasoma is frequently rotated by up to 35° from the longitudinal body axis of the wasp (cf. [45]); this influences the orientation of the terebra. However, the wasp also expresses steering movements of the terebra in several directions that are independent of the orientation of the metasoma (see subchapter ‘Mechanisms of terebra bending and rotation’ below).

Penetration of the targeted host’s skin: Once the wasp has succeeded in reaching its host, it pushes its

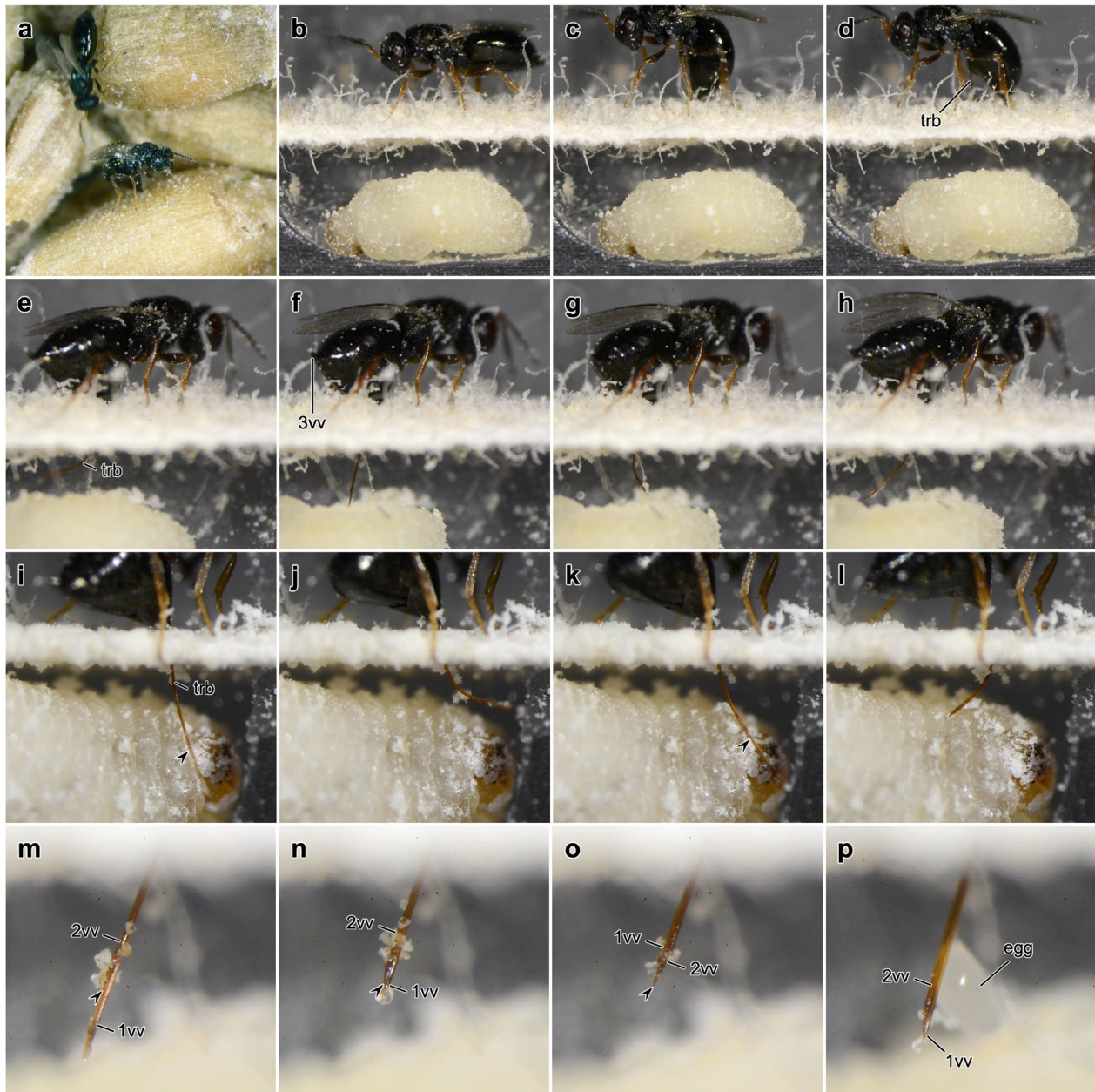


Fig. 2 Oviposition process of *Lariophagus distinguendus*. **a** Female wasps search for potential hosts that live in grains of the common wheat *Triticum aestivum*. **b–p** Single frames of high-resolution video recordings of a female *L. distinguendus* parasitizing a larva of *Sitophilus granaries* in an artificial chamber (cf. Additional file 1). The wasp and the beetle larva were separated by a piece of blotting paper. After the wasp finds a host (**b**), it brings its terebra into drilling position by a downward bending of the metasoma (**c**) and then, once the apex of the terebra is engaged in the substrate, it lifts the metasoma and the 3rd valvulae upwards (**d**). Following penetration of the substrate, the wasp permanently paralyzes the host larva by venom injection and then usually forms a feeding tube for host feeding. During the subsequent assessment of the host and the search for a suitable place for oviposition, the wasp is able to actively bend (**e–l**) its terebra in various directions and also to rotate it to a certain degree (**o**). The individual movements of the single valvulae can be observed (**m–p**). The 1st valvulae is frequently protracted far beyond the apex of the 2nd valvulae (marked with an arrowhead in **i, k, m, n, o**). Finally, an egg is laid (**p**). Rapid alternating movements of the 1st valvulae can be observed during substrate drilling, host envenomation and egg laying. Abbreviations: 1vv: 1st valvulae; 2vv: 2nd valvulae; 3vv: 3rd valvulae; trb: Terebra

terebra straight down to its fullest extent and penetrates the skin of the beetle larva several times with rapid stabbing movements of the terebra (Additional file 1, min.

0:21–0:27, 2:33–2:47; cf. [47, 55]) achieved by fast alternate movements of the 1st valvulae.

Injection of venom: The host larva is usually pierced several times (cf. [45, 47]), with the 1st valvulae performing fast alternate movements. Venom is injected into the host's body and permanently paralyzes the host (Additional file 1, min. 0:21–0:27, 2:33–2:47; cf. [47]) thereby preventing its further development. This is crucial for ectoparasitoids, since movements of the host larva within a small cavity might damage the externally attached parasitoid [65].

Assessment of the host: The permanent paralysis of the host larva presumably allows an easier and more accurate assessment to be carried out by the female wasp, which can now actively steer its terebra (Fig. 2e–l; Additional file 1, min. 0:30–1:10, 2:48–3:17; cf. [47]; see subchapter 'Mechanisms of terebra bending and rotation' below). However, some passive bending of the terebra might also occur because of its deflection on the host surface. A small actively actuated bending of the apex of the terebra would therefore be sufficient to indicate the direction of the bending movement. The assessment of the host is not primarily carried out by the terebra tapping of the host surface, but by the puncture and the assessment of the host's haemolymph (cf. [66, 67]).

Formation of a feeding tube for host feeding: In most parasitization attempts, the female wasps create a feeding tube. Thereby, a secretion, which is produced by the large colleterial glands [68], oozes from the entire terebra [66, 69]. The terebra is moved up and down and is also putatively rotated to a certain degree to ensure an even distribution of the secretion, which hardens in the air and remains for a couple of minutes, forming a feeding tube (cf. [47]). As a result of capillary forces, the haemolymph of the host flows upwards within the tube. The wasp now appears to lick the end of the feeding tube. The absorbed haemolymph serves both as protein-rich nutrition that is needed for egg maturation [70] and allows an assessment of the quality of the potential host [66, 67].

Ovicide/larvicide of the competitors' eggs/larvae: In our artificial setup, we have not tested whether the female wasps attempt to kill their conspecifics' eggs or larvae. Ovicidal and larvicidal behaviour has not as yet been observed in *L. distinguendus*.

Search for a suitable place for oviposition: If the female wasp deems the host larva to be of good quality, it searches for a suitable oviposition site on the host surface. It appears to estimate the available space within the cavity to ensure that the growing larva has enough room for development (Fig. 2e–l; Additional file 1, min. 3:19–3:34; cf. [47]).

Oviposition: Rapid longitudinal alternate movements of the paired 1st valvulae serve to pass the egg along the terebra (Fig. 2m–p; Additional file 1, min. 1:56–2:26, 3:36–4:00; cf. [47, 71]). The diameter of the egg is significantly larger compared with that of the egg canal. The egg is thus strongly deformed during ovipositing. It does not

emerge at the very apex of the terebra but is pushed out ventrally between the two paired 1st valvulae in a region about 100–200 μm proximal to the apex (Fig. 2p). Finally, the egg is attached to the surface of the host. In a few cases, it was also observed to be attached to the surface of the cavity near the host larva. Finally, the wasp withdraws its terebra. Female *L. distinguendus* only lay one egg per host [45, 55].

Morphological structure of the musculoskeletal ovipositor system

The musculoskeletal ovipositor system of *L. distinguendus* consists of three pairs of valvulae, two pairs of valvifers, the female T9, three paired articulations and a set of nine paired muscles.

Because of its bilateral bauplan, all the ovipositor elements and muscles are paired apart from the distal region of the 2nd valvula and the female T9. Paired morphological structures are only described in the singular form in the following, i.e. the elements of the left side only, although they have a mirror image on the right side.

The anatomy of the venom system and of the female internal reproductive system is not discussed thoroughly in the following (for chalcidoids, see [19–25, 35–38, 72–79]; for parasitoid hymenopterans in general, see [26, 27]).

Cuticular elements of the ovipositor

1st valvula (1vv; Figs. 2m–p, 3a, b, f, 4a–d, g–k, and 5a, c): Basally, the thin 1st valvula is continuous with the 1st valvifer via its dorsal ramus (dr1; Figs. 3d, e, g, 5a, c, d, and 6c, j). The 1st valvula has a crescent-shaped cross-section over most of its length (1vv; Fig. 4c). The aulax (au; Figs. 3a and 4g, i, k) of *L. distinguendus* does not reach the apex of the 1st valvula but tapers off around 50 μm before it. The distal end of the aulax features a coeloconic sensillum (cs; Figs. 3a and 4i, j; sensu [80]), presumably monitoring the position of the 1st valvula relative to the 2nd valvula (cf. [81]). Further sensilla can be seen at regular intervals on the lateral sides (blue 'notches' in Fig. 3f), which might have a mechano- and/or chemosensory function. However, the sensillar equipment of the terebra was not further investigated in this study (but see [82–84]). Dorsomedially to the aulax, the medial wall of each 1st valvula is thickened (Fig. 4c). The ventral part of the medial wall is thin and formed into a large membranous fold (when at rest) that projects inwards and overlaps ventrally (Fig. 4a–c; cf. [39]). These thin chitinous folds are considered effectively to seal the crack between the paired 1st valvulae in order to prevent the loss of venom and/or oviposition fluids [39]. The 1st valvula laterally bears two small sawteeth (st1; Fig. 3a) that are of decreasing size at its apex and that are most probably used to penetrate the substrate and the host's skin. On the dorsomedial side of

their apices, the 1st valvulae are connected by the olistheter-like interlock of the 1st valvulae (il1; Fig. 4h, i, k), presumably preventing them from being torn apart during the initial puncturing of the substrate and during drilling. The egg exits the egg canal proximad to these structures and ventrally between the paired 1st valvulae (Fig. 2p; Additional file 1, min. 1:56–2:26, 3:36–4:00). Such interlocking structures are also found in other pteromalids and some species of Aphelinidae, Chalcididae, Eulophidae, Eurytomidae, Ormyridae, Tanaostigmatidae and Trichogrammatidae [39]. In all chalcidoids, the ventral ramus of the 1st valvula is completely reduced [29] and the valvilli inside the egg canal are absent [85].

2nd valvula (2vv; Figs. 2m–p, 3a, c, f–h, 4a–g, i, k, and 5a–c): Proximally, the bulbs of the 2nd valvula (blb; Figs. 3g, h, 4a, and 6e–h) are basally articulated with the 2nd valvifer via the basal articulation (ba; Figs. 3h and 6f). At its basal part, the 2nd valvula bears the processus articularis laterally on the bulbs, and the processus musculares dorsally on the anteriorly directed horn-like processes of the bulbs. On its ventral side, the 2nd valvula bears the rhachises (rh; Figs. 3c and 4g). The 2nd valvula of *L. distinguendus* consists of two longitudinally split, asymmetrically overlapping and more-heavily sclerotized halves (2vv; Figs. 3a, f–h and 4a–c; Additional file 2) that are thickened medially (2vv; Fig. 4c). The two halves are dorsally connected for most of their length by a conjunctiva called the notal membrane (nm; Fig. 4f) [17, 19–25, 40] but are fused at the apex (2vv; Figs. 3a and 4d, i, k). Proximally, the notal membrane is modified into a transversely striate band called the laminated bridge (lb; Figs. 3g, h, 4a, b, e, 5a–c, and 6c, f, h) [19, 20, 22, 40]. The modified 2nd valvula with its longitudinally split and overlapping halves presumably permit a greater distortion of the valvula and appear to be a synapomorphy for

all Chalcidoidea, except for Mymaridae [39]. The ventral side is formed by the ventral wall of the 2nd valvula (vw2; Fig. 4a–c, f; sensu [86]), which extends from the base almost to the apex. This creates a lumen (lu2; Fig. 4a–d, f, i, k). The rhachises are attached to this lamella-like process over most of their length, except for the apex. Ventrolaterally to the rhachises lie lateral extensions of the 2nd valvula (le; Fig. 4c; sensu [86]). The apex of the 2nd valvulae of *L. distinguendus* features seven sawteeth that are placed laterally and staggered relative to one another (st2; Figs. 3a, f and 4i) with sensilla being found in between them. The laterally positioned sawteeth are postulated to act like a screw during the alternate rotational movements of the terebra during substrate penetration [22] and seem to be present in all chalcidoid species that undertake drilling actions [25] (Additional file 3).

Terebra (trb; Figs. 1, 2d–p, 3a and 6c–h): The acicular terebra consists of the paired 1st valvulae and the 2nd valvula and has a smooth surface. The terebra of *L. distinguendus* (and other chalcidoid wasps) features a single opening at the basal end, where the common oviduct (co; Fig. 5) seamlessly merges with the base of the egg canal (cf. [19–23, 25]). In chalcidoid wasps (such as *L. distinguendus* and *Microterys flavus* (Howard, 1881) (Encyrtidae) (data not yet published)), both the orifice of the venom gland reservoir (ovr; Fig. 5b–d; Additional file 4, min. 0:30–0:31) and the dorsolaterally situated Dufour's gland duct (Dgd; Fig. 5) empty into the common oviduct (cf. [73, 77]) before the latter fuses with the egg canal (unlike in ichneumonoid wasps; cf. [16, 87]). The junction lies directly anterior to the basal articulation (ba; Figs. 3h and 6f) and is indicated by the furcula (Fig. 3g; Additional file 2, min. 0:21–0:36). The complete length of the egg canal thus functions as a conduit not only for the egg itself, but also for the expulsion of venom or other

(See figure on next page.)

Fig. 3 Ovipositor of *Lariophagus distinguendus*. **a–e** SEM images of the various ovipositor elements (left is anterior). **a** Apex of the terebra comprising the 2nd valvula and the paired 1st valvulae (dorsolateral view). The 2nd valvula is longitudinally split but fused at the apex, featuring seven sawteeth. The 1st valvula features two small apical sawteeth. Its aulax terminates pre-apically and bears a coeloconic sensillum at its apical end (for cross section cf. Fig. 4i, j). Both the 1st and 2nd valvulae bear various types of sensilla. **b** Upon removal of the 2nd valvula, the aulaces of the inner surface of the 1st valvula become visible (dorsal view), featuring distally directed scale-like structures. **c** Upon removal of the 1st valvula, the rhachis at the ventral side of the 2nd valvula becomes visible (ventral view), featuring distally directed scale-like structures similar to those of the aulax. The egg canal is formed by both the 1st and 2nd valvulae and bears microsculpture consisting of distally oriented ctenidia. **d** Anterior part of the ovipositor (lateral view). The 1st valvifer is continuous with the dorsal ramus of the 1st valvula. It is connected with the 2nd valvifer and the female T9 via the intervalvifer and tergo-valvifer articulation, respectively. The 2nd valvifer possesses a post-ramus flap and two clusters of sensilla: the sensillar patch located anteriorly to the intervalvifer articulation and the sensillar row along its dorsal margin (**e**). **f** WFM image of the apical part of the terebra of *L. distinguendus* (dorsal view, left is anterior; only the images of the DAPI and Cy5 wavelength filters are superimposed here). The cuticle of the aulaces and the sawteeth of the 2nd valvula are heavily sclerotized (as indicated by their red autofluorescence). **g, h** Superimposed CLSM images of the basal part of the ovipositor of *L. distinguendus* (dorsal view, left is anterior; cf. Additional file 2). The cuticle of the valvulae and the valvifers is sclerotized, whereas the ctenidia show a high content of resilin (as indicated by their blue autofluorescence; **h**). Abbreviations: 1vf: 1st valvifer; 1vv: 1st valvula; 2vf: 2nd valvifer; 2vv: 2nd valvula; 3vv: 3rd valvula; au: Aulax; ba: Basal articulation; blb: Bulb; cs: Coeloconic sensillum; ct: Ctenidium; dr1: Dorsal ramus of the 1st valvula; fu: Furcula; iva: Intervalvifer articulation; lb: Laminated bridge; m-p-2vf-2vv: Posterior 2nd valvifer-2nd valvula muscle; prf: Post-ramus flap; rh: Rhachis; sc: Scale-like structure; sp: Sensillar patch of the 2nd valvifer; sr: Sensillar row of the 2nd valvifer; st1: Sawtooth of the 1st valvula; st2: Sawtooth of the 2nd valvula; t-m-d-T9-2vf-a: Tendon of the dorsal 2nd valvifer-T9 muscle part a; T9: Female T9 (9th abdominal tergum); tva: Tergo-valvifer articulation

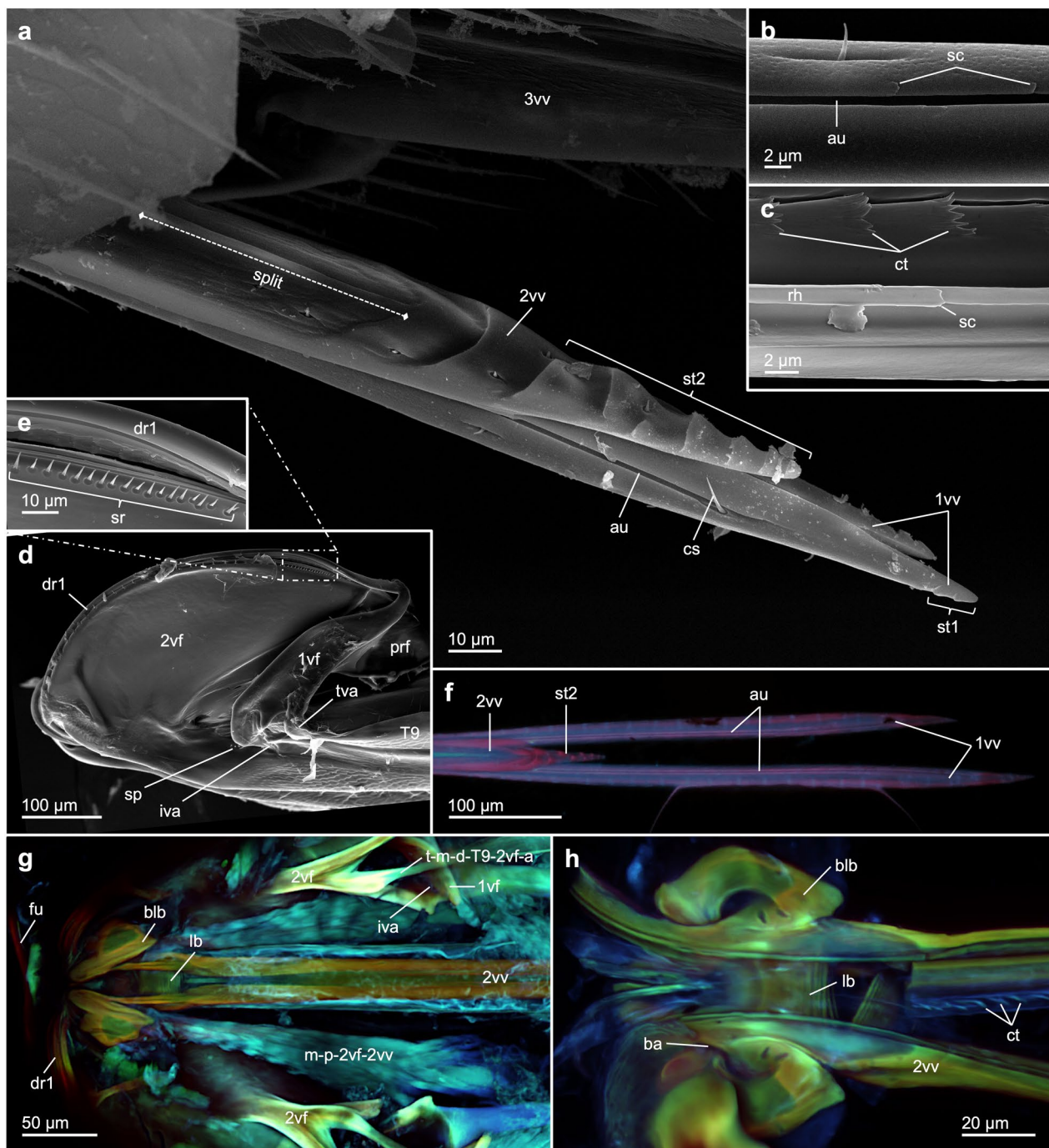


Fig. 3 (See legend on previous page.)

fluids during oviposition. The diameter of the terebra is even along its length (Fig. 4c; Additional file 3) between the broad basal bulbs (Figs. 3g, h and 4a,b) and the distally tapering apex (Figs. 3a and 4d, i, k). The rhachises (rh; Figs. 3c and 4g) on the ventral side of the 2nd valvulae are interlocked with the aulaces (au; Figs. 3a, b and 4g, i, k) on the dorsal side of the opposing 1st valvulae via the

olistheter system (oth; Fig. 4c); this enables the 1st valvulae to move along the 2nd valvulae while they are still connected to each other. The olistheter of *L. distinguendus* does not extend along the entire length of the terebra but end around 50 μm before its apex (Fig. 3a). The distally directed scale-like structures on the contact surfaces of both the rhachises and the aulaces (sc; Fig. 3b, c)

presumably reduce frictional forces by minimizing the contact area of the olistheter elements [88]. However, these scale-like structures potentially also forward a liquid lubricant from the colleterial glands (= accessory glands) to the apex of the olistheter system further to reduce friction in between the moving valvulae (cf. [89]). This arrangement might also enable particles to be continuously flushed out the olistheter system during drilling or venom injection. The scale-like structures might additionally create anisotropic conditions in the olistheter and thus prevent the 1st valvulae from randomly sliding back during drilling and piercing (cf. [31]). The longitudinally split and asymmetrically overlapping halves of the 2nd valvula presumably allow lateral sliding to occur towards or away from each other. Moreover, the rachises of *L. distinguendus* are suspended from lamellar structures of the ventral wall of the 2nd valvula (vw2; Fig. 4b, c) over their entire length, except for the apex (Fig. 4d). Thus, both the 1st and 2nd valvulae, which are connected via the olistheter system, are presumably movable in their position and may diverge tangentially. Moreover, the dorsally thickened walls of the 1st valvulae can be bent away from the midline and, in doing so, can take up the ventral membranous slack, further increasing the volume inside. This is thought to be an adaptation in several chalcidoid taxa to facilitate deformation of the terebra and temporarily to enlargement of the egg canal (ec; Fig. 4c), which is mainly formed by the two paired 1st valvulae, in order to accommodate the passing egg [39]. The olistheter system thereby must sustain the forces exerted by the egg [62, 71]. However, the maximal diameter of the apical half of the terebra is limited by the diameter of the puncture site in the substrate during oviposition. The areas of the rachises at the basal bulbous part of the 2nd valvula presumably are also flexible (purple areas of the cuticle in Fig. 4a, b presumably indicating a higher resilin content). The internal microsculpture of the medial wall of the egg canal consists of distally orientated leaf-like ctenidia (ct; Fig. 3c, h) that contain large amounts of resilin (ct; Fig. 3h; Additional file 2, min. 0:05–0:20) and are found from the proximal basis to the region before the apex. The ctenidia help to push the deformable egg along the egg canal by alternate movements of the 1st valvulae,

prevent regression [71, 88] and are also hypothesized to forward a liquid lubricant for the moving valvulae and thus to reduce friction [88, 90] and/or to produce a feeding tube. Both the 1st and 2nd valvulae have tapered apices. The terebra apex in many hymenopteran taxa is heavily sclerotized and hardened with metal atoms, such as calcium (Ca), manganese (Mn) and zinc (Zn). This enables the piercing of hard substrates, reduces wear and tear and prevents buckling [15, 62, 81, 91–94].

3rd valvula (3vv; Figs. 3a, 4d and 6a–d): The relatively short semi-tubular 3rd valvula of *L. distinguendus* emerges at the posterior end of the 2nd valvifer (Fig. 6a–d) and ensheaths and protects the distal part of the terebra when at rest (Fig. 4d). The distally directed microsetae on the medial surface of the 3rd valvula (Fig. 3a) are thought to be involved in the cleaning of the terebra between oviposition episodes [16, 83]. The 3rd valvula might also have a sensory function [27].

1st valvifer (1vf; Figs. 3d and 6a–d, i, j): The 1st valvifer of *L. distinguendus* and other chalcidoids is bow-shaped [17, 19–25, 35–37]. The anteroventral angle of the 1st valvifer features a horizontal ridge, which has a medial–lateral orientation (Fig. 6i) and which is part of the tergo-valvifer articulation (tva; Figs. 3d and 6b, i, j). The posteroventral corner of the 1st valvifer is bifurcated (Fig. 6i) and is part of the intervalvifer articulation (iva; Figs. 3d, g and 6b, i, j). The interarticular ridge (iar; Fig. 6i) lies between the two articulations and might serve mechanically to stabilize the 1st valvifer. The anterodorsal angle of the 1st valvifer is continuous with the dorsal ramus of the 1st valvula (dr1; Figs. 3d, e, g, 5a, c, d, and 6c, j), which is interlocked with the dorsal projection of the 2nd valvifer (dp2; Fig. 5c, d; cf. [31]) by a system analogous to the olistheter. This tight interlocking guides the dorsal ramus and prevents it from buckling when pushing forces are applied during the protraction of the 1st valvula. Since the dorsal ramus constantly slides around the proximal bulbous end of the 2nd valvula during pro- and retraction, the ramus needs to be flexible in the sagittal plane and thus presumably contains high proportions of the elastic rubber-like protein resilin in its cuticle (cf. [95–98]).

2nd valvifer (2vf; Figs. 3d, 4a–c, 5a, c, d and 6a–d, f): The 2nd valvifer is elongated and its posterior part is

(See figure on next page.)

Fig. 4 Terebra of *Lariophagus distinguendus*. **a–d** Light microscopical images of semithin cross sections through the terebra (from proximal to distal; scale bar in d applies to all light micrographs; positions of the sections are indicated in Fig. 6c; cf. Additional file 3). The bulbs and the laminated bridge are visible proximally. The 2nd valvula is connected with the paired 1st valvulae via the olistheter system. **e–k** TEM images of the terebra of *L. distinguendus*. The cuticle of the valvulae is remarkably homogenous. **e** Parts of the laminated bridge on the proximal part of the 2nd valvula (cf. a). **f** Notal membrane (cf. c). **g** Olistheter system comprising the rachis of the 1st valvula and the aulax of the 2nd valvula. **h–k** Apical part of the terebra. The olistheter-like interlock of the 1st valvulae on their dorsomedial surfaces (**h, i, k**) and the coeloconic sensillum at the apical end of one aulax are visible (**j**; for overview image, cf. Fig. 3a). Abbreviations: 1vv: 1st valvula; 2vf: 2nd valvifer; 2vv: 2nd valvula; 3vv: 3rd valvula; au: Aulax; blb: Bulb; cs: Coeloconic sensillum; den: Dendrite; ec: Egg canal; il1: Interlock of the 1st valvulae; lb: Laminated bridge; le: Lateral extensions of the 2nd valvula; lu2: Lumen of the 2nd valvula; m-1vf-gm: 1st valvifer-genital membrane muscle; nm: Notal membrane; oth: Olistheter; rh: Rachis; st2: Sawtooth of the 2nd valvula; vw2: Ventral wall of the 2nd valvula

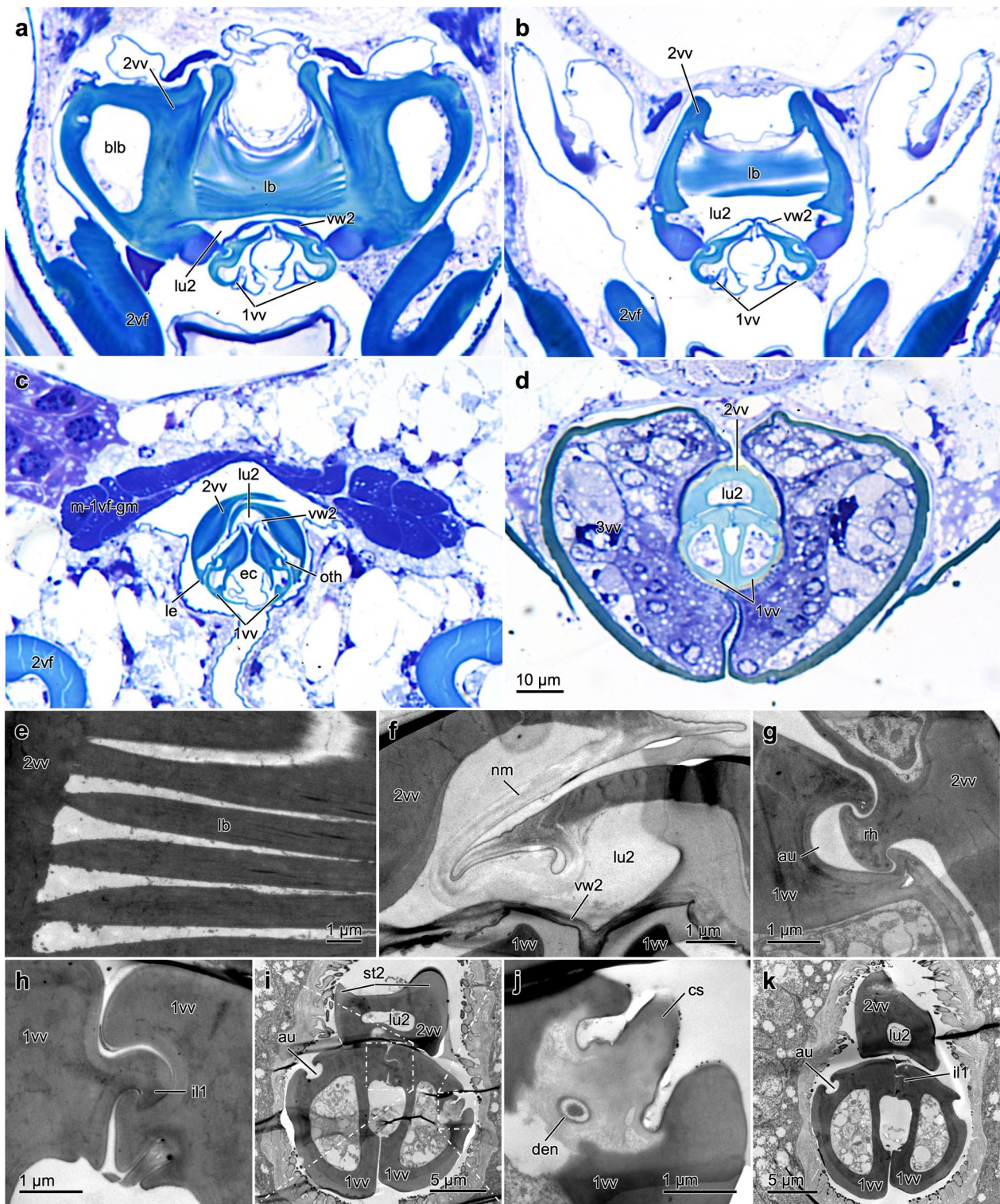


Fig. 4 (See legend on previous page.)

placed medially of the female T9 (Fig. 6b). A conjunctive, called the genital membrane (not shown), connects the ventral margins of the paired 2nd valvifers arching

above the 2nd valvula. The anterior part of the 2nd valvifer of *L. distinguendus* extends dorsally in a semi-circular shape and dorsally bears the dorsal projection of the 2nd

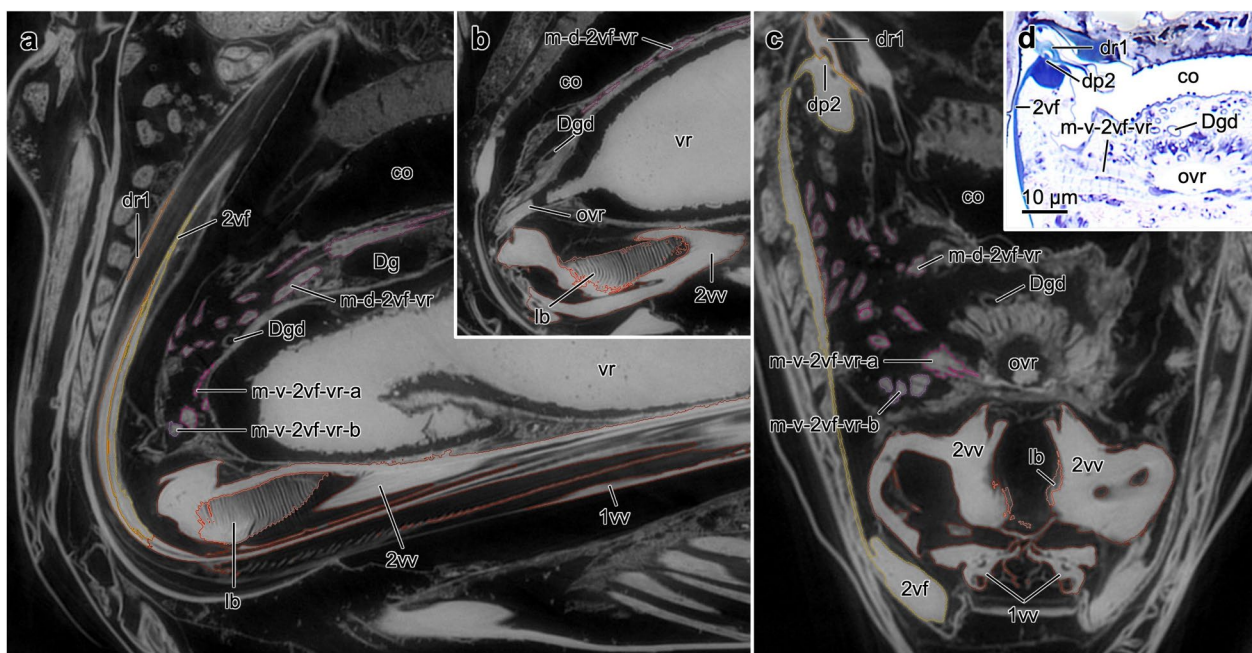


Fig. 5 Ovipositor muscles supporting the venom and reproductive system of *Lariophagus distinguendus*. **a–c** SR- μ CT images of a virtual slices through the anterior part of the ovipositor (**a,b** sagittal view, left is anterior, **c** transversal view) highlighting the muscles supporting the venom and reproductive system, the venom gland reservoir and its orifice, the Dufour's gland and its duct, and the common oviduct (the colour labels correspond to Fig. 6 and Additional file 4). **d** Light microscopical image of a semithin cross section through the ovipositor. The ventral 2nd valvifer-venom gland reservoir muscle with its Z lines is clearly visible. Abbreviations: 1vv: 1st valvula; 2vf: 2nd valvifer; 2vv: 2nd valvula; co: Common oviduct; Dg: Dufour's gland; Dgd: Dufour's gland duct; dp2: Dorsal projection of the 2nd valvifer; dr1: Dorsal ramus of the 1st valvula; lb: Laminated bridge; m-d-2vf-vr: Dorsal 2nd valvifer-venom gland reservoir muscle; m-v-2vf-vr: Ventral 2nd valvifer-venom gland reservoir muscle; m-v-2vf-vr-a: Ventral 2nd valvifer-venom gland reservoir muscle part a; m-v-2vf-vr-b: Ventral 2nd valvifer-venom gland reservoir muscle part b; ovr: orifice of the venom gland reservoir; vr: Venom gland reservoir of the 2nd valvifer

valvifer (dp2; Fig. 5c, d), which is interlocked with the dorsal ramus of the 1st valvula via an interlocking system similar to the olistheter (cf. [31]). At its posterodorsal end and posterior to its medial ridge (mr2; Fig. 6f), the anterior part of the 2nd valvifer features the post-ramus flap (prf; Figs. 3d and 6b; sensu [22]), on which the dorsal projection continues, thus allowing a greater arc of movement of the 1st valvifer and therefore a greater retraction of the 1st valvula. The 2nd valvifer features two sensillar patches: (1) the sensillar patch (sp; Fig. 3d) located anteroventrally to the intervalvifer articulation (iva; Figs. 3d, g and 6b, i, j) and (2) the row of sensilla (sr; Fig. 3e) on the dorsal margin of the 2nd valvifer. These two sensillar patches are in contact with the ventromedial side of the 1st valvifer and the dorsal ramus of the 1st valvula, respectively, and probably monitor the movements of the 1st valvula indirectly. The dorsal margins and the dorsal flanges are strengthened by cuticular ridges that putatively have a stabilizing function and prevent deformation (i.a. at the intervalvifer articulation). The posterodorsal ends of the 2nd valvifers are connected by the median bridge (mb2; Fig. 6c). The venom gland

reservoir (vr; Fig. 5a, b; Additional file 2, min. 0:37–0:52; Additional file 4, min. 0:24–0:31; = acid gland reservoir sensu [19–25, 73]) is situated in between the 2nd valvifers with its proximal end lying near the base of the terebra. The Dufour's gland (Dg; Fig. 5a; Additional file 4, min. 0:21–0:31; = alkaline gland sensu [19–25, 73]) is situated dorsolaterally to the venom gland reservoir (cf. [77, 79]).

Female T9 (T9; Figs. 3d and 6a–d): The female T9 of *L. distinguendus* is U-shaped and situated lateral to the posterior part of the 2nd valvifers (Fig. 6b). Its elongated anteriorly projecting arms articulate with the 1st valvifers via the tergo-valvifer articulations (tva; Figs. 3d and 6b, i, j). The cordate apodeme (not shown) on the anterior margin of the female T9 is located posterior to the articulation. The dorsal margins are strengthened by the anterior flange of T9, which presumably mechanically stabilizes the female T9 during oviposition. Medially, the anterior flange of T9 bifurcates and forms a dorsomedial crest-like ridge that runs almost the entire length of the female T9. This ridge serves as a muscle attachment area both medially and laterally and presumably increases the mechanical stability of the female T9.

Articulations of the musculoskeletal ovipositor system

Basal articulation (ba; Figs. 3h and 6f): The two articular surfaces of this ball-and-socket-like articulation are located on the socket-like pars articularis of the anteroventral part of the 2nd valvifer and the ball-like processus articulated laterally on the bulb of the 2nd valvula. This rotational joint presumably also allows some pivotal and rotational movements of the 2nd valvula and thus of the whole terebra.

Intervalvifer articulation (iva; Figs. 3d, g and 6b, i, j): The 1st and 2nd valvifer are connected via the intervalvifer articulation, a rotational joint that allows a rotation of the 1st valvifer in the sagittal plane only [32]. This articulation consists of the bifurcated posteroventral corner of the 1st valvifer (iva; Fig. 6i), which encloses the articulation site at the 2nd valvifer. Thereby, one furcal structure of the 1st valvifer is placed medially and one laterally to the 2nd valvifer.

Tergo-valvifer articulation (tva; Figs. 3d and 6b, i, j): The 1st valvifer lies adjacent to the female T9 via the tergo-valvifer articulation, which is situated dorsally to the intervalvifer articulation. It is a rotational joint that allows the 1st valvifer to rotate in the sagittal plane only [32]. This articulation consists of a horizontal ridge at the 1st valvifer (tva; Fig. 6i) and a corresponding counterpart at the female T9 situated near the cordate apodeme.

Ovipositor muscles

In total, nine paired ovipositor muscles have been identified that drive and actuate the associated skeletal apparatus (Table 1). Three of these muscles (i.e. the 1st valvifer-genital membrane muscle, the ventral 2nd valvifer-venom gland reservoir muscle and the T9-genital membrane muscle) are described here for the first time in chalcidoids.

1st valvifer-genital membrane muscle (m-1vf-gm; Figs. 4c and 6d, e, f): This muscle is the only muscle of the 1st valvifer. It originates at the medial surface of the posteroventral part of the 1st valvifer, i.e. at the centre between the tergo-valvifer and the intervalvifer articulation (Fig. 6c, d, f), and inserts anteriorly on the genital membrane (Fig. 4c). We here describe the m-1vf-gm for the first time in Chalcidoidea. Previous authors (e.g. [17, 19–25, 36]) might have overlooked its presence because of its minute size.

Dorsal 2nd valvifer-venom gland reservoir muscle (m-d-2vf-vr; Figs. 5a–c and 6d, e, f): This muscle originates at the medial surface of the most anterior part of the 2nd valvifer (Fig. 6c–f) and inserts dorsally at the anterior part of the venom gland reservoir (Fig. 5a, b), which is located ventrally of the common oviduct. Most previous authors (e.g. [17, 19–25]) have overlooked the presence of this muscle; it was only mentioned by [73].

(See figure on next page.)

Fig. 6 Musculoskeletal ovipositor system of *Lariophagus distinguendus*. Segmented 3D model based on SR- μ CT data (perspective view; only the left side of the paired ovipositor elements are depicted; cf. Additional file 4). **a** Orientation of the ovipositor within the metasoma (lateral view, left is anterior; the metasoma is semi-transparent). **b–e** Cuticular elements, articulations and muscles of the ovipositor (**b** lateral view, left is anterior; **c** dorsal view, left is posterior, positions of sections in Fig. 4a–d are indicated here; **d** medial view, left is posterior; **e** frontal view). The ovipositor consists of the following cuticular structures (**b**): 1st valvifer, 1st valvula, 2nd valvifer, 2nd valvula, 3rd valvula and female T9 (9th abdominal tergum). The 1st valvifer is articulated with the 2nd valvifer and the female T9 via the intervalvifer and the tergo-valvifer articulation, respectively (**b**). It is continuous with the dorsal ramus of the 1st valvula (**c**). The 1st and 2nd valvulae form the terebra (1st and 2nd valvulae are not distinguished here). The various ovipositor movements are actuated by a set of nine muscles (**d**): 1st valvifer-genital membrane muscle, dorsal 2nd valvifer-venom gland reservoir muscle, ventral 2nd valvifer-venom gland reservoir muscle part a/b, anterior 2nd valvifer-2nd valvula muscle, posterior 2nd valvifer-2nd valvula muscle, dorsal T9-2nd valvifer muscle part a/b, ventral T9-2nd valvifer muscle, posterior T9-2nd valvifer muscle and T9-genital membrane muscle. **f** Anterior part of the ovipositor (dorsomedial view, left is posterior) highlighting the basal articulation and the three muscles connected to the venom gland reservoir. **g** Base of the terebra featuring the laterally placed bulbs, the laminated bridge and the insertion sites of the anterior and posterior 2nd valvifer-2nd valvula-muscles (i.e. the processus articularis and the processus musculares, respectively) and their orientation (left is anterior; **g** lateral view, **h** dorsal view). **i** Ventral part of the 1st valvifer (posterior view) highlighting the bifurcated posteroventral corner forming one part of the intervalvifer articulation, and the horizontal ridge that is part of the tergo-valvifer articulation. **j** 1st valvifer (lateral view, left is anterior) with dorsal ramus of the 1st valvula. Acting muscle forces are visualized by solid red arrows. Under the simplified assumption that the 2nd valvifer, which acts as the frame of reference, and the female T9 are guided and cannot twist but only slide towards or against each other along the anterior–posterior axis, the input force vectors $F_{m-d-T9-2vf(x)-in}$ and $F_{m-v-T9-2vf(x)-in}$ act in the same plane only at the tergo-valvifer articulation. The distance between the tergo-valvifer articulation (where the force is applied) and the intervalvifer articulation (pivot point/joint axis) is the anatomical inlever a , the effective (= mechanical) inlever is a' ; for torques, see equations (eqs.) 1, 2. The 1st valvifer acts as a lever with the anatomical outlever b being the distance between the intervalvifer articulation and the point at which the 1st valvifer continues as dorsal ramus of the 1st valvula, the effective outlever is b' , resulting in pro- or retraction forces at the dorsal ramus of the 1st valvula $F_{m-d-T9-2vf-out}$ and $F_{m-v-T9-2vf-out}$; see eqs. 3, 4. Abbreviations: 1vf: 1st valvifer; 1vv: 1st valvula; 2vf: 2nd valvifer; 2vv: 2nd valvula; 3vv: 3rd valvula; ba: Basal articulation; blb: Bulb; dr1: Dorsal ramus of the 1st valvula; F : Force; $F_{(x)}$: Horizontal vector component of a force; iar: Interarticular ridge of the 1st valvifer; iva: Intervalvifer articulation; lb: Laminated bridge; m-1vf-gm: 1st valvifer-genital membrane muscle; m-a-2vf-2vv: Anterior 2nd valvifer-2nd valvula muscle; m-d-2vf-vr: Dorsal 2nd valvifer-venom gland reservoir muscle; m-d-T9-2vf-a: Dorsal T9-2nd valvifer muscle part a; m-d-T9-2vf-b: Dorsal T9-2nd valvifer muscle part b; m-p-2vf-2vv: Posterior 2nd valvifer-2nd valvula muscle; m-p-T9-2vf: Posterior T9-2nd valvifer muscle; m-T9-gm: T9-genital membrane muscle; m-v-2vf-vr-a: Ventral 2nd valvifer-venom gland reservoir muscle part a; m-v-2vf-vr-b: Ventral 2nd valvifer-venom gland reservoir muscle part b; m-v-T9-2vf: Ventral T9-2nd valvifer muscle; mb2: Median bridge of the 2nd valvifers; me: Metasoma; mr2: Medial ridge of the 2nd valvifer; prf: Post-ramus flap; T9: Female T9 (9th abdominal tergum); tva: Tergo-valvifer articulation; trb: Terebra

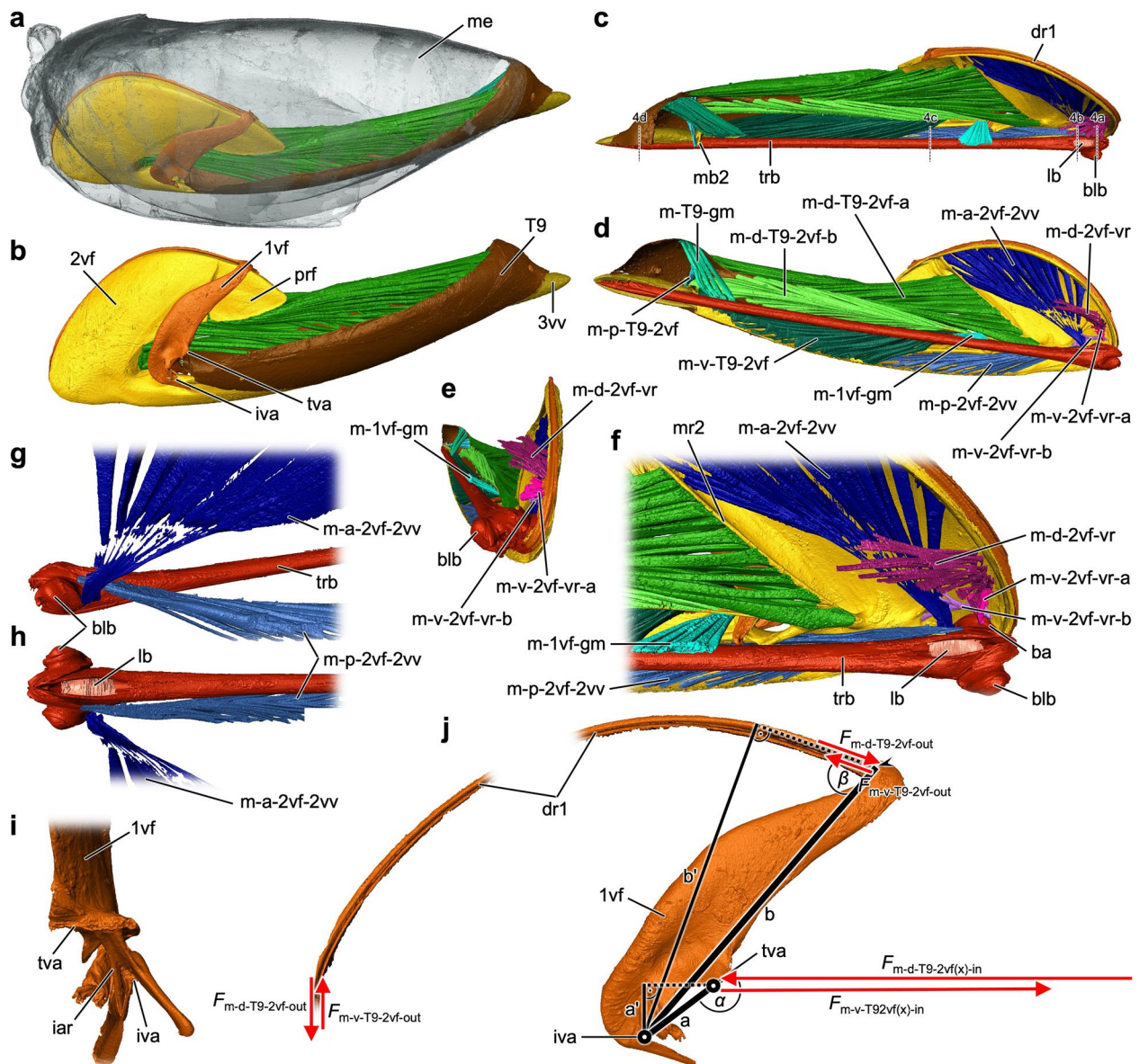


Fig. 6 (See legend on previous page.)

Ventral 2nd valvifer-venom gland reservoir muscle (m-v-2vf-vr-a/b; Figs. 5a, c, d and 6d–f): This muscle forms two distinct bundles. Its anterodorsal part (m-v-2vf-vr-a) originates at the medial surface of the most anterior part of the 2nd valvifer, ventrally to the origin region of the dorsal 2nd valvifer-venom gland reservoir muscle (Fig. 6d–f), and inserts laterally at the orifice the venom gland reservoir (Fig. 5c, d). The other part (m-v-2vf-vr-b) originates at the medial surface of the anterior part of the 2nd valvifer, posteroventrally to the origin region of part a (Fig. 6d–f), and inserts laterally at the orifice of the venom gland reservoir, ventrally to the insertion of part a and shortly before the orifice of

the venom gland reservoir enters the common oviduct (Fig. 5c, d). To our knowledge, this muscle has also not yet been described in chalcidoids (but see [99–101] for the description of a similar set of muscles in ants).

Anterior 2nd valvifer-2nd valvula muscle (m-a-2vf-2vv; Fig. 6d, f, g, h): This muscle originates at the medial region along the anterodorsal arch of the 2nd valvifer (Fig. 6c, d) and inserts at the processus articularis, located laterally on the bulbs of the 2nd valvula (Fig. 6f–h).

Posterior 2nd valvifer-2nd valvula muscle (m-p-2vf-2vv; Fig. 6d, f, g, h): This muscle originates at the medial region along the ventral part of the 2nd valvifer (Fig. 6c, d) and inserts at the processus musculares, located

Table 1 Ovipositor muscles of *Lariophagus distinguendus* (abbreviations in brackets) and their origin, insertion (cf. Additional file 4) and presumed function as verified in the present contribution

Muscle name (abbreviation)	Origin	Insertion	Presumed functions
1st valvifer-genital membrane muscle (m-1vf-gm)*	Medial surface of the posteroventral part of the 1st valvifer, at the centre between the tergo-valvifer and the intervalvifer articulation (Fig. 6c, d, f)	Anteriorly at the genital membrane (Fig. 4c)	Tensor muscle for stabilization of the 1st valvifer during ovipositor movements
Dorsal 2nd valvifer-venom gland reservoir muscle (m-d-2vf-vr)	Medial surface of the most anterior part of the 2nd valvifer (Fig. 6c–f)	Dorsally at the anterior part of the venom gland reservoir (Fig. 5a, b)	Supporting the discharge of venom gland reservoir secretion and probably of Dufour's gland secretion, tensor muscle for stabilization of the 2nd valvifer during ovipositor movements
Ventral 2nd valvifer-venom gland reservoir muscle part a (m-v-2vf-vr-a)*	Medial surface of the most anterior part of the 2nd valvifer, ventrally to the origin of m-d-2vf-vr (Fig. 6d–f)	Laterally at the orifice of the venom gland reservoir (Fig. 5c, d)	Increasing the diameter of the orifice of the venom gland reservoir, thus controlling the venom discharge
Ventral 2nd valvifer-venom gland reservoir muscle part b (m-v-2vf-vr-b)*	Medial surface of the most anterior part of the 2nd valvifer, posterioventrally to the origin of m-v-2vf-vr-a (Fig. 6d–f)	Laterally at the orifice of the venom gland reservoir, ventrally to the insertion of m-v-2vf-vr-a, shortly before the orifice of the venom gland reservoir enters the common oviduct (Fig. 5c, d)	
Anterior 2nd valvifer-2nd valvula muscle (m-a-2vf-2vv)	Medial region along the anterodorsal arch of the 2nd valvifer (Fig. 6c, d)	At the processus articularis on the 2nd valvula, laterally at the bulbs of the 2nd valvula (Fig. 6f–h)	Pulling of the corresponding bulb of the 2nd valvula dorsad (thus inducing lateral bending movements of the terebra) in the active probing position, assistance in the rotation of the terebra during oviposition process, elevator of the terebra back into its resting position (once withdrawn from the substrate), holding the terebra in resting position
Posterior 2nd valvifer-2nd valvula muscle (m-p-2vf-2vv)	Medial region along the ventral part of the 2nd valvifer (Fig. 6c, d)	At the processus musculares on the 2nd valvula, dorsally at the anteriorly directed horn-like processes of the bulbs of the 2nd valvula (Fig. 6f–h)	Rotation of the terebra during oviposition process, inducing partial deformation of the 2nd valvula by moving its two halves tangentially towards each other, holding of the terebra in the active probing position
Dorsal T9-2nd valvifer muscle part a (m-d-T9-2vf-a)	Lateral region along the posterodorsal part of the female T9, laterally along its dorsomedial ridge (Fig. 6a–d)	Anterior section of the dorsal flange of the 2nd valvifer, posterior to its medial ridge (Fig. 6c, d, f)	Protractor of the 1st valvula: moves the 2nd posteriorly and the female T9 anteriorly towards each other, causing the 1st valvifer to tilt anteriorly and thus the 1st valvula to slide distally relative to the 2nd valvula
Dorsal T9-2nd valvifer muscle part b (m-d-T9-2vf-b)	Medial region along the posterodorsal part of the female T9, ventromedially to its dorsomedial ridge (Fig. 6c, d)	Anterior section of the dorsal flange of the 2nd valvifer via a tendon, ventrally to the insertion of m-d-T9-2vf-a (Fig. 6c, d)	
Ventral T9-2nd valvifer muscle (m-v-T9-2vf)	At the cordate apodeme at the anterior margin of the female T9, posteriorly to the tergo-valvifer articulation (Fig. 6c, d)	Medial surface along the posterior section of the dorsal flange of the 2nd valvifer (Fig. 6c, d)	Retractor of the 1st valvula: moves the 2nd anteriorly and the female T9 posteriorly apart from each other, causing the 1st valvifer to tilt posteriorly and thus the 1st valvula to slide proximally relative to the 2nd valvula

Table 1 (continued)

Muscle name (abbreviation)	Origin	Insertion	Presumed functions
Posterior T9-2nd valvifer muscle (m-p-T9-2vf)	Medial surface of the posterodorsal part of the female T9 (Fig. 6c, d)	Median bridge of the 2nd valvifers	Tensor muscle for stabilization by holding the posterior part of the 2nd valvifer in position during ovipositor movements
T9-genital membrane muscle (m-T9-gm)*	Medial surface of the posterodorsal part of the female T9, dorsally of the origin of m-p-T9-2vf (Fig. 6c, d)	Posteriorly at the genital membrane	Tensor muscle for stabilization

The muscles marked with * are described here for the first time in chalcidoids

dorsally on the anteriorly directed horn-like processes of the bulbs of the 2nd valvula (Fig. 6f–h).

Dorsal T9-2nd valvifer muscle (m-d-T9-2vf-a/b; Fig. 6d): This muscle is modified in its insertion and forms two distinct muscle bundles. One part of this muscle (m-d-T9-2vf-a) originates at the lateral region along the posterodorsal part of the female T9, i.e. laterally along its dorsomedial ridge (Fig. 6a–d), and inserts at the anterior section of the dorsal flange of the 2nd valvifer, posterior to its medial ridge (Fig. 6c, d, f). The other part (m-d-T9-2vf-b) originates at the medial region along the posterodorsal part of the female T9, i.e. ventromedially to its dorsomedial ridge (Fig. 6c, d), and inserts at the anterior section of the dorsal flange of the 2nd valvifer via a tendon (t-m-d-T9-2vf-a; Fig. 3g), located ventrally to the insertion region of m-d-T9-2vf-a (Fig. 6c, d).

Ventral T9-2nd valvifer muscle (m-v-T9-2vf; Fig. 6d): This muscle originates at the cordate apodeme, which is located at the anterior margin of the female T9, posteriorly to the tergo-valvifer articulation (Fig. 6c, d), and inserts at the medial surface along the posterior section of the dorsal flange of the 2nd valvifer (Fig. 6c, d).

Posterior T9-2nd valvifer muscle (m-p-T9-2vf; Fig. 6d): This muscle originates at the medial surface of the posterodorsal part of the female T9 (Fig. 6c, d) and inserts at the median bridge of the 2nd valvifers. Previous studies on the chalcidoid ovipositor [17, 19–25] report only one muscle originating in the posterior region of the female T9. The authors presumably were unable to distinguish this muscle from the T9-genital membrane muscle described below.

T9-genital membrane muscle (m-T9-gm; Fig. 6d): This muscle originates at the medial surface of the posterodorsal part of the female T9, dorsally of the origin region of the posterior T9-2nd valvifer muscle (Fig. 6c, d), and inserts posteriorly at the genital membrane. We here describe the m-T9-gm for the first time in Chalcidoidea.

Mechanics and mode of function of the ovipositor system

The set of nine paired ovipositor muscles in *L. distinguendus* comprises two pairs of two antagonistically working muscles that are mainly responsible for the various ovipositor movements, three muscles stabilizing the musculoskeletal system, and two muscles related to the function of the venom gland reservoir (Table 1).

Depression and elevation of the terebra: The 2nd valvula is connected with the 2nd valvifer by a rotational joint called the basal articulation (ba; Figs. 3h, 6f and 7a). Two muscles (m-a-2vf-2vv, m-p-2vf-2vv) insert at the bulbous region around this articulation. The insertion region of the posterior 2nd valvifer-2nd valvula muscle (m-p-2vf-2vv; Fig. 6f–h) at the 2nd valvula is located dorsal of the basal articulation, whereas its region of origin at the 2nd valvifer is located posteroventral to it (Fig. 6c, d). Taxa

from other superfamilies use the m-p-2vf-2vv to depress their terebra towards an active probing position (e.g. Ichneumonidae [31, 32]). However, female *L. distinguendus* have never been observed to depress their terebra in such a manner. Instead, these wasps bend their whole metasoma downwards to bring their terebra into the drilling position. Once the apex of the terebra is engaged in the substrate, the metasoma is lifted upwards again, while the terebra remains in its depressed position (Fig. 2b–d; Additional file 1, min. 0:06–0:11; cf. [45, 47]). This behaviour has also been reported for other pteromalids [40, 46] and species of Torymidae [23], Eurytomidae [21], Encyrtidae (data not yet published) and Eulophidae [19]. Therefore, in pteromalids (and possibly also in other chalcidoid taxa), we assume that the m-p-2vf-2vv is adapted in its function (see paragraph ‘Rotation of the terebra’ of the subchapter ‘Mechanisms of terebra bending and rotation’ below). During this indirect depression of the terebra, the bulbs of the 2nd valvula might be pulled out of the socket-like anterior ends of the 2nd valvifer ventrally by pushing them slightly apart, resulting in a slight translation of the pivot point (= joint axis or fulcrum) of the basal articulation (cf. [32]). The insertion region of the anterior 2nd valvifer-2nd valvula muscle (m-a-2vf-2vv; Fig. 6f–h) at the 2nd valvula is situated posteroventrally of both the basal articulation and the insertion region of m-p-2vf-2vv, whereas its origin at the 2nd valvifer is located posterodorsally of this articulation (Fig. 6c, d). After an oviposition attempt, the terebra is withdrawn from the substrate. Since slender structures such as the terebra can support much higher tensile than compressive stresses, the withdrawal does not damage it [62]. A contraction of the anterior 2nd valvifer-2nd valvula muscle ($F_{m-a-2vf-2vv}$; Fig. 7a) presumably initiates the elevation of the terebra (arrow 9; Fig. 7a; Table 1). The passive rebound of the bulbs of the 2nd valvula into the socket-like anterior ends of the 2nd valvifer presumably further supports the elevation of the terebra passively and helps to stabilize it in its resting position (cf. elevation of the terebra in ceraphronoids, which completely lack the m-a-2vf-2vv [102]). The anatomical cluster comprising the 2nd valvifer, the 2nd valvula and the two muscles connecting them is a simple mechanical system in which the 2nd valvula is a two-armed class 1 lever, whereby the effective (= mechanical) inlever arm and the joint angle (attachment angle) of m-a-2vf-2vv change over the range of motion (cf. [31]).

Pro- and retraction of the 1st valvulae: Three muscles (m-d-T9-2vf, m-v-T9-2vf, m-p-T9-2vf) connect the 2nd valvifer with the female T9. Both of these cuticular structures are connected with the 1st valvifer via the intervalvifer articulation and the tergo-valvifer articulation (iva/tva; Figs. 3d, 6b, i, j and 7a), respectively. The insertion region of both parts of the dorsal T9-2nd valvifer muscle (m-d-T9-2vf-a/b; Fig. 6c, d) at the 2nd valvifer

are situated anterodorsally, whereas their regions of origin at the female T9 are located posterodorsally of both articulations (Fig. 6c, d). A simultaneous contraction of m-d-T9-2vf-a and m-d-T9-2vf-b (summarized as $F_{m-d-T9-2vf}$ Fig. 7a) slides the 2nd valvifer posteriorly with respect to the female T9 (arrow 1; Fig. 7a). This causes the 1st valvifer to tilt anteriorly (arrow 2; Fig. 7a), because it is articulated with both the 2nd valvifer and the female T9 via rotational joints. The 1st valvifer acts as a lever that transforms its tilting movement to the dorsal ramus of the 1st valvula (arrow 3; Fig. 7a). Its tight interlocking with the dorsal projection of the 2nd valvifer prevents it from buckling and transmits the movements to the apex of the 1st valvula, causing it to slide distally relative to the 2nd valvula, i.e. to protract (arrow 4; Fig. 7a; Table 1). In the active probing position, the dorsal ramus is less curved, which presumably reduces friction [32]. The region of origin of the antagonistically acting ventral T9-2nd valvifer muscle at the female T9 (m-v-T9-2vf; Fig. 6c, d) is situated posterodorsally near the intervalvifer articulation and posterior to the tergo-valvifer articulation, whereas its

insertion region at the 2nd valvifer is located posteroventrally of both these articulations (Fig. 6c, d). Its contraction ($F_{m-v-T9-2vf}$; Fig. 7a) slides the 2nd valvifer anteriorly with respect to the female T9 (arrow 5; Fig. 7a), thus indirectly causing the 1st valvifer to tilt posteriorly (arrow 6; Fig. 7a) and the 1st valvula to slide proximally relative to the 2nd valvula, i.e. to retract (arrows 7, 8; Fig. 7a; Table 1). The vibration-like rapid reciprocal alternate pro- and retracting movements of the 1st valvulae are crucial for drilling and precise egg laying (Fig. 2m–p; Additional file 1, min. 1:11–1:35, 1:56–2:22, 3:36–4:00; cf. [32, 44, 47]). The following assumptions have been made for a simplified estimation of the torques (M) exerted by the forces of the dorsal and ventral T9-2nd valvifer muscles ($F_{m-d-T9-2vf}/F_{m-v-T9-2vf}$ Fig. 7a): (1) The 2nd valvifer acts as the frame of reference; therefore, the intervalvifer articulation (iva; Figs. 6i, j and 7a) acts as a pivot point around which the 1st valvifer tilts; (2) the movements of 2nd valvifer and the female T9 are constrained by the musculoskeletal system and cannot twist around the articulations but only slide telescopically towards or against each

(See figure on next page.)

Fig. 7 Mechanisms driving the various ovipositor movements of *Lariophagus distinguendus*, and the importance of the terebra movements during the oviposition process. **a–c** Functional model of the mechanisms driving the various ovipositor movements in the resting and the active probing position (only the left side of the paired ovipositor elements are depicted; not to scale). Acting (input) muscle forces are visualized by solid red arrows and resulting (output) movements by solid black arrows. **a** Mechanism of the tilting movement of the 1st valvifer and the resulting pro- and retraction of the 1st valvulae (lateral view, left is anterior). Only the two pairs of antagonistically working muscles that are responsible for these movements (m-a-2vf-2vv/m-p-2vf-2vv and m-d-T9-2vf/m-v-T9-2vf) are represented in simplified terms. The muscles stabilizing the ovipositor system (m-1vf-gm; m-p-T9-2vf; m-T9-gm) and those supporting the venom and reproductive systems (m-d-2vf-vr; m-v-2vf-vr) are not shown. Contraction of (both parts of) m-d-T9-2vf ($F_{m-d-T9-2vf}$) slides the 2nd valvifer posteriorly and the female T9 anteriorly towards each other (arrow 1), thus indirectly causing the 1st valvifer to tilt anteriorly (arrow 2). This is possible because the 1st valvifer is articulated with both the 2nd valvifer and the female T9 via the intervalvifer and tergo-valvifer articulation, respectively. The 1st valvifer thereby functions as a lever arm that transmits the movement to the dorsal ramus of the 1st valvula (arrow 3) and consequently causes a protraction of the 1st valvula (arrow 4). M-p-T9-2vf and m-T9-gm thereby presumably stabilize the system by holding the 2nd valvifer and the female T9 in position and preventing them from rotating around the articulations. Contraction of m-v-T9-2vf ($F_{m-v-T9-2vf}$) slides the 2nd valvifer anteriorly and the female T9 posteriorly apart from each other (arrow 5), thus causing the 1st valvifer to tilt posteriorly (arrow 6). This movement is transmitted via the dorsal ramus of the 1st valvula (arrow 7) and consequently causes its retraction (arrow 8). When the terebra is withdrawn from the substrate, a contraction of the m-a-2vf-2vv ($F_{m-a-2vf-2vv}$) presumably causes the bulbs to pivot posteriorly around the basal articulation, thus elevating the 2nd valvula and therefore the whole terebra back into its resting position (arrow 9). **b, c** Mechanisms of the bending and rotational movements of the terebra (**b** lateral view, left is anterior; **c** dorsal view; schematic drawing of wasp in lateral view). During oviposition, a contraction of m-a-2vf-2vv cannot elevate the terebra back towards its resting position (as described in other hymenopteran taxa), because the terebra is anchored at the puncture site in the substrate. In this situation, a contraction of one of the paired m-a-2vf-2vv ($F_{m-a-2vf-2vv}$) in the active probing position pulls the corresponding bulb and thus one half of the longitudinally split and asymmetrically overlapping 2nd valvula dorsad along its longitudinal axis (arrow 10) because of the orientation of the muscle and the resulting direction of the force vector. Since the halves of the 2nd valvula are fused at the apex, this movement causes the distal part of the terebra (i.e. the part inside the cavity in the substrate) to bend to the left or right: a contraction of the left m-a-2vf-2vv causes the 2nd valvula and thus the whole terebra to bend to the left (arrow 11), a contraction of the right m-a-2vf-2vv causes a bend to the right. In addition, a contraction of one of the m-p-2vf-2vv ($F_{m-p-2vf-2vv}$) in the active probing position presumably causes the 2nd valvula and thus the whole terebra to rotate back and forth at the basal articulation along its longitudinal axis to a certain degree: a contraction of the left m-p-2vf-2vv causes the 2nd valvula and thus the whole terebra to rotate anti-clockwise when viewed from the dorsal side (arrow 12), whereas a contraction of the right m-p-2vf-2vv results in a clockwise rotation (cf. Additional file 1). Contractions of the m-a-2vf-2vv might support these rotational movements. The rotation allows the bending movements to take effect in different directions. **d** Timeline of the oviposition process of an idiobiont ectoparasitoid wasp highlighting the importance of terebra movements during the various stages (stages in parenthesis do not occur in *L. distinguendus*; stages with * do not occur in all parasitoid lifestyles but are particularly notable in idiobiont ectoparasitoids). Abbreviations: 1vf: 1st valvifer; 1vv: 1st valvula; 2vf: 2nd valvifer; 2vv: 2nd valvula; 3vv: 3rd valvula; ba: Basal articulation; dr1: Dorsal ramus of the 1st valvula; F: Force; iva: Intervalvifer articulation; m-a-2vf-2vv: Anterior 2nd valvifer-2nd valvula muscle; m-d-T9-2vf: Dorsal T9-2nd valvifer muscle; m-p-2vf-2vv: Posterior 2nd valvifer-2nd valvula muscle; m-v-T9-2vf: Ventral T9-2nd valvifer muscle; T9: Female T9 (9th abdominal tergum); tva: Tergo-valvifer articulation; trb: Terebra

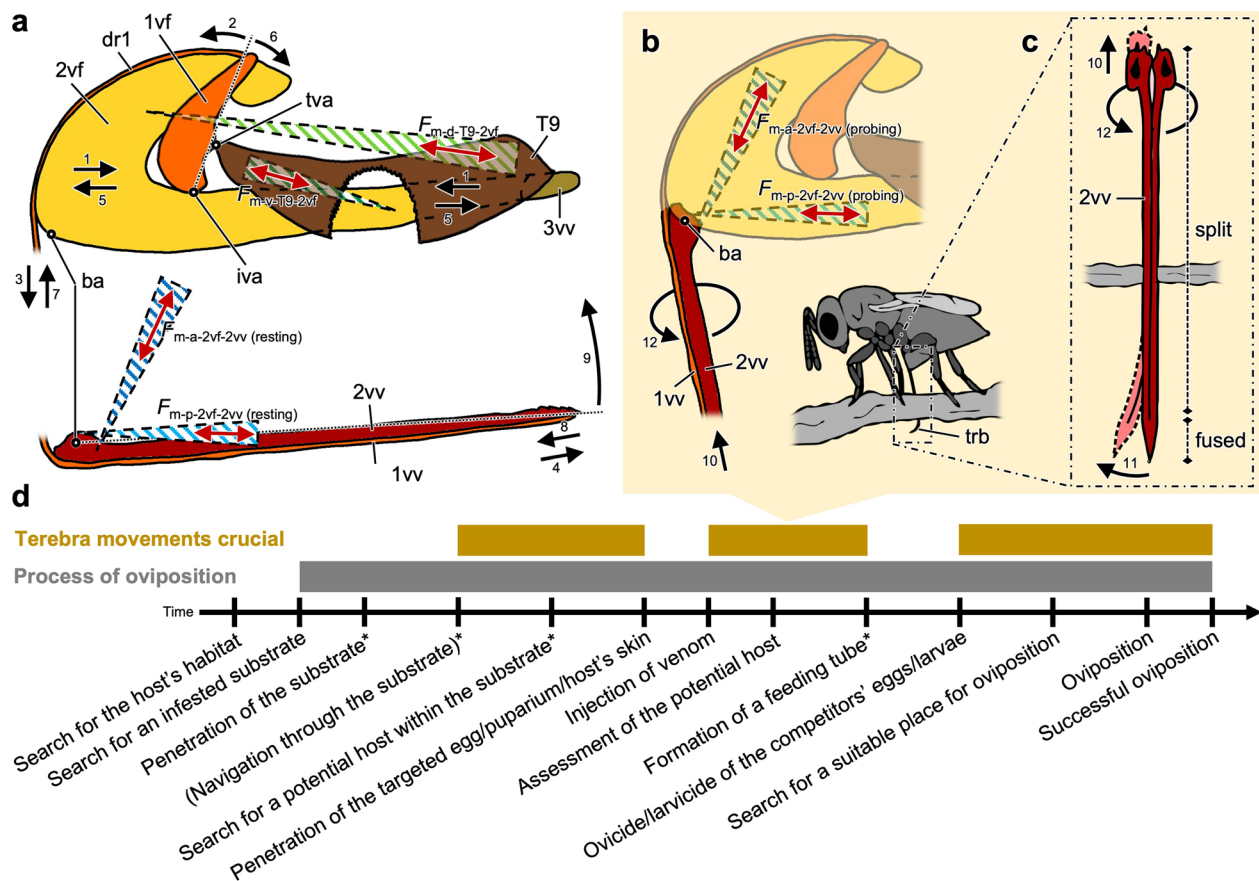


Fig. 7 (See legend on previous page.)

other along the anterior–posterior axis; and (3) frictional forces in the system can be neglected. In reality, all cuticular elements can move relatively to each other. However, under these assumptions, the horizontal force vector components acting in the anterior–posterior axis ($F_{m-d-T9-2vf(x)-in}/F_{m-v-T9-2vf(x)-in}$; Fig. 6j) act at the 1st valvifer at the tergo-valvifer articulation (tva; Figs. 6i, j and 7a). Therefore, the torques (M) of $F_{m-d-T9-2vf}$ and $F_{m-v-T9-2vf}$ that act at the intervalvifer articulation in the resting position can be estimated by using the horizontal vector components ($F_{m-d-T9-2vf(x)-in}/F_{m-v-T9-2vf(x)-in}$; Fig. 6j) of the maximum force of a muscle, the length of the anatomical inlever arm (a ; Fig. 6j), i.e. the distance between the intervalvifer and the tergo-valvifer articulation, and the joint angle (α ; Fig. 6j) according to the equations:

$$M_{m-d-T9-2vf} = F_{m-d-T9-2vf(x)-in} \cdot a \cdot \sin(\alpha) \quad (1)$$

$$M_{m-v-T9-2vf} = F_{m-v-T9-2vf(x)-in} \cdot a \cdot \sin(\alpha) \quad (2)$$

The 1st valvifer acts as a one-armed class 3 lever (force arm smaller than load arm) with the anatomical inlever

(a; Fig. 6j) and the anatomical outlever (b; Fig. 6j), the latter being the distance between the intervalvifer articulation and the point at which the 1st valvifer continues as dorsal ramus of the 1st valvula (arrowhead; Fig. 6j). The resulting pro- and retracting forces at the dorsal ramus of the 1st valvula ($F_{m-d-T9-2vf-out}/F_{m-v-T9-2vf-out}$; Fig. 6j) can be estimated using the horizontal vector components ($F_{m-d-T9-2vf(x)-in}/F_{m-v-T9-2vf(x)-in}$; Fig. 6j) of the forces acting on the 1st valvifer at the tergo-valvifer articulation, the length of the effective inlever arm ($a' = a \cdot \sin(\alpha)$; Fig. 6j) and the effective outlever arm ($b' = b \cdot \sin(\beta)$; Fig. 6j) according to the equations:

$$F_{m-d-T9-2vf-out} = (F_{m-d-T9-2vf(x)-in} \cdot a') / b' \quad (3)$$

$$F_{m-v-T9-2vf-out} = (F_{m-v-T9-2vf(x)-in} \cdot a') / b' \quad (4)$$

The shape of the 1st valvifer and the positions of the intervalvifer and the tergo-valvifer articulations influence the way that the 1st valvula is moved. A comparatively high quotient of the effective outlever to the effective inlever (b'/a' ratio), as observed in *L. distinguendus* (and

other chalcidoid taxa [17, 21–24]), results in a smaller force output but an increase in the potential maximum velocity and mechanical deflection, i.e. an increase in the speed and the movement distance of the 1st valvula [31, 32, 87, 102].

Stabilization of the ovipositor: The small 1st valvifer genital membrane muscle (m-1vf-gm; Figs. 4c and 6d–f) presumably acts as a tensor muscle and stabilizes the 1st valvifers when performing the rapid pivoting movements during substrate drilling, host envenomation and oviposition (Table 1). Additionally, it might also contribute to bringing the 1st valvula into its aligned configuration [32]. The tension of both the T9-genital membrane muscle (m-T9-gm; Fig. 6d) and the posterior T9-2nd valvifer muscle (m-p-T9-2vfv; Fig. 6d) might predominantly serve the stabilization of the ovipositor during oviposition by holding the 2nd valvifers and the female T9 in position and preventing them from rotating around the articulations (Table 1). M-p-T9-2vf is also hypothesized to provide the 3rd valvulae with a certain degree of mobility [20, 22]. However, given its insertion on the median bridge of the 2nd valvifer, this is only possible if a contraction of this muscle is able to cause an elastic deformation of the median bridge, which is connected with the base of the 3rd valvula.

Support of the venom and reproductive system: The dorsal 2nd valvifer-venom gland reservoir muscle (m-d-2vf-vr; Figs. 5a–c and 6d–f) inserts dorsally at the venom gland reservoir. Its contraction presumably supports the discharge of the secretion from both the venom gland reservoir and the Dufour's gland (Table 1; cf. [73, 99, 100, 103]). However, given its medial insertion, it might also act as a tensor muscle stabilizing the 2nd valvifer during the ovipositor movements. The two parts of the ventral 2nd valvifer-venom gland reservoir muscle (m-v-2vf-vr-a/b; Figs. 5a, c, d and 6d–f) insert laterally at the orifice the venom gland reservoir shortly before the latter enters the common oviduct. A contraction of this muscle presumably increases the diameter of the orifice, thereby controlling the venom discharge (Table 1). [35] described a muscle originating at the medial walls of the abdominal sternum 7 and inserting at the vagina; this muscle is postulated to assist in the expulsion of eggs.

Mechanisms of terebra bending and rotation

Various joint-free movement mechanisms have been described in animals (reviewed in [104]), and a variety of steering mechanisms, summarized in the following, have been proposed for the terebra of parasitoid wasps alone (cf. [62]).

The passive bending of the terebra originates from mechanical interactions of the inserted terebra with the surrounding substrate, e.g. the movements of the terebra

of the fruit-fly parasitoid *Diachasmimorpha longicaudata* (Ashmead, 1905) (Braconidae) originate from the interplay between the surrounding substrate and relative movements of the valvulae. The relative position of the individual valvulae featuring geometrically asymmetric bevelled apices create various degrees of geometric asymmetry of the terebra apex. Consequently, the asymmetric substrate reaction forces acting on the apex push it away from a straight path [44], leading to a passive bending of the terebra, which is further facilitated by stiffness gradients in the cuticle of the apical part of the valvulae [105]. The structure and spacing of the ovipositor teeth are also thought to be involved in the passive bending movements of the terebra within plant substrates [106]. Passive bending mechanisms of the terebra are also likely to occur in species of Cynipidae ('ovipositor searching' sensu [107]) and Figitidae [108, 109] while they search for potential host larvae that live in plant substrates, and in species of Torymidae [110] and Agaonidae (fig wasps) [81, 106, 111] during the navigation of the terebra through the plant substrate.

The active bending of the terebra occurs when the bending moments originate from the relative movements of the valvulae, actuated by muscles inside the metasoma, e.g. (1) in species of the Aulacidae and Gasteruptiidae, abrupt terminal stops of the aulaces or protuberances in the ventrolateral side of the 2nd valvula interact with the rhachises or corresponding bosses of the 1st valvulae when the 1st valvulae are protracted and, thus, allow some dorsal bending of the terebra [42]; (2) in several species of the Braconidae, pre-apical 'stop regions' of the rhachis (e.g. swollen regions with scale-like sculptures located centrally within a corresponding widened part of the aulax at rest) increase friction if the 1st valvulae are retracted or extended thereby building up tension and compression and, thus, cause the terebra to curve because of the bending moment distribution [43] (cf. slide-lock working principle according to [104]); (3) in the braconid subfamily Doryctinae, a retraction of the 1st valvula causes the thinned outer walls of the aulaces to restrain the rhachis that features ancillary teeth, consequently resulting in a ventrad bending movement of the terebra [43]; (4) in the braconid genus *Zaglyptogastra*, the distal part of the terebra is formed into multi-arched and unevenly sclerotized regions, with the intermodal arched sections being more heavily sclerotized than the thinner nodes, and thus the protrusion of the 1st valvulae causes a flattening out of the nodal regions and the ventral flexing of the terebra [41]; (5) in several species of the Ichneumonidae, a largely longitudinally divided 2nd valvula, which is fused only at the apex, might allow the terebra to bend left or right when one part of the 2nd valvula is retracted [27]. In all these active bending mechanisms, the extent of bending movement can be controlled

by adjustment of the amplitude of pro-/retraction of the individual valvulae [62]. Most of these parasitoid wasps are able to bend their terebra both dorso-ventrally and laterally, since multilateral steering can be achieved by the interplay of at least three elements [62], or by a rotational movement occurring simultaneously with the bending movement.

Passive and active bending mechanisms can technically act simultaneously or sequentially within the same structure.

During the oviposition process, female *L. distinguendus* were observed actively to bend their terebra in the air (i.e. in a cavity within a substrate) in which passive bending mechanisms can be excluded. The wasps were also observed to be able to pro- and retract the 1st valvula simultaneously with the bending movements (Fig. 2i–l; Additional file 1, min. 0:30–1:10, 1:36–1:44, 3:18–3:34) and independently of the bending state of the 2nd valvula and thus the whole terebra. The 1st valvulae can be protracted far forward and be retracted to a certain degree without significantly changing the bending of the whole terebra (arrowheads; Fig. 2i, k, m–o). This implies that the friction forces between the valvulae, i.e. in the olistheter system, are low. It further implies that no ‘stop regions’ or similar significant mechanical interactions occur between the 1st and 2nd valvulae in *L. distinguendus*. Despite rigorous searches (with scanning electron (SEM) and confocal laser scanning microscope (CLSM)), neither apical ‘stop structures’ in the olistheter nor evidence of a cluster-like occurrence of resilin in the terebra of *L. distinguendus* have been found (Additional file 2). Therefore, we conclude that the active bending mechanisms (1)–(4) mentioned above are not relevant for the terebra bending movements of *L. distinguendus*. The bending mechanisms for lateral and dorso-ventral bending and the rotation of the terebra of *L. distinguendus* are discussed in the following.

Lateral bending of the terebra: During the oviposition process of *L. distinguendus*, the terebra is anchored in the substrate. In this active probing position (Fig. 2a, c–l), a contraction of the anterior 2nd valvifer-2nd valvula muscles cannot elevate the terebra back into the resting position. In this case, however, a contraction of one of the m-a-2vf-2vv ($F_{m-a-2vf-2vv}$; Fig. 7b) presumably pulls the corresponding bulb and thus the longitudinally split and asymmetrically overlapping 2nd valvula dorsad along its longitudinal axis (arrow 10; Fig. 7b, c) because of the orientation of the muscle and the resulting direction of the force vector. Since the two halves of the 2nd valvula are fused at the apex (Figs. 3a and 4d, i, k), this movement causes the distal part of the terebra (the part inside the cavity within the substrate) to bend to the left or right (Fig. 2i–l; Additional file 1, min. 1:02–1:10, 1:36–1:44): a contraction

of the left m-a-2vf-2vv causes the 2nd valvula and thus the whole terebra to bend to the left (arrow 11; Fig. 7b, c; Table 1), whereas a contraction of the right m-a-2vf-2vv causes a bend to the right. The m-a-2vf-2vv in *L. distinguendus* is thus adapted to its lateral bending function of the terebra and no longer serves mainly as its elevator. Furthermore, in the active probing position, a simultaneous contraction of the paired posterior 2nd valvifer 2nd valvula muscles ($F_{m-p-2vf-2vv}$; Fig. 7b) could also move the two overlapping halves of the 2nd valvula tangentially towards each other. However, the extent to which the resulting partial deformation of the 2nd valvula potentially allows local bending needs to be further investigated.

Dorso-ventral bending of the terebra: Female *L. distinguendus* can protract their 1st valvulae far beyond the apex of the 2nd valvula. However, these movements do not cause a dorsad bending movement of the terebra, indicating that no structures in the olistheter impede the movements of the 1st and 2nd valvulae relative to each other. However, a simultaneous retraction of both the 1st valvulae has been postulated to place the terebra under unilateral tension causing the apex to bend ventrad, and a retraction of a single 1st valvula causing the terebra to bend ventrad right or ventrad left [22, 25].

Rotation of the terebra: In the active probing position with the terebra being anchored in the substrate, a contraction of one of the posterior 2nd valvifer-2nd valvula muscles ($F_{m-p-2vf-2vv}$; Fig. 7b) presumably causes the base of the 2nd valvula and thus the whole terebra to rotate at the basal articulation along its longitudinal axis to a certain degree. Even terebra rotations of up to 90° have been observed (Fig. 2n, o; Additional file 1, min. 1:45–1:54), although such extreme rotations are in part attributable to movements of the whole metasoma. Because of the orientation of the muscle in the active probing position and the resulting direction of the force vector, a contraction of the left m-p-2vf-2vv causes the 2nd valvula and thus the terebra to rotate anti-clockwise when viewed from the dorsal side (arrow 12; Fig. 7b, c; Table 1), whereas a contraction of the right m-p-2vf-2vv causes a rotation in a clockwise direction. Contraction of the m-a-2vf-2vv might further support these rotational movements. Alternating contractions of the left and right m-a-2vf-2vv and m-p-2vf-2vv cause a reciprocal rotation of the terebra, as can be observed during substrate penetration and drilling (cf. [25, 36, 60]). A rotation occurring simultaneously with lateral bending movements of the terebra allows the bending to become effective in various directions. The morphological structure of the basal articulations is well adapted for rotational movements (cf. [20]). Since the tendon of m-p-2vf-2vv runs over the curved dorsal side of the bulbous proximal end of the 2nd valvula, the effective inlever will presumably only change

little over the range of motion. However, angular changes have a large impact on the torque that can be generated (cf. [32]) and on the resulting rotation. This mechanism of terebra rotation has also been postulated for other pteromalid [22], chalcidid [36] and aphelinid species [25].

Terebra bending movements in *L. distinguendus* do not result from mechanical interactions between the 1st and 2nd valvulae (as postulated for some species of Aulacidae and Gasteruptionidae [42] and Braconidae [41, 43]). However, the slide-lock working principle (cf. [104]) is attained in a different way. The mechanism relevant for terebra bending in *L. distinguendus* shows similarities with that postulated for species of ophioniform Ichneumonidae, which feature a largely split 2nd valvulae that, like the one of *L. distinguendus*, is fused at the apex only [27, 39]. In these ichneumonid wasps, the pteromalid *L. distinguendus* and possibly also other chalcidoid taxa (see subchapter 'Eco-evolutionary significance of terebra movements' below), the terebra bending is presumably initiated by a bending of the 2nd valvulae solely. The 1st valvulae, which are connected to it via the olistheter, can thus be pro- and retracted to a certain degree without significantly changing the bending state of the 2nd valvulae and thus the whole terebra. This can be advantageous, e.g. for the penetration of the host larva's skin for precise oviposition, whereby, in a bent state of the terebra, often alternating pro- and retraction movements of the 1st valvulae are required.

Whenever the 2nd valvulae is bent in the lateral plane, one side (and thus also the lateral side of the corresponding 1st valvulae) is under compression, with the opposite side being under tension. Both the bending and torsional stiffness of the terebra depend on its geometry, i.e. its cross-sectional shape (cf. [62]), and its material composition, i.e. chitin embedded in a protein matrix of variable mechanical properties (depending on its contents of resilin, arthropodin and sclerotin). The material stiffness of insect cuticle, expressed as Young's modulus, has previously been estimated to range between 0.5–20 GPa [60, 81, 112].

Eco-evolutionary significance of terebra movements

The structure of the terebra of Chalcidoidea, featuring a longitudinally split 2nd valvulae with overlapping, asymmetric halves, is strongly consistent in structure within families and basically similar across families (with the exception of the primitive Mymaridae [18, 39], which recently have been identified as a sister group to all remaining Chalcidoidea [10, 49]), but is unique among other superfamilies of parasitoid Hymenoptera [39]. The similar structure of the terebra of chalcidoid taxa might indicate similar underlying working mechanisms, since form and function are strongly connected [113, 114]. Other chalcidoids are therefore also likely to be able to steer their terebra in a similar manner to that of

L. distinguendus, as such terebra steering movements have also been observed in other species of Pteromalidae during the assessment of a potential host and egg placement [40, 46], in Eurytomidae during egg placement [21], in Eupelmidae during the assessment of a potential host [115] and the ovicide or larvicide of the competitors' eggs and larvae, respectively [116], in species of the Aphelinidae during the ovicide of the competitors' eggs [117–119] and in species of Torymidae [110] and Agaonidae for accurate egg deposition in the plant substrate [81, 106, 111] (although the latter two groups probably use passive bending mechanisms, unlike *L. distinguendus*).

Oviposition is crucial for the reproductive success of insects; thus, oviposition behaviour and ovipositor structure have a central adaptive role [83, 90, 93, 106, 120, 121] that should directly affect fitness. The improved manoeuvrability of the metasoma of the Apocrita, which is essential in the female wasp's probing behaviour when searching or assessing a potential host, is attributed to the evolution of the wasp waist (a constriction between the 1st and 2nd abdominal segment). The presence of a waist was a major innovation in the evolution of Hymenoptera and presumably contributed to the rapid diversification of Apocrita, since it allowed the successful attack of a variety of new hosts [3–5]. However, some chalcidoid wasps, e.g. species of Trichogrammatidae [122], have secondarily lost their wasp waist, presumably during miniaturization. Moreover, the vast majority of Chalcidoidea, although targeting the largest diversity of host taxa among parasitoid wasps [12], are idiobiont ectoparasitoids that develop on enclosed host stages with reduced mobility. Depositing eggs within a substrate provides them and the hatched larvae with the protection of a concealed environment (but without being exposed to the host's immune system, as are endoparasitoids). Thus, in most chalcidoid wasps, as in *L. distinguendus*, a manoeuvrable metasoma does not improve the ability to reach hosts hiding in concealed cavities in hard substrates, since the position of the terebra is anchored at the puncture site. Moreover, drilling is extremely energy- and time-consuming (drilling a hole through a seed grain accounts for approximately 15% of the daily energy budget in a female eupelmid *Eupelmus vuilleti* (Crawford, 1913) [123]) and risky, as the wasps are exposed to predators. In *L. distinguendus* and presumably most chalcidoids that parasitize hosts hidden in hard substrates, the ability actively to bend and rotate the terebra in various directions is crucial during the search for a potential host within the substrate (or the cavity within), a targeted venom injection (e.g. directly into the ganglia [124, 125] or fat bodies of large hosts [126]), the assessment of the potential host, the ovicide and larvicide of the competitors' eggs and larvae, respectively, the search for a

suitable place for oviposition and controlled egg placement (Fig. 7d).

In Chalcidoidea, multiple morpho-physiological and behavioural traits have evolved in correlation with the use of hosts concealed deep within hard substrates, apparently related to several functional demands including host localization, substrate penetration, oviposition and emergence from the substrate (cf. [14]). Modifications or specializations of these traits, such as the ability actively to steer the terebra, may have interacted synergistically to open up new evolutionary pathways (cf. [5]). Adaptations in oviposition behaviour combined with morphological modifications of the terebra and adaptations in the function of certain muscles (i.e. the anterior and posterior 2nd valvifer-2nd valvula muscles) have potentially facilitated the evolution of terebra steering mechanisms, which in turn have facilitated the acquisition of new hosts to a parasitoid's host range. These shifts in host exploitation allow niche partitioning among co-occurring species (cf. [127]) and presumably have led to rapid adaptive radiations in Chalcidoidea [10] (for speciation process in *L. distinguendus* see [128–130]). Thus, the ability actively to steer the terebra potentially has been a central factor in the evolution of the parasitoid life history strategy and the diversification of chalcidoid wasps, resulting in the evolutionary success of this group with its tremendous extant species richness [10, 49]. The Chalcidoidea are the most diverse group of parasitoid hymenopterans, with estimations of more than 500,000 chalcidoid species, the vast majority of them being parasitoids, out of a total of 680,000 parasitoid hymenopteran species [6, 7]. Even larger species numbers might exist because of the possibility of a vast underlying biodiversity of cryptic species (cf. [7, 8, 11]).

Conclusions

Adaptations in oviposition behaviour combined with morphological modifications of the terebra and adaptations in the function of certain muscles allow *L. distinguendus* and presumably also other chalcidoid wasps to steer their terebra in various directions, a crucial skill for the successful oviposition of hosts that are concealed in substrates. Therefore, the evolution of the ability actively to steer the terebra can be considered as a putative key innovation that has largely contributed to the acquisition of new hosts to a parasitoid's host range. Here, we have identified the structural adaptations, i.e. the longitudinally split and asymmetrically overlapping halves of the 2nd valvula that are fused at the apex and the functional adaptations of its associated muscles, and the mechanisms behind these innovations. Further comparative studies are needed to reveal the way in which

morpho-physiological, behavioural, ecological and life history traits have interacted during the evolution and resulted in the enormous radiation of Chalcidoidea.

The terebra of hymenopterans in general and chalcidoids in particular can also act as a suitable biological concept generator, with further investigations into this matter possibly being helpful in the development and the design of slender miniaturized man-made probing tools (cf. [131–134]) for curved steering and drilling.

Methods

The *L. distinguendus* used in this study originate from the laboratory colonies of FuturA GmbH (Borchen, Germany) and Biologische Beratung GmbH (Berlin, Germany), where they were bred on the larvae of *Sitophilus oryzae* (Linnaeus, 1763) (Coleoptera: Curculionidae) that develop endophytically in grain of the common wheat *Triticum aestivum* L.. This host indicates that the *L. distinguendus* used in this study probably belong to the karyotype with 5 chromosomes ('*Sitophilus* Clade 1' sensu [129] or 'GW-lineage' sensu [130], respectively) of the *L. distinguendus* species complex that comprises at least two morphologically indistinguishable cryptic species [135]. The clade/lineage presumably evolved by a host shift from drugstore beetles (*Stegobium paniceum* (Linnaeus, 1758)) to weevils of the genus *Sitophilus* [129]. This shift was probably related to the ability to learn from host-related cues [128].

For lateral overview images, female wasps were imaged with a digital microscope of the type Keyence Digital Microscope VHX-7000 (Keyence Corporation, Osaka, Japan) by using focus stacking.

Images were processed (white/black balancing, cropping) with GIMP version 2.10.30 (<https://www.gimp.org>; RRID:SCR_003182). The schematic drawings were created with Inkscape version 1.1 (<https://www.inkscape.org>; RRID:SCR_014479).

High-resolution videography

The oviposition process of *L. distinguendus* was recorded in an artificial two-part Plexiglas chamber. Each lower chamber element featured a notch (ca. 4 · 1 · 1 mm) at the upper side of the front. Each upper element also featured a notch (ca. 4 · 2 · 4 mm) positioned at the front and lying exactly on that of the lower element. A piece of blotting paper was clamped in between the two elements to divide the space created by the two notches into two compartments. This paper was placed in the breeding substrate of *S. oryzae* for several days before the recording trials for it to take on the hosts' scent (faecal cues) and thus to trigger the wasps to attempt to oviposit. The two chamber elements were then fixed with screws. A female *L. distinguendus* was placed into the upper compartment and

a *S. oryzae* larva in the lower. The front and upper openings of the chamber were subsequently each closed with a clean glass coverslip. The process of oviposition was filmed in a horizontal position by using a Nikon DSC D90 camera (Nikon Corporation, Tokyo, Japan) mounted on a Leica MZ 12.5 stereomicroscope (Leica Microsystems GmbH, Wetzlar, Germany) and with two LED cold-light sources KL 300 LED (Schott AG, Jena, Germany) for sufficient illumination. The focus was adjusted manually.

Scanning electron microscopy (SEM)

For scanning electron microscopy (SEM), we dissected the ovipositor from the genital chamber of ethanol-fixed animals by using fine forceps. Specimens were dehydrated in a graded ethanol (C_2H_6O) series (30, 50, 70, 80, 90, 95 and twice 100% for 30 min each concentration) and air-dried for at least one week in a desiccator with silica gel (Carl Roth GmbH & Co. KG, Karlsruhe, Germany). We mounted the samples with double-sided adhesive carbon tape onto stubs and sputter coated them with 19 nm pure gold (Au) using an Emitech K550X (Quorum Technologies Ltd, West Sussex, UK). Investigation and imaging were performed with a scanning electron microscope of the type Zeiss EVO LS 10 (Carl Zeiss Microscopy GmbH, Jena, Germany) and the software SmartSEM version V05.04.05.00 (Carl Zeiss Microscopy GmbH, Jena, Germany).

Confocal laser scanning microscopy (CLSM) and wide-field epifluorescence microscopy (WFM)

For confocal laser scanning microscopy (CLSM), specimens preserved in 70% ethanol were transferred to glycerol, dissected and further stored in a glycerol (ChemWorld, Kenesaw, GA, USA) droplet on concave microscope slides. Specimens were imaged between two #1.5 coverslips with a confocal laser scanning microscope of the type Nikon A1R-HD (Nikon Corporation, Tokyo, Japan). We used three excitation wavelengths, namely 409, 487 and 560 nm, and three emission ranges, namely 435–470, 500–540 and 570–645 nm. The resulting image sets were assigned pseudo-colours that reflected the fluorescence spectra (blue, green and red, respectively). Volume-rendered micrographs and media files were created using Fiji [136] (https://imagej.net/Fiji;RRID:SCR_002285).

For wide-field epifluorescence microscopy (WFM), we dissected the ovipositor from freshly killed individuals and washed them in distilled water. We mounted them carefully onto cleaned microscope slides (76 mm · 26 mm, VWR International, Radnor, PA, USA), embedded them in glycerol (Croma-Pharma GmbH, Loebendorf, Austria) without staining for observation with an epifluorescence microscope of the type Zeiss Axio

Imager M2 (Carl Zeiss Microscopy GmbH, Jena, Germany) equipped with an ORCA-Flash4.0 V2 Digital CMOS camera C11440-22CU (Hamamatsu Photonics K.K., Hamamatsu, Japan) and the software ZEN 2 pro (blue edition) (Carl Zeiss Microscopy GmbH, Jena, Germany). We used Plan-Apochromat objectives and the following wavelength filters: DAPI (blue, excitation 353 nm, emission 465 nm), ATTO488 (green, excitation 500 nm, emission 525 nm) and Cy5 (red, excitation 650 nm, emission 673 nm).

We superimposed both the CLSM and WFM images in order to show the autofluorescence of the cuticular structures in order to analyse their material composition. Cuticular structures that predominantly show blue autofluorescence are composed of high proportions of the soft and highly elastic rubber-like amorphous protein resilin [98], which has an autofluorescence at a narrow band around 415 nm wavelength [95], whereas cuticular structures that autofluoresce in green are chitinous and non- or weakly sclerotized and those that exhibit red autofluorescence are heavily sclerotized [98, 137].

Sample preparation, light microscopy (LM), transmission electron microscopy (TEM) and image processing

Each female *L. distinguendus* was anaesthetized with carbon dioxide (CO_2) before its metasoma was removed and submersed in fixative solution containing 2.5% glutaraldehyde ($C_5H_8O_2$) and 5% sucrose ($C_{12}H_{22}O_{11}$) buffered with 0.1 M cacodylate ($C_2H_7AsO_2$) buffer (pH 7.4). During this process, the samples were stored in the fixative in small glass vials held in an ice bath at approximately 4 °C for 12 h, following which they were rinsed three times in pre-chilled 0.1 M cacodylate buffer (pH 7.4) for 10 min. After a 4 h period of post-fixation in 1% osmium tetroxide (OsO_4) solution buffered with 0.1 M cacodylate buffer (pH 7.4) in an ice bath, the samples were again rinsed three times in the same buffer. The subsequent steps were performed at room temperature. The samples were dehydrated through a graded ethanol (C_2H_6O) series (30, 50, three times 70, 75, 80, 85, 90, 95 and 100% for three times, 10 min each concentration), containing *en-bloc* staining by using a saturated solution of 70% ethanolic uranyl acetate ($C_4H_6O_6U$) for 12 h. The fully dehydrated samples were then passed through two changes of 100% propylene oxide (C_3H_6O) for 1 h per change and then through increasing concentrations of Spurr low-viscosity embedding resin (Polysciences Inc., Warrington, PA, USA) in propylene oxide with C_3H_6O :Spurr ratios of 3:1, 1:1, 1:3 and 1:7 for 1 h per change and 100% Spurr for 17 h on a rotatory shaker. As a last incubation step, the samples were placed in fresh pure resin for embedment in silicon moulds and polymerized at 70°C for 8 h.

Semithin (600 nm) and ultrathin (60 nm) sections were cut perpendicularly to the terebra of *L. distinguendus* by using an ultramicrotome of the type Leica Ultracut UTC (Leica Microsystems GmbH, Wetzlar, Germany) equipped with a DiATOME histo Jumbo diamond knife (45° knife angle; DiATOME Ltd, Nidau, Switzerland) with a large boat for continuous serial semithin sectioning or a DiATOME ultra diamond knife (35° knife angle; DiATOME Ltd, Nidau, Switzerland) for ultrathin sectioning. We conducted two complete section series through the whole metasoma; one continuous series of semithin sections and one with consecutive alternating series of 20 semithin and 10 ultrathin sections. Microscope slides (76 mm · 26 mm, VWR International, Radnor, PA, USA) for the mounting of semithin serial sections were preliminary stored in a bath containing 96% ethanol and 25% ammonia (NH₃) at a C₂H₆O:NH₃ ratio of 9:1 for at least one week and finally cleaned and stored in distilled water shortly before use. Semithin serial section bands were directly mounted onto these slides and stained with toluidine blue (C₁₅H₁₆ClN₃S) for 60 s on a hot plate at 80°C. After being rinsed with distilled water and dried, the stained sections were embedded in Euparal (Waldeck GmbH & Co. KG, Münster, Germany). Ultrathin sections were placed on Formvar-coated copper slot grids and post-stained with 2% ethanolic uranyl acetate and lead citrate according to Venable and Coggeshall [138] for 20 and 10 min, respectively.

To image the semithin sections, we used a light microscope of the type Zeiss Axioplan (Carl Zeiss Microscopy GmbH, Jena, Germany) equipped with a Nikon D7100 single-lens reflex digital camera (Nikon Corporation, Tokyo, Japan) and the software Helicon Remote version 3.6.2.w (Helicon Soft Ltd, Kharkiv, Ukraine) (for focus stacking Helicon Focus version 6.3.7 Pro; RRID:SCR_014462). After initial image processing (white balancing, colour contrasting, black and white converting, cropping) in Adobe Lightroom version 6.0 (Adobe Systems, San José, CA, USA), the image stack was calibrated with Fiji [136] (<https://imagej.net/Fiji>; RRID:SCR_002285), a distribution of the software ImageJ2 version 2.3.0/1.53f [139, 140] (<https://imagej.net>; RRID:SCR_003070), and imported to the plugin TrakEM2 [141] (RRID:SCR_008954). A preliminary least square rigid alignment followed by an elastic alignment of the image stack was performed using the 'Elastic Stack alignment' plugin [142] in order to create an aligned image stack.

To investigate and image the ultrathin sections, we used a transmission electron microscope of the type Philips/FEI Tecnai 10 (FEI Company, Hillsboro, OR, USA) operated at 80 kV equipped with a side-mounted Gatan Rio9 CMOS camera (Gatan Inc., Pleasanton, CA, USA) and the software Tecnai G² User Interface version 2.1.5 (FEI Company,

Hillsboro, OR, USA) and DigitalMicrograph version 3.32.2403.0 (Gatan Inc., Pleasanton, CA, USA), respectively.

Synchrotron X-ray phase-contrast microtomography (SR- μ CT) and image processing

Two metasomas of ethanol-fixed female *L. distinguendus* were dehydrated stepwise in ethanol and critical-point-dried by using a Polaron 3100 (Quorum Technologies Ltd, West Sussex, UK) to avoid shrinking artefacts by water loss during the tomography procedure. The anterior ends of the metasomas were glued onto plastic pins and mounted onto the goniometer head of the sample stage for tomography. Synchrotron X-ray phase-contrast microtomography (SR- μ CT) [143] was performed at the beamline ID19 at the European Synchrotron Radiation Facility (ESRF; Grenoble, France) at 19.5 keV (wavelength $8 \cdot 10^{-11}$ m). 6000 projections were recorded over a 180° rotation with an effective detector pixel size of 0.3 μ m, and a corresponding field of view of 0.63 · 0.63 mm. The detector consisted of a 4.5 μ m thick LSO:Tb (Tb-doped Lu₂SiO₅) single-crystal scintillator lens (magnification 20 \times , numerical aperture (NA) 0.4) coupled to a sCMOS-based camera type pco.edge 5.5 (Excelitas PCO GmbH, Kelheim, Germany) [144, 145]. The detector-to-sample distance was set to 10 mm. Two separate overlapping image stacks were acquired since the structures of interest were larger than the field of view. The sample was therefore repositioned in between the imaging procedure, resulting in a certain overlap of the two consecutive images. The 3D voxels datasets were reconstructed from 2D radiographs by using the filtered back-projection algorithm [146, 147] developed for parallel-beam tomography.

The two resulting tomograms were registered and calibrated with Fiji [136] (<https://imagej.net/Fiji>; RRID:SCR_002285) and further imported to the plugin TrakEM2 [141] (RRID:SCR_008954) for stitching and cropping. Export of the aligned image stack was performed using a custom script, allowing the export of 16bit image stacks from TrackEM. Subsequently, the resulting image stack was imported to Amira version 6.0 (FEI Company, Hillsboro, OR, USA; RRID:SCR_014305) to pre-segment the various elements of the ovipositor and the whole metasoma in the software's segmentation editor by manually labelling every 25th virtual slice and assigning them to different 'materials'. These labels served as the input for automated segmentation by using the Biomedical Image Segmentation App 'Biomedisa' [148] (<https://biomedisa.org>). After some minor manual corrections to the segmentation results of the 'Biomedisa' output by using Amira, we converted them into polygon meshes. We thereby applied some minor smoothing (unconstrained smoothing, smoothing extent: 2) and polygon reduction to create the final 3D model (surface mesh).

Appendix 1

See Table 2.

Table 2 Morphological terms relevant to the hymenopteran ovipositor system

Anatomical term (abbreviation)	Definition/concept	Synonyms commonly found in literature	URI
1st valvifer (1vf)	The area of the 1st valvifer-1st valvula complex that is proximal to the aulax, bears the 9th tergal condyle of the 1st valvifer and the 2nd valviferal condyle of the 1st valvifer and is connected to the genital membrane by muscle	1. Valvifer [29]; Coin [HAO]; Crosse [HAO]; Écaille du stylet [HAO]; Fulcral plate [17–25, 35–37]; Furcal plate [HAO]; Gonangulum, gonangula [26, 27, 149–152]; Gonocoxite 8 [153]; Gonocoxite XIII [33, 34]; Kidney plate [154]; Plaque triangulaire [50]; Stiletträger [155]; Supporting plate [HAO]; Treibbein [HAO]; Triangular plate [28, 121, 156]; Vorderer Valvifer [29]; Winkel [HAO]; Winkelplatte [155]; Winkelstück [HAO]	http://purl.obolibrary.org/obo/HAO_0000338
1st valvifer-1st valvula complex	The anatomical cluster that is composed of the sclerites that articulates with the 9th abdominal tergite and the 2nd valvifer		http://purl.obolibrary.org/obo/HAO_0002158
1st valvifer-2nd valvifer muscle	The ovipositor muscle that arises from the inter-articular ridge of the 1st valvifer and inserts on the 2nd valvifer		http://purl.obolibrary.org/obo/HAO_0002189
1st valvifer-genital membrane muscle (m-1vfgm)	The ovipositor muscle that arises from the posterior part of the 1st valvifer and inserts anteriorly on the genital membrane anterior to the T9-genital membrane muscle	Anterior tergosternal strictor muscle [34]	http://purl.obolibrary.org/obo/HAO_0001746
1st valvula (1vv)	The area of the 1st valvifer-1st valvula complex that is delimited distally by the proximal margin of the aulax	1. Valvula [29]; 1st gonopophyse [149, 151, 152]; 1st gonapophysis [HAO]; Bohrborste [HAO]; Gonapophysis 8 [153]; Gonapophysis VIII [33, 34]; Gräte [HAO]; Lame de l'aiguillon [HAO]; Lancet [28, 154, 157–159]; Lower valve [16, 26, 27, 42, 43, 85, 88, 90, 93, 160–162]; Première valve [50]; Sägeblatt [HAO]; Sägeplatte [HAO]; Saw [HAO]; Schieber [HAO]; Soie piquante [HAO]; Spicula [HAO]; Stachelgräte [HAO]; Streckborste [29, 45, 155]; Stilet [HAO]; Stylet [17–25, 35–38, 73]; Valvae I [121]; Ventral stylet [163, 164]; Ventral valve [39, 44, 55, 71, 81, 86, 105, 150, 165]; Ventral valvula [163, 164]; Vordere Gonapophyse [HAO]	http://purl.obolibrary.org/obo/HAO_0000339
2nd valvifer (2vf)	The area of the 2nd valvifer-2nd valvula-3rd valvula complex that is proximal to the basal articulation and to the processus musculares and articulates with the female T9	2. Valvifer [29]; 2nd gonocoxa [149–152]; Écaille latérale [HAO]; Gonocoxite 9 [26, 27, 153]; Gonocoxite IX [33, 34]; Hinterer Valvifer [29]; Inner plate [35–37]; ~ Inner ovipositor plate [17–20, 23–25]; Lateral lobes [38]; Oblong plate [28, 121, 156]; Oblongue Platte [29, 155]; Plaque oblongue [HAO]; Portion invaginale [HAO]; Runner plate [154]; Scheide Grundteil [HAO]; Scheidenplatte [HAO]; ~ Semicircular sheet [19–22]; Untere Hälfte der Seitenwand [HAO]; Vordere Platte [HAO]	http://purl.obolibrary.org/obo/HAO_0000927

Table 2 (continued)

Anatomical term (abbreviation)	Definition/concept	Synonyms commonly found in literature	URI
2nd valvifer-2nd valvula-3rd valvula complex	The area that is connected to the 9th tergite and the 1st valvifer via conjunctiva, is articulated to the 1st tergite, and bears the aulax		http://purl.obolibrary.org/obo/HAO_0002175
2nd valvifer-3rd valvula complex	The area of the 2nd valvifer-2nd valvula-3rd valvula complex that is proximal to the basal articulation		http://purl.obolibrary.org/obo/HAO_0002181
2nd valvifer-genital membrane muscle	The ovipositor muscle that arises anteriorly from the dorsal flange of the 2nd valvifer and inserts anteriorly on the dorsal part of the genital membrane		http://purl.obolibrary.org/obo/HAO_0001672
2nd valvifer-venom gland reservoir muscle*	The muscle that arises from the 2nd valvifer and inserts on the venom gland reservoir		http://purl.obolibrary.org/obo/HAO_0002588
2nd valviferal condyle of the 1st valvifer	The condyle that is located on the 1st valvifer and articulates with the 1st valviferal fossa of the 2nd valvifer		http://purl.obolibrary.org/obo/HAO_0002167
2nd valvula (2vw)	The area of the 2nd valvifer-2nd valvula-3rd valvula complex that is distal to the basal articulation and to the processus musculares and is limited medially by the median body axis	2. Valvula [29]; 2nd gonapophyse [149]; 2nd gonapophysis [HAO]; Acus [HAO]; Back piece [HAO]; Branche et tige [HAO]; Corps tige et deux branches [HAO]; Deuxième valve [50]; Dorsal stylet [163, 164]; Dorsal valve [39, 43, 44, 71, 81, 86, 105, 150, 165]; Dorsal valvula [163, 164]; Fused 2nd gonopophyses [151, 152]; Gonapophysis 9 [153]; Gonapophysis IX [33, 34]; Gorgeret [HAO]; Gouttière lamellaire [HAO]; Internal sheath [HAO]; Lance [157]; Median (dorsal) valve [55]; Mittlere Gonapophysen [HAO]; Ovipositor sheath [35]; Ovipositor stylet [HAO]; Schienennrinne [29, 155]; Sheath [17, 18, 25, 38, 73]; Stachelrinne [29, 45]; Stachelschiene [HAO]; String shaft [158]; ~ Stylet (= slender distal part of the united 2nd valvulae) [28, 159]; Stylet sheath [19–24, 36, 37]; Upper valve [16, 26, 27, 42, 43, 85, 88, 90, 93, 160–162]; Valvae II [121]; (Fused) ventral valves [154]	http://purl.obolibrary.org/obo/HAO_0000928

Table 2 (continued)

Anatomical term (abbreviation)	Definition/concept	Synonyms commonly found in literature	URI
3rd valvula (3vv)	The area of the 2nd valvifer-3rd valvula complex that is posterior to the distal vertical conjunctiva of the 2nd valvifer-3rd valvula complex	3. Valvula [29]; Articulating palp [22]; Beborsteres distales Ende der Scheidenplatte [HAO]; Dorsal valve [154]; Fourreau [HAO]; Gaine de l'aiguillon [HAO]; Gonoplac [149–152]; Gonostylus [153, 158]; Gonostylus IX [33, 34]; Hintere Gonapophyse [HAO]; Hülschuppen [HAO]; Klappen [HAO]; Legescheiden [HAO]; Outer sheath [HAO]; Ovipositor sheath [16, 26, 27, 39, 160, 163–165]; Palp [19, 20, 36]; Palp-like appendage [35]; Palp-like termination of the inner plate [35]; Portion évaginale [HAO]; Sensory palp [25, 37]; Sheath [32, 43, 44, 105, 157]; Sheath lobe [28]; Sheath of saw [HAO]; Scheide [HAO]; Scheidenklappe [HAO]; Scheidenspitze [HAO]; Stachelscheide [29, 45, 155]; Stachelstaster [HAO]; Terminal palp [23]; Troisième valve [50]; Valvae III [121]; Valve [HAO]; Valve de fourreau [HAO]; Valve de la gaine du gorgeret [HAO]; Valve du fourreau [HAO]	http://purl.obolibrary.org/obo/HAO_0001012
7th abdominal sternum-vagina muscle*	The muscle that is attached to vagina and to the 7th abdominal sternum	Vaginal muscle [35]	http://purl.obolibrary.org/obo/HAO_0002595
9th tergal condyle of the 1st valvifer	The condyle that is located on the 1st valvifer and articulates with the 1st valviferal fossa of T9		http://purl.obolibrary.org/obo/HAO_0002160
Abdomen	The tagma that is located posterior to the thorax	Hinterleib [29, 45, 155]	http://purl.obolibrary.org/obo/HAO_0000015
Abdominal segment	The segment that is located posterior to the head and does not bear legs		http://purl.obolibrary.org/obo/HAO_0000016
Abdominal segment 7	The abdominal segment that is located between abdominal segment 6 and abdominal segment 8	5th gastral segment [HAO]; 6th metasomal segment [HAO]; 7th abdominal segment [HAO]; Abdominal segment VII [HAO]; Pygidium [HAO]; Segmentum abdominale septimum [HAO]; Segmentum septimum [HAO]	http://purl.obolibrary.org/obo/HAO_0000031
Abdominal segment 8	The abdominal segment that is located between abdominal segment 7 and abdominal segment 9	6th gastral segment [HAO]; 7th metasomal segment [HAO]; 8th abdominal segment [HAO]; Abdominal segment VIII [HAO]; Abdominal-segment 8 [29]; Metasomal segment 7 [HAO]; Segmentum abdominale octavum [HAO]; Segmentum octavum [HAO]	http://purl.obolibrary.org/obo/HAO_0000033

Table 2 (continued)

Anatomical term (abbreviation)	Definition/concept	Synonyms commonly found in literature	URI
Abdominal segment 9	The abdominal segment that is located between abdominal segment 8 and abdominal segment 10	7th gastral segment [HAO]; 8th metasomal segment [HAO]; 9th abdominal segment [HAO]; Abdominal segment IX [HAO]; Abdominal segment 9 [29]; Genital segment [HAO]; Hypopygium [HAO]; Metasomal segment 8 [HAO]; Segmentum abdominale nonum [HAO]; Segmentum nonum [HAO]; Tubular segment 9 [HAO]	http://purl.obolibrary.org/obo/HAO_00000034
Abdominal segment 10	The abdominal segment that is located posterior to abdominal segment 9	8th gastral segment [HAO]; 9th metasomal segment [HAO]; 10th abdominal segment [HAO]; Abdominal segment X [HAO]; Post-genital segment [166]; Segmentum abdominale decimum [HAO]; Segmentum decimum [HAO]	http://purl.obolibrary.org/obo/HAO_00000018
Abdominal sternum	The sternum that is located on the abdominal segment		http://purl.obolibrary.org/obo/HAO_0001425
Abdominal sternum 7	The abdominal sternum that is located on abdominal segment 7	6. Bauchschuppe [HAO]; 7. Sternit [HAO]; 7th abdominal sternite [HAO]; 7th abdominal sternum [HAO]; 7th sternite [35]; 7th sternum [166]; Abdominal sternum 7 [HAO]; Abdominal sternum VII [HAO]; Hypopygium [HAO]; Letzte Bauchschuppe [HAO]; Metasomal sternum VI [HAO]; Plaque ventral [HAO]; Sternum abdominale septimum [HAO]; Sternum septimum [HAO]; Subgenital plate [28, 166]; Subgenitalplatte [HAO]	http://purl.obolibrary.org/obo/HAO_00000044
Abdominal sternum 8	The abdominal sternum that is located on abdominal segment 8	8th abdominal sternite [HAO]; 8th abdominal sternum [HAO]; 8th sternite [35]; Abdominal sternite VIII [HAO]; Abdominal sternum VIII [HAO]; Genital plate [HAO]; Metasomal sternum VII [HAO]; Sternum abdominale octavum [HAO]; Sternum octavum [HAO]	http://purl.obolibrary.org/obo/HAO_0001531
Abdominal sternum 9	The abdominal sternum that is located on abdominal segment 9	9th abdominal sternite [HAO]; 9th abdominal sternum [HAO]; 9th sternal lobe [HAO]; 9th sternite [35]; Annular lamina [HAO]; Hypandrium [HAO]; Hypopygidium [HAO]; Hypopygium [HAO]; Hypotome [HAO]; Lamina subgenitalis [HAO]; Metasomal sternum 8 [HAO]; Metasomal sternum VIII [HAO]; Poculum [HAO]; Postgenital plate [HAO]; Sternum abdominale nonum [HAO]; Sternum nonum [HAO]; Subgenital plate [HAO]	http://purl.obolibrary.org/obo/HAO_00000047
Abdominal sternum 10	The abdominal sternum that is located on abdominal segment 10	10th sternite [35]	http://purl.obolibrary.org/obo/HAO_0001890
Abdominal tergum	The tergum that is located in the abdomen		http://purl.obolibrary.org/obo/HAO_0001426

Table 2 (continued)

Anatomical term (abbreviation)	Definition/concept	Synonyms commonly found in literature	URI
Abdominal tergum 7	The tergum that is located on abdominal segment 7	5th gastral tergite [HAO]; 6th metasomal tergite [HAO]; 7th abdominal tergite [HAO]; 7th abdominal tergum [HAO]; 7th tergite [35]; Abdominal tergum VII [HAO]; Metasomal tergum VI [HAO]; Pygidium [HAO]; Tergum abdominale septimum [HAO]; Tergum septimum [HAO]	http://purl.obolibrary.org/obo/HAO_00000060
Abdominal tergum 8	The tergum that is located on abdominal segment 8	6th gastral tergite [HAO]; 7. Rückensegment [HAO]; 7th metasomal hemitergite [158]; 7th metasomal tergite [HAO]; 7th metasomal tergum [HAO]; 8. Tergit [HAO]; 8° tergite [HAO]; 8th abdominal tergite [HAO]; 8th abdominal tergum [HAO]; 8th hemitergite [HAO]; 8th tergite [35]; 8th tergum [28]; Abdominal terga 8 [HAO]; Abdominal tergite VIII [HAO]; Epigynum [HAO]; Epipygium [HAO]; Lamella basalis superior [HAO]; Metasomal tergum VII [HAO]; Plaque oblongue [HAO]; Plaque stigmatifère [HAO]; Plaque stigmatique [HAO]; Spiracle (plate) [20, 22, 23, 25]; Spiracular plate [28]; Stigmenplatte [HAO]; T8 [HAO]; Tergite 8 [HAO]; Tergitplatte [HAO]; Tergum abdominale octavum [HAO]; Tergum octavum [HAO]; Trachealplatte [HAO]; Tracheenplatte [HAO]	http://purl.obolibrary.org/obo/HAO_00000061
Abdominal tergum 9	(cf. Female T9)	(cf. Female T9)	(cf. Female T9)
Abdominal tergum 10	The tergum that is located on abdominal segment 10	8th gastral tergite [HAO]; 8th gastral tergum [HAO]; 9th metasomal tergite [HAO]; 9th metasomal tergum [HAO]; 10th abdominal tergite [HAO]; 10th tergite [35]; Abdominal tergum X [HAO]; Epipygium [HAO]; Tergum abdominale decimum [HAO]; Tergum decimum [HAO]	http://purl.obolibrary.org/obo/HAO_00000052
Accessory gland	The gland that empties into one of the reproductive ducts		http://purl.obolibrary.org/obo/HAO_00000078
Acellular anatomical structure	Anatomical structure that consists of cell parts and cell substances and together does not constitute a cell or a tissue		http://purl.obolibrary.org/obo/HAO_00000040
Anatomical cluster	The anatomical group that has its parts adjacent to one another		http://purl.obolibrary.org/obo/HAO_00000041
Anatomical entity	Biological entity that is either an individual member of a biological species or constitutes the structural organization of an individual member of a biological species		http://purl.obolibrary.org/obo/HAO_00000000

Table 2 (continued)

Anatomical term (abbreviation)	Definition/concept	Synonyms commonly found in literature	URI
Anatomical group	Anatomical structure consisting of at least two non-overlapping organs, multi-tissue aggregates or portion of tissues or cells of different types that does not constitute an organism, organ, multi-tissue aggregate, or portion of tissue		http://purl.obolibrary.org/obo/HAO_0000054
Anatomical region	A 3D region in space without well-defined compartmental boundaries; for example, the dorsal region of an ectoderm		http://purl.obolibrary.org/obo/HAO_0001980
Anatomical structure	Material anatomical entity which has an inherent 3D shape and is generated by coordinated expression of the organism's own genome		http://purl.obolibrary.org/obo/HAO_0000003
Anatomical system	Anatomical group that has as its parts distinct anatomical structures interconnected by anatomical structures at a lower level of granularity		http://purl.obolibrary.org/obo/HAO_0000011
Annulus	The carina that is transverse and extends across the lateral wall of the terebra		http://purl.obolibrary.org/obo/HAO_0001173
Anterior	Anatomical region anteriorly located on the body or body part		http://purl.obolibrary.org/obo/BSPO_0000071
Anterior 2nd valvifer-2nd valvula muscle (m-a-2vf-2vv)	The ovipositor muscle that arises from the anterodorsal part of the 2nd valvifer and inserts subapically on the processus articularis	Anterior gonocoxapophyseal muscle [33, 34]; Gonapophysys 9 levator [153]; Ramus muscle of the 2nd valvula [28]; Ramus muscle of the 2nd valvulae [166]; Shaft elevator muscle [25]; Sting levator [156]	http://purl.obolibrary.org/obo/HAO_0001166
Anterior angle of the 1st valvifer	The corner on the 1st valvifer that marks the posterior end of the 1st valvula		http://purl.obolibrary.org/obo/HAO_0002168
Anterior area of the 2nd valvifer	The area of the 2nd valvifer which is anterior to the anatomical line that is the shortest distance from the 1st valvifer fossa of the 2nd valvifer and the ventral margin of the 2nd valvifer		http://purl.obolibrary.org/obo/HAO_0002169
Anterior flange of abdominal tergum 9	The flange that extends along the anterolateral margin of female T9	Apodem [29]; Chitinous rib [37]; Chitinous rib of the outer plate [35]	http://purl.obolibrary.org/obo/HAO_0001171
Anterior flange of the 1st valvifer	The flange that extends anteriorly on the 1st valvifer and overlaps with the posterior margin of the anterior area of the 2nd valvifer		http://purl.obolibrary.org/obo/HAO_0002166
Anterior notch of the dorsal valve	The notch that is on the anterior region of the dorsal valve (= composite structure of the fused 2nd valvulae) and accommodates the ventral ramus of the 2nd valvula and the 1st valvula		http://purl.obolibrary.org/obo/HAO_0002178

Table 2 (continued)

Anatomical term (abbreviation)	Definition/concept	Synonyms commonly found in literature	URI
Anterior ridge of T9	The ridge that extends along the anterior margin of female T9 and receives the site of origin of the ventral and the dorsal T9-2nd valvifer muscles		http://purl.obolibrary.org/obo/HAO_0002182
Anterior section of dorsal flange of the 2nd valvifer	The area of the anterior area of the 2nd valvifer that is anterior to the site of origin of the basal line, continuous with the dorsal flange of the 2nd valvifer and marks the site of origin of the dorsal T9-2nd valvifer muscle part b	~ Falcate plate [35]; ~ Pivoting sclerite [36]; ~ Semicircular sheet [19–25]	http://purl.obolibrary.org/obo/HAO_0002173
Apical	Anatomical region located on the apical end on the body or body part	Distal [BSPO]	http://purl.obolibrary.org/obo/BSPO_0000073
Apodeme	The process that is internal		
Aporous sensillum	The sensillum whose cuticular component is without any opening		http://purl.obolibrary.org/obo/HAO_0000142 http://purl.obolibrary.org/obo/HAO_0001964
Appendage	The anatomical structure that is encircled by the evagination of the integument and whose integumental components are attached to the body via muscles		http://purl.obolibrary.org/obo/HAO_0000144
Area	The anatomical structure of the cuticle that is delimited by material or immaterial anatomical entities	Portion of cuticle [HAO]	http://purl.obolibrary.org/obo/HAO_0000146
Articular surface	The area that is located on the sclerite and that makes movable direct contact with another sclerite	Articulation [HAO]	http://purl.obolibrary.org/obo/HAO_0001485
Articulation	The anatomical cluster that is composed of two adjacent articular surfaces		http://purl.obolibrary.org/obo/HAO_0000151
Aulax (au)	The impression that is on the 1st valvifer-1st valvula complex accommodates the rhachis	Falze der Stechborste [155]; Groove [17, 19, 20, 22, 25, 36, 37, 166]	http://purl.obolibrary.org/obo/HAO_0000152
Basal	Anatomical region located basally on the body or body part	Proximal [BSPO]	http://purl.obolibrary.org/obo/BSPO_0000074
Basal articulation (ba)	The articulation that is part of the 2nd valvifer-2nd valvula-3rd valvula complex and adjacent to the rhachis	Basalgelenk [29]; Bulbous articulation [17, 19, 20, 22, 24, 25, 153]	http://purl.obolibrary.org/obo/HAO_0001177
Basal line of the 2nd valvifer	The line on the 2nd valvifer that extends between the pars articularis and the dorsal flange of 2nd valvifer		http://purl.obolibrary.org/obo/HAO_0002171
Body	The anatomical cluster that is composed of the whole organism but which excludes the antennae, legs and wings	Trunk [HAO]	http://purl.obolibrary.org/obo/HAO_0000182

Table 2 (continued)

Anatomical term (abbreviation)	Definition/concept	Synonyms commonly found in literature	URI
Bulb (bib)	The anterior area of the dorsal valve (= composite structure of the fused 2nd valvulae) that is bulbous	Backen [155]; Bulbous basal part of the united 2nd valvulae [28]; Bulbous sockets [20, 22, 24]; Pivoting process [36]; Rotatory process [36, 37]; Sockets [25]	http://purl.obolibrary.org/obo/HAO_0002177
Calyx*	The broadened portion of the lateral oviduct is enlarged and contains virus particles (characterized by bluish autofluorescence)	Calyx gland [26]; Eierkelch [HAO]	http://purl.obolibrary.org/obo/HAO_0000186
Captivated compound organ	Compound organ that contains one or more macroscopic spaces		http://purl.obolibrary.org/obo/HAO_0000072
Carina	The process that is elongate and external	Crest [HAO]; Lamella [HAO]; Lamina [HAO]; Ledge [HAO]; Ridge [HAO]	http://purl.obolibrary.org/obo/HAO_0000188
Cell	Anatomical structure that has its parts a maximally connected cell compartment surrounded by a plasma membrane		http://purl.obolibrary.org/obo/HAO_0000013
Cercus	The sense organ that is located apicolaterally on one of the apicalmost terga and attaches to a large nerve cord	Acrocercus [HAO]; Appendix genitalis [HAO]; Circus [36]; Penicillus [HAO]; Pygopod [HAO]; Pygostyle [20, 22–24]; Pygostylus [HAO]; Sensory appendage [37]; Sensory plate [35, 37]; Socius [29]	http://purl.obolibrary.org/obo/HAO_0000191
Colleterial gland	The glandula mucosa that secretes an adhesive substance used to fasten the eggs to a support	Accessory gland [72, 73]; Collateral gland [27]; Glande accessoire [50]; Glandula mucosa [HAO]; Lubricating gland [72]; Uterine gland [27]; Uterus gland [26]; Vaginal gland [27]	http://purl.obolibrary.org/obo/HAO_0000214
Common oviduct (co)*	The duct that is unpaired and connects the lateral oviducts with the vagina through the gonopore	Median oviduct [HAO]; --Vagina [20, 22, 23, 25, 73, 75]	http://purl.obolibrary.org/obo/HAO_0002601
Compound organ	Anatomical structure that has as its parts two or more multi-tissue structures of at least two different types and which through specific morphogenetic processes forms a single distinct structural unit demarcated by bona fide boundaries from other distinct anatomical structures of different types		http://purl.obolibrary.org/obo/HAO_0000024
Condyle	The articular surface that is convex and is inserted into the fossa of an adjacent sclerite		http://purl.obolibrary.org/obo/HAO_0000220
Conjunctiva	The area of the cuticle that is weakly sclerotized, with thin exocuticle	Arthropodial membrane [HAO]; Corium [HAO]	http://purl.obolibrary.org/obo/HAO_0000221
Cordate apodeme	The apodeme on the anterior margin of female T9. The ventral T9-2nd valvifer muscle attaches partly on the apodeme	Apophyse [29]	http://purl.obolibrary.org/obo/HAO_0001585

Table 2 (continued)

Anatomical term (abbreviation)	Definition/concept	Synonyms commonly found in literature	URI
Corner	The projection that is located at the intersection of two or more edges		http://purl.obolibrary.org/obo/HAO_0000223
Ctenidium (ct)	The process that is located on the annulus	~Oblique ridge [86]; (Ovipositor) scales [71]	http://purl.obolibrary.org/obo/HAO_0001190
Cuticle	The acellular anatomical structure that is the external layer of the integument (covers a body surface as well as lines ectodermal invaginations such as stomodeum, proctodeum and tracheae) and produced by epidermis cells	Cuticula [HAO]; Exoskeleton [HAO]	http://purl.obolibrary.org/obo/HAO_0000240
Cuticular invagination	The area where the cuticle is invaginated	Invagination [HAO]	http://purl.obolibrary.org/obo/HAO_0002021
Depression	The area that is external, concave, point-like and does not correspond to an apodeme	Fovea [HAO]; Pit [HAO]; Trough [HAO]	http://purl.obolibrary.org/obo/HAO_0000241
Distal notch of the dorsal valve	The notch that is distal on the dorsal valve (= composite structure of the fused 2nd valvulae)		http://purl.obolibrary.org/obo/HAO_0002179
Distal vertical conjunctiva of the 2nd valvifer-3rd valvula complex	The conjunctiva that traverses the 2nd valvifer-3rd valvula complex and is located distal to the median bridge of the 2nd valvifers		http://purl.obolibrary.org/obo/HAO_0002180
Dorsal	Anatomical region dorsally located on the body or body part		http://purl.obolibrary.org/obo/BSPO_0000079
Dorsal 2nd valvifer-venom gland reservoir muscle (m-d-2vf-vr)*	The 2nd valvifer-venom gland reservoir muscle that originates at the medial surface of the anterior part of the 2nd valvifer and inserts dorsally at the anterior part of the venom gland reservoir		http://purl.obolibrary.org/obo/HAO_0002597
Dorsal flange of the 2nd valvifer	The flange that extends on the dorsal margin of the 2nd valvifer. Part of the ventral T9-2nd valvifer muscle attaches to the flange	Chitinous rib of the inner plate [35]; Dorsale Verdickungsleiste [29]; Inner longitudinal rib (of the inner plate) [37]	http://purl.obolibrary.org/obo/HAO_0001577
Dorsal projection of the 2nd valvifer (dp2)	The projection that is located on the 2nd valvifer and corresponds to the proximal end of the rhamphus	~ Ramus edge [19–22, 25]	http://purl.obolibrary.org/obo/HAO_0002172
Dorsal ramus of the 1st valvula (dr1)	The region that extends along the dorsal margin of the 1st valvula and bears the aulax	1st ramus [167]; Arc chitineux [50]; Diverging arm of the stylet [35]; Ramus der 1. Valvula [29]; Ramus of the 1st gonapophysis [150]; Ramus of the 1st valvula [28, 168]; Stechborstenbogen [29]	http://purl.obolibrary.org/obo/HAO_0001579
Dorsal ramus of the 2nd valvula	The area that extends along the dorsal margin of the 2nd valvula, bears the processus articularis anteriorly and the processus musculares on the antero-dorsal region and articulates with the 2nd valvifer via the basal articulation	2nd ramus [167]; Diverging arm of the ovipositor sheath [35]; Ramus der 2. Valvula [29]; Ramus of the 2nd gonapophysis [150]; Schienenbogen [29, 155]	http://purl.obolibrary.org/obo/HAO_0002190
Dorsal sclerite of the 1st valvifer	The sclerite of the 1st valvifer that is located dorsally of the transvalviferal conjunctiva		http://purl.obolibrary.org/obo/HAO_0002163

Table 2 (continued)

Anatomical term (abbreviation)	Definition/concept	Synonyms commonly found in literature	URI
Dorsal T8-T9 muscle	The abdominal muscle that arises from the anteromedian margin of female T8 and inserts on the anteromedian margin of female T9		http://purl.obolibrary.org/obo/HAO_0001571
Dorsal T9-2nd valvifer muscle (m-d-T9-2vf)	The ovipositor muscle that arises along the posterodorsal part of the anterior margin of female T9 and inserts on the anterior section of the dorsal flanges of the 2nd valvifer	Anterior tergal muscle [166]; Anterior tergoanocoxal muscle [33, 34]; Dorsal/ventral (= part a/part b) anterior tergal muscle of the 2nd valvifer [28]; Extensor muscles of lancet [154]; Upper/lower (= part a/part b) protractor of gonapophysis 8 [153]; Upper/lower (= part a/part b) stylet protractor muscle [25]	http://purl.obolibrary.org/obo/HAO_0001569
Dorsal valve	The area that is articulated with the right and left 2nd valvifers at the basal articulation and bears the rhachises. (Term sometimes used for the composite structure of the fused 2nd valvulae)	(cf. 2nd valvula)	http://purl.obolibrary.org/obo/HAO_0001658
Duct	The captivated compound organ that is canal-like, layered with epithelial cells and leads to an exocrine gland or organ		http://purl.obolibrary.org/obo/HAO_0000282
Dufour's gland (Dg)*	The accessory gland that is not paired and empties into the female reproductive duct and is composed of class III gland cells	Alkaline gland [19–25, 73]; Glande alkaline [50]; Lubricating gland [89]; Tubular gland [73]	http://purl.obolibrary.org/obo/HAO_0002591
Dufour's gland duct (Dgd)*	The duct that is the proximal-most section of the Dufour's gland between the gland orifice and the Dufour's gland closing muscles	Duct of the acid gland [73]; Stalk (of the Dufour's gland) [77, 79]	http://purl.obolibrary.org/obo/HAO_0002600
Edge	The margin that extends along the border of two areas that are oriented differently		http://purl.obolibrary.org/obo/HAO_0000285
Egg canal (ec)	The anatomical space that is between the left and right olistheters	Central canal [36]; Egg passage [35]; Eikanal [29]; Innenkanal [29, 155]	http://purl.obolibrary.org/obo/HAO_0002191
External female genitalia	The anatomical cluster that is composed of the vagina, spermatheca and the ovipositor apparatus		http://purl.obolibrary.org/obo/HAO_0001768
Female genitalia	The genitalia that is part of the female organism		http://purl.obolibrary.org/obo/HAO_0000324
Female T8	The tergite that is connected to female T9 by muscles	(cf. Abdominal tergum 8)	http://purl.obolibrary.org/obo/HAO_0002188

Table 2 (continued)

Anatomical term (abbreviation)	Definition/concept	Synonyms commonly found in literature	URI
Female T9 (T9)	The tergite that is articulated with the 1st valvifer and is connected to the 2nd valvifer via muscles	8th metasomal hemitergite [158]; 9. Tergit [29]; 9 ^o tergite [HAO]; 9th abdominal tergite [26, 32]; 9th hemitergite [HAO]; 9th tergite [35, 75, 157]; 9th tergum [28]; Abdominal tergum 9 [HAO]; After-platte [HAO]; Anal plate [HAO]; Anterior lobes [38]; Anterior plate [HAO]; Écaille anale [HAO]; Écaille chitineuse [HAO]; Epandrium [HAO]; Epipygium [HAO]; Epipygium [HAO]; Flattened plate [38]; Hintere Platte [155]; Hypopygial valve [HAO]; Lamine externe [HAO]; Lateral plates [89]; Obere Hälfte der Seitenwand [HAO]; Outer ovipositor plate [17–25]; Outer plate (of ovipositor) [35–37]; Plaque carrée [50]; Plaque quadratique [HAO]; Quadrate plate [28, 121, 150, 156]; Quadratische Platte [29, 155]; Quadratplatte [HAO]; Sled plate [154]; T9 [27, 30, 32, 102, 168–170]; Terga 9 [163, 164]; Tergite 9 [83, 153]; Tergite IX [33, 34]; Tergum 9 [30, 168–171]; Tergum IX [167]; Tergum abdominale nonum [HAO]; Tergum nonum [HAO]	http://purl.obolibrary.org/obo/HAO_0000075
Flange	The projection that is lamella-like and is located on a rim, carina, apodeme or edge	Crest [HAO]	http://purl.obolibrary.org/obo/HAO_0000344
Foramen	The anatomical space that is surrounded by sclerites and allows for the passage of haemolymph, nerves and tracheae		http://purl.obolibrary.org/obo/HAO_0000345
Fossa	The articular surface that is concave and accommodates the condyle of another sclerite	Acetabulum [HAO]	http://purl.obolibrary.org/obo/HAO_0000353
Furcula (fu)	The sclerite that is proximal to the 2nd valvifer and receives the site of origin of the posterior 2nd valvifer-2nd valvula muscle	Chitinos fork of the vagina [36]; Gabelbein [29]; V-shaped sclerite [35]	http://purl.obolibrary.org/obo/HAO_0002498
Gaster	The anatomical cluster that is composed of all abdominal segments posterior to abdominal segment 2		http://purl.obolibrary.org/obo/HAO_0000369
Genital membrane	The conjunctiva that connects the ventral margins of the 2nd valvifers arching above the 2nd valvula		http://purl.obolibrary.org/obo/HAO_0001757
Germarium*	Anterior region of the ovariole, that is connected to posterior egg chambers		http://purl.obolibrary.org/obo/FAO_00004866
Gland	The anatomical cluster that is composed of epithelial cell(s) that secrete or excrete materials not related to their ordinary metabolic needs		http://purl.obolibrary.org/obo/HAO_0000375

Table 2 (continued)

Anatomical term (abbreviation)	Definition/concept	Synonyms commonly found in literature	URI
Gonopore*	The anatomical space that is the transition from the common oviduct to the vagina		http://purl.obolibrary.org/obo/HAO_0002602
Groove	The line that is located on the sclerite and is impressed		http://purl.obolibrary.org/obo/HAO_0001525
Hypopygium	The abdominal sternum that is the posteriormost visible sclerite located ventrally in the abdomen	Hypandrium [HAO]; Subgenital plate [HAO]	http://purl.obolibrary.org/obo/HAO_0000410
Immaterial anatomical entity	Anatomical entity that has no mass		http://purl.obolibrary.org/obo/HAO_0000007
Impression	The groove that does not correspond to a ridge	Groove [HAO]	http://purl.obolibrary.org/obo/HAO_0000417
Integument	The anatomical system that forms the covering layer of the animal, ectodermal in origin and composed of epidermal cells producing the cuticle	Body wall [HAO]	http://purl.obolibrary.org/obo/HAO_0000421
Interarticular ridge of the 1st valvifer (iar)	The ridge that extends along the posterior margin of the 1st valvifer between the intervalvifer and tergovalvifer articulations		http://purl.obolibrary.org/obo/HAO_0001562
Interlock of the 1st valvulae (il1)*	The anatomical cluster that consists of the apical regions of the left and right 1st valvulae, which are interlocked with each other in a manner similar to how the 1st and 2nd valvulae are connected by olistheter		http://purl.obolibrary.org/obo/HAO_0002603
Intervalvifer articulation (iva)	The articulation between the 1st valvifer and 2nd valvifer	Articulating process of the fulcral plate with the inner plate [35]; Intervalviferengelenk [29]	http://purl.obolibrary.org/obo/HAO_0001558
Intravalvifer articulation	The articulation between the dorsal sclerite of the 1st valvifer and the ventral sclerite of the 1st valvifer		http://purl.obolibrary.org/obo/HAO_0002165
Laminated bridge (lb)	The area that is located proximally on the notal membrane near the processus articularis, is sclerotized and is continuous with the 2nd valvula	Chitinstäbchen [29]; Chitinous cross striae uniting the rods of the sheath [35]; Transverse chitinous ribs [36, 37]	http://purl.obolibrary.org/obo/HAO_0001548
Lateral	Anatomical region laterally located on the body or body part		http://purl.obolibrary.org/obo/BSPO_0000082
Lateral T8-T9 muscle	The 9th abdominal tergal muscle that arises from the anterolateral margin of female T8 and inserts on the anterolateral margin of female T9		http://purl.obolibrary.org/obo/HAO_0001776
Lateral T9-2nd valvifer muscle	The muscle arises from the posteroventral parts of the female T9 and inserts on the median bridge		http://purl.obolibrary.org/obo/HAO_0002187
Line	The anatomical cluster that is linear		http://purl.obolibrary.org/obo/HAO_0001586

Table 2 (continued)

Anatomical term (abbreviation)	Definition/concept	Synonyms commonly found in literature	URI
Lumen (Anatomical space)	Non-material entity of three dimensions, that is generated by morphogenetic or other physiologic processes; is surrounded by one or more anatomical structures; contains one or more organism substances or anatomical structures		http://purl.obolibrary.org/obo/HAO_0000005
Margin	The line that delimits the periphery of an area The anatomical region that extends along the margin		http://purl.obolibrary.org/obo/HAO_0000510 http://purl.obolibrary.org/obo/HAO_0001981
Medial	Anatomical region medially located on the body or body part		http://purl.obolibrary.org/obo/BSPO_0000083
Medial 2nd valvifer-2nd valvula muscle*	The muscle that arises anteromedially from the 2nd valvifer and inserts inside the lumen of 2nd valvula		http://purl.obolibrary.org/obo/HAO_0002596
Medial conjunctiva of the 1st valvulae	The conjunctiva that extends medially along the 1st valvula		http://purl.obolibrary.org/obo/HAO_0002192
Medial ridge of the 2nd valvifer (mr2)*	The ridge that is on the anterior section of the dorsal flange and serves as the site of insertion of T9-2nd valvifer muscle part b		http://purl.obolibrary.org/obo/HAO_0002594
Median bridge of the 2nd valvifers (mb2)	The area that connects posteriorly the 2nd valvifers and is the site of attachment for the posterior T9-2nd valvifer muscle	Bridge (of the inner plates) [37]; Bridge of 2nd valvifer [HAO]; Transverse ligament [19]	http://purl.obolibrary.org/obo/HAO_0001780
Median conjunctiva of abdominal tergum 9	The conjunctiva of abdominal tergum 9 that has median and longitudinal	Brücke [29]	http://purl.obolibrary.org/obo/HAO_0002267
Metasoma	The tagma that is connected anteriorly to the metapetal-propodeal complex at the propodeal foramen and consists of abdominal segments		http://purl.obolibrary.org/obo/HAO_0000626
Metasomal segment	The abdominal segment that is located in the metasoma		http://purl.obolibrary.org/obo/HAO_0001969
Metasomal sternum	The abdominal sternum that is located in the metasoma		http://purl.obolibrary.org/obo/HAO_0001350
Metasomal tergum	The abdominal tergum that is located in the metasoma		http://purl.obolibrary.org/obo/HAO_0001349
Muscle	The portion of tissue that is composed of contractile fibres		http://purl.obolibrary.org/obo/HAO_0000641
Nervous system	The organ system that is composed of neurons and glial cells		http://purl.obolibrary.org/obo/HAO_0001732
Notal membrane (nm)	The conjunctiva that connects the medial margins of the 2nd valvulae	Elaterium [39, 86]; ~Ligamentum [157]	http://purl.obolibrary.org/obo/HAO_0001733

Table 2 (continued)

Anatomical term (abbreviation)	Definition/concept	Synonyms commonly found in literature	URI
Notch	The part of the margin of a sclerite that is concave		http://purl.obolibrary.org/obo/HAO_0000648
Olistheter (oth)	The anatomical cluster that is composed of the rhachis of the 2nd valvula and the aulax of the 1st valvula	Tongue and groove arrangement [150]; Tongue and groove mechanism [20]	http://purl.obolibrary.org/obo/HAO_0001103
Organ system	A division of the whole organism into specialized systems		http://purl.obolibrary.org/obo/HAO_0001599
Orifice of the venom gland reservoir (ovr)*	The anatomical space at the proximal-most end of the venom gland reservoir	Opening of the reservoir [73]	http://purl.obolibrary.org/obo/HAO_0002599
Ovariole, ovarioles*	An egg assembly line. Consists of a germarium at the anterior tip connected to a chain of egg chambers, each one more mature than the preceding, more anterior egg chamber in the chain. Each ovariole is encased in an ovarian sheath		http://purl.obolibrary.org/obo/FBbt_00004893
Ovary, ovaries*	The female gonad	Ovaire [50]	http://purl.obolibrary.org/obo/FBbt_00004865
Oviduct*	Duct of the female reproductive tract that connects the ovaries to the uterus [172, 173]. The oviduct consists of two lateral oviducts (each connected to an ovary) and one common oviduct, to which the lateral oviducts connect, and which itself connects to the uterus [172, 173]		http://purl.obolibrary.org/obo/FBbt_00004911
Ovipositor	The anatomical cluster that is composed of the 1st valvulae, 2nd valvulae, 3rd valvulae, 1st valvifers, 2nd valvifers and female T9	Legappareil [29, 155]; Ovipositor mechanism [19, 20, 25]; Stachelapparat [29]; Sting [HAO]; Sting apparatus [158, 167, 168, 170]; Stinger [HAO]	http://purl.obolibrary.org/obo/HAO_0000679
Ovipositor apparatus	The anatomical cluster that is composed of the ovipositor, abdominal terga 8–10, abdominal sternum 7 and muscles connecting them		http://purl.obolibrary.org/obo/HAO_0001600
Ovipositor muscle	The abdominal muscle that inserts on the ovipositor		http://purl.obolibrary.org/obo/HAO_0001290
Pars articularis	The articular surface that is situated anteriorly on the ventral margin of the 2nd valvifer and forms the lateral part of the basal articulation	Pars articulares [HAO]	http://purl.obolibrary.org/obo/HAO_0001606
Patch	The area that is round and differs from surrounding regions in sculpture, setae, and/or pigmentation		http://purl.obolibrary.org/obo/HAO_0000704
Portion of tissue	Anatomical structure that consists of similar cells and intercellular matrix, aggregated according to genetically determined spatial relationships		http://purl.obolibrary.org/obo/HAO_0000043

Table 2 (continued)

Anatomical term (abbreviation)	Definition/concept	Synonyms commonly found in literature	URI
Post-ramus flap (prf)*	The distal area of the dorsal projection of the 2nd valvifer that is widened and is flexibly connected to the proximal region of the dorsal projection of the 2nd valvifer	Post-ramus flap of the 2nd valvifer [HAO]; ~ Post-ramus extension [19, 25]	http://purl.obolibrary.org/obo/HAO_0002593
Posterior	Anatomical region posteriorly located on the body or body part		http://purl.obolibrary.org/obo/BSPO_0000072
Posterior 2nd valvifer-2nd valvula muscle (m-p-2vf-2vv)	The ovipositor muscle that arises posteriorly from the 2nd valvifer and inserts on the processus musculares of the 2nd valvula	Gonapophysis 9 depressor [153]; Muscle of the furcula [28, 166]; Posterior gonocoxapophyseal muscle [33, 34]; Retractor of ventral valves [154]; Sting depressor [156]	http://purl.obolibrary.org/obo/HAO_0001815
Posterior area of the 2nd valvifer	The area of the 2nd valvifer that is posterior to the anatomical line that is the shortest distance from the valvifer fossa of the 2nd valvifer to the ventral margin of the 2nd valvifer		http://purl.obolibrary.org/obo/HAO_0002170
Posterior margin of 1st valvifer	The margin of the 1st valvifer that is posterior and extends between the intervalvifer articulation and the anterior angle of the 1st valvifer		http://purl.obolibrary.org/obo/HAO_0002159
Posterior section of dorsal flange of the 2nd valvifer	The area of the dorsal flange of the 2nd valvifer that is posterior to the site of origin of the basal line	~ Inner ovipositor plate [19–25]	http://purl.obolibrary.org/obo/HAO_0002174
Posterior T9-2nd valvifer muscle (m-p-T9-2vf)	The ovipositor muscle that arises medially from the posterodorsal part of female T9 and inserts on the median bridge of the 2nd valvifers	Dorsal/lateral tergonostylar muscle [33, 34]; Posterior dorso-ventral muscle [154]	http://purl.obolibrary.org/obo/HAO_0001813
Posteroventral corner of 1st valvifer	The corner of the 1st valvifer that is adjacent to the intervalvifer articulation		http://purl.obolibrary.org/obo/HAO_0002239
Preadicular incisure	The notch that is located on the margin of the 2nd valvifer immediately anterior to the basal articulation of the 2nd valvula		http://purl.obolibrary.org/obo/HAO_0000799
Process	The area on the sclerite that is raised		http://purl.obolibrary.org/obo/HAO_0000822
Processus articularis	The process that extends laterally from the proximal part of the 2nd valvula and forms the median part of the basal articulation, and corresponds to the site of attachment for the anterior 2nd valvifer-2nd valvula muscle		http://purl.obolibrary.org/obo/HAO_0001704
Processus musculares	The apodeme that extends dorsally from the proximal part of the 2nd valvula to the genital membrane and receives the site of attachment of the posterior 2nd valvifer-2nd valvula muscle	Processus muscularis [HAO]	http://purl.obolibrary.org/obo/HAO_0001703

Table 2 (continued)

Anatomical term (abbreviation)	Definition/concept	Synonyms commonly found in literature	URI
Proctiger	The area that is located around the anal opening posterior to the epipygium and hypopygium		http://purl.obolibrary.org/obo/HAO_0001827
Projection	The process that is located on an edge		http://purl.obolibrary.org/obo/HAO_0000829
Proximal	Anatomical region proximally located on the body or body part		http://purl.obolibrary.org/obo/BSPO_0000077
Region	The anatomical structure that is delimited by at least one immaterial anatomical entity. (Class obsolete.)		http://purl.obolibrary.org/obo/HAO_0000893
Reproductive system	The anatomical system that is involved in reproduction		http://purl.obolibrary.org/obo/HAO_0000895
Rhachis (rh)	The ridge that extends along the ventral surface of the 2nd valvula that is partially enclosed by the aulax	Bead for attaching stylet to rod of sheath [35]; Leiste der Schienenrinne [155]; Rail [166]; Rail guides [81]; T-ridge of ventral valve [154]; Tongue [19, 20, 22, 25]	http://purl.obolibrary.org/obo/HAO_0000898
Ridge	The apodeme that is elongate	Lamella [HAO]; Lamina [HAO]	http://purl.obolibrary.org/obo/HAO_0000899
Rim	The carina that extends along the margin or edge of a sclerite		http://purl.obolibrary.org/obo/HAO_0000900
S7-1st valvula muscle	The muscle that originates from the abdominal tergum 7 and inserts on the 1st valvula		http://purl.obolibrary.org/obo/HAO_0001668
Sawtooth (st1/st2)	The process that is located along the ventral margin of the 1st valvula or the dorsal margin of the 2nd valvula	Barb, barbs [35, 165]; Cutting teeth [20]; Sägezähnen [29, 155]; Serrula [157]; Sheath teeth [17]; Teeth [19–24]; Widerhaken [29]; Zähnen [29]	http://purl.obolibrary.org/obo/HAO_0001681
Sclerite	The area of the cuticle that is strongly sclerotized, with thick exocuticle and is surrounded by conjunctivae	Plate [HAO]; Sclerome [HAO]	http://purl.obolibrary.org/obo/HAO_0000909
Sculpture	The area that is located on the sclerite and that is composed of repetitive anatomical structures		http://purl.obolibrary.org/obo/HAO_0000913
Segment	An anatomical structure that is metameric and is connected to other metameric subdivisions by muscles and is delimited by its sclerites		http://purl.obolibrary.org/obo/HAO_0000929
Sense organ	Multicellular anatomical structure with largely bona fide boundary that transduces some sensory stimulus to the nervous system		http://purl.obolibrary.org/obo/HAO_0000930
Sensillar patch of the 2nd valvifer (sp)	The patch that is composed of placoid sensilla adjacent to the intervalvifer articulation	Sensillar patch [HAO]; Sinneshärtchen des Intervalviferengelenkes [29]	http://purl.obolibrary.org/obo/HAO_0001671
Sensillar row of the 2nd valvifer (sr)*	The row of styloconic sensilla along the proximal margin of the anterior area of the 2nd valvifer	Ramus spines [25]; Sensilla on edge of the 2nd valvifer [HAO]	http://purl.obolibrary.org/obo/HAO_0002592

Table 2 (continued)

Anatomical term (abbreviation)	Definition/concept	Synonyms commonly found in literature	URI
Sensillum	A sense organ embedded in the integument and consisting of one or a cluster of sensory neurons and associated sensory structures, support cells and glial cells forming a single organized unit with a largely bona fide boundary		http://purl.obolibrary.org/obo/HAO_0000933
Sensillum coeloconicum (cs)	The aporous sensillum whose cuticular component is an apically rounded, hair-like structure, which is in a depression below the surface of the surrounding cuticle	Coeloconic sensillum [HAO]	http://purl.obolibrary.org/obo/HAO_0002001
Seta	The sensillum with a hair-like cuticular component	Bristle [HAO]; Hair sensillum [HAO]; Hair-like sensillum [HAO]; Sensillum trichodeum [HAO]; Sinneshärchen [29]; Trichoid sensillum [HAO]	http://purl.obolibrary.org/obo/HAO_0002299
Spermatheca*	The invagination just proximal to the vagina that accommodates sperms	Receptaculum seminis [35]; Spermatheque [50]	http://purl.obolibrary.org/obo/HAO_0000945
Sperone*	The longitudinal ridge on medially on the internal surface of the distal region of the 2nd valvula		http://purl.obolibrary.org/obo/HAO_0002590
Spine	The process that lacks non-sclerotised ring at the base		http://purl.obolibrary.org/obo/HAO_0000949
Sternite	The sclerite is located on the sternum		http://purl.obolibrary.org/obo/HAO_0000955
Sternum	The area that is located on the integument and is ventral of the ventral diaphragm		http://purl.obolibrary.org/obo/HAO_0000956
Sulcus	The groove that corresponds to a ridge		http://purl.obolibrary.org/obo/HAO_0000978
T8-1st valvifer muscle	The ovipositor muscle that originates from the lateral part of female T8 and inserts on the dorsal margin of the 1st valvifer	Furrow [HAO]; Suture [HAO]	http://purl.obolibrary.org/obo/HAO_0001640
T9-genital membrane muscle (m-T9-gm)	The ovipositor muscle that arises from the cordate apodeme and inserts dorsally on the proximal part of the genital membrane and on the opposite cordate apodeme		http://purl.obolibrary.org/obo/HAO_0001639
Tagma	The anatomical structure that is a distinctly delimited group of segments		http://purl.obolibrary.org/obo/HAO_0000988
Tendon	The portion of tissue that is fibrous, strong, composed of tendon cells and connects the muscle to the integument	~ Emergenz (am konkaven Dorsalrand des 2. Valvifers) (= tendon of the dorsal T9-2nd valvifer muscle part b) [29]	http://purl.obolibrary.org/obo/HAO_0000996

Table 2 (continued)

Anatomical term (abbreviation)	Definition/concept	Synonyms commonly found in literature	URI
Terebra (trib)	The anatomical cluster that is composed of the 1st and 2nd valvulae	Boring apparatus and egg tube [37]; External ovipositor [32]; Inner lobes [38]; Legebohrer [29, 45, 155]; Legestachel [29]; Ovipositor [26, 27, 35, 39, 41–44, 55, 77, 79, 81, 86, 90, 93, 105, 106, 111, 151–153, 160–162, 164–166]; Ovipositor s. str. [29]; (Ovipositor) shaft [17–25, 71, 73, 83, 163, 174]; Shaft of ovipositor [28]; Stachel [45, 155]; Sting [36, 37, 156, 158, 159, 167]; Sting shaft [89, 168, 170, 171]; Stylus (of the ovipositor) [175]; ~ Tarière [50]	http://purl.obolibrary.org/obo/HAO_0001004
Tergite	The sclerite that is located on the tergum		http://purl.obolibrary.org/obo/HAO_0001005
Tergo-valvifer articulation (tva)	The articulation that is located between the female T9 and the 1st valvifer and is composed of the 9th tergal condyle of the 1st valvifer and the 1st valviferal fossa of the 9th tergite	Articulating process of the fulcral plate and the outer plate [35]; Tergovalvifergelenk [29]	http://purl.obolibrary.org/obo/HAO_0001636
Tergum	The area that is located on the integument and is dorsal of the ventral diaphragm	Notum [HAO]	http://purl.obolibrary.org/obo/HAO_0001006
Transvalviferal conjunctiva	The conjunctiva that transverses the 1st valvifer and separates the dorsal and ventral sclerites of the 1st valvifer		http://purl.obolibrary.org/obo/HAO_0002162
Uterus*	Anterior part of the genital chamber [173]. It is an ectodermal invagination that is the site of egg fertilization [173]. It is connected to the common oviduct anterodorsally and the vagina posteriorly [173]. It is surrounded by muscles [173]	Egg store [26]	http://purl.obolibrary.org/obo/BBbt_00004924
Vagina*	The duct that is the proximal-most region of the female genital duct, is continuous with the common oviduct and is separated from it by the gonopore	Vagin [50]	http://purl.obolibrary.org/obo/HAO_0002586
Valvillus	The sclerite that articulates on the 1st valvula and projects into the egg/poison canal	Flap [39]; Hemmplättchen [29]; Projection [176]	http://purl.obolibrary.org/obo/HAO_0001619
Venom gland*	The accessory gland that is not paired and that empties into the female reproductive duct and that is of class I gland	Acid gland [19–25, 73, 74]; Glande acide [50]; Multifid gland [73]; Poison gland [75, 89]; Sting gland [89]	http://purl.obolibrary.org/obo/HAO_0002585
Venom gland reservoir of the 2nd valvifer (vr)	The gland reservoir that is between the 2nd valvifers	Acid gland reservoir [73]; Poison reservoir [75, 89]; Reservoir (of the acid gland) [35, 37, 74]; Réservoir [50]; Venom reservoir [77, 79, 156]	http://purl.obolibrary.org/obo/HAO_0002176
Ventral	Anatomical region ventrally located on the body or body part		http://purl.obolibrary.org/obo/BSPO_0000084

Table 2 (continued)

Anatomical term (abbreviation)	Definition/concept	Synonyms commonly found in literature	URI
Ventral 2nd valvifer-venom gland reservoir muscle (m-v-2vf-vr)*	The 2nd valvifer-venom gland reservoir muscle that originates at the medial surface of the 2nd valvifer, ventrally to the site of origin of the dorsal 2nd valvifer-venom gland reservoir muscle, and inserts laterally at the orifice of the venom gland reservoir		http://purl.obolibrary.org/obo/HAO_0002598
Ventral ramus of the 1st valvula	The area that extends external to the dorsal ramus of the 1st valvula	Ramal rod [HAO]; Ventralfortsatz [29]	http://purl.obolibrary.org/obo/HAO_0000891
Ventral ramus of the 2nd valvula	The area of the 2nd valvifer-2nd valvula-3rd valvula complex that bears the rhachis	Rami der 2. Valvulae [29]	http://purl.obolibrary.org/obo/HAO_0001107
Ventral sclerite of the 1st valvifer	The sclerite of the 1st valvifer that is ventral to the transvalviferal conjunctiva		http://purl.obolibrary.org/obo/HAO_0002164
Ventral T9-2nd valvifer muscle (m-v-T9-2vf)	The ovipositor muscle that arises from the lateral region of female T9 and inserts along the posterior part of the dorsal flange of the 2nd valvifer	Gonapophysis 8 retractor [153]; Posterior tergal muscle of the 2nd valvifer [28]; Posterior tergogonocoxal muscle [33, 34]; Retractor muscle of lancet [17]; Stylet retractor muscle [25]	http://purl.obolibrary.org/obo/HAO_0001616
Ventral wall of the 2nd valvulae (vw2)*	The ventral, usually weakly sclerotized region of the 2nd valvulae, that is medially continuous with the rachises		http://purl.obolibrary.org/obo/HAO_0002589
Vestibulum	The anatomical space that is located dorsally of abdominal sternum 7 when the latter extends beyond the abdominal sternum 8		http://purl.obolibrary.org/obo/HAO_0001082
Vitellarium*	Ovariole excluding the germarium		http://purl.obolibrary.org/obo/FFbt_00004900

The terms (abbreviations in brackets) are used and defined according to the Hymenoptera Anatomy Ontology (HAO) [52–54], the synonyms commonly found in the literature and the relevant Uniform Resource Identifier (URI) of the relevant ontologies (Hymenoptera Anatomy Ontology (HAO), *Drosophila gross anatomy* (FFBt), Biological Spatial Ontology (BSPO), Common Anatomy Reference Ontology (CARO), available from <http://gloss.ary.hymaoo.org>, <https://ontobee.org/>, <http://obofoundry.org/>, respectively) are listed. Terms proposed in the present study are marked with *

Abbreviations

1vf	1st valvifer
1vv	1st valvula
2vf	2nd valvifer
2vv	2nd valvula
3vv	3rd valvula
au	Aulax
ba	Basal articulation
blb	Bulb
CLSM	Confocal laser scanning microscopy
co	Common oviduct
cs	Coeloconic sensillum
ct	Ctenidium
den	Dendrite
Dg	Dufour's gland
Dgd	Dufour's gland duct
dp2	Dorsal projection of the 2nd valvifer
dr1	Dorsal ramus of the 1st valvula
ec	Egg canal
F	Force
$F_{(x)}$	Horizontal vector component of a force
fu	Furcula
iar	Interarticular ridge of the 1st valvifer
il1	Interlock of the 1st valvulae
iva	Intervalvifer articulation
lb	Laminated bridge
le	Lateral extensions of the 2nd valvula
LM	Light microscopy
lu2	Lumen of the 2nd valvula
M	Torque
m-1vf-gm	1st valvifer-genital membrane muscle
m-a-2vf-2vv	Anterior 2nd valvifer-2nd valvula muscle
m-d-2vf-vr	Dorsal 2nd valvifer-venom gland reservoir muscle
m-d-T9-2vf-a	Dorsal T9-2nd valvifer muscle part a
m-d-T9-2vf-b	Dorsal T9-2nd valvifer muscle part b
m-p-2vf-2vv	Posterior 2nd valvifer-2nd valvula muscle
m-p-T9-2vf	Posterior T9-2nd valvifer muscle
m-T9-gm	T9-genital membrane muscle
m-v-2vf-vr	Ventral 2nd valvifer-venom gland reservoir muscle
m-v-2vf-vr-a	Ventral 2nd valvifer-venom gland reservoir muscle part a
m-v-2vf-vr-b	Ventral 2nd valvifer-venom gland reservoir muscle part b
m-v-T9-2vf	Ventral T9-2nd valvifer muscle
mb2	Median bridge of the 2nd valvifers
me	Metasoma
mr2	Medial ridge of the 2nd valvifer
oth	Olistheter
ovr	Orifice of the venom gland reservoir
prf	Post-ramus flap
rh	Rhachis
sc	Scale-like structure
SEM	Scanning electron microscopy
sp	Sensillar patch of the 2nd valvifer
sr	Sensillar row of the 2nd valvifer
SR- μ CT	Synchrotron X-ray phase-contrast microtomography
st1	Sawtooth of the 1st valvula
st2	Sawtooth of the 2nd valvula
t-m-d-T9-2vf-a	Tendon of the dorsal 2nd valvifer-T9 muscle part a
T9	Female T9 (9th abdominal tergum)
TEM	Transmission electron microscope
trb	Terebra
tva	Tergo-valvifer articulation
vr	Venom gland reservoir of the 2nd valvifer
vw2	Ventral wall of the 2nd valvula
WFM	Widefield epifluorescence microscopy

Supplementary Information

The online version contains supplementary material available at <https://doi.org/10.1186/s12983-023-00503-1>.

Additional file 1. Video sequences of female *Lariophagus distinguendus* parasitizing larvae of *Sitophilus granarius* in an artificial film chamber (cf. Fig. 2b–p). The terebra bending and rotating movements during host assessment and the alternate movements of the paired 1st valvulae can be observed.

Additional file 2. Superimposed CLSM images of the ovipositor of *Lariophagus distinguendus* (dorsal view, cf. Fig. 3g, h).

Additional file 3. Animation of the aligned semithin sections through the terebra of *Lariophagus distinguendus* (from distal to proximal; cf. Fig. 4a–d). The jittering movements of the two halves of the 2nd valvula in the middle of the image stack result from section and compression artefacts.

Additional file 4. Animation of the rotating segmented 3D model of the musculoskeletal ovipositor system of *Lariophagus distinguendus* (cf. Figs. 5 and 6).

Acknowledgements

The authors thank the following colleagues for their help: Matthias Schöller (Biologische Beratung GmbH) for providing wasps and their hosts; Jana Colatz, Johannes LM Steidle and Urs Wyss for providing inspiring film sequences (Entofilm) and valuable tips; Paavo Bergmann for assistance with histological techniques, Julia Straube with ultramicrotomy, Monika Meinert with SEM, Lorenz Henneberg and York-Dieter Stierhof with WFM, Verena Pietzsch and James H. Nebelsick with the Keyence digital microscope; Robin Kraft, Benjamin Sampalla, Lea von Berg, Erich Lara Spiessberger, Margarita Yavorskaya and Manfred Drack for inspiring discussions; Theresa Jones for improvements and linguistic corrections of the manuscript, and three referees for their helpful comments. The authors gratefully acknowledge the Tübingen Structural Microscopy Core Facility (funded by the Excellence Strategy of the German Federal and State Governments) and the University of New Hampshire Instrumentation Center for their support and assistance in this work.

Author contributions

BE and OB prepared the study design; AR and OB obtained the SR- μ CT data; AR deployed and adjusted the beamline settings for SR- μ CT; BE and SF prepared the samples (fixation, embedding) and processed the SR- μ CT and light microscopical images; BE carried out the ultramicrotomy, LM, WFM, TEM and high-resolution videography, analysed the data and wrote the manuscript; BE and MC carried out the SEM; IM carried out the CLSM; SF, MC, IM, AR and OB discussed the results and revised the manuscript. All authors read and approved the final manuscript.

Funding

This work was funded by the German Research Foundation (DFG) as part of the Transregional Collaborative Research Centre (SFB-TRR) 141 'Biological Design and Integrative Structures' (project A03 'Inspired by plants and animals: actively actuated rod-shaped structures exhibiting adaptive stiffness and joint-free kinematics'). The experiment (LS-2342) at the ESRF was funded by the European Union (EU). The authors acknowledge support from the Open Access Publishing Fund of the University of Tübingen. Open Access funding enabled and organized by Projekt DEAL.

Availability of data and materials

All data supporting the conclusions of this article are included within the article and its additional files. The full resolution videos (Additional file 1, Additional file 2, Additional file 3, and Additional file 4) and the analysed raw datasets are available from the corresponding author on reasonable request.

Declarations

Ethics approval and consent to participate

No approval of research ethics committees was required to achieve the goals of this study, as it involved experimental work with an unregulated invertebrate species.

Consent for publication

Not applicable.

Competing interests

The authors declare that they have no competing or financial interests.

Received: 5 May 2023 Accepted: 13 July 2023

Published online: 08 August 2023

References

- Kristensen NP. Phylogeny of the endopterygote insects, the most successful lineage of living organisms. *Eur J Entomol.* 1999;96:237–53.
- Vilhelmsen L. Before the wasp-waist: comparative anatomy and phylogenetic implications of the skeleto-musculature of the thoraco-abdominal boundary region in basal Hymenoptera (Insecta). *Zoomorphology.* 2000;119:185–221. <https://doi.org/10.1007/PL00008493>.
- Vilhelmsen L, Mikó I, Krogmann L. Beyond the wasp-waist: structural diversity and phylogenetic significance of the mesosoma in apocritan wasps (Insecta: Hymenoptera). *Zool J Linn Soc.* 2010;159:22–194. <https://doi.org/10.1111/j.1096-3642.2009.00576.x>.
- Peters RS, Krogmann L, Mayer C, Donath A, Gunkel S, Meusemann K, et al. Evolutionary history of the Hymenoptera. *Curr Biol.* 2017;27:1013–8. <https://doi.org/10.1016/j.cub.2017.01.027>.
- Blaimer BB, Santos BF, Cruaud A, Gates MW, Kula RR, Mikó I, et al. Key innovations and the diversification of Hymenoptera. *Nat Commun.* 2023;14:1212. <https://doi.org/10.1038/s41467-023-36868-4>.
- Heraty JM, Burks RA, Cruaud A, Gibson GAP, Liljebäck J, Munro J, et al. A phylogenetic analysis of the megadiverse Chalcidoidea (Hymenoptera). *Cladistics.* 2012;29:1–77. <https://doi.org/10.1111/cla.12006>.
- Heraty JM. Parasitoid biodiversity and insect pest management. In: Footitt RG, Adler PH, editors. *Insect biodiversity: science and society.* 2nd ed. Oxford: Wiley-Blackwell; 2017. p. 603–25. <https://doi.org/10.1002/9781118945568.ch19>.
- Huber JT. Biodiversity of Hymenoptera. In: Footitt RG, Adler PH, editors. *Insect biodiversity: science and society.* 2nd ed. Oxford: Wiley-Blackwell; 2017. p. 419–61. <https://doi.org/10.1002/9781118945568.ch12>.
- Noyes JS. Universal Chalcidoidea Database. 2017. <http://www.nhm.ac.uk/our-science/data/chalcidoidea/>. Accessed 1 May 2023.
- Peters RS, Niehuis O, Gunkel S, Bläser M, Mayer C, Podsiadlowski L, et al. Transcriptome sequence-based phylogeny of chalcidoid wasps (Hymenoptera: Chalcidoidea) reveals a history of rapid radiations, convergence, and evolutionary success. *Mol Phylogenet Evol.* 2018;120:286–96. <https://doi.org/10.1016/j.ympev.2017.12.005>.
- Polaszek A, Vilhelmsen L. Biodiversity of hymenopteran parasitoids. *Curr Opin Insect Sci.* 2023;56:101026. <https://doi.org/10.1016/j.cois.2023.101026>.
- Gibson GAP, Heraty JM, Woolley JB. Phylogenetics and classification of Chalcidoidea and Mymarommatoida—a review of current concepts (Hymenoptera, Apocrita). *Zool Scr.* 1999;28:87–124. <https://doi.org/10.1046/j.1463-6409.1999.00016.x>.
- Kenis M, Wermelinger B, Grégoire J-C. Research on parasitoids and predators of Scolytidae—a review. In: Lieutier F, Day KR, Battisti A, Grégoire J-C, Evans HF, editors. *Bark wood boring insects living in trees in Europe, a synthesis.* Dordrecht: Springer; 2007. p. 237–90. https://doi.org/10.1007/978-1-4020-2241-8_11.
- van de Kamp T, Mikó I, Stancic AH, Eggs B, Bajerlein D, Faragó T, et al. Evolution of flexible biting in hyperdiverse parasitoid wasps. *Proc R Soc B Biol Sci.* 2022;289:20212086. <https://doi.org/10.1098/rspb.2021.2086>.
- Broski SA, King BH. Drilling-in and chewing-out of hosts by the parasitoid wasp *Spalangia endius* (Hymenoptera: Pteromalidae) when parasitizing *Musca domestica* (Diptera: Muscidae). *Environ Entomol.* 2015;44:1116–24. <https://doi.org/10.1093/ee/nvv069>.
- Quicke DLJ, LeRalec A, Vilhelmsen L. Ovipositor structure and function in the parasitic Hymenoptera with an exploration of new hypotheses. *Rendiconti.* 2000;47:197–239.
- King PE. The muscular structure of the ovipositor and its mode of function in *Nasonia vitripennis* (Walker) (Hymenoptera: Pteromalidae). *Proc R Entomol Soc Lond Ser A Gen Entomol.* 1962;37:121–8. <https://doi.org/10.1111/j.1365-3032.1962.tb00002.x>.
- King PE, Copland MJW. The structure of the female reproductive system in the Mymaridae (Chalcidoidea: Hymenoptera). *J Nat Hist.* 1969;3:349–65. <https://doi.org/10.1080/00222936900770311>.
- Copland MJW, King PE. The structure and possible function of the reproductive system in some Eulophidae and Tetracampidae. *Entomologist.* 1971;4–28.
- Copland MJW, King PE. The structure of the female reproductive system in the Chalcidoidea (Hym.). *Entomol Mon Mag.* 1971;107:230–9.
- Copland MJW, King PE. The structure of the female reproductive system in the Eurytomidae (Chalcidoidea: Hymenoptera). *J Zool.* 1972;166:185–212. <https://doi.org/10.1111/j.1469-7998.1972.tb04085.x>.
- Copland MJW, King PE. The structure of the female reproductive system in the Pteromalidae (Chalcidoidea: Hymenoptera). *Entomologist.* 1972;105:77–96.
- Copland MJW, King PE. The structure of the female reproductive system in the Torymidae (Hymenoptera: Chalcidoidea). *Trans R Entomol Soc Lond.* 1972;124:191–212. <https://doi.org/10.1111/j.1365-2311.1972.tb00363.x>.
- Copland MJW, King PE, Hill DS. The structure of the female reproductive system in the Agaonidae (Chalcidoidea, Hymenoptera). *J Entomol Ser A Gen Entomol.* 1973;48:25–35. <https://doi.org/10.1111/j.1365-3032.1973.tb00029.x>.
- Copland MJW. Female reproductive system of the Aphelinidae (Hymenoptera: Chalcidoidea). *Int J Insect Morphol Embryol.* 1976;5:151–66. [https://doi.org/10.1016/0020-7322\(76\)90001-5](https://doi.org/10.1016/0020-7322(76)90001-5).
- Quicke DLJ. Parasitic wasps. London: Chapman & Hall; 1997.
- Quicke DLJ. The braconid and ichneumonid parasitoid wasps: biology, systematics, evolution and ecology. Chichester: Wiley-Blackwell; 2015.
- Snodgrass RE. Morphology of the insect abdomen. Part II. The genital ducts and the ovipositor. *Smithson Misc Collect.* 1933;89:1–148.
- Oeser R. Vergleichend-morphologische Untersuchungen über den Ovipositor der Hymenopteren. *Mitt Zool Mus Berlin.* 1961;37:3–119. <https://doi.org/10.1002/mmzn.19610370102>.
- Vilhelmsen L. The ovipositor apparatus of basal Hymenoptera (Insecta): phylogenetic implications and functional morphology. *Zool Scr.* 2000;29:319–45. <https://doi.org/10.1046/j.1463-6409.2000.00046.x>.
- Eggs B, Birkhold AI, Röhrle O, Betz O. Structure and function of the musculoskeletal ovipositor system of an ichneumonid wasp. *BMC Zool.* 2018;3:12. <https://doi.org/10.1186/s40850-018-0037-2>.
- van Meer NMME, Cerkvenik U, Schlepütz CM, van Leeuwen JL, Gussekloo SWS. The ovipositor actuation mechanism of a parasitic wasp and its functional implications. *J Anat.* 2020;237:689–703. <https://doi.org/10.1111/joa.13216>.
- Smith EL. Evolutionary morphology of the external insect genitalia. 2. Hymenoptera. *Ann Entomol Soc Am.* 1970;63:1–27. <https://doi.org/10.1093/aesa/63.1.1>.
- Smith EL. Biosystematics and morphology of Symphyta—III External genitalia of *Euura* (Hymenoptera: Tenthredinidae): sclerites, sensilla, musculature, development and oviposition behavior. *Int J Insect Morphol Embryol.* 1972;1:321–65. [https://doi.org/10.1016/0020-7322\(72\)90016-5](https://doi.org/10.1016/0020-7322(72)90016-5).
- James HC. The anatomy of a British phytophagous chalcidoid of the genus *Harmolita* (*Isosoma*). *Proc Zool Soc Lond.* 1926;96:75–182. <https://doi.org/10.1111/j.1096-3642.1926.tb01540.x>.
- Hanna AD. The male and female genitalia and the biology of *Euchalcidia aryobori* Hanna (Hymenoptera, Chalcididae). *Trans R Entomol Soc Lond.* 1934;82:107–36. <https://doi.org/10.1111/j.1365-2311.1934.tb00030.x>.
- Bucher GE. The anatomy of *Monodontomerus dentipes* Boh., an entomophagous chalcid. *Can J Res.* 1948;26:230–81. <https://doi.org/10.1139/cjr48d-020>.

38. Rakshpal R. The structure and development of the female genital organs of *Tetrastichus pyrillae* Crawford. (Eulophidae-Chalcidoidea) with a comparison of the genital organs in the two sexes. *Indian J Entomol.* 1946;7:65–74.
39. Quicke DLJ, Fitton MG, Tunstead JR, Ingram SN, Gaitens PV. Ovipositor structure and relationships within the Hymenoptera, with special reference to the Ichneumonidae. *J Nat Hist.* 1994;28:635–82. <https://doi.org/10.1080/00222939400770301>.
40. Fulton BB. Notes on *Habrocytus cerealellae*, parasite of the angoumois grain moth. *Ann Entomol Soc Am.* 1933;26:536–53. <https://doi.org/10.1093/aesa/26.4.536>.
41. Quicke DLJ. Ovipositor mechanisms of the braconine wasp genus *Zaglyptogastra* and the ichneumonid genus *Pristomerus*. *J Nat Hist.* 1991;25:971–7. <https://doi.org/10.1080/00222939100770631>.
42. Quicke DLJ, Fitton MG. Ovipositor steering mechanisms in parasitic wasps of the families Gasteruptionidae and Aulacidae (Hymenoptera). *Proc R Soc Lond B Biol Sci.* 1995;261:99–103. <https://doi.org/10.1098/rspb.1995.0122>.
43. Quicke DLJ, Fitton MG, Harris J. Ovipositor steering mechanisms in braconid wasps. *J Hymenopt Res.* 1995;4:110–20.
44. Cerkvenik U, van de Straat B, Gussekloo SWS, van Leeuwen JL. Mechanisms of ovipositor insertion and steering of a parasitic wasp. *Proc Natl Acad Sci USA.* 2017;114:E7822–31. <https://doi.org/10.1073/pnas.1706162114>.
45. Hase A. Zur Kenntnis wirtschaftlich wichtiger Tierformen. I. Über den Stech- und Legeakt, sowie über den Wirtswechsel von *Lariophagus distinguendus*. Chalcididae. Pteromalini. *Naturwissenschaften.* 1924;12:377–84. <https://doi.org/10.1007/BF01493826>.
46. Edwards RL. The host-finding and oviposition behaviour of *Mormoniella vitripennis* (Walker) (Hym., Pteromalidae), a parasite of muscoid flies. *Behaviour.* 1954;7:88–112. <https://doi.org/10.1163/156853955X00049>.
47. Collatz J, Steidle JLM, Wyss U. Der Kornkäfer und sein natürlicher Feind *Lariophagus distinguendus*. Kiel: Entofilm; 2006.
48. Burks R, Mitroiu M-D, Fusu L, Heraty JM, Janšta P, Heydon S, et al. From hell's heart I stab at thee! A determined approach towards a monophyletic Pteromalidae and reclassification of Chalcidoidea (Hymenoptera). *J Hymenopt Res.* 2022;94:13–88. <https://doi.org/10.3897/jhr.94.94263>.
49. Cruaud A, Rasplus J-Y, Zhang J, Burks R, Delvare G, Fusu L, et al. The Chalcidoidea bush of life—a massive radiation blurred by mutational saturation. *bioRxiv.* 2022. <https://doi.org/10.1101/2022.09.11.507458>
50. Kaschef AH. Étude biologique de *Stegobium paniceum* L. (Col. Anobiidae) et son parasite *Lariophagus distinguendus* Först. (Hym. Pteromalidae). *Ann Soc Entomol Fr.* 1955;124:1–88.
51. Steidle JLM, Schöller M. Olfactory host location and learning in the granary weevil parasitoid *Lariophagus distinguendus* (Hymenoptera: Pteromalidae). *J Insect Behav.* 1997;10:331–42. <https://doi.org/10.1007/BF02765601>.
52. Yoder MJ, Mikó I, Seltmann KC, Bertone MA, Deans AR. A gross anatomy ontology for Hymenoptera. *PLoS ONE.* 2010;5:e15991. <https://doi.org/10.1371/journal.pone.0015991>.
53. Seltmann KC, Yoder MJ, Mikó I, Forshage M, Bertone MA, Agosti D, et al. A hymenopterists' guide to the Hymenoptera Anatomy Ontology: utility, clarification, and future directions. *J Hymenopt Res.* 2012;27:67–88. <https://doi.org/10.3897/jhr.27.2961>.
54. Hymenoptera Anatomy Consortium. Hymenoptera Anatomy Ontology. 2022. <http://glossary.hymao.org>. Accessed 1 May 2023.
55. Kaschef AH. *Lariophagus distinguendus* Först., ectoparasite on *Rhizopertha dominica* Fab. *Bull Soc Entomol Egypte.* 1959;43:165–84.
56. Steidle JLM. Host recognition cues of the granary weevil parasitoid *Lariophagus distinguendus*. *Entomol Exp Appl.* 2000;95:185–92. <https://doi.org/10.1046/j.1570-7458.2000.00656.x>.
57. Mair MM, Ruther J. Chemical ecology of the parasitoid wasp genus *Nasonia* (Hymenoptera, Pteromalidae). *Front Ecol Evol.* 2019;7:184. <https://doi.org/10.3389/fevo.2019.00184>.
58. Steidle JLM, Fischer A, Gantert C. Do grains whisper for help? Evidence for herbivore-induced synomones in wheat grains. *Entomol Exp Appl.* 2005;115:239–45. <https://doi.org/10.1111/j.1570-7458.2005.00295.x>.
59. Smirnov E, Polejaeff W. On the behavior of *Lariophagus distinguendus* Först., a parasite of the granary weevil *Calandra granaria* L. *Zool Žurnal.* 1937;16:999–1012.
60. Vincent JFV, King MJ. The mechanism of drilling by wood wasp ovipositors. *Biomimetics.* 1995;3:187–201.
61. Sakes A, Dodou D, Breedveld P. Buckling prevention strategies in nature as inspiration for improving percutaneous instruments: a review. *Bioinspir Biomim.* 2016;11:021001. <https://doi.org/10.1088/1748-3190/11/2/021001>.
62. Cerkvenik U, Dodou D, van Leeuwen JL, Gussekloo SWS. Functional principles of steerable multi-element probes in insects. *Biol Rev.* 2018;94:555–74. <https://doi.org/10.1111/brv.12467>.
63. Billen J, Ito F. The basicoxal gland, a new exocrine structure in poneromorph ants (Hymenoptera, Formicidae): the basicoxal gland, a new exocrine structure in ants. *Acta Zool.* 2006;87:291–6. <https://doi.org/10.1111/j.1463-6395.2006.00244.x>.
64. Nadein K, Gorb S. Lubrication in the joints of insects (Arthropoda: Insecta). *J Zool.* 2022;316:24–39. <https://doi.org/10.1111/jzo.12922>.
65. Hajek AE, Eilenberg J. Insect parasitoids: attack by aliens. In: Natural enemies: an introduction to biological control. Cambridge: Cambridge University Press; 2018. p. 161–88. <https://doi.org/10.1017/9781107280267.009>
66. King PE, Rafai J. Host discrimination in a gregarious parasitoid *Nasonia vitripennis* (Walker) (Hymenoptera: Pteromalidae). *J Exp Biol.* 1970;53:245–54.
67. Jervis MA, Kidd NAC. Host-feeding strategies in hymenopteran parasitoids. *Biol Rev.* 1986;61:395–434. <https://doi.org/10.1111/j.1469-185X.1986.tb00660.x>.
68. Flanders SE. The secretion of the collateral glands in the parasitic chalcids. *J Econ Entomol.* 1934;27:861–2.
69. Pupedis RJ. Tube feeding by *Sisyridivora cavigena* (Hymenoptera: Pteromalidae) on *Climacia areolaris* (Neuroptera: Sisyridae). *Ann Entomol Soc Am.* 1978;71:773–5. <https://doi.org/10.1093/aesa/71.5.773>.
70. Le Ralec A. Egg contents in relation to host-feeding in some parasitic Hymenoptera. *Entomophaga.* 1995;40:87–93. <https://doi.org/10.1007/BF02372684>.
71. Austin AD, Browning TO. A mechanism for movement of eggs along insect ovipositors. *Int J Insect Morphol Embryol.* 1981;10:93–108. [https://doi.org/10.1016/S0020-7322\(81\)80015-3](https://doi.org/10.1016/S0020-7322(81)80015-3).
72. Wilkes A. Sperm transfer and utilization by the arrhenotokous wasp *Dahlbominus fuscipennis* (Zett.) (Hymenoptera: Eulophidae). *Can Entomol.* 1965;97:647–57. <https://doi.org/10.4039/Ent97647-6>.
73. Ratcliffe NA, King PE. The “venom” system of *Nasonia vitripennis* (Walker) (Hymenoptera: Pteromalidae). *Proc R Entomol Soc Lond Ser A Gen Entomol.* 1967;42:49–61. <https://doi.org/10.1111/j.1365-3032.1967.tb01002.x>.
74. Ratcliffe NA, King PE. Morphological, ultrastructural, histochemical and electrophoretic studies on the venom system of *Nasonia vitripennis* Walker (Hymenoptera: Pteromalidae). *J Morphol.* 1969;127:177–204. <https://doi.org/10.1002/jmor.1051270205>.
75. Jackson DJ. Observations on the female reproductive organs and the poison apparatus of *Caraphractus cinctus* Walker (Hymenoptera: Mymaridae). *Zool J Linn Soc.* 1968;48:59–81. <https://doi.org/10.1111/j.1096-3642.1969.tb00705.x>.
76. King PE, Ratcliffe NA. The structure and possible mode of functioning of the female reproductive system in *Nasonia vitripennis* (Hymenoptera: Pteromalidae). *J Zool.* 1969;157:319–44. <https://doi.org/10.1111/j.1469-7998.1969.tb01706.x>.
77. Howard RW, Baker JE. Morphology and chemistry of Dufour glands in four ectoparasitoids: *Cephalonomia tarsalis*, *C. waterstoni* (Hymenoptera: Bethyloidea), *Anisopteromalus calandrae*, and *Pteromalus cerealellae* (Hymenoptera: Pteromalidae). *Comp Biochem Physiol B Biochem Mol Biol.* 2003;135:153–67. [https://doi.org/10.1016/S1096-4959\(03\)00076-9](https://doi.org/10.1016/S1096-4959(03)00076-9).
78. Zhu JY, Ye G-Y, Hu C. Morphology and ultrastructure of the venom apparatus in the endoparasitic wasp *Pteromalus puparum* (Hymenoptera: Pteromalidae). *Micron.* 2008;39:926–33. <https://doi.org/10.1016/j.micron.2007.11.005>.
79. Mao N, Tang P, Tian H-W, Shi M, Chen X-X. General morphology and ultrastructure of the female reproductive apparatus of *Trichomalopsis shirakii* Crawford (Hymenoptera, Pteromalidae). *Microsc Res Tech.* 2016;79:625–36. <https://doi.org/10.1002/jemt.22676>.

80. Romani R, Isidoro N, Bin F. Antennal structures used in communication by egg parasitoids. In: Consoli FL, Parra JRP, Zucchi RA, editors. *Egg parasitoids in agroecosystems with emphasis on Trichogramma* (Progress in biological control, vol. 9). Dordrecht, Netherlands: Springer Science+Business Media; 2010. p. 57–96. https://doi.org/10.1007/978-1-4020-9110-0_3.
81. Kundanati L, Gundiah N. Biomechanics of substrate boring by fig wasps. *J Exp Biol*. 2014;217:1946–54. <https://doi.org/10.1242/jeb.098228>.
82. King PE, Fordy MR. The external morphology of the “pore” structures on the tip of the ovipositor in Hymenoptera. *Entomol Mon Mag*. 1970;106:65–6.
83. Le Ralec A, Rabasse JM, Wajnberg E. Comparative morphology of the ovipositor of some parasitic Hymenoptera in relation to characteristics of their hosts. *Can Entomol*. 1996;128:413–33. <https://doi.org/10.4039/Ent128413-3>.
84. Huang ZY, Li SY, Lu W, Zheng XL. Structure and sense organs of ovipositors of an endoparasitoid *Aprostocetus causalis* and an ectoparasitoid *Quadrasitichus mendeli* in *Leptocybe* spp. *Microsc Microanal*. 2019;25:250–6. <https://doi.org/10.1017/S1431927618015647>.
85. Quicke DLJ, Fitton MG, Ingram S. Phylogenetic implications of the structure and distribution of ovipositor valvelli in the Hymenoptera (Insecta). *J Nat Hist*. 1992;26:587–608. <https://doi.org/10.1080/00222939200770361>.
86. Heraty JM, Quicke DLJ. Phylogenetic implications of ovipositor structure in Eucharitidae and Perilampidae (Hymenoptera: Chalcidoidea). *J Nat Hist*. 2003;37:1751–64. <https://doi.org/10.1080/00222930210130320>.
87. Csader M, Mayer K, Betz O, Fischer S, Eggs B. Ovipositor of the braconid wasp *Habrobracon hebetor*: structural and functional aspects. *J Hymenopt Res*. 2021;83:73–99. <https://doi.org/10.3897/jhr.83.64018>.
88. Rahman MH, Fitton MG, Quicke DLJ. Ovipositor internal microsculpture in the Braconidae (Insecta, Hymenoptera). *Zool Scr*. 1998;27:319–31. <https://doi.org/10.1111/j.1463-6409.1998.tb00464.x>.
89. Bender JC. Anatomy and histology of the female reproductive organs of *Habrobracon jugnalis* (Ashmead) (Hymenoptera, Braconidae). *Ann Entomol Soc Am*. 1943;36:537–45. <https://doi.org/10.1093/aesa/36.3.537>.
90. Beshaw R, Grafen A, Quicke DLJ. Inferring life history from ovipositor morphology in parasitoid wasps using phylogenetic regression and discriminant analysis. *Zool J Linn Soc*. 2003. <https://doi.org/10.1046/j.1096-3642.2003.00078.x>.
91. Quicke DLJ, Wyeth P, Fawke JD, Basibuyuk HH, Vincent JFV. Manganese and zinc in the ovipositors and mandibles of hymenopterous insects. *Zool J Linn Soc*. 1998;124:387–96. <https://doi.org/10.1111/j.1096-3642.1998.tb00583.x>.
92. Quicke DLJ, Palmer-Wilson J, Burroughs A, Broad GR. Discovery of calcium enrichment in cutting teeth of parasitic wasp ovipositors (Hymenoptera: Ichneumonidae). *Afr Entomol*. 2004;12:259–64.
93. Ghara M, Kundanati L, Borges RM. Nature’s Swiss army knives: ovipositor structure mirrors ecology in a multitrophic fig wasp community. *PLoS ONE*. 2011;6:e23642. <https://doi.org/10.1371/journal.pone.0023642>.
94. Polidori C, García AJ, Nieves-Aldrey JL. Breaking up the wall: metal-enrichment in ovipositors, but not in mandibles, co-varies with substrate hardness in gall-wasps and their associates. *PLoS ONE*. 2013;8:e70529. <https://doi.org/10.1371/journal.pone.0070529>.
95. Andersen SO. Characterization of a new type of cross-linkage in resilin, a rubber-like protein. *Biochim Biophys Acta*. 1963;69:249–62. [https://doi.org/10.1016/0006-3002\(63\)91258-7](https://doi.org/10.1016/0006-3002(63)91258-7).
96. Andersen SO, Weis-Fogh T. Resilin. A rubberlike protein in arthropod cuticle. *Adv Insect Physiol*. 1964;2:1–65. [https://doi.org/10.1016/S0065-2806\(08\)60071-5](https://doi.org/10.1016/S0065-2806(08)60071-5).
97. Qin G, Hu X, Cebe P, Kaplan DL. Mechanism of resilin elasticity. *Nat Commun*. 2012;3:1003. <https://doi.org/10.1038/ncomms2004>.
98. Michels J, Gorb SN. Detailed three-dimensional visualization of resilin in the exoskeleton of arthropods using confocal laser scanning microscopy. *J Microsc*. 2012;245:1–16. <https://doi.org/10.1111/j.1365-2818.2011.03523.x>.
99. Billen JPJ. The Dufour gland closing apparatus in *Formica sanguinea* Latreille (Hymenoptera, Formicidae). *Zoomorphology*. 1982;99:235–44. <https://doi.org/10.1007/BF00312297>.
100. Billen J. Morphology and ultrastructure of the Dufour’s and venom gland in the ant *Myrmecia gulosa* (Fabr.) (Hymenoptera: Formicidae). *Aust J Zool*. 1990;38:305–15. <https://doi.org/10.1071/ZO9900305>.
101. Lieberman ZE, Billen J, van de Kamp T, Boudinot BE. The ant abdomen: the skeletomuscular and soft tissue anatomy of *Amblyopone australis* workers (Hymenoptera: Formicidae). *J Morphol*. 2022. <https://doi.org/10.1002/jmor.21471>.
102. Ernst AF, Mikó I, Deans AR. Morphology and function of the ovipositor mechanism in Ceraphronoidea (Hymenoptera, Apocrita). *J Hymenopt Res*. 2013;33:25–61. <https://doi.org/10.3897/JHR.33.5204>.
103. Schoeters E, Billen J. The control apparatus of the venom gland in formicine ants (Hymenoptera: Formicidae). *Neth J Zool*. 1996;46:281–9. <https://doi.org/10.1163/156854295X00230>.
104. Betz O, Birkhold A, Caliaro M, Eggs B, Mader A, Knippers J, et al. Adaptive stiffness and joint-free kinematics: actively actuated rod-shaped structures in plants and animals and their biomimetic potential in architecture and engineering. In: Knippers J, Nickel KG, Speck T, editors. *Biomimetic research for architecture and building construction: biological design and integrative structures* (Biologically-inspired systems, vol. 8). Cham, Switzerland: Springer International Publishing; 2016. p. 135–67. https://doi.org/10.1007/978-3-319-46374-2_8.
105. Cerkvénik U, van Leeuwen JL, Kovalev A, Gorb SN, Matsumura Y, Gussekloo SWS. Stiffness gradients facilitate ovipositor bending and spatial probing control in a parasitic wasp. *J Exp Biol*. 2019;222:jeb.195628. <https://doi.org/10.1242/jeb.195628>.
106. Elias LG, Kjellberg F, Farache FHA, Almeida EAB, Rasplus J-Y, Craud A, et al. Ovipositor morphology correlates with life history evolution in agaonid fig wasps. *Acta Oecol*. 2018;90:109–16. <https://doi.org/10.1016/j.actao.2017.10.007>.
107. van Lenteren JC. The development of host discrimination and the prevention of superparasitism in the parasite *Pseudeucoila bochei* Weld (Hym Cynipidae). *Neth J Zool*. 1976;26:1–83.
108. van Lenteren JC, Isidoro N, Bin F. Functional anatomy of the ovipositor clip in the parasitoid *Leptopilina heterotoma* (Thompson) (Hymenoptera: Eucolidae), a structure to grip escaping host larvae. *Int J Insect Morphol Embryol*. 1998;27:263–8. [https://doi.org/10.1016/S0020-7322\(98\)00019-1](https://doi.org/10.1016/S0020-7322(98)00019-1).
109. Sampalla B, Eggs B, Betz O. Bending the sting: joint-free movement principles in the ovipositor of the parasitoid wasp *Leptopilina heterotoma* (Figitidae). *Mitt dtsh Ges allg angew Ent*. 2018;21:171–4.
110. Compton S, Nefdt R. Extra-long ovipositors in chalcid wasps: some examples and observations. *Antenna*. 1988;12:102–5.
111. Elias LG, Teixeira SP, Kjellberg F, Pereira RAS. Diversification in the use of resources by *Idarnes* species: bypassing functional constraints in the fig-fig wasp interaction. *Biol J Linn Soc*. 2012;106:114–22. <https://doi.org/10.1111/j.1095-8312.2012.01851.x>.
112. Vincent JFV, Wegst UGK. Design and mechanical properties of insect cuticle. *Arthropod Struct Dev*. 2004;33:187–99. <https://doi.org/10.1016/j.asd.2004.05.006>.
113. Lauder GV. Form and function: structural analysis in evolutionary morphology. *Paleobiology*. 1981;7:430–42. <https://doi.org/10.1017/S0094837300025495>.
114. Wake MH. Morphology, the study of form and function, in modern evolutionary biology. In: Futuyma D, Antonovics J, editors. *Oxford surveys in evolutionary biology*, vol. 8. Oxford, UK: Oxford University Press; 1992. p. 289–346.
115. Delanoue P, Arambourg Y. Contribution à l’étude en laboratoire d’*Eupelmus urozonus* Dalm [Hym. Chalcidoidea Eupelmidae]. *Ann Soc Entomol Fr Nouv Sér*. 1965;1:817–42.
116. van Alebeek FAN, Rojas-Rousse D, Leveque L. Interspecific competition between *Eupelmus vuilleti* and *Dinarmus basalis*, two solitary ectoparasitoids of Bruchidae larvae and pupae. *Entomol Exp Appl*. 1993;69:21–31. <https://doi.org/10.1111/j.1570-7458.1993.tb01724.x>.
117. Arakawa R. Attack on the parasitized host by a primary solitary parasitoid, *Encarsia formosa* (Hymenoptera: Aphelinidae): the second female pierces, with her ovipositor, the eggs laid by the first one. *Appl Entomol Zool*. 1987;22:644–5. <https://doi.org/10.1303/aez.22.644>.
118. Netting JF, Hunter MS. Ovicide in the whitefly parasitoid, *Encarsia formosa*. *Anim Behav*. 2000;60:217–26. <https://doi.org/10.1006/anbe.2000.1463>.

119. Collier TR, Hunter MS, Kelly SE. Heterospecific ovicide influences the outcome of competition between two endoparasitoids, *Encarsia formosa* and *Encarsia luteola*. *Ecol Entomol*. 2007;32:70–5. <https://doi.org/10.1111/j.1365-2311.2006.00844.x>.
120. Gauld I, Bolton B. *The Hymenoptera*. Oxford: Oxford University Press; 1988.
121. Brajković M, Nikolić Z, Čurčić SB, Živić I, Stojanović D. Morphological changes of the ovipositor in species of Cheloninae (Hymenoptera: Braconidae) in the course of adaptation to egg-larval parasitism. *Arch Biol Sci*. 2010;62:469–77. <https://doi.org/10.2298/ABS1002469B>.
122. Polilov AA. Features of the structure of Hymenoptera associated with miniaturization: 2. Anatomy of *Trichogramma evanescens* (Hymenoptera, Trichogrammatidae). *Entomol Rev*. 2016;96:419–31. <https://doi.org/10.1134/S0013873816040047>.
123. Boisseau RP, Woods HA, Goubault M. The metabolic costs of fighting and host exploitation in a seed-drilling parasitic wasp. *J Exp Biol*. 2017;220:3955–66. <https://doi.org/10.1242/jeb.160887>.
124. Silvestri F. Contribuzioni alla conoscenza biologica degli imenotteri parassiti: V. Sviluppo del *Platygaster dryomyiae* Silv. (Fam. Proctotrupidae). *Boll Lab Zool Gen Agrar R Scuola Sup Agric Portici*. 1921;11:299–326.
125. Strand MR, Pech LL. Immunological basis for compatibility in parasitoid-host relationships. *Annu Rev Entomol*. 1995;40:31–56. <https://doi.org/10.1146/annurev.en.40.010195.000335>.
126. Carton Y, Nappi AJ. *Drosophila* cellular immunity against parasitoids. *Parasitol Today*. 1997;13:218–27. [https://doi.org/10.1016/S0169-4758\(97\)01058-2](https://doi.org/10.1016/S0169-4758(97)01058-2).
127. Devictor V, Clavel J, Julliard R, Lavergne S, Mouillot D, Thuiller W, et al. Defining and measuring ecological specialization. *J Appl Ecol*. 2010;47:15–25. <https://doi.org/10.1111/j.1365-2664.2009.01744.x>.
128. König K, Krimmer E, Brose S, Gantert C, Buschlüter I, König C, et al. Does early learning drive ecological divergence during speciation processes in parasitoid wasps? *Proc R Soc B Biol Sci*. 2015;282:20141850. <https://doi.org/10.1098/rspb.2014.1850>.
129. König C, Paschke S, Pollmann M, Reinisch R, Gantert C, Weber J, et al. Molecular and cytogenetic differentiation within the *Lariophagus distinguendus* (Förster, 1841) species complex (Hymenoptera, Pteromalidae). *Comp Cytogenet*. 2019;13:133–45. <https://doi.org/10.3897/CompCytogen.v13i2.34492>.
130. König K, Zundel P, Krimmer E, König C, Pollmann M, Gottlieb Y, et al. Reproductive isolation due to prezygotic isolation and postzygotic cytoplasmic incompatibility in parasitoid wasps. *Ecol Evol*. 2019;9:10694–706. <https://doi.org/10.1002/ece3.5588>.
131. Frasson L, Ferroni F, Ko SY, Dogangil G, Rodriguez y Baena F. Experimental evaluation of a novel steerable probe with a programmable bevel tip inspired by nature. *J Robot Surg*. 2012;6:189–97. <https://doi.org/10.1007/s11701-011-0277-4>.
132. Nakajima K, Schwarz O. How to use the ovipositor drilling mechanism of Hymenoptera for developing a surgical instrument in biomimetic design. *Int J Des Nat Ecodyn*. 2014;9:177–89. <https://doi.org/10.2495/DNE-V9-N3-177-189>.
133. Leibinger A, Oldfield MJ, Rodriguez y Baena F. Minimally disruptive needle insertion: a biologically inspired solution. *Interface Focus*. 2016;6:20150107. <https://doi.org/10.1098/rsfs.2015.0107>.
134. Scali M, Pusch TP, Breedveld P, Dodou D. Ovipositor-inspired steerable needle: design and preliminary experimental evaluation. *Bioinspir Biomim*. 2018;13:016006. <https://doi.org/10.1088/1748-3190/aa92b9>.
135. Wendt I, Klopstein S, König K, Al. E. Morphometric differentiation of populations of the parasitoid wasp *Lariophagus distinguendus* (Hymenoptera: Chalcidoidea: Pteromalidae). *Mitt Entomol Ges Stuttgart*. 2014. p. 32.
136. Schindelin J, Arganda-Carreras I, Frise E, Kaynig V, Longair M, Pietzsch T, et al. Fiji: an open-source platform for biological-image analysis. *Nat Methods*. 2012;9:676–82. <https://doi.org/10.1038/nmeth.2019>.
137. Büsse S, Gorb SN. Material composition of the mouthpart cuticle in a damselfly larva (Insecta: Odonata) and its biomechanical significance. *R Soc Open Sci*. 2018;5:172117. <https://doi.org/10.1098/rsos.172117>.
138. Venable JH, Coggeshall R. A simplified lead citrate stain for use in electron microscopy. *J Cell Biol*. 1965;25:407–8. <https://doi.org/10.1083/jcb.25.2.407>.
139. Schneider CA, Rasband WS, Eliceiri KW. NIH Image to ImageJ: 25 years of image analysis. *Nat Methods*. 2012;9:671–5. <https://doi.org/10.1038/nmeth.2089>.
140. Schindelin J, Rueden CT, Hiner MC, Eliceiri KW. The ImageJ ecosystem: an open platform for biomedical image analysis. *Mol Reprod Dev*. 2015;82:518–29. <https://doi.org/10.1002/mrd.22489>.
141. Cardona A, Saalfeld S, Schindelin J, Arganda-Carreras I, Preibisch S, Longair M, et al. TrakEM2 software for neural circuit reconstruction. *PLoS ONE*. 2012;7:e38011. <https://doi.org/10.1371/journal.pone.0038011>.
142. Saalfeld S, Fetter R, Cardona A, Tomancak P. Elastic volume reconstruction from series of ultra-thin microscopy sections. *Nat Methods*. 2012;9:717–20. <https://doi.org/10.1038/nmeth.2072>.
143. Betz O, Wegst U, Weide D, Heethoff M, Helfen L, Lee WK, et al. Imaging applications of synchrotron X-ray phase-contrast microtomography in biological morphology and biomaterials science. I. General aspects of the technique and its advantages in the analysis of millimetre-sized arthropod structure. *J Microsc*. 2007;227:51–71. <https://doi.org/10.1111/j.1365-2818.2007.01785.x>.
144. Martin T, Douissard P-A, Couchaud M, Rack A, Cecilia A, Baumbach T, et al. LSO-based single crystal film scintillator for synchrotron-based hard X-ray micro-imaging. *IEEE Trans Nucl Sci*. 2009;56:1412–8. <https://doi.org/10.1109/TNS.2009.2015878>.
145. Douissard P-A, Cecilia A, Rochet X, Chapel X, Martin T, van de Kamp T, et al. A versatile indirect detector design for hard X-ray microimaging. *J Instrum*. 2012;7:P09016. <https://doi.org/10.1088/1748-0221/7/09/P09016>.
146. Cloetens P, Pateyron-Salomé M, Buffière JY, Peix G, Baruchel J, Peyrin F, et al. Observation of microstructure and damage in materials by phase sensitive radiography and tomography. *J Appl Phys*. 1997;81:5878–86. <https://doi.org/10.1063/1.364374>.
147. Cloetens P, Ludwig W, Boller E, Helfen L, Salvo L, Mache R, et al. Quantitative phase contrast tomography using coherent synchrotron radiation. In: Bonse U, editor. *Proceedings of SPIE: developments in X-ray tomography III*, vol. 4503. Bellingham, WA, USA: SPIE Press; 2002. p. 82–91. <https://doi.org/10.1117/12.452867>.
148. Lösel PD, van de Kamp T, Jayme A, Ershov A, Faragó T, Pichler O, et al. Introducing Biomedisa as an open-source platform for biomedical image segmentation. *Nat Commun*. 2020;11:5577. <https://doi.org/10.1038/s41467-020-19303-w>.
149. Scudder GGE. The comparative morphology of the insect ovipositor. *Trans R Entomol Soc Lond*. 1961;113:25–40. <https://doi.org/10.1111/j.1365-2311.1961.tb00800.x>.
150. Austin AD. Morphology and mechanics of the ovipositor system of *Ceratobaeus* Ashmead (Hymenoptera: Scelionidae) and related genera. *Int J Insect Morphol Embryol*. 1983;12:139–55. [https://doi.org/10.1016/0020-7322\(83\)90006-5](https://doi.org/10.1016/0020-7322(83)90006-5).
151. Field SA, Austin AD. Anatomy and mechanics of the telescopic ovipositor system of *Scelio latreille* (Hymenoptera: Scelionidae) and related genera. *Int J Insect Morphol Embryol*. 1994;23:135–58. [https://doi.org/10.1016/0020-7322\(94\)90007-8](https://doi.org/10.1016/0020-7322(94)90007-8).
152. Austin AD, Field SA. The ovipositor system of scelionid and platygastroid wasps (Hymenoptera: Platygastroidea): comparative morphology and phylogenetic implications. *Invertebr Taxon*. 1997;11:1–87.
153. Fergusson NDM. A comparative study of the structures of phylogenetic importance of female genitalia of the Cynipoidea (Hymenoptera). *Syst Entomol*. 1988;13:13–30.
154. Abbott CE. How *Megarhyssa* deposits her eggs. *J NY Entomol Soc*. 1934;42:127–33.
155. Frühauf E. Legeapparat und Eiablage bei Gallwespen (Cynipidae). *Z Wiss Zool*. 1924;121:656–723.
156. Herrmann HR, Chao J-T. Furcula, a major component of the hymenopterous venom apparatus. *Int J Insect Morphol Embryol*. 1983;12:321–37. [https://doi.org/10.1016/0020-7322\(83\)90027-2](https://doi.org/10.1016/0020-7322(83)90027-2).
157. Ross HH. Sawfly genitalia: terminology and study technique. *Entomol News*. 1945;56:261–8.
158. Packer L. Comparative morphology of the skeletal parts of the sting apparatus of bees (Hymenoptera: Apoidea). *Zool J Linn Soc*. 2003;138:1–38. <https://doi.org/10.1046/j.1096-3642.2003.00055.x>.

159. Zhao Z-L, Zhao H-P, Ma G-J, Wu C-W, Yang K, Feng X-Q. Structures, properties, and functions of the stings of honey bees and paper wasps: a comparative study. *Biol Open*. 2015;4:921–8. <https://doi.org/10.1242/bio.012195>.
160. Shaw MR. Further notes on the biology of *Pseudavga flavicoxa* Tobias, 1964 (Hymenoptera, Braconidae, Rhysipolidae). *J Hymenopt Res*. 2017;54:113–28. <https://doi.org/10.3897/jhr.54.10789>.
161. Fritzén NR, Sääksjärvi IE. Spider silk felting—functional morphology of the ovipositor tip of *Clistopyga* sp. (Ichneumonidae) reveals a novel use of the hymenopteran ovipositor. *Biol Lett*. 2016;12:20160350. <https://doi.org/10.1098/rsbl.2016.0350>.
162. Takasuka K, Fritzén NR, Tanaka Y, Matsumoto R, Maeto K, Shaw MR. The changing use of the ovipositor in host shifts by ichneumonid ectoparasitoids of spiders (Hymenoptera, Ichneumonidae, Pimplinae). *Parasite*. 2018;25:17. <https://doi.org/10.1051/parasite/2018011>.
163. Shah ZA, Blackwell A, Hubbard SF. Ultramorphology of the ovipositor of *Venturia canescens* (Gravenhorst) and possible mechanisms for oviposition. *Int J Agric Biol*. 2012;14:908–14.
164. Shah ZA. Morphology, ultrastructure, and probable functions of the sense organs on the ovipositor stylets of the hymenopteran parasitoid, *Venturia canescens* (Gravenhorst). *Microsc Res Tech*. 2012;75:876–83. <https://doi.org/10.1002/jemt.22007>.
165. Boring CA, Sharkey MJ, Nychka JA. Structure and functional morphology of the ovipositor of *Homolobus truncator* (Hymenoptera: Ichneumonidae: Braconidae). *J Hymenopt Res*. 2009;18:1–24.
166. Venkatraman TV, Subba Rao BR. The mechanisms of oviposition in *Stenobracon deesae* (Cam.) (Hymenoptera: Braconidae). *Proc R Entomol Soc Lond*. 1954;29:1–9.
167. Kumpanenko AS, Gladun DV. Functional morphology of the sting apparatus of the spider wasp *Cryptocheilus versicolor* (Scopoli, 1763) (Hymenoptera: Pompilidae). *Entomol Sci*. 2018;21:124–32. <https://doi.org/10.1111/ens.12288>.
168. Matushkina NA. Sting microsculpture in the digger wasp *Bembix rostrata* (Hymenoptera, Crabronidae). *J Hymenopt Res*. 2011;21:41–52. <https://doi.org/10.3897/JHR.21.873>.
169. Vilhelmsen L, Isidoro N, Romani R, Basibuyuk HH, Quicke DLJ. Host location and oviposition in a basal group of parasitic wasps: the subgenual organ, ovipositor apparatus and associated structures in the Orussidae (Hymenoptera, Insecta). *Zoomorphology*. 2001;121:63–84. <https://doi.org/10.1007/s004350100046>.
170. Matushkina NA, Stetsun HA. Morphology of the sting apparatus of the digger wasp *Oxybelus uniglumis* (Linnaeus, 1758) (Hymenoptera, Crabronidae), with emphasis on intraspecific variability and behavioural plasticity. *Insect Syst Evol*. 2016;47:347–62. <https://doi.org/10.1163/1876312X-47032146>.
171. Stetsun H, Rajabi H, Matushkina N, Gorb SN. Functional morphology of the sting in two digger wasps (Hymenoptera: Crabronidae) with different types of prey transport. *Arthropod Struct Dev*. 2019;52:100882. <https://doi.org/10.1016/j.asd.2019.100882>.
172. Hildreth PE. Fertilization in *Drosophila*. II. Time of inactivation of a gene effect. *Proc Natl Acad Sci USA*. 1965;54:736–41. <https://doi.org/10.1073/pnas.54.3.736>.
173. McQueen EW, Afkhami M, Atallah J, Belote JM, Gompel N, Heifetz Y, et al. A standardized nomenclature and atlas of the female terminalia of *Drosophila melanogaster*. *Fly*. 2022;16:128–51. <https://doi.org/10.1080/19336934.2022.2058309>.
174. Dethier VG. The response of hymenopterous parasites to chemical stimulation of the ovipositor. *J Exp Zool*. 1947;105:199–207. <https://doi.org/10.1002/jez.1401050204>.
175. Le Lannic J, Nénon J-P. Functional morphology of the ovipositor in *Megarhyssa atrata* (Hymenoptera, Ichneumonidae) and its penetration into wood. *Zoomorphology*. 1999;119:73–9. <https://doi.org/10.1007/s004350050082>.
176. Rogers D. The ichneumon wasp *Venturia canescens*: oviposition and avoidance of superparasitism. *Entomol Exp Appl*. 1972;15:190–4. <https://doi.org/10.1111/j.1570-7458.1972.tb00195.x>.
177. Williams JR. The factors which promote and influence the oviposition of *Nemeritis canescens* Grav (Ichneumonidae, Ophioninae). *Proc R Entomol Soc Lond Ser A Gen Entomol*. 1951;26:49–58. <https://doi.org/10.1111/j.1365-3032.1951.tb00120.x>.

Publisher's Note

Springer Nature remains neutral with regard to jurisdictional claims in published maps and institutional affiliations.

Ready to submit your research? Choose BMC and benefit from:

- fast, convenient online submission
- thorough peer review by experienced researchers in your field
- rapid publication on acceptance
- support for research data, including large and complex data types
- gold Open Access which fosters wider collaboration and increased citations
- maximum visibility for your research: over 100M website views per year

At BMC, research is always in progress.

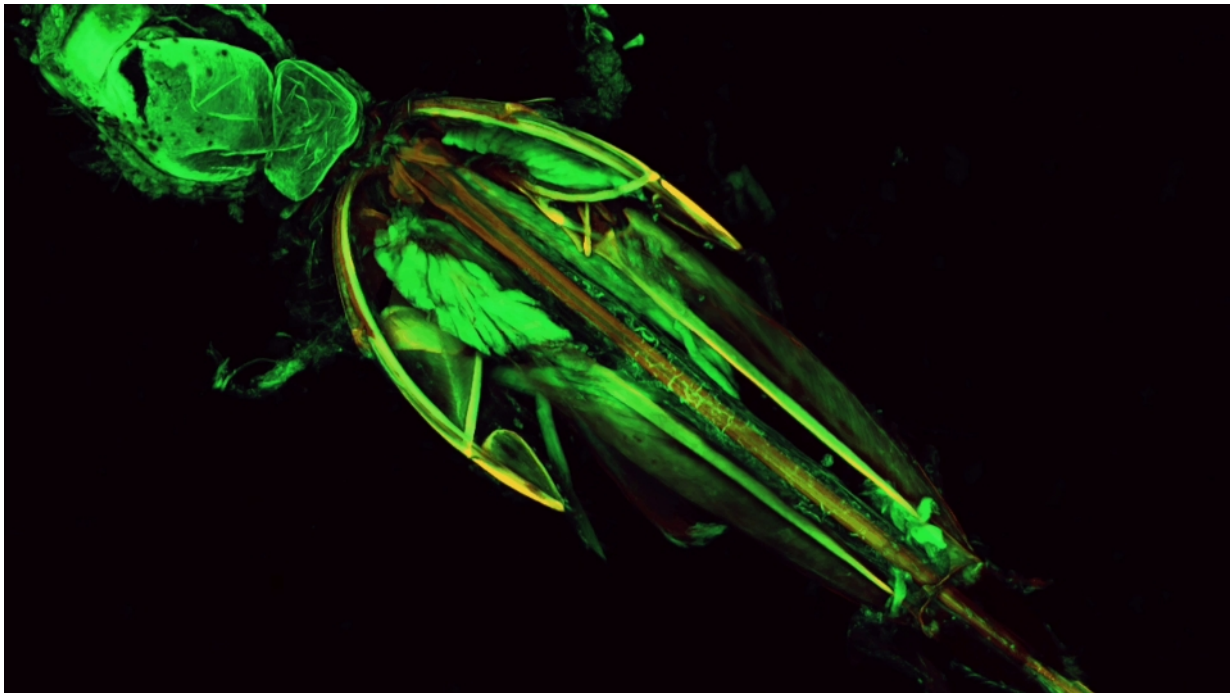
Learn more biomedcentral.com/submissions



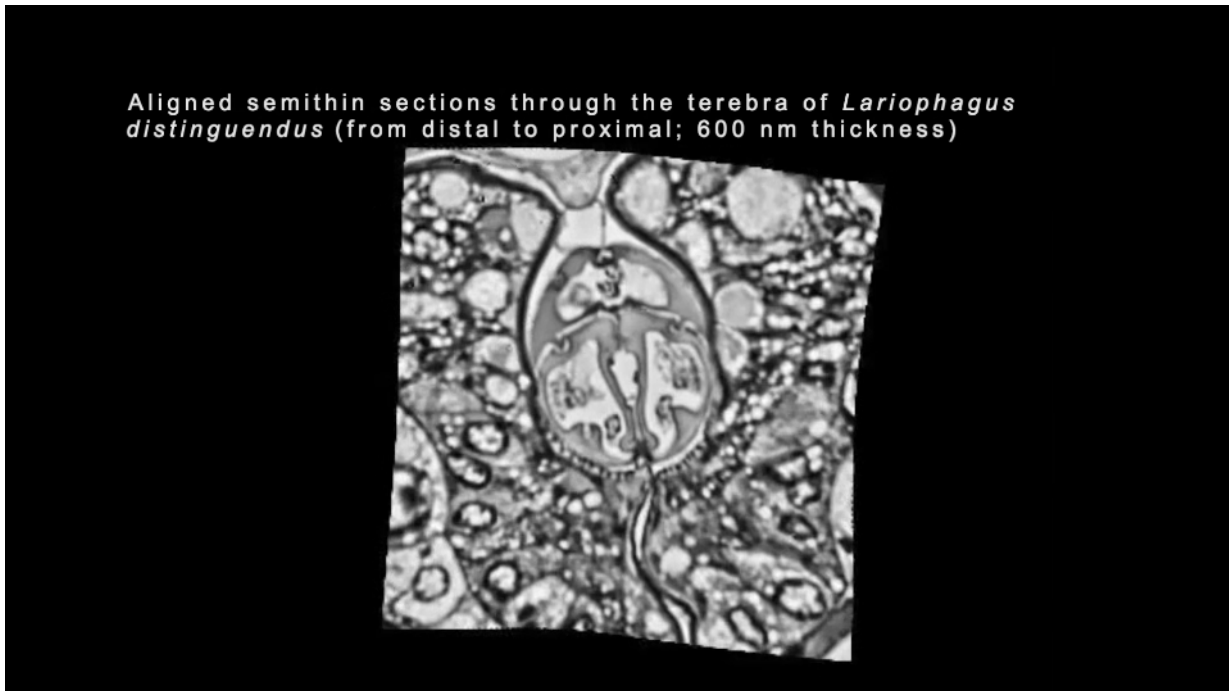
Additional files (supplementary material): video files (snapshots displayed here); available online at <https://frontiersinzooology.biomedcentral.com/articles/10.1186/s12983-023-00503-1>



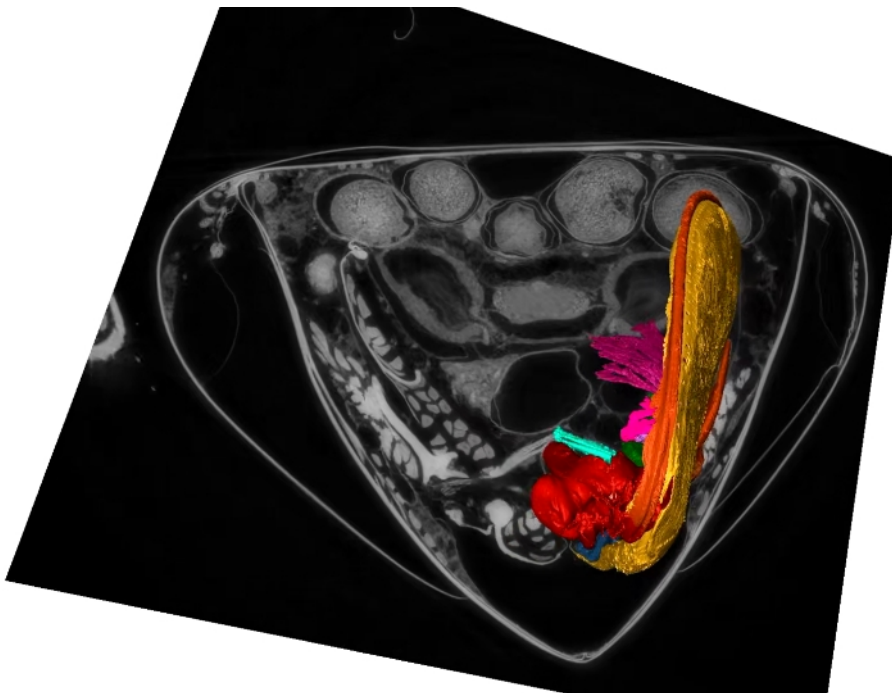
Additional file 1: Video sequences of female *Lariophagus distinguendus* parasitizing larvae of *Sitophilus granarius* in an artificial chamber (cf. Fig. 2b–p). The terebra bending and rotating movements during host assessment and the alternate movements of the paired 1st valvulae can be observed. (MP4)



Additional file 2: Superimposed CLSM images of the ovipositor of *Lariophagus distinguendus* (dorsal view, cf. Fig. 3g,h). (MP4)



Additional file 3: Animation of the aligned section through the terebra of *Lariophagus distinguendus* (from distal to proximal; cf. Fig. 4a–d). The jittering movements of the two halves of the 2nd valvula in the middle of the image stack result from section compression artefacts. (MP4)



Additional file 4: Animation of the rotating segmented 3D model of the musculoskeletal ovipositor system of *Lariophagus distinguendus* (cf. Fig. 5, 6). (MP4)

Publication 6

Sampalla B., **Eggs B.** and Betz O. (2018). Bending the sting: joint-free movement principles of the ovipositor shaft of the parasitoid wasp *Leptopilina heterotoma* (Figitidae). *Mitteilungen der Deutschen Gesellschaft für allgemeine und angewandte Entomologie* 21: 171–174.

(peer-reviewed conference paper)

Abstract

Prinzipien der gelenkfreien Bewegungen des Ovipositors der parasitoiden Wespe *Leptopilina heterotoma* (Figitidae)

Leptopilina heterotoma (THOMSON, 1862) (Hymenoptera: Figitidae), ein koinobionter Endoparasitoid von *Drosophila*-Larven, nutzt seine Terebra (= Eilegestachel), um das Substrat nach geeigneten Wirten zu sondieren. Die Terebra besteht aus den ineinander greifenden ersten und zweiten Valvulae des Ovipositors. Die zweiten Valvulae sind miteinander verwachsen und tragen eine schienenartige Struktur, die Rhachis. Die ersten Valvulae tragen die dazu passende Nut, Aulax genannt. Rhachis und Aulax formen zusammen das Olistheter-System, welches ausschließlich eine longitudinale Bewegung der Untereinheiten zueinander zulässt. Obwohl die Terebra keine intrinsische Muskulatur oder Sehnen aufweist und darüber hinaus auch keinerlei Gelenke besitzt, ist *L. heterotoma* in der Lage, ihre Terebra aktiv und scheinbar frei zu bewegen und zu biegen. Um auf potentielle funktionelle Prinzipien dieses Mechanismus zu schließen, untersuchen wir besagten Bewegungsablauf, sowie die Struktur der Terebra basierend auf bereits beschriebenen Strukturen und extrapolieren elastische sowie harte Anteile in der Terebra aufgrund der unterschiedlichen Autofluoreszenz von Resilin und Sklerotin. Es wurden keine bereits von anderen Autoren beschriebenen Strukturen gefunden, welche für die beobachtete gelenkfreie Biegebewegung der Terebra verantwortlich sein könnten. Auch die Notwendigkeit des "offset steering" für die Biegung kann ausgeschlossen werden, da die Bewegungen der Terebra auch außerhalb des Substrates beobachtet werden konnten. Über die gesamte Länge der Terebra dominiert die blaue, mit Resilin assoziierte Autofluoreszenz mit der Ausnahme eines longitudinalen rot fluoreszierenden Streifens, welcher auf eine stärkere Sklerotisierung des Olistheter-Systems hindeutet. Basierend auf unseren Resultaten stellen wir zwei Hypothesen auf, denen wir weiter nachgehen wollen:

- (1) Ein zur Spitze hin immer enger werdender Formschluss zwischen Rhachis und Aulax führt bei Unterschieden in longitudinal wirkenden Reibungskräften zu einer Biegung der Terebra.
- (2) Bereiche der Cuticula der Terebra stehen unter Vorspannung. Eine von den Muskeln über die Valviferen übertragene Kraft auf die Valvulae führt zu einer Verformung (Biegung, Torsion) der unter Vorspannung stehenden Strukturen.

Significance within the present thesis: In this study, we investigated the terebra bending of a cynipoid wasp: the figitid *Leptopilina heterotoma*. Female wasps have a long coiled terebra and exhibit terebra bending movements when attempting to parasitize their hosts, which live in plant substrates such as rotten fruits. In contrast to chalcidoid wasps (*cf.* Publication 5), these cynipoid wasps do not use active bending mechanisms but passive ones, whereby the movements of the terebra originate from the interplay between the surrounding substrate and the individual valvulae.

Methods used: high-speed videography, scanning electron microscopy (SEM), wide-field epifluorescence microscopy (WFM)

Own contribution: designing and co-supervising the study; discussing and revising the manuscript

Bending the sting: joint-free movement principles in the ovipositor of the parasitoid wasp *Leptopilina heterotoma* (Figitidae)

Benjamin Sampalla, Benjamin Eggs & Oliver Betz

University of Tübingen, Institute for Evolution and Ecology, Evolutionary Biology of Invertebrates

Zusammenfassung: Prinzipien der gelenkfreien Bewegungen des Ovipositors der parasitoiden Wespe *Leptopilina heterotoma* (Figitidae)

Leptopilina heterotoma (THOMSON, 1862) (Hymenoptera: Figitidae), ein koinobionter Endoparasitoid von *Drosophila*-Larven, nutzt seine Terebra (= Eilegestachel), um das Substrat nach geeigneten Wirten zu sondieren. Die Terebra besteht aus den ineinander greifenden ersten und zweiten Valvulae des Ovipositors. Die zweiten Valvulae sind miteinander verwachsen und tragen eine schienenartige Struktur, die Rhachis. Die ersten Valvulae tragen die dazu passende Nut, Aulax genannt. Rhachis und Aulax formen zusammen das Olistheter-System, welches ausschließlich eine longitudinale Bewegung der Untereinheiten zueinander zulässt. Obwohl die Terebra keine intrinsische Muskulatur oder Sehnen aufweist und darüber hinaus auch keinerlei Gelenke besitzt, ist *L. heterotoma* in der Lage, ihre Terebra aktiv und scheinbar frei zu bewegen und zu biegen. Um auf potentielle funktionelle Prinzipien dieses Mechanismus zu schließen, untersuchen wir besagten Bewegungsablauf, sowie die Struktur der Terebra basierend auf bereits beschriebenen Strukturen und extrapolieren elastische sowie harte Anteile in der Terebra aufgrund der unterschiedlichen Autofluoreszenz von Resilin und Sklerotin. Es wurden keine bereits von anderen Autoren beschriebenen Strukturen gefunden, welche für die beobachtete gelenkfreie Biegebewegung der Terebra verantwortlich sein könnten. Auch die Notwendigkeit des „offset steering“ für die Biegung kann ausgeschlossen werden, da die Bewegungen der Terebra auch außerhalb des Substrates beobachtet werden konnten. Über die gesamte Länge der Terebra dominiert die blaue, mit Resilin assoziierte Autofluoreszenz mit der Ausnahme eines longitudinalen rot fluoreszierenden Streifens, welcher auf eine stärkere Sklerotisierung des Olistheter-Systems hindeutet. Basierend auf unseren Resultaten stellen wir zwei Hypothesen auf, denen wir weiter nachgehen wollen:

- (1) Ein zur Spitze hin immer enger werdender Formschluss zwischen Rhachis und Aulax führt bei Unterschieden in longitudinal wirkenden Reibungskräften zu einer Biegung der Terebra.
- (2) Bereiche der Cuticula der Terebra stehen unter Vorspannung. Eine von den Muskeln über die Valviferen übertragene Kraft auf die Valvulae führt zu einer Verformung (Biegung, Torsion) der unter Vorspannung stehenden Strukturen

Key words: joint-free movement, functional morphology, parasitoid wasp, ovipositor, terebra

Benjamin Sampalla, Evolutionary Biology of Invertebrates, Institute of Evolution and Ecology, University of Tübingen, Auf der Morgenstelle 28, 72076 Tübingen, Germany;
E-Mail: benjamin.sampalla@student.uni-tuebingen.de; bnmnsmp@gmail.com

Introduction

Many parasitoid wasps such as *Leptopilina heterotoma* (THOMSON, 1862) (Hymenoptera: Figitidae) are able to bend their highly flexible terebra (ovipositor shaft) actively in various directions in order to find or reach their potential hosts and to permit a better control over egg placement, despite the lack of joints or intrinsic musculature in the terebra itself.

The terebra consists of the interlocked first and second valvulae of the ovipositor. The second valvulae are fused and bear a rail-like structure, called the rhachis. The first valvulae bear the matching groove counterparts, named the aulax. The combination of rhachis and aulax forms the olistheter system, which restricts the movements of the valvulae against each other to the longitudinal axis (OESER, 1961). The longitudinal movements are induced over a mechanism formed by the first and second valvifers and

the female T9 (ninth abdominal tergum). The first valvifers bear the first valvulae, whereas the second valvifers bear the fused second valvulae. Joints are formed between the first and the second valvifers (intervalvifer articulation) and between the first valvifers and the female T9 (tergo-valvifer articulation). T9 and the second valvifers are connected with muscles that can move these elements against each other. This movement is transferred by the described mechanism to the first valvulae. Because of the pairwise construction, the first valvulae can operate in an alternating pattern. On the basal part, the terebra is twisted at 180° (Fig. 1B). This basal twist occurs in several species of the Cynipoidea (RONQUIST, 1999). When not in use, the whole ovipositor of *L. heterotoma* is retracted into the gaster, for which the terebra needs to be coiled (Fig. 1A).

Several potential movement principles are involved in the joint-free kinematics of elongated rod-shaped structures.

- (1) Interlocking mechanisms of elongated elements, which can move against each other, permit some bending induced by differences between the applied longitudinal forces on these elements. Such interlocking structures have been described in the terebra of species of the Braconidae (QUICKE & al., 1995), Aulacidae and Gasteruptiidae (QUICKE & FITTON, 1995).
- (2) Asymmetrical tips such as bevel tips bend away from their theoretical straight path. This phenomenon is described as offset steering (FRASSON & al., 2012); it is a passive bending movement induced by the mechanical resistance of the medium.

The present contribution aims to describe the underlying mechanisms of the joint-free bending ability of the terebra of *L. heterotoma*. It is part of an ongoing project on joint-free movement principles of rod-shaped structures (mouthparts, ovipositors) in insects (BETZ & al, 2016).

Material and Methods

To observe the movements of the terebra, *Drosophila* larvae were hatched and reared for two to three days in small transparent chambers. The substrate consisted of banana juice, which was first filtered, sedimented and decanted to make it transparent for light before it was gelled with agar-agar. Females of *L. heterotoma* were added to the larvae in the chamber and filmed with a high-speed video camera of the type FASTCAM SA3 Model 120K (Photron, Tokyo, Japan) at 125 frames per second and a shutter speed of 1/250 seconds. To achieve a clean shot of the bending procedure without the interfering substrate, one was placed roughly in a pouch between the substrate and the wall of the observation chamber.

Female wasps were killed in 70 % ethanol and dissected to obtain samples for scanning electron microscopy (SEM). The excised ovipositors were stepwise dehydrated in ethanol and critical point dried. The specimens were sputter-coated with 19 nm gold and investigated with a scanning electron microscope of the type EVO LS 10 (Carl Zeiss Microscopy GmbH, Jena, Germany).

Insect cuticle is known to emit autofluorescence at various wavelengths, depending on the material composition (MICHELS & GORB, 2012). Both resilin and sclerotin show autofluorescence but differ in the wavelength of the emitted light. Resilin emits blue light, peaking at 420 nm (ANDERSEN, 1963), whereas heavily sclerotized cuticle is dominated by red autofluorescence (MICHELS & GORB, 2012). The ovipositor was macerated as quickly as possible in hot potassium hydroxide to reduce the possible loss of resilin before it was washed in double-distilled H₂O and embedded in glycerine. Pictures were taken on an epifluorescence microscope Axio Imager M2 (Carl Zeiss Microscopy GmbH, Jena, Germany), equipped with an ORCA-flash4.0 V.2 CMOS camera (Hamamatsu Photonics, Hamamatsu, Japan).

Results

A female wasp was set into a pouch between the gel and the wall of an observation chamber and was observed when bending (Fig. 2) and rotating its terebra, with the terebra being outside the substrate. Interlocking structures such as those that QUICKE & al. (1995) and QUICKE & FITTON (1995) described for other parasitoid wasp taxa could not be found by SEM. The terebra of *L. heterotoma* exhibits a basal twist of 180° (Fig. 1B). Whereas the terebra is dominated by blue autofluorescence (Fig. 1C), the basal parts of the second valvula (bulbs), the apices of the valvulae and a longitudinal line throughout the terebra, which splits when the valvulae are undergoing separation (Fig. 1D, arrows on the terebra), is dominated by red autofluorescence (Fig. 1D).

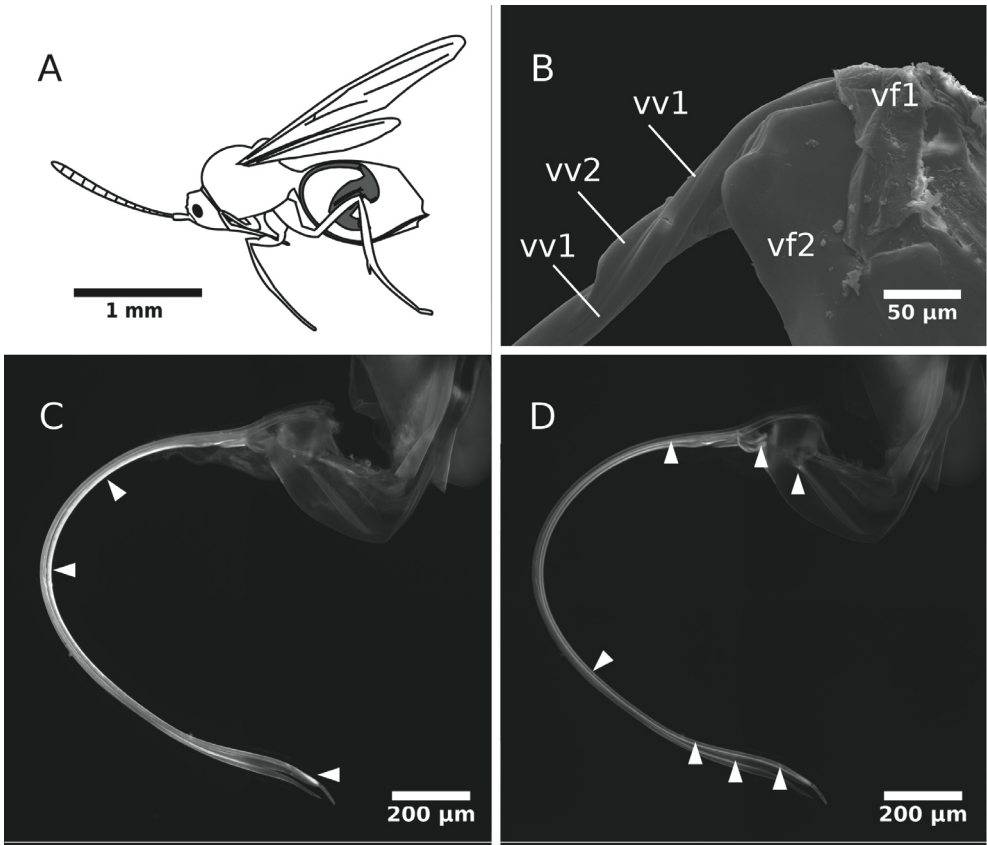


Fig. 1: A – Habitus of *Leptopilina heterotoma* and location of its coiled ovipositor (grey).

B – SEM picture of the basal part of the terebra, where the terebra exhibits a 180° twist when retracted into the gaster. Abbreviations: vf1, first valvifer; vf2, second valvifer; vv1, 1st valvulae; vv2, 2nd valvula.

C – Fluorescence microscopic image of the ovipositor; obtained by using a DAPI Filter. Arrows mark areas that respond strongly to UV excitation, implying the potential occurrence of resilin.

D – Fluorescence image of the ovipositor, obtained by using a Cy5 Filter. Arrows mark strongly sclerotized parts of the cuticle.

Discussion

As the bending of the terebra was observed outside the substrate, an offset steering mechanism caused by the friction between the substrate and the valvulae can be excluded. In the video footage, the wasps often rotated their bent terebra. As a result of their ability to rotate the terebra, a mechanism for bending in all directions is not required, because a combination of rotating and one-dimensional bending allows the wasps to move their terebra in all dimensions. Further, we suggest that the rotation takes place at the same location as the basal twist. The bright areas in Fig. 1C might be caused by the high content of resilin at those areas. Because of the preparation method and the non-specificity of the blue autofluorescence, further experiments are needed for confirmation. The red autofluorescence shows a longitudinal line, which seems to correlate with the olistheter system, as the line is split into two paths when one first valvula is separated from the other two valvulae (Fig. 1D).

Despite the use of a suitable method, we did not find any of the interlocking structures that were described by QUICKE & al. (1995) and QUICKE & FITTON (1995) and that could explain the active bending ability of *L. heterotoma*. Based on the presented results, we hypothesize that:

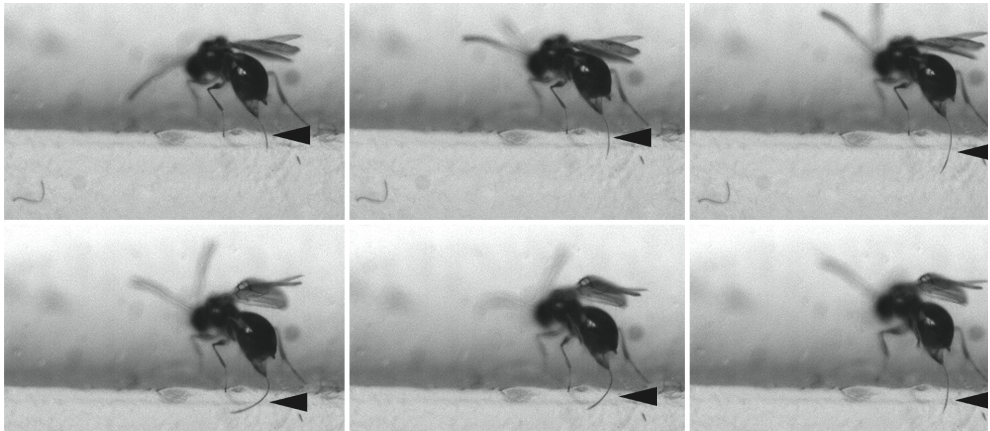


Fig. 2: Single frames of highspeed video recordings, showing *Leptopilina heterotoma* bending its terebra outside of the substrate. The arrows mark the terebra. Interval between single images: 160 ms.

The positive interlocking connection of the rhachis and the aulax may possess some modifications that occur in the distal part of the terebra but that we have not found as yet, e.g. a narrowing of the aulax or a tapering of the rhachis or the aulax. The interactions between the aulax and the rhachis then potentially cause interlocking attributable to increased friction forces, resulting in a bending of the terebra.

Parts of the cuticle of the terebra might be pre-stressed and, thus, bend or twist when a force that is generated by muscles is applied via the valvifers to the valvulae.

Ongoing investigations comprise further SEM and a histological semi-thin section series of the terebra from the apex to the basal joint of the ovipositor with a subsequent 3D reconstruction to reveal the functional principles of the joint-free terebra movements of *L. heterotoma*.

References

- ANDERSEN S. O. (1963): Characterization of a new type of cross-linkage in resilin, a rubber-like protein. – *Biochimica et Biophysica Acta*, **69**: 249-262. doi: [http://dx.doi.org/10.1016/0006-3002\(63\)91258-7](http://dx.doi.org/10.1016/0006-3002(63)91258-7)
- BETZ, O., BIRKHOFF, A., CALIARO, M., EGGS, B., MADER, A., KNIPPERS, J., RÖHRLE, O. & SPECK, O. (2016): Adaptive stiffness and joint-free kinematics – Actively actuated rod-shaped structures in plants and animals and their biomimetic potential in architecture and engineering. – In: KNIPPERS, J., NICKEL, K. & SPECK, T. (Eds.): *Biomimetic Research for Architecture and Building Construction. Biological Design and Integrative Structures. Biologically Inspired Systems* **9**: 135-167). Basel, Switzerland: Springer International Publishing, doi: 10.1007/978-3-319-46374-2_8
- FRASSON L., FERRONI F., KO S. Y., DOGANIL G. & RODRIGUEZ Y BAENA F. (2012): Experimental evaluation of a novel steerable probe with a programmable bevel tip inspired by nature. – *Journal of Robotic Surgery*, **6**(3): 189-197. doi: 10.1007/s11701-011-0277-4
- MICHELS J. & GORB S. (2012): Detailed three-dimensional visualization of resilin in the exoskeleton of arthropods using confocal laser scanning microscopy: detailed three-dimensional visualization of resilin. – *Journal of Microscopy*, **245** (1): 1-16. doi: 10.1111/j.1365-2818.2011.03523.x
- OESER R. (1961): Vergleichend-morphologische Untersuchungen über den Ovipositor der Hymenopteren. – *Mitteilungen aus dem Zoologischen Museum in Berlin*, **37** (1): 3-119.
- QUICKE D. L. & FITTON M. G. (1995): Ovipositor steering mechanisms in parasitic wasps of the families Gasteruptionidae and Aulacidae (Hymenoptera). – *Proceedings of the Royal Society of London B: Biological Sciences*, **261** (1360): 99-103. doi: 10.1098/rspb.1995.0122
- QUICKE D., FITTON M. & HARRIS J. (1995): Ovipositor steering mechanisms in braconid wasps. – *Journal of Hymenoptera Research*, **4**: 110-120.
- RONQUIST F. (1999): Phylogeny, classification and evolution of the Cynipoidea. – *Zoologica Scripta*, **28** (1-2): 139-164.

Publication 7

Tull T., Henn F., Betz O. and **Eggs B.** (2020). Structure and function of the stylets of hematophagous Triatominae (Hemiptera: Reduviidae), with special reference to *Dipetalogaster maxima*. *Arthropod Structure & Development* 58, 100952. doi: 10.1016/j.asd.2020.100952

(peer-reviewed journal article)

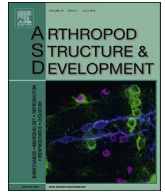
Abstract

Kissing bugs (Hemiptera: Reduviidae: Triatominae) are able to bend their rod-like maxillae while searching for blood vessels in the tissue of their vertebrate hosts. Little is known about the working mechanisms of these bending movements and the distal opening of the food channel. We compared the morphological structure of the stylets (mandibles and maxillae) of four triatomine species and analysed the feeding process of *Dipetalogaster maxima* (UHLER, 1894). The maxillae of triatomine bugs are interlocked by a tongue-and-groove system, allowing longitudinal sliding. While penetrating the host tissue, the animals perform rapid alternate back and forth movements of the maxillae. The resistance of the surrounding tissue pushes the asymmetric apex of the maxillae away from its straight path, *i.e.*, if one individual maxilla is protracted alone, its tip curves inwards, and the other maxilla follows. Once a blood vessel is tapped, the spine-like tip of the left maxilla splays outwards. Apically, each of the maxillae features an abutment, the left one exhibiting a notch that presumably facilitates splaying. The mechanical interaction of the two maxillary abutments enables the distal opening of the food channel but might also support the movements of the maxillary bundle attributable to different bending moment distributions.

Significance within the present thesis: The exclusively haematophagous kissing bugs belonging to the subfamily of Triatominae (Reduviidae) are important vectors of Chagas disease (Lent and Wygodzinsky 1979, Justi and Galvão 2016). In this study, we combined morphological descriptions and observations *in vivo*: we investigated and compared the morphological structure of the elongated stylets (comprising one pair of mandibles and maxillae, respectively) of four triatomine species and the way in which the maxillary bundle can be bent within the tissue as the bugs search for blood vessels. The maxillary bending in tissue is based on passive bending mechanisms. However, in liquids (*e.g.* inside a blood vessel), the bugs also exhibit active bending mechanisms of the maxillae prior to the distal opening of the food channel. This is an example of the way in which passive and active bending mechanisms can work within the same structure and be actuated by the same set of muscles.

Methods used: stereomicroscopy, scanning electron microscopy (SEM), wide-field epifluorescence microscopy, ultramicrotomy, light microscopy (LM), transmission electron microscopy (TEM), synchrotron X-ray phase contrast microtomography (SR- μ CT), high-speed videography

Own contribution: designing and co-supervising the study; preparing the specimens; performing histological, light/fluorescence microscopical and microtomographical studies; writing parts of the manuscript; discussing and revising the manuscript



Structure and function of the stylets of hematophagous Triatominae (Hemiptera: Reduviidae), with special reference to *Dipetalogaster maxima*

Tatjana Tull*, Fabian Henn, Oliver Betz, Benjamin Eggs

Evolutionary Biology of Invertebrates, Institute of Evolution and Ecology, Auf der Morgenstelle 28, 72076 Tübingen, Germany

ARTICLE INFO

Article history:

Received 22 January 2020

Accepted 29 April 2020

Keywords:

Bending

Functional morphology

Hematophagy

Joint-free movement

Mouthparts

Rhodnius

ABSTRACT

Kissing bugs (Hemiptera: Reduviidae: Triatominae) are able to bend their rod-like maxillae while searching for blood vessels in the tissue of their vertebrate hosts. Little is known about the working mechanisms of these bending movements and the distal opening of the food channel. We compared the morphological structure of the stylets (mandibles and maxillae) of four triatomine species and analyzed the feeding process of *Dipetalogaster maxima* (Uhler, 1894). The maxillae of triatomine bugs are interlocked by a tongue-and-groove system, allowing longitudinal sliding. While penetrating the host tissue, the animals perform rapid alternate back and forth movements of the maxillae. The resistance of the surrounding tissue pushes the asymmetric apex of the maxillae away from its straight path, i.e., if one individual maxilla is protracted alone, its tip curves inwards, and the other maxilla follows. Once a blood vessel is tapped, the spine-like tip of the left maxilla splays outwards. Apically, each of the maxillae features an abutment, the left one exhibiting a notch that presumably facilitates splaying. The mechanical interaction of the two maxillary abutments enables the distal opening of the food channel but might also support the movements of the maxillary bundle attributable to different bending moment distributions.

© 2020 Elsevier Ltd. All rights reserved.

1. Introduction

Kissing bugs belonging to the subfamily Triatominae (Hemiptera: Reduviidae) are native to Central and South America and are probably best known for their role as bloodsucking capillary-feeding vectors of Chagas disease (e.g., Lavoipierre et al., 1959; Lent and Wygodzinsky, 1979; Krenn and Aspöck, 2012; Justi and Galvão, 2017). Since the illness-causing trypanosomes, contained in the feces that most species release immediately after feeding, enter the body of the victim through the wound made by the animals' mouthparts (Kraus, 1957; Mesquita et al., 2008; Rabinovich et al., 1979; Rassi et al., 2010), their close examination is crucial for a full understanding of the transmission process of this disease. Moreover, the remarkable manner in which these animals are able to move their mouthparts by using joint-free bending for the efficient localization of blood vessels has attracted the attention of biomimetic researchers (Betz et al., 2016, 2019).

The mouthparts of the exclusively hematophagous Triatominae take the form of elongated stylets (comprising one pair of mandibles and maxillae, respectively), which are specialized for piercing and sucking (Lent and Wygodzinsky, 1979). The maxillae are flexible half-pipes (in cross section) tightly interlocked by a tongue-and-groove system that allows them to move against each other in a longitudinal direction (Wenk et al., 2009, 2010), while also ensuring success of the difficult task of forming and sealing the antidromic channels for food and salivary fluid during blood feeding (Rakitov, 2019). The maxillary apices are strongly asymmetric in shape, i.e., the spine-like left maxillae and the flagellum-like right maxillae can easily be differentiated. The maxillary bundle comprising the two interlocked maxillae is enclosed by the elongated mandibles, which have barb-like teeth at their distal end (Barth, 1952, 1953, 1954; Friend and Smith, 1971; Rakitov, 2019; Wirtz, 1987). When not in use, both the maxillary bundle and the mandibles are ensheathed by the tripartite labium that constitutes the proboscis, which is also called rostrum in hemipterans (e.g., Geigy and Kraus, 1952). At rest, the stylets are retracted in a straight configuration inside their heads until the tips of the stylets lie inside the labium (Wenk et al., 2009, 2010).

* Corresponding author.

E-mail address: tull.tatjana@t-online.de (T. Tull).

The general feeding process of triatomine bugs has been described previously (Barth, 1953; Bernard, 1974; Cobben, 1979; Geigy and Kraus, 1952; Kraus, 1957; Lavoipierre et al., 1959; Wirtz, 1987).

The blood meal is known to play a central role in the survival of the species. The animals are only able to reproduce or molt if they are able to feed sufficiently (Cohen, 1993). With this aim, the animals locate their hosts by the detection of CO₂ (Escandón-Vargas et al., 2017) and, as vessel feeders, locate subcutaneous blood vessels by using their antennae for the detection of temperature differences prior to penetration (Ferreira et al., 2007). The labium unfolds and the mandibles penetrate the skin by alternating back and forth movements. The two maxillae that form the maxillary bundle are then advanced into the host's tissue to locate blood vessels (Lavoipierre et al., 1959), thereby exhibiting bending movements in various directions. These movements can be characterized as 'joint-free movements' (as in Betz et al., 2016), since the stylets are single pieced cuticular rods that are devoid of any intrinsic musculature, and entirely result from the actions of muscles that originate inside the head capsule (Barth, 1952, 1953). Once a blood vessel is found, the distal opening of the food channel (= 'functional mouth' according to Lavoipierre et al., 1959), which is formed by the left and right maxillae, has to open to allow the intake of blood. The tip of the left maxilla splays 'sharply outwards' (Lavoipierre et al., 1959) to expose both the food and the salivary channels. Two strong pumps located in the head, a suction pump and a salivary pump, enable the flow of blood towards the animal and the antidromic stream of saliva into the blood vessel (Barth, 1952; Bennet-Clark, 1963; Krenn and Aspöck, 2012; Wenk et al., 2009, 2010), where its antihemostatic, anticoagulant, immunoregulatory, and anti-inflammatory properties facilitate the further uptake of viscous blood (Fontaine et al., 2011; Ribeiro, 1987; Ribeiro and Garcia, 1981). Evidence also exists for the anesthetic properties of the saliva, which is used to reduce the local sensitivity of the host's tissue (Dan et al., 1999). Since no muscles or any other structures are attached to this most distal part of the maxilla, the splaying of the spine is presumably triggered by solely structural (cuticular) components found in this immediate area in combination with a specific pattern of maxillary movements.

Both the joint-free maxillary movements in the tissue and the distal opening of the food channel have been known for some time based on results from light microscopy and observations with the naked eye (e.g., Lavoipierre et al., 1959). However, many details remain to be explained. Firstly, only limited information is available on the fine-structure of the stylets of the various species of the Triatominae. Secondly, the underlying working mechanisms of (1) the joint-free movements of the maxillary bundle in the host's tissue and (2) the distal opening of the food channel by the splaying of the spine-like tip of the left maxillae are still unclear.

Therefore, in this study, we compare the morphological structure of the stylets and analyze the feeding process of four species of the monophyletic Triatominae subfamily (Hemiptera: Reduviidae), i.e., *Dipetalogaster maxima*, *Rhodnius prolixus*, *Triatoma infestans* and *Panstrongylus megistus* (with special reference to *D. maxima*). These species were selected, because they vary widely in their head morphology and include the most important vectors of the Chagas disease. We have used photography to analyze the proportions of the head, scanning electron microscopy (SEM) to reveal microstructures, wide-field epifluorescence microscopy (WFM) to recognize differences in the material composition of the cuticle, Synchrotron X-ray phase-contrast microtomography (SR- μ CT), ultramicrotomy, light microscopy (LM), and transmission electron microscopy (TEM) to reveal the fine-structure of the cuticle, and high-speed videography to describe the deployment and movements of the stylets *in vivo* during the search for and uptake of food.

Based on this knowledge, we have developed preliminary hypotheses about the underlying working mechanisms of the joint-free movements of the maxillary bundle, the finding of the blood vessels and the splaying of the maxillary spine, which opens the maxillary food channel.

2. Materials and methods

2.1. Study species and maintenance

The following species were investigated in this study: *Dipetalogaster maxima* (Uhler, 1894), *Rhodnius prolixus* Stål, 1859, *Triatoma infestans* (Klug, 1834), and *Panstrongylus megistus* (Burmeister, 1835) (Fig. 1). The limited availability of potential disease vectors restricted our selection of species and their overall number.

The specimens were sourced from the long-term laboratory colonies of the research group 'Zoology and Parasitology' of the University of Bochum (Bochum, Germany) and were fed on a diet consisting solely of sterile defibrinated pig's blood (elocin Tierblutspezialitäten GmbH; Düsseldorf, Germany). The blood was served in latex finger stalls following Christophel et al. (1988) with some modifications. Prior to feeding, the finger stalls were boiled in distilled water for approximately 30 min, a procedure that sterilized them and facilitated the penetration of the membrane by the animal's mouthparts. A sterile pipette was used to fill the finger stall with blood. The filled finger stall was then closed with a clip and placed in a warm water bath. For *D. maxima*, a temperature of approximately 30–40 °C is required to trigger the feeding response (Appendix A. Supplementary material: Video S1), whereas the other species under study require temperatures of approximately 37 °C. A detailed account of specimen maintenance and breeding can be found in Appendix B.

Supplementary video related to this article can be found at <https://doi.org/10.1016/j.asd.2020.100952>

2.2. Measurements of the heads, pronota and stylets

The heads and pronota of exclusively adult animals of all four species under study were directly measured under a stereomicroscope with an integrated measuring bar. The specimens were pinned, so that the head (from the postocciput to the labrum (black-white lines; Fig. 1 d)) or the pronotum, respectively, was perpendicular to the direction of vision.

The dissected mandibles and maxillae of adult animals of all four species under study were mounted onto microscope slides, embedded in glycerol (Croma-Pharma GmbH; Leobendorf, Austria), subsequently photographed, and then measured to compare their proportions. Images were taken by using a Nikon DSC D90 camera (Nikon Corporation; Tokyo, Japan) with a SIGMA MAKRO 105MM F2.8 EX DG OS HSM object lens (SIGMA (Deutschland) GmbH; Rödermark, Germany). The distance between lens and specimen was varied by using STACKSHOT MACRO RAIL (manual steps; Cognisys Inc.; Traverse City, MI, USA) to obtain a sharp image in each focal plane and to ensure a shooting angle of exactly 90°.

Detailed shots of the apices of the maxillae of the same specimens were taken using a light microscope (for details see chapter 2.5.).

The lengths of the whole stylets and their apices were measured by using Fiji (Schindelin et al., 2012; version 2.0.0-rc-59/1.51k; available online at <https://imagej.net/Fiji>; RRID:SCR_002285), a distribution of the software ImageJ (Schneider et al., 2012; Schindelin et al., 2015; version 2.0.0-rc-68/1.52g; available online at <https://imagej.net>; RRID:SCR_003070).

The specimens' heads were submerged in 70% ethanol to take the overview images (Fig. 1 c–f; using the method described

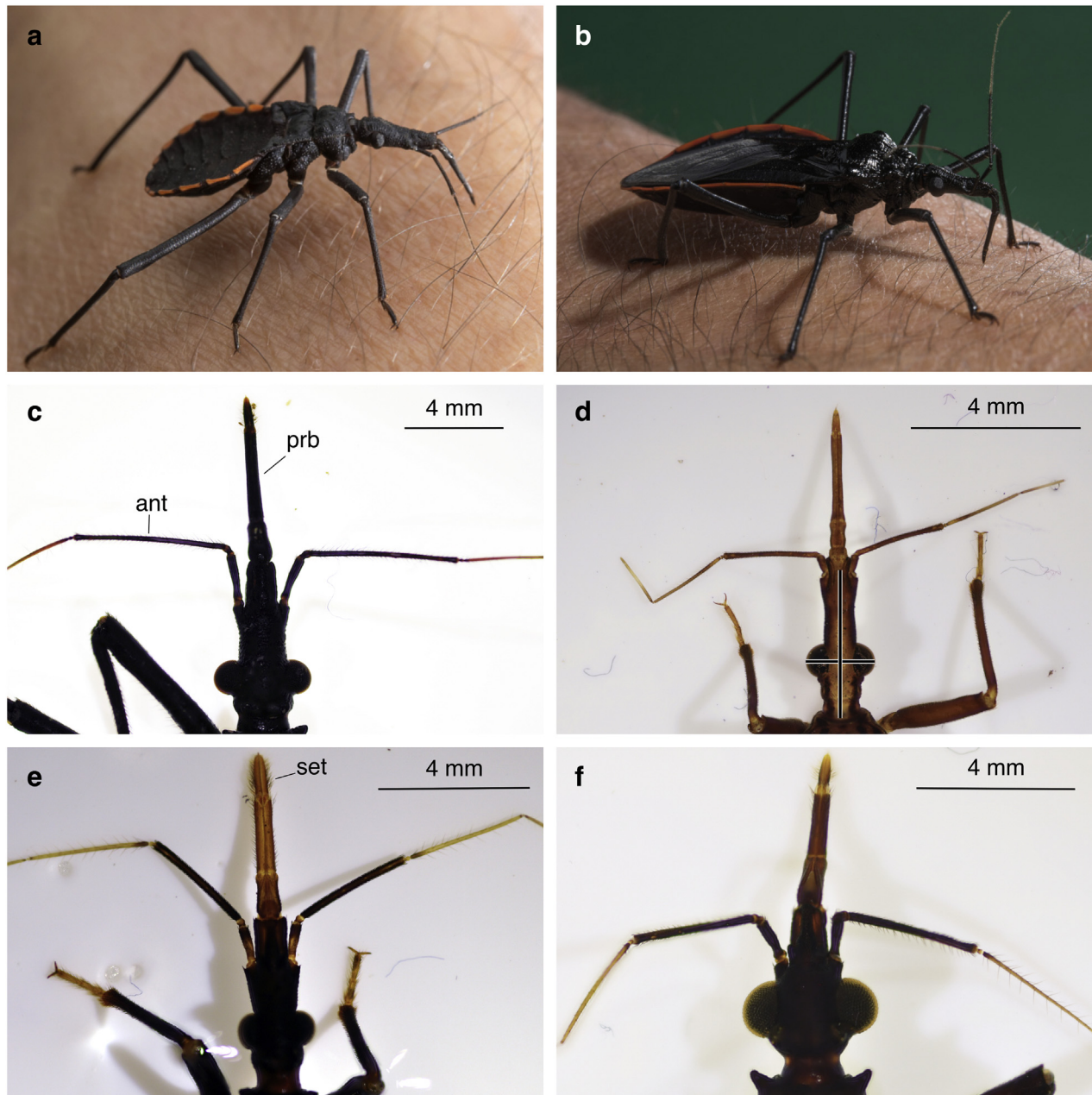


Fig. 1. a–b. Overview of a nymph (a) and an adult (b) *Dipetalogaster maxima* (photographed by Oliver Meckes, eye of science). c–f. Dorsal aspects of heads with antennae and proboscis of the four investigated species (adult animals: *D. maxima* (c); *Rhodnius prolixus* (d); *Triatoma infestans* (e); *Panstrongylus megistus* (f)). The lines in d demonstrate the means by which the lengths and the widths of the heads were determined (see Table 1) (ant: antennae; prb: proboscis; set: setae).

above), stacked, and rendered with HELICON REMOTE (version 3.6.2.w) and HELICON FOCUS (version 6.3.7 Pro; Helicon Soft Ltd; Kharkiv, Ukraine; RRID:SCR_014462). White balance was achieved by using LIGHTROOM (version 6.0; Adobe Systems Incorporated; San Jose, CA, USA).

2.3. Scanning electron microscopy (SEM)

Both adults and nymphs were used for SEM investigations (*D. maxima* adults: $n = 31$, nymphs: $n = 25$; *R. prolixus* adults: $n = 8$; *T. infestans* adults: $n = 7$; *P. megistus* adults: $n = 3$; unequal sample sizes are attributable to their different availability from the various breedings). All animals were stored in 70% ethanol until and during dissection. Both the mandibles and the maxillae were dissected

from the animals by either decapitating the specimens and pulling out the whole stylets or by opening the labium at the distal end and merely extracting the tips of the mouthparts.

Some samples were macerated with 10% aqueous sodium hydroxide (NaOH) for up to 17 h. All samples were dehydrated in ethanol at increasing concentrations (80% – 90% – 95% – 100% – 100%; 10 min each). A desiccator with silica gel (CARL ROTH GmbH + Co. KG; Karlsruhe, Germany; drying time: 1 week) and critical-point-drying (E3100 CPD; Quorum Technologies Ltd; East Sussex, UK) were both used for dehydration. The dried samples were sputtered with 19 nm pure gold in an EMITECH K550X sputter coater (Quorum Technologies Ltd; East Sussex, UK) and then analyzed using an EVO LS 10 scanning electron microscope (Carl Zeiss Microscopy GmbH; Jena, Germany) and the software

SmartSEM (version V05.04.05.00; Carl Zeiss Microscopy GmbH; Jena, Germany). We focused on the distal tips of both mandibles and maxillae and the interlocking structures between the two maxillae.

The images were later analyzed, and selected structures on the mandibles and maxillae were measured by using Fiji (Schindelin et al., 2012; version 2.0.0-rc-59/1.51k; available online at <https://imagej.net/Fiji>; RRID:SCR_002285).

2.4. Wide-field epifluorescence microscopy (WFM)

Wide-field epifluorescence microscopy (WFM) was used to analyze any differences in the material composition of the cuticle of the stylets. Arthropod cuticle shows an autofluorescence ranging from blue-green to deep-red. Heavily sclerotized and therefore robust areas are dominated by red fluorescence (Michels and Gorb, 2012). Resilin, on the other hand, is a structural protein with rubber-like properties (Andersen, 1963; Andersen and Weis-Fogh, 1964). It is known to be an efficient energy storage compound and a highly elastic material with almost complete recovery (Elvin et al., 2005). The autofluorescence of resilin can be made visible under UV illumination, as resilin has an autofluorescence at a narrow band around 415 nm wavelength. Thus, its blue coloration makes it easily distinguishable from the red fluorescence of the rigid cuticle (Andersen, 1963; Andersen and Weis-Fogh, 1964; Michels and Gorb, 2012). However, the validity of this method of resilin detection has limitations, since the intensity and wavelength of the fluorescence is pH-dependent (Andersen, 1963; Neff et al., 2000). Resilin also swells or shrinks depending on its state of hydration (Andersen and Weis-Fogh, 1964), a fact that might also influence its fluorescence patterns. Nonetheless, the detection of resilin via fluorescence microscopy is an accepted tool that has often been used in numerous studies over the last few years (e.g., Burrows et al., 2008; Appel et al., 2015; Deiters et al., 2016) and is acknowledged as a valid approach to the subject. Even though resilin is best known for its role in the flying and jumping abilities of insects (e.g., Elvin et al., 2005), the occurrence of resilin in the mouthparts of insects has long been recognized (e.g., Chapman, 2012; Büsse and Gorb, 2018).

For fluorescence microscopy, we dissected the stylets from eight freshly killed individuals of *D. maxima* (nymphs $n = 4$, adults: $n = 4$) and cleaned them in distilled water. We mounted the stylets carefully onto cleaned microscope slides and embedded them in glycerol (Croma-Pharma GmbH; Leobendorf, Austria) without dyes. Images were taken by using an epifluorescence microscope of the type Axio Imager M2 (Carl Zeiss Microscopy GmbH; Jena, Germany), equipped with an ORCA-Flash4.0 V2 Digital CMOS camera C11440–22CU (Hamamatsu Photonics K.K.; Hamamatsu, Japan) and the software ZEN 2 PRO (blue edition) (Carl Zeiss Microscopy GmbH; Jena, Germany). The following wavelength filters were used: DAPI (blue, excitation 353 nm, emission 465 nm), ATTO488 (green, excitation 500 nm, emission 525 nm), and Cy5 (red, excitation 650 nm, emission 673 nm). The three color channels were superimposed in order to show the autofluorescence of the cuticular structures.

2.5. Sample preparation, light microscopy (LM), and transmission electron microscopy (TEM)

We anesthetized specimens of *D. maxima* with carbon dioxide, submersed and fixed their heads in a modified Karnovsky's fixative (Karnovsky, 1965), and post-fixed them in an osmium tetroxide solution, with rinsing steps in cacodylate buffer after each of these fixation steps. The samples were dehydrated in a graded ethanol series including *en-bloc* staining with uranyl acetate before being

passed through increasing concentrations of Spurr low-viscosity embedding resin (Polysciences Inc.; Warrington, PA, USA) in propylene oxide. As a last incubation step, the samples were placed in fresh pure resin for embedding in silicon molds and polymerized.

Both semithin (600 nm) and ultrathin (60 nm) sections were cut perpendicularly to the head by using an ultramicrotome of the type Leica Ultracut UTC (Leica Microsystems GmbH; Wetzlar, Germany) equipped with a DiATOME diamond knife (45° knife angle; DiATOME Ltd; Nidau, Switzerland). We prepared two section series through the labium; one continuous series of semithin sections and one with consecutive alternating blocks of 28 semithin and 10 ultrathin sections. Semithin sections were mounted on microscope slides and stained with Stevenel's blue (del Cerro et al., 1980). Ultrathin sections were placed on formvar-coated copper slot grids and post-stained with uranyl acetate and lead citrate according to Venable and Coggeshall (1965).

We used a light microscope of the type Zeiss Axioplan (Carl Zeiss Microscopy GmbH; Jena, Germany) equipped with a Nikon D7100 single-lens reflex digital camera (Nikon Corporation; Tokyo, Japan) and the software Helicon Remote version 3.6.2.w (Helicon Soft Ltd, Kharkiv, Ukraine) to image the semithin sections.

To investigate and image the ultrathin sections, we used a transmission electron microscope of the type Philips/FEI Tecnai 10 (FEI Company, Hillsboro, OR, USA) operated at 80kV equipped with a side-mounted MegaView II TEM CCD camera (Olympus Soft Imaging Systems GmbH; Hamburg, Germany) and the software Tecnai G² User Interface version 2.1.5 (FEI Company; Hillsboro, OR, USA) or iTEM version 5.1 (Olympus Soft Imaging Systems GmbH; Hamburg, Germany). Details of the histological protocol for the semi- and ultrathin sections are given in Appendix C.

2.6. Synchrotron X-ray phase-contrast microtomography (SR- μ CT)

The head of an ethanol-fixed *D. maxima* was dehydrated stepwise in ethanol and critically-point-dried by using a Polaron 3100 (Quorum Technologies Ltd; West Sussex, UK) in order to minimize shrinkage artifacts by water loss during the tomography procedure. We unfolded the proboscis manually and glued the posterior end of the head onto a plastic pin, which was then mounted onto the goniometer head of the sample stage for tomography. Synchrotron X-ray phase contrast microtomography (SR- μ CT) (Betz et al., 2007) was performed at the beamline ID19 at the European Synchrotron Radiation Facility (ESRF; Grenoble, France) at 18.1 keV with a wavelength of $8 \cdot 10^{-11}$ m over a 180° rotation. The 3D voxel datasets were reconstructed from 2D radiographs by using the filtered back-projection algorithm (Cloetens et al., 1997, 2002) developed for absorption contrast tomography.

Image processing was performed by using the software Amira version 6.0 (FEI company; Hillsboro, OR, USA; RRID:SCR_014305).

2.7. High-speed videography

Although we had *ad libitum* access to a breeding colony of *D. maxima*, we only had limited access to animals of the other species used in this study (*R. prolixus*, *T. infestans*, and *P. megistus*). Because many living non-adult individuals with a good feeding response are required to record their searching and feeding process *in vivo* by using a high-speed camera, the majority of these studies were conducted on specimens of *D. maxima* (total number of recordings $n = 71$). The movement patterns of six adults of *P. megistus* (female: $n = 1$; male: $n = 5$) were also recorded.

In order to record the movements of the maxillae during the feeding process, we created an appropriate feeding chamber containing the specimen during video trials (Fig. 2). Different chambers enabled us to record the maxillary bundle in different media,

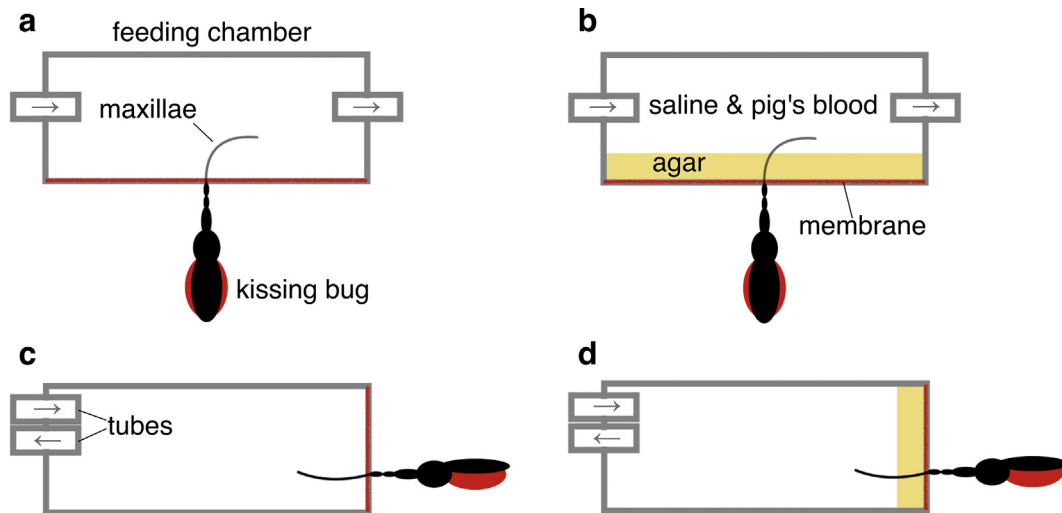


Fig. 2. Film and feeding chambers used to record the maxillary movements during the feeding process via high-speed videography. The tubes were used to fill the chambers with isotonic blood saline. **a–b.** Setup to record the lateral movements of the maxillae: without an agar layer (a) and with an agar layer (b). **c–d.** Setup to record the dorso–ventral movements of the maxillae: without an agar layer (c) and with an agar layer (d).

namely liquid *versus* tissue-like agar (Fig. 2). The feeding chamber was composed of four microscope slides glued together with silicone. The front was covered with a plastic mesh and the opposite end closed with an attached piece of cardboard that could easily be removed to insert or remove the animals. The film chamber allowed us to observe the maxillae during the feeding process and was designed based on Friend and Smith (1971). It was composed of two microscope slides glued together with about 6 mm silicone along the edges of three sides, whereas the front was left clear of silicone. Two small tubes were placed within the silicone of each of the two short sides to fill the chambers with liquids or to drain them. A latex membrane was attached with superglue to the front of the chamber. A transparent medium was necessary in order to be able to see and record the movements of the maxillary bundle. We therefore used an isotonic saline with the addition of one drop of sterile defibrinated pig's blood per 40 ml. This solution was transparent and was well received by the study animals. This chamber, filled with the isotonic blood saline, was used to observe lateral movements of the maxillae in a liquid medium. The same model with a thin agar layer placed directly behind the latex membrane was used to record the lateral movement under tissue-like conditions. Both these chamber types had a vertical version so that we could observe the dorso–ventral movements of the maxillae in both the liquid-like and tissue-like media. The two experimental setups (cf. Fig. 2), which differed in the orientation of the chamber, allowed us to video lateral movements (with the camera above the film chamber) and dorso–ventral movements (recorded from the side) of the maxillae.

The feeding chambers were heated with a heating plate to approximately 40 °C. One animal was placed into the feeding chamber and then positioned in front of the latex membrane. The warm film chamber membrane usually triggered the feeding response and stimulated the animal to unfold its proboscis. Because adult *D. maxima* usually showed a weak feeding response, most specimens used for this observation were nymphs (mostly subadults).

We recorded the movements of the maxillae in the various media via a stereo microscope of the type Leica MZ125 (Leica Mikrosystems; Wetzlar, Germany) with a high-speed camera of the type Photron FASTCAM SA3 Model 120K and the software Photron FASTCAM Viewer (PFV) (Photron Inc.; San Diego, CA, USA). General

movements were recorded at 60 frames per second with a shutter speed of 1/60 s, whereas fast movements (e.g., the distal opening of the food channel) were recorded at 250 frames per second with a shutter speed of 1/250 s and higher LED illumination intensity to ensure sufficient exposure.

3. Results

3.1. Morphological analyses

3.1.1. Head, labium and pronotum

The proportions of the head vary greatly between the species of the Triatominae under study (for the measurement method see Fig. 1 d).

The head of *R. prolixus* (Fig. 1 d) is the most slender of all compared species, being two times as long as it is wide, and also the most elongated compared with the pronotum length (Table 1). *P. megistus* (Fig. 1 f) has the stoutest head, which is also the shortest compared to the pronotum length (Table 1). This species also has the largest eyes relative to its head length, and its antennae originate extremely close to the anterior border of its eyes (Fig. 1 f). In *R. prolixus*, the antennae insert closely to the distal end of the head far away from the eyes (Fig. 1 d), whereas they insert further proximally in *D. maxima* (ant; Fig. 1 c) and *T. infestans* (Fig. 1 e). The apex of the labium in *T. infestans* is covered by small bristly setae (set; Fig. 1 e). The overall morphological structure of the tripartite labium, which ensheathes the mandibles and maxillae, does not vary across the four species. The length of the pronotum is a proxy for the overall body length of the animal (Table 1).

3.1.2. Mandibles

The overall morphological structure of the mandibles is in accord with previous descriptions (Barth, 1952, 1953; Cobben, 1979; Geigy and Kraus, 1952; Lavoipierre et al., 1959); they are long slender rods with barb-like teeth at their apices. However, some interspecific variation is found with respect to the toothed area and the appearance of the teeth themselves (Fig. 3). Both, the maxillae and the mandibles also show a lumen that represents a hemolymph space (Rakitov, 2019) (arrow heads, Fig. 6 a). The following structures can be noted on the mandibles.

Table 1
Measurements of the heads, pronota and stylets of adult triatomine bugs of all species under study. Arithmetic means \pm standard deviations (SD) are presented. The sample size (n = number of heads and stylets, respectively) is provided in brackets behind each mean value \pm SD. Unless stated otherwise, male and female animals were distinguished (n.a.: not available). **Length of head:** distance from the postocipitum to the labrum; **Width of head:** maximum width at the level of the compound eyes; **Ratio head:** length of head/width of head; **Relative length of head:** length of head/length of pronotum; **Relative length of mandibles:** length of mandibles/length of pronotum; **Relative length of left maxilla (maxL):** length of left maxilla/length of pronotum; **Relative length of right maxilla (maxR):** length of right maxilla/length of pronotum; **Length of flagellum (maxR):** distance distal edge of right maxillary abutment to apex; **Length of spine (maxL):** distance 'notch' to tip; **Mandibular row of teeth (rot) length:** first to last tooth; **Mandibular teeth length:** distance from tip of tooth to its base.

	<i>Dipetalogaster maxima</i>		<i>Rhodnius prolixus</i>		<i>Triatoma infestans</i>		<i>Panstrongylus megistus</i>	
	male	female	male	female	male	female	male	female
Head and pronotum (direct measurements)								
Length of head \pm SD [mm]	6.05 \pm 0.23 (3)	6.25 \pm 0.36 (3)	4.17 \pm 0.12 (5)	4.21 (1)	4.98 \pm 0.05 (2)	5.01 \pm 0.15 (4)	4.33 (1)	4.44 (1)
Width of head \pm SD [mm]	3.32 \pm 0.21 (3)	3.48 \pm 0.27 (3)	1.74 \pm 0.06 (5)	1.93 (1)	2.54 \pm 0.16 (2)	2.38 \pm 0.11	3.24 (1)	3.28 (1)
Ratio head	1.82	1.79	2.39	2.19	1.96	2.11	1.34	1.36
Relative length of head	1.15	1.10	1.48	1.37	1.23	1.19	0.92	0.83
Length of pronotum [mm]	5.24 \pm 0.54 (5)	5.67 \pm 0.34 (2)	2.82 \pm 0.16 (11)	3.08 (1)	4.06 \pm 0.18 (9)	4.20 \pm 0.25 (7)	4.73 (1)	5.32 \pm 0.13 (2)
Stylets whole (photography)								
Length of the mandibles \pm SD [mm]	9.66 \pm 0.19 (11)	10.23 \pm 0.19 (9)	6.41 \pm 0.09 (2)	6.62 \pm 0.11 (2)	7.82 \pm 0.21 (4)	7.79 \pm 0.15 (4)	n.a.	7.96 \pm 0.02 (2)
Relative length of mandibles	1.84	1.80	2.27	2.15	1.93	1.85	n.a.	1.49
Length of left maxilla (maxL) \pm SD [mm]	11.55 \pm 0.28 (3)	12.56 \pm 0.12 (4)	n.a.	8.39 (1)	n.a.	9.49 (1)	n.a.	n.a.
Relative length of left maxilla (maxL)	2.20	2.21	n.a.	2.72	n.a.	2.26	n.a.	n.a.
Length of right maxilla (maxR) \pm SD [mm]	12.02 \pm 0.35 (5)	12.69 \pm 0.20 (3)	8.05 (1)	8.45 (1)	n.a.	9.61 \pm 0.23 (3)	n.a.	8.66 (1)
Relative length of right maxilla (maxR)	2.29	2.24	2.85	2.74	n.a.	2.28	n.a.	1.63
Stylets apices (LM and SEM)								
Length of flagellum (maxR) \pm SD [μ m] (LM)	111.20 \pm 8.5 (6)	117.15 \pm 6.5 (5)	85.46 \pm 6.8 (6)	85.37 (1)	54.50 \pm 2.2 (3)	56.30 \pm 1.4 (5)	n.a.	61.40 (1)
Length of spine (maxL) \pm SD [μ m] (LM)	86.32 \pm 2.8 (6)	95.67 \pm 1.6 (5)	53.33 \pm 2.9 (6)	54.72 (1)	54.50 \pm 2.2 (6)	56.30 \pm 1.4 (5)	n.a.	30.28 (1)
Mandibular rot length \pm SD [μ m] (SEM)*		455.74 (1)		125.39 \pm 15.9 (7)		361.38 \pm 57.1 (6)		269.34 \pm 9.2 (2)
Mandibular teeth length \pm SD [μ m] (SEM)*		8.46 (1)		5.45 \pm 0.8 (6)		1.06 \pm 0.2 (5)		2.99 \pm 0.4 (3)
Mandibular teeth number \pm SD (SEM)*		30.00 (1)		22.17 \pm 0.9 (6)		42.20 \pm 4.3 (5)		20.00 \pm 0.0 (2)

Measurements were made either directly on ethanol-preserved specimens (direct measurements) or on the basis of photographs and LM or SEM images (indicated in brackets), respectively. Since the measurements of the stylets are based solely on 2D images, the measurement error is likely to be larger in the apices of the right maxillae, because of its flexible (and therefore often coiled) appearance, resulting in a slight underestimation of these values. *Male and female.

3.1.2.1. Apical row of teeth. All species possess a distal row of teeth (rot), with the teeth pointing proximad. In *D. maxima* (the largest of our study organisms, cf. length of pronotum; Table 1), the mandibles show a well-pronounced row of clearly separated teeth (rot; Fig. 3 a) with a distinct end; this is the longest (Table 1) among all studied species. *D. maxima* also possesses the longest teeth (Fig. 3 a; Table 1). In *R. prolixus*, the row of teeth and the teeth themselves are shorter. Furthermore, the teeth appear less 'stable', i.e., they are thinner and more brittle in *R. prolixus* than in *D. maxima* (compare Fig. 3 a and b). Some teeth at the proximal end of the row are curved in the distal direction in all species (Fig. 3 b). The row of teeth in all species is as clearly differentiated from the rest of the mandible as in *D. maxima* (Fig. 3 a and b). In *T. infestans*, the row of teeth is the second longest and possesses the most and smallest mandibular teeth (Fig. 3 c; Table 1). Accordingly, the end of the row of teeth in proximal direction is much harder to define. The structure of the apices of the mandibles of *P. megistus* strongly resemble those of *D. maxima* (Fig. 3 a, d; Table 1).

3.1.2.2. Surface furrows. In all species, the mandibular surface is covered by parallel furrows that start to intensify posteriorly of the row of teeth and that extend towards the apex of the mandible (Fig. 3 f). Whereas the lateral margins of the mandibles (in areas not covered by processes) seem to be mostly firm and rigid, some images of *D. maxima* (and to some extent also of *R. prolixus*) show a wavy and broad seam-like lateral extension (seam; msm; Fig. 3 e and Fig. 6 a). In all species, the mandibles enclose the maxillae to a different extent. This is especially pronounced in *D. maxima*, in which the mandibles apically form a completely closed sheath with overlapping seam-like extensions around the maxillae (Fig. 6 a, rows 2–4). Saliva can be found inside this sheath and inside the salivary channel of the maxillae (bold arrows; Fig. 6 a).

3.1.2.3. Mandibular processes. At a variable distance proximal of the row of teeth, an area of distally directed small processes can be

found on the seam of the mandibles in all species under study (mnp; Fig. 3 f). They vary in shape from short and stout to long, thin, and brittle. In *D. maxima*, *R. prolixus*, and *T. infestans*, they form a row on one or both the mandibular rims. They are spaced evenly, shaped asymmetrically, and bent towards the tip of the stylet. In *P. megistus*, the shape and arrangement of these processes differ from those of the other species (Fig. 3 g), since, in addition to the one row on each rim, a third row occurs immediately next to it. This row seems to be set deeper than the other two in a groove (mng; Fig. 3 g) parallel to the rim.

3.1.2.4. Material properties. The cuticle of the mandibular teeth and on the outer surface of the mandibles on which the teeth are located is strongly sclerotized as indicated by deep red auto-fluorescence of these structures (not shown). The ultrastructure of the cuticle of the mandibles as investigated by TEM was homogeneous with no apparent layering of cuticle fibers (not shown).

3.1.3. Maxillae

In all species under study, the left and right maxilla can be easily distinguished according to their shape. Whereas the apex of the right maxilla resembles a long flagellum, the apex of the left maxilla forms a sharp spine.

3.1.3.1. Flagellum-like apex of the right maxilla. The description of the right maxilla as a flagellum in the previous literature (e.g., Lavoipierre et al., 1959) was confirmed; its tip appears thin and whip-like in all the investigated species. Its most notable feature is a small indentation close to the end of the flagellum (arrow; Fig. 4 d) and a single projection at some distance to the tip, where its dorsal inner margin widens abruptly to form a right maxillary abutment (rma; Fig. 4 h; 'redan' sensu Bernard, 1974). It is found at the most distal end of the interlocking structures of the flagellum, is present only on one side (the side opposite of the salivary channel)

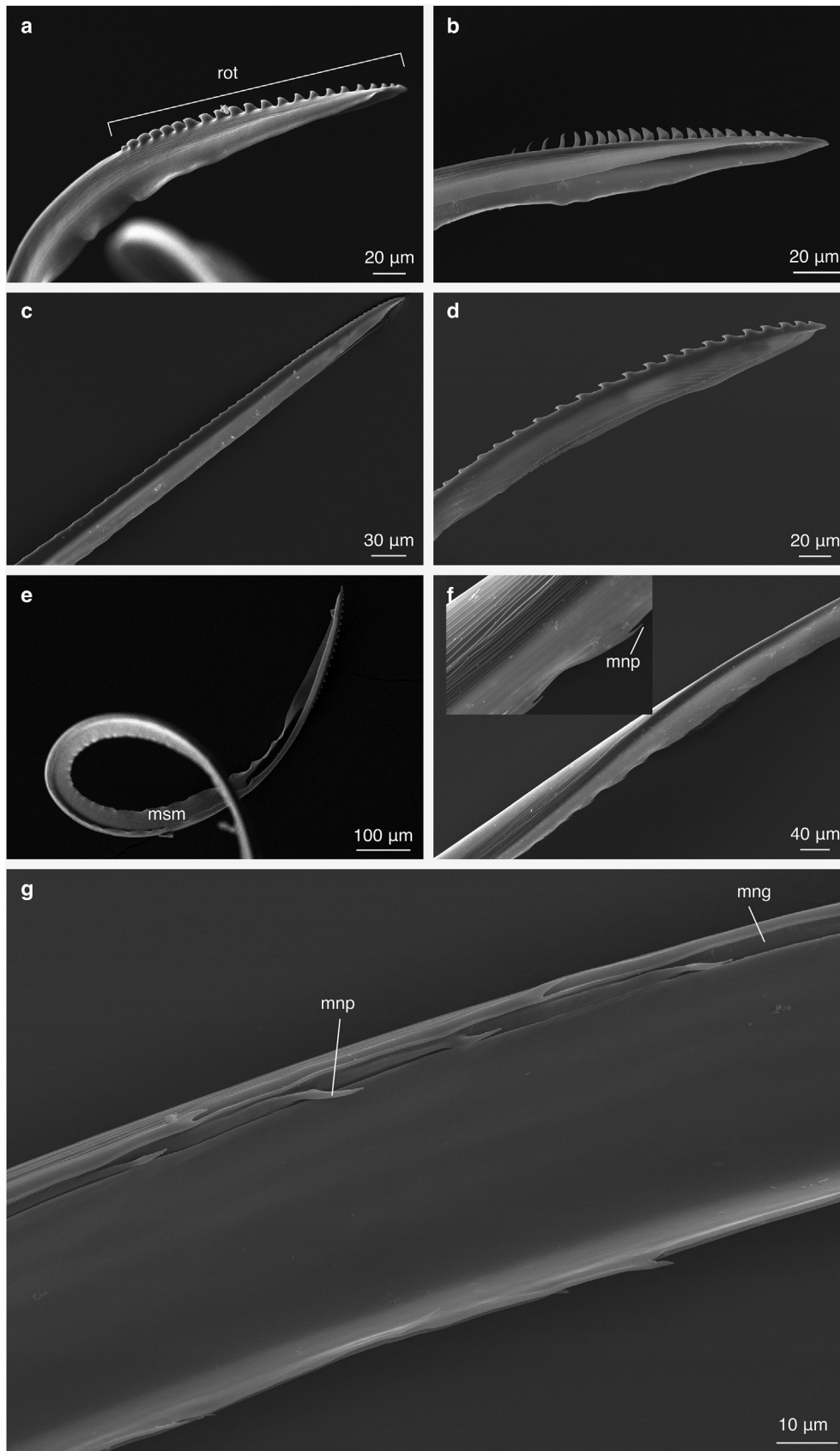


Fig. 3. **a–d.** SEM images of the apices and seam-like lateral extensions of the mandibles of four species of Triatominae: *Dipetalogaster maxima* (a, nymph); *Rhodnius prolixus* (b, adult); *Triatoma infestans* (c, adult); *Panstrongylus megistus* (d, adult). Morphological differences between the species are strongest regarding the length of the row of teeth and the shape and number of the mandibular teeth (see Table 1). **e.** Mandibular seam-like lateral extensions of *D. maxima* (nymph). **f.** Mandibular processes of *D. maxima* (nymph). Only one of two rows of processes on the rim is visible in this image. Their appearance is similar in *R. prolixus* and *T. infestans*. **g.** *P. megistus* (adult); inside aspect of the mandible. In addition to the two outer rows of mandibular processes, a third inner row can be seen in a groove (mng: mandibular groove; mnp: mandibular processes; msm: mandibular seam-like lateral extensions; rot: row of teeth).

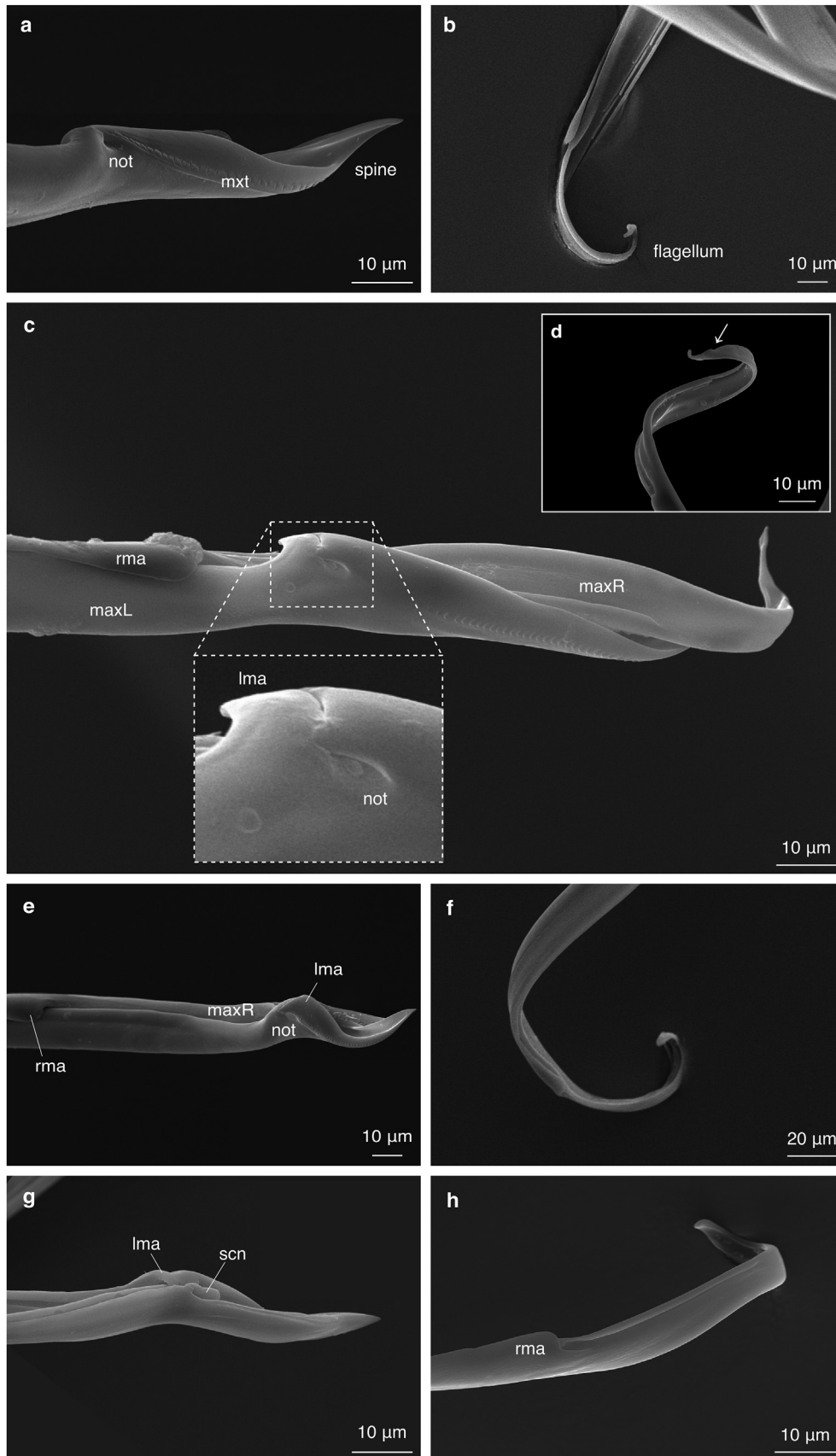


Fig 4. a–h. SEM images of the apices of the maxillae of four species of Triatominae: *Dipetalogaster maxima* (a, nymph; b, adult); *Rhodnius prolixus* (c, d, adult), *Triatoma infestans* (e, f, adult); *Panstrongylus megistus* (g, h, adult). Left maxillae (including the spine; a, c, e, g); right maxillae (including the flagellum, b, d, f, h); both maxillae conjoined (c, e). The abutments of the apices are clearly visible. The maxillary notch can be seen in a, c, and e, whereas g shows the opposite side of the clasp-like structure (lma: left maxillary abutment; maxL: left maxilla; maxR: right maxilla; mxt: maxillary teeth; not: notch; rma: right maxillary abutment; scn: salivary channel).

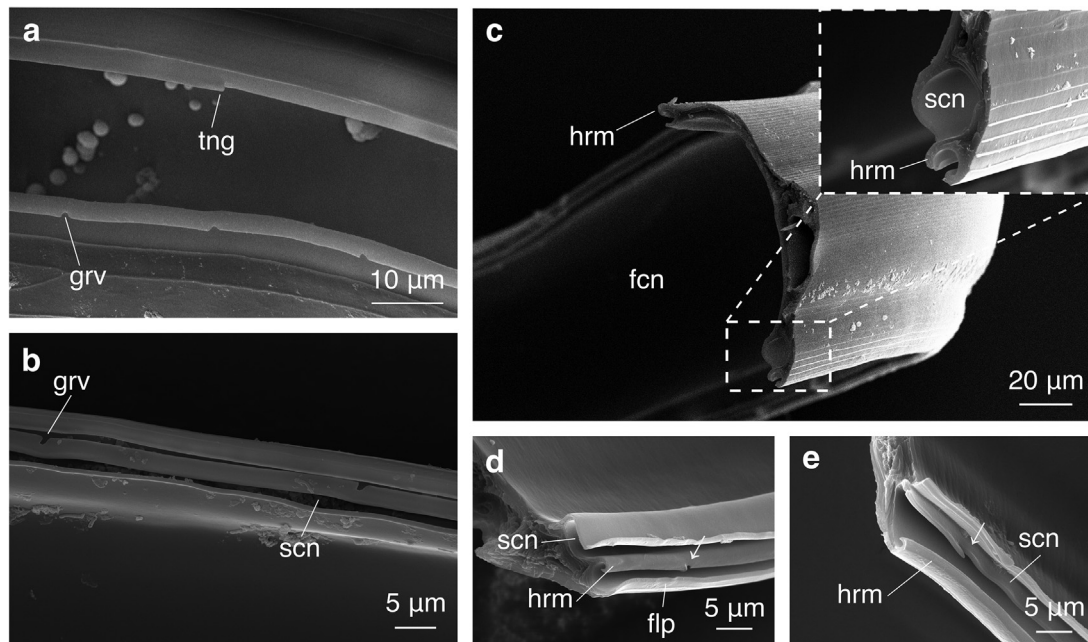


Fig 5. a–e. SEM images of the maxillary interlocking structures of three species of Triatominae: *Dipetalogaster maxima* (a, left maxilla, nymph, salivary channel not clearly visible); *Panstrongylus megistus* (b, left maxilla, adult); *D. maxima* (c, left maxilla); *Rhodnius prolixus* (adult; d, right maxilla; e, left maxilla) (fcn: food channel; flp: flap; grv: groove; hrm: hooked rim; scn: salivary channel; tng: tongue).

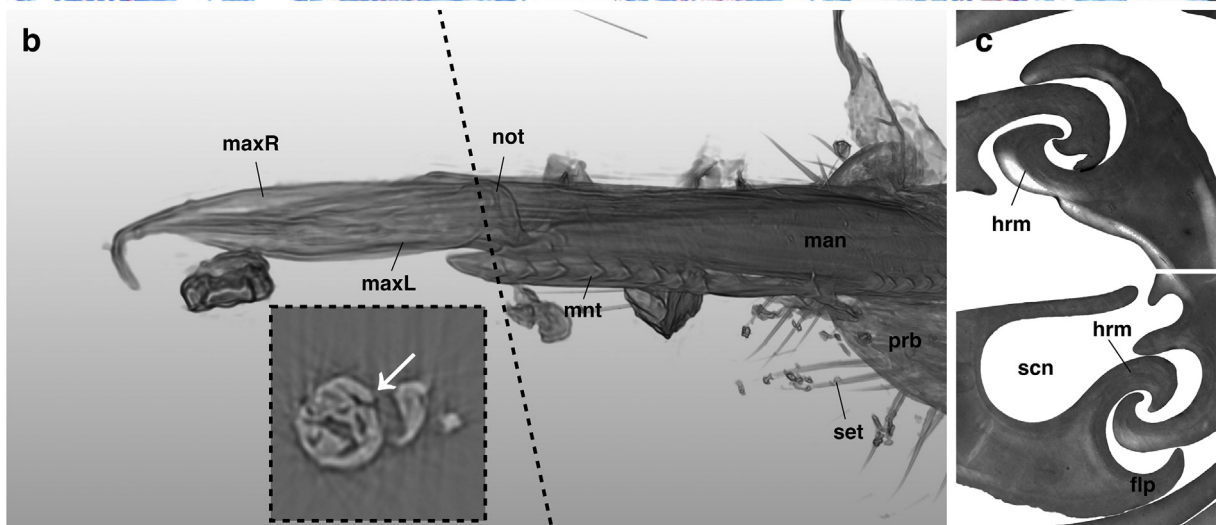
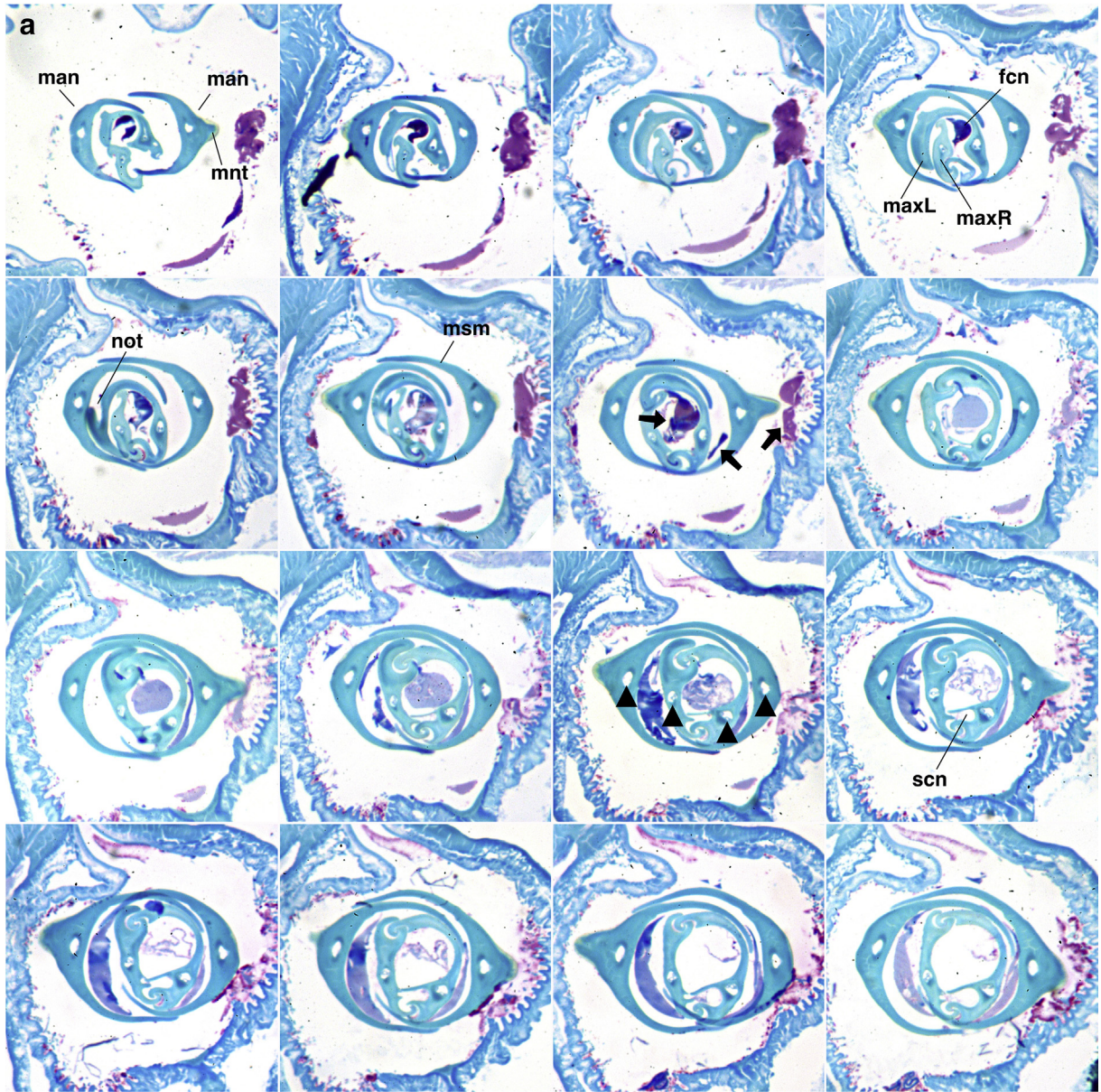
of the stylet, and varies in its distance to the tip between the species (length of flagellum; Table 1).

3.1.3.2. Spine-like apex of the left maxilla. The apices of the left maxillae were almost never deformed in the SEM images suggesting that their spine-like structure is sturdier than the apical flagellum of the right maxillae. This spine seems to be slightly twisted at the very apex from some perspectives (e.g., Figs. 4 a, 8 g). On one side of the apex of the left maxillae, a single row of maxillary teeth (mxt; Fig. 4 a) can be found that is most pronounced in *T. infestans* (Fig. 4 e). An additional small structure occurs (scn; Fig. 4 g) in all species investigated. Since this structure often looks broken or incomplete, we assume that it is delicate. According to its position, it was previously described as the outlet of the salivary channel (Wirtz, 1987). Similar to the right maxilla, the left maxilla has a single unpaired conspicuous ‘appendage’, namely the left maxillary abutment, which is also located on the side opposite of the salivary channel (lma; Fig. 4 c, e, g; ‘talon’ sensu Bernard, 1974). The rim with the outlet of the salivary channel is bent towards this abutment to form an open clasp-like structure that encloses the right maxilla when both stylets are interlocked (Fig. 4 c, e). Another structure of the apical spine that is also found in all species under study is the ‘maxillary notch’ (not; Fig. 4 a, c, e; Fig. 6 a and b; ‘encoche’ sensu Bernard (1974)) lying distally near the left maxillary abutment. It forms a hinge-like area of the left maxilla, so that the maxilla appears notched at this point. The structure of the notch is visible in cross section (not; Fig. 6 a), and its position was verified in the SR- μ CT dataset (Fig. 6 b). It is the only structure that appears flexible on the otherwise sturdy spine. The length of the spine varies between the species and is shorter than the flagellum of the right maxilla (length of spine; Table 1). The surface of both maxillae is smooth (Fig. 4 c) except for the structures described above.

3.1.3.3. Interlocking structures. The interlocking structures of both the maxillae form two channels, i.e., the dorsal food channel and the ventral salivary channel (Fig. 5 d; 6 a, c) (Barth, 1952;

Lavoipierre et al., 1959; Rakitov, 2019; Wenk et al., 2009, 2010). The hooked rims (hrm; Fig. 5 c–e; 6 c) of each edge of each maxilla are accompanied by a flap-like structure (flp; Fig. 5 d) that is clearly visible in cross section (flp; Fig. 6 c). Both the maxillae contribute to the salivary channel across their entire length with the exception of the regions close to the apex, a region in which the salivary channel (which is much smaller than the food channel (fcn; Fig. 5 c)) is no longer formed by both the maxillae but only by the left one (Fig. 5 c; cf. Barth, 1952; Wirtz, 1987). Finally, the twisted spine of the left maxilla contributes the major part of the formed tube of the maxillary bundle at its very apex (see first two rows of cross sections in Fig. 6 a). All species under study show a tongue and groove pattern with regard to the maxillary interlocking structures (tng, grv; Fig. 5 a and b). In the transverse section of the maxillary bundle of *D. maxima*, *R. prolixus*, and *T. infestans*, the left maxilla possesses tongues at the rim that is adjacent to the salivary channel (tng; Fig. 5 a) and grooves at the opposite rim (grv; Fig. 5 a). The opposite pattern of interlocking can be seen at the right maxilla. The spacing and the size of these tongues and grooves stay approximately the same from the tip to the base, which lies deep inside the head of the specimen. Notably, the tongues are oriented in the same way as the mandibular processes, pointing towards the tip of the stylet. *P. megistus* specimens however demonstrate a somewhat reversed pattern. At the left maxilla, grooves can be found at the rim that is adjacent to the salivary channel (grv; Fig. 5 b). These grooves are relatively wide close to the tip and become narrower towards the base of the maxilla. Because of the limited number of available specimens ($n = 2$), no conclusive statements can be made about the shape or position of the tongues of *P. megistus*.

3.1.3.4. Material properties. The cuticle of the maxillary abutments of both the maxillae appear heavily sclerotized, since these structures autofluoresce in deep red compared with the rest of the stylets (arrows; Fig. 8 d). Although the limited resolution of the epifluorescence microscope images does not allow the evaluation of the exact distribution of flexible versus sclerotized materials in



the maxillary apices or abutments (especially of the 'notch' of the left maxillae), both abutments seem to be more heavily sclerotized (red; arrows in Fig. 8 d) than other parts of the stylets. The area of the 'notch' is presumably less sclerotized, since this region auto-fluoresces less in red and more in blue indicating a higher proportion of the flexible protein resilin in the cuticle. Although both maxillae taper apically, their cross-sections change relatively little along most of their length. The ultrastructure of the cuticle of the maxillae is, like the cuticle of the mandibles, homogeneous with no apparent layering of cuticle fibers (Fig. 6 c).

3.2. Behavioral recordings

The movements of the stylets of *D. maxima* were recorded in various observational setups (cf. Fig. 2; Fig. 7). In the resting position, the labium was flexed ventrad in a groove between the coxae. First, the animals extended the labium by almost 180° to a vertical feeding position, pressed its tip against the warm membrane of the chamber, and penetrated the membrane with the mandibles (cf. Geigy and Kraus, 1952; Barth, 1953; Wirtz, 1987). Finally, the maxillae were protracted between the mandibles into the medium (total number of recordings n = 71).

3.2.1. Horizontal chambers with isotonic blood saline

In these chambers (cf. Fig. 2 a; n = 45; with adult males: n = 3, adult females: n = 7, subadults: n = 19, nymphs: n = 16), *D. maxima* specimens protracted the maxillary bundle through alternating stepwise forward movements of the individual maxillae. During these movements, a minor bending of the maxillary tips along one plane (usually the lateral) was frequently observed. In real time, the movements of the maxillary bundle were perceived as a twitching or waving of its tip, whereas the proximal part of the bundle only seemed to swing passively, following the movements of the tip. Movements in the sagittal plane occurred rarely and were always accompanied by a partial or full rotation of the maxillary bundle around its longitudinal axis.

A strong bending of the maxillary bundle was recorded during probing when the animals continuously released saliva from the maxillae, even when the distal opening food channel was closed, i.e., when the spine of the left maxilla was not splayed out. The apical part of the maxillary bundle always bent to the left (bold arrow; Fig. 7 a; single frames 0.144 s, 0.236 s; Appendix A. Supplementary material: Video S2). The strong bending of the maxillae was usually followed by an immediate return to their original straight state. Thereby, the right maxilla slid past the left one resulting in the splaying of the apical spine-like structure of the left maxilla (spine; Fig. 7 a; single frame 0.250 s; Fig. 8 a and b, g). Once the spine was splayed, the animal continuously secreted huge amounts of saliva around the distal opening of the food channel. Even during food uptake, the right maxilla was frequently observed to be protracted and retracted beyond the point at which the left and right maxillary abutments would interact. After probing or food intake, the right maxilla was retracted to its initial position, causing the spine to return to its original position. Thereby, the maxillary bundle slightly bent the apical part to the right (slim

arrow; Fig. 7 a; single frames 1.549 s, 1.564 s). These probing processes were repeated several times until the animal found an ideal spot for feeding. After food intake, it retracted the maxillary bundle back behind the mandibles.

Supplementary video related to this article can be found at <https://doi.org/10.1016/j.asd.2020.100952>

The overall movement patterns of the maxillary bundle of *P. megistus* (adult female: n = 1; adult male: n = 5; not shown) in isotonic blood saline (in horizontal chambers) was comparable with that described for *D. maxima*.

3.2.2. Horizontal chambers with agar

In this chamber type (cf. Fig. 2 b; n = 11, subadults only), the movements of the maxillary bundle of *D. maxima* considerably differed from those recorded in liquid medium. Whereas the maxillary bundle was advanced by short rapid alternating thrusts of the individual maxillae, the speed of both the protrusion of the maxillary bundle and the alternating movements of the maxillae was considerably reduced within the agar. However, the most apparent difference was the way that the maxillae moved and bent within the viscous medium. In the agar, the maxillary bundle was frequently equally bent in both directions (left and right) to a considerable amount. Active movements of the maxillary bundle were only observed at its apex, whereas the rest of the bundle passively followed the tunnel created by the movements of the tip. Thus, the maxillary bundles were bent at several points, e.g., resulting in S-shaped forms (Fig. 7 b; single frames 7.83 s, 10.75 s; Appendix A. Supplementary material: Video S3). The irregular routes produced by the protruding maxillary bundle appeared to follow no particular path. If the animals did not find any liquid medium in the chamber, they retracted their maxillae (often almost to the level of the mandibles at the puncture site) and tested another direction (cf. Friend and Smith, 1971). We never observed an opening of the food channel within the agar, but only in the liquid isotonic saline.

Supplementary video related to this article can be found at <https://doi.org/10.1016/j.asd.2020.100952>

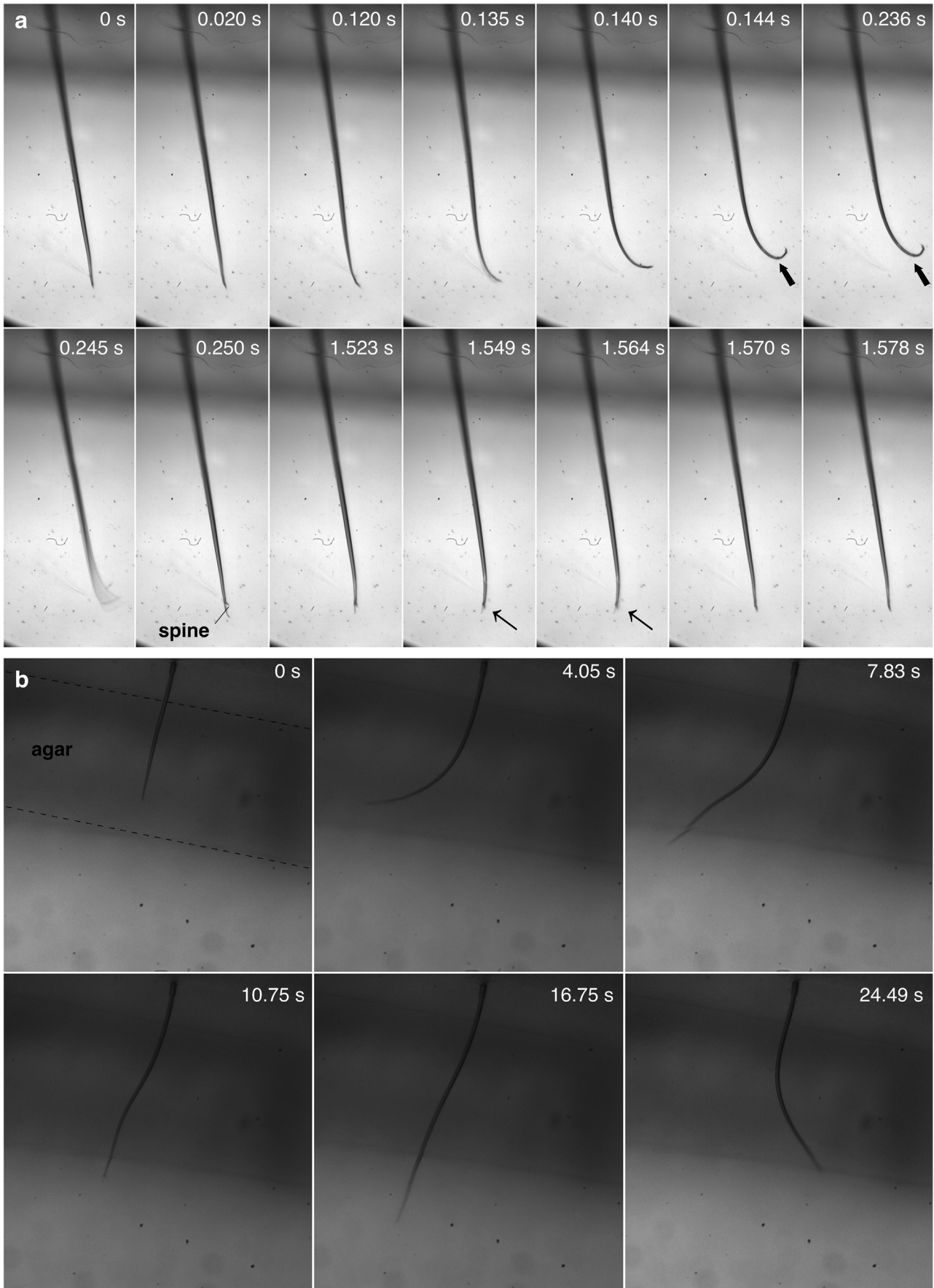
3.2.3. Vertical chambers with and without agar

The potential dorso-ventral bending movements of the maxillae of *D. maxima* could be observed in these setups (Fig. 2 c and d; total n = 15, subadults only). The non-twisted maxillae showed no significant dorso-ventral bending movements. However, a certain twisting of the maxillary bundle around its longitudinal axis could be observed, so that the initial lateral bending might also become effective in dorso-ventral direction.

4. Discussion

Based on previous findings (e.g. Barth, 1952; 1953, 1954; Cobben, 1979; Friend and Smith, 1971; Lavoipierre et al., 1959), we discuss the morphology of the head and the stylets of four triatomine species, the observed joint-free movement of the stylets and the distal opening of the food channel. The following hypotheses are valid for all the investigated species and both sexes, since

Fig. 6. Transverse sectional series of the stylets of the triatomine *Dipetalogaster maxima*. **a.** Light microscopic images of a semithin section series (600 nm; stained with Stevenel's blue). The distance between the sections depicted above is approximately 6 μm. Apically, the left maxilla contributes the major part of the formed tube of the maxillary bundle and creates the salivary channel. The mandibular seam-like lateral extensions fully enclose the maxillary bundle. **b.** Apex of the proboscis of *D. maxima* with the protruded tips of the stylets based on SR-μCT data volume reconstructions. The μCT image (dashed frame) corresponds to the ortho slice (indicated by the dashed line) in the rendered image. The area of the notch is indicated in the light microscopic section series (a) and in the μCT image (white arrow; b). **c.** TEM micrographs of the interlocking structures of the maxillae, whose cuticle appears remarkably homogeneous. For clarity, only the cuticular structures are shown, whereas the background (including some remnants of saliva) was digitally replaced by white color. This was necessary, because the saliva became partially contaminated with lead citrate droplets during the staining process (arrows: →: area of the notch; arrow heads: hemolymph lumen of both stylets; bold arrows: saliva; fcn: food channel; flp: flap; hrm: hooked rim; man: mandible; maxL: left maxilla; maxR: right maxilla; mnt: mandibular tooth; msm: mandibular seam-like lateral extensions; not: notch; prb: proboscis; scn: salivary channel; set: setae).



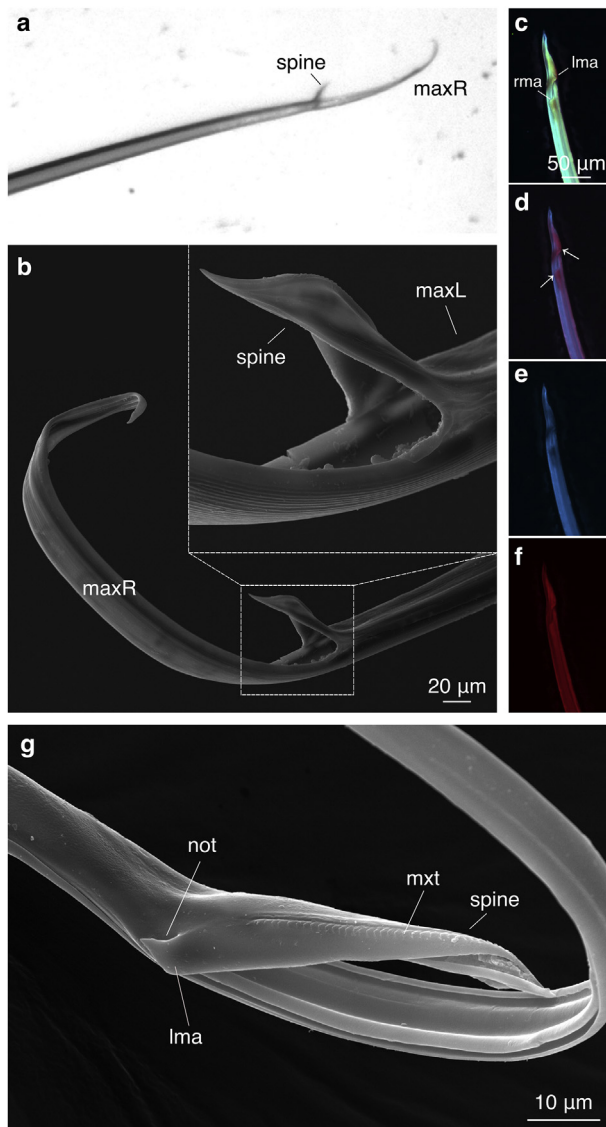


Fig. 8. a, b, g. Opening of the food channel in two species of Triatominae (a single frame of high-speed video recording; b, g, SEM images): *Dipetalogaster maxima* (a, b) and *Rhodnius prolixus* (g). The left and right maxillae form the food channel opening, whereby the left maxilla is splayed outwards and forms the spine (a, b, g). The maxillary notch of the left maxilla is on the opposite side of the structure in b and is directed out of the image plane. c–f. WFM images of the apices of the stylets of *D. maxima*. The cuticle of both the abutments is heavily sclerotized (as indicated by its red fluorescence) compared with the remainder of the stylets (c, arrows in d). This might facilitate the splaying of the spine of the left maxilla when both abutments collide (lma: left maxillary abutment; maxL: left maxilla; maxR: right maxilla; mxt: maxillary teeth; not: notch; rma: right maxillary abutment).

the specimens showed all the involved structures even if their forms differed slightly; they (presumably) also exhibited a similar movement pattern of the maxillary bundle.

4.1. Structural analysis and comparative morphology of the stylets of triatomine species

4.1.1. Head proportions

The relative head proportions vary between the triatomine species investigated (cf. Fig. 1; Table 1). Since the animals do not coil their stylets up but retract them in their straight configuration into their heads (Wenk et al., 2010), this has implications for their maximum possible length (the longer the animal's head, the longer the potential length of the stylets). Also, the maxillary bundle becomes unlocked at the hypopharynx, and the individual maxillae experience a curvature (Wenk et al., 2010). The species with elongated heads (most notably *R. prolixus*) also has the longest stylets proportionally to the pronotum length, whereas the stylets of the short-headed *P. megistus* are comparatively short (Table 1). The length of the head and the labium is linked to the length of the stylets and therefore also to the depth of penetration that the various species are able to achieve in a host's tissue. This is the case, because the muscles responsible for the movement of the stylets are located deep inside the head of the animals. In *R. prolixus*, the retractor muscles of the mandibles are located just anterior to the compound eye, whereas the retractor muscles of the maxillae are attached in the neck region (Barth, 1952; Wenk et al., 2010). Based on measurements of the length of the mouthparts, Wenk et al. (2010) estimated that *R. prolixus* adults attain a maximal penetration depth of at least 2100 μm with their maxillae and 750 μm with their mandibles.

4.1.2. Mandibles

In *D. maxima*, we were able to compare the stylets among the various developmental stages of nymphs. Our comparison revealed that all the described morphological structures were present in all nymphal stages and in the adult animals. This consistency indicates the unchanging function of the stylets throughout the animal's life, since even the youngest larvae need to blood-feed on their hosts and/or conspecifics and also replace their stylets after each molt (Rakitov, 2019).

The single row of hook-like teeth (rot; Fig. 3 a–d) along the midline of each mandible, which is visible in all triatomine species but is unique among Reduviidae (Weirauch, 2008), is used to penetrate the skin of their hosts. In *P. megistus*, the special functions of the mandibular processes (mnp, Fig. 3 g) and the third row of processes (Fig. 3 g) remain unknown.

In all species under study, the mandibular seam-like extensions at the apical part of the mandibles form an approximate half-pipe that partially or, in the distal part, even completely cover the maxillae. This might not only be advantageous for the mechanical stabilization of the mandibles but might also protect and stabilize the maxillary bundle. The resulting tube-like structure presumably also widens the entry wound, forming a channel that keeps the entry open despite the elasticity of the skin. This ensures that the maxillae can be inserted and retracted easily without becoming stuck. The mandibular seam-like lateral extensions are especially pronounced in *D. maxima*, in which the extensions of the right and the left mandible overlap and completely cover the maxillary bundle (msm; Figs. 3 e, 6 a). This might be a special adaptation to their feeding on lizards as their

Fig. 7. Single frames of high-speed video recordings of the typical motion patterns of the maxillary bundle of *Dipetalogaster maxima* (Triatominae) in the feeding chambers shown in Fig. 1. a. Opening of the food channel in a feeding chamber containing isotonic blood saline without agar (recorded with 250 fps). The strong bending to the left (bold arrows at single frames 0.144 s and 0.236 s) was always observed prior to the splaying out of the spine of the left maxilla that opens the food channel. After blood uptake, a minor bending to the right (slim arrows at single frames 1.549 s and 1.564 s) occurs. b. Searching movements of the maxillary bundle in a feeding chamber with agar (recorded with 60 fps): passive bending of the maxillary bundle in the agar and active movements at the apex of the bundle in the fluid medium. The maxillary bundle is advanced by short rapid alternating thrusts of the individual maxillae. In the agar (area indicated by the dashed lines at single frame 0 s), the maxillary bundle was frequently bent to the left and to the right to a considerable extent. The speed of the alternating movements and the advancement of the maxillary bundle were considerably reduced within the agar compared to the isotonic blood saline.

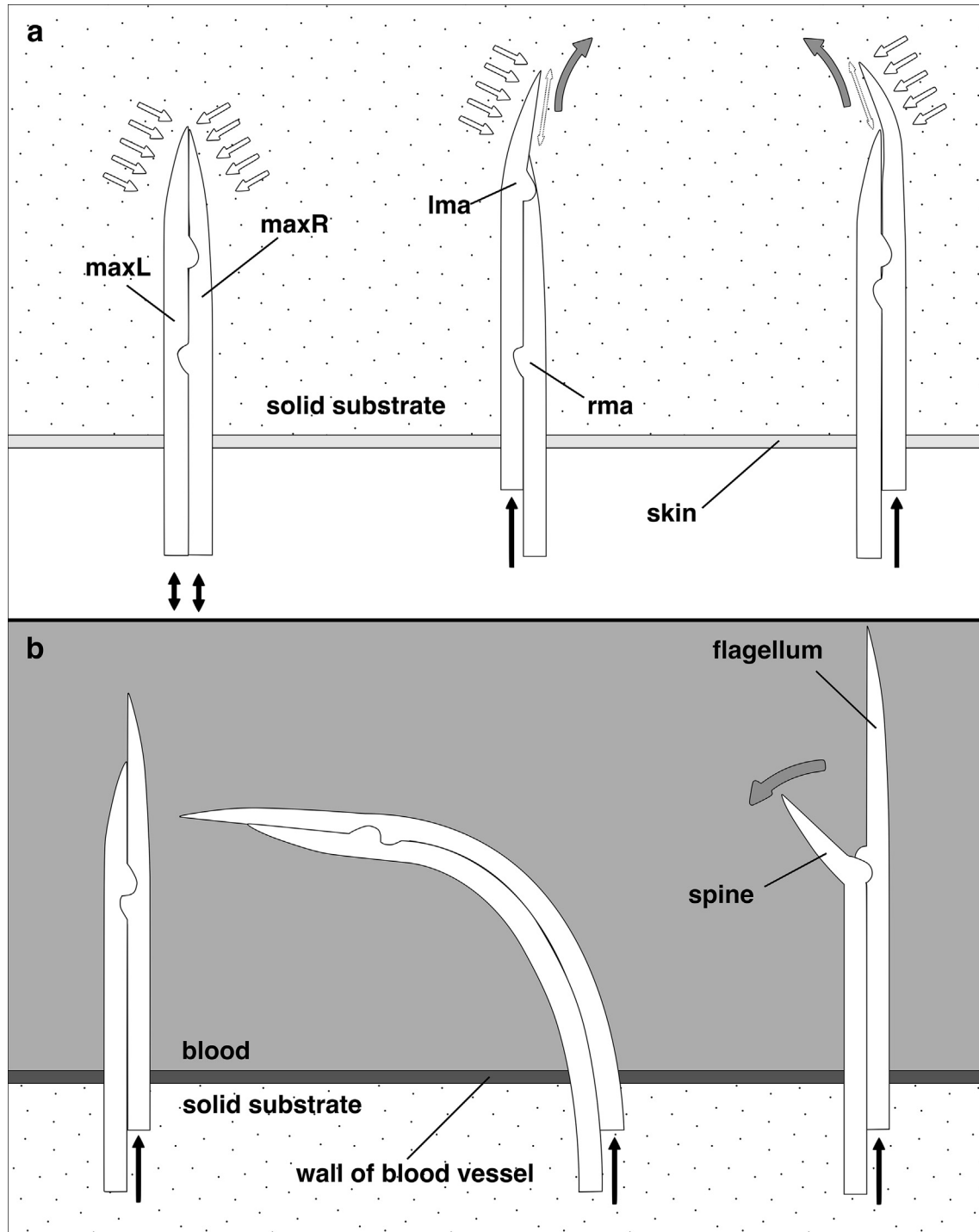


Fig. 9. Schematic representation of the mechanisms involved in the joint-free bending movements of the maxillary bundle in the host tissue and the opening of the food channel. **a.** Stylets at the border of the skin and the tissue, i.e., a solid substrate. The movements of the maxillary bundle in tissue result from the interaction between the surrounding substrate and the alternating movements of the maxillae (black arrows). The beveled tip is pushed away from its straight path (gray arrows) because of asymmetrical forces acting on the variable geometrical asymmetry of the apex (white arrows) (passive bending). These movements are presumably supported by the mechanical interaction of the left and the right maxillary abutments (slide-lock mechanism) whenever the individual maxillae are protracted or retracted to a certain extent, thus causing the maxillary bundle to bend according to the bending moment distribution (active bending). **b.** Stylets at the border of the blood vessel and the fluid blood, showing the consecutive process of the opening of the food channel. Whenever the right maxilla is protracted to a certain extent (black arrows), its path is blocked by the mechanical interaction of the right maxillary abutment with the left one, resulting in a strong bending of the apex of the maxillary bundle to the left (active bending; cf. Fig. 7 a). Once the mechanical resistance is surmounted, the left maxillary apex causes a change from its mechanically stable 'straight' to its equally stable 'splayed out' condition (gray arrow), forming the opening of the food channel (lma: left maxillary abutment; maxL: left maxilla; maxR: right maxilla; rma: right maxillary abutment).

main hosts (Ryckman and Ryckman, 1965), where they potentially prevent buckling by mechanically stabilizing the whole stylet bundle during the penetration of the rough lizard skin. The hosts of the other three species under study comprise birds and mammals (Fresquet and Lazzari, 2011).

4.1.3. Maxillae

The abutments at the apices of both the right and the left maxillae of all the investigated species were, in combination with the 'notch' (i.e., a conspicuous irregularity on the otherwise uniform maxillae) of the left maxillae, the most intriguing functional feature involved in the opening of the food channel (lma, not, rma; Fig. 4 a, c, e). The 'notch' appears to be a conspicuous irregularity on the otherwise uniform maxillae. The abutments are heavily sclerotized, whereas the area of the 'notch' is not (for further discussion, see chapter 4.3).

The sturdy spine-like apex of the left maxilla bears a row of sawteeth (Fig. 4 a, c, e) and is postulated to penetrate the blood vessel wall (Cobben, 1979), although this has not as yet been verified *in vivo*. Former descriptions of an additional small structure (scn, Fig. 4 g) as the outlet of the salivary channel (Wirtz, 1987) have been confirmed.

The specific tongue and groove pattern (tng, grv; Fig. 5 a and b) presumably facilitates the distad movement of the right maxilla during the penetration of the host tissue, based on the shape of the tongues whose tips point distadly. The relative lengthwise movement of the tongue within the groove should be much harder to overcome with a proximad pulling instead of a distad pushing motion of the right maxilla. The tongue and grooves might create anisotropic conditions by increasing the frictional forces whenever one maxilla is pulled proximad; thus, the maxilla is prevented from sliding back during the searching movements in the host tissue. In addition, the maxillary tongue and groove system might also allow saliva to be sent towards the apex of the maxillary bundle to act as a friction-reducing lubricant.

4.2. Insertion and navigation of the maxillary bundle in the tissue

Insects of various orders are able actively to bend rod-shaped structures that comprise several interlocked elements, despite the lack of intrinsic musculature and joints. Examples include the sucking mouthparts of various hemipterans (like the kissing bugs in this study) and nematoceran dipterans, or the terebrae (= ovipositor shafts) of parasitoid hymenopterans used for oviposition (Cerkvenik et al., 2018). These structures are capable of sensing and precisely navigating through diverse substrates to reach their targets without the need of visual information.

Active bending occurs when the bending movements originate from the relative movements of the single interlocked elements, whereby three methods can be distinguished. (1) If the longitudinal sliding of one element is inhibited or even fully prevented by a mechanical block, the result, depending on the stiffness of the cuticle, is a relative bending of the entire rod-shaped structure because of tension and compression forces (e.g., in the terebra of various hymenopterans belonging to Braconidae (Quicke et al., 1995), Aulacidae and Gasteruptidae (Quicke and Fitton, 1995)). This functional principle has recently been termed the 'slide-lock mechanism' (Betz et al., 2016). (2) Bending might also occur because of the uneven sclerotization of various regions across the length of the interlocking elements involving heavily sclerotized stiff arches that alternate with less sclerotized and flexible nodes (e.g., in the multi-arched terebra of wasps of the braconid genus *Zaglyptogastra* (Quicke, 1991)). In this case, a protraction or retraction of one element aligns the stiff arches with the flexible nodes, causing a flattening out of the nodal regions, which leads in

turn to a unilateral bending movement. (3) Bending movements might also originate from the pre-tension of the individual interlocked elements that might lead to incurving upon their protraction when a low enough opposing force is present (e.g., in phytophagous cicadellid hemipterans (Pollard, 1969)). In all three active bending mechanisms described above, the extent of bending can be controlled by adjusting the amplitude of protractions and retractions of the individual interlocked elements (Cerkvenik et al., 2018).

Unlike active bending, passive bending results from the mechanical resistance exerted by the surrounding substrate on the movements of the individual elements of the rod-shaped structure (e.g., the valvulae forming the terebra of the braconid *Diahasmimorpha longicaudata* (Ashmead, 1905) when searching for host larvae in fruits (Cerkvenik et al., 2017), or the stylets of the plant-sucking lygaeid bug *Oncopeltus fasciatus* (Dallas, 1852) (Miles, 1958) and probably also other phytophagous hemipterans (MacGill, 1947; Juárez-Hernández et al., 2014) when penetrating plant tissues). Therefore, these elements need to be thin to limit substrate deformation, and long enough to attain sufficient penetration depths. The shape of the apex of these rod-shaped structures can be actively altered by changing the relative position of the individual elements (Cerkvenik et al., 2017, 2018). While inserted into a substrate, asymmetric forces acting on the varying geometrical asymmetry of the apex deflect the tip away from its straight path.

In the present study on triatomine kissing bugs, we have observed two distinct modes of bending movements of the maxillary bundle:

- (1) In liquid isotonic blood saline, the triatomine bugs exhibit a twitching and bending movement of the apical part of the maxillary bundle. These movements presumably result from the mechanical interaction of the left and the right maxillary abutment (slide-lock mechanism), whenever the individual maxillae are protracted or retracted to a certain amount. These interactions build up tension and compression, causing the maxillary bundle to bend because of the distribution of the bending moment. Since the maxillary bundle tapers and therefore might be more flexible apically, the bending movements are more pronounced at the apical part. Maximum bending movements of the apex of the maxillae have always been observed prior to the food uptake (see below). Pollard (1969) hypothesized that the maxillae of the phytophagous *Eupteryx melissae* (Curtis, 1837) (Hemiptera: Cicadellidae) are 'preloaded elements' that curve in a predetermined direction as soon as parts of them are no longer tightly interlocked, and when no opposing force is present. This results in asymmetric apices with asymmetric forces acting upon them; the tips of the stylets are deflected from their straight path enabling the directional control of the stylet bundle. However, the cuticle of the triatomine species under study does not show any distinct cuticle layers but appears to be remarkably homogeneous. Since we also have not observed any curving of the stylets after the interlocking structures are separated, the stylets of the kissing bugs are presumably not pre-tensioned.
- (2) In agar (simulating the host tissue), the triatomine bugs were able to exhibit considerable bending movements in the lateral plane (equally to the left and to the right). The animals were able to actively bend the maxillary bundle at several points across their length, often resulting in S-shaped forms of the maxillary bundle. Such movements enable the animals to explore a wide range of the substrate/tissue from a single puncture point. The tips of the individual maxillae (and especially the presumably sturdier apex of the spine-like left maxilla) are asymmetrically beveled. The

animals can alter the geometry of the apex of the maxillary bundle by continuously protracting or retracting the individual maxillae. Since the right maxillary abutment is further away from the apex than the left one (Table 1), the triatomine bugs can protract the right maxilla to a certain distance without a mechanical interaction with the abutment of the left maxilla, thereby creating an offset (Fig. 9). If an advancing force (actuated by protractor muscles located in the head) is applied to the maxillae, the protruding stylet will not be pushed into the tissue in a straight path, because the asymmetrically beveled tip deflects it as a result of the asymmetrical forces exerted by the surrounding substrate. If one individual maxilla is protracted alone, its tip curves inwards because of its inwardly directed apex. When the other maxilla follows, it is guided to one side (Fig. 9 a). Thus, the kissing bugs may be able actively to steer the maxillary bundle to the left or right within their host's tissue, since the extent to which one individual maxilla is protracted compared with the other controls the degree of this bending. These passive bending mechanisms might be further supported by the active bending of the apex caused by the slide-lock mechanism described above. Since the maxillary bundle consist of only two elements (in contrast to the hymenopteran terebra comprising three valvulae; cf. Cerkvenik et al. (2017)), this mechanism can account for movements in the lateral plane only. However, the observed rotation of the entire maxillary bundle around its longitudinal axis might be used to increase the working radius of the stylets. Whether this rotation is actively actuated or whether it results from the resistance of the inhomogeneous surrounding substrate remains unclear. The viscosity of the surrounding medium seems to be essential for the described passive bending, since we exclusively observed the strong bending of the maxillary bundle in agar but never in liquid isotonic blood saline. The triatomine bugs advance their maxillary bundle by short rapid alternating thrusts of the individual maxillae, thereby protruding a (curved) tunnel through the surrounding substrate. The maxillary teeth found at the spine (Fig. 4 a, c, e) possibly support the passage of the maxillary bundle through the tissue by reducing cutting forces at the apex and thereby enhancing its efficiency. The further proximal part of the maxillae follows these tunnels and can therefore be passively deformed in various ways. Throughout the insertion process, the surrounding labial tip and the tube formed by the mandibles provide external support.

4.3. Distal opening of the food channel

The kissing bugs in our study never opened their food channel within the agar, but only once the maxillary bundle had left the agar and entered the liquid isotonic blood saline (cf. single frame 0.250 s in Fig. 7 a). This is in accordance with the physiological context during blood-sucking: the mouthparts open once the animal has penetrated a blood vessel but always remain closed within the tissue (Barth, 1952). The apices of the maxillae are shaped (Fig. 4 c, e) such that they seal the openings of the food and salivary channel when the animal is not feeding. Nevertheless, our footage shows that the triatomine bugs continuously release small amounts of saliva during their probing behavior, even when the food channel is closed. The tight form closure of the maxillary tips together with this release of saliva might protect both the salivary and the food channels from becoming clogged during the probing of the tissue. Furthermore, the anesthetic properties of the saliva reduce the local

sensitivity of the host's tissue (Dan et al., 1999), possibly lengthening the feeding time because the host does not immediately detect the presence of the kissing bug.

We have observed that the maxillae are able to perform fast alternating movements (recorded for *D. maxima* and *P. megistus*). A closer inspection of the shape of the maxillae and the reinforcement of the maxilla abutments (lma, rma; Fig. 4 c, e, g, h), which consist of heavily sclerotized material (Fig. 8 c–f), suggests that the abutments do not slide past each other easily in the longitudinal direction. Rather, they block the forward sliding of the maxillae relative to each other once a certain point is reached (slide-lock mechanism). When the animal is not feeding, the right maxillary abutment is always located further proximal relative to the left one (Figs. 4 c, e, 9, Table 1). This situation only changes once the distal entrance to the food channel is open. Pushing the right maxilla further after reaching this blocking point causes the observed strong bending of the apex of the maxillary bundle to the left (arrow; Fig. 7 a, single frame 0.144 s; Fig. 9), as was always observed just before the spine becomes visible and the food channel opened. The opening of the food channel was always achieved by protracting the right maxilla only (and not by retracting the left one as postulated by Barth (1952)). Hence, the food channel always remained at the same position (just where the splayed spine is visible). We therefore conclude that the spine of the left maxilla always splays out within a blood vessel and remains in that position for the duration of the feeding process.

During the time that a triatomine bug feeds, the right maxilla can be protracted and retracted freely about a certain distance as long as the abutments of the maxillae do not collide. These movements might be important to maintain the blood flow or to distribute the saliva evenly. In addition, a further protraction of the right maxilla, whose cross-section widens in the proximal direction (cf. Fig. 6 a), spreads the base of the splayed spine of the left maxilla, i.e., the distal ends of the two interlocking structures of the left maxilla are pushed further apart. This presumably also has an effect on the stability of the splayed spine.

Since the spine-like apex of the left maxilla splays outwards in the region of the maxillary 'notch'—a region that lacks strong sclerotization—this structural modification can be considered a potential 'predetermined playing point'. Based on our findings, we assume that the left maxilla is a bi-stable structure with one stable mechanical condition being 'straight' (cf. Fig. 4 a, c, e, g) and the other one being 'splayed out' (Fig. 8 a and b, g). The force created by the interacting reinforced abutments (leading to the extreme curvature to the left side) presumably triggers a change in the structural conformation of the spine. This would also explain why the mouthparts can stay open once the spine becomes splayed out without any visible mechanisms or forces to hold it open. The open shape of the spine is mechanically stable and needs external energy to be reverted into the 'straight' (i.e., closed) state once again.

The abutments probably also interact when the right maxilla is retracted proximad. This scenario seems to be highly likely, because it was also observed in the fluid medium in the absence of any tissue or agar. Since the left maxillary abutment is not symmetrical but is roughly triangular and pointed proximad (lma; Fig. 4 c, e, g), gliding alongside the right maxilla should thus be easier, resulting in a slighter but still noticeable curvature to the right side (slim arrow; Fig. 7 a, single frame at 1.549 s). This might in turn trigger the change in the structural conformation of the left maxilla back to its 'straight' shape. The maxillary 'notch' potentially facilitates the transition from one mechanical shape into the other. Hence, the small gap (i.e., the notch, not; Fig. 4 a, c, e), which gives the otherwise homogeneous left maxilla room for movement, might provide a secure anatomical location for the spine to snap open without any damage and allow the opening of the food channel.

Another possibility is that the external counter pressure caused by the tissue surrounding the maxillae assists in closing the food channel.

5. Conclusion

Whereas the general appearance of the stylets is similar between the four Triatominae species under study, the size and shape of their respective morphological features differ. The paired mandibles have the form of elongated rods with a prominent row of sawteeth at their apices. The apices of the paired, likewise rod-shaped, and slender maxillae are strongly asymmetrical: the right maxilla ends in a long flagellum, whereas the apex of the left maxilla is a shorter and sturdy spine. The two maxillae are tightly interlocked by a tongue-and-groove system and form a larger food channel and a smaller salivary channel.

The feeding process can be summarized as follows. After penetrating the host's skin, the mandibles with their strong teeth act as an anchor and remain in the outer skin layers to form a stable tube that extends the wound opening and keeps it open. The tightly interlocked maxillae are inserted deeper into the tissue to locate suitable blood vessels. In a solid or highly viscous medium such as agar or tissue, the maxillary bundle moves in a combination of passive and active bending mechanisms: (1) the interplay between the surrounding substrate and the alternating movements of the maxillae pushes the tip away from its straight path because of asymmetrical forces acting on the variable geometrical asymmetry of the apex (passive bending); (2) these movements are probably supported by the mechanical interaction of the left and right maxillary abutment (slide-lock mechanism) whenever the individual maxillae are protracted or retracted to a certain amount (active bending). In a liquid, the movements of the maxillary bundle are solely caused by the active bending mechanisms. Throughout the insertion process, the labial tip and the tube formed by the mandibles are assumed to provide external mechanical support. The food channel opens only once a vessel is found and tapped. This is made possible by the protruding abutments of the left and right maxillae, which block each other's paths. The resistance so created then causes the apex of the left maxilla to change from its mechanically stable 'straight' condition to it equally stable 'splayed out' condition, thereby opening the food channel. The notch of the left maxilla functions as a putative predetermined splaying point.

The examination of the stylets of the four triatomine species under study and the underlying working mechanisms of the joint-free bending movements of the maxillary bundle and the distal opening of the food channel adds to our understanding of the feeding process of these bugs from an eco-morphological point of view. Further comparative studies that thoroughly analyze the triatomine head (muscles, cuticular structures, glands, etc.) are needed in order to determine the way in which the various movements are actuated and the role that these morpho-physiological traits played in influencing the evolution of the behavioral and ecological traits and *vice versa* in the epidemiologically important bloodsucking Triatominae. Previous studies have also shown that specific structures of the reduviid stylets can be used successfully for phylogenetic analyses, since they are closely linked to the food source, the habitat and the evolutionary past of the animals (Johnson et al., 2018; Weirauch, 2008; Weirauch et al., 2019). Further information about their microstructure might also provide new insights in this regard.

In recent years, some efforts have been made to produce biologically inspired steerable instruments for micro-invasive surgery that work without axial rotation (e.g., Frasson et al., 2012; Leibinger et al., 2016; Scali et al., 2017), since multi-part structures

comprising of several interlocked sliding elements seem to be highly effective for volumetric substrate probing. These biomimetic multi-element prototypes are based on the terebrae of hymenoptera. However, the elongated slender mouthparts of hemipterans (and especially those of bloodsucking triatomine bugs) can also act as a suitable biological concept generator, and further investigations into this matter might be helpful in the development and the design of slender man-made probing tools.

Funding

This work was funded by the German Research Foundation (DFG) as part of the Transregional Collaborative Research Centre (SFB-TRR) 141 'Biological design and integrative structures' (project A03 'Inspired by plants and animals: actively actuated rod-shaped structures exhibiting adaptive stiffness and joint-free kinematics'). The experiment (LS-2342) at the ESRF was funded by the European Union.

Author contributions

T.T., F.H., O.B., and B.E. planned the study and prepared the study design. O.B. acquired the funding and supervised the study (together with B.E.) and attained the SR- μ CT data. T.T. and B.E. analyzed the SR- μ CT data and performed the LM, WFM, and TEM studies. T.T. performed the photography and SEM studies. F.H. carried out the high-speed videography. T.T. and F.H. interpreted the data and wrote the first draft of the manuscript. O.B. and B.E. discussed the results and revised the manuscript. All authors read and approved the final version of the manuscript.

CRediT authorship contribution statement

Tatjana Tull: Conceptualization, Methodology, Investigation, Writing - original draft, Writing - review & editing, Visualization. **Fabian Henn:** Conceptualization, Methodology, Investigation, Writing - original draft, Visualization. **Oliver Betz:** Conceptualization, Methodology, Resources, Writing - review & editing, Supervision, Funding acquisition. **Benjamin Eggs:** Conceptualization, Methodology, Investigation, Writing - review & editing, Supervision.

Acknowledgements

We thank the following colleagues for their help: Peter Wenk called our attention to this subject. Günter Schaub provided specimens of all species investigated in this study for our insect stock. Oliver Meckes (eye of science) produced the photographs in Fig. 1 a and b. Monika Meinert assisted with SEM, Stefan Fischer with histological techniques, Julia Straube with ultramicrotomy, Lorenz Henneberg and York-Dieter Stierhof with WFM, and Alexander Rack with the beamline ID19 at ESRF. Manfred Drack provided inspiring discussions, and Theresa Jones linguistic corrections. We also thank two anonymous reviewers for useful comments that greatly helped to improve the quality of this study.

Appendix A. Supplementary data

Supplementary data to this article can be found online at <https://doi.org/10.1016/j.asd.2020.100952>.

Video S1. Time-lapse recording of a *Dipetalogaster maxima* feeding on warm (approximately 37°C) defibrinated pig blood that was served in finger stalls to trigger the feeding response. The recorded process took approximately 90 min in real time.

Video S2. Video sequence of a *Dipetalogaster maxima* probing with its maxillary bundle within isotonic blood saline and the opening of the food channel (cf. Fig. 7 a).

Video S3. Video sequence of a *Dipetalogaster maxima* probing with its maxillary bundle within agar (cf. Fig. 7 b).

Appendix B. Specimen maintenance and breeding

The specimens were sourced from the long-term laboratory colonies of the research group 'Zoology and Parasitology' of the University of Bochum (Bochum, Germany) and were bred in plastic boxes (19 · 12.5 · 7.5 cm) in adult breeding groups of 10–30 individuals per box. Each box was ventilated through two stainless steel mesh-covered openings. The plastic boxes were stored within an incubator of the type Brutmaschine Modell 3000 digital (Brutmaschinen-Janeschitz GmbH (BRUJA); Hammelburg, Germany) to maintain a constant temperature of 29°C and a high humidity. The nymphs were kept under the same conditions. We collected laid eggs and incubated them in Petri dishes on filter paper within the same incubators in which the adults were kept. Since the nymphs need to infect themselves with endosymbionts that are necessary for blood digestion (Baines, 1956), adults and offspring need to be raised in close contact. However, fecal residues on the eggshells seem to be sufficient to infect the nymphs (Brecher & Wigglesworth, 1944; Geigy et al., 1953). No negative effects as described by Baines (1956) were observed in our breeding system. The specimens were fed on a diet consisting solely of sterile defibrinated pig's blood (elocin Tierblutspezialitäten GmbH; Düsseldorf, Germany). The blood was served in latex finger stalls following Christophel et al. (1988) with some modifications

Appendix C. Histological protocols for the semi- and ultrathin sections

Fixation:

2.5% glutaraldehyde and 5% sucrose in 0.1 M cacodylate buffer, pH 7.4, 16 h at 4°C
rinse in 0.1 M cacodylate buffer, pH 7.4, 3 · 10 min at 4°C

Post-fixation:

1% osmium tetroxide in 0.1 M cacodylate buffer, pH 7.4, 4 h at 4°C
rinse in 0.1 M cacodylate buffer, pH 7.4, 3 · 10 min at 4°C

Embedding:

30% ethanol, 15 min at 4°C
50% ethanol, 2 · 10 min at 4°C
70% ethanol, 3 · 10 min at room temperature
70% ethanol saturated with uranyl acetate, 12 h at room temperature
70% – 75% – 80% – 85% – 90% – 95% – 100% ethanol, each dehydration step 3 · 10 min at room temperature
100% propylene oxide, 2 · 1 h at room temperature
Spurr resin/propylene oxide (PO) mixtures with a PO:resin ratio of 3:1, 1 h at room temperature
1:1 PO:resin, 1 h at room temperature
1:3 PO:resin, 1 h at room temperature on a rotatory shaker
1:7 PO:resin, 1 h at room temperature on a rotatory shaker
100% resin, 17 h at room temperature on a rotatory shaker
embedding in 100% fresh resin
polymerization for 8 h at 70°C

Staining of semithin sections:

Stevenel's blue (del Cerro et al., 1980), 40 min at 60°C
rinse in distilled water, 2 · 4 min at 60°C

air-dry

mount in Euparal (Waldeck GmbH & Co. KG, Münster, Germany)

Staining of ultrathin sections:

2% ethanolic uranyl acetate, 20 min at room temperature
rinse in distilled water, 5 s at room temperature
lead citrate, 10 min at room temperature
rinse in distilled water, 5 s at room temperature
air-dry

References

- Andersen, S.O., 1963. Characterization of a new type of cross-linkage in resilin, a rubber-like protein. *Biochim. Biophys. Acta* 69, 249–262.
- Andersen, S.O., Weis-Fogh, T., 1964. Resilin, a rubber like protein in arthropod cuticle. *Adv. Insect Physiol* 2, 1–65.
- Appel, E., Heepe, L., Lin, C.P., Gorb, S.N., 2015. Ultrastructure of dragonfly wing veins: composite structure of fibrous material supplemented by resilin. *J. Anat.* 227, 561–582.
- Baines, S., 1956. The role of the symbiotic bacteria in the nutrition of *Rhodnius prolixus* (Hemiptera). *J. Exp. Biol.* 33, 533–541.
- Barth, R., 1952. Anatomische und histologische Studien ueber die Unterfamilie Triatominae (Heteroptera, Reduviidae). I. Teil: Der Kopf von *Triatoma infestans*. *Mem. Inst. Oswaldo Cruz* 50, 156–197.
- Barth, R., 1953. Anatomische und histologische Studien ueber die Unterfamilie Triatominae (Heteroptera, Reduviidae). III. Teil: Untersuchungen ueber den Stechvorgang bei Triatominae. *Mem. Inst. Oswaldo Cruz* 51, 69–94.
- Barth, R., 1954. Anatomische und histologische Studien ueber die Unterfamilie Triatominae (Heteroptera, Reduviidae). IV. Der Speicheldruesenkomplex von *Triatoma infestans*. *Mem. Inst. Oswaldo Cruz* 52, 541–569.
- Bennet-Clark, H.C., 1963. Negative pressures produced in the pharyngeal pump of the blood-sucking bug, *Rhodnius prolixus*. *J. Exp. Biol.* 40, 223–229.
- Bernard, J., 1974. Mécanisme d'ouverture de la bouche chez l'hémiptère hématophage, *Triatoma infestans*. *J. Insect Physiol.* 20, 1–8.
- Betz, O., Birkhold, A., Caliaro, M., Eggs, B., Mader, A., Knippers, J., Röhrle, O., Speck, O., 2016. Adaptive stiffness and joint-ree kinematics: actively actuated rod-shaped structures in plants and animals and their biomimetic potential in architecture and engineering. In: Knippers, J., Nickel, K.G., Speck, T. (Eds.), *Biomimetic Research for Architecture and Building Construction: Biological Design and Integrative Structures. Biologically-Inspired Systems*, vol. 8. Springer, Cham, pp. 135–167.
- Betz, O., Eggs, B., Henn, F., Birkhold, A., Röhrle, O., 2019. Movement without joints: (how) does it work? In: Knippers, J., Schmid, U., Speck, T. (Eds.), *Biomimetics for Architecture: Learning from Nature*. Birkhäuser Verlag GmbH, Basel, pp. 22–31.
- Betz, O., Wegst, U., Weide, D., Heethoff, M., Helfen, L., Lee, W., Cloetens, P., 2007. Imaging applications of synchrotron X-ray phase-contrast microtomography in biological morphology and biomaterials science. I. General aspects of the technique and its advantages in the analysis of millimetre-sized arthropod structure. *J. Microsc.* 227, 51–71.
- Brecher, G., Wigglesworth, V.B., 1944. The transmission of *Actinomyces rhodii* Erikson in *Rhodnius prolixus* Stål (Hemiptera) and its influence on the growth of the host. *Parasitology* 35, 220–224.
- Burrows, M., Shaw, S.R., Sutton, G.P., 2008. Resilin and chitinous cuticle form a composite structure for energy storage in jumping by frog hopper insects. *BMC Biol.* 6, 41.
- Büsse, S., Gorb, S.N., 2018. Material composition of the mouthpart cuticle in a damselfly larva (Insecta: Odonata) and its biomechanical significance. *R. Soc. Open Sci.* 5, 172117.
- Cerkvenik, U., Dodou, D., van Leeuwen, J.L., Gussekloo, S.W.S., 2018. Functional principles of steerable multi-element probes in insects. *Biol. Rev.* 94, 555–574.
- Cerkvenik, U., van de Straat, B., Gussekloo, S.W.S., van Leeuwen, J.L., 2017. Mechanisms of ovipositor insertion and steering of a parasitic wasp. *Proc. Natl. Acad. Sci. U.S.A.* 114, E7822–E7831.
- Chapman, R.F., 2012. *The Insects: Structure and Function*, fifth ed. Cambridge Univ. Press, Cambridge.
- Christophel, E.-M., Scheede, S., Bommer, W., 1988. Massenfütterung von Reduviiden mit aussortierten menschlichen Blutkonserven in Beuteln aus Haushaltsfolie: zugleich eine Möglichkeit der *in-vitro*-Xenodiagnose der Chagas-Krankheit. *Mitt. Oesterr. Ges. Tropenmed. Parasitol.* 10, 23–32.
- Cloetens, P., Ludwig, W., Boller, E., Helfen, L., Salvo, L., Mache, R., Schlenker, M., 2002. Quantitative phase contrast tomography using coherent synchrotron radiation. *Proc. SPIE* 4503, 82–92. Developments in X-ray tomography III.
- Cloetens, P., Pateyron-Salomé, M., Buffiere, J.Y., Peix, G., Baruchel, J., Peyrin, F., Schlenker, M., 1997. Observation of microstructure and damage in materials by phase sensitive radiography and tomography. *J. Appl. Phys.* 81, 5878–5886.
- Cobben, R.H., 1979. Evolutionary trends in Heteroptera. Part II. Mouthpart-structures and feeding strategies. *Syst. Biol.* 28, 653–656.
- Cohen, A.C., 1993. Organization of digestion and preliminary characterization of salivary trypsin-like enzymes in a predaceous heteropteran, *Zelus renardii*. *J. Insect Physiol.* 39, 823–829.

- Dan, Á., Pereira, M.H., Pesquero, J.L., Diotaiuti, L., Beirão, P.S.L., 1999. Action of the saliva of *Triatoma infestans* (Heteroptera: Reduviidae) on sodium channels. *J. Med. Entomol.* 36, 875–879.
- Deiters, J., Kowalczyk, W., Seidl, T., 2016. Simultaneous optimisation of earwing hindwings for flight and folding. *Biol. Open* 5, 638–644.
- del Cerro, M., Cogen, J., del Cerro, C., 1980. Stevenel's Blue, an excellent stain for optical microscopical study of plastic embedded tissues. *Microsc. Acta* 83, 117–121.
- Elvin, C.M., Carr, A.G., Huson, M.G., Maxwell, J.M., Pearson, R.D., Vuocolo, T., Liyou, N.E., Wong, D.C.C., Merritt, D.J., Dixon, N.E., 2005. Synthesis and properties of crosslinked recombinant pro-resilin. *Nature* 437, 999–1002.
- Escandón-Vargas, K., Muñoz, C.A., Salazar, L., 2017. Blood-feeding of *Rhodnius prolixus*. *Biomedica* 37, 299–302.
- Ferreira, R.A., Lazzari, C.R., Lorenzo, M.G., Pereira, M.H., 2007. Do haematophagous bugs assess skin surface temperature to detect blood vessels? *PLoS ONE* 2, e932.
- Fontaine, A., Diouf, I., Bakkali, N., Missé, D., Pages, F., Fusai, T., Rogier, C., Almeras, L., 2011. Implication of haematophagous arthropod salivary proteins in host-vector interactions. *Parasites Vectors* 4, 187.
- Frasson, L., Ferroni, F., Ko, S.Y., Dogangil, G., Rodríguez y Baena, F., 2012. Experimental evaluation of a novel steerable probe with a programmable bevel tip inspired by nature. *J. Robot. Surg.* 6, 189–197.
- Fresquet, N., Lazzari, C.R., 2011. Response to heat in *Rhodnius prolixus*: the role of the thermal background. *J. Insect Physiol.* 57, 1446–1449.
- Friend, W.G., Smith, J.J.B., 1971. Feeding in *Rhodnius prolixus*: mouthpart activity and salivation, and their correlation with changes of electrical resistance. *J. Insect Physiol.* 17, 233–243.
- Geigy, J.R., Kraus, C., 1952. Rüssel und Stechakt von *Rhodnius prolixus*. *Acta Trop.* 9, 272–277.
- Geigy, R., Halff, L.A., Kocher, V., 1953. Untersuchungen über die physiologischen Beziehungen zwischen einem Überträger der Chagas-Krankheit *Triatoma infestans* und dessen Darmsymbionten. *Schweiz. Med. Wochenschr.* 83, 928–930.
- Johnson, K.P., Dietrich, C.H., Friedrich, F., Beutel, R.G., Wipfler, B., Peters, R.S., Allen, J.M., Petersen, M., Donath, A., Walden, K.K.O., Kozlov, A.M., Podsiadlowski, L., Mayer, C., Meusemann, K., Vasilkopoulos, A., Waterhouse, R.M., Cameron, S.L., Weirauch, C., Swanson, D.R., Percy, D.M., Hardy, N.B., Terry, I., Liu, S., Zhou, X., Misof, B., Robertson, H.M., Yoshizawa, K., 2018. Phylogenomics and the evolution of hemipteroid insects. *Proc. Natl. Acad. Sci. U.S.A.* 115, 12775–12780.
- Juárez-Hernández, P., Valdez-Carrasco, J., Valdovinos-Ponce, G., Mora-Aguilera, J.A., Otero-Colina, G., Téliz-Ortiz, D., Hernández-Castro, E., Ramírez-Ramírez, I., González-Hernández, V.A., 2014. Leaf penetration pattern of *Aulacaspis tubercularis* (Hemiptera: Diaspididae) stylet in mango. *Fla. Entomol.* 97, 100–108.
- Justi, S.A., Galvão, C., 2017. The evolutionary origin of diversity in Chagas disease vectors. *Trends Parasitol.* 33, 42–52.
- Karnovsky, M.J., 1965. A formaldehyde glutaraldehyde fixative of high osmolality for use in electron microscopy. *J. Cell Biol.* 27, 137–139.
- Kraus, C., 1957. Versuch einer morphologischen und neurologischen Analyse des Stechaktes von *Rhodnius prolixus* Stål 1858. *Acta Trop.* 14, 36–87.
- Krenn, H.W., Aspöck, H., 2012. Form, function and evolution of the mouthparts of blood-feeding Arthropoda. *Arthropod Struct. Dev.* 41, 101–118.
- Lavoipierre, M.M.J., Dickerson, G., Gordon, R.M., 1959. Studies on the methods of feeding of blood-sucking arthropods: I—The manner in which triatomine bugs obtain their blood-meal, as observed in the tissues of the living rodent, with some remarks on the effects of the bite on human volunteers. *Ann. Trop. Med. Parasitol.* 53, 235–250.
- Lent, H., Wygodzinsky, P., 1979. Revision of the Triatominae (Hemiptera, Reduviidae), and their significance as vectors of Chagas' disease. *Bull. Am. Mus. Nat. Hist.* 163, 123–520.
- Leibinger, A., Oldfield, M.J., Rodríguez y Baena, F., 2016. Minimally disruptive needle insertion: a biologically inspired solution. *Interface Focus* 6, 20150107.
- MacGill, E.I., 1947. The anatomy of the head and mouth-parts of *Dysdercus intermedius* Dist. *Proc. Zool. Soc. Lond.* 117, 115–128.
- Mesquita, R.D., Carneiro, A.B., Bafica, A., Gazos-Lopes, F., Takiya, C.M., Souto-Padron, T., Vieira, D.P., Ferreira-Pereira, A., Almeida, I.C., Figueiredo, R.T., Porto, B.N., Bozza, M.T., Graça-Souza, A.V., Lopes, A.H.C.S., Atella, G.C., Silvaneto, M.A.C., 2008. *Trypanosoma cruzi* infection is enhanced by vector saliva through immunosuppressant mechanisms mediated by lysophosphatidylcholine. *Infect. Immun.* 76, 5543–5552.
- Michels, J., Gorb, S.N., 2012. Detailed three-dimensional visualization of resilin in the exoskeleton of arthropods using confocal laser scanning microscopy. *J. Microsc.* 245, 1–16.
- Miles, P.W., 1958. The stylet movements of a plant-sucking bug, *Oncopeltus fasciatus* Dall. (Heteroptera: Lygaeidae). *Proc. R. Entomol. Soc. Lond. Ser. A Gen. Entomol.* 33, 15–20.
- Neff, D., Frazier, S.F., Quimby, L., Wang, R.T., Zill, S., 2000. Identification of resilin in the leg of cockroach, *Periplaneta americana*: Confirmation by a simple method using pH dependence of UV fluorescence. *Arthropod Struct. Dev.* 29, 75–83.
- Pollard, D.G., 1969. Directional control of the stylets in phytophagous Hemiptera. *Proc. R. Entomol. Soc. Lond. Ser. A Gen. Entomol.* 44, 173–185.
- Quicke, D.L.J., 1991. Ovipositor mechanics of the braconine wasp genus *Zaglyptogastera* and the ichneumonid genus *Pristomerus*. *J. Nat. Hist.* 25, 971–977.
- Quicke, D.L.J., Fitton, M.G., 1995. Ovipositor steering mechanisms in parasitic wasps of the families Gasteruptionidae and Aulacidae (Hymenoptera). *Proc. R. Soc. Lond. Ser. B Biol. Sci.* 261, 99–103.
- Quicke, D.L.J., Fitton, M.G., Harris, J., 1995. Ovipositor steering mechanisms in braconid wasps. *J. Hymenoptera Res.* 4, 110–120.
- Rabinovich, J.E., Leal, J.A., De Pinerio, D.F., 1979. Domiciliary biting frequency and blood ingestion of the chagas's disease vector *Rhodnius prolixus* Stål (Hemiptera: Reduviidae), in Venezuela. *Trans. R. Soc. Trop. Med. Hyg.* 73, 272–283.
- Rakitov, R., 2019. Morphogenesis of piercing stylets in Hemiptera. In: Krenn, H.W. (Ed.), *Insect Mouthparts*. Zoological Monographs, vol. 5. Springer, Cham, pp. 529–566.
- Rassi, A.J., Rassi, A., Marin-Neto, J.A., 2010. Chagas disease. *Lancet* 375, 1388–1402.
- Ribeiro, J.M.C., 1987. Role of saliva in blood feeding by arthropods. *Annu. Rev. Entomol.* 32, 463–478.
- Ribeiro, J.M.C., Garcia, E.S., 1981. The role of salivary glands in feeding in *Rhodnius prolixus*. *J. Exp. Biol.* 94, 219–230.
- Ryckman, R.E., Ryckman, A.E., 1965. Epizootiology of *Trypanosoma cruzi* in Southwestern North America. *J. Med. Entomol.* 2, 87–108.
- Scali, M., Pusch, T.P., Breedveld, P., Dodou, D., 2017. Ovipositor-inspired steerable needle: design and preliminary experimental evaluation. *Bioinspiration Biomimetics* 13, 016006.
- Schindelin, J., Arganda-Carreras, I., Frise, E., Kaynig, V., Longair, M., Pietzsch, T., Preibisch, S., Rueden, C., Saalfeld, S., Schmid, B., Tinevez, J.-Y., White, D.J., Hartenstein, V., Eliceiri, K., Tomancak, P., Cardona, A., 2012. Fiji: an open-source platform for biological-image analysis. *Nat. Methods* 9, 676–682.
- Schindelin, J., Rueden, C.T., Hiner, M.C., Eliceiri, K.W., 2015. The ImageJ ecosystem: an open platform for biomedical image analysis. *Mol. Reprod. Dev.* 82, 518–529.
- Schneider, C.A., Rasband, W.S., Eliceiri, K.W., 2012. NIH Image to ImageJ: 25 years of image analysis. *Nat. Methods* 9, 671–675.
- Venable, J.H., Coggeshall, R., 1965. A simplified lead citrate stain for use in electron microscopy. *J. Cell Biol.* 25, 407–408.
- Weirauch, C., 2008. Cladistic analysis of Reduviidae (Heteroptera: Cimicomorpha) based on morphological characters. *Syst. Entomol.* 33, 229–274.
- Weirauch, C., Schuh, R.T., Cassis, G., Wheeler, W.C., 2019. Revisiting habitat and lifestyle transitions in Heteroptera (Insecta: Hemiptera): insights from a combined morphological and molecular phylogeny. *Cladistics* 35, 67–105.
- Wenk, P., Lucic, S., Betz, O., 2009. Funktionelle Anatomie des Hypopharynx und der Speichelpumpe beim Saugapparat der Raubwanze *Rhodnius prolixus* (Stål 1858) (Heteroptera: Reduviidae). *Mitt. dtsh. Ges. allg. angew. Entomol.* 17, 281–284.
- Wenk, P., Lucic, S., Betz, O., 2010. Functional anatomy of the hypopharynx and the salivary pump in the feeding apparatus of the assassin bug *Rhodnius prolixus* (Reduviidae, Heteroptera). *Zoomorphology* 129, 225–234.
- Wirtz, H.-P., 1987. Eindringen der Mundwerkzeuge von Raubwanzen durch eine Membran (Hemiptera: Reduviidae). *Entomol. Gen.* 12, 147–153.

Additional files (supplementary data): video files (snapshots displayed here); files available online at <https://www.sciencedirect.com/science/article/abs/pii/S146780392030013X>



Supplementary data – Video S1: Time-lapse recording of a *Dipetalogaster maxima* feeding on warm (approximately 37°C) defibrinated pig blood that was served in finger stalls to trigger the feeding response. The recorded process took approximately 90 min in real time.



Supplementary data – Video S2: Video sequence of a *Dipetalogaster maxima* probing with its maxillary bundle within isotonic blood saline and the opening of the food channel (*cf.* Fig. 7 a).



Supplementary data – Video S3: Video sequence of a *Dipetalogaster maxima* probing with its maxillary bundle within agar (cf. Fig. 7 b).

Publication 8

Betz O., Birkhold A., Caliaro M., **Eggs B.**, Mader A., Knippers J., Röhrle O. and Speck O. (2016). Adaptive stiffness and joint-free kinematics: actively actuated rod-shaped structures in plants and animals and their biomimetic potential in architecture and engineering. In: Knippers J., Nickel K. G. and Speck T. (eds.), *Biomimetic Research for Architecture and Building Construction: Biological Design and Integrative Structures* (pp. 135–167), Biologically-Inspired Systems, vol. 8. Cham, Switzerland: Springer International Publishing. doi: 10.1007/978-3-319-46374-2_8

(peer-reviewed book chapter; review¹)

Abstract

Plants and animals have evolved a variety of rod-like or tube-shaped systems capable of adapting their stiffness and concomitantly achieving deformations without the need of classical engineering-like joints. In architectural concepts, such adaptable systems would provide the technical basis for the construction of building structures and facades with the capacity for continuous adaptive actuation. The present contribution provides an overview of a literature screening for general principles of the deployment of continuous kinematics and adaptive stiffness of rod-like structures in animals and technical systems. With respect to the performance of plants, the initial results of a case study of anatomical properties and wilting modes and of their interrelationship are presented. More specifically, plants are characterized as anatomically heterogeneous and mechanically anisotropic fibre-reinforced materials. In herbaceous plants, movements can be classified into hydraulic movements caused by water transport and movements caused by mechanical instabilities. With our focus on water-dependent adaptive stiffness, the plant tissues of special interest are those that change their properties significantly according to water availability, such as parenchyma and collenchyma. In invertebrate animals and “protozoans”, adaptive stiffness is found in hydroskeletons in which a change in internal hydrostatic pressure interacts with crossed-fibre reinforced external walls and is also achieved by other mechanisms, such as (1) amoeboid cell crawling, (2) muscular hydrostats and (3) slide-lock mechanisms. Slide-lock mechanisms are present, for instance, in insects that have a mechanism for releasing needle-like elongated cuticle structures interlocked along their entire length, thereby achieving joint-free movement (e.g. in needle-like mouthparts responsible for piercing and sucking fluids or in ovipositors used for egg-laying).

The transfer of these biological concepts of adaptive stiffness and continuous kinematics to technical applications in architecture might lead to improved architectural systems, for example, for sun-shading systems. As the proneness to failure is directly dependent on the number of individual

¹Springer Nature license number 5624081054663.

movable components in these systems, a decrease in mechanical complexity is a guiding design criterion. Hinge-less or compliant mechanisms transferred from biology offer this feature. However, abstractions are needed for technical application. Therefore, computational analysis is essential to identify the key characteristics and the underlying actuation principles of the biological role model. The identified principles from several biological role models can finally be implemented in a common demonstrator, thus providing completely novel bio-inspired technical actuation solutions.

Significance within the present thesis: This literature review gives an overview of all joint-free movement mechanisms that we find in plants and animals. We also discuss the potential of these systems as concept generators for biomimetic research and the transfer of biological concepts to technical applications, mainly in engineering and architecture.

Methods used: none (literature review)

Own contribution: writing and preparing parts of the manuscript and figures; discussing the manuscript

Chapter 8

Adaptive Stiffness and Joint-Free Kinematics: Actively Actuated Rod-Shaped Structures in Plants and Animals and Their Biomimetic Potential in Architecture and Engineering

Oliver Betz, Annette Birkhold, Marco Caliaro, Benjamin Eggs, Anja Mader,
Jan Knippers, Oliver Röhrle, and Olga Speck

Abstract Plants and animals have evolved a variety of rod-like or tube-shaped systems capable of adapting their stiffness and concomitantly achieving deformations without the need of classical engineering-like joints. In architectural concepts, such adaptable systems would provide the technical basis for the construction of building structures and facades with the capacity for continuous adaptive actuation. The present contribution provides an overview of a literature screening for general principles of the deployment of continuous kinematics and adaptive stiffness of rod-like structures in animals and technical systems. With respect to the performance of

O. Betz (✉) • B. Eggs

Evolutionary Biology of Invertebrates, Institute of Evolution and Ecology, University of Tübingen, Auf der Morgenstelle 28, 72076 Tübingen, Germany
e-mail: oliver.betz@uni-tuebingen.de

A. Birkhold

Institute of Applied Mechanics (CE), University of Stuttgart, Pfaffenwaldring 7, 70569 Stuttgart, Germany

M. Caliaro • O. Speck

Plant Biomechanics Group, Botanic Garden, Faculty of Biology, University of Freiburg, Schänzlestraße 1, 79104 Freiburg, Germany

Freiburg Centre for Interactive Materials and Bioinspired Technologies (FIT), University of Freiburg, Georges-Köhler-Allee 105, 79110 Freiburg, Germany

A. Mader • J. Knippers

Institute of Building Structures and Structural Design (ITKE), University of Stuttgart, Keplerstraße 11, 70174 Stuttgart, Germany

O. Röhrle

Institute of Applied Mechanics (CE), University of Stuttgart, Pfaffenwaldring 7, D-70569 Stuttgart, Germany

Cluster of Excellence for Simulation Technology, Continuum Biomechanics and Mechanobiology Research Group, University of Stuttgart, Pfaffenwaldring 5a, D-70569 Stuttgart, Germany

plants, the initial results of a case study of anatomical properties and wilting modes and of their interrelationship are presented.

More specifically, plants are characterized as anatomically heterogeneous and mechanically anisotropic fibre-reinforced materials. In herbaceous plants, movements can be classified into hydraulic movements caused by water transport and movements caused by mechanical instabilities. With our focus on water-dependent adaptive stiffness, the plant tissues of special interest are those that change their properties significantly according to water availability, such as parenchyma and collenchyma. In invertebrate animals and “protozoans”, adaptive stiffness is found in hydroskeletons in which a change in internal hydrostatic pressure interacts with crossed-fibre reinforced external walls and is also achieved by other mechanisms, such as (1) amoeboid cell crawling, (2) muscular hydrostats and (3) slide-lock mechanisms. Slide-lock mechanisms are present, for instance, in insects that have a mechanism for releasing needle-like elongated cuticle structures interlocked along their entire length, thereby achieving joint-free movement (e.g. in needle-like mouthparts responsible for piercing and sucking fluids or in ovipositors used for egg-laying).

The transfer of these biological concepts of adaptive stiffness and continuous kinematics to technical applications in architecture might lead to improved architectural systems, for example, for sun-shading systems. As the proneness to failure is directly dependent on the number of individual movable components in these systems, a decrease in mechanical complexity is a guiding design criterion. Hingeless or compliant mechanisms transferred from biology offer this feature. However, abstractions are needed for technical application. Therefore, computational analysis is essential to identify the key characteristics and the underlying actuation principles of the biological role model. The identified principles from several biological role models can finally be implemented in a common demonstrator, thus providing completely novel bio-inspired technical actuation solutions.

8.1 Introduction

Many developments in current architecture and building technology are directed towards adaptive systems that adjust their geometry to changing external environmental conditions or internal comfort requirements. Their general aim is to contribute to a more sustainable architecture through adaptivity. These systems are envisaged in different sizes for a variety of applications, such as moveable panels for daylight-control or sun-shading, solar tracking for photovoltaic cells, flexible cladding for the adjustment of aerodynamic properties and noise reduction. Until now, these structures have been constructed out of rigid elements or soft textiles connected by hinges, bearings and other highly strained elements. They are actuated and locked in certain (often discrete) positions by external mechanical devices. However, proneness to failure is directly dependent on the number of individual movable components. A minimum level of mechanical complexity is therefore a

guiding design criterion. Hinge-less or compliant mechanisms offer this feature. Ideally, these systems exhibit flexibility during movement and develop an increased stiffness and strength when needed. They are thus able continuously to adapt to various geometric configurations through elastic deformation and to resolve the potential conflicts of carrying external loads, mainly self-weight and wind. If these elements deploy a rod-like geometry, they can often be easily integrated in a variety of two-dimensional (2D) or three-dimensional (3D) configurations, similar to hydraulic or electric pistons.

Plants and animals have evolved a variety of linear systems capable of adapting their stiffness and of achieving deformations without the need of classical engineering-like joints. The aim of biomimetic research is to transfer these functional principles to the macro-scale of building constructions through fibre-composite elements with integrated actuators based on pneumatic or other principles.

The present contribution is structured in the following manner. First, general concepts and terms are defined that biology and engineering have in common under the framework of the current biomimetic project (Chap. 8.2). Chapter 8.3 provides the results of a screening of principles of adaptive stiffness and continuous kinematics of (1) a more specific case involving wilting processes in the genus *Gerbera* (botany) and (2) the more general literature of such principles as realized in zoology and engineering. Here, we also introduce two more specific insect examples that are to be investigated in greater detail. Chapter 8.4 exemplifies how the collaboration between biologists and engineers is structured in this concrete project including both data acquisition and engineer-like modelling. Finally, we outline the general way of elucidating their biomimetic potential resulting from the extracted functional principles (Chap. 8.5).

8.2 Definition of Terms

One precondition of the development of interdisciplinary research in the field of biomimetics is to reflect upon project-relevant terms and concepts in order to advance a common understanding of the underlying general functional principles and to ensure their correct use and comprehension (cf. Chap. 19 of this book). Thus, to begin with, we need to define the central concepts and terms used in the present project from the different involved disciplines, i.e. botanical and zoological functional morphology and engineering.

8.2.1 Adaptive Stiffness

The engineers' perspective: Adaptability is a major aim of current research and development in architecture. In general, it reflects the step from a steady and time-

independent conception of architecture towards a built environment that constantly reacts to changing requirements. The current project focuses on the adaption of two selected and individual features: the elastic stiffness and the geometric configuration of a rod.

Stiffness defines the extent to which a body resists deformation in response to an applied force. It is a property dependent on the material, the shape and the applied boundary conditions of the body. In the context of this research, adaptive stiffness means that the stiffness of the system can be altered in such a way that the system is, on the one hand, stiff enough to withstand high external forces in a steady state and, on the other hand, the stiffness can be reduced far enough to allow the system to change its geometric configuration, at least for a defined period of time.

The biologists' perspective: The general capacity of plants and animals directly to adjust to changing habitat conditions is called adaptivity, a term that also refers to concepts such as physiological adaptation, phenotypical adjustment, acclimation or modification. Especially for immobile plants, which cannot escape from unfavourable environmental conditions and cannot hide themselves behind protective structures, adaptive traits confer some evolutionary advantage. Adaptivity, in general, and adaptive stiffness, in particular, mean a significant change of one or more features such as structures, materials and geometric configurations in a controlled fashion in answer to changing environmental conditions such as water availability, temperature or mechanical strains (Gibson 2012; Niklas and Spatz 2012; Fratzl and Barth 2009; Fratzl and Weinkamer 2007; Vincent 2007). In animals, adaptive stiffness occurs when single organs or body parts (usually reversibly) adapt their (flexural) stiffness in response to changing external loads.

In plants and animals, adaptive systems, which are capable of dealing with changing environments, are controlled by feedback loops (Brun et al. 2009). Key components of such open- or closed-loop control systems are (1) sensors in order to detect external or internal stimuli, (2) controllers in order to ensure positive or negative feedback in the system and (3) suitable actuators, which are controllable work-producing elements. Interestingly, this holds true for both natural and technical systems. In contrast to technical applications where sensors, controllers and actuators are realized in terms of block building constructions, biological solutions are often integrated systems. This is of special interest and is especially promising, if one considers biomimetic innovations.

8.2.2 *Joint-Free Movement*

The engineers' perspective: A joint or a kinematic pair is the connection between two (or more) bodies that imposes constraints on their relative movement. Movable technical systems are usually based on the conception of components deploying a maximum ratio of strength versus weight linked by individual elements deploying a minimum resistance to rotation or translation. These hinges and bearings are highly strained elements prone to wearing and failure. A joint-free movement offers a

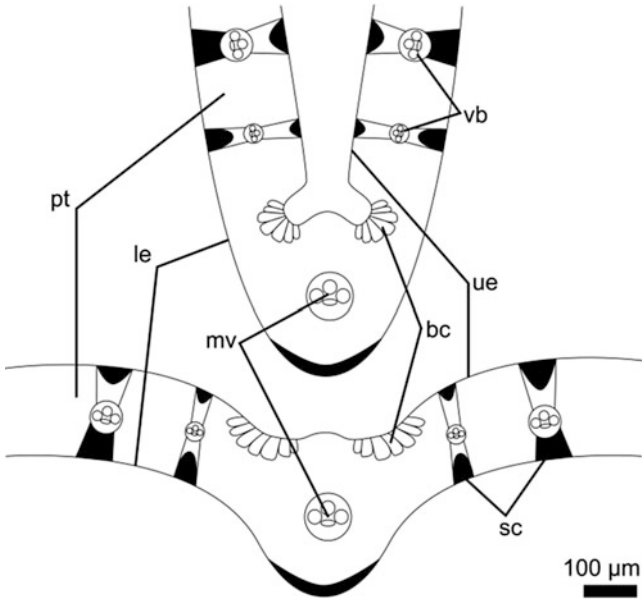


Fig. 8.1 Schematic drawing of the tissue arrangement in leaf blades of *Poa pratensis* L. allowing joint-free adaptive movement. By swelling or shrinking of the bulliform cells (*bc*) the leaf blades can change their conformation between closed (*drawing above*) and open (*drawing below*). Abbreviations: *mv* midvein, *vb* vascular bundles, *ue* upper epidermis, *le* lower epidermis, *pt* parenchymatic tissue, *sc* sclerenchyma strands

radically different approach. In this case, the compliant system consists of only one body. The movement is based on an elastic deformation of the material and is predetermined by a continuous distribution of structural or material properties.

The biologists' perspective: In plants, joints are non-existent according to the engineer's definition. Because of the geometrical arrangements of several tissues that have different mechanical properties and that can react to changing environmental parameters, plant organs, tissues or cells can adaptively – and often reversibly – take various shapes. An excellent example is the joint-free movement of leaves found in monocotyledonous plants such as grass species (Fig. 8.1). Close to the mid-vein, the anatomy is obviously asymmetric: some cells of the upper epidermis are large, highly vacuolated and bubble-shaped (so-called bulliform cells). During drought, the bulliform cells shrink because of decreasing turgor pressure with the result that the two edges of the grass blade fold up towards each other. As soon as adequate water is available, turgor increases and the cells enlarge once again resulting in an opening of the leaves.

In animals, joint-free movements of organs, body parts or entire bodies do not involve flexible links (joints = articulations) between rigid elements (e.g. bones in vertebrates or exoskeletal parts in arthropods) but function via reversible flexible shape-changes together with their enclosing walls. These movements require

deformable body media (i.e. tissues, fluids, sheaths, materials) and might comprise (often localized) lumps, constrictions, dilations, flattenings, elongations, contractions, flexures, coilings, twists, evaginations, eversions and / or undulatory movements.

8.2.3 *Active Actuation*

The engineers' perspective: An actuator converts mechanical, chemical, flow, thermal or electrical energy into a mechanical motion. Active actuation means that adaption is initiated and controlled by an active trigger. The actuation is actively controlled based on sensor data or user demands. In contrast, passive actuation is initiated and controlled by an autonomous reaction to changes in the boundary conditions of the system.

The biologists' perspective: In biology, passive and active actuation is known. Passive actuation is a pure reaction to changing environmental conditions, whereas active actuation needs energy provided by metabolic processes. In botany, active hydraulic actuators are parenchyma or epidermal cells that induce movement by osmotic swelling or shrinking in terms of increasing or decreasing their turgor pressure, i.e. motor cells in carnivorous plants or groups of bulliform cells in leaves of grasses. Other water-driven active actuators include all kinds of growth-mediated movements. Active actuation is also possible by means of fluids such as latex being stored under high pressure in laticifers. Furthermore, mechanically pre-stressed tissues such as fibres under pre-tension and / or parenchyma under pre-compression can serve as actuators. Passive movement, however, is often driven by changes in the humidity of living cells and dead tissues (Dumais and Forterre 2012). A typically passive-actuated motion is the opening and closing of the seed capsules of *Delosperma nakurense* (Engl.) A.G.J.Herre. These capsules possess swellable tissue on the inside and, if saturated with rainwater, the tissue starts to swell and unfold the lids (Harrington et al. 2011). In zoology, active actuation refers to the biological engine-like mechanical effectors that confer motility. On the cellular level, these mechanisms are based on interacting proteins as achieved by the microtubules and microfilaments of single cells and the ratcheting thick (myosin) and thin (actin) filaments that constitute muscles. For the generation of force, muscles usually shorten, thereby performing work. In order to transmit the generated force into movement and support, muscles require interaction with a rigid or incompressible skeletal system.

8.2.4 *Continuous Kinematics*

The engineers' perspective: 'Continuous kinematics' describes a moveable system that displays similar features during all stages of movement. During this continuous movement, the system can take on any geometrical state between two specified

states and is not limited to pre-defined discrete positions as, for example, membrane systems that are stable only in the fully opened or fully closed position. Thus, an indefinite number of geometric configurations can be achieved and no limitation is set to certain pre-defined discrete positions.

The biologists' perspective: Although present in many examples, 'continuous kinematics' has not as yet become a well-defined established concept in functional morphology. So, this term is lacking in the biological literature. Hence, we adopt its technical definition in this paragraph also for the biologists' perspective and, instead of providing a separate definition, just give illustrative examples for its occurrence in biological organisms. In-depth kinematic studies carried out by Dumais and Forterre (2012) as well as by Skotheim and Mahadevan (2005) revealed two categories of plant movement: (1) hydraulic movements caused by water transport and (2) movements caused by mechanical instabilities. This can be displayed graphically in terms of a plot that gives the duration of movement (in seconds) as a function of the tissue size (in meter), defined as the smallest macroscopic moving part. Hydraulic movements are limited by the poroelastic time of water diffusion through porous plant tissues. These include movements caused by growth, swelling and shrinking, which are generally slow. Movements by elastic instabilities are eventually limited by inertia. The release of stored elastic energy or rapid geometric changes can speed up movements beyond the limits imposed by simple hydraulic mechanisms.

In animals, conventional kinematics deal with systems that move via defined joints, whereas continuous kinematics address the versatile joint-free movements of organs, body parts or entire bodies that are continuously deformable (e.g. with respect to changing loads) and are thus less restrained by the rigid interconnection of joints.

8.2.5 Rod-Shaped and Tube-Like Structures

The engineers' perspective: A rod-shaped structure is defined by its geometry, which is typically straight, thin, much longer than wide, and has often a circular cross section. In mechanics, the term 'linear element' is more common.

The biologists' perspective: In biology, cylindrical structures can be massive (rod) or hollow (tube). Important biomechanical properties of a rod are its resistance to (1) bending referred to as flexural stiffness and (2) torsion referred to as torsional stiffness. Both these properties are modified by the cross-sectional shape of the rod and its material anisotropy (Vogel 1988, 2003). More specifically, with respect to their loading regime, rods can be distinguished into (bending) beams and columns. Whereas beams run horizontally and withstand transverse forces that would bend them, columns run vertically and withstand lengthwise forces that would compress them (Vogel 2003). In animals, rods might become elements of superordinate structural systems (frameworks) such as trusses, filled polymers and multibar linkages (Vogel 2003) that confer novel properties by combining static support with mobility.

In plants, rod-shaped structures (without pith) or tube-like structures (with pith) are very common. Examples include stems, pedicels, petioles and roots. With respect to the various bauplans of mono- and dicotyledons, specific patterns of tissue arrangement can be found in the respective plant organ. Bearing in mind that every single tissue has its specific 3D arrangement in the plant organ and that the tissue's mechanical properties are very different from one another, plant organs are characterized as anatomically heterogeneous and mechanically anisotropic fibre-reinforced materials. With regard to adaptive stiffness and because plant movements are caused by water transport and/or mechanical instabilities, the tissues that are of special interest are those that can change their properties significantly according to water availability, such as parenchyma and collenchyma (Caliaro et al. 2013a,b).

8.3 The Diversity of Functional Principles

8.3.1 *Plants: Principles Found in Mono- and Dicotyledons*

From the botanists' viewpoint, the main aim of this project is to investigate mechanisms of plants exhibiting adaptive stiffness and joint-free connections and to abstract the functional principles in order to translate these mechanisms into novel biomimetic actuators for built structures.

Water-dependent systems: Bearing in mind that plants have evolved a remarkable range of mechanisms to create adaptive stiffness in reaction to several external and internal stimuli and considering that water-driven mechanisms play a major role in adaptive design, we first focus on water-dependent adaptive stiffness. This is initially performed within the framework of a screening process of various herbaceous plants followed by the selection of one model plant in which quantitative analyses of the functional morphology and biomechanics with various relative water content are carried out. In future, an abstraction via computational models of variable detail, in particular by using principles of continuum mechanics and the finite element (FE) method, will be investigated.

Suitable model plants were selected on the basis of an extensive literature search and a screening process that has been underpinned by the following pre-defined criteria: (1) herbaceous plant organs, (2) unbranched rod-shaped or tube-like geometry, (3) active actuation, (4) adaptive stiffness dependent on water content and (5) reversible adaptation process.

On the basis of the diverse bauplans of mono- and dicotyledons and the specific pattern of various tissues, a variety of wilting modes and water-dependent recovery can be defined (Fig. 8.2). Whereas wilting is a passive mechanism, the energy-consuming recovery after full water supply can be regarded as an active process.

Table 8.1 shows the result of this screening process carried out on a variety of selected model plants. A relationship between the various wilting modes with or without full recovery and the specific anatomical conditions (Fig. 8.3) can

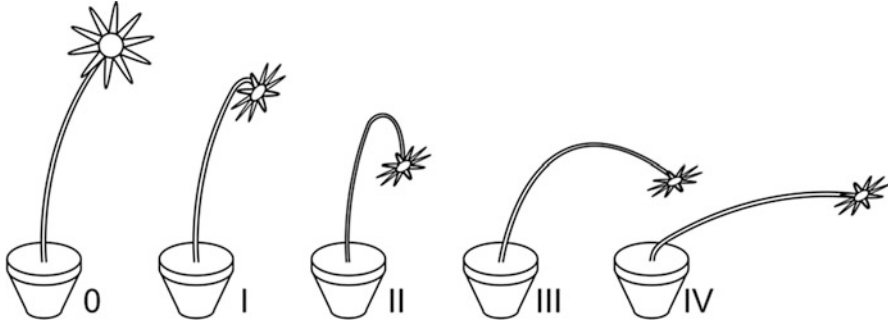


Fig. 8.2 Various wilting modes of rod-shaped or tube-like plant axes (e.g. stem, pedicel, petiole) with a top load (e.g. lamina, flower). *O* original position, *I* bending zone at the apical end of the axis close to the top load, *II* bending zone at a height of about half to two-third of the total length of the axis, *III* bending along the entire axis, *IV* bending zone at the basal end of the axis, thus tilting of the entire axis

be assumed and will be subject of future analyses. Especially promising results concerning the fulfilment of the pre-defined criteria could be found in pedicels of *Gerbera jamesonii* ‘Nuance’. Therefore, this *Gerbera* cultivar was the first model plant to be analysed and initial findings are presented here (cf. Sect. 8.4.1).

8.3.2 Animals: Principles Found in Invertebrates

In animals, we distinguish between three fundamental ways of movement, i.e. (1) ciliate and flagellate via hair-like differentiated structures that beat in a pendulum-like manner, (2) amoeboid (also called cell crawling) via plasma protuberances (= pseudopodia) driven by contracting proteins and (3) muscular involving two sets of filaments (actin and myosin) that slip in between each other, such that muscles shorten. Whereas, in many taxa, muscular movements are regularly linked to jointed limbs, in this overview, we focus on the general principles of joint-free continuous kinematics involving flexible rod-like systems with adaptive stiffness. We limit ourselves to protists and invertebrates, excluding vertebrates. Our screening of the literature has revealed four general principles of such movements, i.e. (1) amoeboid cell crawling, (2) hydroskeleton mechanisms, (3) muscular hydrostats and (4) slide-lock mechanisms (Fig. 8.4).

Amoeboid Cell Crawling (Fig. 8.4a)

Cell crawling occurs in a wide variety of cells including rhizopodean protists and human white blood cells. To enhance the cell’s grip with the substrate, the motile cells produce dynamic surface extensions (e.g. foot-like pseudopodia) of the gel-like ectoplasm containing concentrated networks of actin filaments forming a cell cortex. Forward movements are produced by actin polymerization beneath the cell’s surface causing the leading edge to advance. The actin filaments grow at their plus

Table 8.1 Results of the screening process: plant species were characterized according to the pre-defined criteria

Plant species	Plant organ	Wilting mode	Reversible process	Anatomy
Monocotyledons				
<i>Anthurium andraeanum</i> Linden ex André 'Amalia Elegance'	Pedice/petiole	Wilting shape IV: bending zone at the basal end of the pedice/petiole thus slight tilting, no further change of shape of the pedice/petiole	Fully reversible; recovery of original position	Atactostele: numerous scattered bundles (cf. Fig. 8.3a)
<i>Caladium bicolor</i> (Aiton) Vent. 'Candyland'	Petiole	wilting mode III followed by wilting mode IV: first, bending of the entire petiole; second, bending zone at the basal end of the petiole	Not reversible; permanent bending	Atactostele: numerous scattered bundles; collenchyma prevail in terms of strengthening tissue, nearly no lignified tissues (cf. Fig. 8.3b)
Dicotyledons				
<i>Anemone sylvestris</i> L.	Pedicele	Wilting mode I followed by wilting mode IV: first, bending zone at the apical end of the pedicele close to the flower; second, bending at the basal end of the pedicele and tilting of the entire pedicele	Fully reversible; recovery of original position	Eustele: broad closed ring of vascular bundles together with lignified tissue in the periphery, no pith (cf. Fig. 8.3c)
<i>Armeria maritima</i> (Mill.) Willd. 'Alba'	Pedicele	Wilting shape II: bending zone at a height of about half to two-third of the total length of the pedicele	Fully reversible; recovery of original position	Eustele: broad closed ring of lignified tissue in the periphery, inward following vascular bundles, pith (cf. Fig. 8.3d)
<i>Begonia sanguinea</i> Raddi	Pedice/petiole	Wilting mode IV followed by wilting mode III: first, bending zone at the basal end of the pedice/petiole, thus slight tilting; second, followed by a slight bending along the entire pedice/petiole	Fully reversible; recovery of original position	Eustele: narrow closed ring of vascular bundles together with lignified tissue in the periphery, no pith (pedicele see Fig. 8.3e, petiole see Fig. 8.2f)
<i>Bellis perennis</i> L. 'Habanera'	Pedicele	Wilting shape I: bending zone at the apical end of the pedicele close to the flower	Fully reversible; recovery of original position	Eustele: narrow closed ring of vascular bundles together with lignified tissue in the periphery, pith (cf. Fig. 8.3g)

<i>Pelargonium zonale</i> (L.) L'Hér. ex Aiton	Pedicel	No visible wilting mode	–	Oval cross section; eustele; narrow closed ring of lignified tissue in the periphery, inward following vascular bundles, no pith (cf. Fig. 8.3h)
<i>Gerbera jamesonii</i> Bolus ex Hooker f. 'Nuance'	Pedicel	Wilting shape I: bending zone at the apical end of the pedicel close to the flower	Fully reversible; recovery of original position	Eustele: narrow closed ring of vascular bundles together with lignified tissue in the periphery, pith (cf. Fig. 8.3i)
<i>Primula denticulata</i> Sm. 'Red Select'	Pedicel	Wilting shape III: bending along the entire pedicel	Partially reversible; no recovery of original position	Eustele: narrow closed ring of lignified tissue in the periphery, inward following vascular bundles, huge pith (cf. Fig. 8.3j)
<i>Primula obconica</i> Hance 'Touch me'	Pedicel	Wilting shape IV: bending zone at the basal end of the pedicel, thus tilting of the entire pedicel	Fully reversible; recovery of original position	Eustele: narrow closed ring of lignified tissue in the periphery, inward following vascular bundles, no pith (cf. Fig. 8.3k)
<i>Primula veris</i> L. 'Cabrillo'	Pedicel	Wilting shape IV: bending zone at the basal end of the pedicel, thus tilting of the entire pedicel	Fully reversible; recovery of original position	Eustele: narrow closed ring of lignified tissue in the periphery, inward following vascular bundles, no pith (cf. Fig. 8.3l)

All plant organs possess an unbranched rod-like or tube-like geometry, active actuation and adaptive stiffness dependent on the water content.

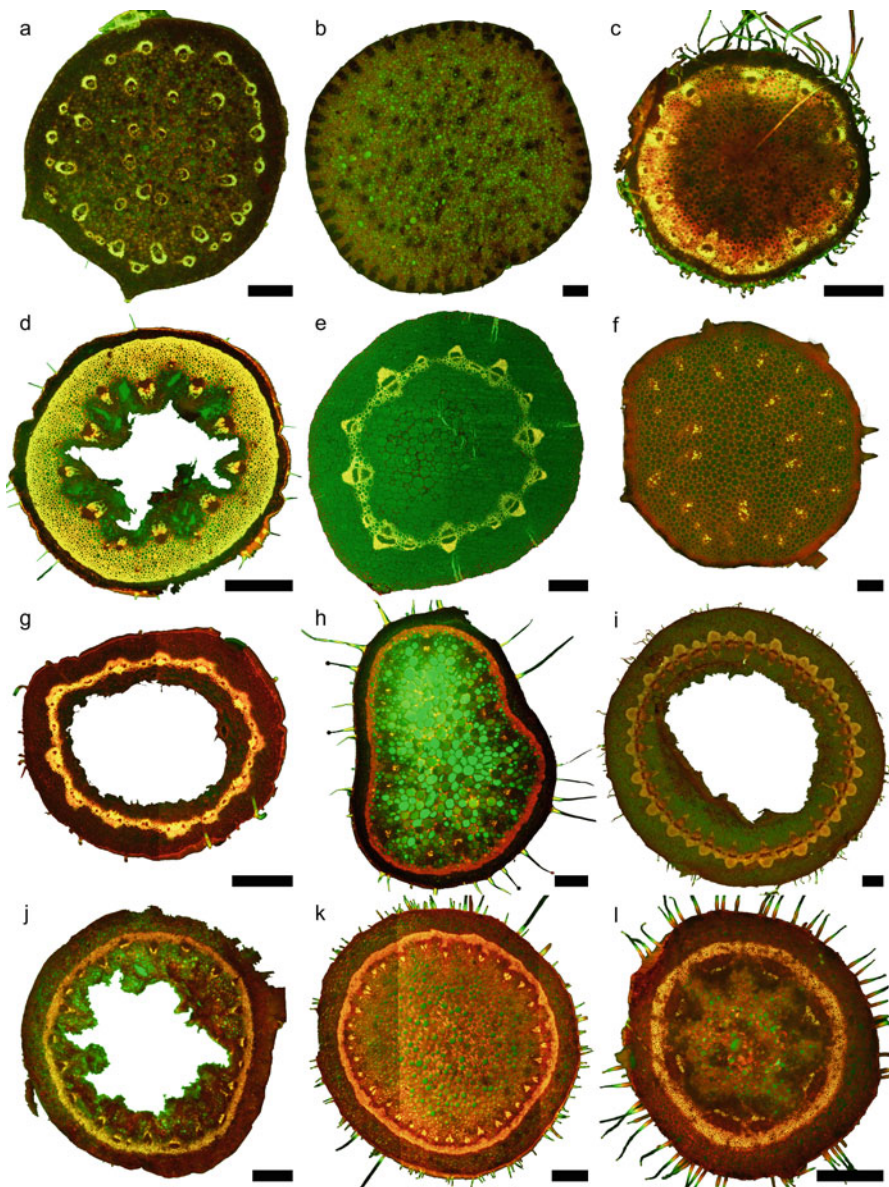


Fig. 8.3 Cross sections of plant organs stained with Acridine Orange highlighting lignified tissues in bright yellow. Monocotyledons: (a) *Anthurium andraeanum* Linden ex André ‘Amalia Elegance’ (petiole), (b) *Caladium bicolor* (Aiton) Vent. ‘Candyland’ (petiole); Dicotyledons: (c) *Anemone sylvestris* L. (pedicel), (d) *Armeria maritima* (Mill.) Willd. ‘Alba’ (pedicel), (e) *Begonia sanguinea* Raddi (pedicel), (f) *Begonia sanguinea* Raddi (petiole), (g) *Bellis perennis* L. ‘Habenera’ (pedicel), (h) *Pelargonium zonale* (L.) L’Hér. ex Aiton (pedicel), (i) *Gerbera jamesonii* Bolus ex Hooker f. ‘Nuance’ (pedicel), (j) *Primula denticulata* Sm. ‘Red Select’ (pedicel), (k) *Primula obconica* Hance ‘Touch me’ (pedicel), (l) *Primula veris* L. ‘Cabrillo’ (pedicel). Scale bars = 500 μ m

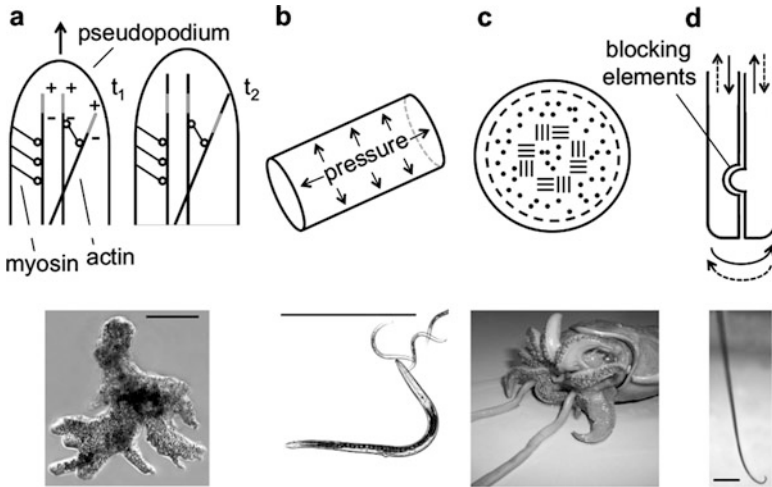


Fig. 8.4 Schemes and photographic examples of four general principles of joint-free movements with adaptive stiffness of rod-like structures in protists and invertebrate animals. **(a)** amoeboid cell crawling, **(b)** hydroskeleton mechanisms, **(c)** muscular hydrostats and **(d)** slide-lock mechanisms. The grey bars in **(a)** are indicative of the outer actin elements to which new elements are added at their plus ends. The drawing in **(c)** shows a schematic cross section of a squid tentacle, in which longitudinal muscles are indicated as dots, and circular and crosswise muscles as dashes. The straight arrows in **(d)** indicate the relative lengthwise movements of the independent rod-like structures, and the curved arrows the resulting bending movement of the entire organ (see Fig. 8.9). The drawings were adapted and modified in **(a)** from Biewener (2003), in **(b)** from Barnes et al. (2002), in **(c)** from Vogel (2003). The photos show **(a)** the amoeba *Amoeba proteus* (Pallas) with protruding pseudopodia (scale bar = 200 μm); photo courtesy to Klaus Eisler, Tübingen, **(b)** the nematode *Pelodera strongyloides* (Schneider) (shown is one adult female and three L1 larvae) during its characteristic undulating body movements through a fluid medium (scale bar = 0.5 mm), **(c)** the arm of the squid *Sepia* sp. Linnaeus, and **(d)** the bending joint-free maxillae of the assassin bug *Dipetalogaster maxima* Uhler (Reduviidae: Triatominae) as recorded during their feeding on pig blood (scale bar = 0.6 mm). Abbreviations: + nucleation sites of actin filaments, - sites of disassembling of actin during the process of “treadmilling”. t1, t2 two succeeding steps of pseudopodium protrusion

ends, while they become disassembled at their minus ends, a process that is called “treadmilling”. Myosin is probably also involved in the generation of propulsive forces by pulling against the local actin networks. More detailed descriptions of this mechanism, which also involves hydrostatic pressure from the interior sol-like endoplasm of the cell and allows animal cells to adopt a variety of shapes, can be found, for example, in Biewener (2003) or Alberts et al. (2014).

Hydroskeleton Mechanisms (Fig. 8.4b)

Once muscles are involved in the production of movement, mechanical counter bearings are needed that are usually provided in the form of skeletons. The phylogenetically oldest skeleton type is the hydrostatic (= fluid) skeleton, whose working principle is a pressurized fluid-filled cavity that is surrounded by a tension-

resisting fibre-reinforced skin or wall. In such systems, changes of the body shape and movements are caused by hydraulics through the transmission of pressure into other parts of the body. In the hydrostatic skeletons of soft-bodied invertebrates, the pressurized body cavity promotes muscle antagonisms, whereupon the body cavity might be either unstructured or segmented. In roundworms (Nematoda), for instance, an unstructured body cavity forms a liquid column that is surrounded by longitudinal muscles only. As a consequence, undulating movements result driven by the alternate contraction of opposing (dorsal and ventral) muscles. In contrast, the segmented worms (Annelida) show a segmental chambered body cavity (coelom) combined with a dermal muscular tunic made of longitudinal and circular muscles. From such an arrangement, a peristaltic movement results from the alternate contraction of the longitudinal and circular muscles. In comparison with non-segmented worms, such segmentation makes it possible to isolate changes in the fluid pressure to individual segments or groups of them and so regions between the contracting segments do not experience high fluid pressures and do not need to contract fully to maintain their body shape. This saves energy. Earthworms and other annelids use this principle to produce peristalsis; thus, instead of the body lengthening and shortening as a whole, waves of lengthening and shortening proceed backwards along the body (Gray 1968; Alexander 1983, 2003). In this way, the worms can produce both the propulsive forces (as exerted by contracting the circular muscles and elongating the segments) and, at the same time, the friction towards the substratum (as caused by the thickening of the fully shortening segments upon contraction of the longitudinal muscles) as necessary for an effective forward penetration through the substrate without slipping backwards.

According to Ruppert et al. (2004), the incompressibility of the fluid- (or, alternatively, parenchyma-) filled body cavity upon muscle pressure leads to two important properties, i.e. (1) the resulting hydrostats are constant in volume and (2) any localized increase in pressure as a result of muscular contraction is transmitted equally throughout the hydrostat. These properties are used by the animals (1) mechanically to support the body and adaptively to increase their stiffness and (2) to generate forces by displacing water in one region to do work in another. In addition to locomotion as described above, the dynamic interrelationship between the muscles of the body wall around a fluid skeleton is responsible for the variety of joint-free body movements shown by worm-shaped invertebrates in various biological contexts (e.g. Clark 1964; Gray 1968). Many animals with hydrostatic skeletons (e.g. such as of sea anemones, “worms”) are characterized by more or less cylindrical bodies and, similar to the windings in the wall of a garden hose, their body wall is often reinforced by a mesh of inextensible (e.g. collagen) fibres (e.g. Clark 1964; Ruppert et al. 2004). Such fibrous mesh not only toughens the body wall, but also prevents uncontrolled bulges and aneurisms as the hydrostatic pressure rises. To prevent aneurisms, the meshwork fibres in natural hydrostats are oriented in a crossed-fibre array, in which the fibres wrap helically around the body in layers of parallel left-handed and right-handed fibres. Figure 8.5 presents a scheme (adopted from Vogel 2003 and originally suggested by Clark 1964) that shows the change in volume and fibre angle as the length of a helically wound cylinder is varied.

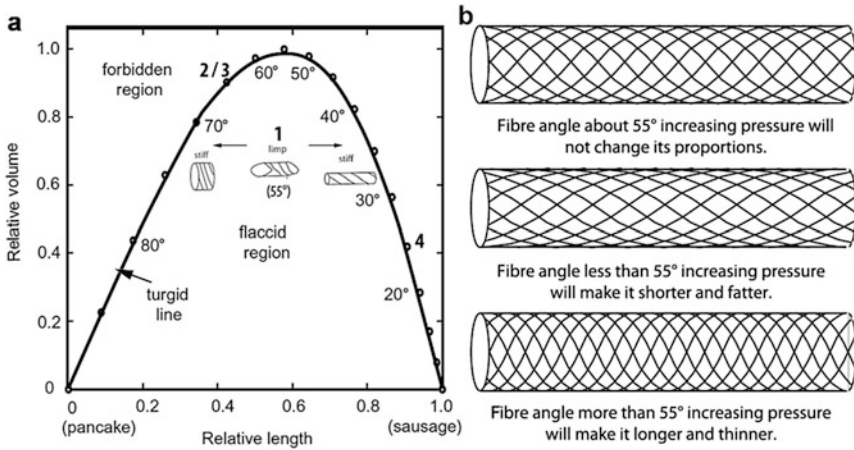


Fig. 8.5 (a) Relationship between the relative volume and the relative length as a function of the fibre angle of helically wound cylinders in natural hydrostats. (b) Three representative cylinders with different fibre angles and their consequences for shape changes. The **bold numbers** in the scheme represent different actual zoological examples. (1) Many “low-pressure” worms (e.g. (acoelomic) limp worms (Nemertini) and flatworms (Plathelminthes)) form flattened (not circular) cylinders, whose volume is not at its maximum (“flaccid”). By contracting the longitudinal muscles, these worms shift to the left towards the turgid line, whereby the mechanical capacity of the fibres is at its maximum. As a consequence, the worms become shorter, thicker, stiffer and more circular in shape. Upon contraction of the circumferential muscles, the worms shift to the right towards the turgid line, becoming longer, thinner and also stiffer and more circular. (2) “High-pressure” roundworms (Nematoda) possess longitudinal muscles only, have a strong external cuticle (with crossed collagen fibres) and show a circular cross section. Upon contraction of the longitudinal muscles, these worms shorten only a little but become stiffer (up to 30 kPa in *Ascaris* Linnaeus). They can increase their volume by relaxing the longitudinal muscles, thereby lowering the fibre angle towards 55°. Worms that possess fibre angles of 55° must be flat to be able to increase their volume by rounding their cross section; otherwise, shape changes would only be possible by further increasing the internal pressure. (3) Similar to roundworms, the small, soft and joint-free tube feet of echinoderms (e.g. starfish) have longitudinal muscles only and collagen fibres of 67° in the fully extended feet. Upon contraction of the longitudinal muscles, the foot shortens, increasing this angle further and making the tubes even stiffer. (4) The mantle of squids (Cephalopoda) possesses circumferential muscles only. Collagen fibres in the mantle make angles of 25° with the long axis. Upon contraction of the circumferential muscles, the fibre orientation resists lengthening, leading to a reduction in the volume of the mantle cavity, which is used to squirt water out of the siphon for jet propulsion. The relationship between volume and fibre angle are calculated as: $\text{volume} = \text{fibre length}^3 (\sin^2\theta \cos\theta)/4\pi$. Figure and examples taken from Vogel (2003); reproduced by courtesy of Princeton University Press

Worm-like invertebrates and other organisms under hydrostatic pressure can use this scheme predictably to adjust their stiffness. Whereas the area beneath the curve in the graph contains cylinders that are not fully inflated (and so not fully cylindrical), the turgid line represents so-called “high-pressure” worms that are under almost maximum pressure (and thus almost cylindrical). More detailed discussions can be found in Clark (1964), Wainwright et al. (1976), Vogel (1988, 2003) and Barnes et al. (2002).

One special biological context of hydrostatic skeletons is the effective protrusion of introvert organs such as the predatory mouthparts of insects (e.g. Kölsch and Betz 1998) and the proboscis of many coelomate worms (Clark 1964). This protrusion is often accomplished by hydraulic linkages and levers (Barnes et al. 2002; Vogel 2003).

In contrast to hydrostats of constant volume, sea anemones (Cnidaria: Anthozoa) possess open cylindrical bodies with circumferential, radial and longitudinal muscles in their walls. The cavity of their gastrointestinal system allows, by the ingress and egress of water via the mouth, an enormous range of hinge-less continuous body sizes and shapes (Wainwright et al. 1976; Alexander 1983). The supporting material in the wall is the mesoglea, i.e. a pliant composite visco-elastic material of fibrillar collagen imbedded in a cell-free matrix. The very low modulus of the mesoglea (0.01 MPa) means that the animal can inflate itself with very low internal pressures (<1 Pa) as generated by ciliary pumping. According to the viscoelasticity of the material, at higher strain rates, the mesoglea becomes more rigid (Wainwright et al. 1976).

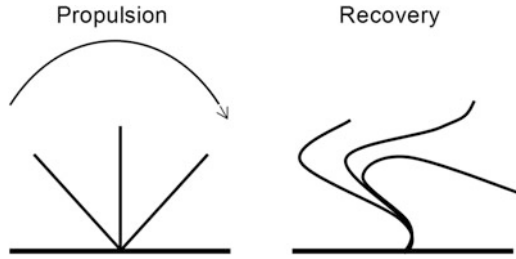
Muscular Hydrostats (Fig. 8.4c)

According to Kier and Smith (1985) and Vogel (1988, 2003), muscular hydrostats are cylinders entirely composed of muscle in which the muscle fibres run in various directions, forming self-supported but fundamentally motile systems. Examples in invertebrates are the tentacles and arms of squids or the feet of snails. Like the fluid-based hydroskeletons, muscular hydrostats cannot change their volume, a feature that enables the muscles to antagonize each other without rigid skeletons or internal water compartments. These systems are able to perform an impressive range of motions and alter their stiffness without much shape change. Moreover, since the relationship between the radius R and the length L accounts for $R = 1/\sqrt{L}$ in cylinders of fixed volume, these motions imply the amplification of force and velocity. For example, by decreasing its diameter by only 20%, a squid tentacle can reach a 70% length extension, which is used by these animals for prey-capture (Vogel 2003).

Slide-Lock Mechanisms (Fig. 8.4d)

These mechanisms involve the lengthwise relative sliding of two or more rod-like elements. If the relative sliding movement between the elements is restrained in some way by some structural modifications at the interfaces, then joint-free bending movements result (similar to the principle of a bimetal strip in a thermostat). In interaction with the mechanical resistance of the penetrated medium, the direction and location of the bending deformations depend on (1) the direction of movement of the sliding elements, (2) the actual position and orientation of the blocking elements and (3) the material properties across the length of the rod-like structures. Examples of this mechanism occur in organisms as dissimilar as protists and insects. Many protists and other eukaryotic cells possess cilia and flagella for driving themselves through a fluid medium (e.g. spermatozoa) and / or producing currents for suspension feeding (e.g. collar cells of sponges). Whereas flagella produce sinusoidal motions across their longitudinal axis, cilia remain stiff and extended during their forward stroke and become flexible, bending near their base

Fig. 8.6 Propulsion and recovery stroke of a cilium. During propulsion, its shaft remains stiff, whereas during the recovery stroke, it becomes more flexible and bends at certain locations along its shaft



during the backward stroke (Fig. 8.6) (Biewener 2003). This movement is understandable from the ultrastructure of a cilium / flagellum that, in transverse section, consists of a set of nine doublet microtubules (made of tubulin) surrounding a pair of single microtubules. Each doublet bears a pair of arms made of the motorprotein dynein, whereupon the dynein arms of one doublet and the tubulin of the adjacent doublet ratchet along each other. If this happens on one side only, the cilium bends. During forward movement, the sliding occurs across the entire length of the cilium shaft at the same time, whereas during the more flexible backward movement the sliding is restricted to certain regions of the shaft (cf. Alberts et al. 2014).

Several insects exhibit slide-lock mechanisms, which employ tongue and groove constructions that lack any joints in the direction of bending. Such mechanisms can be found within extended rod-shaped insect mouthparts responsible for piercing and sucking fluids or in the ovipositors used for egg-laying. Since such kind of functional systems are subjects of our current investigations, they are described in more detail in the following.

Mouthparts of blood sucking Triatominae (Hemiptera: Reduviidae): The haematophagous heteropterans belonging to the subfamily of the Triatominae possess piercing mouthparts (a pair of mandibles that flank a pair of maxillae (Fig. 8.7b)). For feeding, the proboscis is folded outward by 90° - 180° and the apex of the labium is pressed against the host's skin (Fig. 8.7a). The serrated mandibles penetrate the superficial layers of the host's skin by alternate movements but remain in this position to act as anchors. During the extension, the thin and bristle-like maxillae converge at the hypopharynx by a complex interlocking system but are still able to be continuously moved back and forth separately in the formed maxillary bundle (Wenk et al. 2010). They are projected forward as a single bundle and penetrate deeply into the tissue by permanent quiver-like movements. They are capable of a considerable degree of bending when searching for a blood vessel (Lavoipierre et al. 1959). The exact mechanisms behind these actively directed movements, however, remain unclear. When an appropriate blood vessel is tapped, the probing movement ceases. Hereafter, the left maxilla retreats (or the right maxilla further protrudes) suddenly, the thorn-like tip splays out and the connection between the two maxillary parts opens, forming the functional mouth opening (Lavoipierre et al. 1959; Wirtz 1987).

Ovipositors of parasitoid wasps (Hymenoptera): The vast majority of hymenopteran species are parasitoids of other insects, such as most members of the mega-diverse superfamilies of the Chalcidoidea and Ichneumonoidea.

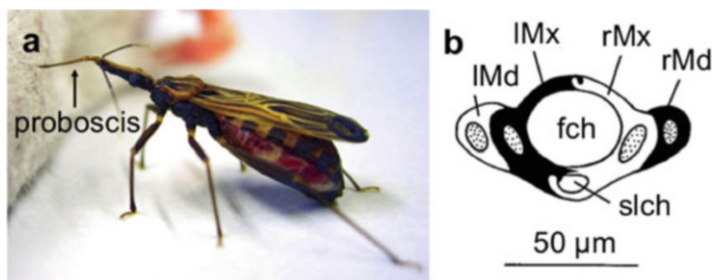


Fig. 8.7 (a) *Rhodnius prolixus* Stål (Reduviidae: Triatominae) feeding on an anaesthetized mouse. The proboscis (labium) is fully extended. (b) Its mandibles and maxillae in transverse section with the dorsally oriented food channel and the ventrally oriented salivary channel. Abbreviations: *fch* maxillary food channel, *IMd* left mandible, *IMx* left maxilla, *rMd* right mandible, *rMx* right maxilla, *slch* maxillary salivary channel. Adapted from Wenk et al. 2010

The ovipositor apparatus of parasitoids can serve several functions: navigating or penetrating the substrate (if the host is concealed), locating, assessing, marking and piercing the host, injecting venom, killing the competitor's eggs and oviposition (Fig. 8.8a), plus defensive stinging and forming a feeding tube (Quicke 2015). The ovipositor shaft (=terebra) consists of an upper valve (=2nd valvula) and a pair of lower valves (=1st valvulae). The upper valve is split into two asymmetric and overlapping halves that are fused at the apex in the Chalcidoidea (Fig. 8.8b), and is also completely divided, except at the apex, in some ophiioniform ichneumonoid taxa (Fig. 8.8d), although it is not divided in the majority of the Ichneumonoidea (Fig. 8.8c) (Oeser 1961; Quicke et al. 1994). The ventral surface of the upper valve interlocks with each of the lower valves by a longitudinal tongue-and-groove mechanism called the olistheter. The sublateral rhachis lies in a groove called the aulax along the dorsal surface of each lower valve. The olistheter mechanism tightly holds the valves together while allowing the three valves to slide independently relative to one another (Oeser 1961; Quicke et al. 1994). Despite the hymenopteran ovipositor completely lacking intrinsic musculature, many parasitoids are capable of actively bending and rotating them in various directions (Quicke et al. 1995; Quicke 2015). The movements of the ovipositor result entirely from the actions of muscles inside the metasoma. Several steering mechanisms have evolved in the various taxa as an adaption for reaching their hosts and permitting far greater control over egg placement. Several taxa have evolved mechanisms involving apposed stops on both the upper and the lower valves. Similar to a bimetal strip in a thermostat, the pushing of one valve beyond the location at which the stops have touched causes the ovipositor to bend. This is attributable to the tight interlocking of the upper and lower valves by the olistheter mechanism. This bending mechanism can be seen in several members of the Braconidae (cf. Fig. 8.8c): some taxa have a strongly swollen short region pre-apically on the rhachis of the upper valve with scale-like sculptures (Macrocentrinae) (Fig. 8.9a–b), others possess ancillary teeth on the lower valves next to the thinned outer wall of the aulax (Doryctinae) (Fig. 8.9c) (Quicke et al. 1995). A second type of ovipositor steering mechanism involves a largely longitudinally divided upper valve that is fused just at the apex (e.g.

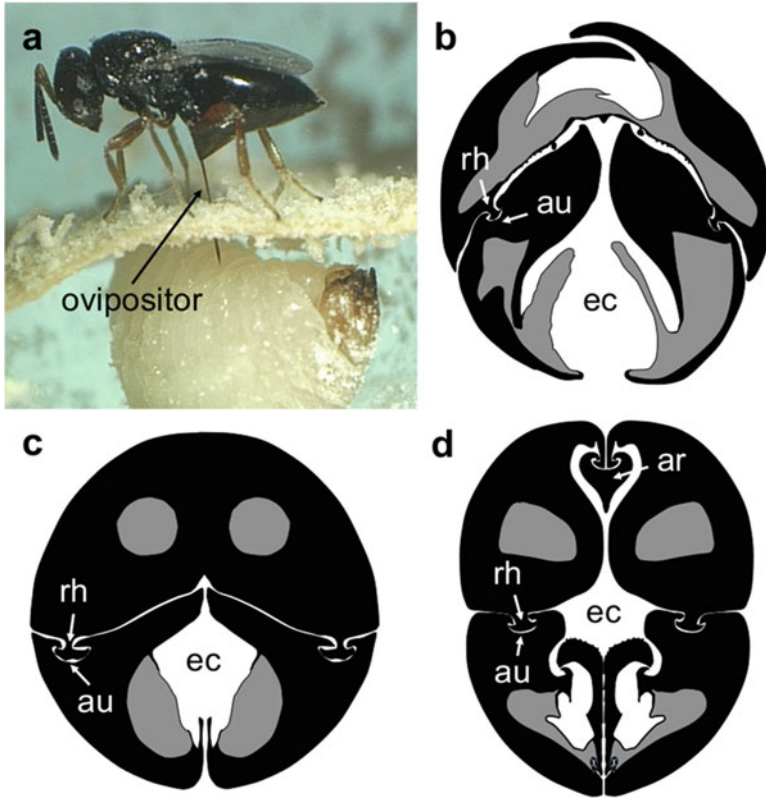


Fig. 8.8 (a) *Lariophagus distinguendus* (Foerster) (Pteromalidae) ovipositing on *Sithophilus granarius* (Linnaeus) (Curculionidae) larva in an artificial film chamber. The upper valve is oriented dorsally and the lower valves ventrally when at rest. (b–d) Diagrams of transverse sections through the medial part of the ovipositors of members of the genera (b) *Plutothrix* Foerster (Pteromalidae), (c) *Spathius* Nees (Braconidae: Doryctinae), (d) *Stethantyx* Townes (Ichneumonidae: Tersilochinae). Abbreviations: *ar* aulaciform rod, *au* aulax, *ec* egg canal, *rh* rhachis. (a) photo courtesy to Collatz et al. 2006, (b–d) provided by Quicke DLJ

in Chalcidoidea (cf. Fig. 8.8b) and several ophioniform Ichneumonidae in which the two parts of the upper valve are linked by the so-called aulaciform rod (cf. Fig. 8.8d)). The pulling of one part of the upper valve will cause the ovipositor to bend to the left or right. These wasps are able to bend their ovipositor both dorso-ventrally and laterally (Quicke 2015).¹

¹Another steering mechanism involves the formation of the distal part of the ovipositor into multi-arched and noticeably unevenly sclerotized regions: the intermodal arched sections are more heavily sclerotized than the thinner nodes (e.g. in the braconid genus *Zaglyptogastra* Ashmead). Therefore, a ventral protrusion of the lower valves will cause a flattening out of the nodal regions and hence a ventral flexing of the entire apex of the ovipositor (Quicke 1991).

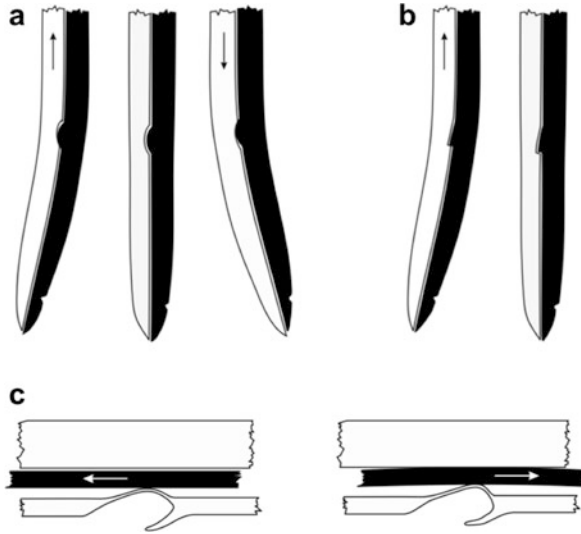


Fig. 8.9 Diagram of the various ovipositor steering mechanisms found in the Braconidae, with the upper ovipositor valve depicted in black. **(a)** System involving the swollen pre-apical part of the rhachis located centrally within a corresponding part of the aulax at rest. Retracting and extending the lower valves will cause a bending of the ovipositor. **(b)** System with a pre-apical scarped butt on the upper valve and a corresponding notch on the lower valve; this permits bending ventrally. **(c)** Flexible construction of the lateral side of the aulax, which is believed to be dragged by the rhachis when the lower valve is retracted, allowing some bending. From Quicke 2015, adapted from Quicke et al. 1995

8.3.3 *Engineering and Architecture: Bio-inspired Mechanical Actuation and Adaptive Stiffness*

Commercially available actuators include electric or fluidic actuators that operate by means of pneumatic or hydraulic pressure. Moreover, novel actuators based on so-called smart materials have been developed. Examples for these materials are shape memory alloys (SMAs), shape memory polymers (SMPs) or electro- and magnetostrictive materials such as piezoelectric materials (Ham et al. 2009). Commercially bio-inspired actuators are rather rare. One of the few commercially available ones are pneumatic muscles and the Bionic Handling Assistant by Festo AG & Co. KG.

Recent advances in technology have led to many bio-inspired actuators in which knowledge gain from active biological systems has been transferred to energy-driven mechanical actuation, including electrospun climbing fibres and contractile polymers (Erb et al. 2013). Additionally, technical systems that take advantage of changes in mechanical behaviour, e.g. by changes in elasticity (Qin et al. 2012), in strength and toughness (Espinosa et al. 2011), or in stimuli responsiveness (Capadona et al. 2008) have also been inspired by biological role models (Egan

et al. 2015). Rod-shaped adaptive actuators are commonly constructed as monolithic structures from compliant materials such as SMAs (Laschi et al. 2009), elastomers (Ilievski et al. 2011), electroactive polymers (Shi et al. 2012), hydrogels (Otake et al. 2002) or composites that undergo a solid-state phase transition (Brown et al. 2010). Actuation can be achieved by various mechanisms, including electrical charges in SMAs (Lin et al. 2011), piezoelectric drivers (Oldham et al. 2007) or micro motors (Yeom and Oh 2009), chemical reactions (Shepherd et al. 2013) and pressurized fluids (Roche et al. 2014; Polygerinos et al. 2015).

In particular, pressure-driven pneumatic- and hydraulic-powered flexible actuators are promising candidates for technical applications because of their high power-to-weight ratio, low material cost and “simple” fabrication process (Polygerinos et al. 2015). The widely used pneumatic artificial muscle actuators (for example, McKibben actuators) are compliant linear soft actuators consisting of elastomer tubes in fibre sleeves, inspired by the hydrostatic skeleton of worms (cf. Sect. 8.3.2). With pressurization, chambers embedded in the soft actuator expand in the directions associated with lower stiffness allowing extending or contracting motions (Tondu and Lopez 2000), bending (Ilievski et al. 2011) or twisting (Sun et al. 2013).

A plant-inspired bending actuation mechanism is based on the reversible adsorption and desorption of environmental humidity (Mazzolai et al. 2014). The combination of active and passive actuation by using a bilayer composite of an active water-absorbing polymer and a passive elastomeric layer allows humidity-dependent bending movements. An animal-inspired bending actuation mechanism has been, for example, adapted from ovipositing wasps, enabling a steering mechanism to be built for a multi-part probe that can undertake minimally invasive percutaneous interventions (e.g. Ko and Baena 2012) involving complex movements. As the probe is inserted into a compliant material, the bio-inspired bending mechanism of the device is influenced by the mechanical tissue-probe interactions and the interaction between the different parts of the probe.

However, most of the examples mentioned above are demonstrators as part of ongoing research.

8.3.3.1 Bending Actuators

The application of hinge-less actuators is often limited to small-scale applications in robotics or medical engineering in which only low forces occur. Research on large-scale applications is carried out in the field of aeronautics, e.g. morphing wings for airplanes (Sofla et al. 2010), or in maritime research, e.g. on fins for marine robots. So far, the principles for a joint-free actuator or for an adaptive stiffness have not been transferred to an architectural scale involving high external forces such as wind and snow. The compliant mechanism of the flectofin, a facade-shading system inspired by the opening mechanism of the flower of the Bird-of-Paradise (*Strelitzia reginae*) (Lienhard et al. 2011) is actuated and locked by external mechanical actuators. This is an example in which a rod-shaped joint-free actuator can be used

to further reduce mechanical complexity and to achieve continuous adaptability of the system. When looking at achieved compliant systems such as the flectofin or the flectofold, we see that the bending of a stiff middle rib is the fundamental driving mechanism. Based on this, the focus of our project will be the development of a bending actuator. Bending describes the behaviour of a structural element subjected to an external load applied perpendicularly to a longitudinal axis of the body. The basic mechanism of bending is the extension of one side with respect to the other. This elongation or shortening can be triggered, for example, by the different thermal expansion of two materials such as in bilayers, SMAs or piezoelectric materials responsible for an elongation or shortening in a defined area of an actuator. Furthermore, fluids can be used to engender an extension. Several possible methods that create a bending motion in fluidic actuators exist. Usually, they require the use of extensible materials that can be elongated by fluid pressure. Limiting this elongation in different parts of the rod-shaped structure enables different actuation movements. Another possibility for creating a bending motion is the construction of an asymmetric inner structure of the actuator. For example, if pressure is applied at locations other than the centroid of the cross section of the structure, a bending motion is generated (Drimer et al. 2016). According to this principle, pneumatic cushions or elongating bellows built from a strong inextensible material can also be integrated into an actuation system. Here, the elongation is based on a shape change. By the arrangement of multiple off-centre elongations within the cross section of an actuator and by their separation in the longitudinal direction, complex motions can be generated. This is the case in several so-called continuous backbone robot manipulators, which are inspired by trunks or tentacles (Walker 2013). A bending actuator can also be built from two separate parts, e.g. with a spring-groove connection. If the two parts are fixed together at one end, a relative motion of the two parts can create the same effect as the elongation or shortening of one side. This principle is also found in biology and has been described for the ovipositors of parasitoid wasps or the feeding apparatus of assassin bugs (cf. Sect. 8.3.2).

8.3.3.2 Adaptive Stiffness

The stiffness of a system depends in general on the material and its geometry. These factors can be controlled in order to vary the stiffness. Adaptively changing the inherent stiffness by a change in material or by control strategies is an active field of research. Variability can be achieved, as for actuators, in many different ways. Compliant actuators in robotics, for example, exploit the possibility of changing their stiffness to allow safe human-machine-interaction. This is achieved through various control strategies: equilibrium-controlled, antagonistic-controlled, structure-controlled and mechanically-controlled strategies (Ham et al. 2009).

Especially in the context of morphing applications, materials of variable stiffness and various structural concepts have been studied. Some examples are the use of shape-memory materials, plant-inspired fluidic flexible matrix composites that derive their tuneable stiffness from the controlled pressurization levels of composite

tubes embedded in a flexible matrix or pneumatic honeycomb structures in which the honeycomb cells are pressurized (Kuder et al. 2013). Materials also change their stiffness because of moisture or temperature changes leading, for example, to glass transition (Saavedra Flores et al. 2013) or phase changes (Schubert and Floreano 2013). The non-linear behaviour of materials can be used to create an adaptable stiffness through pre-tensioning. Based on this principle, a variable stiffness system has been developed inspired by the vertebral column. By compressing the elastic parts of a system consisting of bonded rigid and compliant segments arranged in an alternating way, one can increase the stiffness of the system (Huh et al. 2012). Furthermore, possibilities involving the variation of the moment of inertia by rotating a beam with a rectangular cross section around its axis or by increasing the effective thickness of a system by pressing multi-layered structures together, for example with the help of electrostatic forces or by means of establishing a vacuum, have previously been explored (Ham et al. 2009; Drimer et al. 2016).

8.4 Interdisciplinary Working Program

In this chapter, we exemplify how the collaboration between biologists and engineers is structured in the current project and how this will finally result in a demonstrator that combines major functional principles extracted from the biological role models.

8.4.1 Data Acquisition in the Biological Role Models

Within studies on the selected plant model *Gerbera jamesonii* ‘Nuance’, the water-dependent adaptive behaviour of the pedicels, which have access to more or to less water, are being investigated by using mechanical tests, e.g. three-point-bending tests for studying elastic properties such as the bending elastic modulus and for analysing visco-elastic properties such as the degree of elasticity or energy dissipation (Fig. 8.10).

In addition, morphological-anatomical studies are being carried out for every pedicel. From each pedicel, the corresponding relative water content (RWC) is determined in order to obtain evidence as to the way that the plant water status and the turgor pressure of the parenchyma cells associated therewith (Eastmond and Ross 1997) influence the mechanical properties. Because the mechanical properties also depend significantly on the degree of lignification of the pedicels, samples will be categorized in various age groups on the basis of their anatomical characteristics.

Morphological-anatomical studies of investigated pedicel samples ($n = 8$) reveal, to date, an almost perfect circular cross section (diameter 6.41 ± 0.75 mm, aspect ratio 0.99 ± 0.04), a total length of 45 cm, a varied pronounced taper (tapering mode 0.58 ± 0.18) along the later 3-point-bending-tested length of 280 mm (starting

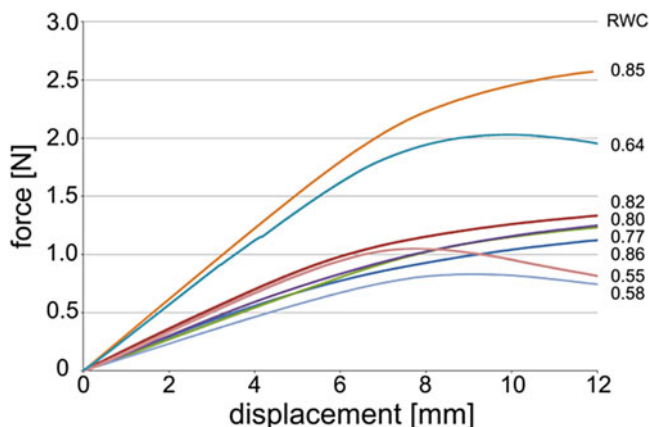


Fig. 8.10 Force-displacement diagram showing elastic behaviour measured during the three-point-bending test. Samples are pedicels of *Gerbera jamesonii* 'Nuance', which have different relative water contents (RWC). The relative water content can take values between 0 to 1, with 0 standing for a fully desiccated or dried plant organ and 1 for a fully hydrated or fully turgescient plant organ

5 cm below the inflorescence) and a density of approximately 0.909 g/cm^3 . Hand-sections show a centripetal arrangement of four tissue layers: (1) an outer epidermis, (2) a peripheral cortex parenchyma with unligified small cells, (3) a closed ring of lignified tissue (vascular bundles and sclerenchyma) and (4) an inner ring of unligified parenchyma with larger cells than the cells of the cortex. The middle part of the pedicel often contains an irregularly shaped pith (Fig. 8.3i).

Video analyses show the water-dependent adaptive behaviour of the pedicels in detail. After the water supply is stopped, the plant wilts within a few days and the pedicels bend close to the flower. In this bending area, the flower stalks show pronounced ovalization events. After being re-watered, the stalks return totally to their original position within the time span of one day. This reversible mechanism and the comparison of the wilting phase relative to the rapid turgidity process are even more interesting, because, in addition to the weight of the pedicel, the weight of the flower head has to be elevated.

In zoology, it is necessary to combine morphological techniques at various scales from gross morphology to ultrastructural details in order to visualize and reconstruct the arthropod morphology under study in our project.

A wide range of histological and histochemical methods are available for the fixation and embedding of biological samples in order to make them processable for serial sectioning by ultramicrotomy. Histologically stained semithin sections (thickness of 500–1500 nm) provide information about the various types of tissue by light microscopic methods (LM, resolution of about 300 nm). Ultrathin sections (thickness of 50–60 nm), stained with uranyl acetate and lead citrate, provide information about the microstructure and chitin fibre directions under the transmission

electron microscope (TEM, resolution of about 1 nm). Finally, all data of the section series are aligned and stacked by specialized 3D reconstruction software that also permits segmentation and 3D modelling. Fluorescence microscopy and confocal laser microscopy (CLSM) of both dissected samples and unstained semithin sections reveal differences in material composition, for example, by taking advantage of the cuticular autofluorescence of arthropod exoskeletons (Donoughe et al. 2011; Michels and Gorb 2012). In addition, scanning electron microscopy (SEM) allows the surface of dried specimens / samples to be viewed at a very high resolution (about 5 nm). Synchrotron X-ray microtomography (SR- μ CT) is a non-invasive technique used to obtain complete sequences of virtual sections and can be applied in addition to classical histological serial sectioning. The tomographic dataset, consisting of voxels, is then visualized by using specialized volume graphics software that allows the 3D object to be sliced along any arbitrary axis (Betz et al. 2007).

A detailed analysis of both the functional morphology and the possible movements *in vivo* are necessary for the investigation of the underlying movement principles and biomechanics of a biological structure under study. Therefore, the quantification of the movements in the living animal is achieved by behavioural recordings with a high-speed video camera with movement tracking software.

All these techniques can be implemented in a detailed computational model.

8.4.2 Two-Step Modelling Approach for Translation from Biology to Architecture

The main purpose of biomimetic research is to solve technical problems by searching for solutions in biological organisms and transferring these into engineering applications. Thereby, a one-to-one reconstruction of the biological role model will not help to achieve a robust solution for technical or architectural applications. Abstractions are needed. To identify the key characteristics and the key underlying principles of the biological role model, a rigorous computational analysis is essential. For example, in order to gain deeper insights into the response of the biological and bio-inspired systems and, hence, to be able efficiently to design specific actuators, many different scenarios should be explored by employing FE simulations.

In living nature, small-scale features often influence large-scale features and, hence, cannot be ignored within FE models. However, because of the differences in scale (sometimes by several orders of magnitude), models resolving highly detailed small-scale features are often, from a computational point of view, not feasible. To achieve this translation, two-scale modelling approaches have been investigated (Table 8.2). Essentially, the two-scale modelling approaches can be categorized into two steps. First, precise micro-scale simulations are carried out to investigate the micro-scale features of the biological role models and to elucidate relevant biological mechanisms from experimental data. In a second simulation step,

Table 8.2 Differences between the detailed biomechanical finite element (FE) simulation and the reduced applied FE simulation

Detailed biomechanical FE simulation		Reduced applied FE simulation
Detailed morphology of biological role model	Geometry	Abstracted geometry
Experimental data & sensitivity analysis with respect to range of possible material parameters	Material properties	Well known technical materials; chosen to match technical requirements most closely
Scale of biological role model	Scale	Upscaling to desired technical application; independent of biological role model
Quantitative analysis of biological role model to analyse functional morphology	Aim	Simulation & analysis of functional principles for translation into technical applications

which aims to achieve the translation to architectural applications, an abstraction of the discovered key features is performed and the principles identified in the first simulations of biological actuation will be up-scaled to a technical actuation application.

By using computational models for investigating functional-morphological aspects of the selected biological concept generators, they can be distinguished into (1) geometrical aspects, (2) material modelling aspects and (3) homogenization techniques providing the link between detailed sub-models and the overall structure. This applies likewise for the use of computational models in order to understand and to abstract further the basic principles originating from plants or animals as biological concept generators. The challenge hereby is to construct models that exhibit the key features on the respective scale, while keeping the amount of data necessary for the respective computational model at a feasible level.

Most imaging techniques, such as light and electron microscopy, create 2D images, whereas micro-computed tomography (μ CT) permits the direct 3D representation of the geometry of the micro-structure. For the computational models of the insect, a geometric image-based modelling approach is used based on high-resolution Synchrotron- μ CT image data. Linking additional information from various 2D imaging techniques, such as high resolution microscopic images of the interlocking mechanism of maxillary or ovipositor parts, or complementary structural information, such as the arrangement of different composites, enables detailed information to be extracted from the biological sample. The behaviour of a bending movement, for example, can be captured in a realistic manner, while providing details about stress concentration points and generated strains. For plants, the computational models are based on 2D geometrical data derived from histological studies and mechanical properties of entire plant organs and single tissues.

Because of the complexity of the experimental data, a fully detailed small-scale model representing, for example, all the geometrical details of the interlocking phenomena between two mouthpart elements or the use of the developed detailed

structural model for simulating the fibre-reinforced (micro) mechanical structure and function for an entire plant is unrealistic. Both the small-scale plant and animal models are employed to analyse and predict large-scale behaviour. Natural actuator systems are based on material systems with wide variability controlled by several parameters, such as the degree of crosslinking of the matrix or the variety of possible fibre arrangements of the chitin (arthropods) and cellulose fibres (plants) within the hierarchical structure of these composites (Fratzl and Barth 2009). Therefore, it is nearly impossible to distinguish between material and structure in these biological systems.

To identify the key features for the macro-scale, a sensitivity analysis with respect to the material parameters has to be carried out. Most likely, additional experimental measurements are necessary to verify constitutive laws qualitatively for the overall structures. This approach of using the output of simulations for the design of future experimental studies will also significantly increase the understanding of the biological concept generators (reverse biomimetics). In a second step, the identified underlying principles are verified by further reducing the FE model and focusing on the functional aspects of the biological role models. Therefore, abstracted large-scale FE models are developed. In these models, the geometry and the overall complexity has to be reduced to the necessary level. The material properties can be changed to support the underlying functional principles based on the range of available technical materials. The reduced large-scale FE models can be used for simulation-based analyses exploring the design variables and the potential of the system. To transfer and adapt the structures, material behaviour and methodologies to bio-inspired technical structures, the geometry model and the material parameters need to be scaled up and adapted to applications in building constructions in a further step. The reduced FE model will reveal the underlying principles of the biological role models and will contribute to a deeper understanding of the biological mechanisms and, at the same time, provide a proof-of-concept for technical transferability. As a final step in the development of a novel biomimetic actuator, functional demonstrators will show the feasibility of the developed system for large-scale applications. The development of a common demonstrator also allows the combination of different functional principles from several biological role models. The combination of principles found in plants and animals might lead to completely new bio-inspired technical solutions.

8.5 Multidisciplinary Functional Principles and Their Biomimetic Potential

The guidelines of the present biomimetic top-down approach, conducted in the framework of an interdisciplinary project, involve the bio-inspired application of linear (rod-like) elements in complex architectural solutions showing hinge-less kinematics driven by systemic and continuous actuation mechanisms and exhibiting adaptive stiffness (Fig. 8.11).

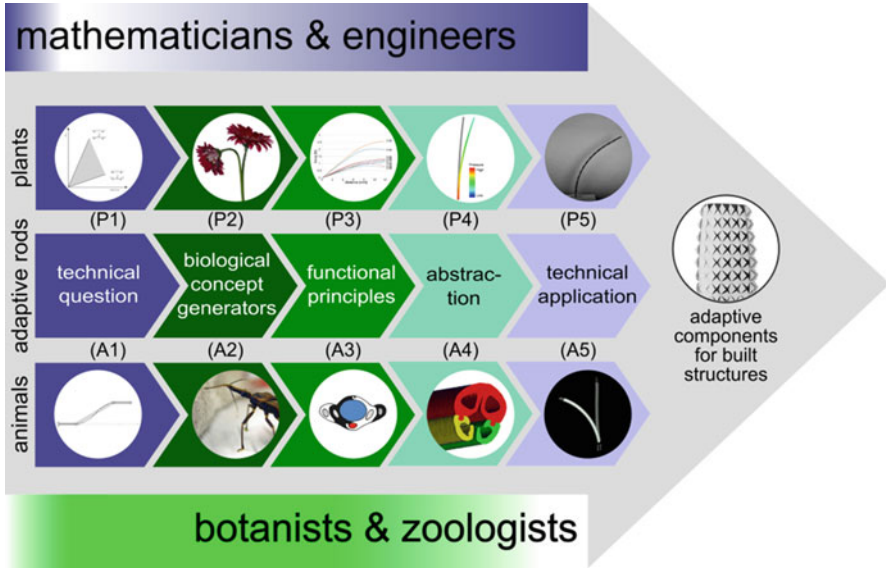


Fig. 8.11 Biomimetic top-down approach (technology pull process) of adaptive components for built structures. The technical challenge is to develop structures with adaptive stiffness and continuous hinge-less kinematics (P1 + A1). Biological concept generators are (P2) herbaceous plants and (A2) mouthparts and ovipositors of insects. The underlying functional principles found in plants (P3) and animals (A3) will be translated into computational models (P4 + A4). The first technical applications (P5 + A5) are feasibility studies for the subsequent demonstrator in which the functional principles from plant and animals will be combined

8.5.1 *Extraction of the General Principles That Are of Technical Relevance*

Most interestingly, in both plants and animals, similar principles and mechanisms are often deployed to consolidate both adaptive stiffness and joint-free continuous kinematics. From the biomimetic point of view, this largely facilitates the implementation of technical applications that concomitantly serve both of these functions. Many principles involve hydrostats that act against tension-resisting fibre-reinforced walls and thus encompass both movement and the possibility of adapting the stiffness to the current demands.

Both plants and animals exhibit examples of a pressure-dependent variable stiffness, whereby pressure is needed to maintain the stiffness of the system by pre-stressing the material or ensuring the transfer of stresses from one part to another. This principle can be transferred into a technical rod-like structure with integrated pneumatic cushions. The pressure of these cushions will be controlled

and thereby allow different modes of operation. Pneumatic cushions are also a promising possibility for creating the actuation. This principle is also used by motor cells such as the bulliform cells that are responsible for the folding of grass leaves in response to drought conditions (cf. Fig. 8.1). The special shape of these cells and their groupwise arrangement and distribution over the cross section of the leaf might provide interesting insights into joint-free actuation with locally defined actuation areas. Discrete pneumatic actuators adapted from these cells can be integrated into fibre-reinforced composites. Fibre-reinforced composites are especially suitable for technical transfer as they allow the local adaptation of the mechanical properties. Thus, we can also learn, from the arrangement of elastic fibres in the insect cuticle and the special placement pattern of highly elastic resilin in the mouthparts or the ovipositors of insects, the way to control or limit deformation to locally defined areas. Furthermore, the prevention of material failure in highly stressed areas can be transferred to a technical application. The mouthparts and ovipositors of insects further show the way in which forces can be transferred between several parts by interlocking structures. The abstraction of these structures to a system that owns its variable stiffness to interlocking structures and, thus, the maintenance of a high stiffness independently of a certain pressure level in the system represents another interesting approach worth further exploration for its technical potentials. The principle of allowing the relative motion of two parts in order to create a bending motion might also be exploited. The potential of principles revealed in plants and animals for achieving a joint-free movement and an adaptive stiffness will be analysed carefully, compared and combined in the best suitable way in order to create a system matching the requirements for an application in load-bearing systems.

8.5.2 Biomimetic Potential from the Perspective of Natural Scientists, Engineers and Architects

With a focus on technical applications, our main interest is that adaptive stiffness, active actuation and joint-like movements of rod-shaped biological structures are not achieved in terms of single components but as a combination of multifunctional structures. Insights revealed in this context might lead to novel kinematic building envelopes and to a feasibility study of the way that markedly different methodologies based on various biological concept generators can be combined into an efficient and novel bio-inspired technical system. During the implementation of the functional principles discovered from biological solutions into biomimetic products (biomimetics), new findings will arise that, in turn, contribute to a deeper understanding of the functioning of the biological samples (reverse biomimetics).

8.6 Outlook

The long-term perspective of this project is to learn from biological systems in order to develop technical systems of higher complexity levels, i.e. multifunctional elements that autonomously adapt both their shape and stiffness according to changing environmental conditions such as temperature, humidity or wind load. This will provide the technical basis for highly efficient building structures and envelopes.

Acknowledgements This work has been funded by the German Research Foundation (DFG) as part of the Transregional Collaborative Research Centre (SFB/Transregio) 141 ‘Biological Design and Integrative Structures’/ project A03 ‘Inspired by plants and animals: actively actuated rod-shaped structures exhibiting adaptive stiffness and joint-free continuous kinematics’. We thank Heike Betz for drawing Fig. 8.4 and for proof reading.

References

- Alberts B, Johnson A, Lewis J, Morgan D, Raff M, Roberts K, Walter P (2014) Molecular biology of the cell. Garland Publishing, New York
- Alexander RMN (1983) Animal mechanics. Blackwell Publishing, Oxford
- Alexander RMN (2003) Principles of animal locomotion. Princeton University Press, Princeton
- Barnes RSK, Calow P, Olive PJW, Golding DW, Spicer JI (2002) The invertebrates. A synthesis. Blackwell Publishing, Malden
- Betz O, Wegst U, Weide D, Heethof M, Helfen L, Lee W-K, Clothen P (2007) Imaging applications of synchrotron X-ray phase-contrast microtomography in biological morphology and biomaterials science. I. General aspects of the technique and its advantages in the analysis of millimetre-sized arthropod structure. *J Microsc* 227:51–71. doi:[10.1111/j.1365-2818.2007.01785.x](https://doi.org/10.1111/j.1365-2818.2007.01785.x)
- Biewener AA (2003) Animal locomotion. Oxford University Press, Oxford
- Brown E, Rodenberg N, Amend J, Mozeika A, Steltz E, Zakin MR, Lipson H, Jaeger HM (2010) Universal robotic gripper based on the jamming of granular material. *Proc Natl Acad Sci USA* 107(44):18809–18814. doi:[10.1073/pnas.1003250107](https://doi.org/10.1073/pnas.1003250107)
- Brun Y, Di Marzo SG, Gacek C, Giese H, Kienle H, Litoiu M, Müller H, Pezzè M, Shaw M (2009) Engineering self-adaptive systems through feedback loops. In: Cheng BHC, de Lemos R, Giese H, Inverardi P, Magee J (eds) Software engineering for self-adaptive systems. Springer, Berlin/Heidelberg, pp 48–70
- Caliaro M, Flues F, Speck T, Speck O (2013a) Novel method for measuring tissue pressure in herbaceous plants. *Int J Plant Sci* 174(2):161–170. doi:[10.1086/668791](https://doi.org/10.1086/668791)
- Caliaro M, Schmich F, Speck T, Speck O (2013b) Effect of drought stress on bending stiffness in petioles of *Caladium bicolor* (Araceae). *Am J Bot* 100(11):2141–2148. doi:[10.3732/ajb.1300158](https://doi.org/10.3732/ajb.1300158)
- Capadona JR, Shanmuganathan K, Tyler DJ, Rowan SJ, Weder C (2008) Stimuli-responsive polymer nanocomposites inspired by the sea cucumber dermis. *Science* 319(5868):1370–1374. doi:[10.1126/science.1153307](https://doi.org/10.1126/science.1153307)
- Clark RB (1964) Dynamics in metazoan evolution. The origin of the coelom and segments. Clarendon, Oxford
- Collatz J, Steidle JJM, Wyss U (2006) Der Kornkäfer und sein natürlicher Feind *Lariophagus distinguendus*. Entofilm, Kiel

- Donoughe S, Crall JD, Merz RA, Combes SA (2011) Resilin in dragonfly and damselfly wings and its implications for wing flexibility. *J Morph* 272:1409–1421. doi:[10.1002/jmor.10992](https://doi.org/10.1002/jmor.10992)
- Drimer N, Mendelson N, Peleg A (2016) A new type of hydraulic muscle. *Actuators* 5(3):1–12
- Dumais J, Forterre Y (2012) “Vegetable dynamics”: the role of water in plant movements. *Annu Rev Fluid Mech* 44:453–478. doi:[10.1146/annurev-fluid-120710-101200](https://doi.org/10.1146/annurev-fluid-120710-101200)
- Eastmond PJ, Ross JD (1997) Evidence that the induction of crassulacean acid metabolism by water stress in *Mesembryanthemum crystallinum* (L.) involves root signalling. *Plant Cell Environ* 20:1559–1565
- Egan P, Sinko R, LeDuc PR, Keten S (2015) The role of mechanics in biological and bio-inspired systems. *Nat Commun* 6:7418. doi:[10.1038/ncomms8418](https://doi.org/10.1038/ncomms8418)
- Erb RM, Sander JS, Grisch R, Studart AR (2013) Self-shaping composites with programmable bioinspired microstructures. *Nat Commun* 4:1712. doi:[10.1038/ncomms2666](https://doi.org/10.1038/ncomms2666)
- Espinosa HD, Juster AL, Latourte FJ, Loh OY, Gregoire D, Zavattieri PD, Zavattieri PD (2011) Tablet-level origin of toughening in abalone shells and translation to synthetic composite materials. *Nat Commun* 2:173. doi:[10.1038/ncomms1172](https://doi.org/10.1038/ncomms1172)
- Fratzl P, Barth FG (2009) Biomaterial systems for mechanosensing and actuation. *Nature* 462:442–448. doi:[10.1038/nature08603](https://doi.org/10.1038/nature08603)
- Fratzl P, Weinkamer R (2007) Nature’s hierarchical materials. *Prog Mater Sci* 52:1263–1334. doi:[10.1016/j.pmatsci.2007.06.001](https://doi.org/10.1016/j.pmatsci.2007.06.001)
- Gibson LJ (2012) The hierarchical structure and mechanics of plant materials. *J R Soc Interface*, rsif20120341. doi:[10.1098/rsif.2012.0341](https://doi.org/10.1098/rsif.2012.0341)
- Gray J (1968) *Animal locomotion*. Weidenfeld and Nicolson, London
- Ham R, Sugar TG, Vanderborght B, Hollander KW, Lefeber D (2009) Compliant actuator designs. *IEEE J Robot Autom* 16(3):81–94
- Harrington MJ, Razghandi K, Ditsch F, Guiducci L, Rueggeberg M, Dunlop JWC, Fratzl P, Neinhuis C, Burgert I (2011) Origami-like unfolding of hydro-actuated ice plant seed capsules. *Nat Commun* 2:337–343. doi:[10.1038/ncomms1336](https://doi.org/10.1038/ncomms1336)
- Huh TM, Park Y, Cho K (2012) Design and analysis of a stiffness adjustable structure using an endoskeleton. *Int J Precis Eng Man* 13(7):1255–1258. doi:[10.1007/s12541-012-0168-2](https://doi.org/10.1007/s12541-012-0168-2)
- Ilievski F, Mazzeo AD, Shepherd RF, Chen X, Whitesides GM (2011) Soft robotics for chemists. *Angew Chem Int Ed Engl* 50(8):1890–1895. doi:[10.1002/anie.201006464](https://doi.org/10.1002/anie.201006464)
- Kier WM, Smith KK (1985) Tongues, tentacles and trunks: the biomechanics of movement in muscular-hydrostats. *Zool J Linn Soc Lond* 83:307–324
- Ko SY, Baena FR y (2012) Trajectory following for a flexible probe with state/input constraints: an approach based on model predictive control. *Rob Auton Syst* 60(4):509–521
- Kölsch G, Betz O (1998) Ultrastructure and function of the adhesion-capture apparatus of *Stenus* species (Coleoptera, Staphylinidae). *Zoomorphology* 118:263–272
- Kuder IK, Arrieta AF, Raither WE, Ermanni P (2013) Variable stiffness material and structural concepts for morphing applications. *Prog Aerosp Sci* 63:33–55. doi:[10.1016/j.paerosci.2013.07.001](https://doi.org/10.1016/j.paerosci.2013.07.001)
- Laschi C, Mazzolai B, Mattoli V, Cianchetti M, Dario P (2009) Design of a biomimetic robotic octopus arm. *Bioinspir Biomim* 4(1):015006. doi:[10.1088/1748-3182/4/1/015006](https://doi.org/10.1088/1748-3182/4/1/015006)
- Lavoipierre MMJ, Dickerson G, Gordon RM (1959) Studies on the methods of blood-sucking arthropods: I. – The manner in which Triatominae bugs obtain their blood-meal, as observed in the tissues of the living rodent, with some remarks on the effects of the bite on human volunteers. *Ann Trop Med Parasitol* 53:235–250
- Lienhard J, Schleicher S, Poppinga S, Masselter T, Milwich M, Speck T, Knippers J (2011) Flectofin: a hingeless flapping mechanism inspired by nature. *Bioinspir Biomim* 6(4):045001. doi:[10.1088/1748-3182/6/4/045001](https://doi.org/10.1088/1748-3182/6/4/045001)
- Lin H, Leisk GG, Trimmer B (2011) GoQBot: a caterpillar-inspired soft-bodied rolling robot. *Bioinspir Biomim* 6(2):026007. doi:[10.1088/1748-3182/6/2/026007](https://doi.org/10.1088/1748-3182/6/2/026007)
- Mazzolai B, Beccai L, Mattoli V (2014) Plants as model in biomimetics and biorobotics: new perspectives. *Front Bioeng Biotechnol* 2:2. doi:[10.3389/fbioe.2014.00002](https://doi.org/10.3389/fbioe.2014.00002)

- Michels J, Gorb SN (2012) Detailed three-dimensional visualization of resilin in the exoskeleton of arthropods using confocal laser scanning microscopy. *J Microsc* 245:1–16. doi:[10.1111/j.1365-2818.2011.03523.x](https://doi.org/10.1111/j.1365-2818.2011.03523.x)
- Niklas KJ, Spatz H-C (2012) *Plant physics*. University of Chicago Press, Chicago
- Oeser R (1961) Vergleichend-morphologische Untersuchungen über den Ovipositor der Hymenopteren. *Mitt Zool Mus Berlin* 37:1–119
- Oldham K, Pulskamp J, Polcawich R, Ranade P, Dubey M (2007) Thin-film piezoelectric actuators for bio-inspired micro-robotic applications. *Integr Ferroelectr* 95:54–65. doi:[10.1080/10584580701756482](https://doi.org/10.1080/10584580701756482)
- Otake M, Kagami Y, Inaba M, Inoue H (2002) Motion design of a starfish-shaped gel robot made of electro-active polymer gel. *Robot Auton Syst* 40(2–3):185–191
- Polygerinos P, Wang Z, Overvelde JTB, Galloway KC, Wood RJ, Bertoldi K, Walsh CJ (2015) Modeling of soft fiber-reinforced bending actuators. *IEEE Trans Robot* 31(3):778–789. doi:[10.1109/TRO.2015.2428504](https://doi.org/10.1109/TRO.2015.2428504)
- Qin G, Hu X, Cebe P, Kaplan DL (2012) Mechanism of resilin elasticity. *Nat Commun* 3:1003. doi:[10.1038/ncomms2004](https://doi.org/10.1038/ncomms2004)
- Quicke DLJ (1991) Ovipositor mechanics of the braconine wasp genus *Zaglyptogastra* and the ichneumonid genus *Pristomerus*. *J Nat Hist* 25:971–977
- Quicke DLJ (2015) *The braconid and ichneumonid parasitoid wasps: biology, systematics, evolution and ecology*. Wiley Blackwell, Chichester
- Quicke DLJ, Fitton MG, Tunstead JR, Ingram SN, Gaitens PV (1994) Ovipositor structure and relationships within the Hymenoptera, with special reference to the Ichneumonoidea. *J Nat Hist* 28:635–682
- Quicke DLJ, Fitton M, Harris J (1995) Ovipositor steering mechanisms in braconid wasps. *J Hymenopt Res* 4:110–120
- Roche ET, Wohlfarth R, Overvelde JTB, Vasilyev NV, Pigula FA, Mooney DJ, Bertoldi K, Walsh CJ (2014) A bioinspired soft actuated material. *Adv Mater Weinheim* 26(8):1200–1206. doi:[10.1002/adma.201304018](https://doi.org/10.1002/adma.201304018)
- Ruppert EE, Fox RS, Barnes RD (2004) *Invertebrate zoology. A functional evolutionary approach*. Brooks/Cole – Thomson, Belmont
- Saavedra Flores EI, Friswell MI, Xia Y (2013) Variable stiffness biological and bio-inspired materials. *J Intel Mat Syst Str* 24(5):529–540. doi:[10.1177/1045389X12461722](https://doi.org/10.1177/1045389X12461722)
- Schubert BE, Floreano D (2013) Variable stiffness material based on rigid low-melting-point-alloy microstructures embedded in soft poly(dimethylsiloxane) (PDMS). *RSC Adv* 3(46):24671–24679. doi:[10.1039/c3ra44412k](https://doi.org/10.1039/c3ra44412k)
- Shepherd RF, Stokes AA, Freake J, Barber J, Snyder PW, Mazzeo AD, Cademartiri L, Morin SA, Whitesides GM (2013) Using explosions to power a soft robot. *Angew Chem Int Ed Engl* 52(10):2892–2896. doi:[10.1002/anie.201209540](https://doi.org/10.1002/anie.201209540)
- Shi L, Guo S, Li M, Mao S, Xiao N, Gao B, Song Z, Asaka K (2012) A novel soft biomimetic microrobot with two motion attitudes. *Sensors* 12(12):16732–16758. doi:[10.3390/s121216732](https://doi.org/10.3390/s121216732)
- Skotheim JM, Mahadevan J (2005) Physical limits and design principles for plants and fungal movements. *Science* 30:1308–1310. doi:[10.1126/science.1107976](https://doi.org/10.1126/science.1107976)
- Sofla AYN, Meguid SA, Tan KT, Yeo WK (2010) Shape morphing of aircraft wing: status and challenges. *Master Design* 31(3):1284–1292. doi:[10.1016/j.matdes.2009.09.011](https://doi.org/10.1016/j.matdes.2009.09.011)
- Sun Y, Song Y, Paik J (2013) Characterization of silicone rubber based soft pneumatic actuator. *Proc IEEE/RSJ Int Conf Intell Robot Syst*, pp 4446–4453
- Tondu B, Lopez P (2000) Modeling and control of McKibben artificial muscle robot actuators. *IEEE Control Syst Mag* 20(2):15–38
- Vincent JFV (2007) Adaptive structures – some biological paradigms. In: Wagg D, Bond I, Weaver P, Friswell M (eds) *Adaptive structures – engineering approach*. Wiley, Chichester, pp 261–286
- Vogel S (1988) *Life's devices. The physical world of animals and plants*. Princeton University Press, Princeton
- Vogel S (2003) *Comparative biomechanics. Life's physical world*. Princeton University Press, Princeton

- Wainwright SA, Biggs WD, Currey JD, Gosline JM (1976) Mechanical design in organisms. Princeton University Press, Princeton
- Walker I (2013) Continuous Backbone “Continuum” Robot Manipulators. ISRN Robotics 2013:1–19
- Wenk P, Lucic S, Betz O (2010) Functional anatomy of the hypopharynx and the salivary pump in the feeding apparatus of the assassin bug *Rhodnius prolixus* (Reduviidae, Heteroptera). Zoomorphology 129:225–234. doi:[10.1007/s00435-010-0115-7](https://doi.org/10.1007/s00435-010-0115-7)
- Wirtz H-P (1987) Eindringen der Mundwerkzeuge von Raubwanzen durch eine Membran (Hemiptera: Reduviidae). Entomol Gener 12(2/3):147–153
- Yeom S, Oh I (2009) A biomimetic jellyfish robot based on ionic polymer metal composite actuators. Smart Mater Struct 18(8):1–10. doi:[10.1088/0964-1726/18/8/085002](https://doi.org/10.1088/0964-1726/18/8/085002)

Publication 9

Betz O., Eggs B., Henn F., Birkhold A. and Röhrle O. (2017). Bewegung ohne Gelenke: (Wie) gehts das? In: Knippers J., Schmid U. and Speck T. (eds.), *Baubionik: Biologie beflügelt Architektur* (pp. 20–29), Stuttgarter Beiträge zur Naturkunde, Serie C, vol. 82. Stuttgart, Germany: Staatliches Museum für Naturkunde Stuttgart und Gesellschaft zur Förderung des Naturkundemuseums in Stuttgart e.V.

(non-peer-reviewed book chapter; companion volume to the special exhibition “Baubionik – Biologie beflügelt Architektur”, Staatliches Museum für Naturkunde Stuttgart, Stuttgart, Germany)

Abstract

Mit der Fähigkeit, sich aktiv zu bewegen, ist bei Einzellern und Tieren die Möglichkeit des freien Ortswechsels verbunden. Das hat viele Vorteile bei der Erschließung von Nahrungsquellen, der Suche nach Sexualpartnern, der Verbreitung von Nachkommen sowie dem Ausweichen vor ungünstigen Umweltbedingungen. Denkt man an die Fortbewegung von Tieren, so kommen einem der schnelle Galopp der Pferde, das geschickte Klettern von Affen oder die gewandten Flugmanöver einer Stubenfliege in den Sinn. Solche Bewegungen setzen Gelenke voraus, wie sie vor allen Dingen bei den Gliederfüßern (Tausendfüßer, Spinnen, Krebse und Insekten) und den Wirbeltieren entwickelt sind. Es geht aber auch ganz anders!

Significance within the present thesis: This book chapter gives an overview of the joint-free movement mechanisms that we can find in animals, *i.e.* amoeboid cell crawling, hydroskeletons, muscular hydrostats and slide-lock mechanisms. Modern methods of the way in which these mechanisms are researched are also presented.

Methods used: high-speed videography, wide-field epifluorescence microscopy (WFM), ultramicrotomy, light microscopy (LM), synchrotron X-ray phase-contrast microtomography (SR- μ CT)

Own contribution: writing and preparing parts of the manuscript and figures; discussing the manuscript

Miscellaneous: The special exhibition “Baubionik – Biologie beflügelt Architektur” of the State Museum of Natural History (SMNS) in Stuttgart, Germany, took place from 19 Oct. 2017 to 6 May 2018. I was involved in the design the exhibition area A03b “Gelenklos glücklich” by preparing the images, video sequences and showpieces and taking care of the live animals during that time. Some images are shown below.

Bewegung ohne Gelenke: (Wie) geht das?

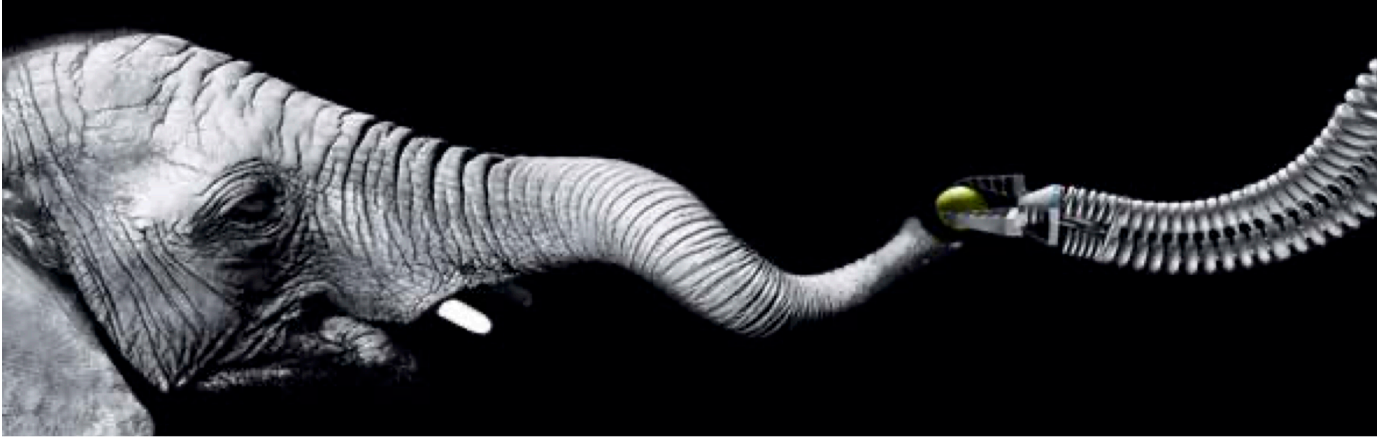
Oliver Betz / Benjamin Eggs / Fabian Henn / Annette Birkhold / Oliver Röhrle

Mit der Fähigkeit, sich aktiv zu bewegen, ist bei Einzellern und Tieren die Möglichkeit des freien Ortswechsels verbunden. Das hat viele Vorteile bei der Erschließung von Nahrungsquellen, der Suche nach Sexualpartnern, der Verbreitung von Nachkommen sowie dem Ausweichen vor ungünstigen Umweltbedingungen. Denkt man an die Fortbewegung von Tieren, so kommen einem der schnelle Galopp der Pferde, das geschickte Klettern von Affen oder die gewandten Flugmanöver einer Stubenfliege in den Sinn. Solche Bewegungen setzen Gelenke voraus, wie sie vor allen Dingen bei den Gliederfüßern (Tausendfüßer, Spinnen, Krebse und Insekten) und den Wirbeltieren entwickelt sind. Es geht aber auch ganz anders!

Unter einem Gelenk verstehen Biologen wie Ingenieure die bewegliche Verbindung zwischen zwei oder mehreren (starrten) Körpern (z.B. Knochen), wodurch deren relative Bewegung zueinander in festgelegten Bahnen vorgegeben wird. Echte Gelenke sind in der Evolution allerdings erst relativ spät entstanden. Am Anfang standen zunächst Bewegungsprinzipien, welche ohne Gelenke funktionierten und dabei eine kontinuierliche Veränderung der Geometrie der beteiligten Strukturen ermöglichten. In den Ingenieurwissenschaften wird dieses Prinzip als „kontinuierliche Kinematik“ bezeichnet. Bei Tieren ist dieses Prinzip weit verbreitet, denken wir nur an die Formveränderungen eines Regenwurms oder die vielfältigen Bewegungen eines Elefantenrüssels [11](#). Solche Systeme können weich und nachgiebig sein, verfügen aber auch häufig über die Fähigkeit, sich an höhere Widerstände anzupassen, indem sie sich, meist durch Muskelkontraktion, mechanisch versteifen. In Verbindung mit den kontinuierlichen Bewegungsformen sind gelenkfreie Mechanismen und Prinzipien für die Ingenieurwissen-

schaften auch deswegen interessant, weil sie im Gegensatz zu den gelenkbasierten Systemen oft einfacher gebaut sind und die darauf beruhenden technischen Systeme über vielfältige Bewegungsmöglichkeiten verfügen, die sich an die jeweiligen Erfordernisse kontinuierlich anpassen lassen.

Das dem Elefantenrüssel zugrundeliegende Prinzip des muskulären Hydrostaten ist nur eines von mehreren Prinzipien der gelenkfreien Bewegung. Unter Hydrostaten werden in der Zoologie inkompressible - mit Flüssigkeit oder Muskulatur gefüllte - Hohlräume verstanden, die infolge von Druckveränderungen Bewegungs- und Steifigkeitsveränderungen herbeiführen können. Auch die menschliche Zunge ist ein solcher muskulärer Hydrostat. Dort führen die Anordnung und Kontraktion einzelner Muskelgruppen zu den vielfältigsten Bewegungen. Elefantenrüssel und Zunge haben beide gemeinsam, dass die Bewegungen oft sehr komplex sind. Sie lassen sich nur sehr schwer in Materialien mit kontrollierbaren und somit funktionellen Eigenschaften in technischen



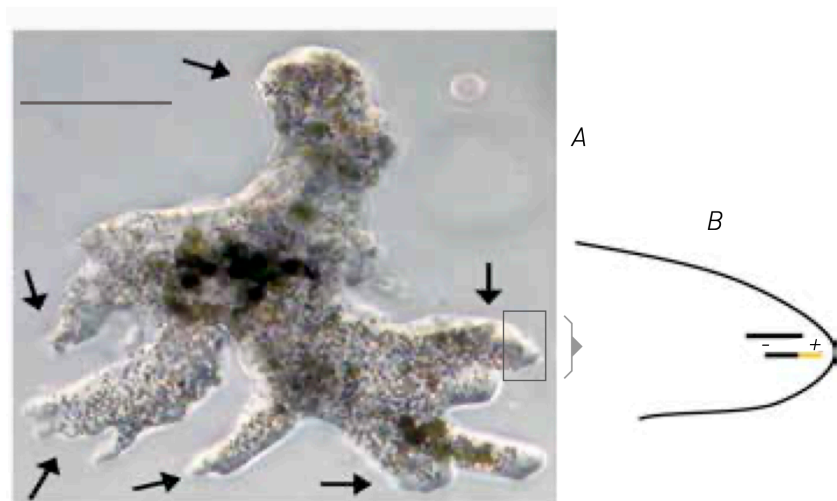
Lösungen überführen. Computersimulationen können dabei helfen, tiefere Einblicke in die Funktionsweisen von Hydrostaten zu erzielen. Der große Vorteil von Computersimulationen ist, dass viele verschiedene Was-Wenn-Simulationen sehr einfach durch die Veränderungen von Eingabeparametern durchgeführt werden können. Allerdings muss man auch anmerken, dass es nicht einfach ist, realitätsnahe Modelle von muskulären Hydrostaten für detaillierte Simulationen zu entwickeln, denn dazu sind genauere Kenntnisse der zugrunde liegenden Prinzipien notwendig. Diese werden im Folgenden etwas genauer vorgestellt. Die meisten gelenkfreien Bewegungen basieren auf Muskelaktivierungen, die Bewegungsmechanismen weisen allerdings häufig passive Strukturen auf. Zunächst soll jedoch ein kurzer Überblick über vier bei Einzellern und Tieren vorkommende Typen von gelenkfreien Bewegungsmechanismen gegeben werden.

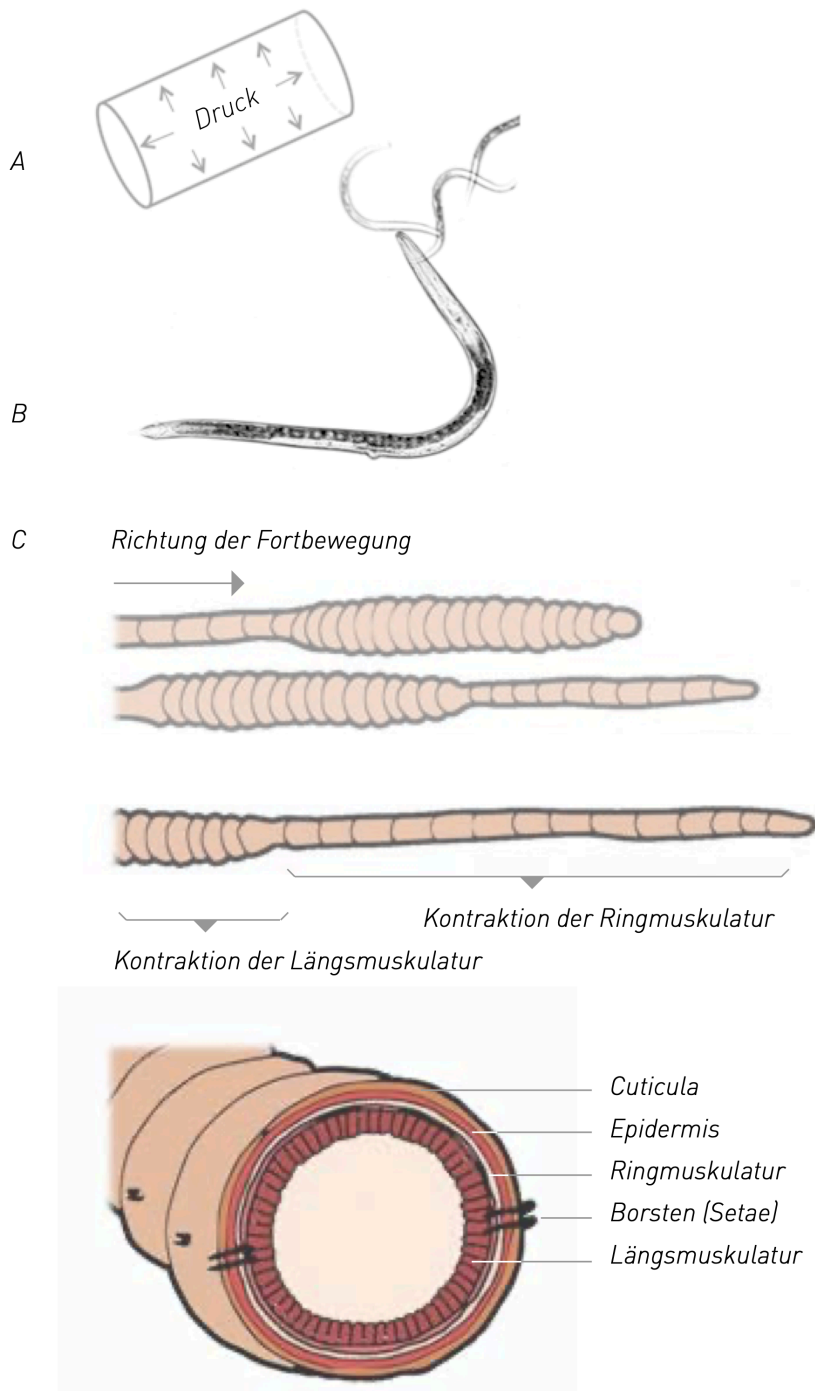
▮11 Der Rüssel des Elefanten ist ein muskulärer Hydrostat. Dieses gelenkfreie Bewegungsprinzip wurde von der Firma FESTO in die Konstruktion eines kontinuierlich beweglichen, technischen Greifarms übersetzt.

1. Amöboide Bewegung

Unter amöboider Bewegung versteht man die kriechend-fließende Fortbewegung, die man bei einer Vielzahl von Zellen findet wie zum Beispiel bei den zu den Einzellern gehörenden Wurzelfüßern (Rhizopoda) ▮A12, aber auch bei menschlichen weißen Blutzellen (Leucozyten). Bei dieser Bewegung produziert die bewegliche Zelle Scheinfüßchen (Pseudopodien), das sind Oberflächenerweiterungen des gelartigen äußeren Zellplasmas. Dieses enthält ein konzentriertes Netzwerk von Eiweißfaser-elementen. Wenn sich diese Filamente unter der Zelloberfläche an ihrer Spitze verlängern und gleichzeitig an ihrer Basis abgebaut werden, bewegt sich die Zelle vorwärts ▮12B.

▮12 (A) Der Wurzelfüßer *Amoeba proteus* bewegt sich mit Hilfe von Scheinfüßchen (Pfeile) fort. Maßlinie: 0,2 mm. (B) Der Vorschub der Scheinfüßchen erfolgt unter permanentem Abbau von Filamenten an ihrem Minus- und nachfolgender Anlagerung (in der Abbildung eingefärbt) an ihrem Plus-Ende.





13 Prinzip und Beispiele von hydrostatisch angetriebenen gelenkfreien Bewegungen. (A) Prinzip des Hautmuskelschlauchs, bei dem die Flüssigkeit der Körperhöhle als Gegendruck zur Körperwand fungiert (adaptive Steifigkeit), gleichzeitig aber auch entlang der Längsachse verlagert werden kann, um Änderungen der Körperform zu ermöglichen. (B) Der Fadenwurm *Pelodera strongyloides* besitzt aus-

schließlich längs verlaufende Muskeln in seiner Körperdecke und ist daher nur zu Schlängelbewegungen befähigt (erwachsenes Weibchen und drei Jungtiere des ersten Larvalstadium). (C) Schema der peristaltischen Bewegung eines Regenwurmes. Wellen von Verkürzungen und Verlängerungen von Körpersegmenten gleiten von vorn nach hinten über den Körper hinweg. Dies ist im Gegensatz zu den in (B)

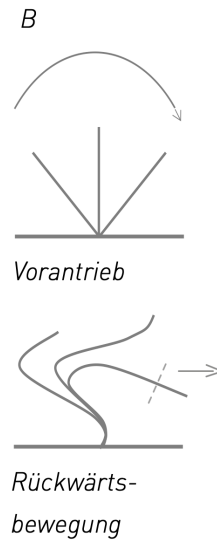
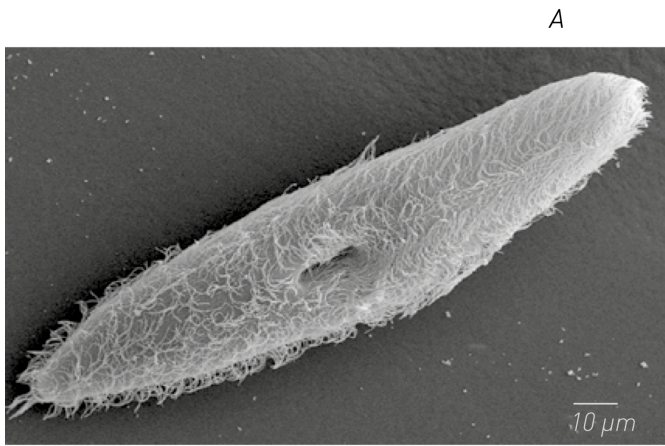
gezeigten Fadenwürmern dadurch möglich, dass die Körperhöhle in viele hintereinanderliegende Kammern (Kompartimente) aufgeteilt ist und sich oberhalb der Schicht von Längsmuskeln auch noch Ringmuskeln in der Körperwand befinden.

2. Bewegungen mittels Hydroskeletten

Wenn Muskeln an der Produktion von Bewegungen beteiligt sind, benötigen sie Gegenlager, normalerweise Skelette. Das müssen keine Knochen sein; Der stammesgeschichtlich älteste Skeletttyp sind die hydrostatischen Skelette. Ihr Prinzip besteht darin, dass eine nach außen begrenzte zug- und druckwiderstehende, faserverstärkte und flüssigkeitsgefüllte Körperhülle unter Druck gesetzt wird. Da die Muskeln in die Körperwand integriert sind, spricht man hier von einem Hautmuskelschlauch. Die Flüssigkeitshöhle kann nicht komprimiert werden. Wird sie durch die in die Körperwand integrierten Muskeln an einer Stelle unter Druck gesetzt, überträgt sich dieser hydraulisch auf andere Körperstellen. Dies verursacht Änderungen der Körperform, die auch zur Fortbewegung genutzt werden können. In der Regel kommen solche Hydroskelette bei wirbellosen Tieren vor, die weiche und nachgiebige Körper besitzen, wie zum Beispiel Regenwürmer. Hier sitzen die für die Bewegung verantwortlichen Muskeln in der Körperwand und das hydrostatische Skelett in Form der flüssigkeitsgefüllten Körperhöhle übernimmt die Rolle des skelettartigen Antagonisten [13](#). Bionische Anwendungen finden beispielsweise Einzug in neue Antriebstechniken, in weiche Roboter oder in Roboterteilen (z.B. Roboterarmen, die eine große Bewegungsfreiheit aufweisen müssen). Sogenannte pneumatische künstliche Muskeln sind aus druckdichten Gewebenetzen bestehende Schläuche. Wird der Innendruck des Schlauchs erhöht, so kontrahiert er. Durch unterschiedliche Anordnung der Gewebenetze können komplexe Verformungen erzielt werden.

3. Muskuläre Hydrostaten

Muskuläre Hydrostaten sind zylinderähnliche Strukturen, die im Inneren vollkommen aus Muskeln (anstatt einer Flüssigkeit) aufgebaut sind, wobei die Muskelfasern in unterschiedlichen Richtungen verlaufen können. Solche Systeme sind selbststabilisierend und dabei vollkommen beweglich. Beispiele hierfür sind unsere Zunge, der Elefantenrüssel [11](#), die Kriechsohlen von Weinbergschnecken oder die Tentakel der Tintenfische. Wie bei den flüssigkeitsbasierten Hydroskeletten (Stichwort: Regenwurm) können auch muskuläre Hydrostaten ihr Volumen nicht verändern. Die Muskeln können deshalb wechselseitig ein Widerlager bilden, ohne dass hierfür ein starres oder flüssigkeitsbasiertes Skelett erforderlich ist. Muskuläre Hydrostaten können eine beeindruckende Vielfalt von Bewegungen ausführen und gleichzeitig ihre Steifigkeit an die mechanischen Erfordernisse anpassen. Dieses Prinzip wird ebenfalls in dem Gebiet der Soft-Robotik angewandt. Hier werden jedoch statt der doch relativ starren Gewebenetze weiche Kunststoffe verwendet, so dass beispielsweise chirurgische Anwendungen im Körperinneren möglich sind. Die Kombination verschiedener Kunststoffe oder verschiedener Wandstärken lassen komplexe Bewegungen (wie etwa die der Tintenfisch-Tentakel) zu, wenn der Schlauch aufgepumpt wird. So soll etwa die „snake“- (Schlangen-) Robotik-Mikrochirurgie es ermöglichen, durch eine kleine Öffnung eine Operation an einer beliebigen Stelle des Herzens durchzuführen.



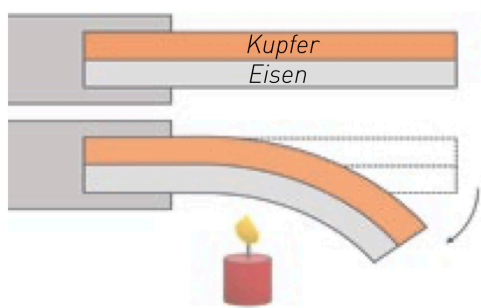
14 (A) Rasterelektronenmikroskopische Aufnahme eines Pantoffeltierchens (*Paramecium*). Die Oberfläche ist dicht mit Cilien besetzt. (B) Vor- und Rücktrieb eines Ciliums. Während der Vorwärtsbewegung bleibt der gesamte Schaft steif. Bei der Rückwärtsbewegung verbiegt er sich an lokalen Stellen geschmeidig.

4. Gleit-Stopp-Mechanismen

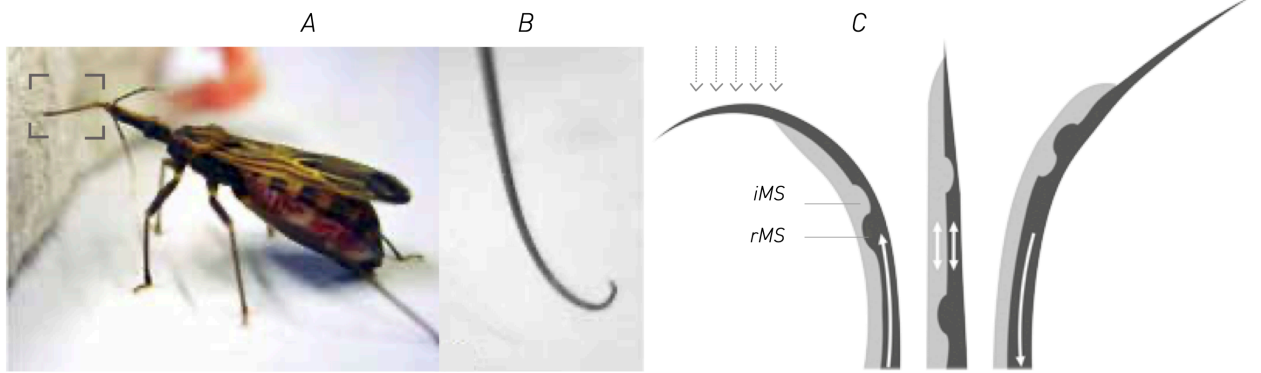
Ein prominentes Beispiel für adaptive gelenkfreie Strukturen sind die Gleit-Stopp-Mechanismen bei Wimpern (Cilien) und Geißeln (Flagellen) **14**. Damit bewegen sich zum Beispiel die einzelligen Pantoffeltierchen souverän durchs Wasser. Diese Art der gelenkfreien Bewegungen gehört zu den ältesten Bewegungsmechanismen überhaupt. Man findet sie bei Einzellern und Mehrzellern (z.B. den Rädertierchen), aber auch bei Samenzellen, die mit ihren Geißeln zur Eizelle schwimmen. Zum Verständnis der Bewegung von Wimpern und Flagellen ist letztlich die Betrachtung ihrer komplexen Feinstruktur in einem Querschnitt erforderlich – was in diesem Rahmen zu weit führt. Einfachere Gleit-Stopp-Mechanismen, die wir untersucht haben, sind die stechend-saugenden Mundwerkzeuge von Wanzen oder die Eilegebohrer von Schlupfwespen und Verwandten. Diese Strukturen verfügen über keinerlei Gelenke und werden über Muskeln im Kopf bzw. Hinterleib gleichsam ferngesteuert. Das in ihnen verwirklichte

Grundprinzip ist letztlich das gleiche wie in den Wimpern und Flagellen.

Bei diesen Systemen sind zwei oder mehrere stabförmige elastische Fasern in Längsrichtung über ein Nut-und-Feder-System miteinander verfalzt. Die Fasern können dabei in Längsrichtung gegeneinander verschoben werden. Wird diese Längsverschiebung jedoch durch eine mechanische Sperre erschwert oder sogar ganz behindert, kommt es – je nach Steifigkeit der Materialien – zu einer relativen Verbiegung beider Fasern ähnlich dem Prinzip eines Bimetalls in der Technik **15**. Bimetalle bestehen aus zwei Schichten unterschiedlicher Metalle, die miteinander verbunden sind. Der Streifen biegt sich bei einer Temperaturänderung. Ursache hierfür ist die unterschiedliche Ausdehnung der beiden Metalle bei veränderter Temperatur. Verwendung finden Bimetalle daher als Thermometer oder Temperaturschalter, etwa zur Steuerung in Wasserkochern.



15 Bimetall-Prinzip. Ein Metallstreifen, der aus zwei Schichten unterschiedlicher Metalle besteht, verformt sich bei einer Temperaturänderung, weil sich die beiden Metalle unterschiedlich stark ausdehnen.



▣ 16 Das Prinzip des Gleit-Stopps nutzen Insekten zur Erzeugung von Biegebewegungen ähnlich dem Mechanismus eines Bimetalls. (A) Die Raubwanze *Rhodnius prolixus* bei der Blutaufnahme an einer anästhesierten Ratte. Die nadelförmig verlängerten Mundwerkzeuge (Rahmen) werden dabei

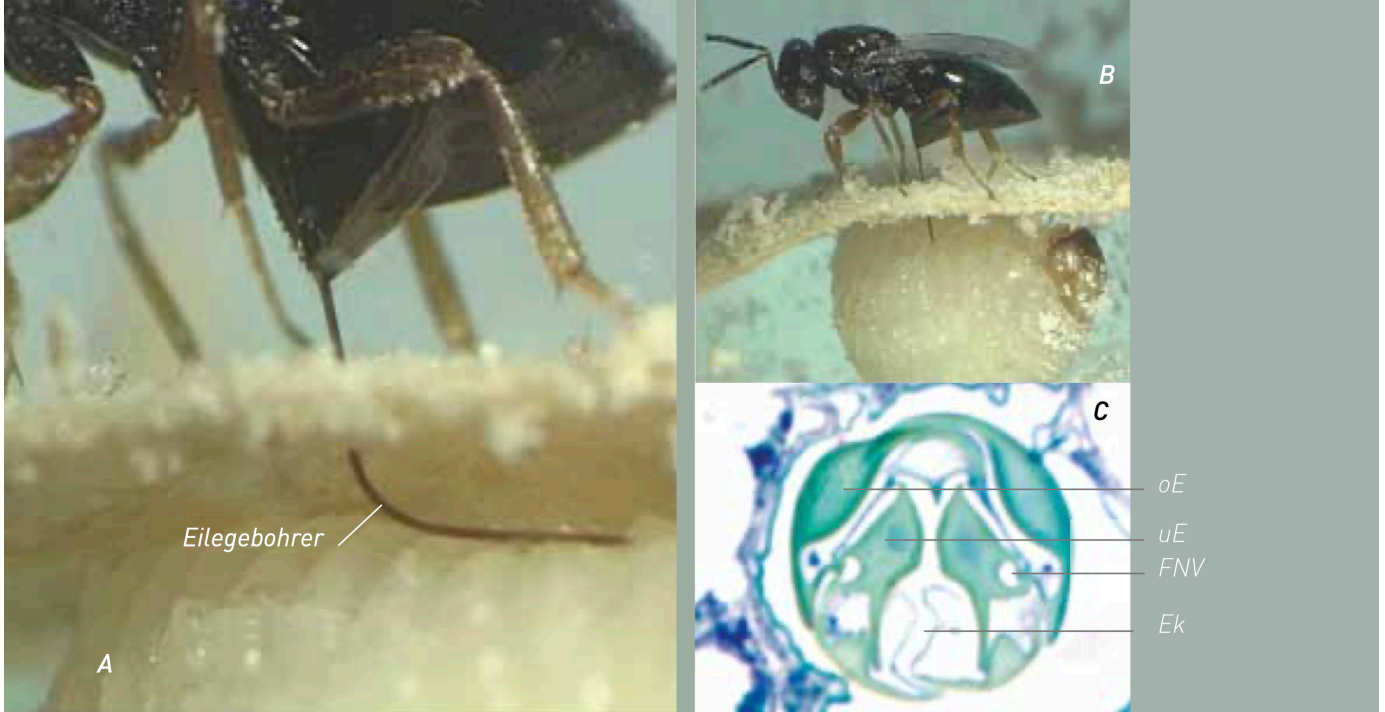
vorgestreckt. (B) Einzelbild einer Videosequenz, das die gelenkfreie Biegebewegung der in Längsrichtung verfalzten Unterkiefer (Maxillen) zeigt. (C) Die zum Aufsuchen eines geeigneten Blutgefäßes erforderlichen Biegebewegungen (gebogene Pfeile) werden dadurch erzeugt, dass sich der rechte

Unterkiefer (dunkel) relativ zum linken (hell) in Längsrichtung verschiebt, dabei aber von der mechanischen Sperre (MS) zurückgehalten wird. Zusätzlich kann der mechanische Widerstand des Umgebungsmediums (gestrichelte Pfeile) die Auslenkung verstärken.

Das Gleit-Stopp-Prinzip ist bei Insekten beispielsweise in Form der nadelförmig verlängerten Mundwerkzeuge von Wanzen verwirklicht. In Südamerika vorkommende blutsaugende Raubwanzen (Reduviidae, Unterfamilie Triatominae) setzen dieses Bewegungsprinzip beim Suchen von kleinen Blutgefäßen im Gewebe ein, nachdem sie die Haut eines Wirtes (z.B. des Menschen) mit ihren Mundwerkzeugen durchbohrt haben ▣ 16. Bei diesen Insekten sind die beiden Unterkiefer (Maxillen) nadelförmig verlängert und längs miteinander verfalzt. Wird nun die Maxille der einen Seite relativ zu der der anderen Seite in Längsrichtung nach vorne geschoben, stößt sie gegen eine am Ende der Verfalzung ausgebildete mechanische Sperre. Je nachdem, welche der beiden Maxillen nach vorne bewegt wurde, bewegt sich das Maxillenbündel in die eine oder die andere Richtung.

Das gleiche Prinzip liegt den Eilegebohrern (Ovipositoren) von parasitoiden Wespen (z.B. Schlupf- und Erzwespen) zugrunde. Diese legen ihre Eier in oder an anderen Insekten(larven) ab, von denen sich der

eigene Nachwuchs später ernährt. Da die Wirte oft verborgen in Pflanzengewebe leben, müssen die Wespenarten zuerst den Wirt selbst aufspüren und dann noch einen geeigneten Eiablageplatz auf der Oberfläche oder im Inneren des Wirts finden. Das geschieht durch Suchbewegungen des Eilegebohrers ▣ 17. In diesem Fall können sogar bis zu vier teilweise unabhängig voneinander bewegliche Elemente (die Eilegescheiden oder Valven) miteinander verfalzt sein. Je nachdem, welche dieser Elemente (gegeneinander) verschoben werden, kann es dadurch zu noch vielfältigeren Biegebewegungen kommen als bei den oben beschriebenen Mundwerkzeugen der blutsaugenden Wanzen.

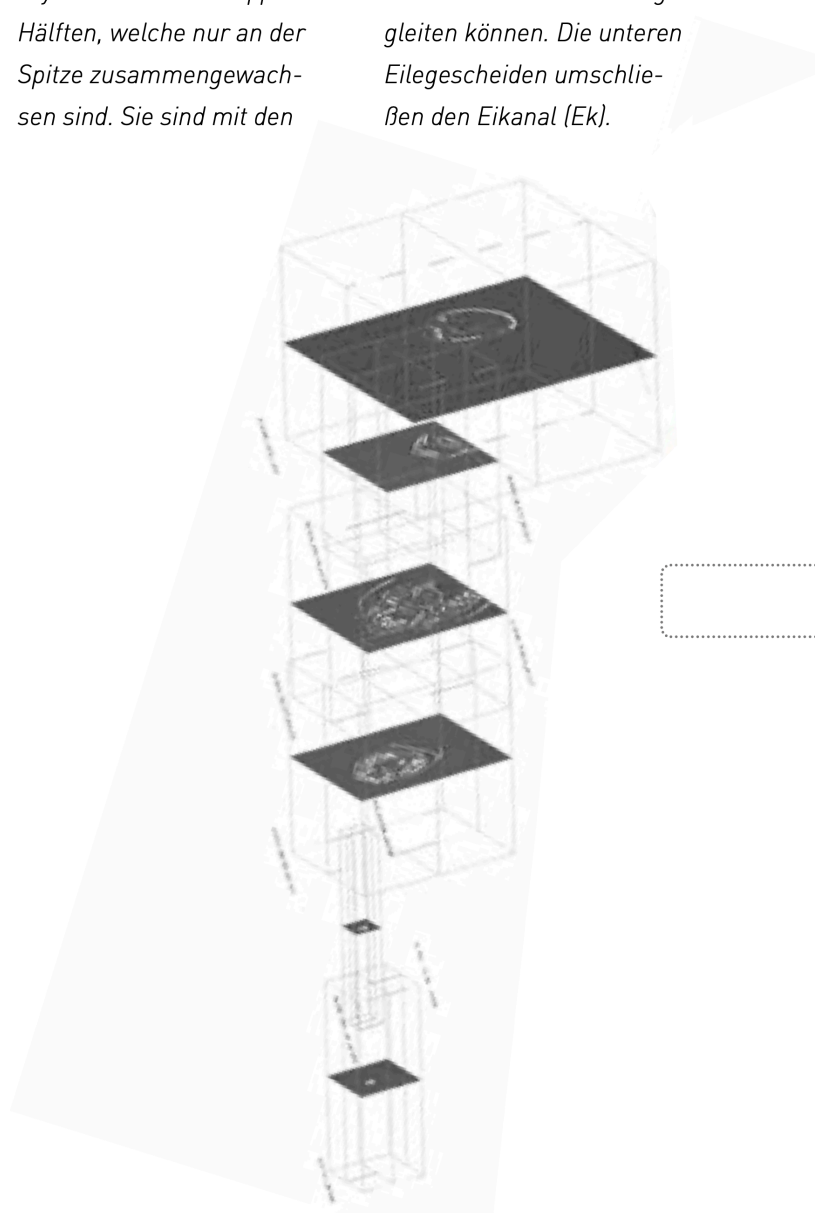


▮ **17** Die Lagererzwespe *Lariophagus distinguendus* ist ein Parasitoid von Larven mehrerer Käferarten, welche im Getreide leben und dieses schädigen. (A-B) Ein Lagererzwespenweibchen legt ein Ei auf eine Larve des Kornkäfers *Sitophilus granarius*; dabei werden die

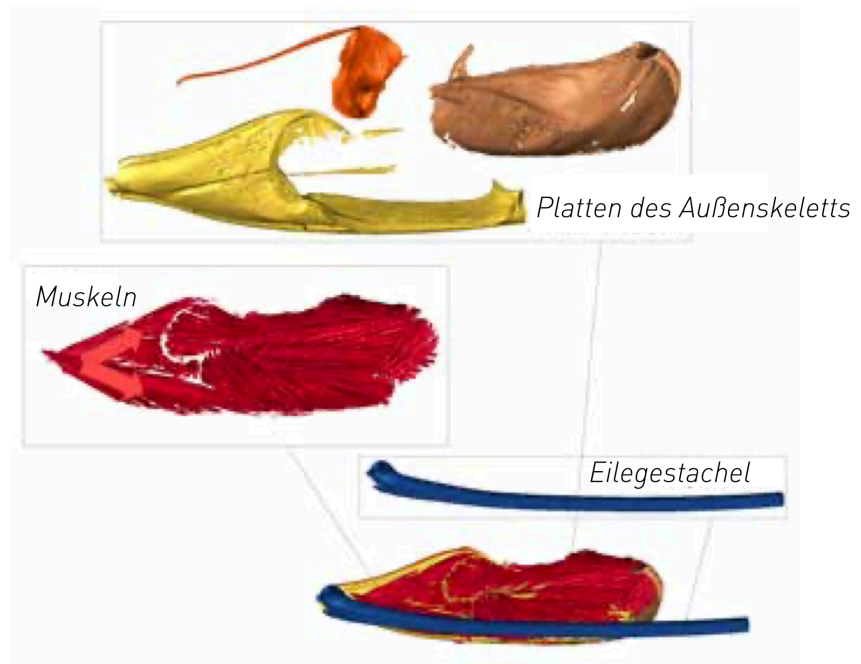
gelenkfreien Bewegungen des Eilegebohrers deutlich. (C) Querschnitt durch den Eilegebohrer. Die obere Eilegescheide (oE) besitzt zwei sich asymmetrisch überlappende Hälften, welche nur an der Spitze zusammengewachsen sind. Sie sind mit den

beiden unteren Eilegescheiden (uE) über eine Feder-Nut-Verbindung (FNV) gekoppelt, was erlaubt, dass die Untereinheiten aneinander entlanggleiten können. Die unteren Eilegescheiden umschließen den Eikanal (Ek).

▮ **18** Aus mehreren hochauflösenden Computertomographie-Aufnahmen des Insekts wird die Gesamtstruktur zusammengesetzt, so dass das Zusammenspiel aller an der Bewegungserzeugung beteiligten Elemente sichtbar wird (hier: Teil des Hinterleibes der Schlupfwespe *Venturia canescens*).



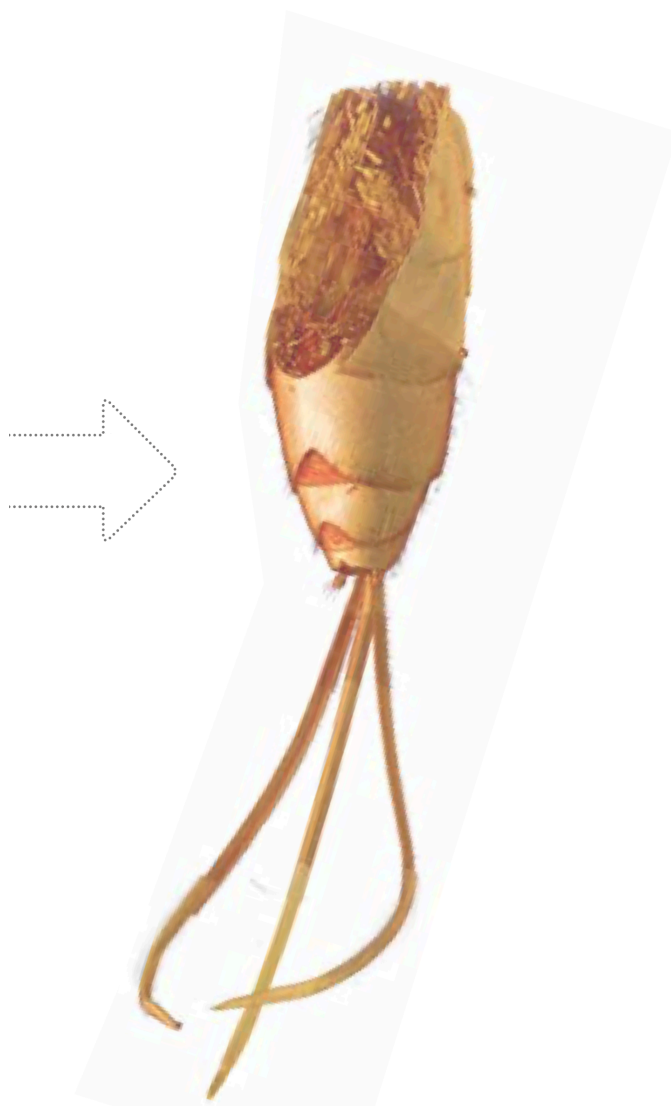
▮ 19 Zerlegung des CT-Bildes eines Eilegebohrers der Schlupfwespe *Venturia canescens* in die einzelnen an der Bewegung beteiligten Strukturen. Hierzu zählen sowohl nach innen verlagerte Teile des Außenskelettes als auch Muskeln. Die Spitze des Eilegestachels ist nicht abgebildet.

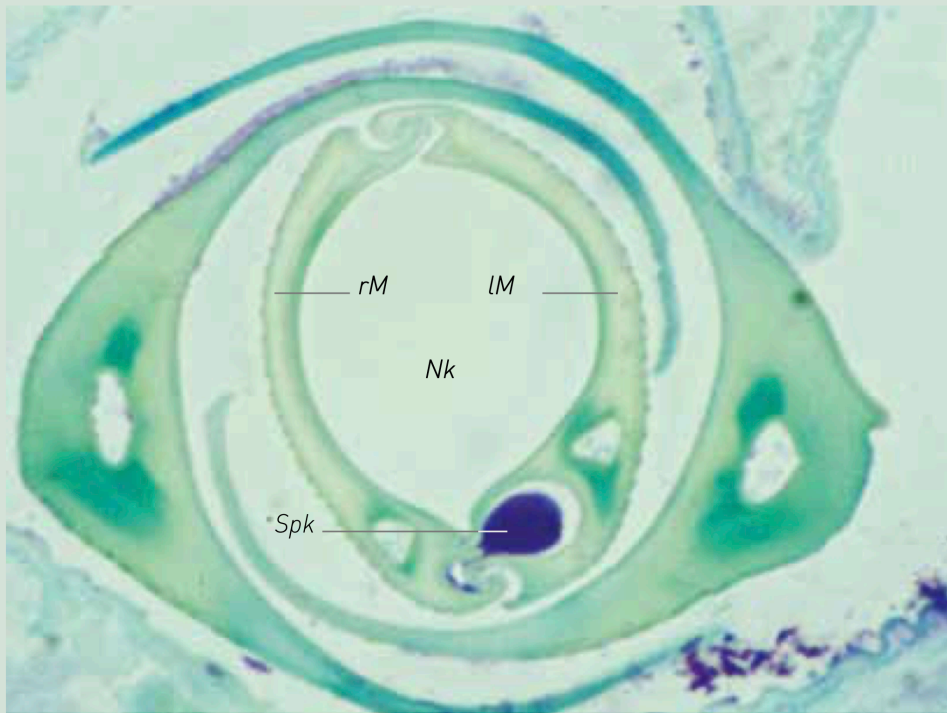


Untersuchung der Bewegungsprinzipien

Um die Bewegungsprinzipien der oben beschriebenen Stech- und Eilegeapparate bei Insekten zu verstehen, erzeugen wir dreidimensionale Bilder der beteiligten Strukturen. Da Insekten sehr klein sind, wenden wir sehr hochauflösende Methoden wie die Synchrotron-Computertomographie (CT) an, eine auch feinste Strukturen zeigende Röntgentechnik. Aufgrund der hohen Auflösung kann nicht das ganze Insekt auf einmal aufgenommen werden. Deshalb müssen mehrere hochaufgelöste Computertomographie-Aufnahmen verschiedener Teile des Insekts zu einem Bild der gesamten Struktur zusammengesetzt werden ▮ 18.

Auf dieser Grundlage erstellen wir dreidimensionale Modelle der untersuchten Objekte. Die 3D-Bilder lassen sich dann wieder in die einzelnen an der Bewegung beteiligten Strukturen zerlegen ▮ 19. Damit können wir zum Beispiel einzelne Muskelstränge untersuchen, um die zur Bewegung





A

▮ **20** Erweiterung des Modells der Mundwerkzeuge der Raubwanze *Dipetalogaster maxima*. Die Mundwerkzeuge bestehen aus den beiden nadelförmig verlängerten und ineinander verfalzten Unterkiefern, auch Maxillen genannt (lM = linke Maxille,

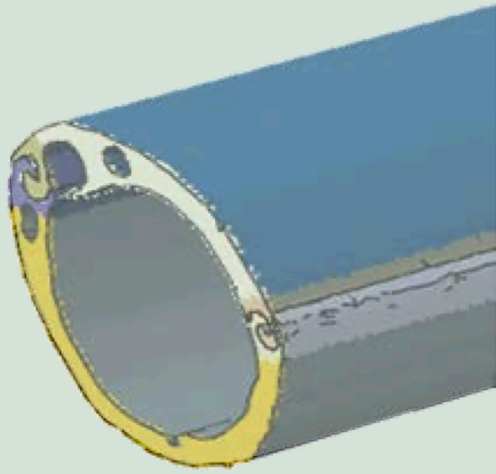
rM = rechte Maxille), welche den Nahrungs- (Nk) und den Speichelkanal (Spk) bilden. Die ineinander verfalzten Mundwerkzeuge werden auch Maxillenbündel (Mb) genannt. Technische Modelle werden laufend verfeinert: Dazu dienen lichtmikrosko-

pische Untersuchungen von Querschnitten (A), die Strukturen im Detail zeigen, und fluoreszenzmikroskopische Aufnahmen (B), mit denen sich mechanische Eigenschaften beurteilen lassen.

führenden Mechanismen zu verstehen und die Bewegung zu berechnen. So kann etwa über die Anzahl und den Durchmesser der einzelnen Muskelfasern die Kraft der Muskelpakete abgeschätzt werden. Über die Angriffspunkte der Muskeln an nach innen verlagerten Platten des Außenskelettes der Insekten und an den zu bewegenden Strukturen (z.B. der Eiablageapparat) kann bestimmt werden, in welche Richtung der Muskel zieht, wenn er kontrahiert.

Trotz der hohen Auflösung der Tomographieaufnahmen können wir sehr kleine Details nicht in den 3D-Datensätzen erkennen. Um eine noch genauere Untersuchung der Mechanismen zu ermöglichen, werden Feinstrukturen wie etwa die Verfalzung der einzelnen Teile des Stechapparates aus licht- und elektronenmikroskopischen Bildern in die 3D-Modelle übernommen

▮ **20A**, um dann die resultierende Bewegung simulieren zu können. Damit überprüfen wir, ob wir die angenommenen Verfalzungsstrukturen und Materialeigenschaften auch richtig interpretiert haben. Insbesondere die Annahme von mechanischen Eigenschaften auf der Mikrostruktur-Ebene ist eine große und oft (noch) unüberwindbare Herausforderung. Eine Möglichkeit, einen Einblick in die mikrostrukturellen Eigenschaften des Stechrüssels zu bekommen, ist die Fluoreszenzmikroskopie **▮20B**. Daraus können weichere und steifere Bereiche identifiziert und in das Modell übernommen werden. Mit diesen Informationen können dann bereits sehr detaillierte Simulationen der Bewegungsabläufe erstellt werden.



Impressions from the special exhibition “Baubionik – Biologie beflügelt Architektur” of the State Museum of Natural History (SMNS) in Stuttgart, exhibition area A03b “Gelenklos glücklich”



Fig. 3. Flyer of the special exhibition “Baubionik – Biologie beflügelt Architektur” of the State Museum of Natural History (SMNS) in Stuttgart, Germany.



Fig. 4. Some impressions of the area “Gelenklos glücklich” (A03b) of the special exhibition “Baubionik – Biologie beflügelt Architektur” of the State Museum of Natural History (SMNS) in Stuttgart, Germany. **a** Live *Dipetalogaster maxima* (Hemiptera: Reduviidae: Triatominae) in a terrarium, various animals that are able to perform joint-free movements under a stereomicroscope and display wall with information concerning joint-free bending mechanisms and the mouthparts of hemipterans. **b** Video recordings of various animals performing joint-free movements and display wall with information about the ovipositors of parasitoid hymenopterans.

Publications 10 and 11

Betz O., **Eggs B.**, Henn F., Birkhold A. and Röhrle O. (2019). Bewegung ohne Gelenke: (Wie) gehts das? In: Knippers J., Schmid U. and Speck T. (eds.), *Bionisch bauen: Von der Natur lernen* (pp. 22–31). Basel, Switzerland: Birkhäuser Verlag GmbH. doi: 10.1515/9783035617870-005

(non-peer-reviewed book chapter; based on Publication 9²)

Betz O., **Eggs B.**, Henn F., Birkhold A. and Röhrle O. (2019). Movement without joints: (how) does it work? In: Knippers J., Schmid U. and Speck T. (eds.), *Biomimetics for Architecture: Learning from Nature* (pp. 22–31). Basel, Switzerland: Birkhäuser Verlag GmbH. doi: 10.1515/9783035617917-005

(non-peer-reviewed book chapter; translation of Publication 10²)

Abstract

The ability to move actively gives unicellular organisms and animals the possibility to freely change their location. This has many advantages with regard to the search for nutrition and mates, the distribution of genes, and the avoidance of unfavorable environmental conditions. The wide range of movements animals perform includes the fast gallop of horses, the skillfull clambering of monkeys, and the impressive maneuvers of flies. Such movements require joints like those familiar to us from arthropods (milipedes, spiders, crabs, and insects) and from vertebrates. However, movement can also be accomplished in quite different ways!

Significance within the present thesis: Cf. Publication 9.

Methods used: high-speed videography, wide-field epifluorescence microscopy (WFM), ultramicrotomy, light microscopy (LM), synchrotron X-ray phase-contrast microtomography (SR- μ CT)

Own contribution: writing and preparing parts of the manuscript and figures; discussing the manuscript; correspondence with the publisher

² Publications 10 and 11 are based on the same text (Publication 9). Hence, they are treated as one here and only the English translation (*i.e.* Publication 11) is included below.

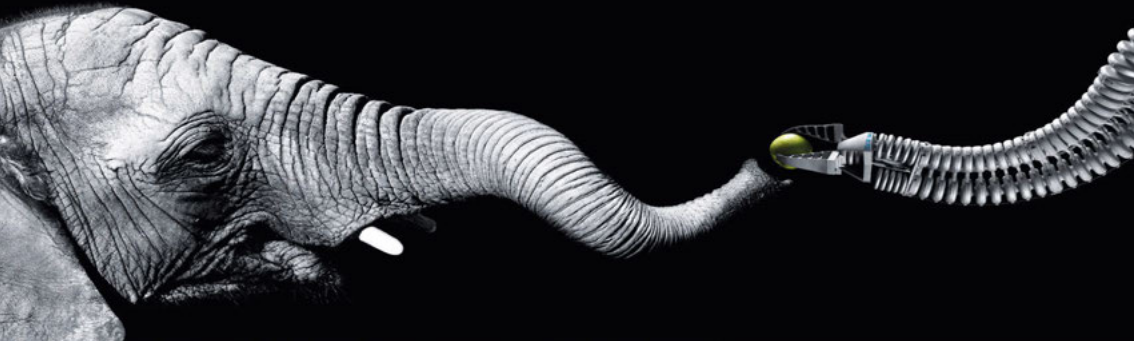
Movement without joints: (how) does it work?

Oliver Betz / Benjamin Eggs / Fabian Henn / Annette Birkhold / Oliver Röhrle

The ability to move actively gives unicellular organisms and animals the possibility to freely change their location. This has many advantages with regard to the search for nutrition and mates, the distribution of genes, and the avoidance of unfavorable environmental conditions. The wide range of movements animals perform includes the fast gallop of horses, the skillful clambering of monkeys, and the impressive maneuvers of flies. Such movements require joints like those familiar to us from arthropods (millipedes, spiders, crabs, and insects) and from vertebrates. However, movement can also be accomplished in quite different ways!

From a biological or engineering perspective, a joint is a movable connection between two or several (rigid) bodies (for instance, bones) that defines their movement in fixed directions in relation to each other. From an evolutionary perspective, however, genuine joints appeared relatively late. Initially movement was achieved without joints but by means of continuously changing the geometry of the structures involved. In engineering, this principle is known as “continuum kinematics.” In animals this principle is common, examples being the changes in shape exhibited by earthworms or the wide range of movements of an elephant’s trunk Γ 11. Such systems are typically soft to flexible, but can often mechanically stiffen to become more resistant. This is usually achieved through the contraction of muscles. The joint-free mechanisms and principles employed in continuous kinematics are of interest to engineering not only because—in contrast to joint-based systems—they are often simpler. The technical systems based on this feature are also capable of achieving much more complex movements

and therefore are better suited to adapt to external constraints and requirements. The principle of the muscular hydrostat, which also governs the complex movements of an elephant’s trunk, is only one of several joint-free movement principles. In zoology, the term “hydrostat” refers to incompressible compartments filled with fluid or muscles that, due to a change in pressure, induce a change in movement and stiffness. For example, the human tongue is another example of a muscular hydrostat. Within the tongue, the wide variety of movements is a result of the arrangement of various muscle groups and its orchestrated activation. A common aspect of the elephant’s trunk and the tongue is that their movements are often highly complex and therefore require a high level of control. It is difficult to transfer the properties of these biological materials to technical solutions with controllable and hence functional characteristics. Computer simulations can help us gain deeper insights into the function of hydrostats. The big advantage of simulations and computational model is that many dif-



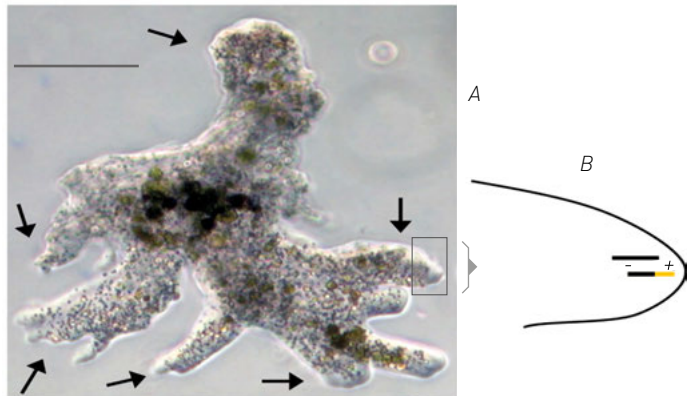
ferent “what if” cases can be performed in a very simple, controllable, and straightforward way by just changing the relevant input parameters. However, realistic computational models of muscular hydrostats are not easy to develop, because this requires in-depth knowledge of the underlying working principles. Below, we outline these principles in more detail. Most joint-free movements are based on muscle activation; however, the resulting movement mechanisms are often governed by the mechanical properties of the passive structures. We provide here a short overview of four joint-free movement mechanisms found in unicellular organisms and animals.

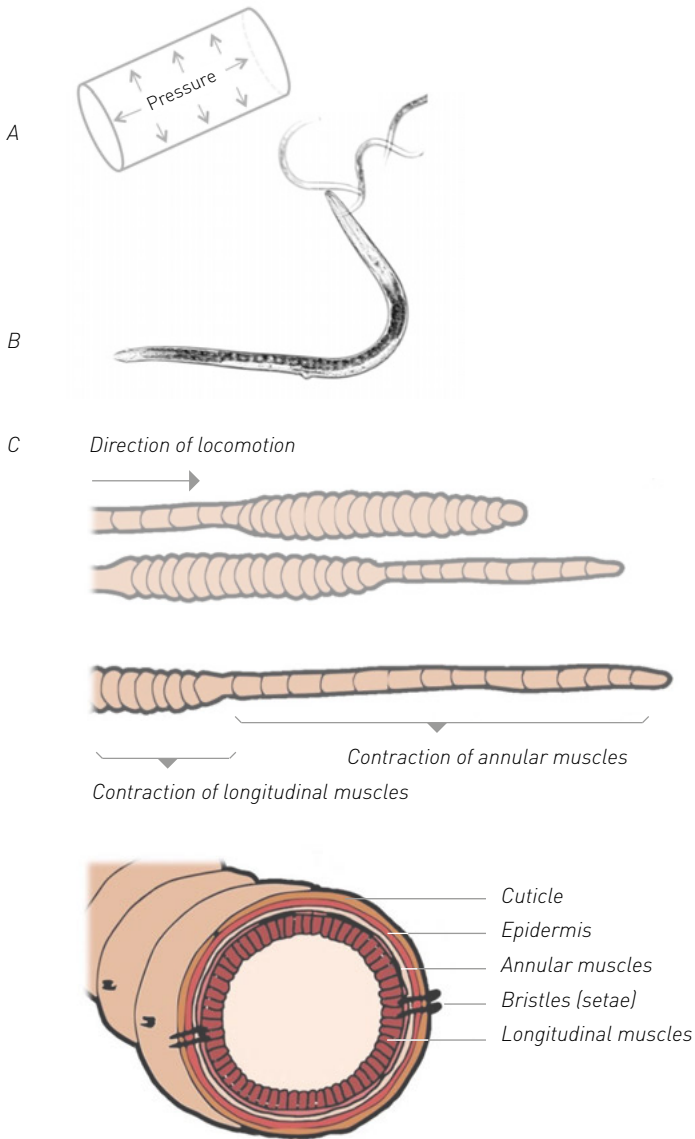
Γ11 *The trunk of the elephant is a muscular hydrostat. This joint-free movement principle was adopted for the construction of a continually movable technical gripper by the FESTO company.*

Amoeboid movement

The term “amoeboid movement” refers to the creeping/flowing form of movement found in many kinds of cells (e.g., in rhizopods) Γ12A, which belong to the unicellular organisms, or in the white blood cells of humans (leucocytes). In this movement, the mobile cell produces pseudopodia (false feet), which are extensions of the surface of the gel-like exterior cell plasma. This contains a concentrated network of protein fiber elements. When these filaments extend beneath the cell surface and, at the same time, are foreshortened at their base, the cell moves forward Γ12B.

Γ12 (A) *The rhizopod Amoeba proteus moves with the help of its false feet (arrows). Scale bar: 0.2 mm. (B) The false feet advance by permanently removing filaments at their minus end and subsequently adding filaments (shown colored in the image) at their plus end.*





13 Principle and examples of hydrostatically driven joint-free movements (A) Principle of the dermal muscular tunic, in which the fluid of the body cavity functions as a counter pressure to the body wall (adaptive rigidity) while, at the same time, it changes its position along the longitudinal axis, facilitating changes in the body shape. (B) In its outer body layer, the nematode *Pelodera strongyloides* only has muscles

in longitudinal direction; this means that it is only capable of performing snaking movements (mature female and three juveniles in the first larval stage). (C) Schematic of the peristaltic movement of an earthworm. Waves of shortening and lengthening body segments move from the front to the rear of the body. In contrast to the nematodes shown in (B), this is possible because of the subdivision of the body cavity

into a series of compartments and because of the presence of annular muscles in the body wall above the layer of longitudinal muscles.

Movement via hydroskeleton

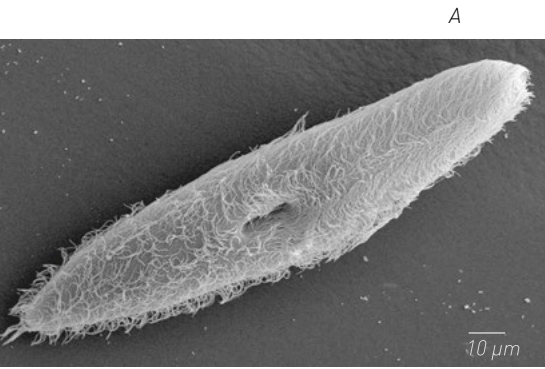
When muscles are involved in the production of movement, they need counter bearings, normally skeletons. These do not have to involve bones; phylogenetically, the oldest types of skeleton are hydrostatic skeletons. They are based on the principle that a fiber-reinforced and fluid-filled body wall that is limited to the outside and resists tension and pressure is itself pressurized. Because the muscles are integrated in the body wall, this system is termed a dermal muscular tunic. In general, due to muscle contractions and the fact that the fluid cavity cannot be compressed, the pressure increases and is hydraulically transferred to other areas of the body. This causes changes in body shape, which can also be used for locomotion. As a rule, such hydroskeletons are common in invertebrates with soft and flexible bodies, such as earthworms. Here, the muscles responsible for movement are located in the body wall, and the hydrostatic skeleton in the form of the fluid-filled body cavity takes on the role of the skeletal antagonist Γ 13.

These principles have been introduced in biomimetic applications, for example in new drive technologies and in soft robots or parts of robots (e.g., robot arms that must have great freedom of movement). So-called “pneumatic” artificial muscles are hoses consisting of a pressure-proof fabric mesh. By increasing the internal pressure the pneumatic muscles contract. Complex deformations can be achieved through various arrangements of the fabric mesh.

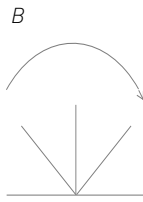
Muscular hydrostats

Muscular hydrostats are cylinder-like structures that predominantly contain muscle tissue (instead of a fluid); the muscle fibers can be arranged in various directions. Such systems are self-stabilizing, yet completely mobile. Examples include the human tongue, the elephant’s trunk Γ 11, the muscular foot of the Roman snail, or the tentacles of an octopus. Like the fluid-based hydroskeletons, such as that of the earthworm, muscular hydrostats cannot change their volume. Therefore, the muscles can act as counter bearings and do not necessarily require a rigid or fluid-based skeleton. Muscular hydrostats can perform an impressive variety of movements and, at the same time, adapt their stiffness to the mechanical requirements.

This principle is also often applied in the field of soft robotics. However, instead of the relatively rigid fabric mesh, soft plastics are used in this case, enabling the development of highly specialized surgical tools for interventions inside the body. The combination of various plastics or diverse wall thicknesses makes complex movements possible when the hose is pumped up. For example, the aim of snake robotic microsurgery is to carry out surgical interventions at any place in the heart through a small opening.



A



Forward movement



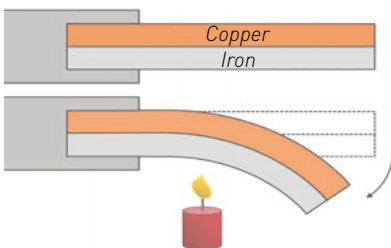
Backward movement

Γ14 (A) Scanning electron micrograph of a *Paramecium*. The surface is densely covered with cilia. (B) Forward and backward movement of a cilium. During the forward movement, the entire shaft remains stiff. During the backward movement, it bends and becomes supple in certain areas.

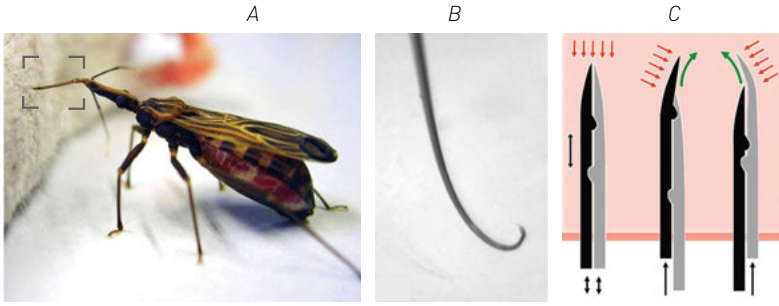
Slide-lock mechanisms

Prominent examples of adaptive joint-free structures are the slide-lock mechanisms of cilia and flagella **Γ14**. The unicellular *Paramecium*, for example, uses this mechanism to move through water freely. This type of joint-free movement is associated with one of the oldest movement mechanisms. It can be found in both uni- and multicellular organisms (such as rotifers) and in sperm cells, which swim towards the egg cell using their flagella. To understand the movement of cilia and flagella, we need to observe their complex and minute structure in cross-section, an aspect that leads us too far away from our main interest in this review. Simpler slide-lock mechanisms we have investigated include the piercing/sucking proboscises of bugs and the ovipositors of parasitoid wasps. These structures do not have any inherent joints and function via remote control (i.e., by means of using muscles in the head or abdomen). Ultimately, the basic working

principles employed in these structures are the same as those in cilia and flagella. In such structures, two or several rod-shaped elastic fibers are linked to each other in longitudinal direction with the help of a tongue-and-groove system. These fibers can be moved in relation to each other longitudinally. However, if longitudinal sliding is inhibited or even fully prevented by a mechanical block, the result is—depending on the stiffness of the materials—a relative bending of both fibers. This is similar to the ideas behind bimetals **Γ15**. Bimetals consist of two layers of different interconnected metals. Changes in temperature, for example, can lead to the bending of the bimetal strip. The reason for bending is due to the fact that the metals are temperature sensitive and each of the metals reacts differently to temperature changes. Bimetals are therefore commonly used as thermometers or temperature switches (e.g., to control the heat in water boilers).



Γ15 Bimetal principle. A metal strip consisting of two layers of different metals changes shape when exposed to temperature changes because the two metals expand at different rates.



▮16 The principle of slide-lock is used by insects to perform bending movements similar to the bimetal mechanism. (A) The assassin bug *Rhodnius prolixus* sucking blood from an anesthetized rat. In this process, the needle-like extended proboscis (frame) is extended forward.

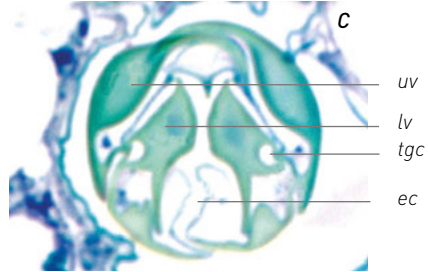
(B) Individual image of a video sequence showing the joint-free bending movement of the maxillae, which are connected along their length with the help of a tongue-and-groove system. (C) The bending movements needed for finding a suitable blood vessel (green

bent arrows) are generated by the right (light) maxilla moving relative to the left (dark) maxilla in longitudinal direction but are restrained by the mechanical block. In addition, the mechanical resistance of the surrounding medium (red arrows) can reinforce the deflection.

In insects, the slide-lock principle can be found, for example, in the needle-like extended proboscises of bugs. Blood-sucking assassin bugs native to South America (Reduviidae, subfamily Triatominae) use this movement principle when searching for small blood vessels in tissue after they have pierced the skin of the host (e.g., a human being) with their proboscises ▮16. In these insects, the two maxillae are extended like needles and interlocked with the help of a tongue-and-groove system. When one of the maxillae is moved forward longitudinally relative to the other, it is subjected at one point to a mechanical block that exists at the end of the tongue-and-groove system. The maxillary bundle moves in one or the other direction depending on which of the two maxillae was moved. In this context, the surrounding medium also plays an important role as the beveled tips of the maxillae are diverted by it. Because of the asymmetrical forces acting on the tip, the movement of the maxillae relative to each other often also

leads to an offset resulting in the bending of the entire bundle.

The same principle is employed in the ovipositors of parasitoid wasps (e.g., ichneumonid and chalcid wasps). These wasps lay their eggs in or on other insects (usually during larval or egg stages), upon which the hatched parasitoid larvae later feed. Because the hosts often live hidden in plant tissue, these wasps must first find the host and then locate a suitable place for depositing the eggs, either on the surface of the host or inside it. This is achieved through search movements of the ovipositor ▮17. In this case, up to four elements can be involved, some of which are independently movable (the valves or valvulae), are connected with each other with the help of a tongue-and-groove system. Depending on which of these elements are shifted (against each other), more diverse bending movements can be achieved, compared to the above-described proboscises of the blood-sucking bugs.

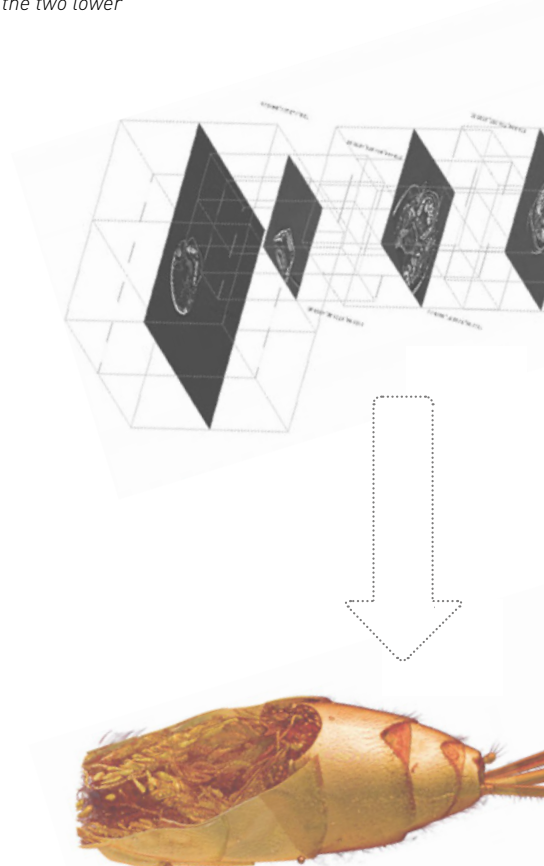


▣ **17** The pteromalid wasp, *Lariophagus distinguendus*, is a parasitoid of the larvae of several beetle species that live in cereal, causing damage. (A–B) A female pteromalid wasp deposits an egg on a larva of the corn weevil *Sitophilus granarius*;

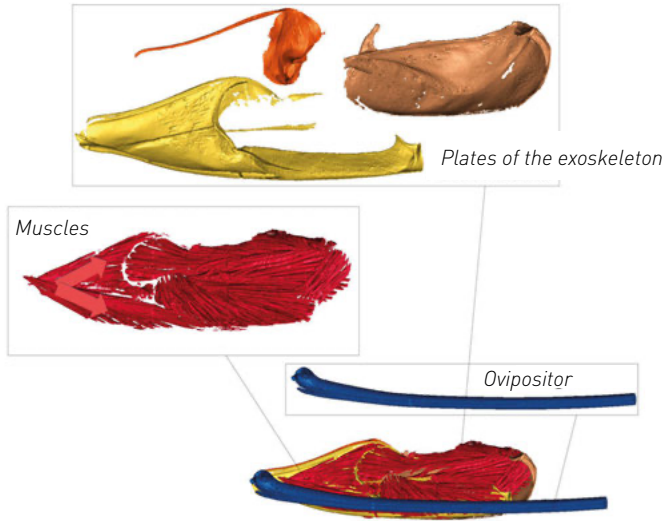
the joint-free movements of the ovipositor can be clearly seen. (C) Cross-section through the ovipositor. The upper valve (uv) comprises two asymmetrically overlapping halves, which are grown together at the tip only. They are joined to the two lower

valves (lv) via a tongue-and-groove connection (tgc), which makes it possible for the lower units to slide along each other. The lower valves enclose the egg canal (ec).

▣ **18** The complete structure comprises several high-resolution computer tomography images of the insect, so that the interaction of all elements involved in generating the movement becomes visible (here, part of the abdomen of the ichneumonid wasp *Venturia canescens*).



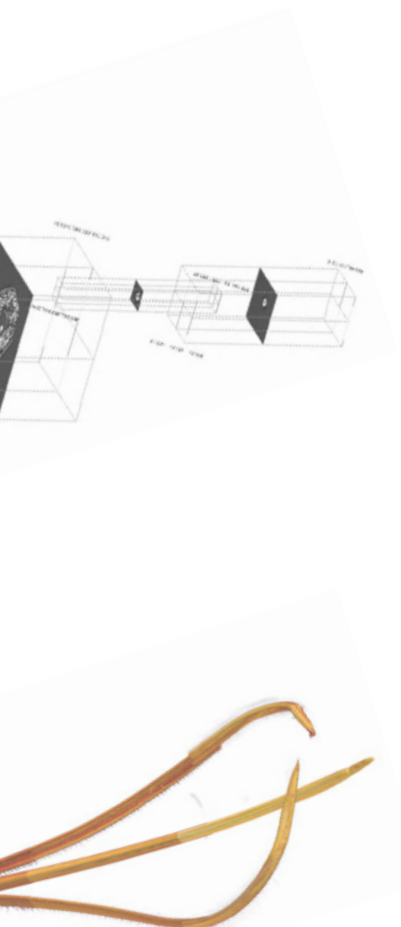
▮ **19** Breakdown of the CT image of an ovipositor of the ichneumonid wasp *Venturia canescens* into the individual structures involved in the movement. These include the parts of the exoskeleton that have been relocated inside and the muscles. The tip of the ovipositor is not shown.



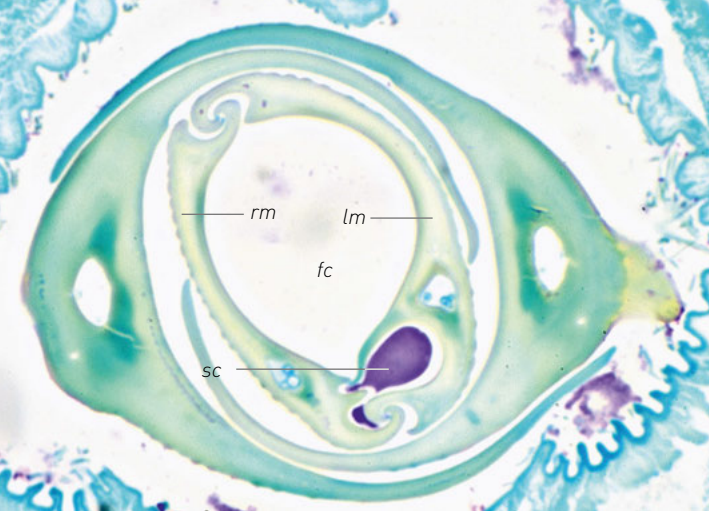
Investigation of the movement principles

In order to understand the movement principles of the proboscises and ovipositors of insects, we have generated three-dimensional images of the structures involved. Since most insects are minute, we employed extremely high-resolution imaging techniques such as synchrotron computer tomography (CT), which is an X-ray technology that can reveal even very small structures. Because of the high resolution, it is not possible to X-ray the whole insect in one take. This means that several high-resolution computer tomography images of different parts of the insect have to be stitched together to form an image of the entire structure ▮ **18**.

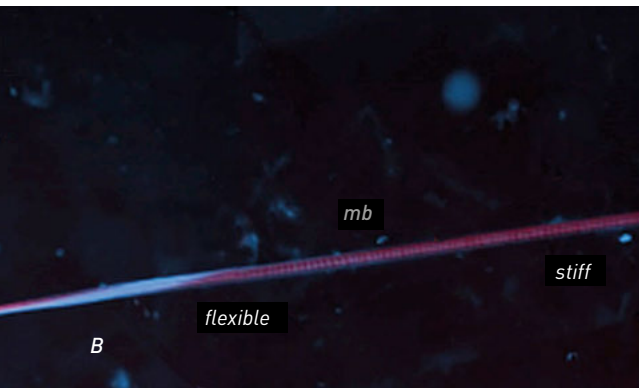
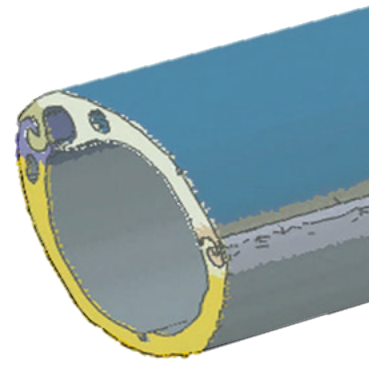
On that basis we have produced three-dimensional models of the objects investigated. The 3D images or the models can also be taken apart to isolate the individual structures involved in the movement ▮ **19**. This method has allowed us to investigate, amongst other things, the individual muscle strands responsible for movement. Moreover, the models can be used within simulations to increase our



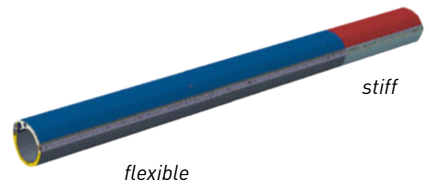
understanding of the mechanisms leading to movement and to predict movements. By using the number and diameter of the individual muscle fibers it is also possible to estimate the strength of the muscle packs. Studies of the points of attachment of the muscles on the plates of the insects' exoskeleton (sometimes relocated to the inside) and on the structures to be moved (such as the ovipositor), enable the determination of the direction of the muscle forces and hence the direction in which the muscle pulls when it contracts. Unfortunately, in spite of the extremely high resolution of the synchrotron CT images, the imaging has its limitations. We cannot detect the smallest details in the 3D data sets. Thus, for investigations of the small-scale mechanisms in even greater detail, for example, the connecting rabbet (or groove) between the different parts of the proboscis, we employed light- and electron-microscopical images Γ_{20A} in order to build models from these structures and to simulate the influence of these small-scale mechanisms on the resulting movement. In this way we can check whether we have correctly interpreted the material properties and the assumed tongue-and-groove structures. Making assumptions with respect to mechanical properties at the microstructure level is a big and often (still) insurmountable challenge. One possible way of gaining more insights into the microstructural properties of the proboscis is to use fluorescence microscopy Γ_{20B} . This imaging method can be used to identify softer and more rigid areas, and to adopt them to build realistic computational models (structural information necessary). With this information it is then possible to produce highly detailed simulations of the movement processes.



A



B



▮ **20** Extension of the model of the proboscis of the assassin bug *Dipetalogaster maxima*. The proboscis consists of the two needle-like extended and connected maxillae (*lm* = left maxilla, *rm* = right maxilla) that

form the food channel (*fc*) and the salivary channel (*sc*). The maxillae connected with each other via a tongue-and-groove system are also called the maxillary bundle (*mb*). Technical models are continually being refined;

this is accomplished using light-microscopy investigations of cross-sections (*A*) that show structures in detail, and by means of fluorescence microscopy images (*B*) that can be used to assess mechanical properties.

Publication 12

Olmi M., Eggs B., Capradossi L., van de Kamp T., Perkovsky E. E., Guglielmino A. and Vasilenko D. V. (2022). A new species of *Bocchus* from upper Eocene Rovno amber (Hymenoptera, Dryinidae). *Journal of Hymenoptera Research* 92: 257–272. doi: 10.3897/jhr.92.87084

(peer-reviewed journal article)

Abstract

A new fossil species of Dryinidae (Hymenoptera, Chrysidoidea) from upper Eocene Rovno amber (Ukraine) is described: *Bocchus rex* **sp. nov.** It is compared with two other species of *Bocchus* known from European amber: *B. primaevus* Martins & Melo from Baltic amber and *B. schmalhauseni* Perkovsky, Olmi, Vasilenko, Capradossi & Guglielmino from Rovno amber. A new key to the Cretaceous and Paleogene species of *Bocchus* is presented. The Dryininae are the most common representatives in all the amber dryinid faunas since the mid-Cretaceous. The Rovno amber fauna is an exception; possible explanations for the abundance of *Bocchus* species within this amber are presented.

Significance within the present thesis: This first description of *Bocchus rex* **sp. nov.**, a dryinid wasp from upper Eocene Rovno amber, demonstrates that the methods used to investigate morphological characters of extant insects can also be applied to (amber) fossils.

Methods used: stereomicroscopy, synchrotron X-ray phase-contrast microtomography (SR- μ CT)

Own contribution: writing parts of the manuscript, preparing all figures; discussing the manuscript; processing of the SR- μ CT data; correspondence

A new species of *Bocchus* from upper Eocene Rovno amber (Hymenoptera, Dryinidae)

Massimo Olmi¹, Benjamin Eggs², Leonardo Capradossi³, Thomas van de Kamp^{4,5},
Evgeny E. Perkovsky⁶, Adalgisa Guglielmino⁷, Dmitry V. Vasilenko^{8,9}

1 Tropical Entomology Research Center, Via De Gasperi 10, 01100 Viterbo, Italy **2** Evolutionary Biology of Invertebrates, Institute of Evolution and Ecology, University of Tübingen, Auf der Morgenstelle 28, 72076 Tübingen, Germany **3** Via Pericle Scriboni 28, 01017 Tuscania, Italy **4** Institute for Photon Science and Synchrotron Radiation (IPS), Karlsruhe Institute of Technology (KIT), Hermann-von-Helmholtz-Platz 1, 76344 Eggenstein-Leopoldshafen, Germany **5** Laboratory for Applications of Synchrotron Radiation (LAS), Karlsruhe Institute of Technology (KIT), Kaiserstrasse 12, 76131 Karlsruhe, Germany **6** I.I. Schmalhausen Institute of Zoology (SIZK), National Academy of Sciences of Ukraine, B. Khmel'nitskogo 15, 01030 Kiev, Ukraine **7** Department of Agriculture and Forestry Sciences (DAFNE), University of Tuscia, Via San Camillo de Lellis, 01100 Viterbo, Italy **8** A.A. Borissiak Paleontological Institute of the Russian Academy of Sciences, Profsoyuznaya Str. 123, 117647 Moscow, Russia **9** Cherepovets State University, 162600 Cherepovets, Russia

Corresponding author: Benjamin Eggs (benjamin.eggs@uni-tuebingen.de)

Academic editor: Michael Ohl | Received 28 May 2022 | Accepted 29 June 2022 | Published 31 August 2022

<https://zoobank.org/40679F47-8A7D-46FE-9CA9-69B0A51A4258>

Citation: Olmi M, Eggs B, Capradossi L, van de Kamp T, Perkovsky EE, Guglielmino A, Vasilenko DV (2022) A new species of *Bocchus* from upper Eocene Rovno amber (Hymenoptera, Dryinidae). *Journal of Hymenoptera Research* 92: 257–272. <https://doi.org/10.3897/jhr.92.87084>

Abstract

A new fossil species of Dryinidae (Hymenoptera, Chrysidoidea) from upper Eocene Rovno amber (Ukraine) is described: *Bocchus rex* **sp. nov.** It is compared with two other species of *Bocchus* known from European amber: *B. primaevus* Martins & Melo from Baltic amber and *B. schmalhauseni* Perkovsky, Olmi, Vasilenko, Capradossi & Guglielmino from Rovno amber. A new key to the Cretaceous and Paleogene species of *Bocchus* is presented. The Dryininae are the most common representatives in all the amber dryinid faunas since the mid-Cretaceous. The Rovno amber fauna is an exception; possible explanations for the abundance of *Bocchus* species within this amber are presented.

Keywords

Bocchinae, *Bocchus rex*, Chrysidoidea, key, systematics

Introduction

Dryinidae (Hymenoptera, Chrysidoidea) are parasitoids of Auchenorrhyncha (Hemiptera) (Olmi 1984; Guglielmino et al. 2013). This family is present in all continents, except for Antarctica, and comprises about 1900 species (Olmi et al. 2021a).

Eighty fossil species of Dryinidae have been described, among which the following six have been recorded from upper Eocene Rovno amber (Ukraine; 35–38 Ma) (Martynova et al. 2019; Perkovsky et al. 2020; Olmi et al. 2022): Bocchinae: *Bocchus schmalhauseni* Perkovsky, Olmi, Vasilenko, Capradossi & Guglielmino, 2020; Dryininae: *Dryinus janzeni* Olmi, 2000, *D. reifti* Olmi & Bechly, 2001, *D. wunderlichi* Olmi & Bechly, 2001; Apodryininae: *Rovnodryinus khomychi* Olmi, Guglielmino, Vasilenko & Perkovsky, 2022; Palaeoanteoninae: *Palaeoanteon janzeni* Olmi, 2000. In contrast, Baltic and Scandinavian amber (coeval of Rovno amber) are known to include 21 and two species of Dryinidae (Martynova et al. 2019; Olmi et al. 2021b), respectively. All known specimens from Ukraine have been collected in the Varash district of the Rovno region (which includes the former Vladimirets and Zarechnoye districts) and most of the important new taxa described from Rovno amber during the last few years (Matalin et al. 2021; Perkovsky and Nel 2021; Tshernyshev and Perkovsky 2021; and references therein).

Recently, we received two pieces of Rovno amber: one from a site in the Volyn region adjacent to the Varash district and the second most probably from the Varash district. They included specimens of Dryinidae that proved to belong to a new species, which we describe below.

Materials and methods

Terms

The description follows the morphological terminology of Olmi et al. (2019). All measurements reported are relative, except for the total length (head to metasomal tip, without antennae and sting). Antennal proportions refer to the lengths of the relevant segments as proportions of each other, with the values rounded to the nearest whole number. The following abbreviations are used: POL, distance between the inner edges of the two lateral ocelli; OL, shortest distance between the edge of a lateral ocellus and the median ocellus; OOL, distance from the outer edge of a lateral ocellus to the compound eye; OPL, distance from the posterior edge of a lateral ocellus to the occipital carina; TL, distance from the posterior edge of the eye to the occipital carina.

The term “disc of metapectal-propodeal complex” is used here in the sense of Kawada et al. (2015) and Lanes et al. (2020). It corresponds to the term “dorsal surface of propodeum” *sensu* Olmi (1984) and Olmi et al. (2019). The term “propodeal declivity” *sensu* Kawada et al. (2015), used here, corresponds to the term “posterior surface of propodeum” *sensu* Olmi (1984) and Olmi et al. (2019). The names of veins of the fore wing are here used in the sense of Azevedo et al. (2018) and Lanes et al. (2020). The “stigmatal vein” (*sensu* Olmi 1984 and Olmi et al. 2019) is named here the “second radial cross & radial sector (2r-rs&Rs)”.

The term “ADOs” (= Antennal Dorsal Organs) is used here in the sense of Riolo et al. (2016). It corresponds to the term “rhinaria” *sensu* Olmi (1984). According to Riolo et al. (2016), ADOs are sensory structures that might mediate the antennal responses to vibratory stimuli. As far as we know, they are usually present in the antennae of dyrinid females attacking Fulgoromorpha (Perkovsky et al. 2019).

Specimens

The specimens studied in this paper have been deposited in the following collections:

Specimen 1: Schmalhausen Institute of Zoology (SIZK), National Academy of Sciences of Ukraine, Kiev, Ukraine.

Specimen 2: State Museum of Natural History Stuttgart (SMNS), Stuttgart, Germany.

Stereomicroscopy

The multifocal photos were taken using a mirrorless Sony Alpha 6100 camera (Sony Group Corporation, Tokyo, Japan), with Canon bellows and three-way revolver for optical microscopy (Canon Inc., Tokyo, Japan). The following objectives were used: LOMO 3.7 × 0.11 (LOMO, St. Petersburg, Russia) for magnifications from 20 to 50×; Zeiss Semiplan 6.3 × 0.11 (Carl Zeiss GmbH, Jena, Germany) for magnifications from 50 to 100×. The motorized focus was managed by a Cognisys stackshot controller (Cognisys Inc., Traverse City, MI, USA). Captured images were merged into a single in-focus image by using ZereneStacker™ version 1.04 (Zerene Systems LLC, Richland, WA, USA). Images were processed with GIMP version 2.10.30 (<https://www.gimp.org>).

Synchrotron X-ray phase-contrast microtomography (SR-μCT) and image processing

Synchrotron X-ray microtomography (SR-μCT) (Betz et al. 2007) was performed at the UFO-I station of the Imaging Cluster at the KIT light source of Karlsruhe Institute of Technology (KIT, Karlsruhe, Germany) by using a parallel polychromatic X-ray beam produced by a 1.5 T bending magnet. Specimen 2 was glued onto a plastic pin and mounted onto the goniometer head of the sample stage for tomography. The beam was spectrally filtered with 0.5 mm aluminium with a spectrum peak around 15 keV and a full-width at half maximum bandwidth of about 10 keV. A fast indirect detector system was employed, consisting of a 13 μm LSO:Tb scintillator (Cecilia et al. 2011), diffraction limited optical microscope (Optique Peter) (Douissard et al. 2012) and a 12bit pco.dimax high-speed camera with a resolution of 2016 × 2016 pixels; 3000 projections were recorded at 70 frames per seconds and an optical magnification of 10×, resulting in an effective detector pixel size of 1.22 μm. Two separate overlapping image stacks were acquired because the specimen was larger than the field of view. Therefore, the sample was repositioned in between the imaging procedure, resulting in

a certain overlap of two consecutive images. The control system concert (Vogelgesang et al. 2016) was used for automated data acquisition and online reconstruction of tomographic slices for data quality assurance. Execution of the pipelines, including online tomographic reconstruction, was performed by the UFO framework (Vogelgesang et al. 2012). Final tomographic reconstruction was carried out with *tofu* (Farágó et al. 2022).

The two resulting tomograms were registered and calibrated with Fiji (Schindelin et al. 2012) (<https://imagej.net/Fiji>) and further imported to the plugin TrakEM2 (Cardona et al. 2012) for stitching and cropping. Subsequently, the resulting image stack was imported to Amira version 6.0 (FEI Company, Hillsboro, OR, USA) to pre-segment the various cuticular and internal structures in the software's segmentation editor by manually labelling every 50th virtual slice. These labels served as an input for automated segmentation by using the Biomedical Image Segmentation App 'Biomedisa' (Lösel et al. 2020) (<https://biomedisa.org>). After some minor manual corrections to the segmentation results of the 'Biomedisa' output by using Amira, we converted them into polygon meshes. We thereby applied some minor smoothing and polygon reduction to create the final 3D model (surface mesh).

Results

Bocchus rex sp. nov.

<https://zoobank.org/C24153EA-53FD-40CD-96FB-08BEA582D2BE>

Type material. *Holotype* (= specimen 1; Fig. 1): f#, in SIZK: UKRAINE: Les-1, specimen in upper Eocene Rovno amber, collected in Lisove amber mine in Volyn Region of W Ukraine, 9 km east of Manevichi (the former Manevichi district, now Kamen-Kashirsky district). Horizon: Priabonian (35–38 Ma). *Paratype* (= specimen 2; Figs 2, 3): 1f#, in SMNS: UKR-1, specimen in Rovno amber (unknown locality).

Diagnosis. Macropterous female of *Bocchus* (Figs 1a–d, 2a–c) with OOL more than three times as long as OPL (Fig. 1b); epicnemium concealed (Fig. 1d); notauli incomplete, reaching about 0.75× length of mesoscutum (Figs 1b, 2c); fore wing with one dark transverse band (Figs 1a, 2c); petiole distinctly visible (Fig. 1a); enlarged claw (Figs 1e, f, 2d, 4a) with one long row of small teeth, in addition to one lamella; pro-tarsomere 5 (Figs 1e, f, 2d, 4a) with distal apex broad and dark pigmented, with one preapical lamella and inner band, without bristles on inner margin.

Description of the female (Figs 1–4a). Fully winged (Figs 1a–d, 2a–c); length 2.8–3.2 mm (holotype 3.2 mm). Holotype ferruginous-black; paratype black. Antenna clavate (Fig. 1a, b), without ADOs; antennomeres in following proportions: 9:6:6:5:5:4.5:4.5:4.5:6; antennomere 9 slightly longer than broad (4.5:3). Head dull, completely granulate, not reticulate rugose; frontal line complete; occipital carina complete; POL = 3; OL = 2; OOL = 5; OPL = 6.5; TL = 6; greatest breadth of lateral ocellus shorter than POL (2:3). Mandible quadridentate, with one



Figure 1. Stereomicroscopical images of *Bocchus rex* sp. nov., female, holotype (= specimen 1) **a, b** habitus, dorsal view **c** habitus, lateral view **d** habitus, ventrolateral view **e** fore leg **f** chela.

smaller intermediate tooth (Fig. 1d). Mesosoma longer than head (18:7), shorter than metasoma (18:23). Pronotum crossed by strong transverse impression, with sculpture not distinct, laterally with some longitudinal keels; pronotal tubercle reaching tegula. Mesoscutum dull, granulate. Notauli incomplete, reaching about 0.80× length of mesoscutum (Figs 1b, 2c). Sculpture of mesoscutellum and metanotum not distinctly visible. Epicnemium concealed (Fig. 1d). Metapectal-propodeal complex not distinctly visible. Fore wing with one dark broad transverse band (Figs 1a, 2c); distal part of 2r-rs&Rs vein much longer than proximal part (17:5). Petiole very long, much shorter than rest of metasoma (4:19). Proleg ratio: 12 (procoxa): 10 (protrochanter): 24 (profemur): 17 (protibia): 13 (protarsomere

1): 2 (protarsomere 2): 3 (protarsomere 3): 7 (protarsomere 4): 11 (protarsomere 5). Enlarged claw (Figs 1e, f, 2d, 4a) with one long row of small teeth (number not distinct) + one lamella. Protarsomere 5 (Figs 1e, f, 2d, 4a) with distal apex broad and dark pigmented, with one preapical lamella and inner band, without bristles on inner margin. Rudimentary claw present, although hardly visible. Mesoleg ratio: 9 (mesocoxa): 4 (mesotrochanter): 19 (mesofemur): 21 (mesotibia): 30 (tarsus). Metaleg ratio: 10 (metacoxa): 6 (metatrochanter): 27 (metafemur): 30 (metatibia): 25 (tarsus). Tibial spurs 1, ?, 1.

Male. Unknown.

Hosts. Unknown.

Etymology. *Bocchus* was the name of two kings of Mauretania (the first being father-in-law to the Numidian King Jugurtha) and *rex* is an appropriate epithet of this nice species with its regal look.

State of preservation of paratype (= specimen 2). The head and thorax are well preserved but each have a fissure dorsally (Fig. 3c, e). The metasoma has been completely crushed (Figs 2c, 3a, c, e, g, Suppl. material 1: Video S1). Its size and form can be roughly estimated from the cavity formed in the amber. However,

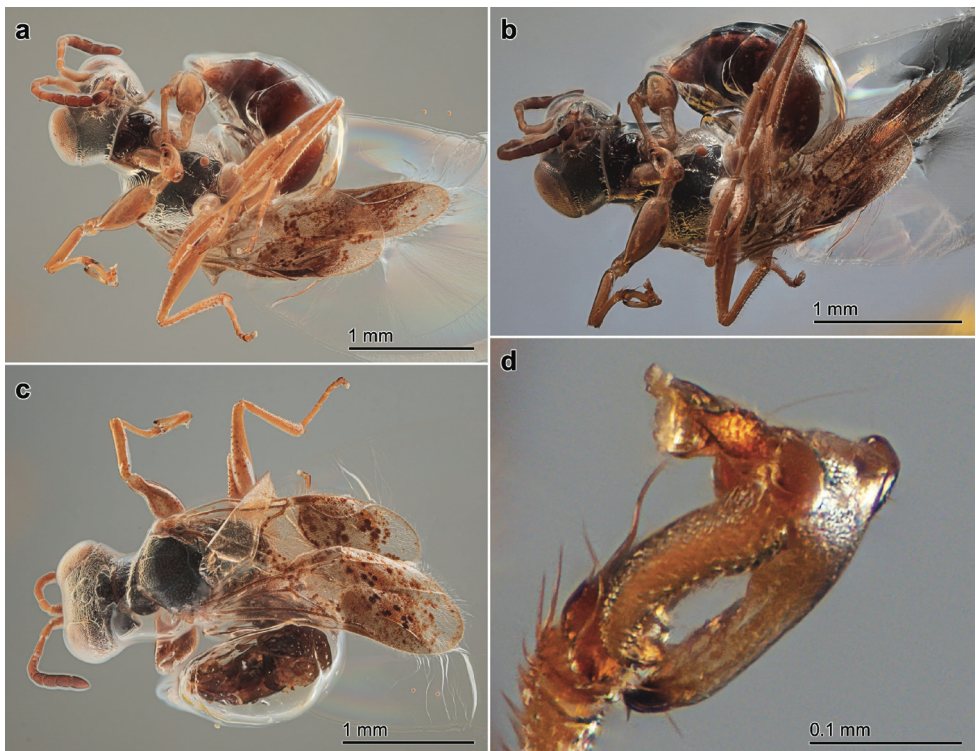


Figure 2. Stereomicroscopical images of *Bocchus rex* sp. nov., female, paratype (= specimen 2) **a, b** habitus, ventral view **c** habitus, dorsal view **d** chela.

cavities are also present laterally between the head and the thorax (Figs 2a–c, 3a, c, e, g, i, Suppl. material 1: Video S1). Unfortunately, the resolution of the SR- μ CT scan was too low to 3D-reconstruct the chelae in great detail. In the head, the partially preserved optical ganglion complex, presumably the optic lobes (= medullae), is clearly visible (Fig. 3b, d, f, h, j, Suppl. material 1: Video S1). It is the second report of optic lobe preservation for Rovno amber arthropods (cf. fig. 1 of Sukhomlyn et al. 2022). Other internal structures are partially preserved; however, it is unclear whether they belong to the optical system or different brain regions, or are partially preserved muscles of the mouthparts (Fig. 3b, d, f, h, j, Suppl. material 1: Video S1). In addition, many muscles in the thorax, the legs and, occasionally, in the metasoma are still preserved (Fig. 3b, d, f, h, j, Suppl. material 1: Video S1). However, as the depicted set of muscles is by no means complete and plays no role in species identification, it will not be discussed further here.

Remarks. After the description of *Bocchus rex* sp. nov., the key published by Perkovsky et al. (2020) can be modified as follows.

Key to the Cretaceous and Paleogene species of the genus *Bocchus* Ashmead, 1893

Female:

- | | | |
|---|---|---|
| 1 | Petiole very short, almost absent (cf. fig. 4 of Perkovsky et al. 2020) | <i>B. cenomanianus</i> Olmi, Rasnitsyn & Guglielmino |
| – | Petiole distinctly visible, one sixth to one ninth of rest of metasoma (cf. fig. 1 of Perkovsky et al. 2020; Fig. 1a) | 2 |
| 2 | Enlarged claw with teeth present only in the distal half of the inner margin (Fig. 4c) | <i>B. schmalhauseni</i> Perkovsky, Olmi, Vasilenko, Capradossi & Guglielmino |
| – | Enlarged claw with teeth distributed along the entire inner margin (Figs 2d, 4a, b) | 3 |
| 3 | Head with OOL about 62% of OPL; notauli complete, posteriorly separated (cf. fig. 9 of Perkovsky et al. 2020); protarsomere 5 with distal apex slender and not pigmented, with two bristles on inner margin (Fig. 4b) | <i>B. primaevus</i> Martins & Melo |
| – | Head with OOL about 77% of OPL (Fig. 1b); notauli incomplete, reaching about 0.80 \times length of mesoscutum (Figs 1b, 2c); protarsomere 5 with distal apex broad and dark pigmented, without bristles on inner margin (Fig. 4a).. | <i>B. rex</i> sp. nov. |

Male:

Unknown.

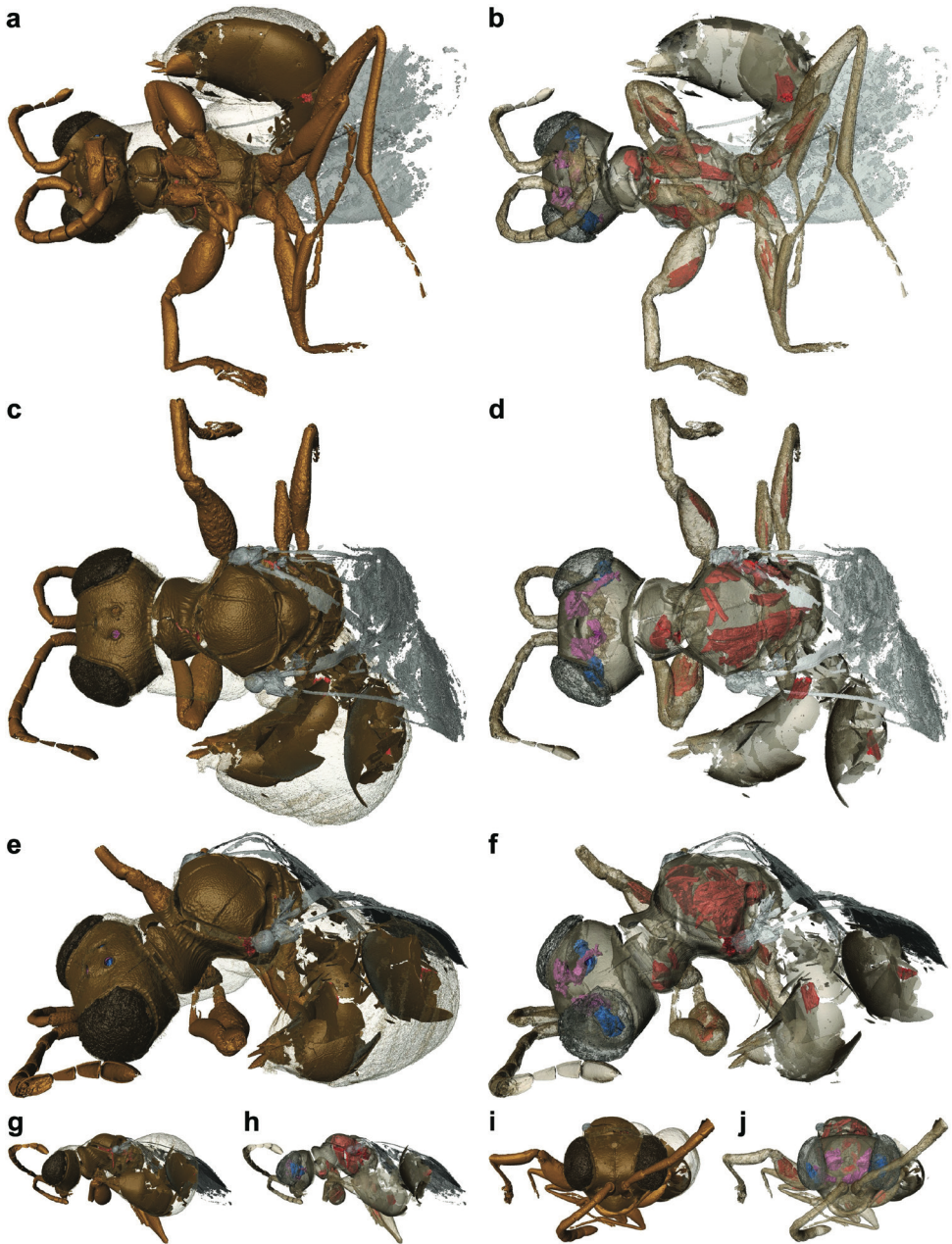


Figure 3. Segmented 3D model of *Bocchus rex* sp. nov., female, paratype (= specimen 2) based on SR- μ CT data (perspective view; cf. Suppl. material 1: Video S1; parts of the left antenna and the tarsus of the right hind leg are outside of the dataset) **a, b** ventral view **c, d** dorsal view **e, f** dorsolateral view **g, h** lateral view **i, j** frontal view. The cuticular elements in a, c, e, g, i are depicted in various shades of brown, whereas the cavity of the wasp in the amber is shown as being semi-transparent. The partially preserved optical ganglion complex is shown in blue, the potential brain regions or head muscles in purple, and the muscles (in the thorax, the legs and the metasoma) in red, whereas the cuticular elements in b, d, f, h, j are semi-transparent and the cavity in the amber is omitted.

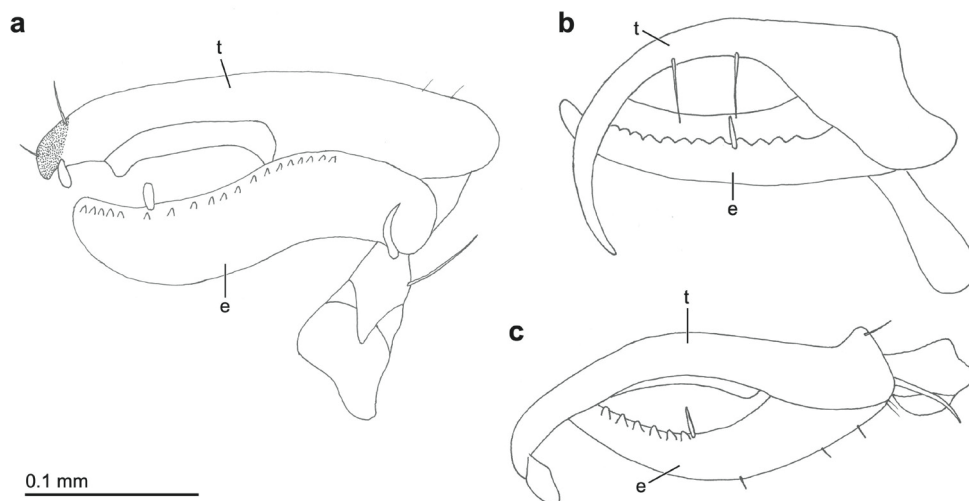


Figure 4. Schematic drawings of chelae of species of *Bocchus* known from amber **a** *Bocchus rex* sp. nov. **b** *B. primaevus* Martins & Melo (from Perkovsky et al. 2020) **c** *B. schmalhauseni* Perkovsky, Olmi, Vasilenko, Capradossi & Guglielmino (from Perkovsky et al. 2020). Abbreviations: e, enlarged claw; t, protarsomere 5.

Discussion

The above-described new species is attributed to the genus *Bocchus* (Hymenoptera, Dryinidae, Bocchinae) because of the following characters: ocelli present; epicnemium concealed; protarsus chelate; chela with rudimentary claw.

The genus *Bocchus* includes 103 species present in all zoogeographical regions, except for Antarctica (Perkovsky et al. 2020). The hosts of *Bocchus* are Tropicuchidae and Caliscelidae (Hemiptera, Auchenorrhyncha) (Guglielmino et al. 2013). These two families of planthoppers are only known from the Cenozoic (Perkovsky et al. 2020).

Fossil species of *Bocchus* are known from the Cenozoic (i.e. from Baltic and Rovno amber) as follows: *B. primaevus* Martins & Melo, 2019 (2021) from upper Eocene Baltic amber, Priabonian, 35–38 Ma; *B. schmalhauseni* Perkovsky, Olmi, Vasilenko, Capradossi & Guglielmino, 2020 and *B. rex* sp. nov. from Rovno amber, coeval of Baltic amber. Probably the hosts of the above three species were Tropicuchidae, as they are known from both Baltic and Rovno amber (Perkovsky and Bogdasarov 2009; Perkovsky et al. 2020; Olmi et al. 2022). The oldest tropiduchid is known from the lower Eocene of the Green River Formation (CO, USA) (Shcherbakov 2006). Fossil Caliscelidae are also known from the Cenozoic, but only from Dominican amber (Burdigalian, lower Miocene; 16–20 Ma) (Bourgoin et al. 2015).

A fourth species has been attributed to the genus *Bocchus*: *B. cenomanianus* Olmi, Rasnitsyn & Guglielmino, 2010. It is a compression fossil in extremely bad condition from Obeschchayushchiy, Magadan region, Russian Federation (Santonian-Campanian, Upper Cretaceous, 72–85 Ma). However, its attribution to *Bocchus* is doubtful, because Caliscelidae and Tropicuchidae are not known from the Cretaceous (Perkovsky et al.

2020). Of course, the host at the Obeschchayushchiy site might well have belonged to other families of planthoppers. However, according to Perkovsky et al. (2020), angiosperms (hosts of extant Caliscelidae and Tropiduchidae) were extremely rare at that site. On the other hand, no evidence exists for possible *Bocchus* hosts feeding on gymnosperms or ancient ferns predominant at the Obeschchayushchiy site (Nadein and Perkovsky 2018; Perkovsky et al. 2020). Hence, *B. cenomanianus* might have been misidentified.

The new *Bocchus* described here is the first hymenopteran and seventh named fossil arthropod from the Volyn Region, Ukraine (Martynov et al. 2021; Telnov et al. 2021; Legalov et al. 2022). The discovery of *B. rex* is indicative of the richness of *Bocchus* species in Rovno amber in comparison with Baltic amber: two species (29% of all dryinid species) in Rovno amber versus one (4.8% of all dryinid species) in Baltic amber. In addition, one specimen from Varash district could not be determined to the species level. This difference might be related to the climate of the Rovno amber forest being warmer than that of the Baltic amber forest (Kupryjanowicz et al. 2022; Yamamoto et al. 2022; and references therein), especially since their potential hosts (i.e. Tropiduchidae) are mainly tropical and subtropical (Bourgoin 2020).

To date, *Bocchus* is the most common genus of Dryinidae in Rovno amber fauna and Bocchinae is the dominant subfamily (44.4% of specimens versus 33.3% for *Dryinus* and Dryininae) at the specimen level. This is unusual, as Dryininae strongly dominate not only in Baltic amber, but also in Kachin (33 Dryininae species according to Olmi et al. 2022) and Dominican (ten Dryininae species versus one belonging to Bocchinae; Martynova et al. 2019; Martins and Melo 2020) ambers, both at the specimen and species levels.

The biology of *Bocchus* species is poorly known so far. The species with known biology live in open environments. An even more important reason for the abundance of *Bocchus* is that open environments were more common in the Priabonian Ukraine than in the Baltic amber forest (Lyubarsky and Perkovsky 2012; Perkovsky 2013; Lyubarsky and Perkovsky 2019; Dietrich and Perkovsky 2020).

A comparison with the extant *Bocchus* species shows that their body shape is similar to the species known from European Eocene amber. The chela of *B. rex* and *B. schmalhauseni* follows the same general scheme as in the extant species. The only difference can be observed in the chela of *B. primaevus* and is attributable to the anomalous long and slender protarsomere 5 (Fig. 4b). A similar type of protarsomere 5 has not been found in any extant or fossil species of *Bocchus*. However, the significance of this anomalous chela remains unknown.

Acknowledgements

We are grateful to Nikolai R. Khomich (Rovno, Ukraine) and Jonas Damzen (Vilnius, Lithuania) for their help in obtaining the specimens studied in this paper, to Anatoly P. Vlaskin (SIZK) for cutting and polishing the amber piece and to Sergei A. Simutnik (SIZK) for his help with the photographic images. We are also grateful to Alexander P. Rasnitsyn (A.A. Borissiak Paleontological Institute of the Russian Academy

of Sciences, Moscow, Russia) for his helpful discussion of the results. We thank Elias Hamann and Marcus Zuber (both KIT) for their assistance at the beamline and Tomáš Faragó (KIT) for tomographic raw data reconstruction. We acknowledge the KIT light source for provision of instruments at their beamlines and we also thank the Institute for Beam Physics and Technology (IBPT) for operation of the storage ring, the Karlsruhe Research Accelerator (KARA). Our thanks are also extended to Oliver Betz (University of Tübingen) for his support and Theresa Jones for linguistic corrections of the manuscript. Many thanks to Eduardo G. Virla and Wesley Dondoni Colombo for their helpful comments and suggestions. We acknowledge the support of the Open Access Publishing Fund of the University of Tübingen.

References

- Ashmead WH (1893) Monograph of the North American Proctotrypidae. Bulletin of the United States National Museum 45: 1–472. <https://doi.org/10.5479/si.03629236.45.1>
- Azevedo CO, Alencar IDCC, Ramos MS, Barbosa DN, Colombo WD, Vargas JM, Lim J (2018) Global guide to the flat wasps (Hymenoptera, Bethyridae). *Zootaxa* 4489(1): 1–294. <https://doi.org/10.11646/zootaxa.4489.1.1>
- Betz O, Wegst U, Weide D, Heethof M, Helfen L, Lee W-K, Cloetens P (2007) Imaging applications of synchrotron X-ray phase-contrast microtomography in biological morphology and biomaterials science. I. General aspects of the technique and its advantages in the analysis of millimetre-sized arthropod structure. *Journal of Microscopy* 227(1): 51–71. <https://www.doi.org/10.1111/j.1365-2818.2007.01785.x>
- Bourgoin T (2020) FLOW (Fulgoromorpha Lists On the Web): a world knowledge base dedicated to Fulgoromorpha. Version 8, updated 11 November 2020. <http://flow.snv.jussieu.fr/> [accessed 25 November, 2020]
- Bourgoin T, Wang R-R, Gnezdilov VM (2015) First fossil record of Caliscelidae (Hemiptera: Fulgoroidea): a new Early Miocene Dominican amber genus extends the distribution of Augilini to the Neotropics. *Journal of Systematic Palaeontology* 14(3): 211–218. <https://doi.org/10.1080/14772019.2015.1032376>
- Cardona A, Saalfeld S, Schindelin J, Arganda-Carreras I, Preibisch S, Longair M, Tomancak P, Hartenstein V, Douglas RJ (2012) TrakEM2 Software for neural circuit reconstruction. *PLoS ONE* 7(6): e38011. <https://doi.org/10.1371/journal.pone.0038011>
- Cecilia A, Rack A, Douissard P-A, Martin T, dos Santos Rolo T, Vagovič P, Hamann E, van de Kamp T, Riedel A, Fiederle M, Baumbach T (2011) LPE grown LSO:Tb scintillator films for high resolution X-ray imaging applications at synchrotron light sources. *Nuclear Instruments and Methods in Physics Research, Section A: Accelerators, Spectrometers, Detectors and Associated Equipment* 648 (Supplement 1): S321–S323. <https://doi.org/10.1016/j.nima.2010.10.150>
- Dietrich CH, Perkovsky EE (2020) A new genus and species representing the first leafhopper (Hemiptera: Cicadellidae) from Eocene Rovno amber. *Palaeontology* 3(2): 180–187. <https://doi.org/10.11646/palaeontology.3.2.7>

- Douissard P-A, Cecilia A, Rochet X, Martin T, van de Kamp T, Helfen L, Baumbach T, Luquot L, Xiao X, Meinhardt J, Rack A (2012) A versatile indirect detector design for hard X-ray microimaging. *Journal of Instrumentation* 7: P09016. <https://doi.org/10.1088/1748-0221/7/09/P09016>
- Faragó T, Gasilov S, Emslie I, Zuber M, Helfen L, Vogelgesang M, Baumbach T (2022) *Tofu*: a fast, versatile and user-friendly image processing toolkit for computed tomography. *Journal of Synchrotron Radiation* 29: 916–927. <https://doi.org/10.1107/S160057752200282X>
- Guglielmino A, Olmi M, Bückle C (2013) An updated host-parasite catalogue of world Dryinidae (Hymenoptera: Chrysidoidea). *Zootaxa* 3740(1): 1–113. <https://doi.org/10.11646/zootaxa.3740.1.1>
- Kawada R, Lanes GO, Azevedo CO (2015) Evolution of metapostnotum in flat wasps (Hymenoptera, Bethyridae): implications for homology assessments in Chrysidoidea. *PLoS ONE* 10(10): e0140051. <https://doi.org/10.1371/journal.pone.0140051>
- Kupryjanowicz J, Lyubarsky GYu, Perkovsky EE (2022) A new genus of the subfamily Languriinae (Coleoptera: Erotylidae) from the Late Eocene Baltic amber. *Far Eastern Entomologist* 447: 1–9. <https://doi.org/10.25221/fee.447.1>
- Lanes GO, Kawada R, Azevedo CO, Brothers DJ (2020) Revisited morphology applied for Systematics of flat wasps (Hymenoptera, Bethyridae). *Zootaxa* 4752(1): 1–127. <https://doi.org/10.11646/zootaxa.4752.1.1>
- Legalov AA, Vasilenko DV, Perkovsky EE (2022) New proxy for Moraceae in Priabonian of Europe: first record of the genus *Demimaea* Pascoe, 1870 (Coleoptera: Curculionidae) from Eocene Rovno amber. *Historical Biology*. <https://doi.org/10.1080/08912963.2022.2089983>
- Lösel PD, van de Kamp T, Jayme A, Ershov A, Faragó T, Pichler O, Jerome NT, Aadepeu N, Bremer S, Chilingaryan SA, Heethoff M, Kopmann A, Odar J, Schmelzle S, Zuber M, Wittbrodt J, Baumbach T, Heuveline V (2020) Introducing Biomedisa as an open-source online platform for biomedical image segmentation. *Nature Communications* 11: 5577. <https://doi.org/10.1038/s41467-020-19303-w>
- Lyubarsky GYu, Perkovsky EE (2012) The first Eocene species of the genus *Cryptophagus* (Coleoptera, Clavicornia, Cryptophagidae). *Vestnik zoologii* 46(1): 83–87. <https://doi.org/10.2478/v10058-012-0007-z>
- Lyubarsky GYu, Perkovsky EE (2019) *Spaniophagus*, first new Eocene genus of silken fungus beetle from Baltic amber (Coleoptera: Clavicornia: Cryptophagidae). *Russian Entomological Journal* 28(3): 263–268. <https://doi.org/10.15298/rusentj.28.3.05>
- Martins AL, Melo GAR (2020) Revision of the fossil species of *Thaumatomyrus* Perkins from Dominican amber, with a new combination and description of a new species (Hymenoptera, Dryinidae). *Journal of Hymenoptera Research* 79: 77–88. <https://doi.org/10.3897/jhr.79.57686>
- Martins AL, Melo GAR (2021) The oldest confirmed fossil of Bocchinae (Hymenoptera, Dryinidae), with description of a new species of *Bocchus* Ashmead from Baltic amber. *Historical Biology* 33(2): 268–271. <https://doi.org/10.1080/08912963.2019.1613392>

- Martynov AV, Vasilenko DV, Perkovsky EE (2021) First Odonata from Upper Eocene Rovno amber (Ukraine). *Historical Biology*. <https://doi.org/10.1080/08912963.2021.2005040>
- Martynova KV, Perkovsky EE, Olmi M, Vasilenko DV (2019) New records of Upper Eocene chrysidoid wasps (Hymenoptera: Chryridoidea) from basins of Styr and Stokhod rivers (Rovno Amber). *Paleontological Journal* 53(10): 998–1023. <https://doi.org/10.1134/S0031030119100125>
- Matalin AV, Perkovsky EE, Vasilenko DV (2021) First record of tiger beetles (Coleoptera, Cicindelidae) from Rovno amber, with the description of a new genus and species. *Zootaxa* 5016(2): 243–256. <https://doi.org/10.11646/zootaxa.5016.2.5>
- Nadein KS, Perkovsky EE (2018) A new tribe of Galerucinae leaf beetle (Insecta: Coleoptera: Chrysomelidae) from the Upper Cretaceous Taimyr amber. *Cretaceous Research* 84: 97–106. <https://doi.org/10.1016/j.cretres.2017.10.023>
- Olmi M (1984) A revision of the Dryinidae (Hymenoptera). *Memoirs of the American Entomological Institute* 37(I–XII): 1–1913.
- Olmi M (2000 [“1998”]) New fossil Dryinidae from Baltic and Lebanese amber (Hymenoptera Chryridoidea). *Frustula entomologica*, N.S. 21: 48–67.
- Olmi M, Bechly G (2001) New parasitic wasps from Baltic amber (Insecta: Hymenoptera: Dryinidae). *Stuttgarter Beiträge zur Naturkunde, Serie B* 306: 1–58.
- Olmi M, Copeland RS, van Noort S (2019) Dryinidae of the Afrotropical region (Hymenoptera, Chryridoidea). *Zootaxa* 4630(1): 1–619. <https://doi.org/10.11646/zootaxa.4630.1.1>
- Olmi M, Rasnitsyn AP, Guglielmino A (2010) Revision of rock fossils of Dryinidae and Embolemidae (Hymenoptera: Chryridoidea). *Zootaxa* 2499(1): 21–38. <https://doi.org/10.11646/zootaxa.2499.1.2>
- Olmi M, Chen H-Y, Shih C, Müller P, Capradossi L, Ren D, Perkovsky EE, Guglielmino A (2021a) New species of *Hybristodryinus* Engel (Hymenoptera, Dryinidae) from mid-Cretaceous amber of northern Myanmar, with notes on their possible hosts. *Journal of Hymenoptera Research* 81: 43–55. <https://doi.org/10.3897/jhr.81.57792>
- Olmi M, Vasilenko DV, Capradossi L, Perkovsky EE, Guglielmino A (2021b) A new species of *Lonchodryinus* (Hymenoptera, Dryinidae) from Upper Eocene Baltic amber. *Zootaxa* 5020(2): 328–336. <https://doi.org/10.11646/zootaxa.5020.2.5>
- Olmi M, Guglielmino A, Vasilenko DV, Perkovsky EE (2022) Discovery of the first apterous pincer wasp from amber, with description of a new tribe, genus and species of Apodryininae (Hymenoptera, Dryinidae). *Zootaxa* 5162(1): 054–066. <https://doi.org/10.11646/zootaxa.5162.1.3>
- Perkovsky EE (2013) *Eohelea sinuosa* (Meunier, 1904) (Diptera, Ceratopogonidae) in Late Eocene Ambers of Europe. *Paleontological Journal* 47(5): 503–512. <https://doi.org/10.1134/S0031030113040163>
- Perkovsky EE, Bogdasarov MA (2009 [“2008”]) New finds of insects and plants in amber from Belarus. *The Kharkov Entomological Society Gazette* 16: 7–13.
- Perkovsky EE, Nel A (2021) A new Rovno amber termite genus (Isoptera, Rhinotermitidae) from Styr River basin. *Palaeontologia Electronica* 24(1): 24.1.a05. <https://doi.org/10.26879/1127>

- Perkovsky EE, Olmi M, Müller P, Martynova KV (2019) A review of the genus *Hybristodryinus* Engel, 2005 (Hymenoptera, Dryinidae) from mid-Cretaceous Burmese amber, with a discussion on its phylogenetic significance. *Cretaceous Research* 99: 169–189. <https://doi.org/10.1016/j.cretres.2019.01.023>
- Perkovsky EE, Olmi M, Vasilenko DV, Capradossi L, Guglielmino A (2020) First *Bocchus* Ashmead (Hymenoptera: Dryinidae) from Upper Eocene Rovno amber: *B. schmalhauseni* sp. nov. *Zootaxa* 4819(3): 544–556. <https://doi.org/10.11646/zootaxa.4819.3.6>
- Riolo P, Isidoro N, Ruschioni S, Minuz RL, Bin F, Romani R (2016) Anatomy of the antennal dorsal organ in female of *Neodryinus typhlocybae* (Hymenoptera: Dryinidae): a peculiar sensory structure possibly involved in perception of host vibration. *Journal of Morphology* 277(1): 128–137. <https://doi.org/10.1002/jmor.20485>
- Schindelin J, Arganda-Carreras I, Frise E, Kaying V, Longair M, Pietzsch T, Preibisch S, Rueden C, Saalfeld S, Schmid B, Tinevez J-Y, White DJ, Hartenstein V, Eliceiri K, Tomancak P, Cardona A (2012) Fiji: an open-source platform for biological-image analysis. *Nature Methods* 9(7): 676–682. <https://doi.org/10.1038/nmeth.2019>
- Shcherbakov DE (2006) The earliest find of Tropicuchidae (Homoptera: Auchenorrhyncha), representing a new tribe, from the Eocene of Green River, USA, with notes on the fossil record of higher Fulgoroidea. *Russian Entomological Journal* 15(3): 315–322.
- Sukhomlyn MM, Vorontsov DD, Vasilenko DV, Perkovsky EE (2022) Review of information on Eocene entomopathogenic Hypocreales (Ascomycota). *Paleontological Journal* 56(3): 305–310. <https://doi.org/10.1134/S0031030122030133>
- Telnov D, Perkovsky EE, Vasilenko DV, Yamamoto S (2021) The first fossil Coleoptera record from the Volyn Region, Ukraine, with description of a new *Glesoconomorphus* (Coleoptera, Mycteridae) in syninclusion with Winterschmidtidae (Acari) and a key to species. *ZooKeys* 1068: 189–201. <https://doi.org/10.3897/zookeys.1068.75391>
- Tshernyshev SE, Perkovsky EE (2021) *Protomauroania mikhailovi*—a new species of malachite beetles (Coleoptera, Dasytidae) in Rovno amber. *Zootaxa* 5006(1): 189–194. <https://doi.org/10.11646/zootaxa.5006.1.20>
- Vogelgesang M, Chilingaryan S, dos Santos Rolo T, Kopmann A (2012) UFO: a scalable GPU-based image processing framework for on-line monitoring. *Proceedings of HPCC-ICISS: 824–829*. <https://doi.org/10.1109/HPCC.2012.116>
- Vogelgesang M, Farago T, Morgener TF, Helfen L, dos Santos Rolo T, Myagotin A, Baumbach T (2016) Real-time image-content-based beamline control for smart 4D X-ray imaging. *Journal of Synchrotron Radiation* 23: 1254–1263. <https://doi.org/10.1107/S1600577516010195>
- Yamamoto S, Nazarenko VYu, Vasilenko DV, Perkovsky EE (2022) First fossil species of ship-timber beetles (Coleoptera: Lymexylidae) from Eocene Rovno amber (Ukraine). *Fossil Record* 25(1): 65–74. <https://doi.org/10.3897/fr.25.81054>

Supplementary material I

Video S1

Authors: Massimo Olmi, Benjamin Eggs, Leonardo Capradossi, Thomas van de Kamp, Evgeny E. Perkovsky, Adalgisa Guglielmino, Dmitry V. Vasilenko

Data type: video file (mp4)

Explanation note: Animation of the rotating segmented 3D model of *Bocchus rex* sp. nov., female, paratype (= specimen 2) based on SR- μ CT data (perspective view; cf. Fig. 3; parts of the left antenna and the tarsus of the right hind leg are outside of the dataset). The cuticular elements are depicted in various shades of brown, whereas the cavity of the wasp in the amber is shown as being semi-transparent. The partially preserved optical ganglion complex is shown in blue, the potential brain regions or head muscles in purple, and the muscles in red.

Copyright notice: This dataset is made available under the Open Database License (<http://opendatacommons.org/licenses/odbl/1.0/>). The Open Database License (ODbL) is a license agreement intended to allow users to freely share, modify, and use this Dataset while maintaining this same freedom for others, provided that the original source and author(s) are credited.

Link: <https://doi.org/10.3897/jhr.92.87084.suppl1>

Additional files (supplementary material): video file (snapshot displayed here); file available online at <https://jhr.pensoft.net/article/87084/>



Supplementary material 1 – Video S1: Animation of the rotating segmented 3D model of *Bocchus rex* sp. nov., female, paratype (= specimen 2) based on SR- μ CT data (perspective view; cf. Fig. 3; parts of the left antenna and the tarsus of the right hind leg are outside of the dataset). The cuticular elements are depicted in various shades of brown, whereas the cavity of the wasp in the amber is shown as being semi-transparent. The partially preserved optical ganglion complex is shown in blue, the potential brain regions or head muscles in purple, and the muscles in red. (mp4)

Conclusions

This thesis provides an overview of the various joint-free steering mechanisms of rod-shaped structures in invertebrates in the form of literature reviews (see Publications 8–11) with a focus on the slide-lock mechanisms (*sensu* Betz *et al.* 2016).

Various mechanisms have been described or postulated for the joint-free steering movements of rod-shaped multi-element structures in insects, such as the terebrae of hymenopterans or the piercing-sucking mouthparts of hemipterans. Basically, two different types of bending mechanisms can be distinguished: passive and active bending mechanisms.

The observed **passive bending** results from the interplay between the surrounding substrate and the relative movements of the individual elements of a multi-element probe. The relative position of the individual elements, which typically feature geometrically asymmetric bevelled apices, create various degrees of geometric asymmetry of the apex as a whole. Consequently, the asymmetric substrate reaction forces acting on the apex push it away from a straight path during protraction (Fig. 3a), leading to a passive bending of the probe (Cerkvenik *et al.* 2017, 2018; *cf.* “offset steering” *sensu* Frasson *et al.* 2012).

The observed **active bending** occurs when the bending movements originate from the relative movements of the individual elements of a multi-element probe. Several different mechanisms have been described hitherto; *e.g.* pre-apical ‘stop regions’ that increase friction if the individual elements are pro- or retracted (Fig. 3b; *cf.* Quicke *et al.* 1995; *cf.* slide-lock working principle according to Betz *et al.* 2016), largely longitudinally divided elements (*cf.* Quicke 2015), ‘preloaded’ elements (Fig. 3d; *sensu* Pollard 1969), or elements with multi-arched regions of various material composition (Fig. 3c; *cf.* Quicke 1991) (see below for detailed explanations).

Theoretically, passive and active bending mechanisms can act simultaneously or sequentially within the same structure.

The possession of basic knowledge about the various bending and steering mechanisms (passive vs active bending mechanisms, *etc.*) is important for the recognition and comprehension of the morphological evolutionary adaptations found in the organisms under study and for the cognisance of any mechanisms that are not yet described.

The main focus of this thesis has been the various case studies of the structure and function of the ovipositor of parasitoid hymenopterans (Publications 1–6) and the mouthparts of triatomine heteropterans (Publication 7). These integrative studies combining morphological descriptions and biomechanical analyses with behavioural observations *in vivo* are central for identifying the working principles (*sensu* Drack *et al.* 2018) of joint-free steering and thus for the development and design of biomimetic products.

Joint-free steering movements of the terebrae of parasitoid hymenopterans

Despite many descriptive studies on the comparative morphology of the hymenopteran terebra (e.g. Snodgrass 1933, Oeser 1961, Quicke *et al.* 1994, Le Ralec *et al.* 1996), detailed in-depth morphological descriptions and mechanical analyses of the musculoskeletal ovipositor system are rare, especially for the completely understudied and often minute parasitoid wasps, *i.a.* members of Ichneumonoidea, Chalcidoidea or Cynipoidea. In addition, only a few studies have been published on the mechanisms of terebra steering, most of them focusing on ichneumonoid species (Quicke 1991, Quicke *et al.* 1995, Cerkvenik *et al.* 2017). Various passive and active terebra steering mechanisms have been proposed.

Passive bending mechanisms:

- A well studied example of passive bending are the movements of the terebra of the fruit-fly parasitoid *Diachasmimorpha longicaudata* (ASHMEAD, 1905) (Braconidae). The relative position of the individual valvulae featuring geometrically asymmetric bevelled apices creates various degrees of geometric asymmetry of the terebra apex. Consequently, the asymmetric substrate reaction forces acting on the apex push it away from a straight path (Fig. 3a), leading to a passive bending of the terebra (Cerkvenik *et al.* 2017).

Active bending mechanisms:

- Parasitoid hymenopterans can move their valvulae in relation to each other longitudinally. However, if relative sliding is restrained or even fully prevented in some way by structural modifications (e.g. at the interfaces of the valvulae), then joint-free bending movements result as a result of elastic deformations of the single elements. Various forms of this so-called slide-lock mechanism (according to Betz *et al.* 2016) have been postulated in parasitoids:
 - In several species of the Braconidae, pre-apical ‘stop regions’ of the rhachis (e.g. swollen regions located centrally within a corresponding widened part of the aulax at rest) increase

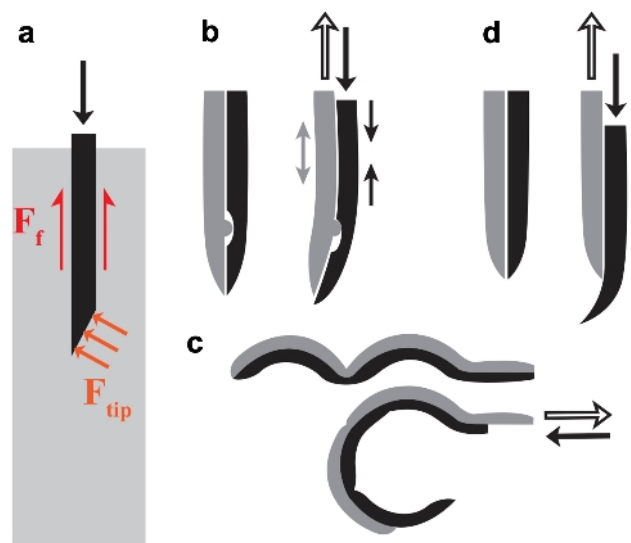


Fig. 3. Hypothesised steering mechanisms in 2D (full arrows represent push forces, empty arrows pull forces, grey arrows tensile forces and small black arrows compression forces). **a** Bevel shape of a probe leads to bending because of asymmetrical tip forces. **b** Restriction in inter-element displacement causes bending attributable to tensile and compression forces. **c** Arched probes bend as a result of differential material composition of their segments. **d** Pre-tension of individual elements leads to inwards curving upon protraction. From Cerkvenik *et al.* 2017, with kind permission of the authors. Abbreviations: F_f : friction along the shaft; F_{tip} : tip forces

friction if the 1st valvulae are retracted or extended, thereby building tension and compression and thus causing the terebra to curve because of the bending moment distribution (Fig. 3b; Quicke *et al.* 1995).

- In the braconid subfamily Doryctinae, a retraction of the 1st valvulae causes the thinned outer walls of the aulaces to restrain the rhachis, which possesses ancillary teeth, consequentially resulting in a ventrad bending movement of the terebra (Quicke *et al.* 1995).
- In several ichneumonid species, a largely longitudinally divided 2nd valvula, which is fused only at the apex, might allow the terebra to be bend left or right when one half of the 2nd valvula is retracted (Quicke 2015).
- In species of the Aulacidae and Gasteruptidae, abrupt terminal stops of the aulaces or protuberances in the ventrolateral side of the 2nd valvula interact with the rhachises of the corresponding bosses of the 1st valvulae whenever they are protracted, thus causing an active dorsal bending of the terebra (Quicke and Fitton 1995).
- In the braconid genus *Zaglyptogastra*, the distal part of the terebra is formed into multi-arched and unevenly sclerotized regions, with the internodular arched sections being more heavily sclerotized than the thinner nodes and, thus, the protrusion of the 1st valvulae causes a flattening out of the nodal regions and a ventral flexing of the terebra (Fig. 3c; Quicke 1991).

The wide variety of parasitoid hymenopterans have evolved many different terebra steering mechanisms, sometimes even within the same family, such as in the Braconidae. The slide-lock mechanisms (Fig. 3b) can also be developed in various ways, as described above.

Most of these parasitoid wasps are able to bend their terebra both dorso–ventrally and laterally, since multilateral steering can be achieved by the interplay of at least three elements (Cerkvenik *et al.* 2018) or by rotational movement occurring simultaneously with the bending movement (*cf.* Publication 5).

New contributions of the present thesis (regarding joint-free steering): Terebra bending movements of parasitoid hymenopterans and of the movements of the individual valvulae (pro- and retraction, bending, rotation) have rarely been recorded *in vivo*. Furthermore, all of the studies on the mechanisms of terebra steering mentioned above have solely focused on the cuticular elements of the ovipositor and have completely neglected the ovipositor musculature.

In our study on the terebra steering of the pteromalid *Lariophagus distinguendus* (Publication 5), we combined behavioural analyses of the oviposition behaviour with thorough morphological investigations (including material properties) of the entire musculoskeletal ovipositor system. Thus, we were able to identify the morphological modifications of the terebra and functional modifications of certain muscles allowing *L. distinguendus* and presumably also other chalcidoid wasps actively to steer their terebra in various directions. We presented the first holistic functional model of the actuation and the underlying mechanisms of terebra bending and rotation (but also all other ovipositor movements) (Fig. 4; *cf.* Fig. 7 of Publication 5). The terebra of *L. distinguendus* and other chalcidoids features a longitudinally split valvula with overlapping

asymmetric halves that are fused only at the apex. The function of the anterior and the posterior 2nd valvifer-2nd valvula muscles of *L. distinguendus* (and presumably in chalcidoid wasps in general) are adapted in their function. (1) In the active probing position, they enable the wasps to pull the base of each of the halves of the 2nd valvula dorsad, thus enabling lateral bending of the terebra. (2) These muscles can also rotate the 2nd valvula and therefore the whole terebra at the basal articulation, allowing the bending movements to become effective in various directions. This terebra steering mechanism, *i.e.* a specific version of the slide-lock mechanisms unique to chalcidoid wasps, is new to science. In contrast to the previously described mechanisms (see above), it allows the 1st valvulae to be pro- or retracted simultaneously with bending movements, regardless of the bending state. These hypotheses were confirmed by *in vivo* observations. A freely steerable terebra increases the chance of contacting a potential host within a concealed cavity, as is often the case in chalcidoid wasps. The ability to steer the terebra can thus be considered a key innovation in the evolution of the hyperdiverse Chalcidoidea (Publication 5).

We have also recorded the bending movements of the unusual coiled terebra of the figitid wasp *Leptopilina heterotoma* *in vivo* and investigated the passive bending mechanisms that it uses to reach its host in plant substrates (Publication 6; Csader *et al.* in prep.).

New contributions of the present thesis (miscellaneous): We have presented the first quantitative analysis of the mechanics and kinematics of the musculoskeletal ovipositor system of any hymenopteran, namely the ichneumonid *Venturia canescens*, including leverages and muscle forces (Publication 1).

We have also found three paired ovipositor muscles in the pteromalid *L. distinguendus*, muscles that have not been previously described in chalcidoids: the 1st valvifer-genital membrane muscle, the ventral 2nd valvifer-venom gland reservoir muscle and the T9-genital membrane muscle. These findings highlight the

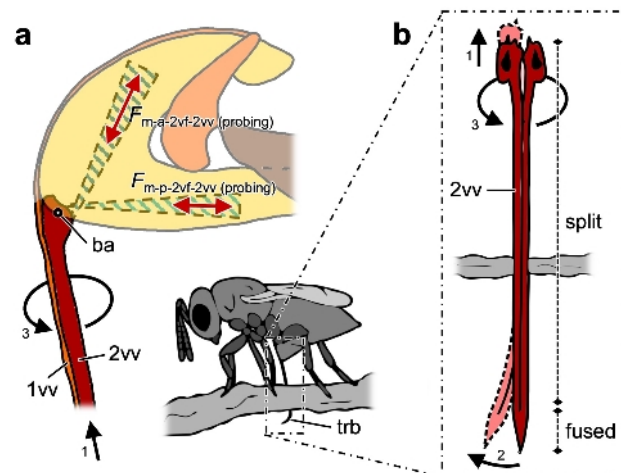


Fig. 4. Functional model of the mechanisms of terebra bending and rotation of *Lariophagus distinguendus*. Acting (input) forces are visualized by solid red arrows and resulting (output) movements by solid black arrows (a lateral view; b dorsal view, schematic drawing of wasps in lateral view). During oviposition, the terebra is anchored at the puncture site in the substrate. A contraction of one of the paired m-a-2vf-2vv ($F_{m-a-2vf-2vv}$) in the active probing position pulls the corresponding bulb and thus one half of the longitudinally split and asymmetrically overlapping 2nd valvula dorsad along its longitudinal axis (arrow 1) because of the orientation of the muscle and the resulting direction of the force vector. Since the halves of the 2nd valvula are fused at the apex, this movement causes the distal part of the terebra (*i.e.* the part inside the cavity of the substrate) to bend to the left or right (arrow 2). A contraction of one of the m-p-2vf-2vv ($F_{m-p-2vf-2vv}$) presumably causes the 2nd valvula and thus the whole terebra to rotate back and forth at the basal articulation along its longitudinal axis to a certain degree (arrow 3). Adapted from Eggs *et al.* 2023 (Publication 5). Abbreviations: 1vv: 1st valvula; 2vv: 2nd valvula; ba: basal articulation; F : force; m-a-2vf-2vv: anterior 2nd valvifer-2nd valvula muscle; m-p-2vf-2vv: posterior 2nd valvifer-2nd valvula muscle; trb: terebra

importance of thorough morphological (re-)investigations with modern state-of-the-art techniques and the need to study a wide range of organisms rather than solely focusing on a handful of well-known study organisms.

The dorsal and the ventral 2nd valvifer-venom gland reservoir muscles found in the chalcidoids *L. distinguendus* (Pteromalidae) (Publication 5) and *Microterys flavus* (Encyrtidae) (Kraft *et al.* in prep.) and in the cynipoid *L. heterotoma* (Figitidae) (Csader *et al.* in prep.) presumably support the discharge of the venom gland reservoir and probably of the secretions of the Dufour's gland. However, these muscles are absent in the two ichneumonoid taxa that we have studied, namely *V. canescens* (Ichneumonidae) (Publication 1, 2) and *Habrobracon hebetor* (Braconidae) (Publication 3). We consider that the valvilli inside the egg canal, which are completely absent in chalcidoid wasps (Quicke *et al.* 1992), support a controlled discharge of venom and oviposition fluids in ichneumonoids.

In addition to their modified terebra used to parasitize hosts living concealed in substrates (Publication 5), chalcidoid wasps possess highly modified mandibles; *i.e.* a secondary reversal to monocondylic mandibles (reduction of the posterior condyle accompanied by modified musculature with functional separation), which allow emerging wasps to bite through hard substrates by precise cutting movements (Publication 4). Several evolutionary novelties and morphological adaptations linked with the use of hosts that live concealed within a substrate have appeared in Chalcidoidea. We have described adaptations in the ovipositor system (for entering the substrate to find a potential host) (Publication 5) and in the mandibles (for leaving the substrate when hatching) (Publication 4) that presumably have been strong drivers of diversification in the Chalcidoidea.

Following modern concepts of designating morphological structures in a standardized way, we have applied (Publications 1–6) and supplemented (Publication 5) the Hymenoptera Anatomy Ontology (HAO; Yoder *et al.* 2010, Seltmann *et al.* 2012, Hymenoptera Anatomy Consortium 2022; <http://glossary.hymao.org>) and list their definitions and all the synonyms found in the literature (210 terms relevant of the hymenopteran ovipositor system and 513 synonyms; Publication 5) to facilitate future reading and to enable comparisons of findings of different studies dealing with the ovipositor of Hymenoptera.

The integrative and comprehensive studies presented in this thesis combining behavioural analyses of the oviposition behaviour with in-depth morphological and biomechanical analyses of the ovipositor system (Publications 1, 5) might become reference works for the study of the hymenopteran ovipositor in the future.

Joint-free steering movements of the maxillary bundles of triatomine heteropterans

Many studies have been published concerning the (comparative) morphology of the mouthparts of the haematophagous kissing bugs (Reduviidae: Triatominae) (e.g. Barth 1952, Geigy and Kraus 1952, Cobben 1978, Rakitov 2019) and their feeding processes (e.g. Barth 1953, Kraus 1957, Lavoipierre *et al.* 1959), even though the majority focuses on *Rhodnius prolixus*, one of the main vectors of Chagas disease (Lent and Wygodzinsky 1979). However, little is known about the manner in which the animals are able actively to steer their mouthparts (a pair of maxillae flanked by a pair of mandibles) for the efficient localization of blood vessels.

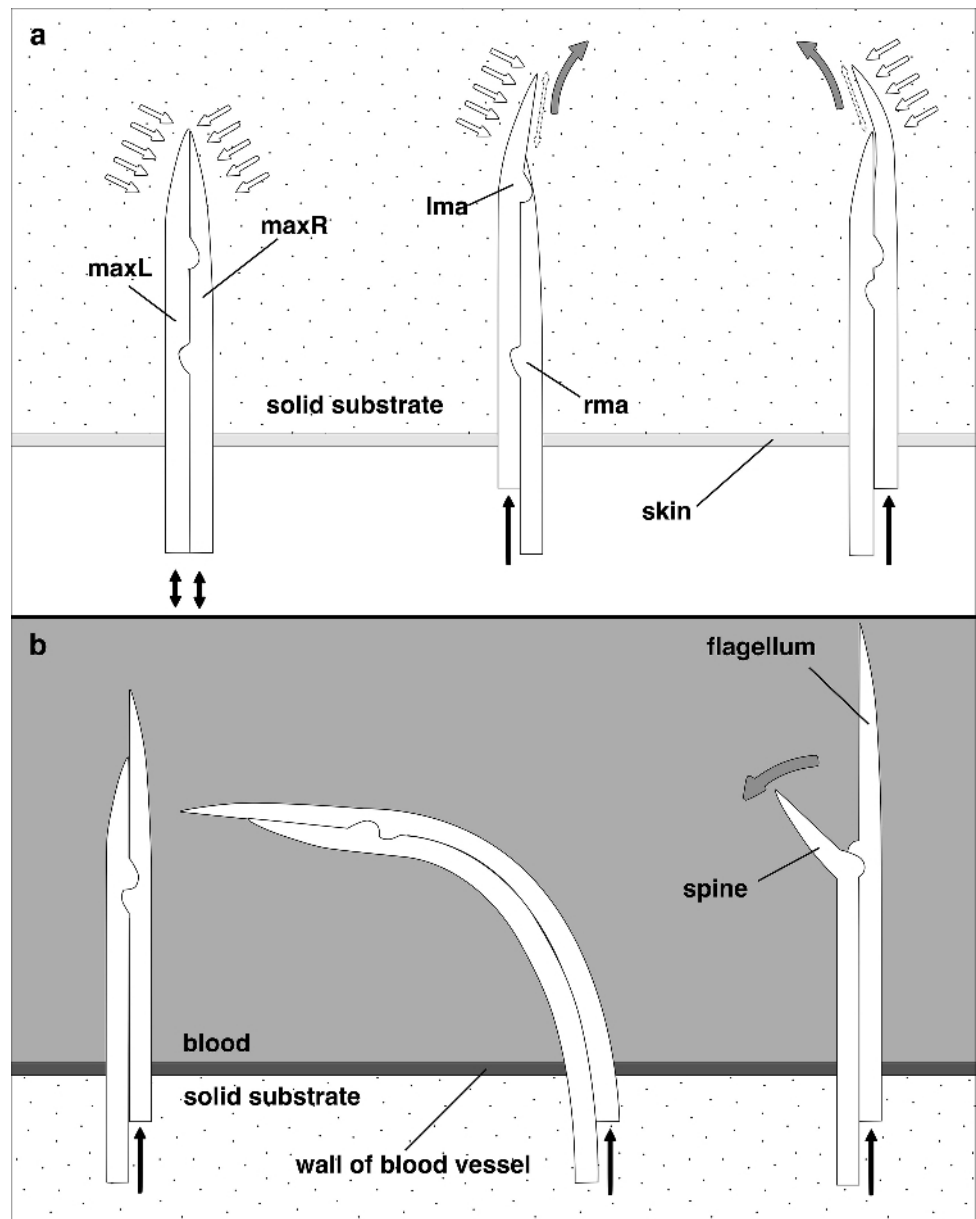


Fig. 5. Mechanisms involved in the bending of the maxillary bundle of triatomine bugs. **a** Movements of the maxillary bundle in tissue (*i.e.* a solid substrate) result from the interaction between substrate and the alternate movements of the maxillae (black arrows). The bevelled tip is pushed away from its straight path (grey arrows) because of asymmetrical forces acting on the variable geometrical asymmetry of the apex (white arrows) (passive bending). **b** In liquids, whenever the right maxilla is protracted to a certain extent (black arrow), its path is blocked by the mechanical interaction of the abutments, resulting in a strong bending of the apex of the maxillary bundle to the left (active bending). Once the mechanical resistance is surmounted, the left maxillary apex changes into its 'splayed out' condition (grey arrow), forming the opening of the food channel. From Tull *et al.* 2020 (Publication 7). Abbreviations: lma/rma: left/right maxillary abutment; maxL/maxR: left/right maxilla

New contributions of the present thesis (regarding joint-free steering): We analysed the morphological structure of the stylets and the feeding process of four different species of Triatominae, namely *Dipetalogaster maxima*, *Rhodnius prolixus*, *Triatoma infestans* and *Panstrongylus megistus* (Publication 7). We recorded and described the steering movements of the maxillary bundle *in vivo* in both liquids and tissue-like substrates. Furthermore, we clearly distinguished between steering movements when searching for a blood vessel and those movements occurring when the distal end of the food channel opens. In agar (simulating the host tissue), we have found that the triatomine bugs are able to steer their maxillary bundle to the left and right. The animals can alter the geometry of the apex of the maxillary bundle by continuously pro- or retracting the individual maxillae. The protruding maxilla is not pushed into the tissue in a straight path, because the asymmetrically bevelled apex is deflected as a result of the asymmetrical forces exerted by the surrounding substrate (*i.e.* passive bending mechanisms). If one maxilla is protracted alone, it curves inwards and the other maxilla follows (Fig. 5b, *cf.* Fig. 9b of Publication 7). In liquids, however, the maxillary bundle is only bent at the apical part and prior to the opening of the distal end of the food channel. These movements presumably result from the mechanical interaction of the apical right and left maxillary abutment (slide-lock mechanism, *i.e.* an active bending mechanism; Fig. 5a, *cf.* Fig. 9a of Publication 7). This demonstrates that both passive and active bending mechanisms not only can occur in the same system, but can also be actuated by the same set of muscles.

Joint-free steering movements of acicular cuticular structures in insects and their potential for biomimetic research

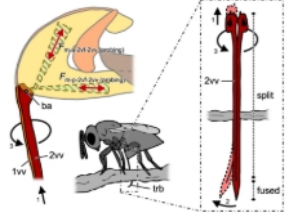
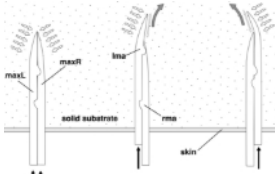
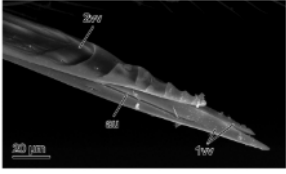
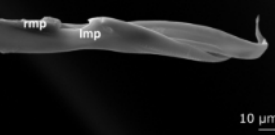
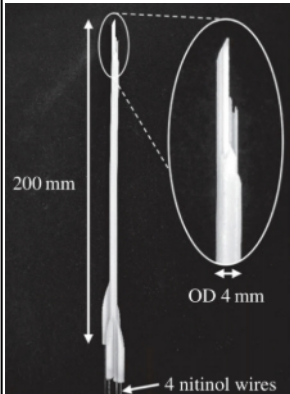
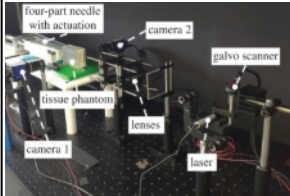
Both the terebrae of parasitoid hymenopterans and the maxillary bundles of triatomine heteropterans were examined in this thesis as examples for rod-like acicular cuticular structures in insects, with specific reference to their joint-free and target-oriented bending movements and their underlying mechanisms and actuation.

Both these structures consist of two or more sub-elements, which are connected by a tongue-and-groove mechanism that allows them to slide longitudinally against each other. Various passive and/or active bending mechanisms enable these rod-like structures to be bent reversibly because of elastic body deformations (see above). The bending stiffness of the elements depends on their geometry, *i.e.* their cross-sectional shape, and their material composition (Publication 8; Cerkvenik *et al.* 2018). A slender probe is more flexible than a wide structure of the same material and length, because of its smaller second moment of area (Cerkvenik *et al.* 2018). Long slender multi-element structures presumably enable precise volumetric steering through a substrate with a very low net external pushing force, preventing buckling during substrate penetration (Cerkvenik *et al.* 2018, *cf.* ‘push-pull’ mechanism; Vincent and King 1995, Wen *et al.* 2023). Shared functional demands, such as buckling avoidance and reaching targets deep within solid substrates without visual information, have presumably led to an evolutionary convergence of slender multi-element probing structures in these different insect taxa.

Both the terebrae of parasitoid hymenopterans and the maxillary bundle of triatomine heteropterans are potentially interesting for biomimetic research and might serve as suitable biological concept generators (Publications 8–11).

Biomimetics can be defined as follows: ‘biomimetics combines the disciplines of biology and technology with the goal of solving technical problems through the abstraction, transfer and application of knowledge gained from biological models’ (VDI 6220 2012). The concepts of ‘function’ and ‘working principle’ (usually termed working mechanisms in the publications presented above) are the core elements in biomimetic knowledge transfer. In the form-function-relationship, the working principle must be considered as the connector between form and function (Drack *et al.* 2018). Many approaches can be used to infer both functions (“What has to be done?”) and working principles (“How?”), *i.a.* morphological investigations, behavioural analyses, material surveys, simulations, and inferences based on analogies (see Duncker 1992). Detailed and thorough case studies (such as Publications 1–7) are thus crucial eliciting function and working principles and thus the development of biomimetic products (Drack *et al.* 2018) (the conceptual levels used for both the terebra and the maxillary bundle and their technical application are shown in Table 1 below).

Table 1. Conceptual levels of engineering design used for two biological examples and their technical application (cf. Drack *et al.* 2018).

Level	Display format	Biological sample 1:	Biological sample 2:	Biomimetic application:
		Terebra of <i>Lariophagus distinguendus</i> (Pteromalidae)	Maxillary bundle of <i>Dipetalogaster maxima</i> (Reduviidae: Triatominae)	Minimally invasive, steerable needle for soft tissue surgery developed by Leibinger <i>et al.</i> 2016
Task	Verbal description	Assessment of a potential host, precise egg laying etc.	Search for a blood vessel	Reach targets in soft tissues with minimal disruption
Function	Verbal description (formalized)	To steer (<i>i.e.</i> bend and rotate) the terebra	To steer (<i>i.e.</i> bend and rotate) the maxillary bundle	To steer (<i>i.e.</i> bend and rotate) the needle
Working principle	Physical (biological) effect and geometry	(Adapted) slide-lock mechanisms, active bending mechanisms  (cf. Eggs <i>et al.</i> 2023)	Passive bending mechanisms attributable to asymmetric substrate reaction forces on the asymmetrical apices (cf. "offset steering" <i>sensu</i> Frasson <i>et al.</i> 2012)  (From Tull <i>et al.</i> 2020)	Passive bending mechanism attributable to controlled tip deflection  (From Leibinger <i>et al.</i> 2016)
Construction	Imaging / detailed drawing	Actual structures of the valvulae involved, <i>i.e.</i> the longitudinally split and asymmetrically overlapping halves of the 2nd valvula that are fused at the apex and the functional adaptations of the associated muscles  (cf. Eggs <i>et al.</i> 2023)	Actual structures of the maxillae involved <i>i.e.</i> the asymmetrically bevelled apices of the two interlocked maxillae  (Image: Tatjana Tull)	Actual structure of the four-part needle prototype  (From Leibinger <i>et al.</i> 2016)
Overarching system	General arrangement picture / drawing	Ovipositor apparatus  (cf. Eggs <i>et al.</i> 2023)	Feeding apparatus  (Image: Fabian Henn)	Set-up for needle actuation  (From Leibinger <i>et al.</i> 2016)

Images from Tull *et al.* 2020 (Publication 7) and Leibinger *et al.* 2016, with kind permission of the authors, and adapted from Eggs *et al.* 2023 (Publication 5). Abbreviations: 1vv: 1st valvula; 2vv: 2nd valvula; au: aulax; ba: basal articulation; F: force; lma/rma, lmp/rmp: left/right maxillary abutment; m-a-2vf-2vv: anterior 2nd valvifer-2nd valvula muscle; m-p-2vf-2vv: posterior 2nd valvifer-2nd valvula muscle; maxL/maxR: left/right maxilla; trb: terebra; OD: outer diameter

The rod-like, acicular cuticular structures capable of joint-free and target-oriented bending movements as studied here, *i.e.* terebrae of parasitoid hymenopterans and the maxillary bundles of triatomine heteropterans, might represent suitable biological concept generators for the design and development of slender miniaturized needle-like probing tools. Biomimetic prototypes based on the hymenopteran terebra comprise various prototypes of actively actuated steerable needle-like probes for minimally disruptive insertion (*e.g.* Young Ko *et al.* 2011, Frasson *et al.* 2012, Leibinger *et al.* 2016, Scali *et al.* 2018, 2019, de Kater *et al.* 2021, Bloemberg *et al.* 2022) that might be beneficial for minimally invasive surgery.

For architecture, however, the biomimetic potential of these structures is probably much lower (see Publication 8), since slender structures are more flexible than a wider ones of the same material and length, because of their smaller second moment of area (Cerkvenik *et al.* 2018). Moreover, all acicular structures under study in the work presented in this thesis comprise of two or more elements that are connected by a tongue-and-groove mechanism. Although the scale-like sculptures at the contact surfaces of the elements, which presumably reduce frictional forces by minimizing contact areas, friction is a major problem for the up-scaling of multi-element structures. Thus, acicular cuticular structures in insects are most likely unsuitable biological concept generators for most large-scale projects, such as those in architecture.

Outlook

Further (comparative) integrative and thorough studies on slender multi-element cuticular structures in insects are needed (1) to investigate their eco-evolutionary significance and reveal the way in which morpho-physiological, behavioural, ecological and life history traits have interacted during their evolution; and (2) to determine their mode of function and working principles in order to develop new biomimetic products.

In addition to the ability to bend without the need of joints conventionally used in engineering, another feature makes the multi-element cuticular structures examined in this thesis exciting biological concept generators, namely the ability to drill without torque and with low axial forces (*cf.* Nakajima and Schwarz 2014). The so-called 'push-pull' mechanism (*cf.* Vincent and King 1995, Cerkvénik *et al.* 2018, Wen *et al.* 2023; also briefly explained in the paragraph 'Penetration of the substrate' of Publication 5) allows certain wasp species to drill through substrates presumably with material removal (and not just material displacement), completely without torque and with an extremely low axial force required.

Moreover, a combination of substrate penetration by the 'push-pull' mechanism with controlled bending movements of the probe would be of interest for drilling n-angled holes with a curved drill path. Such multifunctional systems certainly have a high innovation and application potential, especially in medical technology, *e.g.* for developing tools for minimally invasive surgery.

References

- Barth R. (1952). Anatomische und histologische Studien ueber die Unterfamilie Triatominae (Heteroptera, Reduviidae). I. Teil: Der Kopf von *Triatoma infestans*. *Memórias do Instituto Oswaldo Cruz* 50: 156–194.
- Barth R. (1953). Anatomische und histologische Studien ueber die Unterfamilie Triatominae (Heteroptera, Reduviidae). III. Teil: Untersuchungen ueber den Stechvorgang bei Triatominae. *Memórias do Instituto Oswaldo Cruz* 51: 69–94.
- Belshaw R., Grafen A. and Quicke D. L. J. (2003). Inferring life history from ovipositor morphology in parasitoid wasps using phylogenetic regression and discriminant analysis. *Zoological Journal of the Linnean Society* 139: 213–228. doi: 10.1046/j.1096-3642.2003.00078.x
- Betz O., Wegst U., Weide D., Heethoff M., Helfen L., Lee W. K. and Cloetens P. (2007). Imaging applications of synchrotron X-ray phase-contrast microtomography in biological morphology and biomaterials science. I. General aspects of the technique and its advantages in the analysis of millimetre-sized arthropod structure. *Journal of Microscopy* 227: 51–71. doi: 10.1111/j.1365-2818.2007.01785.x
- Betz O., Birkhold A., Caliaro M., **Eggs B.**, Mader A., Knippers J., Röhrle O. and Speck O. (2016). Adaptive stiffness and joint-free kinematics: actively actuated rod-shaped structures in plants and animals and their biomimetic potential in architecture and engineering. In: Knippers J., Nickel K. G. and Speck T. (eds.), *Biomimetic Research for Architecture and Building Construction: Biological Design and Integrative Structures* (pp. 135–167), Biologically-Inspired Systems, vol. 8. Cham, Switzerland: Springer International Publishing. doi: 10.1007/978-3-319-46374-2_8
- Betz O., **Eggs B.**, Henn F., Birkhold A. and Röhrle O. (2017). Bewegung ohne Gelenke: (Wie) gehts das? In: Knippers J., Schmid U. and Speck T. (eds.), *Baubionik: Biologie beflügelt Architektur* (pp. 20–29), Stuttgarter Beiträge zur Naturkunde, Serie C, vol. 82. Stuttgart, Germany: Staatliches Museum für Naturkunde Stuttgart und Gesellschaft zur Förderung des Naturkundemuseums in Stuttgart e.V.
- Betz O., **Eggs B.**, Henn F., Birkhold A. and Röhrle O. (2019). Bewegung ohne Gelenke: (Wie) gehts das? In: Knippers J., Schmid U. and Speck T. (eds.), *Bionisch bauen: Von der Natur lernen* (pp. 22–31). Basel, Switzerland: Birkhäuser Verlag GmbH. doi: 10.1515/9783035617870-005
- Betz O., **Eggs B.**, Henn F., Birkhold A. and Röhrle O. (2019). Movement without joints: (how) does it work? In: Knippers J., Schmid U. and Speck T. (eds.), *Biomimetics for Architecture: Learning from Nature* (pp. 22–31). Basel, Switzerland: Birkhäuser Verlag GmbH. doi: 10.1515/9783035617917-005

-
- Bloemberg J., Trauzettel F., Coolen B., Dodou D. and Breedveld P. (2022). Design and evaluation of an MRI-ready, self-propelled needle for prostate interventions. *PLoS ONE* 17 (9): e0274063. doi: 10.1371/journal.pone.0274063
- Cardona A., Saalfeld S., Schindelin J., Arganda-Carreras I., Preibisch S., Longair M., Tomancak P., Hartenstein V. and Douglas R. J. (2012). TrakEM2 software for neural circuit reconstruction. *PLoS ONE* 7 (6): e38011. doi: 10.1371/journal.pone.0038011
- Cerkvenik U., van de Straat B., Gussekloo S. W. S. and van Leeuwen J. L. (2017). Mechanisms of ovipositor insertion and steering of a parasitic wasp. *Proceedings of the National Academy of Sciences of the United States of America* 114 (17): E7822–E7831. doi: 10.1073/pnas.1706162114
- Cerkvenik U., Dodou D., van Leeuwen J. L. and Gussekloo S. W. S. (2018). Functional principles of steerable multi-element probes in insects. *Biological Reviews* 94 (2): 555–574. doi: 10.1111/brv.12467
- Cobben R. H. (1978). Evolutionary trends in Heteroptera. Part II. Mouthpart-structures and feeding strategies. *Mededelingen Landbouwhogeschool Wageningen* 78 (5): 1–407. doi: 10.1017/9781139542364.011
- Csader M., Mayer K., Fischer S., Betz O. and **Eggs B.** (2021). The ovipositor of the braconid wasp *Habrobracon hebetor*: structural and functional aspects. *Journal of Hymenoptera Research* 83: 73–99. doi: 10.3897/jhr.83.64018
- Drack M., Limpinsel M., de Bruyn G., Nebelsick J. H. and Betz O. (2018). Towards a theoretical clarification of biomimetics using conceptual tools from engineering design. *Bioinspiration & Biomimetics* 13 (1): 016007. doi: 10.1088/1748-3190/aa967c
- Eggs B.**, Birkhold A. I., Röhrle O. and Betz O. (2018). Structure and function of the musculoskeletal ovipositor system of an ichneumonid wasp. *BMC Zoology* 3: 12. doi: 10.1186/s40850-018-0037-2
- Eggs B.**, Birkhold A. I., Röhrle O. and Betz O. (2018). The musculoskeletal ovipositor system of an ichneumonid wasp: structural and functional aspects. *Mitteilungen des Entomologischen Vereins Stuttgart* 53 (1): 34–36.
- Eggs B.**, Fischer S., Csader M., Mikó I., Rack A. and Betz O. (2023). Terebra steering in chalcidoid wasps. *Frontiers in Zoology* 20: 26. doi: 10.1186/s12983-023-00503-1
- Duncker H.-R. (1992). Funktionelle Morphologie und ihre methodischen Grundlagen—functional morphology and its methodology. *Verhandlungen der Deutschen Zoologischen Gesellschaft* 85: 339–348.
-

-
- Frasson L., Ferroni F., Young Ko S., Dogangil G. and Rodriguez y Baena F. (2012). Experimental evaluation of a novel steerable probe with a programmable bevel tip inspired by nature. *Journal of Robotic Surgery* 6 (3): 189–197. doi: 10.1007/s11701-011-0277-4
- Gauld I. and Bolton B. (1988). *The Hymenoptera*. Oxford, UK: Oxford University Press.
- Geigy R. and Kraus C. (1952). Rüssel und Stechakt von *Rhodnius prolixus*. *Acta Tropica* 9 (3): 272–277.
- Ghara M., Kundanati L. and Borges R. M. (2011). Nature's Swiss army knives: ovipositor structure mirrors ecology in a multitrophic fig wasp community. *PLoS ONE* 6 (8): e23642. doi: 10.1371/journal.pone.0023642
- Hajek A. E. and Eilenberg J. (2018). Insect parasitoids: attack by aliens. In: *Natural Enemies: An Introduction to Biological Control* (pp. 161–188). Cambridge, UK: Cambridge University Press. doi: 10.1017/9781107280267.009
- Heraty J. M. (2017). Parasitoid biodiversity and insect pest management. In: Footitt R. G. and Adler P. H. (eds.), *Insect Biodiversity: Science and Society* (pp. 603–625). Oxford, UK: Wiley-Blackwell. doi: 10.1002/9781118945568.ch19
- Hymenoptera Anatomy Consortium (2022). Hymenoptera Anatomy Ontology. <http://glossary.hymao.org>. Accessed 1 May 2023.
- Justi S. A. and Galvão C. (2016). The evolutionary origin of diversity in Chagas disease vectors. *Trends in Parasitology* 33 (1): 42–52. doi: 10.1016/j.pt.2016.11.002
- de Kater E. P., Sakes A., Bloemberg J., Jager D. J. and Breedveld P. (2021). Design of a flexible wasp-inspired tissue transport mechanism. *Frontiers in Bioengineering and Biotechnology* 9: 782037. doi: 10.3389/fbioe.2021.782037
- Kraus C. (1957). Versuch einer morphologischen und neurologischen Analyse des Stechaktes von *Rhodnius prolixus* STAL 1858. *Acta Tropica* 14: 36–87.
- Krenn H. W. and Aspöck H. (2012). Form, function and evolution of the mouthparts of blood-feeding Arthropoda. *Arthropod Structure & Development* 41 (2): 101–118. doi: 10.1016/j.asd.2011.12.001
- Lavoipierre M. M. J., Dickerson G. and Gordon R. M. (1959). Studies on the methods of feeding of blood-sucking arthropods: I.—The manner in which Triatomine bugs obtain their blood-meal, as observed in the tissue of the living rodent, with some remarks on the effects of the bite on human volunteers. *Annals of Tropical Medicine and Parasitology* 53 (2): 235–250.
-

-
- Le Ralec A., Rabasse J. M. and Wajnberg E. (1996). Comparative morphology of the ovipositor of some parasitic Hymenoptera in relation to characteristics of their hosts. *The Canadian Entomologist* 128: 413–433. doi: 10.4039/Ent128413-3
- Leibinger A., Oldfield M. J. and Rodriguez y Baena F. (2016). Minimally disruptive needle insertion: a biologically inspired solution. *Interface Focus* 6 (3): 20150107. doi: 10.1098/rsfs.2015.0107
- Lent H. and Wygodzinsky P. (1979). Revision of the Triatominae (Hemiptera, Reduviidae), and their significance as vectors of Chagas' disease. *Bulletin of the American Museum of Natural History* 163: 123–520.
- Lösel P. D., van de Kamp T., Jayme A., Ershov A., Faragó T., Pichler O., Jerome N. T., Aadepeu N., Bremer S., Chilingaryan S. A., Heethoff M., Kopmann A., Odar J., Schmelzle S., Zuber M., Wittbrodt J., Baumbach T. and Heuveline V. (2020). Introducing Biomedisa as an open-source platform for biomedical image segmentation. *Nature Communications* 11: 5577. doi: 10.1038/s41467-020-19303-w
- Michels J. and Gorb S. N. (2012). Detailed three-dimensional visualization of resilin in the exoskeleton of arthropods using confocal laser scanning microscopy. *Journal of Microscopy* 245 (1): 1–16. doi: 10.1111/j.1365-2818.2011.03523.x
- Nakajima K. and Schwarz O. (2014). How to use the ovipositor drilling mechanism of Hymenoptera for developing a surgical instrument in biomimetic design. *International Journal of Design and Nature and Ecodynamics* 9 (3): 177–189. doi: 10.2495/DNE-V9-N3-177-189
- Oeser R. (1961). Vergleichend-morphologische Untersuchungen über den Ovipositor der Hymenopteren. *Mitteilungen aus dem Zoologischen Museum in Berlin* 37 (1): 3–119. doi: 10.1002/mmz.19610370102
- Olmi M., **Eggs B.**, Capradossi L., van de Kamp T., Perkovsky E. E., Guglielmino A. and Vasilenko D. V. (2022). A new species of *Bocchus* from upper Eocene Rovno amber (Hymenoptera, Dryinidae). *Journal of Hymenoptera Research* 92: 257–272. doi: 10.3897/jhr.92.87084
- Peters R. S., Niehuis O., Gunkel S., Bläser M., Mayer C., Podsiadlowski L., Kozlov A., Donath A., van Noort S., Liu S., Zhou X., Misof B., Heraty J. and Krogmann L. (2018). Transcriptome sequence-based phylogeny of chalcidoid wasps (Hymenoptera: Chalcidoidea) reveals a history of rapid radiations, convergence, and evolutionary success. *Molecular Phylogenetics and Evolution* 120: 286–296. doi: 10.1016/j.ympev.2017.12.005
-

-
- Peters R. S., Krogmann L., Mayer C., Donath A., Gunkel S., Meusemann K., Kozlov A., Podsiadlowski L., Petersen M., Lanfear R., Diez P. A., Heraty J., Kjer K. M., Klopstein S., Meier R., Polidori C., Schmitt T., Liu S., Zhou X., Wappler T., Rust J., Misof B. and Niehuis O. (2017). Evolutionary history of the Hymenoptera. *Current Biology* 27 (7): 1013–1018. doi: 10.1016/j.cub.2017.01.027
- Polaszek A. and Vilhemsen L. (2023). Biodiversity of hymenopteran parasitoids. *Current Opinion in Insect Science* 56: 101026. doi: 10.1016/j.cois.2023.101026
- Pollard D. G. (1969). Directional control of the stylets in phytophagous Hemiptera. *Proceedings of the Royal Entomological Society of London. Series A, General Entomology* 44 (10–12): 173–185. doi: 10.1111/j.1365-3032.1969.tb00825.x
- Quicke D. L. J. (1991). Ovipositor mechanisms of the braconine wasp genus *Zaglyptogastra* and the ichneumonid genus *Pristomerus*. *Journal of Natural History* 25: 971–977. doi: 10.1080/00222939100770631
- Quicke D. L. J. (1997). *Parasitic Wasps*. London, UK: Chapman & Hall.
- Quicke D. L. J. (2015). *The Braconid and Ichneumonid Parasitoid Wasps: Biology, Systematics, Evolution and Ecology*. Chichester, UK: Wiley-Blackwell. doi: 10.1002/9781118907085
- Quicke D. L. J. and Fitton M. G. (1995). Ovipositor steering mechanisms in parasitic wasps of the families Gasteruptionidae and Aulacidae (Hymenoptera). *Proceedings of the Royal Society of London B: Biological Sciences* 261: 99–103. doi: 10.1098/rspb.1995.0122
- Quicke D. L. J., Fitton M. G. and Ingram S. (1992). Phylogenetic implications of the structure and distribution of ovipositor valvilli in the Hymenoptera (Insecta). *Journal of Natural History* 26: 587–608. doi: 10.1080/00222939200770361
- Quicke D. L. J., Fitton M. G. and Harris J. (1995). Ovipositor steering mechanisms in braconid wasps. *Journal of Hymenoptera Research* 4: 110–120.
- Quicke D. L. J., Fitton M. G., Tunstead J. R., Ingram S. N. and Gaitens P. V. (1994). Ovipositor structure and relationships within the Hymenoptera, with special reference to the Ichneumonoidea. *Journal of Natural History* 28: 635–682. doi: 10.1080/00222939400770301
- Rakitov R. (2019). Morphogenesis of piercing stylets in Hemiptera. In: Krenn H. W. (ed.), *Insect Mouthparts* (pp. 529–566), Zoological Monographs, vol. 5. Cham, Switzerland: Springer Nature Switzerland. doi: 10.1007/978-3-030-29654-4_16
-

-
- Sampalla B., **Eggs B.** and Betz O. (2018). Bending the sting: joint-free movement principles of the ovipositor shaft of the parasitoid wasp *Leptopilina heterotoma* (Figitidae). *Mitteilungen der Deutschen Gesellschaft für allgemeine und angewandte Entomologie* 21: 171–174.
- Scali M., Breedveld P. and Dodou D. (2019). Experimental evaluation of a self-propelling bio-inspired needle in single- and multi-layered phantoms. *Scientific Reports* 9: 19988. doi: 10.1038/s41598-019-56403-0
- Scali M., Pusch T. P., Breedveld P. and Dodou D. (2018). Ovipositor-inspired steerable needle: design and preliminary experimental evaluation. *Bioinspiration & Biomimetics* 13: 016006. doi: 10.1088/1748-3190/aa92b9
- Schindelin J., Arganda-Carreras I., Frise E., Kaynig V., Longair M., Pietzsch T., Preibisch S., Rueden C., Saalfeld S., Schmid B., Tinevez J.-Y., White D. J., Hartenstein V., Eliceiri K., Tomancak P. and Cardona A. (2012). Fiji: an open-source platform for biological-image analysis. *Nature Methods* 9 (7): 676–682. doi: 10.1038/nmeth.2019
- Seltmann K. C., Yoder M. J., Mikó I., Forshage M., Bertone M. A., Agosti D., Austin A. D., Balhoff J. P., Borowiec M. L., Brady S. G., Broad G. R., Brothers D. J., Burks R. A., Buffington M. L., Campbell H. M., Dew K. J., Ernst A. F., Fernández-Triana J. L., Gates M. W., Gibson G. A. P., Jennings J. T., Johnson N. F., Karlsson D., Kawada R., Krogmann L., Kula R. R., Mullins P. L., Ohl M., Rasmussen C., Ronquist F., Schulmeister S., Sharkey M. J., Talamas E., Tucker E., Vilhelmsen L., Ward P. S., Wharton R. A. and Deans A. R. (2012). A hymenopterists' guide to the Hymenoptera Anatomy Ontology: utility, clarification, and future directions. *Journal of Hymenoptera Research* 27: 67–88. doi: 10.3897/jhr.27.2961
- Snodgrass R. E. (1933). Morphology of the insect abdomen. Part II. The genital ducts and the ovipositor. *Smithsonian Miscellaneous Collections* 89 (8): 1–148.
- Tull T., Henn F., Betz O. and **Eggs B.** (2020). Structure and function of the stylets of hematophagous Triatominae (Hemiptera: Reduviidae), with special reference to *Dipetalogaster maxima*. *Arthropod Structure & Development* 58, 100952. doi: 10.1016/j.asd.2020.100952
- van de Kamp T., Mikó I., Staniczek A. H., **Eggs B.**, Bajerlein D., Faragó T., Hagelstein L., Hamann E., Spiecker R., Baumbach T., Janšta P. and Krogmann L. (2022). Evolution of flexible biting in hyperdiverse parasitoid wasps. *Proceedings of the Royal Society B: Biological Sciences* 298 (1967): 20212086. doi: 10.1098/rspb.2021.2086
- VDI 6220 (2012). Biomimetics—conception and strategy—differences between biomimetic and conventional methods/products. *VDI-Richtlinien*. Berlin, Germany: Beuth.
-

- Vilhelmsen L. (2000). The ovipositor apparatus of basal Hymenoptera (Insecta): phylogenetic implications and functional morphology. *Zoologica Scripta* 29: 319–345. doi: 10.1046/j.1463-6409.2000.00046.x
- Vincent J. F. V., and King M. J. (1995). The mechanism of drilling by wood wasp ovipositors. *Biomimetics* 3 (4): 187–201.
- Wen R., Wang Z., Yi J. and Hu Y. (2023). Bending-activated biotensegrity structure enables female *Megarhyssa* to cross the barrier of Euler's critical force. *Science Advances* 9 (42): eadi8284. doi: 10.1126/sciadv.adi8284
- Wenk P., Lucic S. and Betz O. (2010). Functional anatomy of the hypopharynx and the salivary pump in the feeding apparatus of the assassin bug *Rhodnius prolixus*. *Zoomorphology* 129: 225–234. doi: 10.1007/s00435-010-0115-7
- Wirtz H.-P. (1987). Eindringen der Mundwerkzeuge von Raubwanzen durch eine Membran (Hemiptera: Reduviidae). *Entomologia Generalis* 12 (2–3): 147–153. doi: 10.1127/entom.gen/12/1987/147
- Yoder M. J., Mikó I., Seltmann K. C., Bertone M. A. and Deans A. R. (2010). A gross anatomy ontology for Hymenoptera. *PLoS ONE* 5 (12): e15991. doi: 10.1371/journal.pone.0015991
- Young Ko S., Frasson L. and Rodriguez Y Baena F. (2011). Closed-loop planar motion control of a steerable probe with a “programmable bevel” inspired by nature. *IEEE Transactions on Robotics* 27 (5): 970–983. doi: 10.1109/TRO.2011.2159411